Olga A. Smirnova

Environmental Radiation Effects on Mammals

A Dynamical Modeling Approach

Second Edition

Springer

Environmental Radiation Effects on Mammals

Olga A. Smirnova

Environmental Radiation Effects on Mammals

A Dynamical Modeling Approach

Second Edition

Springer

Olga A. Smirnova
Research and Technical Center
of Radiation-Chemical Safety
and Hygiene,
Moscow, Russian Federation

ISBN 978-3-319-45759-8 ISBN 978-3-319-45761-1 (eBook)
DOI 10.1007/978-3-319-45761-1

Library of Congress Control Number: 2016951310

Printed on acid-free paper

This Springer imprint is published by Springer Nature
The registered company is Springer International Publishing AG
The registered company address is: Gewerbestrasse 11, 6330 Cham, Switzerland

Dedicated to my mother and father,
Inna Mikhailovna Smirnova and
Andrey Grigorievich Smirnov

Preface

The monograph presents the biologically motivated dynamic modeling approach to the study and prediction of radiation effects on mammals. This approach embodies the author's mathematical models, which are capable of predicting the dynamics of vital body systems in mammals (namely, the hematopoietic system in rodents and humans, the immune system in rodents, the small intestine in rodents, and the skin in young swine) under normal conditions and under various irradiation regimes (acute/chronic/fractionated/non-uniform irradiation). The developed approach also includes the author's mathematical models, which are capable of prognosticating the mortality dynamics and the average life-span shortening for homogeneous and nonhomogeneous (in radiosensitivity) mammalian populations exposed to acute and chronic irradiation in wide ranges of doses and dose rates on the basis of the statistical characteristics and the modeling dynamics of the respective critical body system (the hematopoietic system or the small intestine) in exposed specimens composing the population. The developed approach demonstrates its efficiency in the assessment of the excess relative risks for leukemia among acutely and continuously irradiated humans (the atomic bomb survivors and patients treated with brachytherapy) proceeding from two key characteristics of the respective modeling dynamics of human major hematopoietic lineages (the granulopoietic and lymphopoietic systems). The developed approach also proves its reliability in the prediction of the dynamics of the pathophysiological reaction (moist desquamation) in skin exposed to single and fractionated irradiation in wide ranges of doses and total doses on the basis of the respective modeling dynamics of epidermal cells of the upper skin layer.

The material presented in the monograph is of an evident theoretical significance. In particular, the performed modeling studies elucidate the basic regulatory mechanisms of the damage and recovery processes running in the vital body systems of exposed mammals and reveal the key parameters characterizing these processes. The proposed explications of a number of nonlinear effects of low-level single and chronic irradiation on the vital body systems, on the organism as a whole, and on a nonhomogeneous mammalian population are of a particular theoretical importance, since these effects still have no unambiguous interpretation.

The proposed explanation of experimentally observed distinctive features of effects of non-uniform and uniform acute irradiation on the major hematopoietic lineages in rodents is of an obvious theoretical significance, too. Furthermore, the developed models of radiation-induced mortality lay down the theoretical foundations of a new individual-based approach to radiation risk assessment. The most appealing feature of these mortality models consists in the fact that they account for the intrinsic properties of the exposed organism and the individual variability of radiosensitivity.

The material presented in the monograph is of a wide practical applicability, too. In particular, the developed models of the human hematopoietic system, as well as the developed models of other vital body systems (after appropriate identification), could be employed to investigate and foretell the effects of space radiation on these systems for astronauts on long-term space missions (e.g., voyages to Mars or lunar colonies). The obtained modeling predictions would provide a better understanding of the risks to health from the space radiation environment and enable one to evaluate the need for operational applications of countermeasures for astronauts. The models of the human hematopoietic system and the properly identified models of the other vital body systems could also be used for predicting the radiation injury of these systems for people residing in contaminated areas after nuclear power plant accidents. Obtained results would help the decision makers to evaluate the hazard for the health of the people and to take proper decisions for operational applications of all necessary countermeasures including their settling out, as well as for their subsequent resettling. Such models could be also applied to assessment of the health hazard for clean-up crew members taking part in the elimination of consequences of such accidents.

The demonstrated efficiency of the employment of the biologically motivated dynamic modeling approach in estimating the excess relative risks for leukemia among acutely and continuously irradiated humans attests to its applicability to the assessment of the radiogenic leukemia risk among people residing in contaminated areas after nuclear power plant accidents, among clean-up crew members taking part in the elimination of consequences of such accidents, among astronauts on long-term space missions, among person subjected to occupational irradiation (uranium miners, radiologists, and others), as well as among patients treated with radiotherapy.

The developed models of radiation-induced mortality (after appropriate identification) could be used to predict the mortality dynamics and the average life-span shortening for an individual and for nonhomogeneous (in radiosensitivity) populations of humans under various irradiation conditions, including low-level chronic irradiation. Therefore, such mortality models could be employed as a tool for estimating the risks for a population residing in contaminated areas. This would help the decision makers to distribute, in an optimal way, the available resources to reduce the hazard for the population. Such models could also be applied to estimate the radiation risks for astronauts on long-term space missions (e.g., voyages to Mars or lunar colonies). This would allow one to carry out more effectively preventive and protective measures among them.

In this monograph, a wide range of fundamental problems in the fields of radiation biology and ecology is investigated in the framework of the single biologically motivated dynamic modeling approach. Thus, the developed methodology of the studies, the elaborated models themselves, and the obtained theoretical results can be of benefit to academic institutions, scientists, and researchers working in the field of mathematical modeling of biological systems, as well as in the fields of radiation biology, ecology, medicine, and radiation safety. The monograph can be of benefit to aerospace agencies and to corporations that deal with the problems of ensuring the space environmental radiation safety, as well as to practitioners and professionals working in the related fields. The monograph can be used as a basis for a lecture course on mathematical modeling in radiation biology and ecology. It can also be of benefit to graduate and postgraduate students of appropriate specializations.

Dubna, Moscow region
Russian Federation
May 2016

Olga Andreevna Smirnova

Acknowledgments

I am deeply grateful to Prof. Natalia Vyacheslavovna Stepanova, who was my scientific advisor during my graduate and postgraduate studies at the Faculty of Physics of Moscow State University (MSU) and remained my main teacher throughout her life.

I am indebted to MSU Prof. Yury M. Romanovsky and Dmitry S. Chernavsky, who also influenced me in forming my scientific outlook and in choosing the direction and methods of my research.

I am very much obliged to the specialists in space research Prof. Juergen Kiefer, Stanley B. Curtis, and Boris S. Fedorenko for their interest in my investigations and valuable discussions.

I am thankful to the specialists in radiation biology Prof. Natalia G. Darenskaya, Elena B. Burlakova, Alexander A. Yarilin, Evgeny A. Krasavin, Katharine E. Carr, Dr. Thomas M. Seed, and Dr. Glen I. Reeves for their interest in my investigations and fruitful discussions.

I am also thankful to the specialists in mathematical modeling in biology Prof. Galina Y. Riznichenko, Alexey A. Romanukha, Thomas G. Hallam, Marcus Loeffler, Herbert I. Freedman, and Rafael Bravo de la Parra for their interest in my investigations and useful discussions.

My coauthors on a number of publications were specialists in the field of radiobiology, immunology, hematology, and space research: Prof. Morio Yonezawa, Dr. Shaowen Hu, Dr. Georgy P. Dimov, Dr. Tatiana M. Zukhbaya, Dr. Nikolai I. Rizhov, Dr. Raisa D. Govorun, and Prof. Mikhail I. Levi. I am thankful to them for collaboration.

I am grateful to Prof. Francis A. Cucinotta for many years of fruitful collaboration and for valuable discussions.

I am indebted to Prof. Alexander V. Akleyev, Evgeny E. Kovalev, and Vadim A. Sakovich for useful discussions and support.

Contents

Introduction

The problem of ensuring the environmental radiation safety remains a challenge. This is primarily caused by the radioactive contamination of areas due to major nuclear power plant accidents, such as the Fukushima and Chernobyl disasters, and by the increasing number of people exposed to occupational radiation due to the development of atomic engineering and the use of radioactive materials in industry, science, and medicine. Additionally, the problem of ensuring the space environmental radiation safety becomes particularly actual in view of the development of programs of long-term space missions, such as Mars missions and lunar colonies. The solution to this problem entails certain complications due to the nonlinearity of the effects of low-level irradiation on biota and due to the individual variability of radiosensitivity. All this calls for the development of new individual-based approaches to the radiation risk assessment and to the investigation of the health effects of environmental radiation [1–29].

This monograph presents the biologically motivated dynamic modeling approach to the study and prediction of radiation effects on mammals. This approach embodies the author's mathematical models, which describe the dynamics of vital body systems in mammals (namely, the hematopoietic system in rodents and humans, the immune system in rodents, the small intestine in rodents, and the skin in young swine) under normal conditions and under various irradiation regimes (acute/chronic/fractionated/non-uniform irradiation). Radiation-induced damage of these systems can result in the development of hematopoietic, gastrointestinal, and cutaneous subsyndromes of the acute radiation syndrome. The models are implemented in the form of systems of nonlinear differential equations, with the modern methodology of the construction of biologically motivated dynamical models being employed. In general, such models involve only several key variables and parameters. This fact allows one to perform, in most cases, a thorough analytical investigation of such models by making use of the qualitative theory of differential equations, oscillation theory, and bifurcation theory and to reveal all the peculiarities of corresponding solutions. In turn, a clear biophysical meaning of the variables and parameters of the developed models enables one to directly compare the modeling

results with relevant experimental data and to successfully perform identification and verification of the models on hand.

The developed approach also includes the author's mathematical models, which describe the dynamics of radiation-induced mortality in homogeneous and non-homogeneous (in radiosensitivity) populations of mammals (rodents) on the basis of the statistical characteristics and the dynamics of critical body systems of specimens composing these populations. In accordance with the experimental observations, either the hematopoietic system or the intestinal system is considered the critical one, depending on the dose and dose rate of acute and chronic irradiation. The dynamics of the critical body systems is computed by making use of the aforementioned mathematical models, the latter being constituent parts of the model of radiation-induced mortality.

The developed approach is applied to estimate the excess relative risks for leukemia among acutely and continuously irradiated humans (the atomic bomb survivors and patients treated with brachytherapy) proceeding from two key characteristics of the respective modeling dynamics of human major hematopoietic lineages (the granulopoietic and lymphopoietic systems). The developed approach is also employed to predict the dynamics of the pathophysiological reaction (moist desquamation) in skin exposed to single and fractionated irradiation in wide ranges of doses and total doses on the basis of the respective modeling dynamics of epidermal cells of the upper skin layer.

This monograph presents the comprehensive formulation and construction of the models mentioned above, their analytical and numerical analysis, and the obtained results [30–96].

References

1. National Council on Radiation Protection and Measurements. Guidance on Radiation Received in Space Activity (NCRP report no. 98), NCRP, Bethesda, MD, 1989.
2. Committee on the Biological Effects of Ionizing Radiations, National Research Council: Health Effects of Exposure to Low Levels of Ionizing Radiation (BEIR V). Washington, DC: Natl Acad Press, 1990.
3. Committee to Assess Health Risks from Exposure to Low Levels of Ionizing Radiation, National Research Council: Health risks from exposure to low levels of ionizing radiation (BEIR VII—Phase 2). Washington, DC: Natl Acad Press, 2006.
4. ICRP Publication 118. ICRP Statement on Tissue Reactions. Early and Late Effects of Radiation in Normal Tissues and Organs - Threshold Doses for Tissue Reactions in a Radiation Protection Context. Annals of the ICRP, v. 41(1/2), 2012.
5. Carnell L., Blattnig S., Hu S., Huff J.L., Kim M.H., Norman R., Patel Z., Simonsen L., Wu H., Casey R., Cucinotta F.A. Risk of Acute Radiation Syndromes Due to Solar Particle Events. NASA Technical Report JSC-CN-35747, 2016.
6. Martin A., Harbison S, Beach K., Cole P. An introduction to radiation protection. Sixth edition, Boca Raton: CRC Press, Taylor & Francis Group, 2012.
7. Kamiya K., Ozasa K., Akiba S., Niwa O., Kodama K., Takamura N., Zaharieva E.K., Kimura Y., Wakeford R. Long-term effects of radiation exposure on health. The Lancet, v. 386, No. 9992, pp. 469–478, 2015.

8. Hasegawa A., Tanigawa K., Ohtsuru A., Yabe H., Maeda M., Shigemura J., Ohira T., Tominaga T., Akashi M., Hirohashi N., Ishikawa T., Kamiya K., Shibuya K., Yamashita S., Chhem R.K. Health effects of radiation and other health problems in the aftermath of nuclear accidents, with an emphasis on Fukushima. The Lancet, v. 386, No. 9992, pp. 479-488, 2015.
9. Ohtsuru A., Tanigawa K., Kumagai A., Niwa O., Takamura N., Midorikawa S., Nollet K., Yamashita S., Ohto H., Chhem R.K., Clarke M. Nuclear disasters and health: lessons learned, challenges, and proposals. The Lancet, v. 386, No. 9992, pp. 489–497, 2015.
10. Thomas G.A., Symonds P. Radiation exposure and health effects - is it time to reassess the real consequences? Clinical Oncology, v. 28(4), pp. 231–236, 2016.
11. Cucinotta F.A., Schimmerling W., Wilson J.W., Peterson L.E., Saganti P.B., Dicello J.F. Uncertainties in estimates of the risks of late effects from space radiation. Advances in Space Research, v. 34(6), pp. 1383–1389, 2004.
12. Cucinotta F.A., Dicello J.F. On the development of biophysical models for space radiation risk assessment. Advances in Space Research, v. 25(10), pp. 2131–2140, 2000.
13. Schimmerling W., Cucinotta F.A., Wilson J.W. Radiation risk and human space exploration. Advances in Space Research, v. 31(1), pp. 27–34, 2003.
14. Hu S., Kim M.H., McClellan G.E., Cucinotta F.A. Modeling the acute health effects of astronauts from exposure to large solar particle events. Health Physics, v. 96(4), pp. 465–476, 2009.
15. Simonsen L.C., Wilson J.W., Kim, M.H., Cucinotta F.A. Radiation exposure for human Mars exploration. Health Physics, v. 79(5), pp. 515–525, 2000.
16. Blakely E.A. Biological effects of cosmic radiation: Deterministic and stochastic. Health Physics, v. 79(5), pp. 495–506, 2000.
17. Eidemuller M., Ostroumova E., Krestinina L., Akleyev A., Jacob P. Analysis of solid cancer mortality in the Techa River Cohort using the two-step clonal expansion model. Radiation Research, v. 169(2), pp. 138–148, 2008.
18. Canu I.G., Ellis E.D., Tirmarche M. Cancer risk in nuclear workers occupationally exposed to uranium—Emphasis on internal exposure. Health Physics, v. 94(1), pp. 1–17, 2008.
19. Fliedner T.M., Graessle D.H. Hematopoietic cell renewal systems: Mechanisms of coping and failing after chronic exposure to ionizing radiation. Radiation and Environmental Biophysics, v. 47(1), pp. 63–69, 2008.
20. Wilson J.W., Kim M., Schimmerling W., Badavi F.F., Thibeault S.A., Cucinotta F.A., Shinn J.L., Kiefer R. Issues in space radiation protection: Galactic cosmic rays. Health Physics, v. 68(1), pp. 50–58, 1995.
21. Wilson J.W., Thibeault S.A., Cucinotta F.A., Shinn J.L., Kim M., Kiefer R., Badavi F.F. Issues in protection from galactic cosmic rays. Radiation and Environmental Biophysics, v. 34, pp. 217–222, 1995.
22. Hagen U., Harder D., Jung H., Streffen C. (Eds.). Radiation Research 1895-1995. Eds.: U. Hagen, D. Harder, H. Jung, C. Streffer. Congress Proceedings. Volume 2: Congress Lectures. Wurzburg: Universitatsdruckerei H. Sturtz AG, 1995, pp. 1–1210.
23. Luckey T.D. Physiological benefits from low levels of ionizing radiation. Health Physics, v. 43(6), pp. 771–789, 1982.
24. Gottlober P., Steinert M., Weiss M., Bebeshko V., Belyi D., Nadejina N., Stefani F.H., Wagemaker G., Fliedner T.M., Peter R.U. The outcome of local radiation injuries: 14 years of follow-up after the Chernobyl accident. Radiation Research, v. 155(3), pp. 409–416, 2001.
25. Meineke V., Van Beuningen D., Sohns T., Fliedner T.M. Medical management principles for radiation accidents. Military Medicine, v. 168(3), pp. 219–222, 2003.
26. Fliedner T.M., et al. Stem cells, multiorgan failure in radiation emergency medical preparedness: A U.S./European consultation workshop. Stem Cells, v. 27(5), pp. 1205–1211, 2009.
27. Ivanov V.K., Tzyb A.F. Medical radiobiological effects of the Chernobyl catastrophe on the population of Russia: Estimation of radiation risks. Moscow: Meditsina, 2002 (Russian).
28. Akleev A.V., Kisselyov M.F. (Eds.). Medical–biological and ecological impacts of radioactive contamination of the Techa River. Moscow: Medbioextrem, 2001 (Russian).
29. Akleyev A.V. Chronic Radiation Syndrome. Heidelberg: Springer, 2014.

30. Smirnova O.A., Stepanova N.V. Mathematical model of oscillations under infection's immunity. In: Proceedings of the Second All-Union Symposium on Oscillatory Processes in Biological and Chemical Systems, Pushchino-na-Oke, 1970. NTsBI AN SSSR, Pushchino-na-Oke, v. 2, pp. 247–251, 1971 (Russian).
31. Smirnova O.A., Stepanova N.V. Computer modeling of immune response dynamics. Vestnik Moskovskogo Universiteta (Fizika, Astronomiya), no. 5, pp. 520–526, 1971 (Russian).
32. Smirnova O.A., Stepanova N.V. Mathematical model of the cooperative interaction in the immune reaction. Zhurnal Mikrobiologii, Epidemiologii i Immunologii, no. 11, pp. 50–53, 1974 (Russian).
33. Levi M.I., Smirnova O.A., Stepanova N.V. Mathematical models of the primary immunological reaction (a review). Zhurnal mikrobiologii, Epidemiologii, i Immunobiologii, no. 11, pp. 113–120, 1974.
34. Smirnova O.A., Stepanova N.V. Mathematical model of infection's immunity. In: Proceedings of the Intercollegiate Meeting on Theoretical and Experimental Biophysics. Kaliningrad: Kaliningrad State University, no. 5, pp. 61–75, 1975 (Russian).
35. Smirnova O.A. Mathematical model of the immune reaction. Vestnik Moskovskogo Universiteta (Fizika, Astronomiya), no. 4, pp. 485–486, 1975 (Russian).
36. Smirnova O.A., Stepanova N.V. Mathematical model of autoimmunity. Biofizika, v. 20, pp. 1095–1098, 1975 (Russian).
37. Levi M.I., Smirnova O.A. The conveyer hypothesis of the primary immune response to soluble antigen. Zhurnal Obschei Biologii, v. 38, pp. 88–99, 1977 (Russian).
38. Levi M.I., Smirnova O.A. Cyclic kinetics and mathematical expression of the primary immune response to soluble antigen: VII. The conveyer hypothesis and its mathematical expression. Folia Microbiologica, v. 22, pp. 117–127, 1977.
39. Smirnova O.A., Govorun R.D., Ryshov N.I. Mathematical model to study the postirradiation dynamics of lymphopoiesis. Radiobiologiya, v. 22, pp. 488–473, 1982 (Russian).
40. Smirnova O.A. Mathematical model of radiation effect on immune system. Immunologiya, no. 2, pp. 38–42, 1984 (Russian).
41. Smirnova O.A. Mathematical model of cyclic kinetics of granulocytopoiesis. Kosmicheskaya Biologiya i Aviakosmicheskaya Meditsina, no. 1, pp. 77–80, 1985 (Russian).
42. Smirnova O.A. Mathematical modeling of thrombocytopoiesis dynamics in mammals exposed to radiation. Radiobiologiya, v. 25, p. 571. Dep. in VINITI N 2552-85, 16.04.85, 1985 (Russian).
43. Smirnova O.A. The mathematical model of mortality dynamics for irradiated mammals which is based on the model of hematopoiesis. Radiobiologiya, v. 27, p. 713. Dep. in VINITI N 2443-1387, 06.07.87, 1987 (Russian).
44. Smirnova O.A. Mathematical model for postirradiation autoimmunity. Radiobiologiya, v. 28(3), pp. 331–335, 1988 (Russian).
45. Smirnova O.A. Mathematical modeling of autoimmunity dynamics under continuous irradiation. In: Modeling of Population Dynamics. Gorky: Gorky University Press, pp. 47–54, 1988 (Russian).
46. Smirnova O.A. Mathematical simulation of the dynamics of postirradiation damage and recovery of intestinal epithelium. Radiobiologiya, v. 28, pp. 817–821, 1988 (Russian).
47. Zukhbaya T.N., Smirnova O.A. Experimental and theoretical investigation of the dynamics of lymphopoiesis upon prolonged exposure to ionizing radiation. Radiobiologiya, v. 28, pp. 626–631, 1988 (Russian).
48. Zukhbaya T.N., Smirnova O.A. Mathematical model for the dynamics of granulocytopoiesis in mammals. Radiobiologiya, v. 28, pp. 796–802, 1988 (Russian).
49. Smirnova O.A. Mathematical modelling of cyclic kinetics of haemopoiesis. Kosmicheskaya Biologiya i Aviakosmicheskaya Meditsina, no. 1, pp. 41–45, 1989 (Russian).
50. Smirnova O.A. The model of homeostasis of hematopoiesis system under chronic irradiation. In: Modeling of Population Dynamics. Gorky: Gorky University Press, pp. 39–45, 1989 (Russian).

51. Zukhbaya T.M., Smirnova O.A. The stimulation effect of prolonged radiation of small dose rates on mammalian lymphopoiesis. Kosmicheskaya Biologiya i Aviakosmicheskaya Meditsina, no. 1, pp. 47–51, 1989 (Russian).
52. Smirnova O.A. Mathematical modelling of dynamics of erythropoiesis and granulocytopoiesis under acute irradiation. Radiobiologiya, v. 30, pp. 627–633, 1990 (Russian).
53. Smirnova O.A. Mathematical modelling of the death rate dynamics in mammals with intestinal form of radiation sickness. Radiobiologiya, v. 30, pp. 814–820, 1990 (Russian).
54. Smirnova O.A. Mathematical modelling of bone-marrow erythropoiesis dynamics in non-irradiated and irradiated mammals. In: Dynamics of Biological Populations. Gorky: Gorky University Press, pp. 51–58, 1990 (Russian).
55. Smirnova O.A. Study of cyclic kinetics of immunity by mathematical modelling methods. Kosmicheskaya Biologiya i Aviakosmicheskaya Meditsina, no. 5, pp. 53–56, 1991 (Russian).
56. Smirnova O.A., Zukhbaya T.M. The stimulation effect of prolonged radiation of small dose rates on mammalian granulocytopoiesis. Kosmicheskaya Biologiya i Aviakosmicheskaya Meditsina, no. 3, pp. 40–42, 1991 (Russian).
57. Zukhbaya T.M., Smirnova O.A. An experimental and mathematical analysis of lymphopoiesis dynamics under continuous irradiation. Health Physics, v. 61(1), pp. 87–95, 1991.
58. Smirnova O.A. Mathematical simulation of the intestinal epithelium dynamics in nonirradiated and irradiated mammals. Radiobiologiya, v. 32, pp. 751–756, 1992 (Russian).
59. Smirnova O.A. Effect of chronic irradiation at high dose rate on the hemopoietic system: Mathematical simulation. Radiobiologiya, v. 32, pp. 757–763, 1992 (Russian).
60. Kovalev E.E., Smirnova O.A. Life-span of irradiated mammals. Mathematical modelling. Acta Astronautica, v. 32, pp. 649–652, 1994.
61. Smirnova O.A. Hematopoiesis dynamics in mammals under combined exposures to radiation: Mathematical modelling. Aviakosmicheskaya i Ekologicheskaya Meditsina, no. 3, pp. 45–49, 1995 (Russian).
62. Kovalev E.E., Smirnova O.A. Radiation risk assessment based on the concept of individual variability of radiosensitivity. Radiation research 1895–1995. Congress Proceedings. Vol. 1. U. Hagen, H. Jung, C. Streffer (Eds.). Tenth International Congress of Radiation Research, Wurzburg, Germany, August 27 - September 1, 1995. Wurzburg: Universitatsdruckerei H. Strtz AG, p. 335, 1995.
63. Smirnova O.A. Mathematical modeling of the effect of ionizing radiation on the immune system of mammals. Physics of Particles and Nuclei. American Institute of Physics, v. 27(1), pp. 100–120, 1996.
64. Kovalev E.E., Smirnova O.A. Estimation of radiation risk based on the concept of individual variability of radiosensitivity. AFRRI Contract Report 96-1. Bethesda, MD: Armed Forces Radiobiology Research Institute, 1996.
65. Smirnova O.A. Problems of mathematical modeling in modern space radiobiology. Proceedings of Sissakian Memorial Symposium under the auspices of UNESCO “Problems of Biochemistry, Radiation and Space Biology.” Moscow, Dubna, Russia, January 22–25, 1997. D-19-97-284. Dubna: JINR, pp. 239–253, 1997 (Russian).
66. Smirnova O.A. Mathematical modeling of the mortality dynamics of mammals exposed to acute and chronic irradiation. Mathematics, Computers, Education. Moscow: Progress-Tradiciya, v. 5, pp. 299–303, 1998 (Russian).
67. Smirnova O.A. Mathematical models of hematopoiesis dynamics in nonirradiated and irradiated mammals. BioMedSim’99. 1st Conference on Modelling and Simulation in Biology, Medicine and Biomedical Engineering, Noisy-le-Grand, France, April 20-22, 1999. Proceedings. Paris: Groupe ESIEE, pp. 105–109, 1999.
68. Smirnova O.A. Autoimmunity dynamics in irradiated mammals: Mathematical modeling. BioMedSim’99. 1st Conference on Modelling and Simulation in Biology, Medicine and Biomedical Engineering, Noisy-le-Grand, France, April 20–22, 1999. Proceedings. Paris: Groupe ESIEE, pp. 110–113, 1999.
69. Smirnova O.A. Mathematical modeling of mortality dynamics of mammalian populations exposed to radiation. Mathematical Biosciences, v. 167(1), pp. 19–30, 2000.

70. Smirnova O.A. Mathematical models of hematopoiesis dynamics in irradiated mammals. Abstracts of the 24th Meeting of the European Study Group for Cell Proliferation (ESGCP), Leipzig, Germany, June 12–17, 2001. Cell Proliferation, v. 34(3), p. 193, 2001.
71. Smirnova O.A. Mathematical models of dynamics of small intestine epithelium system in nonirradiated and irradiated mammals. Abstracts of the 24th Meeting of the European Study Group for Cell Proliferation (ESGCP), Leipzig, Germany, June 12–17, 2001. Cell Proliferation, v. 34(3), pp. 193–194, 2001.
72. Smirnova O.A. Simulation of mortality dynamics for mammalian populations exposed to radiation. The 4th International EUROSIM Congress "Shaping Future with Simulation," Delft, the Netherlands, June 26–29, 2001. Abstracts, Delft: TUDelft, pp. 109–110, 2001.
73. Smirnova O.A. Paradoxical effects of low level irradiation on radiosensitivity of mammals: Modeling investigations. "Problems of Biochemistry, Radiation, and Space Biology," II International Symposium under the auspices of UNESCO dedicated to the memory of Academician N. Sissakian and II Sissakian Readings, Moscow, Dubna, Russia, 29 May–1 June 2001. Proceedings, ISBN 5-85165-697-2, Dubna, JINR, v. 1, pp. 177–182, 2002 (Russian).
74. Smirnova O.A. Mathematical model for assessment of radiation risk on long space mission. Advances in Space Research, v. 30(4), pp. 1005–1010, 2002.
75. Smirnova O.A. Mathematical modeling of radiation-induced autoimmunity. In: Mathematical Modelling and Computing in Biology and Medicine. 5th ECMTB Conference 2002. V. Capasso (Ed.). Milan: Milan Research Centre for Industrial and Applied Mathematics, pp. 392–402, 2003.
76. Smirnova O.A., Yonezawa M. Radioprotection effect of low level preirradiation on mammals: Modeling and experimental investigations. Health Physics, v. 85(2), pp. 150–158, 2003.
77. Sakovich V.A., Smirnova O.A. Modeling radiation effects on life span of mammals. Physics Particles and Nuclei, v. 34(6), pp. 743–766, 2003.
78. Smirnova O.A. Simulation of mortality dynamics for populations of mammals (mice) exposed to radiation. Simulation Modelling Practice and Theory: Advances in Modelling and Simulation in Biology and Medicine. Y. Hamam and F. Rocaries (Eds.), v. 12(2), pp. 171–182, 2004.
79. Smirnova O.A. Comparative risk assessment for homogeneous and nonhomogeneous mammalian populations exposed to low level radiation. In: I. Linkov and A.B. Ramadan (Eds.) Comparative Risk Assessment and Environmental Decision Making. NATO Science Series. IV. Earth and Environmental Sciences, Vol. 38. Dordrecht, the Netherlands: Kluwer Academic Publishers, pp. 385–392, 2004.
80. Smirnova O.A., Yonezawa M. Radioresistance in mammals induced by low-level chronic irradiation: Modeling and experimental investigations. Health Physics, v. 87(4), pp. 366–374, 2004.
81. Smirnova O.A. Mathematical modelling the radiation effects on humoral immunity. Advances in Space Research, v. 37, pp. 1813–1822, 2006.
82. Smirnova O.A. Radiation and Organism of Mammals: Modeling Approach. Moscow-Izhevsk: Scientific-Publishing Centre "Regular and Chaotic Dynamics," Institute of Computer Science, 2006 (Russian).
83. Smirnova O., Yonezawa M. Effects of chronic low-level irradiation on radiosensitivity of mammals: Modeling and experimental studies. In: Radiation Risk Estimates in Normal and Emergency Situations. Proceedings of the NATO Advanced Research Workshop on Impact of Radiation Risk Estimates in Normal and Emergency Situations, Yerevan, Armenia, September 8–11, 2005. A.A. Cigna and M. Durante (Eds.), Springer, XX, pp. 291–301, 2006.
84. Smirnova O.A. Effects of low-level chronic irradiation on the radiosensitivity of mammals: Modeling studies. Advances in Space Research, v. 40, pp. 1408–1413, 2007.
85. Smirnova O.A. Radiation effects on small intestine epithelium system: Mathematical modeling. Proceedings of III International Symposium "Problems of Biochemistry, Radiation and Space Biology" dedicated to the centenary of Academician N.M. Sissakian's birth, Dubna, pp. 250–256, 2007.
86. Smirnova O.A. Blood and small intestine cell kinetics under radiation exposures: Mathematical modeling. Advances in Space Research, v. 44, pp. 1457–1469, 2009.

87. Smirnova O.A. Modeling study of radiation effects on thrombocytopoietic and granulocytopoietic systems in humans. Advances in Space Research, v. 48, pp. 184–198, 2011.
88. Smirnova O.A. Comparative analysis of the dynamics of thrombocytopoietic, granulocytopoietic, and erythropoietic systems in irradiated humans: a modeling approach. Health Physics, v. 103(6), pp. 787–801, 2012.
89. Hu S., Smirnova O.A., Cucinotta F.A. A biomathematical model of lymphopoiesis following severe radiation accidents–potential use for dose assessment. Health physics, v. 102(4), pp. 425–436, 2012.
90. Smirnova O.A. Modeling Analysis of the dynamics of thrombocytopoietic, granulocytopoietic, and erythropoietic systems in irradiated humans. Journal of Radiation Research, v. 55, p. i36, 2014.
91. Smirnova O.A., Hu S., Cucinotta F.A. Analysis of the lymphocytopoiesis dynamics in nonirradiated and irradiated humans: a modeling approach. Radiation Research, v. 181, pp. 240–250, 2014.
92. Smirnova O.A., Akleyev A.V., Dimov G.P. Analysis of hematopoiesis dynamics in residents of Techa riverside villages chronically exposed to nonuniform radiation: modeling approach. Health Physics, v. 106, pp. 445–458, 2014.
93. Smirnova O.A., Akleyev A.V., Dimov G.P. Modeling analysis of the lymphocytopoiesis dynamics in chronically irradiated residents of Techa riverside villages. Radiation and Environmental Biophysics, v. 53, pp. 515–523, 2014.
94. Smirnova O.A., Hu S., Cucinotta F.A. Dynamics of acutely irradiated skin epidermal epithelium in swine: modeling studies. Health Physics, v. 107, pp. 47–59, 2014.
95. Smirnova O.A. Myeloid leukemia risk assessment and dynamics of the granulocytopoietic system in acutely and continuously irradiated humans: modeling approach Health Physics, v. 108(5), pp. 492–502, 2015.
96. Smirnova O.A. Comparative modeling analysis of the hematopoiesis dynamics in mammals exposed to nonuniform and uniform acute irradiation. Health Physics, v. 109(3), pp. 218–232, 2015.

Chapter 1
Effects of Acute and Chronic Irradiation on the Blood-Forming System

1.1 Introduction

The hematopoietic system plays an important part in maintaining the vitality of mammals [1–3]. Functional cells of this system transport oxygen in the blood, provide specific and nonspecific immune protection to the organism against foreign substances (viruses, bacteria, and so on), ensure the blood coagulates, and sustain intact blood vessels. Hematopoietic system is one of the most radiosensitive systems in mammalian organisms [4–8]. A radiation injury of hematopoietic system can lead to hemorrhage, to endo- and exoinfections, and to anemia. They are the main manifestations of the hematopoietic subsyndrome of the acute radiation syndrome. The latter can become a cause of death in some cases. That is why it is important not only to reveal, by making use of mathematical modeling, the basic regulation mechanisms of hematopoietic system in exposed mammals, but also to investigate in detail the dynamics of injury and recovery processes in this system depending on the dose and dose rate of irradiation. All this is aimed to predict the state of the blood-forming system in mammals exposed to various irradiation conditions. Very often such information cannot be obtained by direct experimental methods.

Mathematical modeling came into use in hematopoietic studies about half a century ago. By now, a large number of models have been developed (see Sect. 1.3). When constructing the models of the blood-forming system, different methodologies were used. Basically, simulation models and biologically motivated dynamical models were constructed. However, models of a "black box" type were also considered. In those studies, various mathematical tools were employed: algebraic equations, linear and nonlinear ordinary differential equations without and with a delay, partial differential equations, integro-differential equations, and stochastic modeling.

The primary objectives of our studies [9–33] were to develop and investigate the mathematical models, which describe the dynamics of the major hematopoietic lineages in mammals unexposed and exposed to acute and chronic irradiation.

O.A. Smirnova, *Environmental Radiation Effects on Mammals*,
DOI 10.1007/978-3-319-45761-1_1

The models were required to account for the principal regulatory mechanisms of the hematopoietic system and to include explicitly the characteristics of ionizing radiation and the basic kinetic and radiobiological parameters of the major hematopoietic lineages. The results of our investigations of this subject are summarized in this chapter.

1.2 The Essentials of Hematopoiesis

Hematopoietic system is one of the most complex body systems both in its structure and in the variety of its functions [1–3, 34–38]. This system includes the bone marrow, the major blood-forming organ, and mature functional cells circulating in the blood vessels.

The mature functional blood cells can be split into three main groups taking into account their morphological and functional peculiarities, namely thrombocytes, erythrocytes, and leukocytes. The last group includes granulocytes and lymphocytes. Accordingly, the four major hematopoietic lineages are called as the thrombopoietic, erythropoietic, granulopoietic, and lymphopoietic systems.

Pedigree cells of the major hematopoietic lineages are stem cells. They are not morphologically identified. It is assumed that stem cells locate in a so-called growth environment (a niche formed by stromal cells of the bone marrow). Some stem cells are at rest. Other cells enter into mitosis. A part of them can begin to differentiate into the direction of an individual hematopoietic lineage. There is no a unique point of view on the mechanism of regulation of the way out into differentiation. Some researchers consider this process a stochastic one, while others relate it to an action of specific humoral factors. It is also assumed that the direction of differentiation of a stem cell is predetermined by its growth microenvironment.

In the course of differentiation, cells are proliferating and transforming into morphologically identified precursor cells of the respective hematopoietic lineage. After that, these cells stop dividing and form the pool of maturing cells. Mature cells leave the bone marrow through the so-called sinuses and enter into the peripheral blood. Some types of mature blood cells can migrate into other organs and tissues. The mature cells fulfill their functions and then die.

There are different points of view on the regulation mechanism of proliferation of the bone marrow precursor cells. One of them is the chalone theory. According to this theory, certain tissue-specific substances, chalones, are the material carriers of the feedback in cell division control. Chalones, which belong to cytokines, are specific inhibitors of cell division. They are the product of vital activity and decay of cells of some self-renewing systems of the mammalian organism, including thrombopoietic, lymphopoietic, erythropoietic, and granulopoietic systems.

1.3 Review of Mathematical Models of the Blood-Forming System

In the field of the mathematical modeling of hematopoiesis, one can distinguish three main directions. The first one deals with general problems of regulation of differentiation and self-maintenance of blood-forming stem cells. The basis of these studies was created by the works in [39–41]. Models developed later differ in basic assumptions and in the degree of detail for processes studied (see the survey in [42]). The achievements obtained in this field during recent years are basically due to the close collaboration of theoreticians and experimentalists [43–47].

The second direction is the modeling studies of the major hematopoietic lineages. The most interesting results obtained in this area can be found in [42, 48–63]. The models were applied to reproduce typical dynamics of the major hematopoietic lineages. In particular, the models proposed in [49, 50, 52–55] were used to find solutions describing the cyclic kinetics of hematopoiesis observed in some mammalian species. However, the major part of these studies did not contain the analytical investigation of the conditions needed for the appearance of the stable oscillatory regimes. The models were also employed to simulate the influence on the hematopoiesis dynamics of such factors as hypoxia [57–59], blood transfusion [51, 58], hemorrhage [51, 58], weightlessness [59], drug treatment [51], and virus infection [57]. But only in [51, 58] were the modeling results compared with the corresponding experimental data on a quantitative level.

At present, special attention is paid to the third direction of investigation, which deals with the modeling study of the effects of ionizing radiation on hematopoiesis. The dynamics of hematopoietic lineages in mammals exposed to acute irradiation was modeled, for example, in [42, 58, 64–68]. In turn, the dynamics of hematopoietic lineages in mammals exposed to chronic irradiation was simulated, for instance, in [58, 67, 68]. A disadvantage of majority of those models is that they do not include, in an explicit form, the basic parameters: the dose and dose rate of ionizing radiation and the characteristics of radiosensitivity of hematopoietic cells. This hinders the application of these models in predicting the response of hematopoietic lineages to various doses and dose rates of acute and chronic irradiation.

All these directions of investigations have been further developed in recent works [69–94].

1.4 Master Model of Hematopoiesis

According to current concepts concerning the structure and regulatory mechanisms of the hematopoietic system, the latter can be regarded as a complex of four major hematopoietic lineages: thrombopoietic, lymphopoietic, erythropoietic, and granulopoietic systems [1–3, 34–38]. Each such system contains the entire set of

cells, from stem cells (in the microenvironment predetermining their differentiation toward the respective hematopoietic lineage) to mature blood cells of this lineage.

Let us construct a master model of an individual hematopoietic lineage taking into account only the principal regulatory mechanisms of its functioning. For this purpose, we split all the cells of a hematopoietic lineage into the following three groups according to the degree of maturity and differentiation:

- X_1, bone marrow precursor cells (from stem cells in the respective microenvironment to morphologically identifiable dividing cells);
- X_2, nondividing maturing bone marrow cells;
- X_3, mature blood cells.

Bringing together all bone marrow precursor cells capable of dividing into a single group X_1 obviates the necessity to consider separately the complicated (and not yet clearly understood) processes of self-maintenance and pre-differentiation of stem cells. In constructing the model, we assume the following:

1. the dynamics of X_1 cells is determined by the rate of their reproduction and transition to group X_2;
2. the dynamics of X_2 cells is determined by the arrival of cells from group X_1 and transition to group X_3;
3. the dynamics of X_3 cells is determined by the arrival of cells from group X_2 and their natural death.

In accordance with the chalone theory of hematopoiesis regulation, we assume that the X_1 cell reproduction rate depends on the concentration of chalone, the specific inhibitor of cell division, which is product of the vital activity and decay of these cells and their progeny.

We take the concentrations of X_1, X_2, and X_3 cells and of the specific chalone (x_1, x_2, x_3, and I, respectively) as the model variables. By cell concentration, we mean the ratio of the total number of cells of a certain group to the total blood volume. With these assumptions, the dynamics of the concentrations x_1, x_2, x_3, and I is described by the following differential equations:

$$\frac{dx_1}{dt} = Bx_1 - Cx_1, \tag{1.1}$$

$$\frac{dx_2}{dt} = Cx_1 - Fx_2, \tag{1.2}$$

$$\frac{dx_3}{dt} = Fx_2 - Ex_3, \tag{1.3}$$

$$\frac{dI}{dt} = G(x_1 + \theta_2 x_2 + \theta_3 x_3) - HI. \tag{1.4}$$

The coefficients C and F in Eqs. (1.1)–(1.3) are the specific rates of transfer of cells from group X_1 to group X_2 and from X_2 to X_3, respectively. When simulating the dynamics of different hematopoietic lineages, the parameters C and F are either

constant coefficients or nonlinear functions of the concentrations of respective cells. The coefficient E in Eq. (1.3) is the specific decay rate of cells. Equation (1.4) accounts for the different contributions of X_1, X_2, and X_3 cells to the chalone production by multipliers G, $G\theta_2$, and $G\theta_3$ in front of the variables x_1, x_2, and x_3. Equation (1.4) also allows for the natural decay of the chalone with the specific rate H.

The influence of the chalone inhibitor on the reproduction rate of X_1 cells is described by the Ierusalimskii equation [95–97]:

$$B = \frac{\alpha}{1 + I/K}, \tag{1.5}$$

where K is the inhibition constant and α is the maximum specific rate of cell division. Experiments revealed that chalones preserve their activity for several hours [34, 35]. Bearing in mind that the processes of differentiation and maturation of the bone marrow cells last for several days, Eq. (1.4) can be considered "fast" compared to Eqs. (1.1)–(1.3). Hence, according to the Tikhonov theorem [95–97], Eq. (1.4) can be replaced by its stationary solution $I = (G/H)(x_1 + \theta_2 x_2 + \theta_3 x_3)$. Then we have

$$B = \frac{\alpha}{1 + \beta(x_1 + \theta_2 x_2 + \theta_3 x_3)}, \qquad \beta = \frac{G}{HK}. \tag{1.6}$$

Thus, the model of the dynamics of a hematopoietic lineage for nonirradiated mammals is the system of three nonlinear differential equations (1.1)–(1.3).

When modeling the effect of ionizing radiation on hematopoiesis, we take into account the following well-known facts [4–8, 98–100]. Irradiation with sublethal doses does not in practice affect the differentiation and life span of hematopoietic cells undamaged by radiation [4]. The effect of ionizing radiation is primarily manifested in the death of part of the radiosensitive cells of the blood-forming system. The cells most sensitive to radiation are the early precursors of blood cells (X_1 cells). A lower sensitivity (sometimes even radioresistance) is shown by nondividing maturing bone marrow X_2 cells and by mature cells X_3 of some hematopoietic lineages [4, 98, 99]. Needless to say, the radiosensitivity of cells depends, in a complicated way, on their age, as well as on the stage of their life cycle at the time of irradiation. For the sake of simplicity, we characterize the radiosensitivity of hematopoietic cells at each of three stages of their development by certain averaged values. In addition, we assume that all of the cells receive the same radiation dose.

Equations (1.1)–(1.3) and (1.6) form the basis for describing the effect of ionizing radiation with a dose rate N on a hematopoietic lineage. It is assumed for generality that cells of a hematopoietic lineage are radiosensitive at every stage of their development. In accordance with the experimental observations [99], the radiosensitive X_i cells can be split into three groups, according to their response to irradiation. The first group includes undamaged X_i^{ud} cells, the second group contains damaged X_i^{d}

cells that die within 1 or 2 days (mitotic death), and the third group includes heavily damaged X_i^{hd} cells that die within the first 4–7 h following the irradiation (interphase death) [99]. As the model variables, we take the concentrations of undamaged, damaged, and heavily damaged cells, x_i^{ud}, x_i^{d}, x_i^{hd}, respectively. The separation of cells into groups according to the degree of their damage and consideration of the dynamics of concentrations of undamaged, damaged, and heavily damaged cells are novel elements in modeling the hematopoiesis in irradiated mammals. This approach enables one to predict the damage and recovery processes in radiosensitive cell populations in detail. Moreover, as will be shown below, our approach also enables one to describe the contribution of radiation-damaged cells to the chalone regulation of hematopoiesis, which, evidently, is of great importance. According to the one-target–one-hit theory of cell damage [101], the specific damage rate is proportional to the radiation dose rate N. Therefore, the dynamics of hematopoietic cell concentrations is described by the following differential equations:

$$\frac{dx_1^{ud}}{dt} = Bx_1^{ud} - Cx_1^{ud} - \frac{N}{D_1^0}x_1^{ud}, \tag{1.7}$$

$$\frac{dx_2^{ud}}{dt} = Cx_1^{ud} - Fx_2^{ud} - \frac{N}{D_2^0}x_2^{ud}, \tag{1.8}$$

$$\frac{dx_3^{ud}}{dt} = Fx_2^{ud} - Ex_3^{ud} - \frac{N}{D_3^0}x_3^{ud}, \tag{1.9}$$

$$\frac{dx_i^{d}}{dt} = \frac{N}{D_i^0}\frac{1}{1+\rho_i}x_i^{ud} - \mu x_i^{d}, \tag{1.10}$$

$$\frac{dx_i^{hd}}{dt} = \frac{N}{D_i^0}\frac{\rho_i}{1+\rho_i}x_i^{ud} - \nu x_i^{hd} \quad (i = 1, 2, 3). \tag{1.11}$$

Here N/D_i^0 is a specific rate of transition of X_i cells from the undamaged state to the damaged and heavily damaged states. The parameter ρ_i represents the ratio of parts of X_i^{ud} cells that transfer to the groups of heavily damaged X_i^{hd} and damaged X_i^{d} cells. The coefficients μ and ν are the specific death rates of damaged and heavily damaged cells, respectively.

When modifying Eq. (1.6), which describes the reproduction rate of X_1^{ud} cells, we take into account the contribution of X_i^{d} and X_i^{hd} cells to the chalone production:

$$B = \frac{\alpha}{1 + \beta\left[x_1^{ud} + \phi x_1^{d} + \varphi x_1^{hd} + \theta_2(x_2^{ud} + \phi x_2^{d} + \varphi x_2^{hd}) + \theta_3(x_3^{ud} + \phi x_3^{d} + \varphi x_3^{hd})\right]}. \tag{1.12}$$

Here the dimensionless multipliers ϕ and φ in front of the variables x_i^{d} and x_i^{hd} represent the dissimilar contributions of damaged X_i^{d} and heavily damaged X_i^{hd} cells to the production of the inhibitor I.

When the dynamics of a hematopoietic lineage in mammals exposed to chronic radiation is described in the framework of the model (1.7)–(1.11), the initial concentrations of X_i^{ud}, X_i^{d}, and X_i^{hd} cells are equal to their values before the onset of exposure:

$$x_i^{\mathrm{ud}}(0) = (x_i^{\mathrm{ud}})_0, \quad x_i^{\mathrm{d}}(0) = (x_i^{\mathrm{d}})_0, \quad x_i^{\mathrm{hd}}(0) = (x_i^{\mathrm{hd}})_0 \quad (i = 1, 2, 3). \tag{1.13}$$

To simulate the dynamics of a hematopoietic lineage in mammals exposed to acute radiation at dose D, one can employ the developed model (1.7)–(1.11) with the corresponding parameter N and the initial conditions (1.13). One can also use a simplified version of the model. To derive the latter, it is necessary to take into account an extremely short duration of acute irradiation. In this case the characteristic time scales of Eqs. (1.7)–(1.11) considerably exceed the duration τ of acute irradiation. Therefore, the dynamics of cell concentrations during the exposure can be described by the system of "fast" equations

$$\frac{dx_i^{\mathrm{ud}}}{dt} = -\frac{N}{D_i^0} x_i^{\mathrm{ud}}, \tag{1.14}$$

$$\frac{dx_i^{\mathrm{d}}}{dt} = \frac{N}{D_i^0} \frac{1}{1+\rho_i} x_i^{\mathrm{ud}}, \tag{1.15}$$

$$\frac{dx_i^{\mathrm{hd}}}{dt} = \frac{N}{D_i^0} \frac{\rho_i}{1+\rho_i} x_i^{\mathrm{ud}} \quad (i = 1, 2, 3). \tag{1.16}$$

The initial conditions for these equations are given by Eqs. (1.13). For the case of the constant dose rate ($N = \mathrm{const}$), Eqs. (1.14)–(1.16) can be integrated explicitly. The obtained expressions for the concentrations of X_i^{ud}, X_i^{d}, X_i^{hd} ($i = 1, 2, 3$) cells can be used as the initial conditions for Eqs. (1.7)–(1.11) with zero value for the parameter N:

$$x_i^{\mathrm{ud}}(0) = (x_i^{\mathrm{ud}})_0 \exp(-D/D_i^0), \tag{1.17}$$

$$x_i^{\mathrm{d}}(0) = (x_i^{\mathrm{ud}})_0 \frac{1}{1+\rho_i}[1 - \exp(-D/D_i^0)] + (x_i^{\mathrm{d}})_0, \tag{1.18}$$

$$x_i^{\mathrm{hd}}(0) = (x_i^{\mathrm{ud}})_0 \frac{\rho_i}{1+\rho_i}[1 - \exp(-D/D_i^0)] + (x_i^{\mathrm{hd}})_0 \quad (i = 1, 2, 3). \tag{1.19}$$

Here $D = N\tau$ is the dose of acute irradiation. In turn, the parameter D_i^0, as follows from Eq. (1.17), is equivalent to the conventional radiobiological dose D_0. After exposure to this dose, the number of X_i cells left undamaged is $e = 2.718\ldots$ times smaller than their initial number [4, 98, 99].

It is worthwhile to note the following. In the case of irradiation of a healthy organism that has not previously been exposed to radiation, the initial concentrations of undamaged X_i^{ud} cells are equal to their normal values and the concentrations

of damaged X_i^{d} and heavily damaged X_i^{hd} cells are zero in Eqs. (1.13) and in Eqs. (1.17)–(1.19), namely:

$$(x_i^{\mathrm{ud}})_0 = \bar{x}_i, \quad (x_i^{\mathrm{d}})_0 = 0, \quad (x_i^{\mathrm{hd}})_0 = 0 \quad (i = 1, 2, 3). \tag{1.20}$$

The parameter ρ_i $(i = 1, 2, 3)$ can be specified in the following way. Specifically, Eq. (1.17) implies that the fraction Γ_i^{ud} of undamaged X_i^{ud} cells is

$$\Gamma_i^{\mathrm{ud}} = \exp(-D/D_i^0) \quad (i = 1, 2, 3). \tag{1.21}$$

According to Eq. (1.21), the formula for the joint fraction Γ_i^{dhd} of damaged X_i^{d} cells and heavily damaged X_i^{hd} cells reads

$$\Gamma_i^{\mathrm{dhd}} = 1 - \Gamma_i^{\mathrm{ud}} = 1 - \exp(-D/D_i^0) \quad (i = 1, 2, 3). \tag{1.22}$$

As it was found from experimental data in [102], the joint fraction Γ_i^{dud} of damaged X_i^{d} cells and undamaged X_i^{ud} cells, i.e., the fraction of X_i cells, which did not die in the interphase following acute irradiation with dose D, is an exponential function of D:

$$\Gamma_i^{\mathrm{dud}} = \exp(-D/D_i^{00}) \quad (i = 1, 2, 3). \tag{1.23}$$

Here the parameter D_i^{00} $(i = 1, 2, 3)$ is the dose, after exposure to which the number of X_i $(i = 1, 2, 3)$ cells that did not undergo the interphase death is $\exp(-1)$ (i.e., 36.79 %) of their initial number. Respectively, the fraction Γ_i^{hd} of heavily damaged X_i^{hd} cells is

$$\Gamma_i^{\mathrm{hd}} = 1 - \Gamma_i^{\mathrm{dud}} = 1 - \exp(-D/D_i^{00}) \quad (i = 1, 2, 3). \tag{1.24}$$

The fraction Γ_i^{d} of damaged X_i^{d} cells is the difference between Γ_i^{dhd} and Γ_i^{hd}:

$$\Gamma_i^{\mathrm{d}} = \Gamma_i^{\mathrm{dhd}} - \Gamma_i^{\mathrm{hd}} = \exp(-D/D_i^{00}) - \exp(-D/D_i^0) \quad (i = 1, 2, 3). \tag{1.25}$$

By virtue of Eqs. (1.24) and (1.25), the formula for the parameter ρ_i takes the form

$$\rho_i = \frac{\Gamma_i^{\mathrm{hd}}}{\Gamma_i^{\mathrm{d}}} = \frac{1 - \exp(-D/D_i^{00})}{\exp(-D/D_i^{00}) - \exp(-D/D_i^0)} \quad (i = 1, 2, 3), \tag{1.26}$$

where the parameters D, D_i^0, and D_i^{00} $(i = 1, 2, 3)$ are defined above.

For $D << \min(D_i^0, D_i^{00})$, the parameter ρ_i, at a first approximation, is

$$\rho_i = \frac{1}{(D_i^{00}/D_i^0) - 1} \quad (i = 1, 2, 3). \tag{1.27}$$

As one can infer from Eq. (1.27), the parameter ρ_i depends, in such approximation, only on the ratio of the parameters characterizing the radiosensitivity of X_i cells. Note that Eq. (1.27) for the parameter ρ_i can also be used in the case of simulating of the dynamics of the major hematopoietic lineages under chronic irradiation in the framework of Eqs. (1.1)–(1.6) with the initial conditions (14)–(17) (see, e.g., [25–33]).

It is worth noting that in hematopoietic lineages the cells of some groups X_i can be considered completely radioresistant. In the framework of the model, this fact can be accounted for by assuming that the corresponding parameters D_i^0 tend to infinity. In turn, this will result in the absence of terms describing the radiation effects on these cells in the model under consideration.

Thus, the model describing the dynamics of cell concentrations in a hematopoietic lineage of mammals unexposed and exposed to acute/chronic irradiation has been developed. It is important to emphasize that this model contains, in an explicit form, the main characteristics of irradiation, namely the dose D and the dose rate N, as well as the conventional radiobiological parameters D_i^0, D_i^{00}, and D_1^{000} characterizing the radiosensitivity of the hematopoietic cells.

In what follows we examine the dynamics of the major hematopoietic lineages with their own specific features of regulation and various cell radiosensitivities.

1.5 The Dynamics of the Thrombopoietic System in Mammals Unexposed and Exposed to Acute/Chronic Irradiation

The generic cells of thrombocytes (blood platelets) are megakaryocytes, the giant cells of the bone marrow [1–3]. The youngest morphologically identifiable cell of the thrombopoietic lineage is the dividing megakaryocytoblast. At the next differentiation stage (promegakaryocyte), the cells do not divide but grow in size by increasing their ploidy. A megakaryocyte can have 4, 8, 16, 32, or 64 nuclei. When the number of nuclei reaches 8, the megakaryocyte starts producing thrombocytes, which subsequently leave the bone marrow and pass into the blood. The number of thrombocytes produced by one megakaryocyte is proportional to the volume of its cytoplasm, which in turn is proportional to the number of nuclei of the mature megakaryocyte. On average, a megakaryocyte produces about 3000–4000 thrombocytes and then dies. Blood thrombocytes also undergo a natural process of dying. The control of the reproduction rate in the megakaryocytoblasts and their precursors is provided by a chalone—thrombocytopenin [34].

Let us denote the bone marrow precursor cells (from stem cells in the respective microenvironment to megakaryocytoblasts) by X_1, the nondividing cells (from promegakaryocytes to mature megakaryocytes) by X_2, and the blood thrombocytes by X_3. Then, in accordance with Eqs. (1.1)–(1.3) and relation (1.6), the dynamics of the respective cell concentrations x_1, x_2, x_3 is described by the system of three differential equations

$$\frac{dx_1}{dt} = \frac{\alpha\, x_1}{1 + \beta(x_1 + \theta_2\, x_2 + \theta_3\, x_3)} - \gamma\, x_1, \tag{1.28}$$

$$\frac{dx_2}{dt} = f\,\gamma\, x_1 - \delta\, x_2, \tag{1.29}$$

$$\frac{dx_3}{dt} = \sigma\,\delta\, x_2 - \psi\, x_3. \tag{1.30}$$

The coefficients α, β, θ_2, θ_3, $\gamma \equiv C$, $\delta \equiv F$, $\psi \equiv E$ in Eqs. (1.28)–(1.30) have the same meaning as in Eqs. (1.1)–(1.6).

The mathematical description of the complicated process of nucleus duplication in megakaryocytes, which eventually determines the megakaryocyte ploidy and the number of thrombocytes produced, is substituted by introducing a new integral quantity, namely the coefficient of megakaryocyte ploidy f. It is known from experiments [103, 104] that in healthy mammals the normal concentration of the blood thrombocytes, $\bar{x}_3$, the average ploidy of bone marrow megakaryocytes, $P(\bar{x}_3)$, and the thrombocyte yield per megakaryocyte, σ, are stable quantities. When the number of blood thrombocytes is reduced ($x_3 < \bar{x}_3$), the average ploidy $P(x_3)$ increases: $P(x_3) > P(\bar{x}_3)$. The ratio of $P(x_3)$ to $P(\bar{x}_3)$ is the ploidy coefficient f. In accordance with experimental data [103, 104], the coefficient f is represented as a decreasing function of the thrombocyte concentration

$$f = \frac{P(x_3)}{P(\bar{x}_3)} = \frac{1}{\lambda + \omega\, x_3}. \tag{1.31}$$

In this equation, λ and ω are certain constant parameters. By definition, at $x_3 = \bar{x}_3$, $f = 1/(\lambda + \omega\bar{x}_3) = 1$; hence $\omega\,\bar{x}_3 = 1 - \lambda$. In addition, at $x_3 = 0, f = \lambda^{-1}$, so the dimensionless parameter λ must satisfy the following condition: $0 < \lambda < 1$. As a results, Eq. (1.31) reads

$$f = \frac{1}{\lambda + (1 - \lambda)\,(x_3/\bar{x}_3)}. \tag{1.32}$$

In fact, the function f (1.32) describes the feedback mechanism that regulates the megakaryocyte ploidy with respect to the thrombocyte concentration. In turn, the parameter λ in this function specifies the strength of the feedback. Decreasing of λ leads to strengthening of the latter. On the contrary, increasing of λ results in weakening of the feedback.

When deriving Eq. (1.30), it is assumed that all X_2 cells have the same ploidy $P(\bar{x}_3)$ and after maturation produce the same number σ of thrombocytes. A change in the average ploidy is described in the model by an equivalent change of the concentration of X_2 cells. The concentration of X_1 cells that have just passed into phase X_2 is multiplied by the coefficient f. This way of introducing the coefficient f into Eq. (1.29) enables one to take into account, in a dynamic form, the delay effect between the control signal (deviation of thrombocyte concentration from the normal level) and the response (change of average megakaryocyte ploidy).

The system of Eqs. (1.28)–(1.30) is investigated by methods of the qualitative theory of differential equations, oscillation theory, and bifurcation theory [105–111]. It is found that this system has two singular points in the space of variables. The first singular point is trivial (the variables x_1, x_2, and x_3 vanish). Coordinates of the second singular point in the space of variables are the following:

$$\bar{x}_1 = \frac{(\alpha/\gamma) - 1}{\beta\left[1 + \theta_2\,(\gamma/\delta) + \theta_3\,\sigma\,(\gamma/\psi)\right]}, \tag{1.33}$$

$$\bar{x}_2 = \frac{\gamma}{\delta}\,\frac{(\alpha/\gamma) - 1}{\beta\left[1 + \theta_2\,(\gamma/\delta) + \theta_3\,\sigma\,(\gamma/\psi)\right]}, \tag{1.34}$$

$$\bar{x}_3 = \sigma\,\frac{\gamma}{\psi}\,\frac{(\alpha/\gamma) - 1}{\beta\left[1 + \theta_2\,(\gamma/\delta) + \theta_3\,\sigma\,(\gamma/\psi)\right]}. \tag{1.35}$$

These coordinates can be positive, negative, or trivial depending on values of the model parameters.

When $\alpha < \gamma$, the first (trivial) singular point is stable (node), whereas the second singular point has no physical sense because its coordinates are negative. If $\alpha = \gamma$, then the second singular point coincides with the first one. In both cases the stable trivial singular point can be identified with the state of the extinction of the thrombopoietic system. This range of the parameters is not considered in what follows.

When $\alpha > \gamma$, the first (trivial) singular point is unstable (saddle). The coordinates of the second singular point are positive. The second singular point can be either stable (focus) or unstable (saddle-focus), depending on the values of the model parameters.

It is found that the second singular point becomes unstable when the model parameters obey the following conditions:

$$\theta_3 > \frac{1}{\sigma}\left\{\theta_2 + \frac{1}{g}\left[(g+c)^2 + 2\sqrt{gc(g+c)(g+c+\theta_2)(2-\lambda)}\,\right]\right\}, \tag{1.36}$$

$$\frac{\gamma}{2-\lambda} > \delta + \psi, \tag{1.37}$$

$$\frac{\gamma}{1 - (1 + \theta_2/g + \sigma\theta_3/c)A_2} < \alpha < \frac{\gamma}{1 - (1 + \theta_2/g + \sigma\theta_3/c)A_1}, \tag{1.38}$$

where $A_{1,2} = \left[u \pm (u^2 - w^2)^{1/2}\right]\left[2(g + c + \theta_2)\right]^{-1}$, $u = g(\sigma\theta_3 - \theta_2) - (g + c)^2$, $w^2 = 4gc(g + c)(g + c + \theta_2)(2 - \lambda)$, $g = \delta/\gamma$, and $c = \psi/\gamma$. It is worth noting that the quantities A_1 and A_2 are real and positive when Eq. (1.36) holds.

If the second singular point is stable, it can be identified with the state of the stable dynamic equilibrium (the homeostasis state) of the thrombopoietic system in mammals. In this case, the values of its positive coordinates $\bar{x}_1$, $\bar{x}_2$, and $\bar{x}_3$ can be considered the normal concentrations of blood thrombocytes and their bone marrow precursor cells.

When the second singular point becomes unstable, one more particular solution appears: a stable limit cycle (stable oscillations of the variables x_1, x_2, and x_3). This particular solution can be identified with stable oscillations of the concentrations of blood thrombocytes and their bone marrow precursors. Thus, inequalities (1.36)–(1.38) can be considered the conditions of appearance of the cyclic thrombopoiesis in mammals. Specifically, inequality (1.36) may become valid when the parameter θ_3 takes a larger value, i.e., when the influence of the chalone produced by thrombocytes on the reproduction rate of X_1 cells is increased. In turn, inequality (1.37) may become valid when the parameter λ takes a larger value, i.e., when the feedback, which regulates the megakaryocyte ploidy with respect to the thrombocyte concentration, is weakened. Inequality (1.37) may also become valid when the parameter γ takes a larger value and/or the parameters δ and ψ take smaller values, i.e., when the specific rate of transfer of X_1 cell to group X_2 increases and/or the specific rate of transfer of X_2 cell to group X_3 and the specific rate of X_3 cell death decrease. Finally, inequality (1.38) may become valid when the parameter α, the maximal specific reproduction rate of X_1 cells, is within a certain range.

The developed model [Eqs. (1.28)–(1.30)] is investigated numerically. For the convenience, Eqs. (1.28)–(1.30) are rewritten in terms of the new dimensionless variables, the latter being the ratios of the dimension cell concentrations to their stationary values. Numerical studies of the model confirm the predictions made in the course of its analytical investigations. The stable limit cycle is obtained in the model with the following values of independent parameters: $\alpha = 4\ \text{day}^{-1}$, $\gamma = 2\ \text{day}^{-1}$, $\delta = 0.4\ \text{day}^{-1}$, $\psi = 0.5\ \text{day}^{-1}$, $\sigma = 3000$, $\theta_2 = 0.4$, $\theta_3 = 0.133$, $\lambda = 0.9$. The parameters are chosen in such a way that the values of the period and amplitude of oscillations of the dimensionless concentration of X_3 cells are 14 days and 0.2, respectively (Fig. 1.1). These modeling predictions correspond to the experimental data for gray collies, which showed the stable oscillations in thrombocyte concentration with a period of 13 days and an amplitude of 0.5 [112].

In the case when the second singular point is a stable focus, the recovery processes have the character of damped oscillations. In fact, experiments on rats in which thrombocytes were removed from the blood [113] and, conversely, introduced into the blood [114] revealed damped oscillations in thrombocyte concentration. These results are reproduced within the thrombopoiesis model. The values of the parameters α, γ, δ, ψ, and σ are either taken directly from the literature or derived from experimental data [3, 4, 98]. They are given in Table 1.1. The coefficient λ is varied from 0 to 1 in accordance with relation (1.32). The parameters θ_2 and θ_3 were varied over a wide range. A good agreement with experimental data [114] is obtained at the values of the coefficients λ, θ_2, and θ_3 presented in Table 1.1.

The model describes both the recovery of the thrombocyte pool in the blood following its reduction by metabolic blood transfusion (Fig. 1.2) and the process of the return of the thrombocyte concentration to the normal level after injection of fresh thrombocytes into the blood (Fig. 1.3). In both cases the computed dynamics of dimensionless thrombocyte concentration has the character of damped oscillations. The statistical χ^2-test [115] is chosen for a quantitative comparison of the model and the respective experimental results [113, 114]. The computed values of $\chi^2 = 8.06$

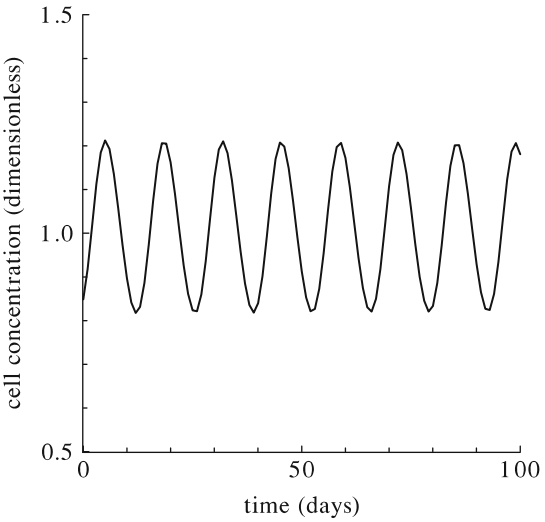

Fig. 1.1 Stable oscillations of X_3 cell concentration in the thrombopoiesis model

Table 1.1 Parameters of the thrombopoiesis model for small laboratory animals (mice)

Parameter	Value	Dimension
α	2.4	day^{-1}
γ	1.4	day^{-1}
δ	0.35	day^{-1}
ψ	0.35	day^{-1}
μ	0.5	day^{-1}
ν	6	day^{-1}
D_1^0	2.4	Gy
D_1^{00}	4.8	Gy
ϕ	209	1
φ	2508	1
θ_2	0.1	1
θ_3	0.01	1
λ	0.5	1
σ	3000	1

and $\chi^2 = 8.8$ do not exceed their critical values of $\chi^2_{0.05} = 12.592$ (the number of degrees of freedom $n = 7 - 1 = 6$) and $\chi^2_{0.05} = 15.507$ ($n = 12 - 1 - 3 = 8$); i.e., there is a quantitative agreement.

Let us now address the effects of ionizing radiation on the thrombopoiesis. As known from experiments [4, 98], thrombocytes and all cells of the thrombopoietic lineage, starting from promegakaryocytes, are radioresistant. The megakaryocytoblasts and their precursors are radiosensitive. Therefore, the model of thrombopoiesis dynamics in irradiated mammals comprises five differential equations describing the concentrations of undamaged X_1^{ud}, damaged X_1^{d}, and heavily damaged X_1^{hd} cells, and also the concentrations of radioresistant X_2 and X_3 cells (see Sect. 1.4).

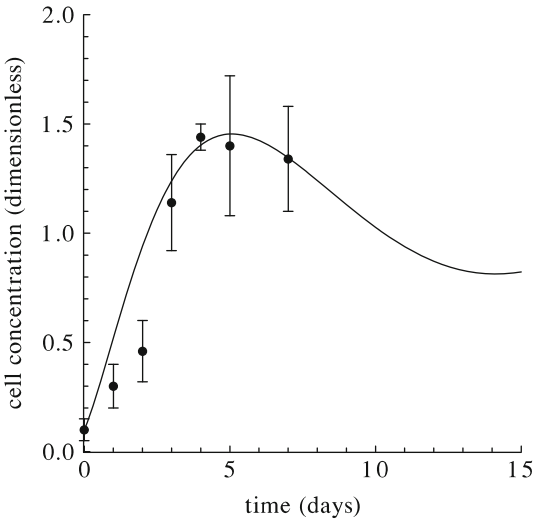

Fig. 1.2 Dynamics of thrombocyte concentration in the blood of rats, with the concentration deliberately reduced to 10 % of the normal level. Modeling results (*curve*) and the respective experimental data [113] (*circle*)

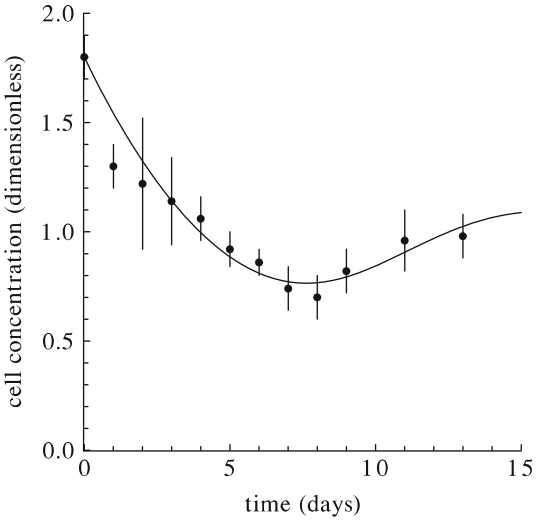

Fig. 1.3 Dynamics of thrombocyte concentration in the blood of rats, with the concentration deliberately increased to 180 % of the normal level. Modeling results (*curve*) and the respective experimental data [114] (*circle*)

For numerical studies, the equations describing the concentrations of the cells listed above are rewritten in terms of the new dimensionless variables, the latter being the ratios of the dimension cell concentrations to their normal values.

The model is applied to examine the dynamics of thrombopoiesis in mice exposed to chronic irradiation. The values of eight independent coefficients, α, γ, δ, ψ, σ, λ, θ_2, θ_3, are taken to be the same as in the aforementioned case of the simulation of thrombopoiesis dynamics in nonirradiated mice (Table 1.1). The values of the coefficients μ and ν are taken directly from the literature [99]. The values of the parameters ϕ, φ, D_1^0, and D_1^{00} are estimated in the course of the numerical study of the model and the subsequent juxtaposition of the modeling

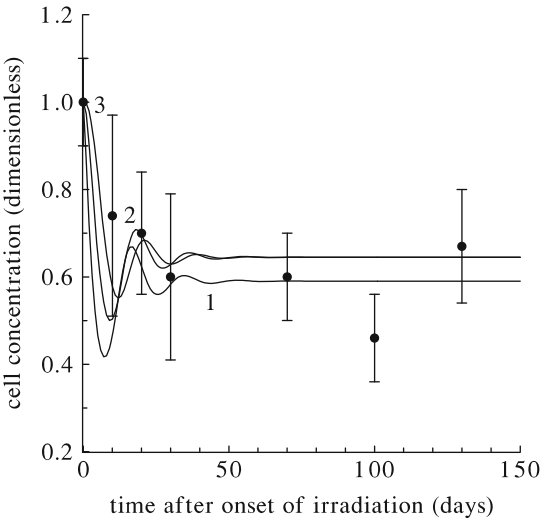

Fig. 1.4 Thrombopoiesis dynamics in mice under chronic irradiation at dose rate $N = 0.25\,\mathrm{Gy/day}$. Computed concentrations of X_1, X_2, and X_3 cells (*curves 1–3*) and experimentally measured values of blood thrombocyte concentration (*circle*) [116]

results with experimental data on the dynamics of thrombopoiesis after acute irradiation [4]. The values of these parameters are also given in Table 1.1.

Figure 1.4 demonstrates the dynamics of X_1, X_2, and X_3 cell concentrations computed for a moderate radiation dose rate. The figure also shows the corresponding experimental data on the dynamics of the thrombocyte concentration in the blood of chronically irradiated mice [116]. The model reproduces the transition process having the character of damped oscillations. When the transition process is over, the dimensionless concentrations of X_1, X_2, and X_3 cells acquire new, lower than normal, stationary values. The large spread in the experimental data [116] does not allow one to perform their detailed comparison with the modeling predictions. Therefore, to check whether there is agreement between the modeling results and experimental data presented in Fig. 1.4, the statistical χ^2-test [115] is used. The computed value of $\chi^2 = 4.195$ does not exceed the critical value $\chi^2_{0.05} = 12.592$ ($n = 6$); i.e., the modeling predictions quantitatively agree with the respective experimental data. A rather similar thrombopoiesis dynamics is also obtained within the model for other (low and moderate) dose rates N of chronic irradiation.

Analytical investigations show that, for any relation between parameters and for any nonvanishing value of dose rate of chronic irradiation N, the values of new stationary concentrations of X_1, X_2, and X_3 cells in the thrombopoietic system are below their normal levels. In turn, these values vanish when N becomes equal to or exceeds a certain critical dose rate N_c. The latter is defined in terms of the model parameters by the simple formula

$$N_c = D_1^0(\alpha - \gamma). \tag{1.39}$$

From this formula it follows, in particular, that the critical dose rate N_c increases when the radiosensitivity of the bone marrow cell precursors capable of dividing

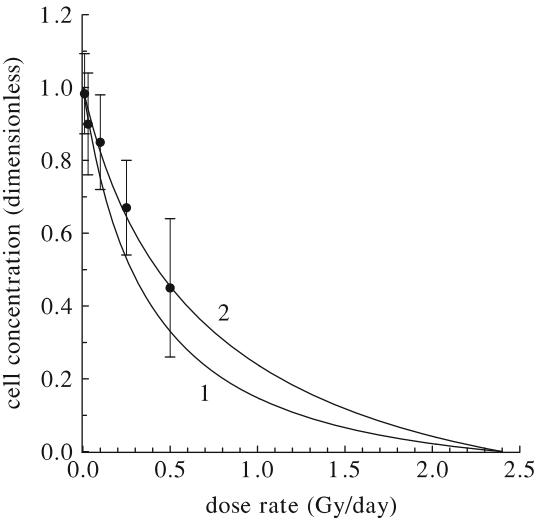

Fig. 1.5 New stationary concentrations of cells in the thrombopoietic system of mice versus the dose rate N of chronic irradiation. Computed values for X_1 cells (*curve 1*), X_2 cells (*curve 2*), and X_3 cells (*curve 2*) and experimentally measured values for blood thrombocytes (*circle*) [99, 117]

(X_1 cells) decreases and/or when the proliferation potential of these cells increases. The critical dose rate N_c for the thrombopoietic system turns out to be 2.4 Gy/day.

The values of new stationary concentrations of X_1, X_2, and X_3 cells computed for various radiation dose rates N are presented in Fig. 1.5. As one can see, these quantities decrease with growing N and vanish when N becomes equal to or exceeds the critical level N_c. It is important to emphasize that the modeling predictions qualitatively and quantitatively agree with relevant experimental data [99, 117, 118]. The computed value $\chi^2 = 1.194$ does not exceed its critical value $\chi^2_{0.05} = 9.488$ ($n = 4$).

The establishment of new stationary cell concentrations in the thrombopoietic system at low and moderate dose rates N can be regarded as the adaptation of this system to chronic irradiation, and such state itself can be regarded as a new stable dynamic equilibrium state (a new homeostasis state) of this system. Note that the adaptation to chronic radiation exposures of cellular self-renewing systems, including that of thrombopoietic system, was observed in mammals (see, e.g., [116, 117, 119, 120]). It is worthwhile emphasizing that the new homeostasis in the thrombopoietic system is also characterized by enhanced mitotic activity of X_1 cells. Hence, the model describes the "overstrain" in functioning of the thrombopoietic system required to maintain the new stable dynamic equilibrium in this system under chronic irradiation at low and moderate dose rates N. This prediction of the model is also supported experimentally [119, 120].

Computations show that when N is close to or exceeds N_c, then the dynamics of the thrombopoietic system differs substantially from the one obtained for low and moderate dose rates. The kinetics of X_1, X_2, and X_3 cell concentrations have an aperiodic character that corresponds to experimental observations [116, 118] (see Fig. 1.6). At $N \sim N_c$, the concentrations of these cells reduce to low levels

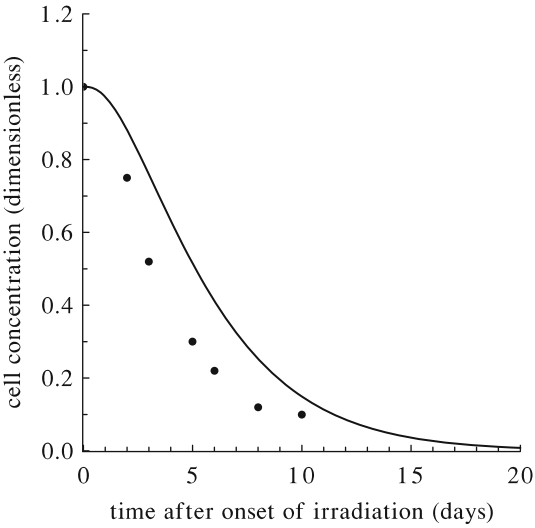

Fig. 1.6 Dynamics of concentration of blood thrombocytes (X_3 cells) in mice under chronic irradiation at dose rate $N = 6\,\mathrm{Gy/day}$. Modeling results (*curve*) and experimental data [118] (*circle*)

incompatible with life, and at $N \geq N_c$, they become equal to zero. These modeling predictions can be identified with the irreversible depletion of the thrombopoietic system. Depletion of this kind was observed in mice exposed to chronic irradiation at high dose rates [116, 118].

In the course of the numerical study of the model, the values of all parameters were varied within reasonable ranges. It is found that the minimal concentrations of X_1, X_2, and X_3 cells are basically determined by the parameter D_1^0, which specifies the radiosensitivity of the bone marrow thrombocyte precursor cells capable of dividing. The parameter D_1^0, as well as the coefficients θ_2, θ_3, ϕ, and φ, determines, to a large extent, the values of new stationary concentrations of X_1, X_2, and X_3 cells. All the quantities listed above also depend on the variable parameter N, the dose rate of chronic irradiation. The results obtained within this model are in qualitative agreement with the experimentally observed dynamics of the thrombopoiesis in various mammalian species during chronic irradiation [99, 120].

The model is also employed to examine the effects of acute irradiation on the thrombopoietic system. The dynamics of this system computed for a moderate dose is shown in Fig. 1.7. The relevant experimental data [4] are also represented in this figure by averaged values of thrombocyte concentration in the peripheral blood of mice. The modeling results are shown by three kinetic curves. The first curve represents the dynamics of the concentration of the X_1 cell pool, which includes undamaged X_1^{ud}, damaged X_1^{d}, and heavily damaged X_1^{hd} cells. Starting from the time when the concentrations of X_1^{d} and X_1^{hd} cells become zero, this curve describes the concentration of undamaged X_1^{ud} cells. This representation of the modeling results allows one to describe in detail not only the recovery process, but also the dynamics of the reduction in the concentration of the X_1 cell pool as a result of the death of part of these cells. The same representation will be used to describe the

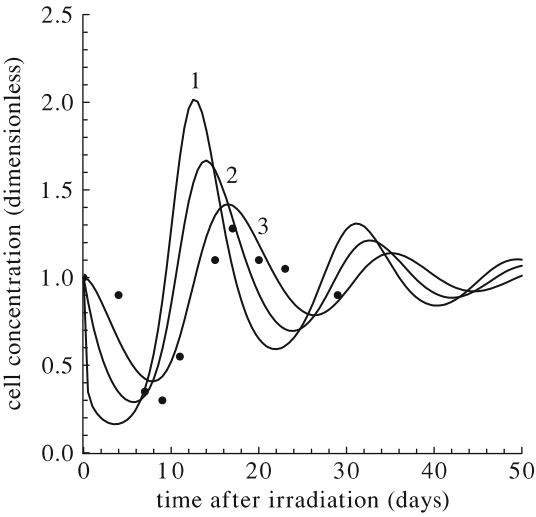

Fig. 1.7 Thrombopoiesis dynamics in mice after acute irradiation at dose $D = 4$ Gy. Computed concentrations of X_1, X_2, and X_3 cells (*curves 1–3*) and experimentally measured values of blood thrombocyte concentration (*circle*) [4]

dynamics of radiosensitive cell concentrations in lymphopoietic, erythropoietic, and granulopoietic systems in exposed specimens (see Sects. 1.6, 1.7, and 1.8).

The second and third kinetic curves in Fig. 1.7 describe the concentrations of radioresistant X_2 and X_3 cells, respectively. As one can see, the concentration of X_3 cells decreases during the first 8 days after irradiation. Then the thrombocyte concentration increases. By the 16th postirradiation day, it reaches a maximum and then decreases again. The recovery process, having the character of damped oscillations, completes within 50 days. The modeling results on the postirradiation dynamics of X_3 cell concentration agree with the respective experimental data [4] on the kinetics of the thrombocyte concentration in acutely irradiated mice (see Fig. 1.7).

The numerical studies of the model revealed the following. The principal indices of postirradiation damage of the thrombopoietic system, namely the minimal concentrations of X_1, X_2, and X_3 cells, are basically determined by the parameter D_1^0 specifying the radiosensitivity of X_1 cells, as well as by the radiation dose D. In particular, the minimal concentrations of X_1, X_2, and X_3 cells decrease as the parameter D_1^0 decreases and/or the dose D increases.

These modeling results qualitatively agree with the experimentally observed dynamics of the thrombopoiesis in various mammalian species after acute irradiation [4].

1.6 The Dynamics of the Lymphopoietic System in Mammals Unexposed and Exposed to Acute/Chronic Irradiation

The lymphocyte is a type of white blood cell (leukocyte) [1–3, 34]. The first morphologically identifiable lymphocyte precursors in the bone marrow are lymphoblasts. Later these cells reach the stage of nondividing maturing lymphocytes. Mature lymphocytes leave the bone marrow and pass into the blood. The lymphocytes are capable of passing from the blood flow to the lymph and back, and also of residing in lymphatic organs (thymus, spleen, lymph nodes, etc.). The reproduction of the bone marrow lymphocyte precursors is controlled by the lymphocytic chalone.

In describing the bone marrow lymphopoiesis, we restrict ourselves to examination of the lymphocyte dynamics in the absence of any antigenic stimulation. We denote the bone marrow precursor cells (from stem cells in the respective microenvironment to lymphoblasts) by X_1, the nondividing maturing lymphoid cells of the bone marrow by X_2, and the mature lymphocytes in the blood by X_3. We denote the concentration of X_1, X_2, and X_3 cells by x_1, x_2, and x_3, respectively. By virtue of Eqs. (1.1)–(1.3) and relation (1.6), the dynamics of the concentrations x_1, x_2, and x_3 is described by the system of three differential equations

$$\frac{dx_1}{dt} = \frac{\alpha\, x_1}{1 + \beta\,(x_1 + \theta_2\, x_2 + \theta_3\, x_3)} - \gamma\, x_1, \tag{1.40}$$

$$\frac{dx_2}{dt} = \gamma\, x_1 - \delta\, x_2, \tag{1.41}$$

$$\frac{dx_3}{dt} = \delta\, x_2 - \psi\, x_3. \tag{1.42}$$

The meaning of the constants α, β, θ_2, θ_3, $\gamma \equiv C$, $\delta \equiv F$, $\psi \equiv E$ in the system (1.40)–(1.42) is the same as in Eqs. (1.1)–(1.6) (see Sect. 1.4).

The system of Eqs. (1.40)–(1.42) is investigated by methods of the qualitative theory of differential equations, oscillation theory, and bifurcation theory [105–111]. It is found that this system has two singular points in the space of variables. The first singular point is trivial. The coordinates of the second singular point in the space of variables are the following:

$$\bar{x}_1 = \frac{(\alpha/\gamma) - 1}{\beta\big[1 + \theta_2\,(\gamma/\delta) + \theta_3\,(\gamma/\psi)\big]}, \tag{1.43}$$

$$\bar{x}_2 = \frac{\gamma}{\delta}\,\frac{(\alpha/\gamma) - 1}{\beta\big[1 + \theta_2\,(\gamma/\delta) + \theta_3\,(\gamma/\psi)\big]}, \tag{1.44}$$

$$\bar{x}_3 = \frac{\gamma}{\psi}\,\frac{(\alpha/\gamma) - 1}{\beta\big[1 + \theta_2\,(\gamma/\delta) + \theta_3\,(\gamma/\psi)\big]}. \tag{1.45}$$

When $\alpha < \gamma$, the first (trivial) singular point is stable (node) and the second singular point has no physical sense because its coordinates are negative ($\bar{x}_1 < 0$, $\bar{x}_2 < 0, \bar{x}_3 < 0$). If $\alpha = \gamma$, then the second singular point coincides with the first one. In both these cases the stable trivial singular point can be identified with the state of extinction of the lymphopoietic system. This range of the parameters is not considered further.

When $\alpha > \gamma$, the first (trivial) singular point is unstable (saddle). The coordinates of the second singular point are positive. The second singular point can be stable (focus) or unstable (saddle-focus), depending on the values of the model parameters.

It is found that the second singular point becomes unstable when the model parameters satisfy the following conditions:

$$\theta_3 > \theta_2 + \frac{1}{g}\Big[(g+c)^2 + 2\sqrt{gc(g+c)(g+c+\theta_2)}\Big], \tag{1.46}$$

$$\gamma > \delta + \psi, \tag{1.47}$$

$$\frac{\gamma}{1-(1+\theta_2/g+\theta_3/c)A_2} < \alpha < \frac{\gamma}{1-(1+\theta_2/g+\theta_3/c)A_1}, \tag{1.48}$$

where $A_{1,2} = \big[u \pm (u^2 - w^2)^{1/2}\big]\big[2(g+c+\theta_2)\big]^{-1}$, $u = g(\theta_3 - \theta_2) - (g+c)^2$, $w^2 = 4gc(g+c)(g+c+\theta_2)$, $g = \delta/\gamma$, and $c = \psi/\gamma$. It is worth noting that the quantities A_1 and A_2 are real and positive when Eq. (1.46) holds.

If the second singular point with positive coordinates $\bar{x}_i$ [Eqs. (1.43)–(1.45)] is stable, then it can be identified with the state of the stable dynamic equilibrium (the homeostasis state) of the lymphopoietic system in mammals. In this case the values $\bar{x}_i$ ($i = 1, 2, 3$) can be considered the normal concentrations of blood lymphocytes and their bone marrow precursors.

When the second singular point becomes unstable, one more particular solution appears: a stable limit cycle (stable oscillations of the variables x_1, x_2, and x_3). This particular solution can be identified with stable oscillations of the concentrations of the respective cells. Thus, inequalities (1.46)–(1.48) can be considered the conditions of appearance of the cyclic lymphopoiesis in mammals. In particular, inequality (1.46) may become valid when the parameter θ_3 takes a larger value, i.e., when the influence of the chalone produced by the blood lymphocytes on the reproduction rate of X_1 cells is increased. In turn, inequality (1.47) may become valid when the parameter γ takes a larger value and/or the parameters δ and ψ take smaller values, i.e., when the specific rate of the transfer of X_1 cell to the pool X_2 increases and/or the specific rate of the transfer of X_2 cell to the pool X_3 and the specific rate of X_3 cell death decrease. Finally, inequality (1.48) may become valid when the parameter α (the maximal specific reproduction rate of X_1 cells) is within a certain range.

The developed model [Eqs. (1.40)–(1.42)] is investigated numerically. For the convenience, Eqs. (1.40)–(1.42) are rewritten in terms of the new dimensionless variables, the latter being the ratios of the dimension cell concentrations to their stationary values. Numerical studies of the model confirm the predictions made

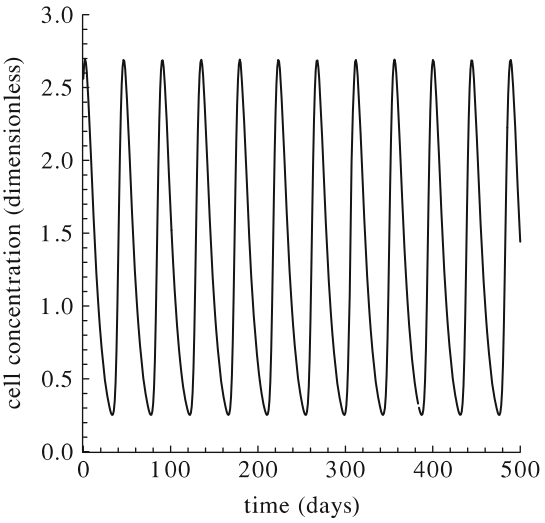

Fig. 1.8 Stable oscillations of X_3 cell concentration in the lymphopoiesis model

in the course of its analytical investigation. First of all, the model describes the state of the stable dynamic equilibrium (the homeostasis state) of the lymphopoietic system. After deviation from this state, the system returns to it. Additionally, the model reproduces the cyclic lymphopoiesis. Specifically, the stable limit cycle was obtained in the model with the following values of the independent parameters: $\alpha = 2.4\,\text{day}^{-1}$, $\gamma = 1.4\,\text{day}^{-1}$, $\delta = 0.23\,\text{day}^{-1}$, $\psi = 0.1\,\text{day}^{-1}$, $\theta_2 = 0.5$, $\theta_3 = 10$ (Fig. 1.8). The parameters are chosen in such a way that the period and the amplitude of oscillations of the X_3 cell dimensionless concentrations are about 50 days and 1.2, respectively. Note that a cyclic lymphopoiesis kinetics was observed in dogs and in humans [121, 122].

Let us now address the effect of ionizing radiation on the lymphopoiesis. It is well known that both mature blood lymphocytes and their bone marrow precursor cells are radiosensitive [4, 98, 99]. Therefore, the lymphopoiesis model for irradiated mammals comprises nine differential equations describing the dynamics of concentrations of undamaged, damaged, and heavily damaged cells of all three groups: X_i^{ud}, X_i^{d}, and X_i^{hd} ($i = 1, 2, 3$) (see Sect. 1.4). For numerical studies, the equations describing the dynamics of concentrations of cells listed above are rewritten in terms of the new dimensionless variables, the latter being the ratios of the dimension cell concentrations to their normal values.

The model is used to examine the lymphopoiesis dynamics in small laboratory animals (rats, mice) exposed to chronic irradiation. The coefficients α, γ, δ, ψ, μ, and ν, as well as D_i^0 and D_i^{00} ($i = 1, 2, 3$), are either taken directly from the literature or derived from hematologic and radiobiological data [3, 4, 98, 99, 123, 124]. The coefficients θ_2, θ_3, ϕ, and φ are estimated in the course of the numerical study of the model and the subsequent juxtaposition of the modeling results with experimental data on the dynamics of lymphopoiesis after acute irradiation [125]. The parameter values are given in Table 1.2.

Table 1.2 Parameters of the lymphopoiesis model for small laboratory animals (rats and mice)

Parameter	Value	Dimension
α	2.4	day^{-1}
γ	1.4	day^{-1}
δ	0.2	day^{-1}
ψ	0.08	day^{-1}
μ	0.5	day^{-1}
ν	6	day^{-1}
D_1^0	1.4	Gy
D_1^{00}	13	Gy
D_2^0	1.4	Gy
D_2^{00}	13	Gy
D_3^0	1	Gy
D_3^{00}	6.5	Gy
θ_2	0.1	1
θ_3	0.16	1
ϕ	1	1
φ	12	1

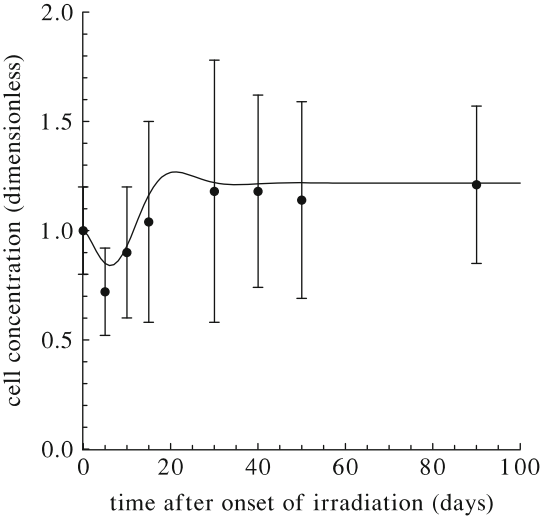

Fig. 1.9 Lymphopoiesis dynamics in rats under chronic irradiation at dose rate $N = 0.1\,\text{Gy/day}$. Computed values of the total concentration of X_1 and X_2 cells (*curve*) and experimentally measured values of concentration of bone marrow lymphocyte precursors (*circle*) [20]

Figures 1.9 and 1.10 show the dynamics of the total concentration of X_1 and X_2 cells and of the concentration of X_3 cells computed for $N = 0.1\,\text{Gy/day}$. Here and below we mean that X_i cells are all cells of the respective group, i.e., both undamaged cells and cells with different levels of injury by irradiation but not dead yet. Figures 1.9 and 1.10 also present the concentrations of lymphoid cells in the bone marrow and lymphocytes in the blood of rats exposed to chronic irradiation with the same, as in the computation, dose rate N [20]. All these quantities are given in the dimensionless form. As one can infer from these figures, the modeling results

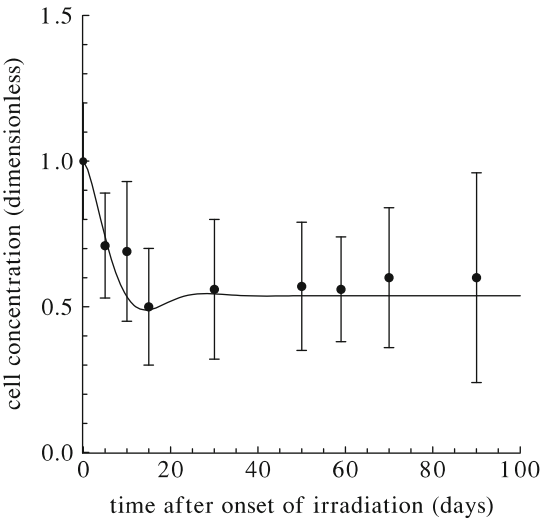

Fig. 1.10 Lymphopoiesis dynamics in rats under chronic irradiation at dose rate $N = 0.1$ Gy/day. Computed values of X_3 cell concentration (*curve*) and experimentally measured values of blood lymphocyte concentration (*circle*) [20]

qualitatively agree with experimental data [20]. When applying the statistical χ^2-test [115] to compare the dynamics of the lymphoid cell concentration in the bone marrow of rats [20] with modeling kinetics of the total concentration of X_1 and X_2 cells, the value $\chi^2 = 0.544$ is obtained. It does not exceed its critical value $\chi^2_{0.05} = 14.067$ (the number of degrees of freedom $n = 7$). When comparing the dynamics of the lymphocyte concentration in the blood of rats [20] with the modeling kinetics of the concentration of X_3 cells, the value $\chi^2 = 0.589$ is obtained. It also does not exceed its critical value $\chi^2_{0.05} = 15.507$ ($n = 8$). Thus, the modeling results quantitatively agree with experimental data [20].

Figures 1.9 and 1.10 show that the model describes the experimentally observed ability of the lymphopoietic system to adapt itself to low dose rate chronic irradiation. This adaptation manifests itself in the establishment of a new homeostasis state (a new stable dynamic equilibrium state). The latter is characterized by new stationary concentrations of lymphoid cells in the bone marrow (X_1 and X_2 cells) and of lymphocytes in the blood (X_3 cells). The stationary concentration of bone marrow lymphoid cells appears to be higher than the normal level, whereas the stationary concentration of lymphocytes in the blood is lower than the norm. Note that the effect of chronic irradiation on the lymphopoiesis is also manifested in an enhanced mitotic activity of X_1^{ud} cells. This finding also agrees with experimental data [126, 127].

The model is used to study the lymphopoiesis dynamics for other low and moderate dose rates of chronic irradiation. It is found that when the transition process having the character of overdamped oscillations is over, the dimensionless concentrations of X_1, X_2, and X_3 cells take new stationary values. Similar to experimental observations [20, 126], the new stationary concentration of blood lymphocyte (X_3 cells) decreases as N increases (Fig. 1.11). The new stationary concentrations of bone marrow lymphocyte precursor cells capable and incapable

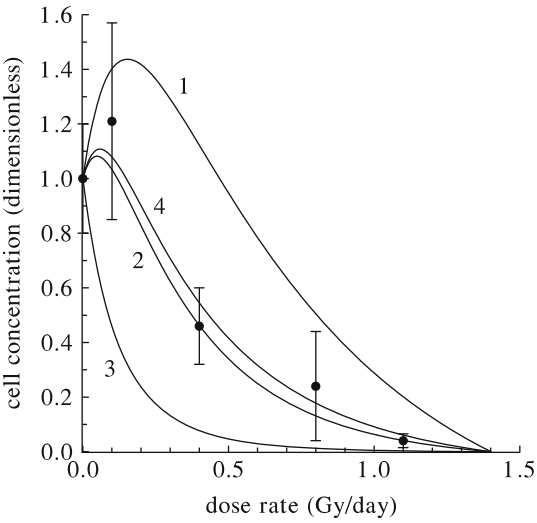

Fig. 1.11 New stationary concentrations of cells in the lymphopoietic system of rats versus the dose rate N of chronic irradiation. Computed values for X_1 cells (*curve 1*), X_2 cells (*curve 2*), X_3 cells (*curve 3*), and for the total amount of X_1 and X_2 cells (*curve 4*), as well as experimentally measured values for bone marrow lymphocyte precursors (*circle*) [20, 126]

of dividing (X_1 and X_2 cells) depend on the dose rate N in a more complicated way (Fig. 1.11). Analysis of the model shows that new stationary concentrations of X_1 and X_2 cells exceed their normal levels when $0 < N < N_1$ and $0 < N < N_2$, respectively. Here $N_1 = 0.39$ Gy/day and $N_2 = 0.06$ Gy/day. When $N > N_1$ and $N > N_2$, the new stationary concentrations of X_1 and X_2 cells take values lower than their normal levels. These new stationary values decrease as the dose rate N increases. Figure 1.11 shows that the dependence of the new stationary values of the total concentration of X_1 and X_2 cells on N qualitatively agrees with the experimental data [20, 126]. For a quantitative comparison of these modeling predictions with experimental data, the statistical χ^2-test [115] is used. The computed value $\chi^2 = 1.28$ does not exceed its critical value $\chi^2_{0.05} = 9.488$ (the number of degrees of freedom $n = 4$). Consequently, modeling results quantitatively agree with experimental data [20, 126].

The establishment of the new stable dynamic equilibrium state in the lymphopoietic system, which is characterized by elevated (with respect to the norm) concentrations of lymphocyte precursor cells capable of dividing (X_1 cells) and of their nondividing progeny (X_2 cells) in the bone marrow, can be regarded as a paradoxical adaptation of the lymphopoietic system to chronic low-level irradiation. This phenomenon can be considered the radiation hormesis (opposite effects of low and high doses and dose rates of radiation on the biota), which has been the subject of intensive studies [119, 128–130]. Note that the curves in Fig. 1.11, which show the dependence of stationary concentrations of lymphoid cells in the bone marrow on the dose rate N of chronic irradiation, have the same shape as a hypothetical generalized dose-effect curve illustrating the existence of radiation hormesis in chronic irradiation [129].

Figure 1.11 shows that the stationary concentrations of X_1, X_2, and X_3 cells as well as the stationary values of the total concentration of X_1 and X_2 cells become

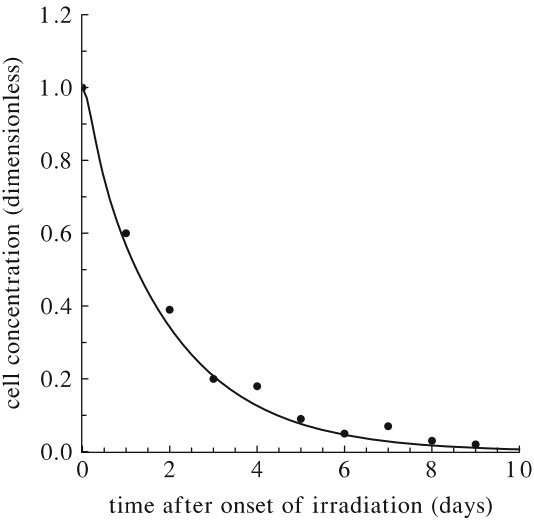

Fig. 1.12 Dynamics of concentration of blood lymphocytes (X_3 cells) in mice under chronic irradiation at dose rate $N = 6\,\mathrm{Gy/day}$. Modeling results (*curve*) and experimental data [118] (*circle*)

equal to zero at $N \geq N_c$. The critical dose rate N_c in the lymphopoiesis and thrombopoiesis models is defined by the same formula (1.39) but is smaller for the lymphopoietic system: $N_c = 1.4\,\mathrm{Gy/day}$.

In both the lymphopoiesis and thrombopoiesis models, the kinetic curves describing the concentrations of X_1, X_2, and X_3 cells at high dose rates N have an aperiodic character. The concentrations of lymphoid cells in the bone marrow and of lymphocytes in the blood decrease to levels incompatible with life (at $N \sim N_c$) or to zero (at $N \geq N_c$). These modeling results agree with experimental data [118] and correspond to irreversible depletion of the lymphopoietic system in mammals, resulting in the death of irradiated animals (Fig. 1.12).

In the numerical studies of the model, all the parameters were varied. It is found that the minimal concentrations of X_1, X_2, and X_3 cells depend basically on the parameters D_1^0, D_2^0, D_3^0 specifying the radiosensitivity of these cells. In turn, the new stationary concentrations of X_1, X_2, X_3 cells depend, to a large extent, on the parameters D_1^0, D_2^0, D_3^0, θ_2, θ_3, ϕ, and φ. All the aforementioned quantities also depend on the variable parameter N—the dose rate of chronic irradiation.

The results obtained in the framework of the model are qualitatively consistent with the experimentally observed dynamics of the lymphopoiesis in various mammalian species during chronic irradiation [99, 116–118, 120].

The developed model is also applied to examine the effects of acute irradiation on the lymphopoietic system. Figure 1.13 presents the dynamics of the total concentrations of X_1 and X_2 cells and of the X_3 cell concentration computed for a moderate dose D of acute irradiation. This figure also shows the respective experimental data [125], which are represented by the mean values of concentrations of bone marrow lymphoid cells and blood lymphocytes in rats at various intervals after the same exposure. As one can infer from Fig. 1.13, within the first postirradiation days, the concentrations of lymphoid cells in the bone marrow and mature lymphocytes

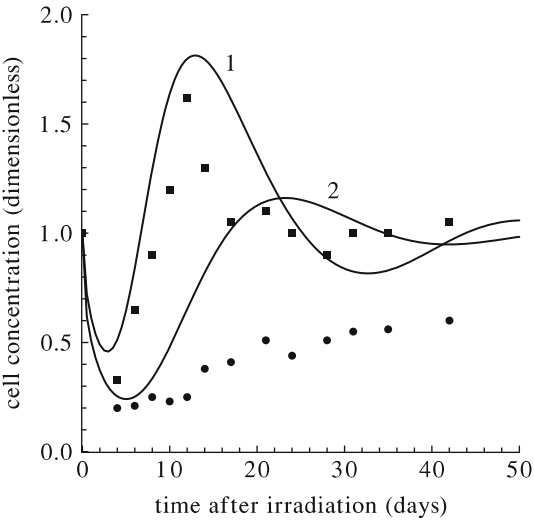

Fig. 1.13 Lymphopoiesis dynamics in rats after acute irradiation at dose $D = 2$ Gy. Computed values of the total concentration of X_1 and X_2 cells (*curve 1*) and of X_3 cell concentration (*curve 2*), as well as experimentally measured concentrations of bone marrow lymphocyte precursors (*box*) and of blood lymphocytes (*circle*) [125]

in the blood decrease. Thereafter the recovery process sets up, which is mainly over within 50 days after the end of irradiation. The overestimated (with respect to experiment) computed values of the concentration of blood lymphocytes (X_3 cells) seem to be explained by an enhanced migration of lymphocytes from the blood to the lymph, which is not taken into account in the model.

In the numerical studies of the model, the values of all parameters were varied. It has been revealed that the indices of radiation injury of the lymphopoietic system—the minimal concentrations of X_1, X_2, and X_3 cells—are basically determined by the parameters D_1^0, D_2^0, and D_3^0 specifying the radiosensitivity of these cells and by the dose D. Namely, they decrease as the parameters D_1^0, D_2^0, D_3^0 decrease and/or the dose D increases.

The features of the postirradiation lymphopoiesis dynamics predicted by the model qualitatively agree with the results of experiments on the effects of acute irradiation on the lymphopoiesis in various mammalian species [4].

1.7 The Dynamics of the Erythropoietic System in Mammals Unexposed and Exposed to Acute/Chronic Irradiation

Erythrocytes are the red blood cells [1–3] that have a vital function: transport of oxygen in the blood. The first morphologically identifiable precursors of erythrocytes in the bone marrow are proerythroblasts. The reproducing cells of the erythrocytic series also include the basophilic erythroblasts and the early and middle polychromatophil normoblasts. The rate of reproduction of erythrocyte precursors is controlled by the erythrocytic chalone [34]. The cell division ceases

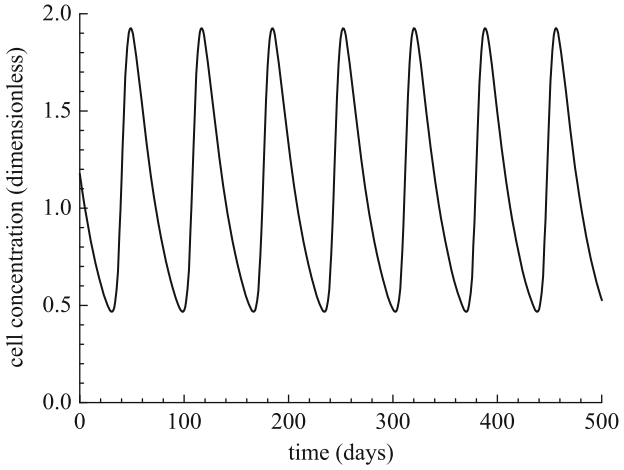

Fig. 1.14 Stable oscillations of X_3 cell concentration in the erythropoiesis model

at the subsequent stages of differentiation and maturation (late polychromatophil normoblast, oxyphilic normoblast, pronormocyte, normocyte, reticulocyte, and erythrocyte). Mature cells leave the bone marrow, circulate in the peripheral blood, and then die. As before, we split all the cells of the erythrocytic series into groups X_1, X_2, and X_3. In accordance with the above-stated concepts and model (1.1)–(1.3), (1.6), the dynamics of X_1, X_2, and X_3 cell concentrations (x_1, x_2, and x_3, respectively) is described by the differential equations (1.40)–(1.42). Therefore, all the results of the analytic investigation of the lymphopoiesis model are valid for the erythropoiesis model. In particular, the model reproduces stable oscillations of the cell concentrations (a stable limit cycle). The respective modeling results are presented in Fig. 1.14. This solution is obtained at the following values of the independent parameters: $\alpha = 2.4\,\text{day}^{-1}$, $\gamma = 1.4\,\text{day}^{-1}$, $\delta = 0.3\,\text{day}^{-1}$, $\psi = 0.033\,\text{day}^{-1}$, $\theta_2 = 0.1$, and $\theta_3 = 2$. The values are chosen in such a way that the modeling results correspond to the cyclic kinetics of erythropoiesis in dogs [131]. Note that the cyclic erythropoiesis was also observed in humans [122].

As for the effects of radiation on the erythropoiesis, experiments [4, 98, 99] show that the erythrocytes in the blood are radioresistant, whereas their bone marrow precursor cells are sensitive to radiation. Therefore, the model of erythropoiesis in irradiated mammals comprises seven differential equations. The latter describe the dynamics of concentrations of undamaged X_i^{ud}, damaged X_i^{d}, and heavily damaged X_i^{hd} cells ($i = 1, 2$), and also the concentration of radioresistant X_3 cells (see Sect. 1.4). For numerical studies, the equations are rewritten in terms of the new dimensionless variables, the latter being the ratios of the dimension cell concentrations to their normal values.

Our model is used to examine the erythropoiesis dynamics in small laboratory animals (rats, mice) exposed to chronic irradiation. The coefficients α, γ, δ, ψ,

μ, and ν, as well as D_i^0 and D_i^{00} ($i = 1, 2$), are either taken directly from the literature or derived from hematologic and radiobiological data [3, 4, 98, 99, 132]. The coefficients θ_2, θ_3, ϕ, and φ are estimated in the course of the numerical study of the model and the subsequent juxtaposition of the modeling results with experimental data on the dynamics of the erythropoiesis after acute irradiation [133]. The values of the independent parameters are given in Table 1.3.

Figures 1.15 and 1.16 present the dynamics of the total concentration of X_1 and X_2 cells and of the X_3 cell concentration computed for a low dose rate N. These figures also show the kinetics of concentrations of bone marrow erythroid cells and blood erythrocytes in rats exposed to chronic irradiation with the same dose

Table 1.3 Parameters of the erythropoiesis model for small laboratory animals (rats and mice)

Parameter	Value	Dimension
α	2.4	day^{-1}
γ	1.5	day^{-1}
δ	1.1	day^{-1}
ψ	0.04	day^{-1}
μ	1	day^{-1}
ν	6	day^{-1}
D_1^0	1.7	Gy
D_1^{00}	6	Gy
D_2^0	0.6	Gy
D_2^{00}	8	Gy
θ_2	0.01	1
θ_3	0.06	1
ϕ	2.5	1
φ	30	1

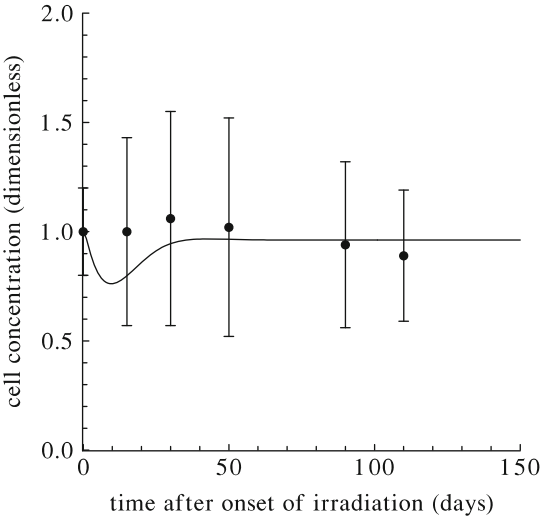

Fig. 1.15 Erythropoiesis dynamics in rats under chronic irradiation at dose rate $N = 0.1$ Gy/day. Computed values of the total concentration of X_1 and X_2 cells (*curve*) and experimentally measured values of concentration of bone marrow erythrocyte precursors (*circle*) [134]

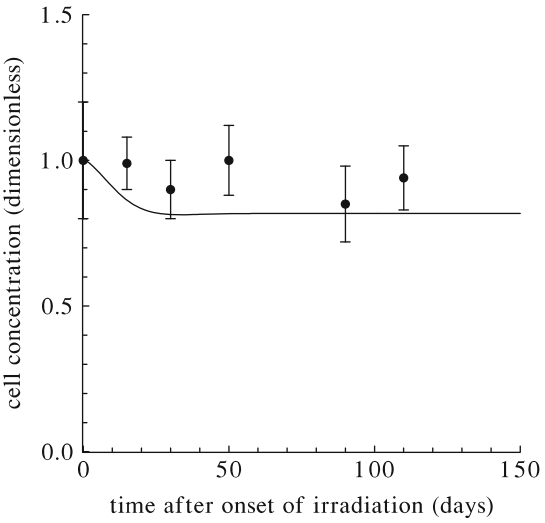

Fig. 1.16 Erythropoiesis dynamics in rats under chronic irradiation at dose rate $N = 0.1$ Gy/day. Computed values of X_3 cell concentration and experimentally measured values of blood erythrocyte concentration (*circle*) [134]

rate [134, 135]. All these quantities are given in the dimensionless units. As one can infer from Figs. 1.15 and 1.16, the modeling results qualitatively agree with experimental data [134, 135]. Furthermore, there is also a quantitative agreement between them. The computed values $\chi^2 = 0.345$ and $\chi^2 = 6.35$ do not exceed their critical level $\chi^2_{0.05} = 11.070$ (the number of degrees of freedom $n = 5$).

The transition process in the erythropoietic system has some peculiarities. After the onset of irradiation, the total concentration of X_1 and X_2 cells decreases to a certain minimal value. Then it increases and approaches a new stationary level. In turn, the concentration of X_3 cells slowly decreases until it reaches a new stationary level. This seems to be due to the "inertia" of the X_3 cell population resulting from the large life span of blood erythrocytes and their radioresistance.

Figures 1.15 and 1.16 demonstrate that a new stable dynamic equilibrium state (a new homeostasis state) is established in the erythropoietic system upon the completion of the transition process. The establishment of the new homeostasis state in the erythropoietic system can be considered an adaptation of this system to chronic irradiation. It is worthwhile noting that the new homeostasis state in the erythropoietic system, as those in thrombopoietic and lymphopoietic systems, is characterized by an enhanced mitotic activity of X_1 cells. Hence, the model describes an "overstrain" in the functioning of the erythropoietic system. This "overstrain" is required to maintain the new stable dynamic equilibrium in this system under chronic irradiation at low and moderate dose rates N. These modeling results are supported experimentally [119, 120, 134, 135].

Figure 1.17 presents the values of new stationary concentrations of X_1, X_2, and X_3 cells and of the total concentration of X_1 and X_2 cells that are computed for various dose rates N. Figure 1.17 also shows the new stationary concentrations of bone marrow erythrocyte precursors in rats exposed to chronic irradiation with several dose rates N [134, 135]. As one can see, a new stationary concentration of

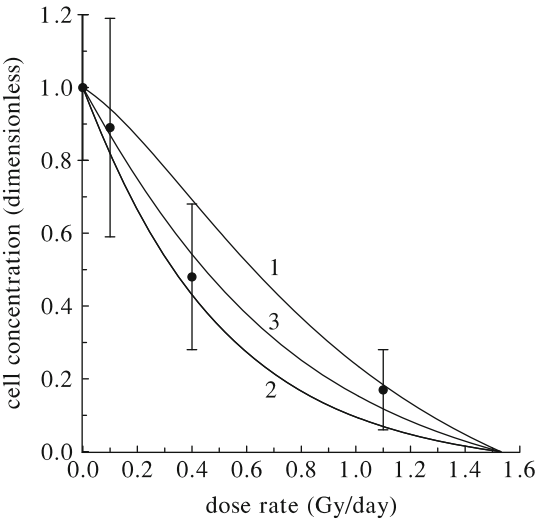

Fig. 1.17 New stationary concentrations of cells in the erythropoietic system of rats versus the dose rate N of chronic irradiation. Computed values for X_1 cells (*curve 1*), X_2 cells (*curve 2*), X_3 cells (*curve 2*), and for the total amount of X_1 and X_2 cells (*curve 3*), as well as experimentally measured values for bone marrow erythrocyte precursors (*circle*) [134, 135]

X_3 cells decreases (compared to normal) as the dose rate N increases. The same relation is valid for new stationary concentrations of X_1 and X_2 cells. As one can infer from Fig. 1.17, the computed dependence of the new stationary values of the total concentration of X_1 and X_2 cells on the dose rate N qualitatively agrees with the relevant experimental data [134, 135]. Moreover, they are also in quantitative agreement. The computed value of $\chi^2 = 0.327$ does not exceed its critical value $\chi^2_{0.05} = 7.815$ ($n = 3$).

Figure 1.17 shows that the new stationary concentrations of the above-mentioned cells are zero at $N \geq N_c$. The critical radiation dose rate N_c for the erythropoietic system is defined by the same formula (1.39) as that for the lymphopoietic and thrombopoietic systems. It is found that $N_c = 1.53\,\mathrm{Gy/day}$. Note that this value is close to that for the lymphopoietic system.

At values of the dose rate N that are close to or exceed the critical dose rate N_c, the erythropoiesis dynamics is aperiodic, as in the models considered above. Concentrations of X_1, X_2, and X_3 cells decrease to low values at $N \sim N_c$ and to zero at $N \geq N_c$. Comparison of the dynamics of X_3 cell concentration computed for lethal dose rates with the pertinent experimental data on the kinetics of the erythrocyte concentration in the blood of mice [118] demonstrates their qualitative and quantitative agreement for the first 10 days from the onset of irradiation (Fig. 1.18). The comparison could not be continued further because of the death of the mice.

In the numerical study of the model, the values of all the parameters were varied within reasonable ranges. It has been revealed that the minimal concentrations of X_1 and X_2 cells are basically determined by parameters D_1^0 and D_2^0 specifying the radiosensitivity of these cells. The same parameters, as well as coefficients θ_2, θ_3, ϕ, and φ, determine to a large extent the values of the new stationary concentrations

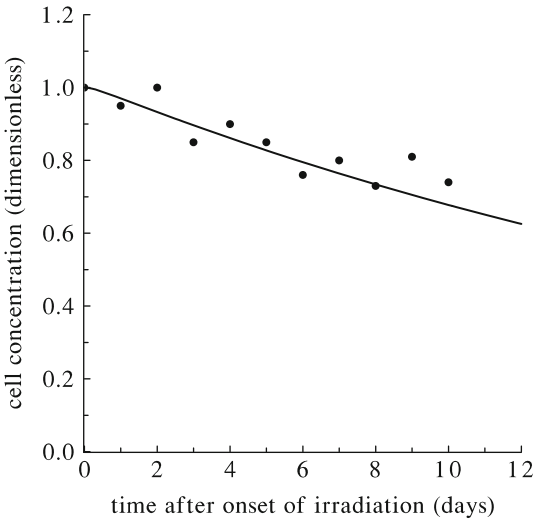

Fig. 1.18 Dynamics of the concentration of blood erythrocytes (X_3 cells) in mice under chronic irradiation at dose rate $N = 3$ Gy/day. Modeling results (*curve*) and experimental data (*circle*) [118]

for X_1, X_2, and X_3 cells. All these quantities also depend on the variable parameter N, the dose rate of chronic irradiation.

The presented results of numerical studies of the model qualitatively correspond to the erythropoiesis dynamics in other mammalian species during chronic irradiation [99, 116, 117, 120].

The model is applied to examine the erythropoiesis dynamics in rats after acute irradiation. The values of the model parameters are taken to be the same as those in Table 1.3. The model qualitatively reproduces the postirradiation dynamics of erythropoietic cells in the bone marrow and erythrocytes in the peripheral blood [4, 125, 133]. Specifically, the model describes a postirradiation decrease in the concentration of all three cell groups. Having decreased to minimal values, the concentrations of X_1 and X_2 cells increase, reach a maximum, decrease, and return to their normal levels. In turn, having decreased to a minimal value, the X_3 cell concentration increases and reaches the normal level practically without oscillations. The dose dependence of the minimal concentrations of X_1 and X_2 cells in the model of the erythropoietic system is the same as those in the models of the lymphopoietic and thrombopoietic system, namely the minimal level decreases as the radiation dose D increases.

The modeling results agree quantitatively with experimental data, which is evident from Fig. 1.19. This figure shows the modeling and experimental results on the dynamics of concentrations of bone marrow erythrocyte precursors (X_1 and X_2 cells) and of blood erythrocytes (X_3 cells) in rats after acute irradiation with a moderate dose D [4, 125].

Our model does not account for the influence of erythropoietin on the erythropoietic system. This simplification is explained by the following considerations. It is believed that erythropoietin substantially affects the erythropoiesis in mammals during conditions of emergency (hemorrhages, hypoxia, etc.) when a quick response

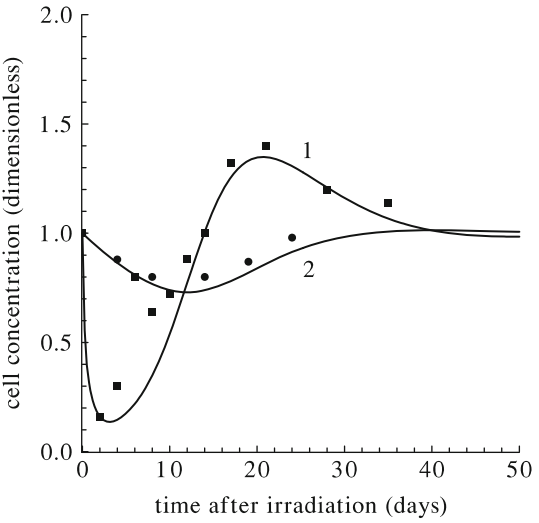

Fig. 1.19 Erythropoiesis dynamics in rats after acute irradiation at dose $D = 4$ Gy. Computed values of the total concentration of X_1 and X_2 cells (*curve 1*) and of X_3 cell concentration (*curve 2*), as well as experimentally measured concentrations of bone marrow erythrocyte precursors (*box*) and of blood erythrocytes (*circle*) [125, 133]

of this system is needed to provide the required oxygen to the organism. In the experimental conditions we deal with, no such emergencies are likely to arise. For low and moderate doses D of acute radiation and various dose rates N of chronic radiation, hemorrhages do not occur and hypoxia is very weak, if present at all, because the reduction in erythrocyte concentration in the blood is insignificant. At high D and N, the animals die either before a hemorrhage takes place or at the time of hemorrhage.

In the course of numerical studies of the model, the values of all the parameters were varied. It is revealed that the basic indices of radiation-induced damage of the erythropoietic system—the minimal concentrations of X_1, X_2, and X_3 cells—are largely determined by the parameters D_1^0 and D_2^0, which specify the radiosensitivity of X_1 and X_2 cells, as well as by the radiation dose D.

The obtained modeling results are qualitatively consistent with the experimentally observed postirradiation dynamics of the erythropoiesis in different mammalian species [4].

1.8 The Dynamics of the Granulopoietic System in Mammals Unexposed and Exposed to Acute/Chronic Irradiation

The granulocytes are a class of leukocytes [1–3]. Their function in the organism is a nonspecific immune protection by digestion of foreign substances with the help of hydrolytic enzymes. The first morphologically identifiable granulocyte precursor cells in the bone marrow are myeloblasts. The dividing cells of the granulocyte series also include promyelocytes and myelocytes. Reproduction of the granulocyte

precursors is controlled by the granulocytic chalone [34]. At subsequent stages of differentiation and maturation (metamyelocyte, granulocyte), the cells do not divide. For some time, mature cells remain in the bone marrow, in the so-called bone marrow depot, and then pass into the blood. There is a negative feedback between the rate of granulocyte emergence from the bone marrow and their number in the peripheral blood. From the blood the granulocytes migrate to tissues. The tissue granulocytes no longer circulate, and this is the final stage of their life.

First we develop a simplified version of the granulopoiesis model. The bone marrow precursor cells (from stem cells in the respective microenvironment to the myelocytes) that are capable of dividing are denoted by X_1, the metamyelocytes and the mature bone marrow granulocytes are denoted by X_2, and the mature granulocytes outside the bone marrow are denoted by X_3. In accordance with Eqs. (1.1)–(1.3) and relation (1.6), the dynamics of the concentrations of X_1, X_2, and X_3 cells (x_1, x_2, and x_3, respectively) can be described as follows:

$$\frac{dx_1}{dt} = \frac{\alpha\, x_1}{1 + \beta\,(x_1 + \theta_2 x_2 + \theta_3 x_3)} - \gamma\, x_1, \tag{1.49}$$

$$\frac{dx_2}{dt} = \gamma\, x_1 - F\, x_2, \tag{1.50}$$

$$\frac{dx_3}{dt} = F\, x_2 - \Psi\, x_3. \tag{1.51}$$

The constant coefficients α, β, θ_2, θ_3, $\gamma \equiv C$, and $\Psi \equiv E$ in the system (1.49)–(1.51) have the same meaning as in Eqs. (1.1)–(1.6). We represent the specific rate of granulocyte supply from the bone marrow to the blood flow, with consideration for the bone marrow depot, as the following function of X_3 cell concentration:

$$F = \delta\, \frac{1 + M x_3^2}{1 + L x_3^2}. \tag{1.52}$$

The quantities δ and $\delta\, M/L$ are, respectively, the maximal and minimal specific rates of granulocyte supply from the bone marrow to the blood flow. The constants L and M are related by the inequality $L > M$.

The system (1.49)–(1.51) is investigated by methods of the qualitative theory of differential equations, oscillation theory, and bifurcation theory [105–111]. It has two singular points in the space of variables. The first of them is trivial (the variables x_1, x_2, and x_3 vanish). The coordinate $\bar{x}_3$ of the second singular point in the space of variables is determined by the following cubic equation:

$$\bar{x}_3^3\, \beta \left[\left(\frac{\Psi}{\gamma} + \theta_3 \right) M + \theta_2 \frac{\Psi}{\delta} L \right] - \bar{x}_3^2\, M \left(\frac{\alpha}{\gamma} - 1 \right)$$
$$+ \bar{x}_3\, \beta \left(\frac{\Psi}{\gamma} + \theta_2 \frac{\Psi}{\delta} + \theta_3 \right) - \left(\frac{\alpha}{\gamma} - 1 \right) = 0. \tag{1.53}$$

Two other coordinates, $\bar{x}_1$ and $\bar{x}_2$, can be expressed in terms of $\bar{x}_3$ in the following way:

$$\bar{x}_1 = \bar{x}_3 \frac{\Psi}{\gamma}, \tag{1.54}$$

$$\bar{x}_2 = \bar{x}_3 \frac{\Psi}{\delta} \frac{1 + L\bar{x}_3^2}{1 + M\bar{x}_3^2}. \tag{1.55}$$

When $\alpha < \gamma$, the first (trivial) singular point is the stable (node). In turn, all the roots of Eq. (1.53) have negative real parts according to the Routh–Hurwitz criterion (see, e.g., [111]) and, hence, the second singular point has no physical sense. If $\alpha = \gamma$, then the second singular point coincides with the first one, the latter being the stable node. In both cases the stable trivial singular point can be identified with the state of the extinction of the granulopoietic system. These ranges of the parameter values are not considered in what follows.

When $\alpha > \gamma$, then the first (trivial) singular point is unstable (saddle). According to the Routh–Hurwitz criterion, all the roots of Eq. (1.53) have positive real parts. This means that Eq. (1.53) has at least one positive real root and, hence, the second singular point has physical sense.

The second singular point can be either stable or unstable, depending on the values of the model parameters. It has been found that the second singular point becomes unstable when the model parameters obey the following conditions:

$$\theta_3 > \theta_2 + \frac{1}{q}\left[(q+s)^2 + 2\sqrt{qc(q+s)(q+s+\theta_2)}\right], \tag{1.56}$$

$$\gamma > \delta \frac{1+m}{1+l} + \Psi\left[1 + 2\frac{l-m}{(1+m)(1+l)}\right], \tag{1.57}$$

$$\frac{\gamma}{1-(1+\theta_2/q+\theta_3/c)A_2} < \alpha < \frac{\gamma}{1-(1+\theta_2/q+\theta_3/c)A_1}, \tag{1.58}$$

where

$$A_{1,2} = \frac{u \pm (u^2 - w^2)^{1/2}}{2(q+s+\theta_2)}, \quad q = \frac{\delta}{\gamma}\frac{1+m}{1+l}, \quad s = \frac{\Psi}{\gamma}\left[1 + 2\frac{l-m}{(1+l)(1+m)}\right], \tag{1.59}$$

$u = q(\theta_3 - \theta_2) - (q+s)^2$, $w^2 = 4qc(q+s)(q+s+\theta_2)$, $m = M\bar{x}_3^2$, and $l = L\bar{x}_3^2$. It is worth noting that the quantities A_1 and A_2 are real and positive when Eq. (1.56) is valid.

If the second singular point with positive coordinates $\bar{x}_i$ is stable, then it can be identified with the state of the stable dynamic equilibrium (the homeostasis state) of the granulopoietic system and the values $\bar{x}_i$ can be considered the normal concentrations of the respective cells.

When the second singular point becomes unstable, one more particular solution appears: a stable limit cycle (stable oscillations of the variables x_1, x_2, and x_3). This particular solution can be interpreted as the stable oscillations of the cell concentrations in the granulopoietic system. Thus, the inequalities (1.56)–(1.58) can be considered the conditions of appearance of the cyclic granulopoiesis in mammals. They are similar to those derived in the models of other hematopoietic lineages and have the same physical meaning. Specifically, inequality (1.56) may become valid when the parameter θ_3 takes a larger value, i.e., when the influence of the chalone produced by X_3 cells on the reproduction rate of X_1 cells is intensified. In turn, inequality (1.57) may hold when the parameter γ takes a larger value and/or the parameters δ and Ψ take smaller values, i.e., when the specific rate of transfer of cells from group X_1 to group X_2 increases and/or the specific rate of transfer of cells from group X_2 to group X_3 and the specific rate of X_3 cell death decrease. Finally, inequality (1.58) may become valid when the parameter α, the maximal specific reproduction rate of X_1 cells, is within a certain range.

The developed model [Eqs. (1.49)–(1.51)] is investigated numerically. For the convenience, Eqs. (1.49)–(1.51) are rewritten in terms of the new dimensionless variables. The latter are the ratios of the dimension cell concentrations to their stationary values. The numerical studies of the model confirm the predictions made in the course of its analytical investigations. First of all, the model describes the state of the stable dynamic equilibrium (the homeostasis state) of the granulopoietic system, which is characterized by stationary concentrations of the mature granulocytes and their bone marrow precursors. After deviation from this state, the system returns to it. The model also reproduces the cyclic kinetics of the granulopoietic system. To simulate this behavior of the granulopoietic system in dogs, the following values of the independent parameters are used: $\alpha = 2.4\,\text{day}^{-1}$, $\gamma = 0.93\,\text{day}^{-1}$, $\delta = 0.37\,\text{day}^{-1}$, $\Psi = 0.15\,\text{day}^{-1}$, $m = 0.5$, $l = 1$, $\theta_2 = 0.1$, and $\theta_3 = 10$. The obtained modeling results are presented in Fig. 1.20. As one can infer from this figure, the period and the amplitude of oscillations of the dimensionless concentration of X_3 cells are 29 days and 0.4, respectively. Note that a cyclic granulopoiesis was observed in both dogs and humans [121, 136].

Researchers often restrict themselves to the study of two indices only: the concentration of granulocytes in the peripheral blood and the total number of granulopoietic elements in the bone marrow. For an effective comparison of modeling results with experimental data, we modify the system (1.49)–(1.51). Instead of Eq. (1.51), which describes the dynamics of the concentration of the mature granulocytes outside the bone marrow, we introduce two equations that describe the dynamics of concentrations of granulocytes in the peripheral blood and in tissues (cells X_3 and X_4 and their respective concentrations x_3 and x_4). We also assume that the specific rate of granulocyte supply from the bone marrow to the blood flow is largely determined by the blood granulocyte concentration. Finally, the model takes the form

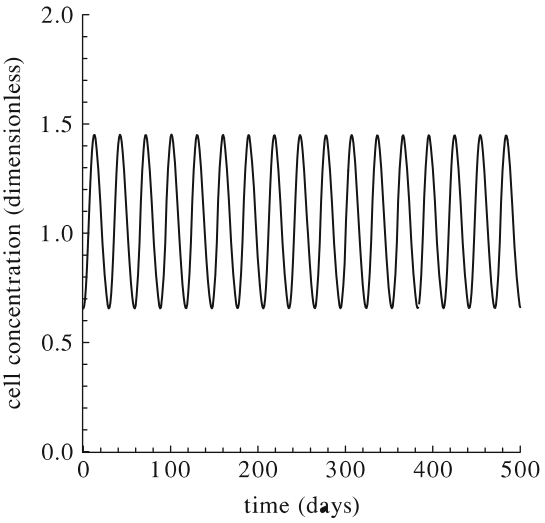

Fig. 1.20 Stable oscillations of X_3 cell concentration in the granulopoiesis model

$$\frac{dx_1}{dt} = \frac{\alpha\, x_1}{1 + \beta\,(x_1 + \theta_2\, x_2 + \theta_3\, x_3 + \theta_4\, x_4)} - \gamma\, x_1, \tag{1.60}$$

$$\frac{dx_2}{dt} = \gamma\, x_1 - \delta\, \frac{1 + M\, x_3^2}{1 + L\, x_3^2}\, x_2, \tag{1.61}$$

$$\frac{dx_3}{dt} = \delta\, \frac{1 + M\, x_3^2}{1 + L\, x_3^2}\, x_2 - \psi\, x_3, \tag{1.62}$$

$$\frac{dx_4}{dt} = \psi\, x_3 - \xi\, x_4. \tag{1.63}$$

In Eqs. (1.62) and (1.63), the parameter ψ denotes the specific rate of transfer of cells from group X_3 to group X_4, whereas the parameter ξ is the specific rate of natural death of X_4 cells.

Similar to the system (1.49)–(1.51), the system (1.60)–(1.63) has two singular points. The first of them is trivial. The coordinate $\bar{x}_3$ of the second singular point in the space of variables is determined by the following cubic equation:

$$\bar{x}_3^3\, \beta \left[\left(\frac{\psi}{\gamma} + \theta_3 + \theta_4 \frac{\psi}{\xi} \right) M + \theta_2 \frac{\psi}{\delta} L \right] - \bar{x}_3^2\, M \left(\frac{\alpha}{\gamma} - 1 \right)$$
$$+ \bar{x}_3\, \beta \left(\frac{\psi}{\gamma} + \theta_2 \frac{\psi}{\delta} + \theta_3 + \theta_4 \frac{\psi}{\xi} \right) - \left(\frac{\alpha}{\gamma} - 1 \right) = 0. \tag{1.64}$$

Three other coordinates, $\bar{x}_1$, $\bar{x}_2$, and $\bar{x}_4$, of the second singular point can be expressed in terms of $\bar{x}_3$ in the following way:

$$\bar{x}_1 = \bar{x}_3 \frac{\psi}{\gamma}, \tag{1.65}$$

$$\bar{x}_2 = \bar{x}_3 \frac{\psi}{\delta} \frac{1 + L\bar{x}_3^2}{1 + M\bar{x}_3^2}, \tag{1.66}$$

$$\bar{x}_4 = \bar{x}_3 \frac{\psi}{\xi}. \tag{1.67}$$

When $\alpha < \gamma$, the first (trivial) singular point is stable (node). The second singular point has no physical sense because all the roots of Eq. (1.64) have negative real parts according to the Routh–Hurwitz criterion [111]. If $\alpha = \gamma$, then the second singular point coincides with the first (trivial) singular point. In both these cases the stable first singular point can be identified with the state of extinction of the granulopoietic system. This range of the parameter values is not considered in what follows.

When $\alpha > \gamma$, the first (trivial) singular point is unstable (saddle). According to the Routh–Hurwitz criterion [111], all the roots of Eq. (1.64) have positive real parts. This means that Eq. (1.64) has at least one positive real root and, hence, the second singular point is physically meaningful.

Experiments have shown that all cells of the granulocytic series exhibit radiosensitivity, though in different degrees [137]. Therefore, the model of the dynamics of the granulopoietic system in irradiated mammals based on system (1.60)–(1.63) comprises 12 differential equations that describe the dynamics of concentrations of undamaged X_i^{ud}, damaged X_i^{d}, and heavily damaged X_i^{hd} cells ($i = 1, 2, 3, 4$). For numerical studies, the equations describing the concentrations of cells listed above are rewritten in terms of the new dimensionless variables, the latter being the ratios of the dimension cell concentrations to their normal values.

The developed model is applied to simulate the dynamics of the granulopoietic system in small laboratory animals (rats, mice) exposed to chronic irradiation. The coefficients α, γ, δ, ψ, ξ, μ, and ν, as well as D_i^0 and D_i^{00} ($i = 1, 2, 3, 4$), are either taken directly from the literature or derived from hematologic and radiobiological data [3, 4, 98, 99, 137]. The coefficients $m = M\bar{x}_3^2$, $l = L\bar{x}_3^2$, θ_2, θ_3, ϕ, and φ are estimated in the course of the numerical study of the model and the subsequent juxtaposition of the modeling results with experimental data on the dynamics of the granulopoietic system after acute irradiation [125]. The parameter values are given in Table 1.4.

Figures 1.21 and 1.22 present the dynamics of the total concentration of X_1 and X_2 cells and of the X_3 cell concentration computed for a low dose rate N. These figures also show concentrations of bone marrow granulocyte precursor cells and blood granulocytes measured in rats exposed to chronic irradiation with the same dose rate N [134]. All these quantities are given in the dimensionless units. As one can infer from Figs. 1.21 and 1.22, the modeling results qualitatively agree with the experimental data [134]. After initially decreasing, the concentrations under consideration increase, then decrease again, and eventually approach new

Table 1.4 Parameters of the granulopoiesis model for small laboratory animals (rats and mice)

Parameter	Value	Dimension
α	2.4	day^{-1}
γ	0.36	day^{-1}
δ	0.33	day^{-1}
ψ	2.4	day^{-1}
ξ	0.03	day^{-1}
μ	0.5	day^{-1}
ν	6	day^{-1}
D_1^0	2.5	Gy
D_1^{00}	5	Gy
D_2^0	10	Gy
D_3^0	10	Gy
D_4^0	10	Gy
D_2^{00}	100	Gy
D_3^{00}	100	Gy
D_4^{00}	100	Gy
m	0.33	1
l	2	1
θ_2	0.01	1
θ_3	0.06	1
θ_4	0.23	1
ϕ	1	1
φ	12	1

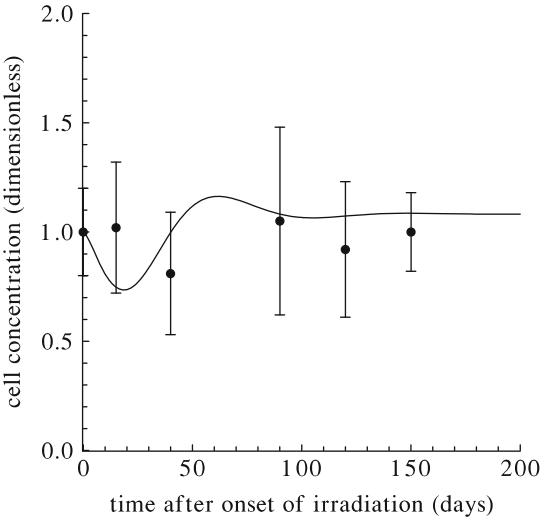

Fig. 1.21 The dynamics of the granulopoietic system in rats under chronic irradiation at dose rate $N = 0.1\,\text{Gy/day}$. Computed values of the total concentration of X_1 and X_2 cells (*curve*) and experimentally measured values of concentration of bone marrow granulocyte precursors (*circle*) [134]

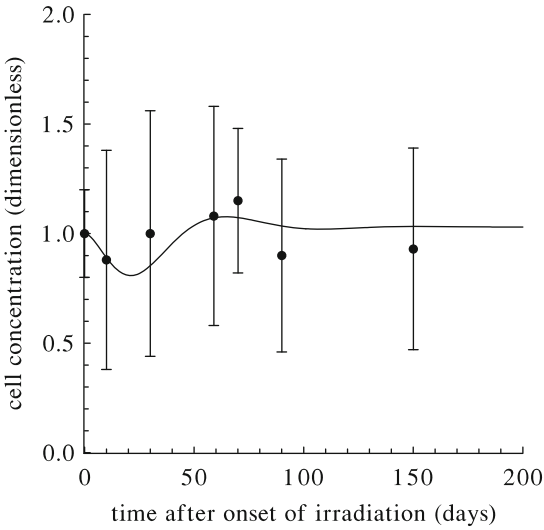

Fig. 1.22 The dynamics of the granulopoietic system in rats under chronic irradiation at dose rate $N = 0.1$ Gy/day. Computed values of X_3 cell concentration and experimentally measured values of blood neutrophil concentration (*circle*) [134]

stationary levels, the latter being higher than the normal ones. These modeling results quantitatively agree with the experimental data [134]. The computed values $\chi^2 = 1.75$ and $\chi^2 = 0.267$ do not exceed their critical values $\chi^2_{0.05} = 11.070$ ($n = 5$) and $\chi^2_{0.05} = 12.592$ ($n = 6$).

The effect of chronic irradiation on the granulopoietic system is also manifested in an enhanced mitotic activity of X_1 cells. This modeling prediction agrees with experimental data [127, 134].

Figure 1.23 presents new stationary concentrations of X_i cells ($i = 1, 2, 3, 4$), as well as new stationary values of the total concentration of X_1 and X_2 cells, computed for various dose rates N. This figure also shows new stationary concentrations of bone marrow granulocyte precursors in rats exposed to chronic irradiation with several dose rates N [134, 135]. As one can see, the new stationary concentrations of X_4 cells are smaller than its normal level. They decrease with increasing N. In turn, the dependence of new stationary values of concentrations of X_1, X_2, and X_3 cells on the dose rate N and the dependence of the total concentration of X_1 and X_2 cells on N are more complicated. In the range of low dose rates, these quantities exceed their normal levels, the latter being equal to unity in view of the applied definition of the dimensionless concentrations of X_i cells ($i = 1, 2, 3, 4$). In the range of moderate and high dose rates, the dependence of new stationary concentrations of these cell groups on the dose rate N is the same as that for X_4 cells. It is worthwhile emphasizing that the modeling results are in qualitative and quantitative agreement with experimental data [134, 135]. The computed value $\chi^2 = 0.94$ does not exceed its critical value $\chi^2_{0.05} = 11.070$ ($n = 5$).

The establishment of the state of the new stable dynamic equilibrium in the granulopoietic system, which is characterized by an elevated (compared to normal) concentrations of bone marrow granulocyte precursors (X_1 and X_2 cells) and of

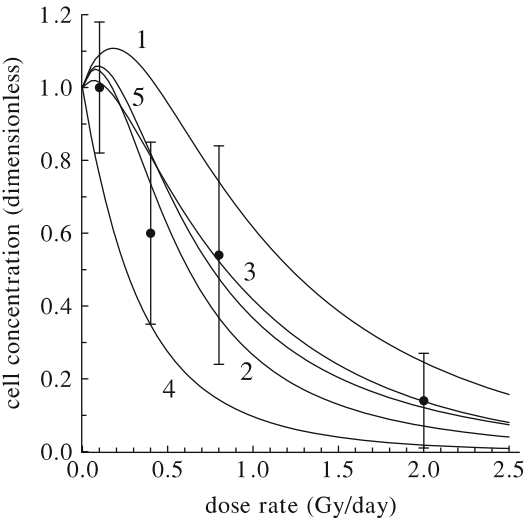

Fig. 1.23 New stationary concentrations of cells in the granulopoietic system of rats vs. dose rate N of chronic irradiation. Computed values for X_1 cells (*curve 1*), X_2 cells (*curve 2*), X_3 cells (*curve 3*), X_4 cells (*curve 4*), and for the total amount of X_1 and X_2 cells (*curve 5*), as well as experimentally measured values for bone marrow granulocyte precursors (*circle*) [134, 135]

blood granulocytes (X_3 cells), can be regarded as the paradoxical adaptation of this system to low-level chronic irradiation. This finding can be related to the effects of radiation hormesis.

As it is found, the stationary concentrations of X_1, X_2, X_3, and X_4 cells become equal to zero at $N \geq N_c$. The critical dose rate N_c in the granulopoiesis model is determined by the same formula (1.39) as that in the models described earlier, but it has the highest value: $N_c = 5.1\,\mathrm{Gy/day}$.

When the dose rate N is close to or exceeds N_c, the cell concentration dynamics in the granulopoietic system has an aperiodic character, as does that in the other hematopoietic lineages. The concentrations of all cells in this system decrease to low levels at $N \sim N_c$ and to zero at $N \geq N_c$. Such solutions can be identified with an irreversible depletion of the granulopoietic system, which was observed in mammals at high dose rates of chronic irradiation [4]. As one can infer from Fig. 1.24, the modeling results and relevant experimental data [118] presented there are in qualitative and quantitative agreement.

In the numerical study of the model, the values of all the parameters were varied. It has been revealed that the minimal concentrations of X_1, X_2, X_3, and X_4 cells depend basically on the parameter D_1^0 specifying the radiosensitivity of X_1 cells. The parameter D_1^0 as well as the coefficients θ_2, θ_3, θ_4, ϕ, and φ determine to a large extent the new stationary concentrations of X_1, X_2, X_3, and X_4 cells. All of the above quantities also depend on the variable parameter N—the dose rate of chronic irradiation.

The results obtained in the framework of the model are qualitatively consistent with the experimentally observed dynamics of the granulopoietic system in various mammalian species during chronic irradiation [99, 116–118, 120].

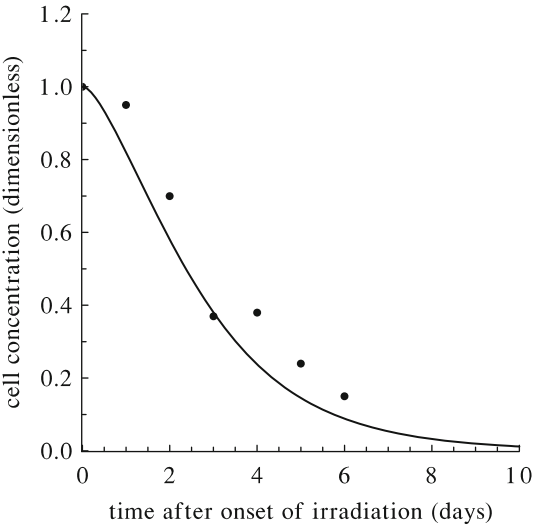

Fig. 1.24 Dynamics of the concentration of blood granulocytes in mice under chronic irradiation at dose rate $N = 10\,\text{Gy/day}$. Modeling results (*curve*) and experimental data (*circle*) [118]

The model is also used to simulate the dynamics of the granulopoietic system in rats exposed to acute irradiation. The values of the model parameters are taken to be the same as those in Table 1.4. Similar to the previously studied case of other hematopoietic lineages, the concentrations of all cells in the granulopoietic system decrease to minimal values. The latter decrease as the dose D increases. Then a recovery process ensues. When this process is over, the concentrations of all cells return to their initial levels. As an example, Fig. 1.25 presents the dynamics of the X_3 cell concentration computed for a moderate acute radiation dose D. This figure also shows the relevant experimental data [125] on the kinetics of the concentration of neutrophils prevailing in the pool of blood granulocytes. As one can see, the model adequately reproduces the experimental results [125]. Comparison of the model predictions with the experimental data shows that they agree on a quantitative level. The computed value $\chi^2 = 6.98$ does not exceed its critical value $\chi^2_{0.05} = 18.307$ (the number of degrees of freedom $n = 10$).

In the model simulation of the effect of acute irradiation on the granulopoietic system, all the parameters were varied. It has been found that the indices of radiation injury of the granulopoietic system—the minimal concentrations of X_1, X_2, X_3, and X_4 cells—are basically determined by the coefficient D_1^0 specifying the radiosensitivity of X_1 cells and by the dose D.

The specific features of postirradiation dynamics in the granulopoietic system revealed by the model agree with relevant experiment data on this hematopoietic lineage in various mammalian species [4].

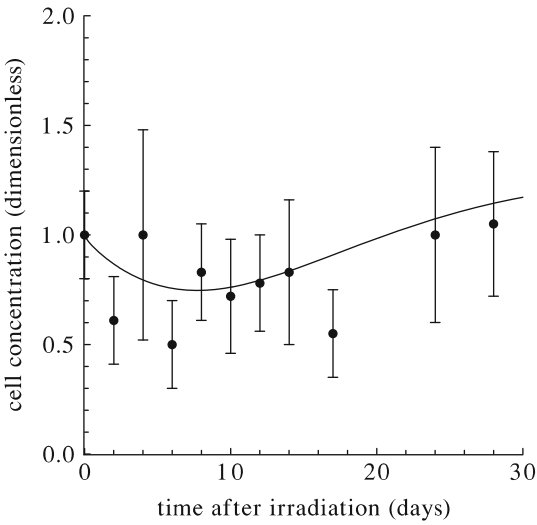

Fig. 1.25 Modeling dynamics of the concentration of X_3 cells after acute irradiation at dose $D = 2$ Gy (*curve*) and pertinent experimental data on the kinetic of neutrophil concentration in the blood of rats (*circle*) [125]

1.9 Acquired Radioresistance of Hematopoietic System After Single Preirradiation

It was found experimentally that low-level single preirradiation can induce either radioprotection or radiosensitization effects on mice [28, 138–143]. Major manifestations of these effects are, respectively, reduced and raised mortality of animals after subsequent acute exposure. The manifestations of the radioprotection effect of single preirradiation were named *acquired radioresistance* and *adaptive response*. However, there is still no unambiguous interpretation of the aforementioned experimental results.

In experiments [28, 138–143], the main reason for animal death was the hematopoietic subsyndrome of the acute radiation syndrome. This form of mortality is caused by radiation-induced damage of the hematopoietic system. Therefore, to reveal the mechanisms of acquired radioresistance, theoretical investigations based on mathematical models of the hematopoiesis can be used.

The models of the major hematopoietic lineages presented above are applied to examine the dynamics of these cell systems under priming and challenge exposures to radiation. In the numerical studies, the values of the priming dose D' that are taken are those used in the respective experiments. The dose D of the challenge exposure is taken from the range of doses causing the hematopoietic subsyndrome of the acute radiation syndrome. The time interval T between these exposures is varied in a broad range.

The analysis of the obtained modeling results is based on the conventional radiobiological concepts [4]. According to the latter, the radiosensitivity of an organism's cell system can be characterized by the severity of postirradiation injury of this system, namely by the depth of postirradiation depletion of its functional

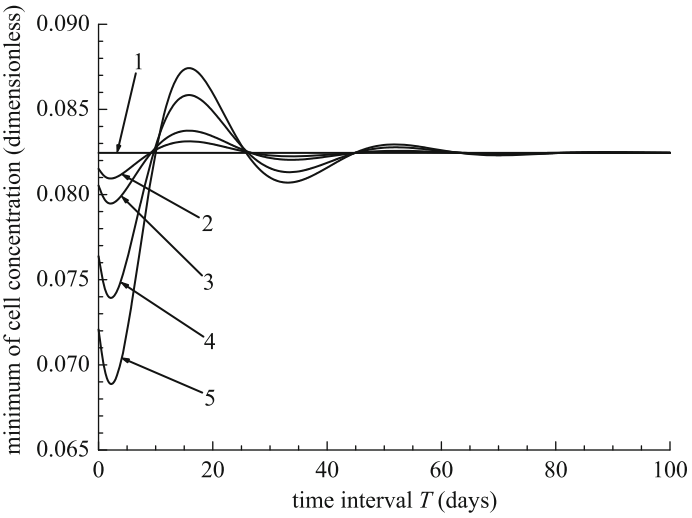

Fig. 1.26 Dependence of the minimum of the lymphocyte concentration after challenge acute irradiation at dose $D = 4$ Gy on the time interval T between this challenge exposure and preliminary single irradiation at doses $D' = 0, 0.05, 0.1, 0.3, 0.5$ Gy (*straight line* 1 and *curves* 2–5, respectively)

cell pool. Manifestations of elevated and lowered radiosensitivity of a system are, respectively, more severe and less severe depletion of its functional cell pool. Proceeding from all this, one can take, as the index of radiosensitivity of an individual hematopoietic lineage in preirradiated animals, the minimal level up to which the concentration of functional cells in this system is reduced after challenge irradiation. Note that we consider the following cell pools in the lymphopoietic, thrombopoietic, granulopoietic, and erythropoietic systems to be functional cells: the total number of lymphocytes in the blood, the total number of thrombocytes in the blood, the total number of granulocytes in the blood and tissues, and the total number of erythrocytes in the blood.

Figures 1.26, 1.27, 1.28, and 1.29 show the minimal values up to which the dimensionless concentrations of the aforementioned functional cells in the major hematopoietic lineages are reduced after challenge irradiation at a dose D following in a time interval T after priming irradiation at a dose D'. The modeling results are presented as curves describing the dependence of the pointed-out indexes on T computed for several values of D' and for a fixed dose D. These figures also show the standard levels (straight lines). These levels determine the minimal values up to which the dimensionless concentrations of functional cells in the major hematopoietic lineages decrease in specimens exposed only to challenge irradiation with the same dose D. In accordance with the arguments presented above, the ranges of values of T, at which the curves lie below the standard levels, correspond to the periods of elevated radiosensitivity of the major hematopoietic lineages. In turn, the

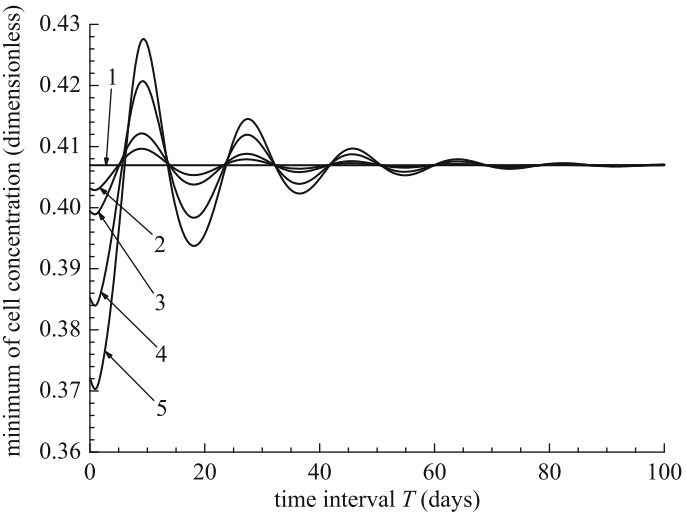

Fig. 1.27 Dependence of the minimum of the thrombocyte concentration after challenge acute irradiation at dose $D = 4$ Gy on the time interval T between this challenge exposure and preliminary single irradiation at doses $D' = 0, 0.05, 0.1, 0.3, 0.5$ Gy (*straight line* 1 and *curves* 2–5, respectively)

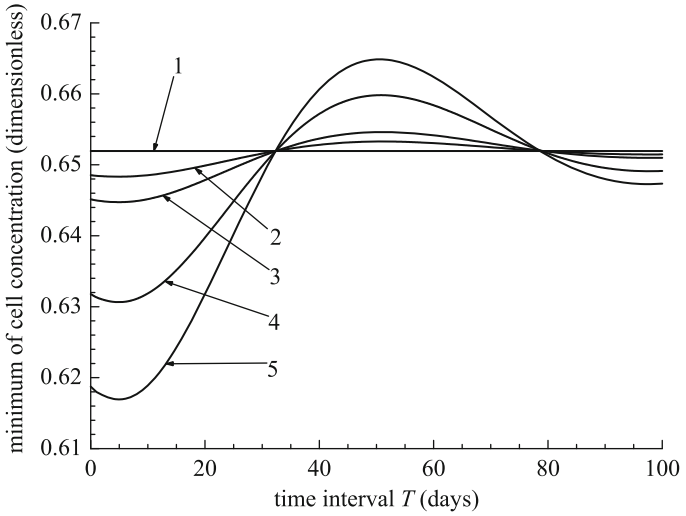

Fig. 1.28 Dependence of the minimum of the granulocyte concentration after challenge acute irradiation at dose $D = 4$ Gy on the time interval T between this challenge exposure and preliminary single irradiation at doses $D' = 0, 0.05, 0.1, 0.3, 0.5$ Gy (*straight line* 1 and *curves* 2–5, respectively)

ranges of values of T, when the curves lie above the standard levels, correspond to the periods of lowered radiosensitivity of these systems.

Figures 1.26, 1.27, 1.28, and 1.29 show that, with increasing T, the indexes under consideration oscillate with damping about their standard levels. These

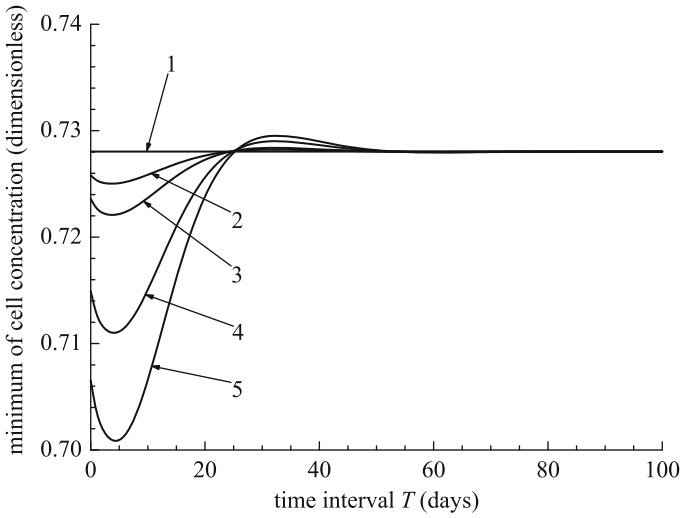

Fig. 1.29 Dependence of the minimum of the erythrocyte concentration after challenge acute irradiation at dose $D = 4$ Gy on the time interval T between this challenge exposure and preliminary single irradiation at doses $D' = 0, 0.05, 0.1, 0.3, 0.5$ Gy (*straight line* 1 and *curves* 2–5, respectively)

results have the following interpretation. Damped oscillations in radiosensitivity of the major hematopoietic lineages take place after priming irradiation. The period of elevated radiosensitivity is replaced by the period of lowered radiosensitivity (radioresistance) and so on, their duration being different for different hematopoietic lineages.

The analysis of the modeling results allowed us to find two independent sets of conditions on the concentrations of functional cells and their bone marrow precursor cells that are incapable and capable of dividing, and also on the mitotic activity of the latter in the major hematopoietic lineages of preirradiated animals. When either set of conditions is fulfilled prior to challenge irradiation, then one can infer that the respective hematopoietic lineage in preirradiated animals is in the radioresistance state. In turn, the violation of both sets of conditions can be used as an indicator of the state of elevated radiosensitivity. The first set involves the following conditions: The concentration of X_3 cells is greater than its normal level; the mitotic activity of X_1 cells is lower than normal; the concentrations of X_1 and X_2 cells can be greater or slightly less than their normal levels. The second set consists of the following conditions: The concentrations of X_1 and X_2 cells are greater than their normal levels; the concentration of X_3 cells and the mitotic activity of X_1 cells are slightly less than normal. Thus, these modeling results show that the radioprotection

effects of preliminary low dose irradiation on the major hematopoietic lineages are the consequences of hypercompensation of radiation damage of certain cell pools during recovery processes running in these systems after low dose priming exposure.

The developed models enable one to predict the radiosensitivity modifications on the level of an organism as a whole. One of the basic reasons for mammalian death after acute irradiation at doses resulting in the hematopoietic subsyndrome of the acute radiation syndrome is infections [4]. A significant contribution to specific and nonspecific immune defense against infections is given by lymphocytes and granulocytes. Therefore, if animals are treated with challenge acute irradiation during the period when the radioprotection effects of preliminary irradiation on lymphopoietic and/or granulopoietic systems are manifested, then one can expect the following. The challenge exposure induces less severe depletions of the aforementioned functional cell pools. This leads to a higher level of immune defense against infections and, as a consequence, to decreased mortality of preirradiated animals in comparison with postirradiation mortality of earlier nonirradiated specimens. Another basic reason for mammalian death after acute irradiation at doses resulting in the hematopoietic subsyndrome of the acute radiation syndrome is hemorrhage [4]. The latter is caused by postirradiation injury of the thrombopoietic system. Therefore, if animals are treated with challenge acute irradiation during the period, when the radioprotection effect of preliminary irradiation on this hematopoietic lineage takes place, then one can expect a prevention of hemorrhage and, hence, a rescue from death.

For the adequate interpretation of the modeling results, we must also take into account the following. As Figs. 1.26, 1.27, 1.28, and 1.29 show, lymphopoietic system is the most radiosensitive system among the major hematopoietic lineages. The challenge irradiation induces the most severe depletion of the functional cell pool in the lymphopoietic system in preliminary unexposed specimens. The concentration of blood lymphocytes drops to the level that can be critical for ensuring the specific immune defense against infections and hence for the survival of these animals. Therefore, one can assume that even small changes in the radiosensitivity of the lymphopoietic system, which are induced by preirradiation, can influence very strongly the formation of the effects of radioprotection or radiosensitization manifested on the level of an organism as a whole. Additionally, according to the modeling results, the thrombopoietic system is considerably less radiosensitive than the lymphopoietic system, the granulopoietic system is less radiosensitive than the thrombopoietic system, and the erythropoietic system is the most radioresistant hematopoietic lineage (Figs. 1.26, 1.27, 1.28, and 1.29). Therefore, one can expect that changes in the radiosensitivity of the thrombopoietic and granulopoietic systems, which are induced by low dose priming irradiation, influence changes in the survival of animals after challenge irradiation considerably less than the changes in the radiosensitivity of the lymphopoietic system do. In turn, the respective influence of the erythropoietic system is the smallest one.

As follows from Fig. 1.26, the first period of lowered radiosensitivity (radioresistance) of the lymphopoietic system starts after day 11 and terminates on day 23 after preliminary irradiation. The radiosensitivity of the granulopoietic system is elevated

during this period (Fig. 1.28). Nevertheless, bearing in mind the above-mentioned argument, one can expect some protective effect from the preirradiation on mice due to prevention of infections. In addition, during the period of days 8–14, when the radiosensitivity of the lymphopoietic system changes from a slightly elevated level to a maximal lowered level, the radiosensitivity of the thrombopoietic system is lowered (Figs. 1.26 and 1.27). In turn, during the period of days 19–22, when the radiosensitivity of the lymphopoietic system is slightly lowered, the radiosensitivity of the thrombopoietic system is slightly elevated (Figs. 1.26 and 1.27). Taking all this into account, one can suggest that the mortality of preirradiated animals, which are exposed to acute radiation in the period between 8 and 22 days after preirradiation, will be lowered (due to prevention of hemorrhage and infections) in comparison with the mortality of previously unexposed specimens after the same challenge irradiation.

These modeling predictions agree with the data that were obtained in experiments on ICR mice [138–142] and on C57BL/6 mice [28, 143]. In particular, acquired radioresistance is observed in the ICR mice treated with X-irradiation on day 14 after preirradiation, when the priming doses are $D' = 0.05, 0.3, 0.5$ Gy and the respective challenge doses are $D = 7.2, 8.0, 8.0$ Gy [139]. In these cases the 30-day survival rate in the preirradiated groups of mice is greater than that in the respective unexposed (control) groups after challenge irradiation. The values of the increment of the survival rate, which is the difference in the survival rate of preirradiated and unexposed mice after challenge irradiation, are equal to 13, 39, and 30 %, respectively. Obviously, the positive value of the increment of the survival rate indicates the state of radioresistance of preirradiated specimens at the moment of challenge exposure and the negative one determines the state of elevated radiosensitivity. Thus, the positive values of the increment of survival rate obtained on the ICR mice show that the preirradiated specimens are in the state of radioresistance on day 14 after preirradiation, which falls into the early period of acquired radioresistance predicted by the models, and for the above-mentioned priming doses, which are the same as in our computation.

In turn, the duration of the early period of acquired radioresistance predicted on the basis of the model analysis practically coincides with those found in the experiment on C57BL/6 mice [28]. This is illustrated by experimental data presented in Fig. 1.30. The values of the increment of the survival rate obtained for the time intervals between priming and challenge exposures $T = 8, 9, 12, 14, 17, 21$ days are positive.

To compare the experimental data in Fig. 1.30 with modeling results in detail, we introduce the new dimensionless index, which can be named the increment of radioresistance of the critical body system. It represents the ratio of the difference in the minimal levels of the concentration of the respective functional cells in preirradiated and unexposed specimens after identical challenge irradiation to the minimal level of the functional cell concentration in unexposed specimens after the same challenge exposure. Obviously, the positive value of the increment of radioresistance indicates the radioresistance state of the critical body system at the moment of challenge irradiation and the negative one determines the state of

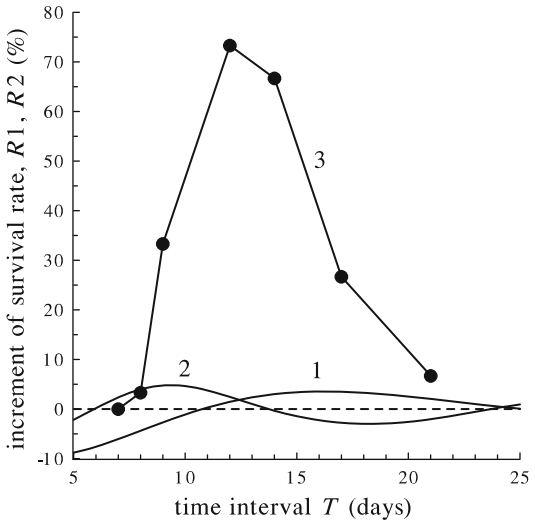

Fig. 1.30 Dependence of the increment of radioresistance on time interval T between priming single irradiation and challenge acute exposure. *Curves 1 and 2* show results obtained in the framework of the lymphopoiesis model (function $R1$) and in the framework of the thrombopoiesis model (function $R2$) at priming dose D' of 0.45 Gy and challenge dose D of 6.75 Gy. The relevant dependence of the increment of survival rate on T obtained for mice at the same values of D' and D [143] are given by *circles* and *polygonal line* 3

elevated radiosensitivity. The values of the increment of radioresistance, which are obtained in the framework of the lymphopoiesis and thrombopoiesis models at the same priming and challenge doses as those in the experiment on C57BL/6 mice, are shown in Fig. 1.30 as the functions $R1(T)$ and $R2(T)$, respectively. The comparison of the experimental and modeling results presented in Fig. 1.30 clearly indicates that the radioprotection effect of preirradiation on the organism as a whole in the early period of acquired radioresistance is caused by the superposition of the radioprotection effects of the preirradiation on thrombopoietic and lymphopoietic systems. This conclusion corresponds with the experimental observation. Specifically, preirradiation of ICR mice with 0.3–0.5 Gy 2 weeks before challenge irradiation suppresses hemorrhage [140]. In addition, the correlation between the state of radioresistance and the raised level of immune protection against a T-dependent antigen was revealed in C57BL/6 mice [143] and in ICR mice [142] 2 weeks after the 0.5 Gy preexposure.

As follows from the modeling results, the period of lowered radiosensitivity (radioresistance) of the granulopoietic system, during which the radiosensitivity of the lymphopoietic system in preirradiated animals is slightly lower than the standard level or close to it, starts on day 45 and ends on day 77 after preirradiation (Figs. 1.26 and 1.28). Note that the radiosensitivity of the thrombopoietic system and that of the erythropoietic system are close to their standard levels at that time (Figs. 1.27 and 1.29). Therefore, one can expect the following. The mortality of

preirradiated animals, which are irradiated in this period, will be less than that of previously unexposed specimens due to prevention of infections. In fact, the correlation between the state of radioresistance and the raised level of immune protection against a *T*-dependent antigen was observed in ICR mice 8 weeks after preirradiation at the priming doses of 0.05 Gy and 0.1 Gy [142].

The duration of the late period of acquired radioresistance found in the framework of the models corresponds to those revealed in the experiments on ICR mice treated with *X*-irradiation [138–141]. For example, at the priming dose D' of 0.05 Gy, the values of the increment of the survival rate are positive and equal 5, 27, and 21 % for the time interval T of 1.5, 2.0, and 2.5 months, respectively. The second and third results obtained at the challenge doses of 7.75 Gy and 8.5 Gy, respectively, are statistically significant. Though the first result obtained at the challenge dose of 7.75 Gy is not statistically significant, a tendency is quite obvious.

The modeling results can also be used to predict the periods of elevated radiosensitivity in preirradiated mice. The first of them takes place during the first week after exposure to priming doses D' of 0.05–0.5 Gy, when the radiosensitivity of the major hematopoietic lineages in preirradiated mice is higher than in unexposed ones (Figs. 1.26, 1.27, 1.28, and 1.29). This model prediction does not contradict experimental observations on C57BL/6 mice. In turn, the second period of elevated radiosensitivity starts on day 24 and terminates on day 32 after the preliminary irradiation with doses of 0.05–0.5 Gy, when the effects of radiosensitization take place on the level of both the lymphopoietic and granulopoietic systems (Figs. 1.26, 1.27, 1.28, and 1.29). This model prediction also agrees with experimental data [139]. The radiosensitization effect of the priming dose of 0.05 Gy on ICR mice takes place if the time interval T between the priming exposure and challenge irradiation at the dose of 7.75 Gy is equal to 1 month. In this case the increment of the survival rate is negative (namely, −16 %), the result being statistically significant.

One more modeling prediction concerns the return of the radiosensitivity of preirradiated mice to the normal level. It happens 3 months after priming irradiation with doses D' of 0.05–0.5 Gy, when the radiosensitivity of the major hematopoietic lineages practically returns to standard levels (Figs. 1.26, 1.27, 1.28, and 1.29). In fact, neither a significant radiosensitization effect nor a radioprotection effect is revealed in ICR mice after challenge irradiation following time intervals of 3, 4, and 5 months after priming exposure to 0.05 Gy [139].

Thus, the results of performed investigations convincingly show that ordinary and paradoxical effects of low-level preirradiation on the radiosensitivity of mammals are caused by peculiarities of postirradiation dynamics of the lymphopoietic, granulopoietic, and thrombopoietic systems, which play a key role in the formation of these effects. Specifically, the interchange of periods of elevated and reduced radiosensitivity in preirradiated mice is due to the oscillating dynamics of the aforementioned hematopoietic lineages in these animals.

It is worth noting that the studies carried out in this work clearly demonstrate the effectiveness of employing mathematical models, parallel with relevant experiments, in the elucidation of the mechanisms of the radioprotection effect of low-level preliminary exposures on mammals and in the planning of new

experiments. In addition, the developed approach can be useful in elaborating the optimal schedules of clean-up crews' work in the elimination of consequences of accidents at nuclear plants. This approach can also be useful in estimating the hazard of space radiation for astronauts' health on long-term space missions.

1.10 Acquired Radioresistance of Hematopoietic System After Chronic Preirradiation

It was found experimentally that low-level chronic preirradiation can induce either radioprotection or radiosensitization effects on mice [144–146]. Major manifestations of these effects were, respectively, reduced and raised mortality of animals after subsequent acute exposure. The manifestations of the radioprotective effect of low-level chronic preirradiation are called *acquired radioresistance* and *adaptive response*, as in the case of single preirradiation. The above-mentioned experimental results still have no unambiguous interpretation.

In experiments [144–146] the principal reason for specimen death was the hematopoietic subsyndrome of the acute radiation syndrome. As mentioned in Sect. 1.9, this form of mortality is caused by radiation-induced damage to the hematopoietic system. Therefore, to reveal the mechanisms of acquired radioresistance, theoretical investigations based on mathematical models of the hematopoiesis can be employed.

Specifically, the models of the major hematopoietic lineages presented in Sects. 1.5–1.8 are used to simulate the dynamics of lymphopoietic, granulopoietic, erythropoietic, and thrombopoietic systems in small laboratory animals (mice) exposed to challenge acute irradiation following the chronic one. The dose D of challenge acute exposure is chosen from the range of doses causing the hematopoietic subsyndrome of the acute radiation syndrome. The dose rate N and the duration T of priming chronic exposure are varied.

As mentioned in Sect. 1.9, manifestations of increased and decreased radiosensitivity of an individual hematopoietic lineage in preirradiated animals are, respectively, more severe and less severe depletion of the functional cell pool in this system after acute exposure in comparison with that for earlier nonirradiated specimens.

The modeling results elucidate the following facts. Priming chronic irradiation, in chosen ranges of N and T, leads to an increase in the radiosensitivity of the lymphopoietic and erythropoietic systems (Figs. 1.31 and 1.32). In turn, the effect of chronic preirradiation on the thrombopoietic system can manifest itself both in an increase or a decrease of the radiosensitivity of this major hematopoietic lineage (Fig. 1.33). The slightly lowered radiosensitivity occurs at low dose rates N (below 0.03 Gy/day) and in a fairly narrow range of durations of chronic exposure (13–16 days).

As modeling studies show, chronic preirradiation can cause both a radiosensitization effect and a radioprotection effect on the granulopoietic system.

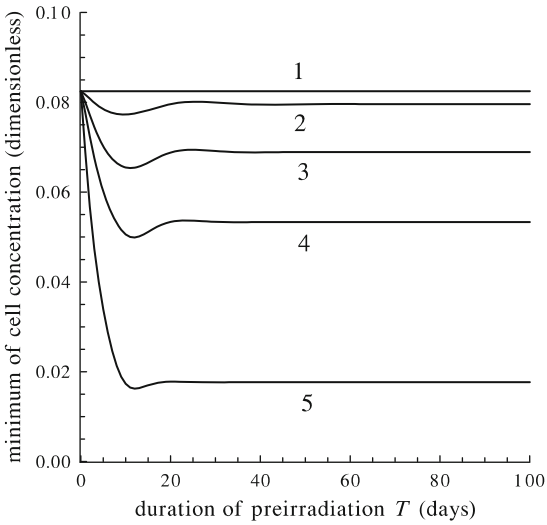

Fig. 1.31 Dependence of the minimum of the lymphocyte concentration after challenge acute exposure at dose $D = 4$ Gy on the duration T of priming chronic irradiation at dose rates $N =$ 0, 0.03, 0.1, 0.2, 0.6 Gy/day (*straight line* 1 and *curves* 2–5, respectively)

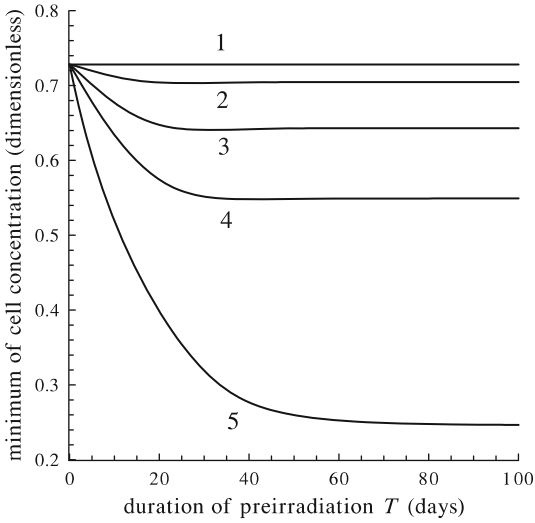

Fig. 1.32 Dependence of the minimum of the erythrocyte concentration after challenge acute exposure at dose $D = 4$ Gy on the duration T of priming chronic irradiation at dose rates $N =$ 0, 0.03, 0.1, 0.2, 0.6 Gy/day (*straight line* 1 and *curves* 2–5, respectively)

The radioprotection effect manifests itself in less severe depletion of the blood granulocyte pool when the dose rate N of chronic preirradiation is less than or equal to 0.3 Gy/day and its duration T exceeds, depending on N, 32–33 days (Fig. 1.34). The same preirradiation conditions lead to more severe depletion of the tissue granulocyte pool and, hence, the radiosensitization effect takes place on the level of this functional cell pool (Fig. 1.35). At all other preirradiation regimes, the radiosensitization effect is revealed on the level of both functional cell pools in the granulopoietic system (Figs. 1.34 and 1.35).

Thus, in the framework of the same models, the ordinary and paradoxical modifications of radiosensitivity of the thrombopoietic and granulopoietic systems

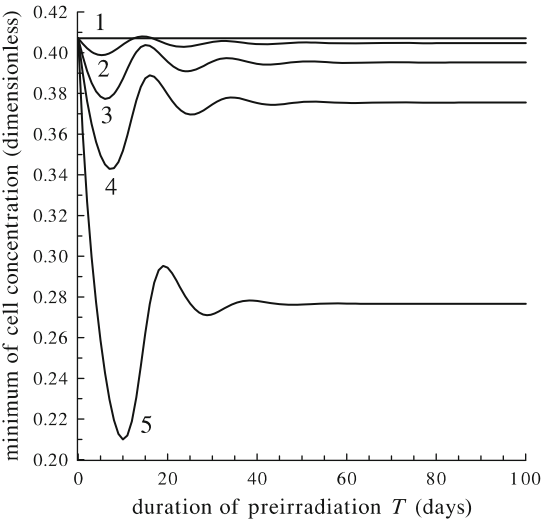

Fig. 1.33 Dependence of the minimum of the thrombocyte concentration after challenge acute exposure at dose $D = 4$ Gy on the duration T of priming chronic irradiation at dose rates $N =$ 0, 0.03, 0.1, 0.2, 0.6 Gy/day (*straight line* 1 and *curves* 2–5, respectively)

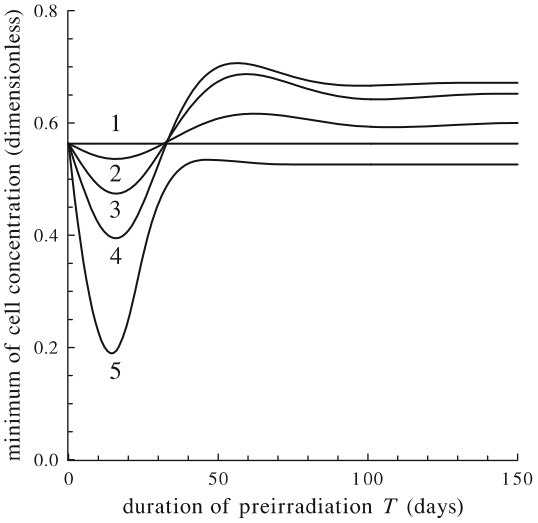

Fig. 1.34 Dependence of the minimum of the blood granulocyte concentration after challenge acute exposure at dose $D = 4$ Gy on the duration T of priming chronic irradiation at dose rates $N =$ 0, 0.03, 0.1, 0.2, 0.6 Gy/day (*straight line* 1 and *curves* 2–5, respectively)

in preirradiated mammals are reproduced. This implies that the explanation of these paradoxical effects of chronic preirradiation with low dose rates does not require us to use any additional assumptions. In other words, these paradoxical effects are the natural reaction of the complicated self-regulated systems to external action.

In the framework of the models it is proved that the character of radiosensitivity modification of the thrombopoietic and granulopoietic systems in chronically preirradiated mammals is predetermined by concentrations of the respective functional cells and their bone marrow precursor cells that are incapable and capable of dividing, and also by mitotic activity of the latter at the moment of challenge irradiation. In particular, the granulopoietic system is in the state of radioresistance

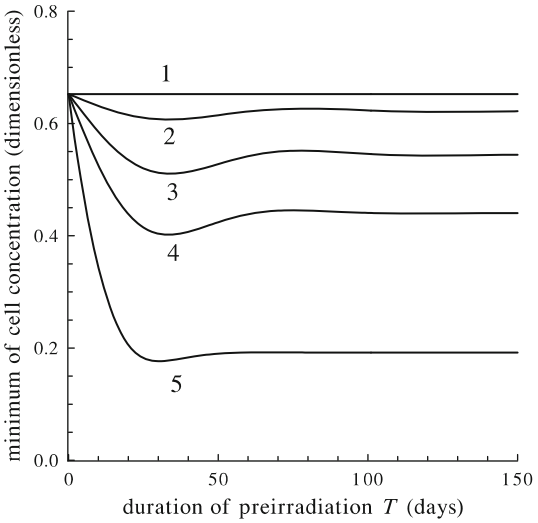

Fig. 1.35 Dependence of the minimum of tissue granulocyte concentration after challenge acute exposure at dose $D = 4$ Gy on the duration T of priming chronic irradiation at dose rates $N =$ 0, 0.03, 0.1, 0.2, 0.6 Gy/day (*straight line* 1 and *curves* 2–5, respectively)

prior to challenge irradiation if the concentrations of undamaged cells in X_2 and X_3 pools are higher or slightly lower than their normal levels, but the concentration of undamaged X_1 cells and the mitotic activity of these cells are higher than those in intact animals. In turn, the thrombopoietic system is in the state of radioresistance if the concentration of undamaged by radiation X_1 cells and concentrations of X_2 and X_3 cells are slightly below the corresponding indexes in intact animals, but the mitotic activity of X_1 cells exceeds the norm. These modeling results show that the radioprotection effect of preliminary low dose rate chronic preirradiation on the thrombopoietic and granulopoietic systems is the consequence of hypercompensation of radiation damage of certain groups of cells and/or enhanced mitotic activity of bone marrow precursor cells (X_1) in the course of adaptation processes running in these hematopoietic lineages after the onset of preirradiation.

One more important conclusion that can be drawn on the basis of the modeling results is the following. Changing the radiosensitivity of the hematopoietic lineages by increasing the duration of chronic irradiation, i.e., by increasing the total dose, does not at all follow the linear law. Furthermore, for pools of blood granulocytes and blood thrombocytes, the radiosensitization effect is replaced by the radioprotection one when the total dose of the preliminary chronic irradiation increases.

The modeling results enable one to make a number of predictions concerning the modification of the radiosensitivity of mammalian organisms as a result of preliminary chronic irradiation. As noted in Sect. 1.9, one of the basic reasons for mammalian death after acute irradiation with doses leading to the hematopoietic subsyndrome of the acute radiation syndrome is infections [4]. Functional cells of the lymphopoietic and granulopoietic systems play a decisive role in specific and nonspecific immune protection against infections. Therefore, if animals are treated with acute irradiation within the periods when the radioprotection effect of

preliminary irradiation on one of the functional cell pools of these systems (blood granulocytes) takes place, but the radiosensitization effect on the other pools of functional cells (tissue granulocytes and blood lymphocytes) is negligible, then one can expect the following. Challenge acute irradiation will induce less severe depletion of the pool of blood granulocytes in preirradiated animals than in earlier unexposed ones. In turn, postirradiation depletion of the blood lymphocyte pool and tissue granulocyte pool will be almost the same in both cases. All this will cause a higher level of immune protection against infections and, as a consequence, lower mortality of preirradiated animals in comparison with analogous indexes for previously unexposed specimens.

The results of the modeling studies elucidate the following. When the dose rate N of chronic preirradiation does not exceed 0.03 Gy/day and the duration T of this preexposure exceeds 31 days, then the radiosensitivity of the granulopoietic system will be decreased. In addition, such exposures do not in practice affect the radiosensitivity of the thrombopoietic, lymphopoietic, and erythropoietic systems and have a radioprotection effect on the bone marrow reserve of functional cells of the lymphopoietic and granulopoietic systems. Therefore, one can expect that after challenge acute irradiation, the mortality should be lower in animals that were preliminarily irradiated in regimes stated above than in earlier unexposed ones. This modeling prediction qualitatively agrees with experimental data [145]. In studies [145] the mice of the SHK strain were subjected to protracted radiation ($T = 100$ days) at a low dose rate ($N = 0.03$ Gy/day). Then these animals and intact ones were exposed to acute irradiation at dose $D = 8$ Gy. This challenge exposure led to the development of the hematopoietic subsyndrome of the acute radiation syndrome and to the death of some of the specimens. Thirty days after the exposure, the survival in the given two groups of animals was, respectively, 39.3 and 28.5 %. In other words, the chronic exposure induced the radioprotection effect: The survival was higher in preirradiated animals than that in previously nonirradiated ones.

In the course of the modeling studies, it was revealed that after chronic irradiation with a duration of less than 33 days and with dose rates from 0.01 Gy/day to 0.5 Gy/day, the lymphopoietic, granulopoietic, and erythropoietic systems in mammals (mice) have an elevated radiosensitivity, but the radiosensitivity of the thrombopoietic system is either increased or close to the standard level. Therefore, one can anticipate that subsequent acute irradiation with a dose leading to the hematopoietic subsyndrome of the acute radiation syndrome will cause higher mortality in specimens preirradiated in the above-indicated regimes than that of unexposed ones. This modeling prediction agrees with experimental data [144, 146]. The mice of the (CBA.C57/BL6)F_1 strain were kept, during short time intervals (from 1 to 14 days), in the 10-km zone of the Chernobyl accident [144]. The dose rate of chronic irradiation was 0.024 Gy/day. Then, two days after evacuation from this zone, these groups of animals, as well as the group of intact mice of the same strain, were exposed to irradiation at doses leading to the hematopoietic subsyndrome of the acute radiation syndrome ($D = 3, 5, 7, 9$ Gy). Within 30 days after acute irradiation, the mortality of preirradiated animals was significantly higher than that of previously unexposed specimens. In [146] an increase in sensitivity to

acute irradiation at a dose of 2 Gy was revealed in the $(CBA.C57/B1)F_1$ mice, which 2 days before had been kept in the zone of the Chernobyl accident for a duration of 1 or 5 days. The dose rate of the preliminary exposure was 0.024 Gy/day.

To compare the experimental data with modeling results in detail, we compute the dimensionless index, the increment of the radioresistance of the critical body system. Remember that it is the ratio of the difference in the minimal levels of the concentration of the functional cells in the critical system of preirradiated and unexposed specimens after identical challenge irradiation to the minimal level of the functional cell concentration in unexposed specimens after the same challenge exposure. Obviously, the positive value of the increment of radioresistance shows that the critical body system is in the radioresistance state at the moment of challenge irradiation and the negative value of the increment of radioresistance corresponds to the state of elevated radiosensitivity.

The modeling results on the increment of radioresistance, which are computed for pools of blood granulocytes, tissue granulocytes, and blood lymphocytes at various durations of priming chronic irradiation T and at fixed priming dose rate and fixed challenge dose, are shown in Fig. 1.36 as the functions $R1$, $R2$, and $R3$, respectively. The qualitative comparison of these modeling and experimental results

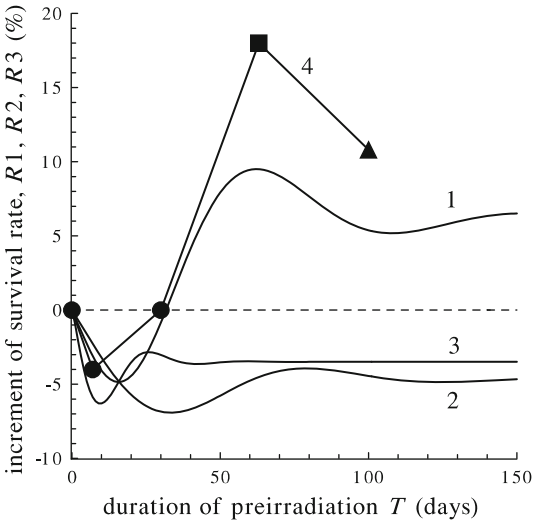

Fig. 1.36 Dependence of the increment of radioresistance on the duration T of priming chronic irradiation. *Curves 1–3* show the results obtained in the framework of the granulopoiesis model using the values of the minimum of the granulocyte concentration in the blood (function $R1$) and in the tissues (function $R2$) and in the framework of the lymphopoiesis model (function $R3$) at priming dose rate of 0.03 Gy/day and challenge dose D of 4 Gy. Pertinent dependence of the increment of survival rate on T obtained for mice is presented by polygonal line 4 and by symbols. Namely, the experimental data on the increment of survival rate were obtained for female NA-2 mice at challenge dose D of 8 Gy [29] (*box*), for SHK mice at D of 8 Gy [145] (*triangle*), and for $(CBA.C57/BL6)F_1$ mice at D of 9 Gy [146] (*circle*)

shows the following. At the chosen regimes of preirradiation, the radioresistance of an organism as a whole at the moment of the challenge exposure is determined mainly by the radioresistance of the granulopoietic system manifested on the level of the pool of blood granulocytes. In particular, the radioprotection and radiosensitization effects of preirradiation on this cell system correlate, respectively, with the radioprotection and radiosensitization effects of the preexposure on the mouse organism as a whole. Moreover, the duration of the chronic preirradiation, at which the radiosensitization effect on mice changes into the radioprotection one, practically coincides with the duration of the chronic preirradiation, at which the radiosensitization effect on the above-mentioned cell system changes into the radioprotection one. In Fig. 1.36, it is the time interval of 30 days at which the sign of the effect is reversed.

Thus, the modeling predictions are supported experimentally. This implies that the developed models can be used for planning the experiments to study the effects of chronic irradiation on mammalian radiosensitivity. They can also be useful in determining the optimal schedules of clean-up crews' work on the elimination of consequences of accidents at nuclear plants. This approach can also be useful in estimating the hazard of space radiation for astronaut health on long-term space missions.

1.11 Conclusions

Biologically motivated mathematical models of the hematopoiesis dynamics in nonirradiated and irradiated mammals (rodents) are developed. The blood-forming system is regarded here as a complex of the major hematopoietic lineages: thrombopoietic, lymphopoietic, erythropoietic, and granulopoietic systems. The models consider the principal stages of development of hematopoietic cells. They also account for the general and specific regulatory mechanisms in the major hematopoietic lineages. The models are implemented as the systems of nonlinear differential equations describing the dynamics of concentrations of mature cells in the blood and their precursor cells in the bone marrow. The radiation dose and dose rate are variable parameters of the models, and the constant coefficients have the meanings generally accepted in hematology and radiobiology.

In the absence of radiation, the models are reduced to systems of three nonlinear differential equations. These equations are investigated by methods of qualitative theory of differential equations and oscillation theory. The stability and type of stability of singular points, which have specific biological interpretations, are investigated. For each model system, being in the first (trivial) singular point is equivalent to a complete depletion of the respective hematopoietic lineage. The coordinates of the second singular point, when it is stable, correspond to normal concentrations of cells of a hematopoietic lineage. Analytical studies of the models reveal the conditions when the second singular point becomes unstable and one more particular solution (a stable limit cycle) appears. Stable oscillations of

concentrations of blood cells and their precursors in the bone marrow correspond to this particular solution. This modeling result can be identified with the cyclic hematopoiesis observed in dogs and humans. Computer studies also show that if the second singular point is stable, then the recovery processes in the thrombopoietic, lymphopoietic, erythropoietic, and granulopoietic systems have the character of damped oscillations. These modeling predictions also agree with experimental data.

The models are employed to examine the hematopoiesis dynamics in small laboratory animals (rats, mice) exposed to acute and chronic radiation. A principal advantage of the models consists of the fact that their identification requires only the data obtained in the studies of these systems in intact specimens and in specimens exposed to either acute or chronic irradiation.

The dynamics of concentrations of mature blood cells and their bone marrow precursor cells is investigated for various doses of acute irradiation. A comparative analysis of the kinetics of the major hematopoietic lineages is performed and an interpretation of the results is suggested. It is shown that the models provide a qualitative and quantitative description of postirradiation injury and recovery of the thrombopoietic, lymphopoietic, erythropoietic, and granulopoietic systems in small laboratory animals (rats, mice).

In the simulation of the effects of chronic irradiation on hematopoiesis, the dose rate is varied from low to high levels. Computations show that the models reproduce an irreversible depletion of the major hematopoietic lineages if the dose rate exceeds the respective critical levels. It has been found that the value of the critical dose rate depends on radiosensitivity of bone marrow precursor cells capable of dividing and on two kinetic parameters specifying the proliferative potential of these cells in the respective hematopoietic lineage. The formula for calculating the critical dose rate derived within the models can be used to determine the levels of chronic radiation that may be harmful to various mammalian species, including humans.

Computations also show that the models can describe the experimentally observed ability of the hematopoietic system to adapt itself to chronic irradiation at low and moderate dose rates. Actually, the models reproduce the ability of the major hematopoietic lineages to recover the homeostasis, the stable dynamic equilibrium state, under such exposures. This equilibrium state is characterized by new (depending on the dose rate) stationary concentrations of functional cells in the blood and their precursors in the bone marrow. For the erythropoietic and thrombopoietic systems, these values decrease as the radiation dose rate increases. For the lymphopoietic and granulopoietic systems, the same rule applies at moderate dose rates. With chronic irradiation at low dose rates, the stationary concentrations of bone marrow precursors of lymphocytes and granulocytes and of blood granulocytes exceed their normal levels. These modeling predictions, which are also corroborated by experimental data, can be regarded as effects of radiation hormesis.

The models are also used to examine the radiosensitivity modifications of the major hematopoietic lineages induced by low-level single/chronic preirradiation and manifested after the subsequent challenge exposure. The conditions, which allow the models to reproduce both radioprotection and radiosensitization effects

of preirradiation on the major hematopoietic lineages, are found. Proceeding from the modeling results, a number of qualitative predictions concerning the effects of low-level single/chronic preirradiation on the radiosensitivity of the organism as a whole is made. It is shown that these predictions agree with experimentally obtained integral characteristics of the mortality of preirradiated mice after challenge exposure. It is revealed that the state of acquired radioresistance in mice previously exposed to low dose single irradiation is caused by reduced radiosensitivity of the lymphopoietic and thrombopoietic systems in the early period and by reduced radiosensitivity of the granulopoietic system in the late period after preirradiation. The state of acquired radioresistance in mice previously exposed to low dose rate chronic irradiation is caused by reduced radiosensitivity of the granulopoietic system in the late period after the onset of preirradiation. In turn, reduced radiosensitivity of the above-mentioned hematopoietic lineages is the consequence of hypercompensation of radiation damages of certain cell pools during the recovery processes running in preirradiated animals. It is important to emphasize that the evaluations of the duration of the periods of postirradiation radioresistance in mice, carried out on the basis of the modeling and experimental investigations, practically coincide. Thus, for the first time, a consistent explanation of the paradoxical effect of low-level preirradiation on mammals, the acquired radioresistance, is suggested. Obviously, the developed mathematical models can be effective in the planning of new experiments, specifically, in revealing the optimal scenarios of irradiation that would maximize the effect under study. The latter is of particular importance for the investigation of the low dose effects. Furthermore, the mathematical models can provide some hints about the behavior of a biological system in the experimentally inaccessible environment.

The reproduction of a wide range of experimentally observed processes by the models implies that they do take into account the main cause–effect relationships that govern the functioning of the hematopoietic system both in the absence and in the presence of ionizing radiation. It also proves the fact that the model parameters and variables are indeed the key quantities characterizing the hematopoietic system. The clear biological meaning of the model variables allows one to directly compare the modeling predictions with experimental data at the qualitative and quantitative levels. The obtained agreement bears witness to the validity of the employment of the developed models, after proper identification, in the studies and predictions of dynamics of the hematopoiesis in various mammalian species, including humans, exposed to acute/chronic irradiation in wide ranges of doses and dose rates.

References

1. Munker R., Hiller E., Glass J., Paquette R. (Eds.). Modern Hematology, 2nd ed. Totowa, NJ: Humana Press 2007.
2. Young N.S., Gerson S.L., High K.A. (Eds.). Clinical Hematology. Philadelphia: Mosby/Elsevier, 2005.

3. Fedorov N.A. Normal Haemopoiesis and Its Regulation, 1st ed. Moscow: Meditsina, 1976 (Russian).
4. Bond V.P., Fliendner T.M., Archambeau J.O. Mammalian Radiation Lethality: A Disturbance in Cellular Kinetics. New York: Academic Press, 1965.
5. Yarmonenko S.P., Vainson A.A. Radiobiology of Humans and Animals. Moscow: Vysshaya shkola, 2004 (Russian).
6. Nias A.H.W. An Introduction to Radiobiology, 2nd ed. Chichester, UK: Wiley, 1998.
7. Fliedner T.M., Graessle D., Paulsen C., Reimers K. Structure and function of bone marrow hemopoiesis: Mechanisms of response to ionizing radiation exposure. Cancer Biotherapy and Radiopharmaceuticals, v. 17(4), pp. 405–426, 2002.
8. Fliedner T.M., Graessle D., Meineke V., Dorr H. Pathophysiological principles underlying the blood cell concentration responses used to assess the severity of effect after accidental whole-body radiation exposure: An essential basis for an evidence-based clinical triage. Experimental Hematology, v. 35(4), pp. 8–16, 2007.
9. Smirnova O.A., Govorun R.D., Ryshov N.I. Mathematical model to study the postirradiation dynamics of lymphopoiesis. Radiobiologiya, v. 22, pp. 488–493, 1982 (Russian).
10. Smirnova O.A. Mathematical model of cyclic kinetics of granulocytopoiesis. Kosmicheskaya Biologiya i Aviakosmicheskay Meditsina, no. 1, pp. 77–80, 1985 (Russian).
11. Smirnova O.A. Mathematical modeling of thrombocytopoiesis dynamics in mammals exposed to radiation. Radiobiologiya, v. 25, p. 571. Dep. in VINITI N 2552-85, 16.04.85, 1985.
12. Zukhbaya T.N., Smirnova O.A. Experimental and theoretical investigation of the dynamics of lymphopoiesis upon prolonged exposure to ionizing radiation. Radiobiologiya, v. 28, pp. 626–631, 1988 (Russian).
13. Zukhbaya T.N., Smirnova O.A. Mathematical model for the dynamics of granulocytopoiesis in mammals. Radiobiologiya, v. 28, pp. 796–802, 1988 (Russian).
14. Smirnova O.A. Mathematical modeling of cyclic kinetics of hematopoiesis. Kosmicheskaya Biologiya i Aviakosmicheskaya Meditsina, no. 1, pp. 41–45, 1989 (Russian).
15. Smirnova O.A. The model of homeostasis of hematopoiesis system under chronic irradiation. In: Modeling of Population Dynamics. Gorky: Gorky University Press, pp. 39–45, 1989 (Russian).
16. Zukhbaya T.M., Smirnova O.A. The stimulation effect of prolonged radiation of small dose rates on mammalian lymphopoiesis. Kosmicheskaya Biologiya i Aviakosmicheskaya Meditsina, no. 1, pp. 47–51, 1989 (Russian).
17. Smirnova O.A. Mathematical modeling of dynamics of erythropoiesis and granulocytopoiesis under acute irradiation. Radiobiologiya, v. 30, pp. 627–633, 1990 (Russian).
18. Smirnova O.A. Mathematical modeling of bone–marrow erythropoiesis dynamics in non-irradiated and irradiated mammals. In: Dynamics of Biological Populations. Gorky: Gorky University Press, pp. 51–58, 1990 (Russian).
19. Smirnova O.A., Zukhbaya T.M. The stimulation effect of prolonged radiation of small dose rates on mammalian granulocytopoiesis. Kosmicheskaya Biologiya i Aviakosmicheskaya Meditsina, no. 3, pp. 40–42, 1991 (Russian).
20. Zukhbaya T.M., Smirnova O.A. An experimental and mathematical analysis of lymphopoiesis dynamics under continuous irradiation. Health Physics, v. 61, pp. 87–95, 1991.
21. Smirnova O.A. Effect of chronic irradiation at high dose rate on the hematopoietic system: Mathematical simulation. Radiobiologiya, v. 32, pp. 757–763, 1992 (Russian).
22. Smirnova O.A. Hematopoiesis dynamics in mammals under combined exposures to radiation: Mathematical modeling. Aviakosmicheskaya i Ekologicheskaya Meditsina, no. 3, pp. 45–49, 1995 (Russian).
23. Kovalev E.E., Smirnova O.A. Estimation of radiation risk based on the concept of individual variability of radiosensitivity. AFRRI Contract Report 96-1. Bethesda, MD: Armed Forces Radiobiology Research Institute, 1996.
24. Smirnova O.A. Problems of mathematical modeling in modern space radiobiology. Proceedings of Sissakian Memorial Symposium under the auspices of UNESCO, “Problems of

Biochemistry, Radiation and Space Biology," Moscow, Dubna, Russia, January 22–25, 1997. D-19-97-284. Dubna: JINR, pp. 239–253, 1997 (Russian).
25. Smirnova O.A. Mathematical models of hematopoiesis dynamics in nonirradiated and irradiated mammals. BioMedSim'99. 1st Conference on Modeling and Simulation in Biology, Medicine and Biomedical Engineering, Noisy-le-Grand, France, April 20–22, 1999. Proceedings. Paris: Groupe ESIEE, pp. 105–109, 1999.
26. Smirnova O.A. Mathematical Models of Hematopoiesis Dynamics in Irradiated Mammals. Abstracts of the 24th Meeting of the European Study Group for Cell Proliferation (ESGCP), Leipzig, Germany, June 12–17, 2001. Cell Proliferation, v. 34(3), p. 193, 2001.
27. Smirnova O.A. Paradoxical effects of low level irradiation on radiosensitivity of mammals: Modeling investigation. In: "Problems of Biochemistry, Radiation, and Space Biology," II International Symposium under the auspices of UNESCO dedicated to the memory of Academician N. Sissakian and II Sissakian Readings, Moscow, Dubna, Russia, 2001: Proceedings. ISBN 5-85165-697-2. Dubna: JINR, v. I, pp. 177–182, 2002 (Russian).
28. Smirnova O.A., Yonezawa M. Radioprotection effect of low level preirradiation on mammals: Modeling and experimental investigations. Health Physics, v. 85(2), pp. 150–158, 2003.
29. Smirnova O.A., Yonezawa M. Radioresistance in mammals induced by low–level chronic irradiation: Modeling and experimental investigations. Health Physics, v. 87(4), pp. 366–374, 2004.
30. Smirnova O.A. Radiation and organism of mammals: Modeling approach. Moscow-Izhevsk: Scientific-Publishing Centre "Regular and Chaotic Dynamics," Institute of Computer Science, 2006 (Russian).
31. Smirnova O., Yonezawa M. Effects of chronic low-level irradiation on radiosensitivity of mammals: Modeling and experimental studies. In: Radiation Risk Estimates in Normal and Emergency Situations. Proceedings of the NATO Advanced Research Workshop on Impact of Radiation Risk Estimates in Normal and Emergency Situations, Yerevan, Armenia, September 8–11, 2005. A.A. Cigna and M. Durante (Eds.), Springer, XX, pp. 291–301, 2006.
32. Smirnova O.A. Effects of low-level chronic irradiation on the radiosensitivity of mammals: Modeling studies. Advances in Space Research, v. 40, pp. 1408–1413, 2007.
33. Smirnova O.A. Blood and small intestine cell kinetics under radiation exposures: Mathematical modeling. Advances in Space Research, v. 44, pp. 1457–1469, 2009.
34. Romanov J.A., Ketlinsky S.A., Antokhin A.I., Okulov V.B. Chalones and Regulation of Cell Division. Moscow: Meditsina, 1984 (Russian).
35. Ketlinsky S.A., Simbircev A.S., Vorob'ev A.A. Endogenous Immunomodulators. Sankt-Peterburg: Hippokrat, 1992 (Russian).
36. Loeffler M., Potten C.S. Stem cells and cellular pedigrees — A conceptual introduction. In: Potten C.S. (Ed.) Stem Cells. Cambridge: Academic Press, pp. 1–27, 1997.
37. Loeffler M., Roeder I. Tissue stem cells: Definition, plasticity, heterogeneity, self-organization and models — A conceptual approach. Cells Tissues Organs, v. 171, pp. 8–26, 2002.
38. Fliedner T.M. The role of blood stem cells in hematopoietic cell renewal. Stem Cells (Dayton, Ohio), v. 16(6), pp. 361–374, 1998.
39. Lajtha L.G., Oliver R., Gurney C.W. Model of a bone–marrow stem-cell population. British Journal of Haematology, v. 8, pp. 442–460, 1962.
40. Till J.E., McCulloch E.A., Siminovitch L. A stochastic model of stem cell proliferation, based on the growth of spleen colony-forming cells. Proceedings of the National Academy of Science, v. 51, pp. 29–36, 1964.
41. Kiefer J. A model of feedback-controlled cell populations. Journal of Theoretical Biology, v. 18, pp. 263–279, 1968.
42. Wichmann H.E. Computer modeling of erythropoiesis. In: Current Concepts in Erythropoiesis, C.D.R. Dunn (Ed.). Chichester, UK: John Wiley and Sons, pp. 99–141, 1983.
43. Roeder I., Kamminga L.M., Braesel K., Dontje B., Haan G., Loeffler M. Competitive clonal hematopoiesis in mouse chimeras explained by a stochastic model of stem cell organization. Blood, v. 105(2), pp. 609–616, 2005.

44. Glauche I., Cross M., Loeffler M., Roeder I. Stem cells. Lineage specification of hematopoietic stem cells: Mathematical modeling and biological implications. Stem Cells, v. 25, pp. 1791–1799, 2007.
45. Roeder I., Horn K., Sieburg H.-B., Cho R., Muller-Sieburg C., Loeffler M. Characterization and quantification of clonal heterogeneity among hematopoietic stem cells: A model-based approach. Blood, v. 112(13), pp. 4874–4883, 2008.
46. Hoffmann M., Chang H.H., Huang S., Ingber D.E., Loeffler M., Galle J. Noise-driven stem cell and progenitor population dynamics. PLoS ONE, 3(8), e2922, 2008.
47. Glauche I., Moore K., Thielecke L., Horn K., Loeffler M., Roeder I. Stem cell proliferation and quiescence — two sides of the same coin. PLoS Comput. Biol., 5(7), e1000447, 2009.
48. Belair J., Mackey M.C., Mahaffy J.M. Age-structured and two-delay models for erythropoiesis. Mathematical Biosciences, v. 128(1-2), pp. 317–346, 1995.
49. King-Smith E.A., Morley A. Computer simulation of granulopoiesis: Normal and impaired granulopoiesis. Blood, v. 36(2), pp. 254-262, 1970.
50. Kirk J., Orr J.S., Wheldon T.E., Gray W.M. Stress cycle analysis in the biocybernetic study of blood cell populations. Journal of Theoretical Biology, v. 26, pp. 265–276, 1970.
51. Gray W.M., Kirk J. Analysis of analogue and digital computers of bone marrow stem cell and platelet control mechanisms. Computers for analysis and control in medical and biological research. IEEE publication, pp. 120–124, 1971.
52. Wheldon T.E. Mathematical model of oscillatory blood cell production. Mathematical Biosciences, v. 24, pp. 289–305, 1975.
53. Kazarinoff N.D., Driessche P. Control of oscillations in hematopoiesis. Science, v. 203, pp. 1348–1349, 1979.
54. Mahaffy J.M., Belair J., Mackey M.C. Hematopoietic model with moving boundary condition and state dependent delay: Applications in erythropoiesis. Journal of Theoretical Biology, v. 190(2), pp. 135–146, 1998.
55. Hearn T., Haurie C., Mackey M.C. Cyclical neutropenia and the peripheral control of white blood cell production. Journal of Theoretical Biology, v. 192(2), pp. 167–181, 1998.
56. Wichmann H.E., Gerhardts M.D., Spechtmeyer H., Gross R. A mathematical model of thrombopoiesis in rats. Cell Tissue Kinetics, v. 12, pp. 551–567, 1979.
57. Marchuk G.I. Mathematical Models in Immunology. Moscow: Nauka, pp. 134–206, 1980 (Russian).
58. Wichmann H.E., Loeffler M. Mathematical Modeling of Cell Proliferation: Stem Cell Regulation in Hemopoiesis, 1st ed. Boca Raton, FL: CRC Press, 1985.
59. Verigo V.V. Systemic Methods in Cosmic Biology and Medicine. Problems of Cosmic Biology. Moscow: Nauka, pp. 132–150, 1987 (Russian).
60. Wichmann H.E., Loeffler M., Schmitz S. A concept of hemopoietic regulation and its mathematical realization. Blood Cells, v. 14, pp. 411–429, 1988.
61. Loeffler M., Pantel K., Wulff H., Wichmann H.E. A mathematical model of erythropoiesis in mice and rats. Cell Tissue Kinetics, v. 22, pp. 13–30, 1989.
62. Schmitz S., Loeffler M., Jones J.B., Lange R.D., Wichmann H.E. Synchrony of bone marrow proliferation and maturation as the origin of cyclic haemopoiesis. Cell Tissue Kinetics, v. 23, pp. 425–441, 1990.
63. Schmitz S., Franke H., Loeffler M., Wichmann H.E., Diehl V. Reduced variance of bone marrow transit time of granulopoiesis — A possible pathomechanism of human cyclic neutropenia. Cell Proliferation, v. 27, pp. 655–667, 1994.
64. Monichev A.J. Dynamics of Haemopoiesis. Moscow: Meditsina, 1984 (Russian).
65. Tyazelova V.G. Kinetic Principle in Interspecies Extrapolations. Moscow: Nauka, 1988 (Russian).
66. Vakha I., Znoil V. The mathematical model of erythropoiesis application for investigation of the postirradiation recovery process in mice. Biofizika, v. 20, pp. 872–879, 1975 (Russian).
67. Sacher G.A., Trucco E. Theory of radiation injury and recovery in self-renewing cell populations. Radiation Research, v. 29, pp. 236–256, 1966.

68. Shafirkin A.V. Some regularities of hemopoietic stem cell dynamics under continuous irradiation with different values of dose rate. Radiobiologiya, v. 23, pp. 630–636, 1983 (Russian).
69. Schirm S., Engel C., Loeffler M., Scholz M. A Biomathematical Model of Human Erythropoiesis under Erythropoietin and Chemotherapy Administration. PLoS One, v. 8(6), e65630, 2013.
70. Schirm S., Engel C., Loeffler M., Scholz M. A combined model of human erythropoiesis and granulopoiesis under growth factor and chemotherapy treatment. Theoretical Biology and Medical Modelling, v. 11:24, 2014. doi: 10.1186/1742-4682-11-24.
71. Scholz M., Engel C., Loeffler M. Modelling human granulopoiesis under poly-chemotherapy with G-CSF support. Journal of Mathematical Biology v. 50(4), pp. 397–439, 2005.
72. Engel C., Scholz M., Loeffler M. A computational model of human granulopoiesis to simulate the hematotoxic effects of multicycle polychemotherapy. Blood, v. 104(8), pp. 2323-2331, 2004.
73. Roeder I., Loeffler I. A novel dynamic model of hematopoietic stem cell organization based on the concept of within-tissue plasticity. Experimental Hematology, v. 30(8), pp. 853–861, 2002.
74. Roeder I., Loeffler M. Quantitative tissue stem cell modeling. Blood, v. 102(3), pp. 1143–1145, 2003.
75. Loeffler M., Roeder I. Conceptual models to understand tissue stem cell organization. Current Opinion in Hematology, v. 11(2), pp. 81–87, 2004.
76. Roeder I., Horn M., Glauche I., Hochhaus A., Mueller M.C., Loeffler M. Dynamic modeling of imatinib-treated chronic myeloid leukemia: Functional insights and clinical implications. Nature Medicine, v. 12, pp. 1181–1184, 2006.
77. Horn M., Loeffler M., Roeder I. Mathematical modeling of genesis and treatment of chronic myeloid leukemia. Cells Tissues Organs, v. 188, pp. 236–247, 2008.
78. Haurie C., Dale D.C., Rudnicki R., Mackey M.C. Modeling complex neutrophil dynamics in the grey collie. Journal of Theoretical Biology, v. 204(4), pp. 505–519, 2000.
79. Santillan M., Mahaffy J.M., Belair J., Mackey M.C. Regulation of platelet production: The normal response to perturbation and cyclical platelet disease. Journal of Theoretical Biology, v. 206(4), pp. 585–603, 2000.
80. Bernard S., Belair J., Mackey M.C. Oscillations in cyclical neutropenia: New evidence based on mathematical modeling. Journal of Theoretical Biology, v. 223(3), pp. 283–298, 2003.
81. Colijn C., Mackey M.C. A mathematical model of hematopoiesis. I. Periodic chronic myelogenous leukemia. Journal of Theoretical Biology, v. 237(2), pp. 117–132, 2005.
82. Colijn C., Mackey M.C. A mathematical model of hematopoiesis. II. Cyclical neutropenia. Journal of Theoretical Biology, v. 237(2), pp. 133–146, 2005.
83. Foley C., Bernard S., Mackey M.C. Cost-effective G-CSF therapy strategies for cyclical neutropenia: Mathematical modelling based hypotheses. Journal of Theoretical Biology, v. 238(4), pp. 754–763, 2006.
84. Apostu R., Mackey M.C. Understanding cyclical thrombocytopenia: A mathematical modeling approach. Journal of Theoretical Biology, v. 251(2), pp. 297–316, 2008.
85. Foley C., Mackey M.C. Mathematical model for G-CSF administration after chemotherapy. Journal of Theoretical Biology, v. 257(1), pp. 27–44, 2009.
86. Fliedner T.M, Friesecke I., Graessle D., Paulsen C., Weiss M. Hematopoietic cell renewal as the limiting factor in low-level radiation exposure: Diagnostic implications and therapeutic options. Military Medicine, v. 167, pp. 46–48, 2002.
87. Ackleh A.S., Deng K., Ito K., Thibodeaux J. A structured erythropoiesis model with nonlinear cell maturation velocity and hormone decay rate. Mathematical Biosciences, v. 204(1), pp. 21–48, 2006.
88. Alaoui H.T., Yafia R. Stability and Hopf bifurcation in an approachable haematopoietic stem cells model. Mathematical Biosciences, v. 206(2), pp. 176–184, 2007.
89. Dingli D., Traulsen A., Pacheco J.M. Compartmental architecture and dynamics of hematopoiesis. PLoS ONE 2:e345, 2007.

90. Fliedner T.M., Graessle D., Meineke D., Dorr H. Pathophysiological principles underlying the blood cell concentration responses used to assess the severity of effect after accidental whole-body radiation exposure: An essential basis for an evidence-based clinical triage. Experimental Hematology, v. 35(4), pp. 8–16, 2007.
91. Fliedner T.M., Graessle D.H. Hematopoietic cell renewal systems: Mechanisms of coping and failing after chronic exposure to ionizing radiation. Radiation and Environmental Biophysics, v. 47(1), pp. 63–69, 2008.
92. Fliedner T.M. et al. Stem cells, multiorgan failure in radiation emergency medical preparedness: A U.S./European consultation workshop. Stem Cells, v. 27(5), pp. 1205–1211, 2009.
93. Thibodeaux J.J. Modeling erythropoiesis subject to malaria infection. Mathematical Biosciences, v. 225(1), pp. 59–67, 2010.
94. Graessle D.H., Fliedner T.M. Computer-assisted severity of effect assessment of hematopoietic cell renewal after radiation exposure based on mathematical models. Health Physics, v. 98(2), pp. 282–289, 2010.
95. Romanovsky J.M., Stepanova N.V., Chernavsky D.S. Mathematical Modeling in Biophysics. Introduction to Theoretical Biophysics. Moscow-Izhevsk: Scientific-Publishing Centre "Regular and Chaotic Dynamics," Institute of Computer Science, 2004 (Russian).
96. Romanovsky J.M., Stepanova N.V., Chernavsky D.S. Mathematical Biophysics. Moscow: Nauka, 1984 (Russian).
97. Romanovsky J.M., Stepanova N.V., Chernavsky D.S. Kinetische Modelle in der Biophysik. Stuttgart: Gustav Fischer Verlag, 1974.
98. Yarmonenko S.P. Radiation Haematology Hand-book, 1st ed. Moscow: Meditsina, 1974 (Russian).
99. Belousova O.I., Gorizontov P.D., Fedorova M.I. Radiation and Haemopoietic System. Moscow: Atomizdat, 1979 (Russian).
100. Fliedner T.M, Graessle D., Paulsen C., Reimers K. Structure and function of bone marrow hemopoiesis: Mechanisms of response to ionizing radiation exposure. Cancer Biotherapy and Radiopharmaceuticals, v. 17(4), pp. 405–426, 2002.
101. Lea D.E. Action of Radiation on Living Cells, 2nd ed. Cambridge: The Syndics of the Cambridge University Press, 1955.
102. Strdzidzovsky A.D. Dynamical and dose characteristics of the distraction process in lymphoid tissue in rodents. Radiobiologiya, v. 14, pp. 409–412, 1974 (Russian).
103. Mosyagina E.N., Vladimirskaya E.B., Torubarova N.A., Mizina N.V. Kinetics of the Blood Constituents of the Blood. Moscow: Meditsina, 1976 (Russian).
104. Harker L.A. Platelet production. New England Journal of Medicine, v. 282(9), pp. 492–494, 1970.
105. Pontryagin L.S. Ordinary Differential Equations. Moscow: Nauka, 1982 (Russian).
106. Andronov A.A., Vitt A.A., Khikin S.E. Theory of Oscillations. Moscow: Nauka, 1981 (Russian).
107. Andronov A.A., Leontovich E.A., Gordon I.I., Maier A.G. Theory of Bifurcations of Dynamical Systems on Plane. Moscow: Nauka, 1967 (Russian).
108. Hayashi C. Nonlinear Oscillations in Physical Systems. New York: McGraw-Hill Book Company, 1964.
109. Arrowsmith D.K., Place C.M. Ordinary Differential Equations. A Qualitative Approach with Applications. London: Chapman and Hall, 1982.
110. Dulac H. Sur les cycles limités. Bulletin de la Société Mathématique de France, v. 51, pp. 45–188, 1923.
111. Korn G.A., Korn T.M. Mathematical Handbook. New York: McGraw-Hill Book Company, 1968.
112. Patt H.M., Lund J.E., Maloney M.A. Cyclic hematopoiesis in grey collie dogs: A stem-cell problem. Blood, v. 42(6), pp. 873–884, 1973.
113. Matter M., Hartmann J.R., Kautz J., De Marsh Q.B., Finch C.A. A study of thrombopoiesis in induced acute thrombocytopenia. Blood, v. 15(1), pp. 174–185, 1960.

114. De Gabriele G., Penington D.G. Physiology of the regulation of platelet production. British Journal of Haematology, v. 13, pp. 202–209, 1967.
115. Hudson D.J. Statistics. Lectures on Elementary Statistics and Probability. Geneva: CERN, 1964.
116. Kalina I., Praslichka M. Changes in haemopoiesis and survival of continuously irradiated mice. Radiobiologiya, v. 17, pp. 849–853, 1977 (Russian).
117. Praslichka M., Kalina I. Influence of low dose-rate radiation on the change of CFC and peripheral blood in mice. Radiobiologiya, v. 16, pp. 376–380, 1976 (Russian).
118. Kalina I., Praslicka M., Marko L., Hudak S. Hamatologische veranderungen und iiberlebensdauer bei mausen nach kontinuierlicher bestrahlung. Radiobiologia Radiotherapia, v. 16(3), pp. 347–354, 1975.
119. Fabrikant J.I. Adaptation of cell renewal systems under continuous irradiation. Health Physics, v. 52(5), pp. 561–570, 1987.
120. Muksinova K.N., Mushkacheva G.S. Cellular and molecular bases of haemopoiesis transformation under continuous irradiation. Moscow: Energoatomizdat, 1990 (Russian).
121. Dale D.S., Alling D.W., Wolff S.M. Cyclic hematopoiesis: The mechanism of cyclic neutropenia in grey collie dogs. Journal of Clinical Investigations, v. 51, pp. 2197–2204, 1972.
122. Lange R.D., Jones J.B. Erythropoiesis in dogs and humans with cyclic hematopoiesis. Current Concepts in Erythropoiesis, C.D.R. Dunn (Ed.). Chichester, UK: John Wiley and Sons, pp. 144–165, 1983.
123. Hulse E.V. Lymphocyte depletion of the blood and bone marrow of the irradiated rat: A quantitative study. British Journal of Haematology, v. 5, pp. 278–283, 1959.
124. Smirnova O.A. Mathematical modeling of radiation effects on immune system. Immunologiya, no. 2, pp. 38–42, 1984 (Russian).
125. Hulse E.V. Lymphocytic recovery after irradiation and its relation to other aspects of haemopoiesis. British Journal of Haematology, v. 9, pp. 376–384, 1963.
126. Zukhbaya T.M. The kinetics of lymphocytes during long-term γ-irradiation. Radiobiologiya, v. 21, pp. 863–867, 1981 (Russian).
127. Lamerton L.F., Pontifex A.H., Blackett N.M., Adams K. Effects of protracted irradiation: I. Continuous exposure. British Journal of Radiology, v. 33(389), pp. 287–301, 1960.
128. Kuzin A.M. Stimulation Effect of Ionizing Radiation on Biological Processes. Moscow: Atomizdat, 1977 (Russian).
129. Luckey T.D. Physiological benefits from low levels of ionizing radiation. Health Physics, v. 43(6), pp. 771–789, 1982.
130. Luckey T.D. Radiation Hormesis. Boca Raton, FL: Taylor and Francis, 1991.
131. Morley A., Stohlman F. Erythropoiesis in the dog: The periodic nature of the steady state. Science, v. 165, pp. 1025–1027, 1968.
132. Hulse E.V. Quantitative studies on the depletion of the erythropoietic cells in the bone marrow of the irradiated rat. British Journal of Haematology, v. 3, pp. 348–358, 1957.
133. Hulse E.V. Recovery of erythropoiesis after irradiation: A quantitative study in the rat. British Journal of Haematology, v. 9, pp. 365–375, 1963.
134. Zukhbaya T.M. Regularities in the development of radiation affection and recovery of haemopoietic tissues of rates subjected to long-term γ-irradiation of a dose rate of 0.1 Gy/day. Radiobiologiya, v. 29, pp. 74–78, 1989 (Russian).
135. Zukhbaya T.M. Quantitative changes in some generations of cells of erythroid and granulopoietic compartments in bone marrow of rats exposed to constant γ-radiation at varying dose rates. Radiobiologiya, v.19, pp. 278–282, 1979 (Russian).
136. Morley A. A neutrophil cycle in healthy individuals. Lancet, v. 2, pp. 1220–1222, 1966.
137. Hulse E.V. The depletion of the myelopoietic cells of the irradiated rat. British Journal of Haematology, v. 5, pp. 369–378, 1959.
138. Yonezawa M., Misonoh J., Hosokawa Y. Two types of acquired radioresistance after low doses of X-rays in mice. In: Low Dose Irradiation and Biological Defense Mechanisms. T. Suguhara, L.A. Sagan, T. Aoyama (Eds.). Amsterdam: Elsevier Science Publishers, pp. 215–218, 1992.

139. Yonezawa M., Misonoh J., Hosokawa Y. Two types of X-ray-induced radioresistance in mice: Presence of 4 dose ranges with distinct biological effects. Mutation Research, v. 358, pp. 237–243, 1996.
140. Yonezawa M., Misonoh J., Hosokawa Y., Asano T. Decreased bone marrow death and suppression of hemorrhage in radioadaptive response in mice. Hoken Butsuri, v. 34, pp. 375–380, 1999.
141. Yonezawa M. Radio-adaptive survival response in mice. In: Biological Effects of Low Dose Radiation. Proceedings of an Excepta Medica International Congress, Series 1211, T. Yamada, C. Mothersill, B.D. Michael, C.S. Potten (Eds.). Amsterdam: Elsevier Science Publishers, pp. 93–99, 2000.
142. Matsubara J., Turcanu V., Poindron P., Ina Y. Immune effects of low-dose radiation: Short-term induction of thymocyte apoptosis and long-term augmentation of T-cell-dependent immune responses. Radiation Research, v. 153, pp. 332–338, 2000.
143. Nose M., Wang B., Itsukaichi H., Yukawa O., Hayata I., Yamada T., Ohyama H. Rescue of lethally irradiated mice from hematopoietic death by pre-exposure to 0.5 Gy X rays without recovery from peripheral blood cell depletion and its modification by OK432. Radiation Research, v. 156, pp. 195–204, 2001.
144. Pelevina I.I., Afanasiev G.G., Gotlib V.Y. et al. (1993) Radiation exposure of cultured tissue cells and animals (mice) within the ten-kilometer zone of Chernobyl disaster: Effect on radiosensitivity to posterior irradiation. Radiatsionnaya Biologiya Radioekologiya, v. 33, pp. 508–520, 1993 (Russian).
145. Fomenko L.A., Kozhanovskaya Y.K., Gaziev A.I. Formation of micronuclei in bone–marrow cells of chronically irradiated mice and subsequent acute exposure to γ-radiation. Radiobiologiya, v. 31, pp. 709–715, 1991 (Russian).
146. Konradov A.A., Lyubimova N.V., Pelevina I.I. Modification of radiosensitivity of animals after exposure within the zone of Chernobyl disaster. Radiatsionnaya Biologiya Radioekologiya, v. 33, pp. 499–507, 1993 (Russian).

Chapter 2
Effects of Non-uniform Acute Irradiation on the Blood-Forming System

2.1 Introduction

No doubt, the patterns of organism's responses to non-uniform and uniform acute irradiation are rather different [1]. The study and prediction of such differences, as well as the revealing of their dependence on the exposure conditions (e.g., the degree of non-uniformity of irradiation and the respective whole-body dose), still remain the challenging problems. The solution of the latter requires the analysis of relevant experimental and clinical data, as well as the creation of effective research tools of studies and predictions of the effects of such exposures on the organism's vital systems, which can lead to the malfunction and illness of the latter. Such tools can be, in particular, the biologically motivated mathematical models, which are capable of predicting the dynamics of these systems after non-uniform acute irradiation.

The primary objectives of our work [2] were the development and thorough investigation of mathematical models, which describe the dynamics of the major hematopoietic lineages (the thrombopoietic, erythropoietic, granulopoietic, and lymphopoietic systems) under non-uniform acute irradiation. These models are based on the developed mathematical models of the dynamics of these systems in mammals (rodents) exposed to uniform acute irradiation (see Chap. 1, as well as [3–8]). The description of the mathematical models of the dynamics of the major hematopoietic lineages in mammals (rodents) exposed to non-uniform and uniform acute irradiation, the comparative analysis of the results obtained in their framework, revealing the causes, which can lead to differences in the responses of these systems to uniform and non-uniform acute irradiation, as well as the discussion of possible ways of extension of these models to the study of the effects of non-uniform acute irradiation on the major hematopoietic lineages in humans are given below.

O.A. Smirnova, *Environmental Radiation Effects on Mammals*,
DOI 10.1007/978-3-319-45761-1_2

2.2 Mathematical Models

The models of the dynamics of the thrombopoietic, erythropoietic, granulopoietic, and lymphopoietic systems in mammals (rodents) after non-uniform acute irradiation are based on the developed models of the dynamics of these major hematopoietic lineages after uniform acute irradiation (see Chap. 1, as well as [3–8]).

Summarizing all the stated in Chap. 1, the mathematical models of the dynamics of the major hematopoietic lineages in mammals (rodents) after uniform acute irradiation can be presented in the following way. Specifically, these models consider the basic cell compartments according to the degree of maturity and differentiation of cells of the respective hematopoietic lineages:

- X_1, the precursor cells capable of dividing (from stem cells in the microenvironment, which predetermine their differentiation toward the aforementioned hematopoietic lineages, to morphologically identifiable dividing maturing bone marrow cells in these hematopoietic lineages, namely to megakaryocytoblasts in the thrombopoietic system, to polychromatophilic erythroblasts in the erythropoietic system, to myelocytes in the granulopoietic system, and to lymphoblasts in the lymphopoietic system);
- X_2, the precursor cells incapable of dividing (nondividing maturing bone marrow cells in the hematopoietic lineages on hand, namely from promegakaryocytes to mature megakaryocytes in the thrombopoietic system, from orthochromatic erythroblasts to reticulocytes in the erythropoietic system, from metamyelocytes to granulocytes in the granulopoietic system, and lymphoid cells in the lymphopoietic system);
- X_3, the mature cells (the functional blood cells of the hematopoietic lineages on hand, namely thrombocytes (blood platelets) in the thrombopoietic system, blood erythrocytes in the erythropoietic system, blood granulocytes in the granulopoietic system, and blood lymphocytes in the lymphopoietic system);
- X_4, the tissue granulocytes (appears only in the granulopoiesis model).

The cells of a radiosensitive compartment X_i ($i = 1, \ldots, n$) are split into three groups, according to their response to irradiation:

- X_i^{ud}, undamaged cells;
- X_i^{d}, damaged cells that die within 1 or 2 days (mitotic death);
- X_i^{hd}, heavily damaged cells that die within several hours (interphase death).

In turn, the cells of a radioresistant compartment X_i ($i = n+1, \ldots, m$) are considered as undamaged cells X_i^{ud} ($i = n + 1, \ldots, m$). Here m is the total number of cell compartments considered in the model of the respective hematopoietic lineage and n is the number of radiosensitive cell compartments among them. In particular, only X_1 cells are radiosensitive in the thrombopoietic system (i.e., $n = 1$, $m = 3$). In the erythropoietic system, X_1 and X_2 cells are radiosensitive (i.e., $n = 2$, $m = 3$). In the granulopoietic system, X_1, X_2, X_3, and X_4 cells are radiosensitive, though in

a different degree (i.e., $n = m = 4$). In the lymphopoietic system, X_1, X_2, and X_3 cells are radiosensitive (i.e., $n = m = 3$).

The variables of the models are the concentrations of radiosensitive X_i^{ud}, X_i^{d}, X_i^{hd} $(i = 1, \ldots, n)$ cells and the concentrations of radioresistant X_i^{ud} $(i = n+1, \ldots, m)$ cells: x_i^{ud}, x_i^{d}, x_i^{hd} $(i = 1, \ldots, n)$ and x_i^{ud} $(i = n+1, \ldots, m)$, respectively. By cell concentration, we mean the ratio of the total number of cells of a certain group to the total blood volume. The dynamics of the concentrations of X_i^{ud} $(i = 1, \ldots, n)$, X_i^{d} $(i = 1, \ldots, n)$, X_i^{hd} $(i = 1, \ldots, n)$, and X_i^{ud} $(i = n+1, \ldots, m)$ cells in the respective major hematopoietic lineages after uniform acute irradiation is described by the following differential equations (see Chap. 1 and the references therein for the details):

$$\frac{dx_1^{\mathrm{ud}}}{dt} = Bx_1^{\mathrm{ud}} - \gamma x_1^{\mathrm{ud}}, \tag{2.1}$$

$$\frac{dx_2^{\mathrm{ud}}}{dt} = \gamma x_1^{\mathrm{ud}} - Fx_2^{\mathrm{ud}}, \tag{2.2}$$

$$\frac{dx_3^{\mathrm{ud}}}{dt} = Fx_2^{\mathrm{ud}} - \psi x_3^{\mathrm{ud}}, \tag{2.3}$$

$$\frac{dx_4^{\mathrm{ud}}}{dt} = \psi x_3^{\mathrm{ud}} - \xi x_4^{\mathrm{ud}}, \tag{2.4}$$

$$\frac{dx_i^{\mathrm{d}}}{dt} = -\mu x_i^{\mathrm{d}} \quad (i = 1, \ldots, n), \tag{2.5}$$

$$\frac{dx_i^{\mathrm{hd}}}{dt} = -\nu x_i^{\mathrm{hd}} \quad (i = 1, \ldots, n). \tag{2.6}$$

In Eqs. (2.1)–(2.3), the parameter B is the specific reproduction rate of X_1^{ud} cells, the coefficients γ and F are the specific rates of transfer of cells from group X_1^{ud} to group X_2^{ud} and from group X_2^{ud} to group X_3^{ud}, respectively. In the thrombopoiesis, erythropoiesis, and lymphopoiesis models, the coefficient ψ in Eq. (2.3) denotes the specific rate of the natural death of X_3^{ud} cells. In the granulopoiesis model, the coefficient ψ in Eqs. (2.3) and (2.4) stands for the specific rate of transfer of cells from group X_3^{ud} to group X_4^{ud} (from blood to tissues) and the coefficient ξ in Eq. (2.4) is the specific rate of the natural death of X_4^{ud} cells. In Eqs. (2.5) and (2.6), the coefficients μ and ν are the specific death rates of damaged and heavily damaged cells, respectively.

The formula describing the parameter B in Eq. (2.1) takes into account the negative-feedback control of the specific reproduction rate of X_1^{ud} cells in the major hematopoietic lineages (see Chap. 1 and the references therein for the details):

$$B = \frac{\alpha}{1 + \beta\left[\sum_{i=1}^{n} \theta_i \left(x_i^{\mathrm{ud}} + \phi x_i^{\mathrm{d}} + \varphi x_i^{\mathrm{hd}}\right) + \sum_{i=n+1}^{m} \theta_i x_i^{\mathrm{ud}}\right]}. \tag{2.7}$$

Here $\theta_1 = 1$ by definition, the parameters θ_i ($i = 2, \ldots, m$), β, ϕ, and φ are constants.

The model of the granulopoietic system considers the regulatory mechanism of the specific rate of the granulocyte supply from the bone marrow to the blood flow by the introduction of the variable parameter F. The latter accounts for the contributions of the undamaged, damaged, and heavily damaged blood granulocytes (X_3^{ud}, X_3^{d}, and X_3^{hd} cells) to this regulatory mechanism (see Chap. 1 and the references therein for the details):

$$F = \delta \frac{1 + [m/(\bar{x}_3)^2]\left(x_3^{\mathrm{ud}} + x_3^{\mathrm{d}} + x_3^{\mathrm{hd}}\right)^2}{1 + [l/(\bar{x}_3)^2]\left(x_3^{\mathrm{ud}} + x_3^{\mathrm{d}} + x_3^{\mathrm{hd}}\right)^2}, \tag{2.8}$$

where constants δ and $\delta m/l$ are the maximal and minimal values of the specific rate of granulocyte supply from the bone marrow to the blood flow. Note that the parameter F is constants ($F \equiv \delta$) in the models of the thrombopoietic, erythropoietic, and lymphopoietic systems.

In turn, the model of the thrombopoietic system takes into account the regulatory mechanism of megakaryocyte ploidy by the introduction of the ploidy coefficient f. The latter is described by the decreasing function of the thrombocyte concentration x_3^{ud} (see Chap. 1 and the references therein for the details):

$$f = \frac{1}{\lambda + (1 - \lambda)(x_3^{\mathrm{ud}}/\bar{x}_3)}. \tag{2.9}$$

Here λ is a dimensionless constant and $\bar{x}_3$ is the normal concentration of thrombocytes (X_3 cells). In the thrombopoiesis model, the first term on the right-hand side of Eq. (2.2) is multiplied by the factor f and the first term on the right-hand side of Eq. (2.3) is multiplied by the factor σ, the latter being the average number of thrombocytes produced by one megakaryocyte.

The initial conditions for Eqs. (2.1)–(2.6) read (see Chap. 1 and the references therein for the details):

$$x_i^{\mathrm{ud}}(0) = \bar{x}_i \exp(-D/D_i^0) \quad (i = 1, \ldots, n), \tag{2.10}$$

$$x_i^{\mathrm{d}}(0) = \bar{x}_i \frac{1}{1 + \rho_i}[1 - \exp(-D/D_i^0)] \quad (i = 1, \ldots, n), \tag{2.11}$$

$$x_i^{\mathrm{hd}}(0) = \bar{x}_i \frac{\rho_i}{1 + \rho_i}[1 - \exp(-D/D_i^0)] \quad (i = 1, \ldots, n), \tag{2.12}$$

$$x_i^{\mathrm{ud}}(0) = \bar{x}_i \quad (i = n + 1, \ldots, m), \tag{2.13}$$

where

$$\rho_i = \frac{1 - \exp(-D/D_i^{00})}{\exp(-D/D_i^{00}) - \exp(-D/D_i^0)} \quad (i = 1, \ldots, n). \tag{2.14}$$

Here $\bar{x}_i$ $(i = 1, \ldots, m)$ is the normal concentration of X_i $(i = 1, \ldots, m)$ cells. The parameter D is a dose of acute irradiation. The coefficient D_i^0 $(i = 1, \ldots, n)$ is equivalent to the conventional dose D_0, after exposure to which the number of X_i cells left undamaged is $e = 2.718\ldots$ times smaller than their initial number [9]. The coefficient D_i^{00} $(i = 1, \ldots, n)$ is the dose, after exposure to which the number of X_i^{ud} $(i = 1, \ldots, n)$ cells, which do not undergo the interphase death, is $e = 2.718\ldots$ times smaller than their initial number.

It is important to emphasize that the developed models, which describe the dynamics of the major hematopoietic lineages after uniform acute irradiation, explicitly embody the main characteristic of irradiation, namely the dose D of such exposure, as well as the radiobiological parameters D_i^0 and D_i^{00} $(i = 1, \ldots, n)$, which characterize the radiosensitivity of the respective cells of these systems.

To extend the models of the dynamics of the major hematopoietic lineages (the thrombopoietic, erythropoietic, granulopoietic, and lymphopoietic systems) in mammals (rodents) after uniform acute irradiation with the aim of the describing, in their framework, of the dynamics of these system after non-uniform acute irradiation, the following approach is used. It is assumed that non-uniform acute irradiation of the hematopoietic tissue, which contains the radiosensitive cells of the systems on hand, can be considered as a composition of k uniform acute exposures of its k parts with dose rates N_j $(j = 1, \ldots, k)$ and a duration τ, respectively. The ratio of the mass of j-th part of the hematopoietic tissue to the total mass of the latter (i.e., the fraction of mass of j-th part of the hematopoietic tissue) before the onset of non-uniform acute irradiation is denoted by Ω_j $(j = 1, \ldots, k)$. In accordance with these assumptions, the extended models, which describe the dynamics of the major hematopoietic lineages after non-uniform acute irradiation, consider undamaged, damaged, and heavily damaged radiosensitive cells [X_{ij}^{ud}, X_{ij}^{d}, X_{ij}^{hd} $(i = 1, \ldots, n; j = 1, \ldots, k)$ cells] and radioresistant cells [X_{ij}^{ud} $(i = n + 1, \ldots, m; j = 1, \ldots, k)$ cells] belonging to the j-th $(j = 1, \ldots, k)$ part of the hematopoietic tissue. Here the index i specifies a certain cell compartment and the index j specifies a certain part of the hematopoietic tissue. The variables of these models are the concentrations of cells of the aforementioned groups: x_{ij}^{ud}, x_{ij}^{d}, x_{ij}^{hd} $(i = 1, \ldots, n; j = 1, \ldots, k)$ and x_{ij}^{ud} $(i = n+1, \ldots, m; j = 1, \ldots, k)$. It is obvious that the concentrations x_i^{ud}, x_i^{d}, x_i^{hd} $(i = 1, \ldots, n)$ and x_i^{ud} $(i = n + 1, \ldots, m)$ can be expressed in terms of the concentrations x_{ij}^{ud}, x_{ij}^{d}, x_{ij}^{hd} $(i = 1, \ldots, n; j = 1, \ldots, k)$ and x_{ij}^{ud} $(i = n + 1, \ldots, m; j = 1, \ldots, k)$ in the following way:

$$x_i^{\mathrm{ud}} = \sum_{j=1}^{k} x_{ij}^{\mathrm{ud}} \quad (i = 1, \ldots, n), \tag{2.15}$$

$$x_i^{\mathrm{d}} = \sum_{j=1}^{k} x_{ij}^{\mathrm{d}} \quad (i = 1, \ldots, n), \tag{2.16}$$

$$x_i^{\mathrm{hd}} = \sum_{j=1}^{k} x_{ij}^{\mathrm{hd}} \quad (i = 1, \ldots, n), \tag{2.17}$$

$$x_i^{\mathrm{ud}} = \sum_{j=1}^{k} x_{ij}^{\mathrm{ud}} \quad (i = n+1, \ldots, m). \tag{2.18}$$

Taking into account the one-target–one-hit theory of cell damage [10], according to which the damage rate of radiosensitive cells is proportional to the dose rate of irradiation, and taking into consideration the extremely short duration τ of non-uniform acute irradiation, the dynamics of the concentrations of undamaged, damaged, and heavily damaged radiosensitive X_{ij}^{ud}, X_{ij}^{d}, X_{ij}^{hd} $(i = 1, \ldots, n; j = 1, \ldots, k)$ cells during the exposure can be described by the system of "fast" equations, whereas the concentrations of radioresistant X_{ij}^{ud} $(i = n+1, \ldots, m; j = 1, \ldots, k)$ cells can be considered constant ones:

$$\frac{dx_{ij}^{\mathrm{ud}}}{dt} = -\frac{N_j}{D_i^0} x_{ij}^{\mathrm{ud}} \quad (i = 1, \ldots, n; j = 1, \ldots, k), \tag{2.19}$$

$$\frac{dx_{ij}^{\mathrm{d}}}{dt} = \frac{N_j}{D_i^0} \frac{1}{1+\rho_{ij}} x_{ij}^{\mathrm{ud}} \quad (i = 1, \ldots, n; j = 1, \ldots, k), \tag{2.20}$$

$$\frac{dx_{ij}^{\mathrm{hd}}}{dt} = \frac{N_j}{D_i^0} \frac{\rho_{ij}}{1+\rho_{ij}} x_{ij}^{\mathrm{ud}} \quad (i = 1, \ldots, n; j = 1, \ldots, k), \tag{2.21}$$

$$\frac{dx_{ij}^{\mathrm{ud}}}{dt} = 0 \quad (i = n+1, \ldots, m; j = 1, \ldots, k), \tag{2.22}$$

where N_j $(j = 1, \ldots, k)$ is the dose rate of the uniform acute exposure of j $(j = 1, \ldots, k)$ part of the hematopoietic tissue; the parameter D_i^0 $(i = 1, \ldots, n)$ is equivalent to the conventional dose D_0, after exposure to which the number of X_i cells left undamaged is exp(-1) (i.e., 36.79 %) of their initial number [9]. The ratio N_j/D_i^0 on the right-hand side of Eq. (2.19), which describes the dynamics of concentration of radiosensitive cells X_{ij}^{ud}, is the specific rate of decrease of the concentration of these cells due to their radiation-induced damage. One part of them transfers into the group of damaged cells X_{ij}^{d} [Eq. (2.20)] and the other part passes to the group of heavily damaged cells X_{ij}^{hd} [Eq. (2.21)]. The ratio of these parts is denoted by ρ_{ij}.

The initial conditions for Eqs. (2.19)–(2.22) are concentrations of X_{ij}^{ud} $(i = 1, \ldots, n; j = 1, \ldots, k)$ cells, X_{ij}^{d} $(i = 1, \ldots, n; j = 1, \ldots, k)$ cells, X_{ij}^{hd} $(i = 1, \ldots, n; j = 1, \ldots, k)$ cells, and X_{ij}^{ud} $(i = n+1, \ldots, m; j = 1, \ldots, k)$ cells before the onset of non-uniform acute irradiation. In particular, in the case of irradiation of a healthy individual that has not previously been exposed to radiation, the concentrations of damaged X_{ij}^{d} $(i = 1, \ldots, n; j = 1, \ldots, k)$ cells and heavily

damaged X_{ij}^{hd} $(i = 1,\ldots,n; j = 1,\ldots,k)$ cells are equal to zero, whereas the concentrations of radiosensitive X_{ij}^{ud} $(i = 1,\ldots,n; j = 1,\ldots,k)$ cells and radioresistant X_{ij}^{ud} $(i = n+1,\ldots,m; j = 1,\ldots,k)$ cells are equal to their normal values. As a result, the initial conditions for Eqs. (2.19)–(2.22) take the following form:

$$x_{ij}^{\mathrm{ud}}(0) = \bar{x}_i \Omega_j \quad (i = 1,\ldots,n; j = 1,\ldots,k), \tag{2.23}$$

$$x_{ij}^{\mathrm{d}}(0) = 0 \quad (i = 1,\ldots,n), \tag{2.24}$$

$$x_{ij}^{\mathrm{hd}}(0) = 0 \quad (i = 1,\ldots,n), \tag{2.25}$$

$$x_{ij}^{\mathrm{ud}}(0) = \bar{x}_i \Omega_j \quad (i = n+1,\ldots,m; j = 1,\ldots,k). \tag{2.26}$$

For the considered case of the constant dose rate N_j, which the j-th part of the hematopoietic tissue is exposed to, Eqs. (2.19)–(2.22) with the initial conditions (2.23)–(2.26) can be integrated explicitly. The obtained expressions for the concentrations of X_{ij}^{ud}, X_{ij}^{d}, X_{ij}^{hd} $(i = 1,\ldots,n; j = 1,\ldots,k)$ cells and X_{ij}^{ud} $(i = n+1,\ldots,m; j = 1,\ldots,k)$ cells can be used as the initial conditions for the concentrations of these cells:

$$x_{ij}^{\mathrm{ud}}(0) = \bar{x}_i\, \Omega_j\, \exp(-D_j/D_i^0) \quad (i = 1,\ldots,n; j = 1,\ldots,k), \tag{2.27}$$

$$x_{ij}^{\mathrm{d}}(0) = \bar{x}_i\, \Omega_j\, \frac{1}{1+\rho_{ij}}[1 - \exp(-D_j/D_i^0)] \quad (i = 1,\ldots,n; j = 1,\ldots,k), \tag{2.28}$$

$$x_{ij}^{\mathrm{hd}}(0) = \bar{x}_i\, \Omega_j\, \frac{\rho_{ij}}{1+\rho_{ij}}[1 - \exp(-D_j/D_i^0)] \quad (i = 1,\ldots,n; j = 1,\ldots,k), \tag{2.29}$$

$$x_{ij}^{\mathrm{ud}}(0) = \bar{x}_i\, \Omega_j \quad (i = n+1,\ldots,m; j = 1,\ldots,k), \tag{2.30}$$

where

$$\rho_{ij} = \frac{1 - \exp(-D_j/D_i^{00})}{\exp(-D_j/D_i^{00}) - \exp(-D_j/D_i^0)} \quad (i = 1,\ldots,n; j = 1,\ldots,k). \tag{2.31}$$

Here D_j is the dose of irradiation of j-th part of the hematopoietic tissue. The parameter D_i^0 $(i = 1,\ldots,n)$, as it was specified above, is equivalent to the conventional dose D_0, after exposure to which the number of X_i^{ud} $(i = 1,\ldots,n)$ cells left undamaged is $\exp(-1)$ (i.e., 36.79 %) of their initial number [9]. The parameter D_i^{00} $(i = 1,\ldots,n)$ is the dose, after exposure to which the number of X_i^{ud} $(i = 1,\ldots,n)$ cells, which do not undergo the interphase death, is $\exp(-1)$ (i.e., 36.79 %) of their initial number.

By virtue of Eqs. (2.15)–(2.18), Eqs. (2.27)–(2.30) are reduced to the following equations:

$$x_i^{\mathrm{ud}}(0) = \bar{x}_i \sum_{j=1}^{k} \Omega_j \exp(-D_j/D_i^0) \quad (i = 1, \ldots, n), \tag{2.32}$$

$$x_i^{\mathrm{d}}(0) = \bar{x}_i \sum_{j=1}^{k} \Omega_j \frac{1}{1+\rho_{ij}} [1 - \exp(-D_j/D_i^0)] \quad (i = 1, \ldots, n), \tag{2.33}$$

$$x_i^{\mathrm{hd}}(0) = \bar{x}_i \sum_{j=1}^{k} \Omega_j \frac{\rho_{ij}}{1+\rho_{ij}} [1 - \exp(-D_j/D_i^0)] \quad (i = 1, \ldots, n), \tag{2.34}$$

$$x_i^{\mathrm{ud}}(0) = \bar{x}_i \quad (i = n+1, \ldots, m). \tag{2.35}$$

Thus, the dynamics of the major hematopoietic lineages after non-uniform acute irradiation can be described by Eqs. (2.1)–(2.6) with the initial conditions (2.32)–(2.35). It is important to emphasize that these models explicitly embody the main characteristic of such exposure, namely the doses D_j ($j = 1, \ldots, k$) of irradiation of k parts of the hematopoietic tissue, as well as the radiobiological parameters D_i^0 and D_i^{00} ($i = 1, \ldots, n$), which characterize the radiosensitivity of the respective cells of these systems.

Note that the models of the dynamics the major hematopoietic lineages after non-uniform acute irradiation [Eqs. (2.1)–(2.6) with the initial conditions (2.32)–(2.35)] are reduced to the models of the dynamics of these systems after uniform acute irradiation [Eqs. (2.1)–(2.6) with the initial conditions (2.10)–(2.13)] if the model parameters k and Ω_1 are taken to be equal to unity ($k = 1$, $\Omega_1 = 1$) and $D_1 \equiv D$.

For the numerical studies, the models of the major hematopoietic lineages in mammals (rodents) exposed to uniform and non-uniform acute irradiation are rewritten in terms of the new dimensionless variables, the latter being the ratios of the dimension concentrations of the considered cells to their normal values.

The values of the independent parameters of the models of the major hematopoietic lineages in rodents (rats, mice) are given in Tables 1.1, 1.2, 1.3, and 1.4.

2.3 Distinctive Features of Responses of Major Hematopoietic Lineages to Non-uniform and Uniform Acute Irradiation

The developed models of the thrombopoietic, erythropoietic, granulopoietic, and lymphopoietic systems are applied to study the responses of these major hematopoietic lineages in rodents (mice, rats) to non-uniform and uniform acute irradiation and to analyze the distinctions between them. In this series of the modeling simulations, the number k of parts of the hematopoietic tissue, which were exposed to different

doses D_j ($j = 1, \ldots, k$), is fixed and taken to be equal to four. The exposure doses D_j ($j = 1, \ldots, 4$) of these equal parts are chosen so that the averaged exposure dose (i.e., the whole-body dose) is equal to the dose of uniform acute irradiation D reported in [9, 11]. The variation of the degree of non-uniformity of acute irradiation is simulated by the respective variation of exposure doses D_j ($j = 1, \ldots, k$). In turn, the dose of uniform acute irradiation is taken to be equal to the whole-body dose of non-uniform exposure. The obtained modeling results are presented in Figs. 2.1, 2.2, 2.3, and 2.4.

Figure 2.1 shows the modeling dynamics of concentrations of blood thrombocytes (X_3 cells) and their undamaged bone marrow precursor cells capable of dividing (X_1^{ud} cells) in the thrombopoietic system after uniform acute irradiation and after two non-uniform acute radiation exposures with the equal values of their whole-body doses. As one can see, the concentrations of X_3 cells and of X_1^{ud} cells decrease and approach their minimal levels, which are higher in the cases of non-uniform exposures than those in the case of uniform acute irradiation. The time intervals required to reach these minimal levels are shorter in the cases of non-uniform acute exposures than those in the case of uniform acute irradiation. Then the concentrations of these cells increase and achieve their maximal values, which are smaller in the cases of non-uniform exposures than those in the case

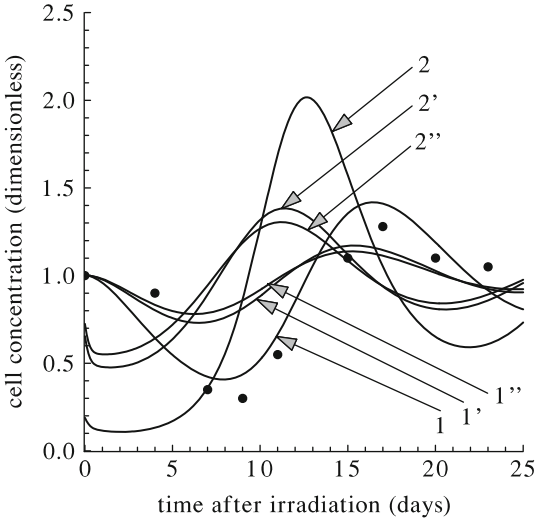

Fig. 2.1 The modeling results on the dynamics of the dimensionless concentrations of blood thrombocytes (X_3 cells) and their undamaged bone marrow precursor cells capable of dividing (X_1^{ud} cells) in rodents (*mice*) exposed to uniform acute irradiation with the dose of 4 Gy (*curves 1 and 2*) and in mice exposed to two non-uniform acute exposures with the averaged doses of 4 Gy, at which the doses of irradiation of 4 equal parts of the hematopoietic tissue are equal to 0.25, 0.25, 0.5, 15.0 Gy (*curves 1' and 2'*) and to 0.0625, 0.0625, 0.125, 15.75 Gy (*curves 1" and 2"*). The experimental data [9] are given by mean values of concentration of blood thrombocytes in mice after uniform acute irradiation with the dose of 4 Gy (*circles*)

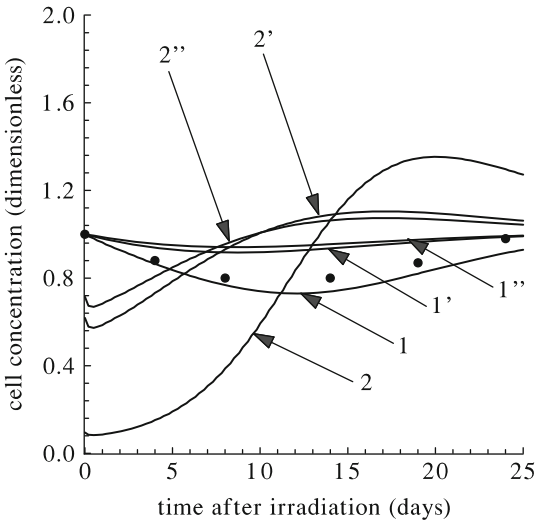

Fig. 2.2 The modeling results on the dynamics of the dimensionless concentrations of blood erythrocytes (X_3 cells) and their undamaged bone marrow precursor cells capable of dividing (X_1^{ud} cells) in rodents (*rats*) exposed to uniform acute irradiation with the dose of 4 Gy (*curves 1 and 2*) and in rats exposed to two non-uniform acute exposures with the averaged doses of 4 Gy, at which the doses of irradiation of 4 equal parts of the hematopoietic tissue are equal to 0.25, 0.25, 0.5, 15.0 Gy (*curves 1' and 2'*) and to 0.0625, 0.0625, 0.125, 15.75 Gy (*curves 1" and 2"*). The experimental data [11] are given by mean values of concentration of blood erythrocytes in rats after uniform acute irradiation with the dose of 4 Gy (*circles*)

of uniform acute irradiation. The time intervals required to reach these maximal levels are shorter in the cases of non-uniform acute exposures than those in the case of uniform acute irradiation. Further, the concentrations of X_3 cells and of X_1^{ud} cells decrease again and, after damped oscillations, return to their normal values in shorter time intervals after non-uniform acute exposures than after uniform one, as computations show. It is important to emphasize that, as it follows from Fig. 2.1, the modeling results on the dynamics of the concentration of X_3 cells after uniform acute irradiation agree with the respective experimental data [9] on the kinetics of the concentration of thrombocytes in mice.

Figure 2.2 displays the modeling dynamics of concentrations of blood erythrocytes (X_3 cells) and their undamaged bone marrow precursor cells capable of dividing (X_1^{ud} cells) in the erythropoietic system after uniform acute irradiation and after two non-uniform acute radiation exposures with the equal values of their whole-body doses. Figure 2.2 shows that the concentration of X_1^{ud} cells decreases and approaches its minimal level, which is higher in the case of non-uniform acute exposure than that in the case of uniform acute irradiation. The time interval required to reach this minimal level is slightly shorter in the case of non-uniform acute exposure than that in the case of uniform acute irradiation. Then the concentration of X_1^{ud} cells increases and achieves its maximal value, which is smaller in the case

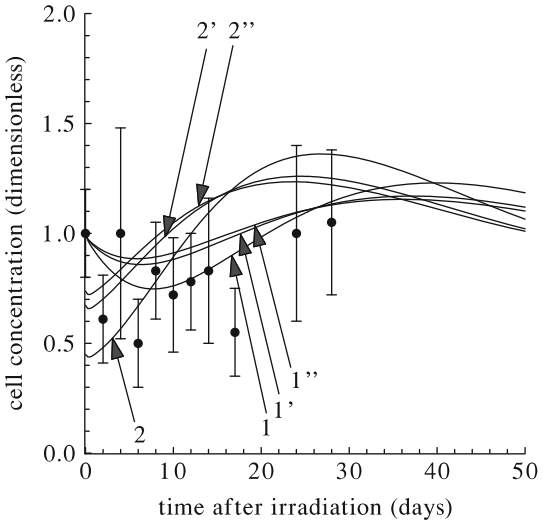

Fig. 2.3 The modeling results on the dynamics of the dimensionless concentrations of blood granulocytes (X_3 cells) and their undamaged bone marrow precursor cells capable of dividing (X_1^{ud} cells) in rodents (*rats*) exposed to uniform acute irradiation with the dose of 2 Gy (*curves 1 and 2*) and in rats exposed to two non-uniform acute exposures with the averaged doses of 2 Gy, at which the doses of irradiation of 4 equal parts of the hematopoietic tissue are equal to 0.25, 0.25, 0.5, 7.0 Gy (*curves 1' and 2'*) and to 0.0625, 0.0625, 0.125, 7.75 Gy (*curves 1" and 2"*). The experimental data [11] are given by mean values of dimensionless concentration of blood neutrophilic granulocytes (*circles*) and by mean square deviations from these mean values in rats after uniform acute irradiation with the dose of 2 Gy

of non-uniform exposure than that in the case of uniform acute irradiation. The time interval required to reach this maximal level is shorter in the case of non-uniform acute exposure than that in the case of uniform acute irradiation. Further, the concentration of X_1^{ud} cells decreases again and, after overdamped oscillations, returns to its normal value in shorter time interval after non-uniform acute irradiation than after uniform one, as computations show. Figure 2.2 also demonstrates that the concentration of X_3 cells decreases and approaches its minimal level, which is higher in the case of non-uniform acute exposure than that in the case of uniform acute irradiation. The time interval required to reach this minimal level is slightly shorter in the case of non-uniform acute exposure than that in the case of uniform acute irradiation. Then the concentration of X_3 cells increases and returns, aperiodically, to the normal level in shorter time interval after non-uniform acute exposure than after uniform one, as computations show. It is important to outline that, as it follows from Fig. 2.2, the modeling results on the dynamics of the concentration of X_3 cells after uniform acute irradiation agree with the respective experimental data [11] on the kinetics of the concentration of erythrocytes in rats.

Figure 2.3 presents the modeling dynamics of concentrations of blood granulocytes (X_3 cells) and their undamaged bone marrow precursor cells capable of

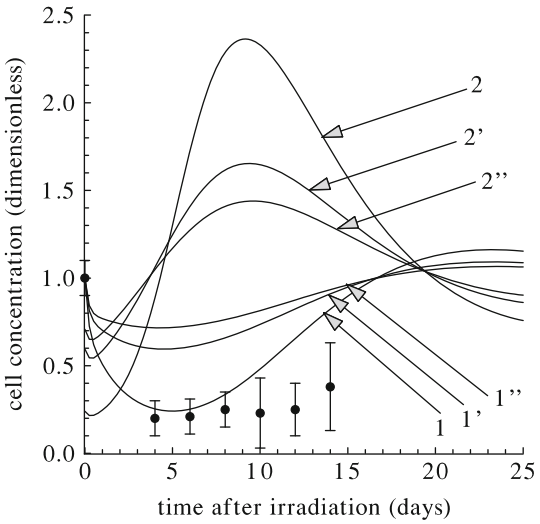

Fig. 2.4 The modeling results on the dynamics of the dimensionless concentrations of blood lymphocytes (X_3 cells) and their undamaged bone marrow precursor cells capable of dividing (X_1^{ud} cells) in rodents (*rats*) exposed to uniform acute irradiation with the dose of 2 Gy (*curves 1 and 2*) and in rats exposed to two non-uniform acute exposures with the averaged doses of 2 Gy, at which the doses of irradiation of 4 equal parts of the hematopoietic tissue are equal to 0.25, 0.25, 0.5, 7.0 Gy (*curves 1' and 2'*) and to 0.0625, 0.0625, 0.125, 7.75 Gy (*curves 1" and 2"*). The experimental data [11] are given by mean values of dimensionless concentration of blood lymphocytes (*circles*) and by mean square deviations from these mean values in rats after uniform acute irradiation with the dose of 2 Gy

dividing (X_1^{ud} cells) in the granulopoietic system after uniform acute irradiation and after two non-uniform acute radiation exposures with the equal values of their whole-body doses. As one can see, the concentrations of X_3 cells and of X_1^{ud} cells decrease and approach their minimal levels, which are higher in the cases of non-uniform exposures than those in the case of uniform acute irradiation. The time intervals required to reach these minimal levels are slightly shorter in the cases of non-uniform acute exposures than those in the case of uniform acute irradiation. Then the concentrations of X_3 cells and of X_1^{ud} cells increase and achieve their maximal values, which are smaller in the cases of non-uniform acute exposures than those in the case of uniform acute irradiation. The time intervals required to reach these maximal levels are shorter in the cases of non-uniform acute exposures than those in the case of uniform acute irradiation. Further, the concentrations of X_3 cells and of X_1^{ud} cells decrease again and, after damped oscillations, return to their normal values in shorter time intervals after non-uniform acute exposures than after uniform one, as computations show. It is important to underscore that, as it follows from Fig. 2.3, the modeling results on the dynamics of the concentration of X_3 cells after uniform acute irradiation agree with the respective experimental data [11] on the kinetics of the concentration of granulocytes in rats.

Figure 2.4 displays the modeling dynamics of concentrations of blood lymphocytes (X_3 cells) and their undamaged bone marrow precursor cells capable of dividing (X_1^{ud} cells) in the lymphopoietic system after uniform acute irradiation and after two non-uniform acute radiation exposures with the equal values of their whole-body doses. As one can infer from this figure, the concentrations of X_3 cells and of X_1^{ud} cells decrease and approach their minimal levels, which are higher in the cases of non-uniform acute exposures than those in the case of uniform acute irradiation. The time intervals required to reach these minimal levels are slightly shorter in the cases of non-uniform acute exposures than those in the case of uniform acute irradiation. Then the concentrations of X_3 cells and of X_1^{ud} cells increase and achieve their maximal values, which are smaller in the cases of non-uniform acute exposures than those in the case of uniform acute irradiation. The time intervals required to reach these maximal levels are slightly shorter in the cases of non-uniform acute exposures than those in the case of uniform acute irradiation. Further, the concentrations of X_3 cells and of X_1^{ud} cells decrease again and, after damped oscillations, return to their normal values in shorter time intervals after non-uniform acute exposures than after uniform one, as computations show. It is important to note that, as it follows from Fig. 2.4, the modeling results on the dynamics of the concentration of X_3 cells after uniform acute irradiation agree with the respective experimental data [11] on the kinetics of the concentration of lymphocytes in rats.

The analysis of the modeling results presented in Figs. 2.1, 2.2, 2.3, and 2.4 allows one to reveal the following. The modeling dynamics of the concentrations of X_3 cells and X_1^{ud} cells in the systems on hand after non-uniform and uniform acute irradiation have the similar character. However, there are quantitative distinctions between them, these distinctions being more significant in the case of more pronounced non-uniformity of acute irradiation. Specifically, the minimal levels, up to which the concentrations of X_3 cells and X_1^{ud} cells in each considered major hematopoietic lineage decrease after non-uniform acute irradiation, are higher than those after uniform acute irradiation at equal values of whole-body doses of these exposures. The differences between these levels are more valuable in the case of more pronounced non-uniformity of acute irradiation. In turn, as computations show, the concentrations of X_3 cells and X_1^{ud} cells in the major hematopoietic lineages reach their normal levels faster after non-uniform acute irradiation than those after uniform acute exposure at equal values of whole-body doses of these exposures. The time intervals required to reach their normal levels are shorter in the case of more pronounced non-uniformity of acute irradiation. Thus, the developed models of the major hematopoietic lineages predict the smaller depletion of pools of functional blood cells and their bone marrow precursor cells capable of dividing in the major hematopoietic lineages of rodent and the faster recovering of the pools of these cells after non-uniform acute irradiation than those after uniform acute irradiation at the same whole-body doses of such exposures. These modeling findings conform with experimental observation [12].

The juxtaposition of the modeling results on the dynamics of concentrations of functional blood cells (X_3 cells) and their undamaged bone marrow precursor cells capable of dividing (X_1^{ud} cells) in the major hematopoietic lineages after uniform

and non-uniform acute irradiation at the same whole-body doses of these exposures elucidates the following feature. The levels, up to which the concentrations of functional blood cells (X_3 cells) decrease, are higher and the time intervals needed for returning of these concentrations to their normal levels are shorter, if the concentrations of their bone marrow precursor cells capable of dividing, which are left undamaged after acute irradiation (X_1^{ud} cells), are higher (Figs. 2.1, 2.2, 2.3, and 2.4). In turn, the concentrations of the bone marrow precursor cells capable of dividing (X_1 cells), which are left undamaged after non-uniform acute irradiation are higher in comparison with those, which are left undamaged after uniform acute irradiation Figs. 2.1, 2.2, 2.3, and 2.4.

These modeling findings allow one to reveal the reason–consequence relationships, which are resulted in observed distinctions in the responses of the major hematopoietic lineages to non-uniform and uniform acute irradiation at the same whole-body doses of such exposures. Specifically, the less pronounced depletions of the pools of the functional blood cells (X_3 cells) and the faster recovery of these cell pools in the major hematopoietic lineages after non-uniform acute irradiation to compare with those after uniform acute irradiation (at the same whole-body doses of such exposures) are due to the higher levels of concentrations of the bone marrow precursor cells capable of dividing (X_1 cells), which are left undamaged after non-uniform acute irradiation, in comparison with those, which are left undamaged after uniform acute irradiation. Taking into account that the compartment of X_1 cells includes stem cells and their committed progenies capable of dividing, the obtained modeling results testify to the principal role of these cells in the process of damage and recovery in the major hematopoietic lineages after non-uniform and uniform acute irradiation, as well as elucidate the role of these cells in weakening the hematopoietic subsyndrome of acute radiation syndrome under non-uniform acute irradiation. Additionally, the modeling results attest to the inefficiency of the employment, for the prognostic purposes, of the whole-body dose D of non-uniform acute irradiation.

2.4 Distinctive Features of Responses of Major Hematopoietic Lineages to Partial and Uniform Acute Irradiation

The models of the major hematopoietic lineages (the thrombopoietic, erythropoietic, granulopoietic, and lymphopoietic systems) are used to compare, in detail, the responses of these systems to uniform acute irradiation and to partial acute irradiation. The latter is a particular case of non-uniform acute irradiation (one part of the body is shielded and the other one is unshielded). Therefore the number k of parts of the hematopoietic tissue exposed to different doses of acute irradiation is taken to be equal to two in the models on hand.

In these series of modeling simulations, the doses of irradiation of shielded and unshielded parts of the hematopoietic tissue, D_1 and D_2, are fixed, the dose D_1 being substantially lower than the dose D_2. The variation of the degree of non-uniformity of partial acute irradiation is simulated by the variation of the fraction Ω_2 of the mass of unshielded part of the hematopoietic tissue, the fraction Ω_1 of the mass of shielded part of the hematopoietic tissue being equal to $(1 - \Omega_2)$. To compare effectively the responses of the major hematopoietic lineages to uniform acute irradiation and to non-uniform (partial) acute irradiation, the dose D of uniform acute irradiation is taken to be equal to the averaged dose (i.e., the whole-body dose) of partial acute irradiation:

$$D = D_1(1 - \Omega_2) + D_2\Omega_2. \tag{2.36}$$

In the framework of the models, the minimal levels and the first-day levels of concentrations of blood cells in the major hematopoietic lineages after partial acute irradiation and after the respective uniform acute irradiation are computed at fixed values of doses D_1 and D_2 and at various values of the parameter Ω_2 ($0 \leq \Omega_2 \leq 1$), i.e., at various values of the whole-body dose D of partial acute irradiation and at the respective values of the dose of uniform acute irradiation D [Eq. 2.36]. The obtained modeling results are presented in Figs. 2.5, 2.6, 2.7, and 2.8.

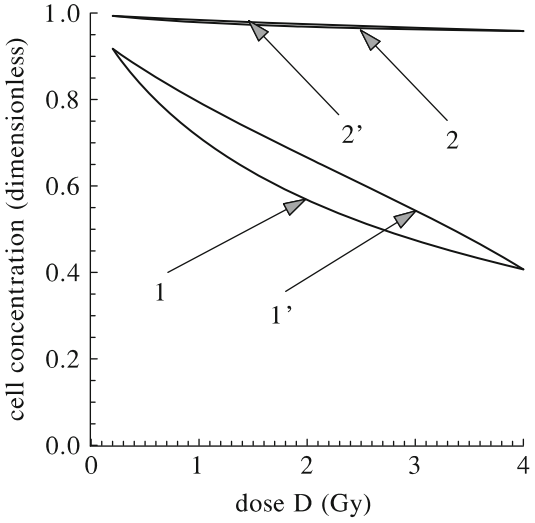

Fig. 2.5 The minimal levels and the first-day levels of the dimensionless concentration of blood thrombocytes (X_3 cells) in rodents (*mice*) after partial acute irradiation with various averaged doses D (*curves 1' and 2'*, respectively) and in mice after uniform acute irradiation with the same doses D (*curves 1 and 2*, respectively). Modeling results are computed at the fixed doses of irradiation of shielded and unshielded parts of the hematopoietic tissue (0.55 Gy and 11 Gy, respectively) and at various values of the parameter Ω_2, which specifies the fraction of the mass of unshielded hematopoietic tissue

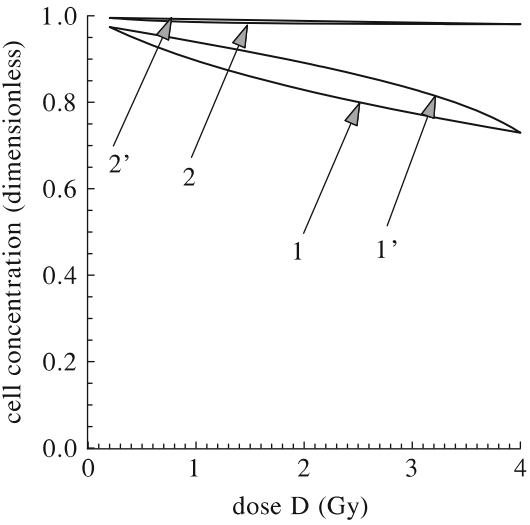

Fig. 2.6 The minimal levels and the first-day levels of the dimensionless concentration of blood erythrocytes (X_3 cells) in rodents (*rats*) after partial acute irradiation with various averaged doses D (*curves 1' and 2'*, respectively) and in rats after uniform acute irradiation with the same doses D (*curves 1 and 2*, respectively). Modeling results are computed at the fixed doses of irradiation of shielded and unshielded parts of the hematopoietic tissue (0.55 Gy and 11 Gy, respectively) and at various values of the parameter Ω_2, which specifies the fraction of the mass of unshielded hematopoietic tissue

As it follows from Figs. 2.5, 2.6, 2.7, and 2.8, the minimal levels and the first-day levels of concentrations of blood cells in the major hematopoietic lineages after partial acute irradiation and after the respective uniform acute irradiation are lower when the value of D is higher, i.e., when the parameter Ω_2 is larger. These modeling findings conform with experimental observations [13].

At fixed values of D, i.e., at fixed values of the parameter Ω_2 from the range $(0 < \Omega_2 < 1)$, the minimal levels of concentrations of the blood cells in the major hematopoietic lineages after partial acute irradiation are higher than those after uniform acute irradiation. In turn, at fixed values of D, i.e., at fixed values of the parameter Ω_2 from the range $(0 < \Omega_2 < 1)$, the first-day levels of concentrations of the blood cells in the thrombopoietic, erythropoietic, and granulopoietic systems after partial acute irradiation are slightly higher than those after uniform acute irradiation (Figs. 2.5, 2.6, and 2.7), whereas the first-day level of concentration of the blood lymphocytes in the lymphopoietic system after partial acute irradiation is considerably higher than that after uniform acute irradiation (Fig. 2.8). Obviously, in the case of the absence of shielding ($\Omega_2 = 1$) and in the case of the whole-body shielding ($\Omega_2 = 0$), these indices become equal to each other.

The obtained modeling results demonstrate that the lymphopoietic system is the most susceptible major hematopoietic lineage to both non-uniform (partial) acute irradiation and to uniform acute irradiation. Additionally, the differences

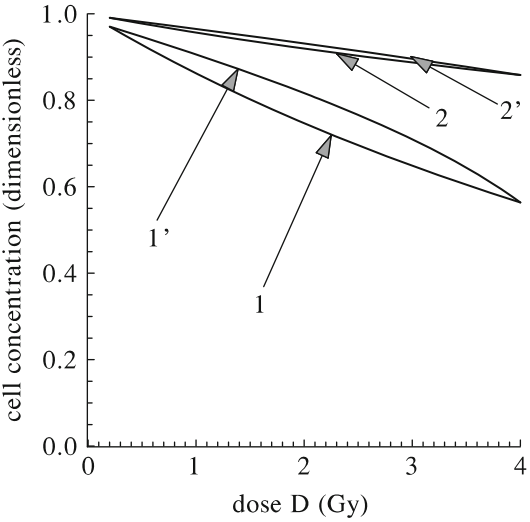

Fig. 2.7 The minimal levels and the first-day levels of the dimensionless concentration of blood granulocytes (X_3 cells) in rodents (*rats*) after partial acute irradiation with various averaged doses D (*curves 1' and 2'*, respectively) and in rats after uniform acute irradiation with the same doses D (*curves 1 and 2*, respectively). Modeling results are computed at the fixed doses of irradiation of shielded and unshielded parts of the hematopoietic tissue (0.55 Gy and 11 Gy, respectively) and at various values of the parameter Ω_2, which specifies the fraction of the mass of unshielded hematopoietic tissue

between the minimal levels of the concentration of blood cells in this major hematopoietic lineage and even between the first-day levels of concentration of these cells after non-uniform (partial) acute irradiation and after uniform acute irradiation (at the same whole-body doses of such exposures) are the most pronounced in the lymphopoietic system in comparison with those in the other major hematopoietic lineages. These modeling findings testify to the efficiency of the use of the first-day level of concentration of blood lymphocytes for the early predicting of the development of the lymphocytopenia after non-uniform (partial) acute irradiation.

2.5 Prognostic Importance of Lymphocytopenia After Partial Acute Irradiation

Partial acute irradiation is employed in the treatment of some form of cancer. The increase of the whole-body radiation dose received by patients in the course of such treatment can lead to the development of harmful reactions [14]. One of them is the development of leukopenia, which is the result of the development of granulocytopenia and/or lymphocytopenia. The former is characterized by the decrease of concentration of blood granulocytes up to dangerous levels, whereas

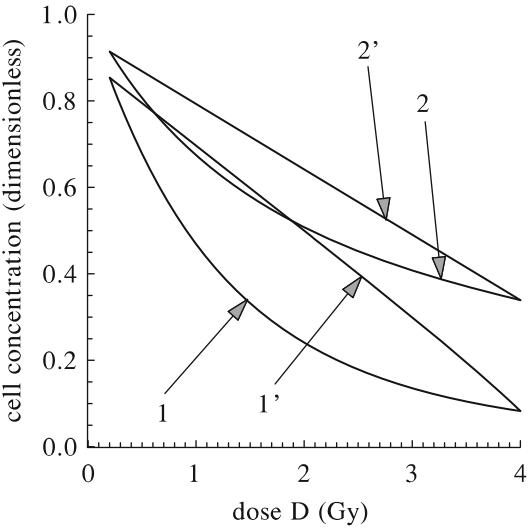

Fig. 2.8 The minimal levels and the first-day levels of the dimensionless concentration of blood lymphocytes (X_3 cells) in rodents (*rats*) after partial acute irradiation with various averaged doses D (*curves 1' and 2'*, respectively) and in rats after uniform acute irradiation with the same doses D (*curves 1 and 2*, respectively). Modeling results are computed at the fixed doses of irradiation of shielded and unshielded parts of the hematopoietic tissue (0.55 Gy and 11 Gy, respectively) and at various values of the parameter Ω_2, which specifies the fraction of the mass of unshielded hematopoietic tissue

the latter is characterized by the decrease of concentration of blood lymphocytes up to dangerous levels. The development of the leukopenia serves an indicator for the interruption of treatment. Therefore there is no doubt in a great practical significance of the prediction of the development of leukopenia after partial acute irradiation.

Interesting results of the experimental studies of peculiarities of radiation injury of two major hematopoietic lineages (the granulopoietic and lymphopoietic systems) after partial acute irradiation are presented in [14]. That work was devoted to the investigation of the early responses of these systems to partial acute irradiation, as well as to uniform acute irradiation. In the experiment, rodents (mice) were exposed to uniform acute gamma-irradiation and to three types of partial acute gamma-irradiation. In the case of uniform acute irradiation, the mass of unshielded part of the hematopoietic tissue was 100 % of its total mass, that corresponds to the parameter Ω_2 of 1.0 in the developed models. In the first case of partial acute irradiation, the mass of unshielded part of the hematopoietic tissue was 85 % of its total mass [14], that corresponds to the parameter Ω_2 of 0.85. In the second case of partial acute irradiation, when the front part of the body was exposed without shielding, the mass of unshielded part of the hematopoietic tissue was 54 % of its total mass [14], that corresponds to the parameter Ω_2 of 0.54. In the third case of partial acute irradiation, when the back part of the body was exposed without shielding, the mass of unshielded part of the hematopoietic tissue was 31 % of its

total mass [14], that corresponds to the parameter Ω_2 of 0.31. In [14], the dose D_2 of irradiation of unshielded part of the body was equal to 11 Gy, whereas the dose D_1 of irradiation of shielded part of the body was equal to 0.55 Gy. In experiments [14], the first-day levels of concentrations of functional blood cells in the granulopoietic and lymphopoietic systems in mice after the acute exposures listed above were examined.

The experimental data presented in [14] are used to verify the capability of the developed models of the granulopoietic and lymphopoietic systems to predict the first-day levels of concentrations of functional blood cells in these systems after partial acute exposures. For this purpose, the dynamics of the granulopoietic and lymphopoietic systems are computed in the framework of the developed models of these systems at the values of irradiation doses D_1 and D_2 of shielded and unshielded parts of an animal body, which were reported in [14], whereas the parameter Ω_2 is varied in the range ($0 \leq \Omega_2 \leq 1$).

As it follows from the obtained modeling results, the first-day levels of the dimensionless concentration of blood granulocytes after partial acute exposures and after uniform acute irradiation are equal to 0.9728, 0.9618, 0.9471, and 0.9400, when the values of parameter Ω_2 are taken the same as those in experiments [14], namely 0.31, 0.54, 0.85, and 1.00, i.e., when the values of parameter D [Eq. (2.36)] are equal to 3.79 Gy, 6.19 Gy, 9.43 Gy, and 11.00 Gy, respectively. The obtained modeling results imply that the first-day levels of blood granulocyte concentration 1 day after the considered exposures are close enough to the norm. These modeling predictions are consistent with experimental observations [14].

Figure 2.9 shows the first-day levels of the concentration of blood lymphocytes in the lymphopoietic system in mice after partial acute irradiation and after uniform acute irradiation, which are computed at the aforementioned values of doses D_1 and D_2 and at the values of parameter Ω_2 varied from zero to unity. Note that the case of $\Omega_2 = 0$ corresponds to uniform acute irradiation with the dose D_1, whereas the case of $\Omega_2 = 1$ corresponds to uniform acute irradiation with the dose D_2. Figure 2.9 also displays the experimental data [14] on the concentration of blood lymphocytes measured 1 day after four types of radiation exposure specified above.

As it follows from the modeling results, the first-day levels of the dimensionless concentration of blood lymphocytes after partial acute exposures and after uniform irradiation are equal to 0.583, 0.426, 0.216, and 0.114, when the values of parameter Ω_2 are equal to 0.31, 0.54, 0.85, and 1.00, i.e., when the values of parameter D are equal to 3.79 Gy, 6.19 Gy, 9.43 Gy, and 11.00 Gy, respectively. The corresponding experimental values of the first-day levels of the dimensionless concentration of blood lymphocytes are equal to 0.57 ± 0.13, 0.37 ± 0.13, 0.14 ± 0.10, and 0.12 ± 0.06 [14]. Thus, the modeling results are in a good agreement with those experimental data. The obtained agreement between modeling predictions and the respective experimental data [14] testifies to the capability of the lymphopoiesis model of predicting the first-day level of blood lymphocyte concentration after partial acute irradiation. In turn, this level can be used in the early prediction of the development lymphocytopenia after such radiation exposures.

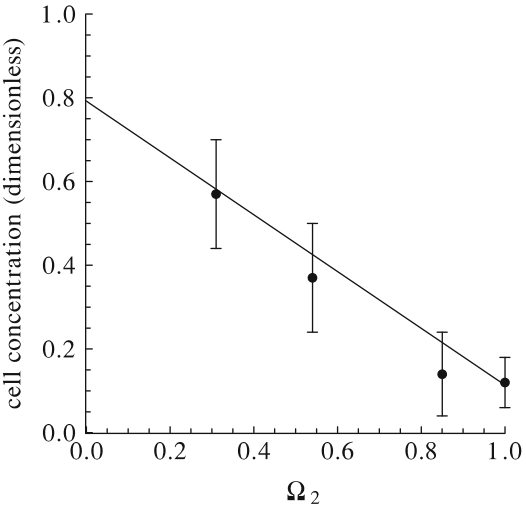

Fig. 2.9 The dependence of the first-day level of the dimensionless concentration of blood lymphocytes (X_3 cells) in rats after partial acute irradiation on the parameter Ω_2, which specifies the fraction of the mass of unshielded hematopoietic tissue. The modeling results (*curve*) are computed at $0 \leq \Omega_2 \leq 1$ and at the fixed doses of irradiation of shielded and unshielded parts of the hematopoietic tissue (0.55 Gy and 11 Gy, respectively). The relevant experimental data [14] are given by mean values of dimensionless concentration of blood lymphocytes (*circles*) in the aforementioned time moment and by mean square deviations from these mean values

2.6 Conclusions

Biologically motivated mathematical models of the dynamics of the major hematopoietic lineages (the thrombopoietic, erythropoietic, granulopoietic, and lymphopoietic systems) in mammals (rodents) exposed to non-uniform acute irradiation are developed and thoroughly investigated. These models are based on the mathematical models, which are capable of predicting the dynamics of these systems in mammals (rodents) exposed to uniform acute irradiation in a wide dose range (see Chap. 1).

The developed models account for the principal stages of development of hematopoietic cells. They also consider the general and specific regulatory mechanisms in the major hematopoietic lineages. The models are the systems of nonlinear ordinary differential equations, whose variables and constant parameters have clear biological meaning. A new element of these models is the consideration of non-uniform acute irradiation of the hematopoietic tissue as a composition of a certain number of uniform acute irradiations of its parts. The variable parameters of the models are the number of considered parts of the hematopoietic tissue, the fractions of masses of the considered parts of the hematopoietic tissue, and the doses of acute irradiation, which these parts of the hematopoietic tissue are exposed to.

The developed models are employed to compare the dynamics of the major hematopoietic lineages (the thrombopoietic, erythropoietic, granulopoietic, and lymphopoietic systems) in mammals (rats, mice) after non-uniform and uniform acute irradiation. It is found that the models reproduce the experimentally observed smaller depletion of the major hematopoietic lineages and their faster recovering after non-uniform acute irradiation than those after uniform acute irradiation at the same whole-body doses of these exposures. The obtained modeling results imply that the lesser injury and the faster recovery of the major hematopoietic lineages after non-uniform acute irradiation than those after uniform acute irradiation at the same whole-body doses of these exposures are due to higher levels of concentrations of the undamaged bone marrow precursor cells capable of dividing (X_1^{ud} cells) left in these systems after non-uniform acute irradiation than those after uniform acute irradiation. Taking into account that the compartment of X_1^{ud} cells includes undamaged stem cells and their undamaged committed progenies capable of dividing, the obtained modeling findings testify to the principal role of these cells in the processes running in the major hematopoietic lineages after non-uniform and uniform acute irradiation. Additionally, the modeling findings testify to inefficiency of the employment, for the prognostic purposes, of the whole-body dose D of partial acute irradiation.

The developed models are also used to study, in detail, the dynamics of the major hematopoietic lineages in mammals (rats, mice) after uniform acute irradiation and after partial acute irradiation, at which one part of the body and, hence, of the hematopoietic tissue is shielded and an other one is not shielded. In the framework of the models, the minimal levels and the first-day levels of concentrations of blood cells in the major hematopoietic lineages after partial acute irradiation and after uniform acute irradiation with equal values of the whole-body doses are computed, the doses of shielded and unshielded parts of the hematopoietic tissue being fixed and the fraction of mass of unshielded part being varied from zero to unity. It is revealed that the models provide the description of a deeper postirradiation injury of the major hematopoietic lineages in the rodents exposed to partial acute irradiation, when the mass of unshielded part of the hematopoietic tissue is larger, i.e., when the whole-body dose of partial acute irradiation is higher. The models also provide the description of a deeper postirradiation injury of the major hematopoietic lineages in the rodents exposed to uniform acute irradiation, when the dose of such exposure is higher. The modeling results also demonstrate that the lymphopoietic system is the most susceptible major hematopoietic lineage to both uniform and non-uniform (partial) acute irradiation.

Additionally, the models predict lesser depletions of the hematopoietic lineages after partial acute irradiation than those after uniform acute irradiation at equal whole-body doses of such exposures. Distinctions between the minimal levels and even between the first-day levels of the concentrations of the functional blood cells in the major hematopoietic lineages after partial acute irradiation and after uniform acute irradiation at the same whole-body doses of such exposures are the most pronounced in the lymphopoietic system. In other words, the lymphopoietic system is the most susceptible major hematopoietic lineage to the non-uniformity of acute

irradiation. Moreover, the modeling finings testify to the efficiency of the use of the first-day level of concentration of blood lymphocytes for the early predicting of the development of the lymphocytopenia after partial acute irradiation.

The developed models of the lymphopoietic and granulopoietic systems are used to simulate the responses of these major hematopoietic lineages to non-uniform (partial) acute irradiation and to uniform acute irradiation reported in [14]. The experimental work [14] was devoted to the investigation of early responses of the lymphopoietic and granulopoietic systems in rodents (mice) to uniform acute gamma-irradiation and to three types of partial acute gamma-irradiation. It is found that the first-day levels of the blood granulocyte concentration after the aforementioned exposures, which were predicted by granulopoiesis model, slightly deviate from its normal level, that conforms with experimental observation [14]. In turn, the first-day levels of the blood lymphocyte concentration after the aforementioned exposures, which were predicted by lymphopoiesis model, strongly deviate from its normal level. The modeling results are in a very good agreement with experimental data. The obtained agreement between modeling predictions and experimental data [14] testifies to the capability of the lymphopoiesis model of predicting the first-day level of blood lymphocyte concentration after partial acute irradiation. In turn, this level can be used in the early prediction of the development of the lymphocytopenia after partial acute irradiation.

The obtained modeling results bear witness to the validity of employment of the developed models of the major hematopoietic lineages in studies and predictions of the effects of non-uniform acute irradiation, including partial acute irradiation, on these systems in rodents (rats, mice), as well as in planning new experiments.

It is worthwhile to note that the employment of the developed mathematical model is limited to the modeling studies of the effects of non-uniform acute irradiation on the major hematopoietic lineages in rodents (mice, rats). At the same time, the proposed approach, which was successfully used to develop the models capable of describing the effects of non-uniform acute irradiation on the dynamics of the major hematopoietic lineages in rodents, can also be used to develop the mathematical models, which describe the effects of non-uniform acute irradiation on the dynamics of these systems in humans. In this case, the recently developed mathematical models (see Chap. 7, as well as [15–20]), which describe the effects of uniform acute/chronic irradiation on the dynamics of the major hematopoietic lineages in humans, form a basis of this approach. The models of the dynamics of the major hematopoietic lineages in humans exposed to non-uniform acute irradiation could be applied to predict the radiation injury of the hematopoietic system in individuals underwent to non-uniform acute exposures in radiation incidents and radiation accidents, as well as in the course of radiotherapy. Such modeling results would provide a better understanding of the risks to health from non-uniform irradiation and could help to elaborate an appropriate methods of their treatment. These models could also be helpful in the assessment of the radiation risks for the health of astronauts in cases of their exposures to non-uniform irradiation caused by solar particle events and in the development of operational countermeasures for them in long-term space missions.

References

1. Martin A., Harbison S, Beach K., Cole P. An introduction to radiation protection. Sixth edition, Boca Raton: CRC Press, Taylor & Francis Group, 2012.
2. Smirnova O.A. Comparative modeling analysis of the hematopoiesis dynamics in mammals exposed to nonuniform and uniform acute irradiation. Health Physics, v. 109(3), pp. 218–232, 2015.
3. Smirnova OA. Radiation and organism of mammals: Modeling approach. Moscow-Izhevsk: Scientific-Publishing Centre Regular and Chaotic Dynamics: 2006 (In Russian).
4. Smirnova O.A. Effects of low-level chronic irradiation on the radiosensitivity of mammals: Modeling studies. Advances in Space Research, v. 40, pp. 1408–1413, 2007.
5. Smirnova OA. Blood and small intestine cell kinetics under radiation exposures: Mathematical modeling. Advances in Space Research, v. 44, pp. 1457–1469, 2009.
6. Smirnova O.A., Yonezawa M. Radioprotection effect of low level preirradiation on mammals: modeling and experimental investigations. Health Physics, v. 85, pp. 150–158, 2003.
7. Smirnova O.A., Yonezawa M. Radioresistance in mammals induced by low-level chronic irradiation: modeling and experimental investigations. Health Physics, v. 87, pp. 366–374, 2004.
8. Smirnova O.A., Yonezawa M. Effects of chronic low-level irradiation on radiosensitivity of mammals: Modeling and experimental studies. In: Cigna A.A., Durante M., eds. Radiation Risk Estimates in Normal and Emergency Situations. Proceedings of the NATO Advanced Research Workshop on Impact of Radiation Risk Estimates in Normal and Emergency Situations (Yerevan, Armenia, 2005). NATO Security through Science Series B: Physics and Biophysics, Vol. 9. Dordrecht, The Netherlands: Springer; 2006: pp. 291–301.
9. Bond V.P., Fliendner T.M., Archambeau J.O. Mammalian Radiation Lethality: A Disturbance in Cellular Kinetics. New York: Academic Press, 1965.
10. Lea D.E. Action of Radiation on Living Cells, 2nd edn. Cambridge: The Syndics of the Cambridge University Press, 1955.
11. Hulse E.V. Lymphocytic recovery after irradiation and its relation to other aspects of haemopoiesis. British Journal of Haematology, v. 9, pp. 376–384, 1963.
12. Avetisov G.M., Darenskaya N.G., Nelyubov A.A. An influence of the distribution of an absorbed dose to biological effect. In: Darenskaya N.G., ed. Biological effects of non-uniform radiation exposures. Moscow: Atomizdat, 1974 (In Russian)
13. Ilyinsky D.A., Vishnevsky L.V., Sokolova E.N., Pozharsskya G.D., Nezdatny M.M. Peculiarities of time-course and pathogenetic structures of radiation injuries under non-uniform exposures. In: Darenskaya NG, ed. Biological effects of non-uniform radiation exposures. Moscow: Atomizdat, 1974 (In Russian)
14. Yarmonenko S.P., Revelskaya T.A., Redkina E.N. About the nature and prognostic significance of leukopenia under partial irradiation. In: Darenskaya N.G., ed. Biological effects of non-uniform radiation exposures. Moscow: Atomizdat, 1974 (In Russian)
15. Smirnova O.A. Modeling study of radiation effects on thrombocytopoietic and granulocytopoietic systems in humans. Advances in Space Research, v. 48, pp. 184–198, 2011.
16. Smirnova O.A. Comparative analysis of the dynamics of thrombocytopoietic, granulocytopoietic, and erythropoietic systems in irradiated humans: a modeling approach. Health Physics, v. 103(6), pp. 787–801, 2012.
17. Smirnova O.A. Modeling Analysis of the dynamics of thrombocytopoietic, granulocytopoietic, and erythropoietic systems in irradiated humans. Journal of Radiation Research, v. 55, p. i36, 2014.
18. Smirnova O.A., Hu S., Cucinotta F.A. Analysis of the lymphocytopoiesis dynamics in nonirradiated and irradiated humans: a modeling approach. Radiation Research, v. 181, pp. 240–250, 2014.

19. Smirnova O.A., Akleyev A.V., Dimov G.P. Analysis of hematopoiesis dynamics in residents of Techa riverside villages chronically exposed to nonuniform radiation: modeling approach. Health Physics, v. 106, pp. 445–458, 2014.
20. Smirnova O.A., Akleyev A.V., Dimov G.P. Modeling analysis of the lymphocytopoiesis dynamics in chronically irradiated residents of Techa riverside villages. Radiation and Environmental Biophysics, v. 53, pp. 515–523, 2014.

Chapter 3
The Small Intestine as a Target for Radiation

3.1 Introduction

The function of the alimentary canal in mammalian organisms is of vital importance [1]. This system comprises the oral cavity, gullet, esophagus, stomach, small intestine, large intestine, and rectum. The damage to the alimentary canal in mammals exposed to high-level irradiation is a major contributor to the pathogenesis of acute radiation sickness [2–8]. The main clinical symptoms of the gastrointestinal subsyndrome of the acute radiation syndrome are anorexia, diarrhea, and dehydration. Death of mammals occurs in 3–6 days. Anatomic studies show that the characteristic symptoms of the gastrointestinal subsyndrome of the acute radiation syndrome and the following death of exposed mammals are basically due to damage to the small intestine. Whereas in the oral cavity, gullet, esophagus, stomach, large intestine, and rectum, only isolated ulcers and erosions are usually observed, the mucus membrane of the small intestine appears to be damaged completely. Therefore, damage to the small intestinal epithelium system (SIES), one of the critical body systems, is important in determining the effects of high-level irradiation on mammals. In these studies, the employment of the mathematical models of SIES can prove to be useful, especially in view of the limited applicability of clinical methods in the investigation of such radiation effects in human.

The primary objectives of our studies [9–15] were to develop and investigate the mathematical models, which describe the dynamics of the small intestinal epithelium system in mammals unexposed and exposed to acute and chronic irradiation. The models were required to account for the principal regulatory mechanisms of this system and to include explicitly the characteristics of ionizing radiation and the basic kinetic and radiobiological parameters of the small intestinal epithelium. The results of our studies on this subject are presented in this chapter.

O.A. Smirnova, *Environmental Radiation Effects on Mammals*,
DOI 10.1007/978-3-319-45761-1_3

3.2 The Essentials of the Small Intestine

The small intestine consists of the duodenum, jejunum, and ileum [1]. In general, their structures are similar to each other. The external surface is formed by a serous cover, under which the longitudinal and ring layers of the muscular cover are situated. Further, the subepithelial and epithelial covers are gone. The latter consists of a large number of villi and flask-shaped crypts that lie under the villous bottom. The cells of crypts and villi represent the single system of the small intestinal epithelium renewal [1, 16]. Basic (columnar) cells prevail in this system. The numbers of cells of two other types, Paneth cells and goblet cells, do not exceed 5–10 % and 5 %, respectively. One assumes that Paneth cells and goblet cells form two independent systems with specific functions and their own ways of development.

Pedigree cells of the columnar cells in the small intestinal epithelium system are stem cells located in the crypt bottom [16–19]. The stem cells are capable of self-maintaining their population, as well as of differentiating in the direction of proliferating-maturing crypt cells. The latter migrate to the top of the crypt. Close to the villous bottom, they stop to proliferate and form the pool of maturing cells. The mature cells transfer from the crypt to the villous and continue to migrate to the villous top, where they exfoliate into the intestinal lumen. The regulation mechanisms of proliferating the crypt cells have not been studied in detail yet though special substances have been found that are capable of rendering stimulatory [20] and inhibitory [21, 22] effects on the proliferation of the cells under consideration.

3.3 Review of Mathematical Models of the Small Intestinal Epithelium

There are a number of works that deal with modeling the dynamics of the small intestinal epithelium system in nonirradiated mammals (see, e.g., [23–35]) and in mammals exposed to acute irradiation (see, e.g., [36–40]).

Specifically, in the works [23–27], cellular automata models are proposed to describe the intestinal epithelium system. They simulate the behavior of single cells arranged on a two-dimensional rigid lattice with rectangular cell layouts, which is an analog of a single-layered epithelium in a crypt. The models are based on the concept of specialized stem cells undergoing mostly asymmetric self-maintaining cell division. The models also use the so-called pedigree concept according to which the transit cells undergo a predetermined number of divisions with a predetermined cycle time before these cells enter the status of nonproliferating maturation. The models explain a lot of experimental data for the intestinal epithelium being in steady-state homeostasis. These data concern positional changes in mitotic and thymidin labeling indices, migration of the cells from the bottom to the tip of crypts, and generation of Goblet cells in mid-crypt positions.

However, the models [23–27] cannot be used to reproduce the spatial and cell kinetic data on damaging and recovering the intestinal epithelium after irradiation. As noted in [27], this is due to conceptual problems from which these models suffer. The major problem is as follows. In the models, cell division and cell migration are directly coupled. Therefore, it is impossible to reproduce experimentally observed mitotic arrest induced by high-dose irradiation and the subsequent enhanced reproduction of cells in the framework of these models.

To get rid of the above-noted conceptual problems, an interesting approach to modeling the intestinal epithelium system is proposed in [36]. The epithelium is modeled there by a one-dimensional chain of cells that is an analog of the array of cells in a section of the intestinal crypt and villous along the vertical proliferation and migration axis, namely, from the bottom of the crypt to the top of the villous. It is also assumed that cell proliferation is controlled by a growth environment. The latter is introduced in the model as a gradient of a hypothetical growth factor, stimulatory substance, diffusing from the bottom of the crypt to the top. It is assumed that an individual cell can divide if a critical threshold of the growth factor is exceeded. Stochastic elements are used in the model to simulate the cell loss at the villous top and to describe the cell transition from the G_1-phase to the S-phase during a cell cycle. A random element is also used to account for the choice of cells damaged by radiation. Note that the latter can be considered only a simplified description of the radiation effect on the small intestinal epithelium system because only some of the crypt cells are radiosensitive [2]. Additionally, the model does not explicitly include the dependence of the fraction of damaged cells on a radiation dose. All this makes it difficult to investigate in detail the response of the intestinal epithelium system to radiation exposures.

A quasi-phenomenological model of the dynamics of the small intestinal system in acutely irradiated mammals is proposed in [37]. The processes of radiation damage to this system are described by one algebraic equation and two differential equations. The algebraic equation is a sum of several exponents, their arguments being the linear and quadratic functions of time. To simulate the dynamics of the small intestinal epithelium system in mammals exposed to a certain radiation dose, it is necessary to determine the parameters of the algebraic equation again by making use of the respective experimental data. This reduces the predictive power of the model [37].

The model presented in [38] describes the postirradiation dynamics of the small intestinal system in humans. The model represents a system of linear differential equations with a delay argument. However, the model includes a lot of independent parameters. As mentioned in the paper [38], the parameter identification faces certain difficulties due to a very limited number of sets of the respective clinical data. The comparison of the modeling results with clinical observations meets difficulties, too. Therefore, their juxtaposition is performed in [38] by one index only. The latter is the time the functional cell concentration stays below a certain critical value. So the predictive power of this model is not high.

A good agreement with experimental data was obtained in the framework of two simple mathematical models [39, 40] that describe the process of postirradiation

recovery in the small intestine of small laboratory animals (mice). The models are the systems of two nonlinear differential equations with a delay argument. The concentrations of crypt and villous cells are the variables of the models and the radiation dose is the variable parameter therein. Note that these models take into account a simplified mechanism of regulation of the small intestinal epithelium system. In particular, the models do not consider the migration of cells from the bottom of the crypt to the top of the villous.

3.4 Dynamical Model of the Small Intestinal Epithelium in Nonirradiated Mammals

First we develop the dynamical model of the small intestinal epithelium system in nonirradiated mammals. The model is based on current concepts of the structure and functioning of the system of the small intestinal epithelium described in [16–18].

The object of our modeling is a population of basic (columnar) cells of the small intestinal epithelium system. We split the cells under consideration into three groups according to the degree of their maturity and differentiation:

- group X, the crypt cells capable of dividing, from the stem cell to the dividing -maturing cell;
- group Y, maturing crypt cells incapable of dividing;
- group Z, functional villous cells (enterocytes).

In constructing the model, we assume that

1. the dynamics of X cells is determined by the rates of their reproduction and transition to group Y;
2. the dynamics of Y cells is determined by the rate of the arrival of cells from group X and by the rate of their transfer to group Z (i.e., cell displacement from crypt to villous);
3. the dynamics of Z cells is determined by the rate of the arrival of cells from group Y and by the rate of leaving group Z (i.e., cell exfoliation from the villous into the intestinal lumen).

We also suppose that the negative-feedback control of the reproduction rate of X cells is affected by the chalone, the specific inhibitor of cell division, which is a product of the vital activity and decay of these cells and their progeny [21].

The concentrations of X, Y, and Z cells (x, y, and z, respectively) and the concentration of the specific chalone (I) are used as variables of the model. The dynamics of the small intestinal epithelium is described by the system of nonlinear differential equations similar to Eqs. (1.1)–(1.4) used in the hematopoiesis model:

$$\frac{dx}{dt} = B\,x - \gamma\,x, \tag{3.1}$$

$$\frac{dy}{dt} = \gamma x - F y, \tag{3.2}$$

$$\frac{dz}{dt} = F y - E z, \tag{3.3}$$

$$\frac{dI}{dt} = G(x + \theta y + \vartheta z) - HI. \tag{3.4}$$

In Eqs. (3.1)–(3.3), the coefficients B, γ, F, and E are the specific rates of X cell reproduction, cell transfer from group X to group Y, cell displacement from crypt to villous, and cell exfoliation from the villous into the intestinal lumen, respectively. In Eq. (3.4), the multipliers G, $G\theta$, and $G\vartheta$ determine the specific rates of chalone production by X, Y, and Z cells, respectively, during their vital activity and decay, and H is the rate of natural decay of the chalone.

The model embodies the peculiarities of small intestinal epithelium system functioning related to the motion of cells over the crypt and villous in the course of their division and maturation. It has been found that cell migration is observed even after complete mitotic arrest [41]. In turn, the specific rate of cell displacement from crypt to villous, F, and the specific rate of cell exfoliation from villous to intestinal lumen, E, increase as the mitotic activity of X cells increases, i.e., as the parameter B increases [42]. The exact form of the dependence of F and E on B has not been determined experimentally yet. As a first approximation, we assume them to be linear in B:

$$F = \delta(1 + LB), \qquad E = \psi(1 + MB). \tag{3.5}$$

Here δ and ψ are the specific rates of, respectively, cell displacement from crypt to villous and from villous to intestinal lumen when mitosis of the crypt cells is suppressed ($B = 0$); L and M are constants.

The relationship between the specific rate of reproduction of X cells, B, and the concentration of the specific inhibitor, I, is given, as in Chap. 1, by the Ierusalimskii equation [43–45]:

$$B = \frac{\alpha}{1 + I/K}, \tag{3.6}$$

where α is the maximum specific rate of cell division and K is a constant.

In view of the fact that the chalone keeps its activity for a few hours [21], whereas the small intestinal epithelium cells live, differentiate, and maturate over tens of hours [2], Eq. (3.4) can be considered "fast" compared to Eqs. (3.1)–(3.3). Therefore, according to the Tikhonov theorem [43–45], Eq. (3.4) can be substituted by its stationary solution $I = (G/H)(x + \theta y + \vartheta z)$, by virtue of which Eq. (3.6) acquires the form

$$B = \frac{\alpha}{1 + \beta(x + \theta y + \vartheta z)}, \qquad \beta = \frac{G}{HK}. \tag{3.7}$$

The model of the small intestinal epithelium system in its final version includes three nonlinear differential equations that are fully specified by eight independent parameters: α, γ, δ, ψ, L, M, θ, and ϑ. Six of them (namely, α, γ, δ, ψ, L, and M) are found from experimental data. The values of the parameters θ and ϑ can be obtained by fitting the modeling results to the experimental data on the small intestinal epithelium system dynamics when this system's stationary state is upset by some external factor.

The model (3.1)–(3.3) is investigated by methods of the qualitative theory of differential equations, oscillation theory, and bifurcation theory [46–52]. It has been found that this system has two singular points in the space of variables. The first singular point is trivial (variables x, y, and z vanish). The coordinates of the second singular point in the space of variables are the following:

$$\bar{x} = \frac{(\alpha/\gamma) - 1}{\beta\{1 + \theta\gamma/[\delta(1 + L\gamma)] + \vartheta\gamma/[\psi(1 + M\gamma)]\}}, \tag{3.8}$$

$$\bar{y} = \bar{x}\frac{\gamma}{\delta(1 + L\gamma)}, \tag{3.9}$$

$$\bar{z} = \bar{x}\frac{\gamma}{\psi(1 + M\gamma)}. \tag{3.10}$$

When $\alpha < \gamma$, the first (trivial) singular point is stable (node) and the second singular point has no physical sense because its coordinates are negative ($\bar{x} < 0$, $\bar{y} < 0$, $\bar{z} < 0$). If $\alpha = \gamma$, the second singular point coincides with the first one. In both cases, the stable trivial singular point can be identified with the state of the extinction of the small intestinal epithelium system. This range of parameters is not considered in what follows.

When $\alpha > \gamma$, the first (trivial) singular point is unstable (saddle). The coordinates of the second singular point are positive. The second singular point can be either stable (focus) or unstable (saddle-focus), depending on the values of the model parameters. The respective ranges of parameter values are found in the course of the numerical solution of the characteristic equation. It has been revealed that the second singular point loses stability if the X-cell reproduction is predominantly controlled by the inhibitor produced by Z cells and if the cells stay in the Y group for a sufficiently long time.

If the second singular point with positive coordinates $\bar{x}$, $\bar{y}$, and $\bar{z}$ [Eqs. (3.8)–(3.10)] is stable, then it can be identified with the stable dynamic equilibrium state (the homeostasis state) of the small intestinal epithelium system in mammals. In this case, the values $\bar{x}$, $\bar{y}$, and $\bar{z}$ can be considered the normal concentrations of villous enterocytes and their capable and incapable of dividing precursors in crypts.

When the second singular point as well as the first one is unstable, there is one more particular solution: stable oscillations of the variables x, y, and z (a stable limit cycle). This particular solution can be identified with stable oscillations in the concentrations of villous enterocytes and their capable and incapable of dividing precursors in crypts. Specifically, the model (3.1)–(3.3) reproduces the

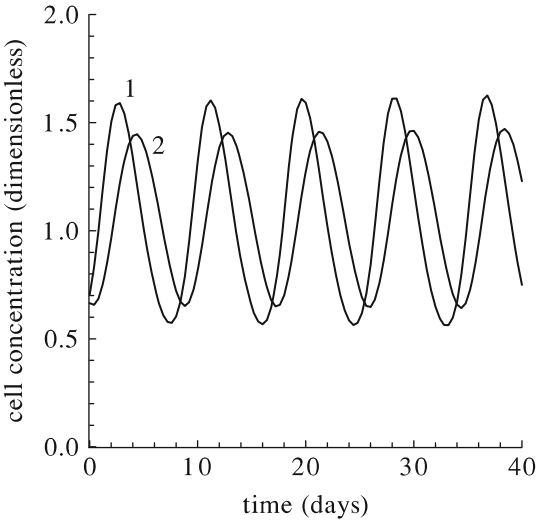

Fig. 3.1 Cyclic kinetics of the small intestinal epithelium system in nonirradiated mammals: *curve 1* is the total concentration of crypt cells (*X* and *Y* cells), and *curve 2* represents the concentration of villous cells (*Z* cells)

stable oscillations of cell concentrations for $\theta = 0.01$ and $\vartheta = 10$, and the values of the rest of parameters that will be given in Sect. 3.5. The respective modeling results are presented in Fig. 3.1. As one can see, the period of oscillations is about 9 days.

The developed model reproduces the basic dynamic regimes of the small intestinal epithelium system in nonirradiated mammals and can be used when modeling the effects of ionizing radiation on this vital body system.

3.5 Dynamics of the Small Intestinal Epithelium Under Chronic Irradiation

According to experimental studies, the crypt cells capable of dividing (*X* cells) are radiosensitive to some extent, whereas the maturing crypt cells incapable of dividing (*Y* cells) and villous enterocytes (*Z* cells) are radioresistant [2–5]. We split the radiosensitive *X* cells into two groups according to their response to irradiation. The first group includes the undamaged X^{ud} cells and the second one involves the damaged X^{d} cells. The concentrations of these cells are denoted by x^{ud} and x^{d}, respectively. In the model we do not make any distinction between damaged and heavily damaged cells, as we did in the hematopoiesis models (see Sect. 1.4), since practically all the radiosensitive crypt cells damaged by radiation undergo the so-called interphase death with the same specific rate [2–4]. Describing the dynamics of the radiosensitive cell concentration, we proceed from the one-target–one-hit theory of cell damage [53]. According to this theory, the specific damage rate is proportional to the radiation dose rate *N*.

Let us introduce the dimensionless variables $\tilde{x}^{\,\mathrm{ud}} = x^{\mathrm{ud}}/\bar{x}$, $\tilde{y} = y/\bar{y}$, $\tilde{z} = z/\bar{z}$, and $\tilde{x}^{\,\mathrm{d}} = x^{\mathrm{d}}/\bar{x}$, as well as the dimensionless parameters $l = \gamma L$ and $m = \gamma M$. Then the dynamics of the dimensionless concentrations of cells in the small intestinal epithelium system of mammals exposed to chronic irradiation at dose rate N is described by the following equations:

$$\frac{d\tilde{x}^{\,\mathrm{ud}}}{dt} = \gamma\,\tilde{x}^{\,\mathrm{ud}}(\tilde{B} - 1) - \frac{N}{D_x^0}\,\tilde{x}^{\,\mathrm{ud}}, \tag{3.11}$$

$$\frac{d\tilde{y}}{dt} = \delta\Big[(1 + l)\tilde{x}^{\,\mathrm{ud}} - (1 + l\widetilde{B})\tilde{y}\Big], \tag{3.12}$$

$$\frac{d\tilde{z}}{dt} = \psi\left[\frac{1 + m}{1 + l}(1 + l\widetilde{B})\tilde{y} - (1 + m\widetilde{B})\tilde{z}\right], \tag{3.13}$$

$$\frac{d\tilde{x}^{\,\mathrm{d}}}{dt} = \frac{N}{D_x^0}\tilde{x}^{\,\mathrm{ud}} - \nu\tilde{x}^{\,\mathrm{d}}. \tag{3.14}$$

In Eqs. (3.11) and (3.14), the term $(N/D_x^0)\,\tilde{x}^{\,\mathrm{ud}}$ is the rate of X^{ud} cell transition into the group of damaged X^{d} cells, and $\nu\tilde{x}^{\,\mathrm{d}}$ in Eq. (3.14) is the death rate of damaged X^{d} cells. The coefficient D_x^0 of the dimension of the radiation dose characterizes the radiosensitivity of X cells. It is equivalent to the conventionally measured quantity: After exposure to dose D_x^0, the number of X cells left undamaged is $e = 2.718\ldots$ times smaller than their initial number [2, 4, 5].

In modifying Eq. (3.7), which describes the rate B of X cell reproduction, we allow for the contribution of X^{d} cells to the chalone production. Then the dimensionless specific rate of X^{ud} cell reproduction is

$$\widetilde{B} = \frac{B}{\gamma} = \frac{a}{1 + b\{\tilde{x}^{\,\mathrm{ud}} + \phi\tilde{x}^{\,\mathrm{d}} + \theta\tilde{y}/[g(1 + l)] + \vartheta\tilde{z}/[c(1 + m)]\}}. \tag{3.15}$$

Here $a = \alpha/\gamma$, $g = \delta/\gamma$, $c = \psi/\gamma$, and

$$b = \beta\,\bar{x} = \frac{a - 1}{1 + \theta/[g(1 + l)] + \vartheta/[c(1 + m)]} \tag{3.16}$$

are dimensionless parameters. The initial conditions for Eqs. (3.11)–(3.14) are the concentrations of X^{ud}, Y, Z, X^{d} cells before irradiation, namely:

$$\tilde{x}^{\,\mathrm{ud}}(0) = 1, \qquad \tilde{y}(0) = 1, \qquad \tilde{z}(0) = 1, \qquad \tilde{x}^{\,\mathrm{d}}(0) = 0. \tag{3.17}$$

It should be noted that the use of the concentration of damaged cells as a variable in the model of the small intestinal epithelium system and the allowance for the contribution of these cells to regulatory processes [Eq. (3.15)] constitute a novel approach to modeling the dynamics of this system under irradiation. It seems important to emphasize that when implementing this approach and modifying

the model (3.1)–(3.3) in order to describe the effects of chronic irradiation on the dynamics of this system, apart from the variable parameter N, we introduced only three new independent coefficients, D_x^0, ν, and ϕ. The parameter D_x^0 specifies the radiosensitivity of X cells. The coefficient ν is the specific death rate of damaged X^{d} cells. The dimensionless multiplier ϕ expresses the dissimilar contributions of undamaged X^{ud} and damaged X^{d} cells to the chalone production. There are 10 independent coefficients in system (3.11)–(3.14), and most of them, as will be shown below, can be evaluated from experimental data.

Model (3.11)–(3.14) is used to examine the effects of chronic irradiation on the small intestinal epithelium system in small laboratory animals (mice and rats). The model parameters are determined from the pertinent experimental data obtained for these animals in the absence of radiation and under radiation exposure. For example, the mitotic activity of dividing cells can be characterized by a mitotic index M, the latter being related to the specific rate B by the formula [54]

$$M = B \cdot T \cdot 100\,\%. \tag{3.18}$$

In Eq. (3.18), the parameter T is the true time of mitosis. Bearing in mind that in nonirradiated mice the mitotic index of dividing crypt cells is 5.3 % and $T = 0.8$ h [55], from (3.18) we derive the value of the specific rate of proliferation of X cells: $B = 1.6\ \mathrm{day}^{-1}$. As follows from Eq. (3.1), under normal conditions, the specific rate of cell transfer from group X to group Y is equal to the specific rate of proliferation of X cells; hence, $\gamma = B = 1.6\ \mathrm{day}^{-1}$.

Analysis of experimental data [42] shows the following. When the mitotic activity of the crypt cells is suppressed ($B = 0$), the specific rates of cell transfer from crypt to villous and of villous cell exfoliation into the intestinal lumen are $F = 0.8\ \mathrm{day}^{-1}$ and $E = 0.28\ \mathrm{day}^{-1}$, respectively. In addition, these quantities are $F = 2.4\ \mathrm{day}^{-1}$ and $E = 0.86\ \mathrm{day}^{-1}$ under normal conditions ($B = \gamma$). On the other hand, according to Eq. (3.5), these quantities can be expressed in terms of the model parameters in the following way: $F = \delta$, $E = \psi$ when $B = 0$, and $F = \delta(1 + l)$, $E = \psi(1 + m)$ when $B = \gamma$. This implies that $\delta = 0.8\ \mathrm{day}^{-1}$, $l = 2$, $\psi = 0.28\ \mathrm{day}^{-1}$, and $m = 2$. In turn, the values of the parameters α, ν, and D_x^0 are found from experimental data [2, 42, 56]. The values of the parameters θ, ϑ, and ϕ are estimated in the course of numerical study of the model and subsequent juxtaposition of the modeling results with experimental data on the dynamics of the small intestinal epithelium system after acute irradiation [57, 58]. The values of all these parameters are given in Table 3.1.

The dynamics of the small intestinal epithelium system is studied within the model (3.11)–(3.14) at various dose rates N of chronic irradiation. Computations show that at low N, the small intestinal epithelium remains practically intact. For instance, at $N = (0.001 \div 0.1)$ Gy/day, the loss of enterocytes is less than $(0.05 \div 5)$ % of their normal level. At higher radiation dose rates, $N = (0.1 \div 10)$ Gy/day, the injury to the system is characterized by two different stages. The first one is an oscillatory transition process. The second stage is a new stationary state of the small intestinal epithelium system.

Table 3.1 Parameters of the small intestine model for small laboratory animals (mice, rats)

Parameter	Value	Dimension
α	5.6	day^{-1}
γ	1.6	day^{-1}
δ	0.8	day^{-1}
ψ	0.28	day^{-1}
ν	2.0	day^{-1}
D_x^0	11.2	Gy
ϕ	20.0	1
θ	0.1	1
ϑ	1.0	1
m	2.0	1
l	2.0	1

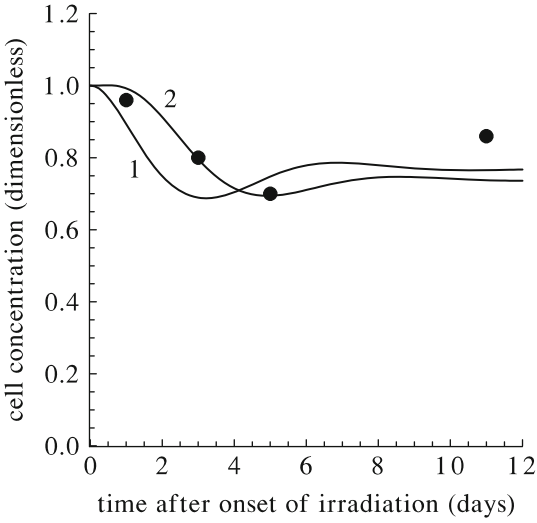

Fig. 3.2 Dynamics of the small intestinal epithelium system in rats under chronic irradiation at a dose rate of 0.84 Gy/day. Computed values of the total concentration of X and Y cells (*curve 1*) and of Z cell concentration (*curve 2*), as well as experimentally measured values of the villous cell concentration (*circle*) [59]

Figures 3.2, 3.3, 3.4, and 3.5 show the dynamics of the total concentration of crypt cells (X and Y cells) and the concentration of villous cells (Z cells), as well as the dynamics of the mitotic index M of X^{ud} cells computed for the dose rates N of 0.84 Gy/day and 1.76 Gy/day, respectively. Figures 3.2 and 3.4 also present the the experimentally measured concentrations of villous cells in rats [59]. As one can infer from Figs. 3.2 and 3.4, the crypt cell concentration decreases within the first 3 days after the onset of irradiation. The decrease in villous cell concentration starts 1 day after the onset of irradiation and ends within 5 days. The decrease in the concentrations of crypt and villous cells is greater as the dose rate N increases. Then the concentrations of crypt and villous cells increase but do not reach their normal values. Further, the concentrations of these cells slightly decrease and approach new stationary levels. The latter are lower as the dose rate N increases. These results are consistent with experimental data [59]. For instance, after 20 days of chronic

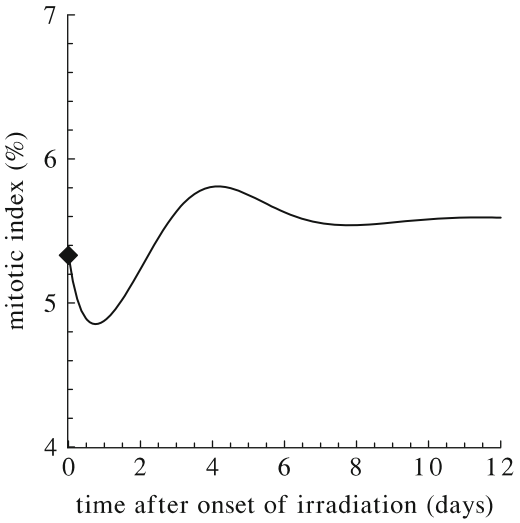

Fig. 3.3 Dynamics of the mitotic index M of X^{ud} cells under chronic irradiation at a dose rate of 0.84 Gy/day. The normal value of M is indicated by the *diamond*

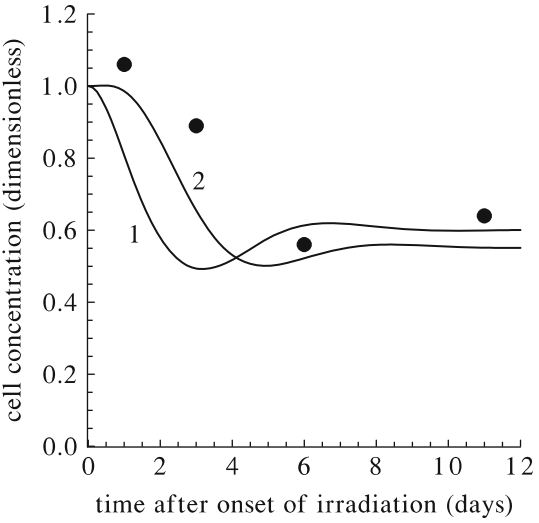

Fig. 3.4 Dynamics of the small intestinal epithelium system in rats under chronic irradiation at a dose rate of 1.76 Gy/day. Computed values of the total concentration of X and Y cells (*curve 1*) and of the Z cell concentration (*curve 2*), as well as experimentally measured values of the villous cell concentration (*circle*) [59]

irradiation at $N = 0.84\,\mathrm{Gy/day}$ and $N = 1.76\,\mathrm{Gy/day}$, the new stationary levels of the dimensionless concentration of villous cells in rats were (0.83 ± 0.15) and (0.67 ± 0.2), respectively. The corresponding computed values are 0.75 and 0.56. The steady reduction in the crypt cell concentration under chronic irradiation is also rather well reproduced by the model. For example, at $N = 4\,\mathrm{Gy/day}$, the new stationary levels of the crypt cell concentration measured in rats [60] and computed in the framework of the model are $(0.16 \div 0.37)$ and 0.34, respectively. Thus, the model provides a theoretical description of the ability of the intestinal epithelium to adapt itself to chronic radiation exposure, which has been observed in experiments [59, 60].

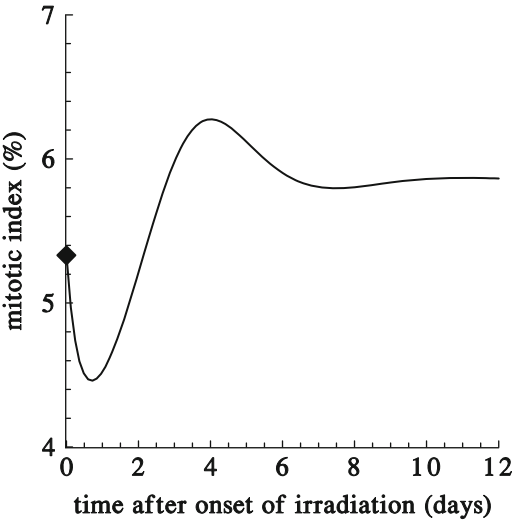

Fig. 3.5 Dynamics of the mitotic index M of X^{ud} cells under chronic irradiation at a dose rate of 1.76 Gy/day. The normal value of M is indicated by the *diamond*

Figures 3.3 and 3.5 show that within 1 day after the onset of irradiation, the mitotic index M of X cells decreases. The decrease is greater as the dose rate N increases. Then M starts growing and reaches a maximum. Later, the mitotic index M decreases and reaches a new stationary value. The latter is larger as the dose rate N increases. In other words, the new stable dynamic equilibrium (homeostasis) established in the small intestinal epithelium system under chronic irradiation is characterized by an enhanced mitotic activity of the crypt cells capable of dividing (X cells). These modeling predictions are in qualitative agreement with experimental data [61].

Modeling studies revealed that the kinetics of cell concentrations in the small intestinal epithelium system has an aperiodic character when the dose rate of chronic irradiation exceeds 10 Gy/day. In such cases, the concentrations of crypt and villous cells decrease to low levels. In turn, the concentrations of these cells decrease to zero when the dose rate N of chronic irradiation equals or exceeds a critical value N_c. The formula defining the quantity N_c is derived within the model of the small intestinal epithelium system. As has been found, the critical dose rate N_c is the product of the coefficient D_x^0, which is a measure of the radiosensitivity of crypt cells capable of dividing (X cells) and the difference of two kinetic parameters $(\alpha - \gamma)$ that characterizes the proliferative potential of these cells:

$$N_c = D_x^0(\alpha - \gamma). \tag{3.19}$$

As one can see, Eq. (3.19) coincides with Eq. (1.39), which was derived within the models of the major hematopoietic lineages. Equation (3.19) can be used to evaluate the critical dose rates of chronic radiation that induce an irreversible depletion of the small intestinal epithelium system in various mammalian species, including humans. Specifically, this quantity for small laboratory animals (mice, rats) is equal to 44.8 Gy/day.

In the course of numerical studies of the model (3.11)–(3.14), the values of all parameters were varied. It has been found that the minimum concentrations of X, Y, Z cells are mainly determined by the parameter D_x^0 characterizing the radiosensitivity of X cells. The parameter D_x^0 and the coefficients l, m, θ, ϑ, ϕ affect the levels of new stationary concentrations of X, Y, Z cells. Obviously, these quantities also depend on the variable parameter N—the dose rate of chronic irradiation.

3.6 Dynamics of the Small Intestinal Epithelium After Acute Irradiation

To simulate the dynamics of the small intestinal epithelium system in mammals exposed to acute radiation at dose D, one can apply the developed model (3.11)–(3.14) with the corresponding parameter N and the initial conditions given by Eq. (3.17). In addition, a simplified version of the model can be used. To derive the latter, it is necessary to take into account an extremely short duration of acute irradiation. In this case, the characteristic time scales of Eqs. (3.11)–(3.14) considerably exceed the duration τ of acute irradiation. Therefore, the dynamics of the dimensionless concentrations of undamaged X^{ud} and damaged X^{d} cells ($\tilde{x}^{\,\mathrm{ud}}$ and $\tilde{x}^{\,\mathrm{d}}$, respectively) during the exposure can be described by the system of "fast" equations

$$\frac{d\tilde{x}^{\,\mathrm{ud}}}{dt} = -\frac{N}{D_x^0}\,\tilde{x}^{\,\mathrm{ud}}, \qquad \frac{d\tilde{x}^{\,\mathrm{d}}}{dt} = \frac{N}{D_x^0}\,\tilde{x}^{\,\mathrm{ud}}. \tag{3.20}$$

In turn, the dimensionless concentrations of radioresistant Y and Z cells ($\tilde{y}$ and $\tilde{z}$) can be considered constant ones:

$$\frac{d\tilde{y}}{dt} = 0, \qquad \frac{d\tilde{z}}{dt} = 0. \tag{3.21}$$

The corresponding initial conditions read

$$\tilde{x}^{\,\mathrm{ud}}(0) = 1, \qquad \tilde{x}^{\,\mathrm{d}}(0) = 0, \qquad \tilde{y}(0) = 1, \qquad \tilde{z}(0) = 1. \tag{3.22}$$

With $N = \mathrm{const}$, Eqs. (3.20) and (3.21) can be integrated explicitly. The obtained expressions for the dimensionless concentrations of undamaged X^{ud} and damaged X^{d} cells ($\tilde{x}^{\mathrm{ud}}$ and $\tilde{x}^{\mathrm{d}}$), as well as for the dimensionless concentrations of radioresistant Y and Z cells ($\tilde{y}$ and $\tilde{z}$) can be used as the initial conditions for Eqs. (3.11)–(3.14) with zero value for the parameter N:

$$\tilde{x}^{\,\mathrm{ud}}(0) = \exp(-D/D_x^0), \qquad \tilde{x}^{\,\mathrm{d}}(0) = 1 - \exp(-D/D_x^0), \qquad \tilde{y}(0) = 1, \qquad \tilde{z}(0) = 1. \tag{3.23}$$

Here $D = N\tau$ is the dose of acute irradiation.

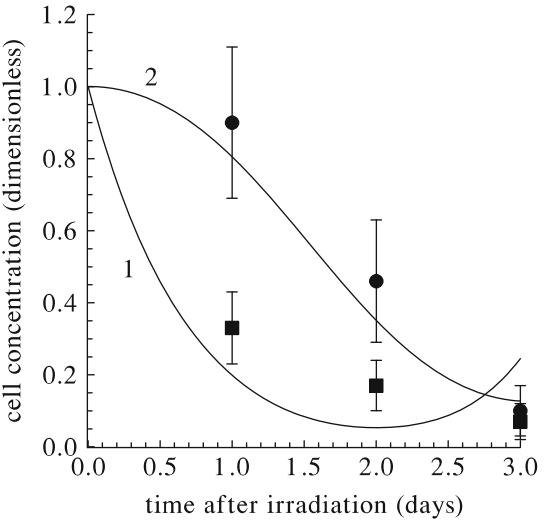

Fig. 3.6 Dynamics of the small intestinal epithelium system in mice after acute irradiation at a dose of 30 Gy. Computed values of the total concentration of X and Y cells (*curve 1*) and of the Z cell concentration (*curve 2*), as well as experimentally measured concentrations of crypt cells (*box*) and villous cells (*circle*) [62]

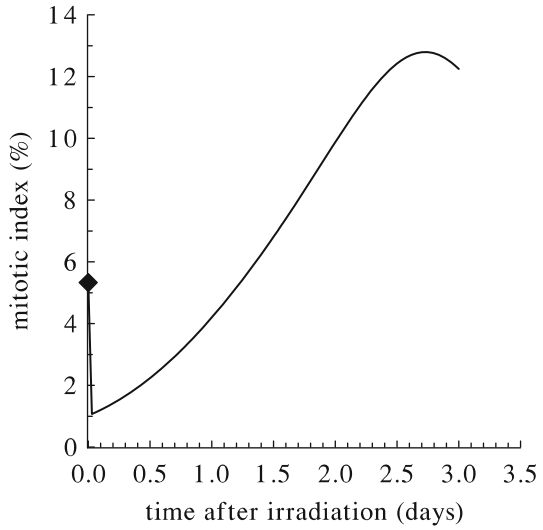

Fig. 3.7 Dynamics of the mitotic index M of X^{ud} cells after acute irradiation at a dose of 30 Gy. The normal value of M is indicated by the *diamond*

The developed model is used to examine the dynamics of the small intestinal epithelium system in mice exposed to acute radiation at high doses D. Specifically, the modeling results computed for $D = 30$ Gy are presented in Figs. 3.6 and 3.7. Figure 3.6 presents the dynamics of the dimensionless total concentration of crypt cells (X and Y cells) and of the dimensionless concentration of villous cells (Z cells). This figure also shows the corresponding experimental data [62] on radiation-induced changes of crypt and villous cell concentrations in mice of the CFW strain. As one can infer from Fig. 3.6, the model reproduces the experimentally observed rapid depletion of the crypt cell pool. As early as the second postirradiation day,

the concentration of crypt cells goes below 20 % of its normal level. In the first day, the villous cell concentration slowly decreases. But already by the second day, the concentration of villous cells is reduced nearly by half and continues to drop rapidly to a level incompatible with life. This level is usually reached within the third postirradiation day, and all mice die [62]. The use of the statistical χ^2-test demonstrates the quantitative agreement between the modeling results and the experimental data [62]. The computed values of $\chi^2 = 0.844$ and $\chi^2 = 1.839$ do not exceed the critical value of $\chi^2_{0.05} = 5.991$ (the number of degrees of freedom $n = 2$).

Figure 3.7 shows the dynamics of the mitotic index M of X^{ud} cells computed in the framework of the model at the same dose of acute irradiation. As one can see, first the mitotic decreases to a minimum. After that it begins to increase, reaches a maximum exceeding its normal value, and then starts to decrease. Furthermore, all mice die [62].

The model is also used to examine the peculiarities of the dynamics of the small intestinal epithelium system in mice exposed to acute radiation at lower doses. The results of a computation are given in Figs. 3.8 and 3.9. Figure 3.8 also shows the corresponding experimental data obtained in the study of the intestinal epithelium in white mice [57, 58]. One can see that the model describes the radiation-induced decrease in the concentrations of crypt and villous cells. The depletion stage is followed by the repair stage when the concentrations of these cells start to grow. These modeling results agree with experimental data [57, 58]. As has been found experimentally [57, 58], intestinal epithelium regeneration in mice irradiated at doses lower than 10 Gy and that survived in the first 3 days was observed.

Figure 3.9 shows the dynamics of the mitotic index M of X^{ud} cells computed for the same dose D of acute irradiation. As one can see, first the mitotic index decreases

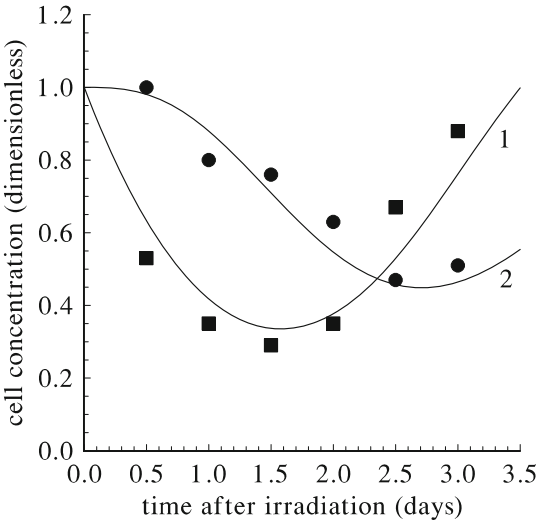

Fig. 3.8 Dynamics of the small intestinal epithelium system in mice after acute irradiation at a dose of 7 Gy. Computed values of the total concentration of X and Y cells (*curve 1*) and of the Z cell concentration (*curve 2*), as well as experimentally measured concentrations of crypt cells (*box*) and villous cells (*circle*) [57, 58]

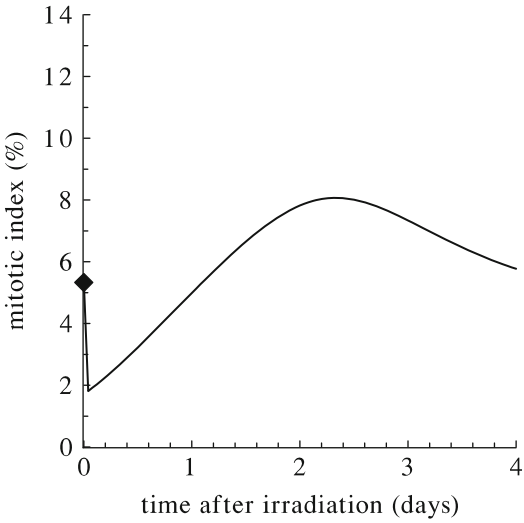

Fig. 3.9 Dynamics of the mitotic index M of X^{ud} cells after acute irradiation at a dose of 7 Gy. The normal value of M is indicated by the *diamond*

and then it reaches a minimum. After that it begins to increase and then reaches a maximum exceeding its normal value. Then, as computations show, it decreases and, after damped oscillations, reaches the normal level. The modeling dynamics of the mitotic index M of X^{ud} cells qualitatively corresponds to the experimentally observed changes in the mitotic index of crypt cells in mice [56] and rats [2] after irradiation at doses of $(6 \div 10)$ Gy. It is worthwhile emphasizing that this is the first time that the pattern of changes in the mitotic activity of crypt cells in the course of postirradiation injury and regeneration of the intestinal epithelium has been reproduced by a dynamic model at the qualitative level.

In the course of numerical studies of the model, the values of all parameters were varied. It has been found that the principal characteristics of radiation injury of the intestinal epithelium—minimal concentrations of X, Y, Z cells—are mainly determined by the parameter D_x^0 characterizing the radiosensitivity of X cells and by the radiation dose D.

3.7 Conclusions

A biologically motivated mathematical model describing the dynamics of the small intestinal epithelium system in nonirradiated and irradiated mammals was developed and investigated. A principal advantage of the model consists of the fact that its identification requires only the data obtained in the studies of this system in intact mammals and in mammals exposed to either acute or chronic irradiation. The verification of the model was successfully performed by making use of the data for small laboratory animals (mice, rats). The model reproduces common regularities, as well as peculiarities, in the kinetics of the small intestinal epithelium

in nonirradiated and irradiated mammals. All this implies that the developed model of the small intestinal epithelium does account for the principal regulatory mechanisms governing the function of this system under normal conditions and under irradiation. This also bears witness to the validity of the employment of the model, after proper identification, in studies and predictions of the dynamics of the small intestinal epithelium system in various mammalian species, including humans, exposed to acute or chronic irradiation in wide ranges of doses and dose rates. In particular, the properly identified model of the small intestinal epithelium system and the granulopoiesis model presented in Chap. 7 can be used as constituent parts of a joint model. The latter would be able to simulate the dynamics of the small intestinal epithelium system in humans in cases of radiation-induced damage of the granulopoiesis system, which plays an important role in defending the small intestinal epithelium system from infections. Such a model could be helpful in the estimation of the health effects of space radiation in astronauts during long-term space missions, such as Lunar colonies and Mars missions.

References

1. Travis S., Ahmad T., Collier J., Steinhart A.H. Gastroenterology, 3rd edition. Malden, MA: Wiley-Blackwell, 2005.
2. Bond V.P., Fliendner T.M., Archambeau J.O. Mammalian Radiation Lethality: A Disturbance in Cellular Kinetics. New York: Academic Press, 1965.
3. Yarmonenko S.P., Vainson A.A. Radiobiology of Humans and Animals. Moscow: Vyisshaya shkola, 2004 (Russian).
4. Yarmonenko S.P. Radiobiology of Human and Animals. Moscow: Viysshaya shkola, 1988 (Russian).
5. Darenskaya N.G., Korotkevich A.O. Nonspecific Body Reactivity and Principles of Forming of Individual Radiosensitivity. Moscow: Voentexinizdat, 2001 (Russian).
6. Quastler H. The nature of intestinal radiation death. Radiation Research, v. 4, pp. 303–320, 1956.
7. Baer A.R., Cheeseman C.I., Thomson B.R. The assessment of recovery of the intestine after acute radiation injury. Radiation Research, v. 109, pp. 319–329, 1987.
8. Geraci J.P., Jackson K.L., Mariano M.S. The intestinal radiation syndrome: Sepsis and endotoxin. Radiation Research, v. 101, pp. 442–450, 1985.
9. Smirnova O.A. Mathematical simulation of the dynamics of postirradiation damage and recovery of intestinal epithelium. Radiobiologiya, v. 28, pp. 817–821, 1988 (Russian).
10. Smirnova O.A. Mathematical simulation of the intestinal epithelium dynamics in nonirradiated and irradiated mammals. Radiobiologiya, v. 32, pp. 751–756, 1992 (Russian).
11. Kovalev E.E., Smirnova O.A. Estimation of radiation risk based on the concept of individual variability of radiosensitivity. AFRRI Contract Report 96-1. Bethesda, MD: Armed Forces Radiobiology Research Institute, 1996.
12. Smirnova O.A. Mathematical models of dynamics of small intestine epithelium system in nonirradiated and irradiated mammals. Abstracts of the 24th Meeting of the European Study Group for Cell Proliferation (ESGCP), Leipzig, Germany, June 12–17, 2001. Cell Proliferation, v. 34(3), pp. 193–194, 2001.
13. Smirnova O.A. Radiation and Organism of Mammals: Modeling Approach. Moscow-Izhevsk: Scientific-Publishing Centre “Regular and Chaotic Dynamics,” Institute of Computer Science, 2006 (Russian).

14. Smirnova O.A. Radiation effects on small intestine epithelium system: Mathematical modeling. Proceedings of III International Symposium "Problems of Biochemistry, Radiation and Space Biology" dedicated to the centenary of Academician N.M. Sissakian's birth, Dubna, pp. 250–256, 2007.
15. Smirnova O.A. Blood and small intestine cell kinetics under radiation exposures: Mathematical modeling. Advances in Space Research, v. 44, pp. 1457–1469, 2009.
16. Loeffler M., Potten C.S. Stem cells and cellular pedigrees — A conceptual introduction; in Potten C.S. (Ed.): Stem Cells, ISBN 0-12-563455-2, Cambridge: Academic Press, pp. 1–27, 1997.
17. Potten C.S., Loeffler M. Stem cells: Attributes, cycles, spirals, pitfalls and uncertainties. Lessons for and from the crypt. Development, v. 110, pp. 1001–1020, 1990.
18. Loeffler M., Roeder I. Tissue stem cells: Definition, plasticity, heterogeneity, self-organization and models — A conceptual approach. Cells Tissues Organs, v. 171, pp. 8–26, 2002.
19. Potten C.S., Gandara R., Mahida Y.R., Loeffler M., Wright N.A. The stem cells of small intestinal crypts: Where are they? Cell Proliferation, v. 42, pp. 731–750, 2009.
20. Kwan W.B., Shui C., Ning S., Knox S.J. Enhancement of murine intestinal stem cell survival after irradiation by keratinocyte growth factor. Radiation Research, v. 148, p. 248, 1997.
21. Romanov J.A., Ketlinsky S.A., Antokhin A.I., Okulov V.B. Chalones and Regulation of Cell Division. Moscow: Meditsina, 1984 (Russian).
22. Potten C.S., Booth C., Haley J.D. Pretreatment with transforming growth factor beta-3 protects small intestinal cells against radiation damage in vivo. British Journal of Cancer, v. 75, p. 1454, 1997.
23. Loeffler M., Stein R., Wichmann H.E., Potten C.S., Kaur P., Chwalinski S. Intestinal cell proliferation: I. A comprehensive model of steady-state proliferation in the crypt. Cell and Tissue Kinetics, v. 19, pp. 627–645, 1986.
24. Loeffler M., Potten C.S., Paulus U., Glatzer J., Chwalinski S. Intestinal crypt proliferation: II. Computer modelling of mitotic index data provides further evidence for lateral and vertical cell migration in the absence of mitotic activity. Cell Proliferation, v. 21(4), pp. 247–258, 1988.
25. Potten C.S., Loeffler M. A comprehensive model of the crypts of the small intestine of the mouse provides insight into the mechanisms of cell migration and the proliferation hierarchy. Journal of Theoretical Biology, v. 127, pp. 381–391, 1987.
26. Paulus U., Loeffler M., Zeidler J., Owen G., Potten C.S. The differentiation and lineage development of goblet cells in the murine small intestinal crypt: Experimental and modelling studies. Journal of Cell Science, v. 106, pp. 473–484, 1993.
27. Meineke F.A., Potten C.S., Loeffler M. Cell migration and organization in the intestinal crypt using a lattice-free model. Cell Proliferation, v. 34, pp. 253–266, 2001.
28. Drasdo D., Loffler M. Individual-based models to growth and folding in one-layered tissues: Intestinal crypts and early development. Nonlinear Analysis, v. 47, pp. 245–256, 2001.
29. Shu-Han Lin A., Buist M.L., Smith N.P., Pullan A.J. Modelling slow wave activity in the small intestine. Journal of Theoretical Biology, v. 242(2), pp. 356–362, 2006.
30. Miftahof R., Akhmadeev N. Dynamics of intestinal propulsion. Journal of Theoretical Biology, v. 246(2), pp. 377–393, 2007.
31. Onofrio A., Tomlinson I.P.M. A nonlinear mathematical model of cell turnover, differentiation and tumorigenesis in the intestinal crypt. Journal of Theoretical Biology, v. 244(3), pp. 367–374, 2007.
32. Simpson M.J., Landman K.A., Bhaganagarapu K. Coalescence of interacting cell populations. Journal of Theoretical Biology, v. 247(3), pp. 525–543, 2007.
33. Qu K., Ortoleva P. Understanding stem cell differentiation through self-organization theory. Journal of Theoretical Biology, v. 250(4), pp. 606–620, 2008.
34. Guebel D.V., Torres N.V. A computer model of oxygen dynamics in human colon mucosa: Implications in normal physiology and early tumor development. Journal of Theoretical Biology, v. 250(3), pp. 389–409, 2008.
35. Binder B.J., Landman K.A. Exclusion processes on a growing domain. Journal of Theoretical Biology, v. 259(3), pp. 541–551, 2009.

36. Gerike T.G., Paulus U., Potten C.S., Loeffler M. A dynamical model of proliferation and differentiation in the intestinal crypt based on a hypothetical intraepithelial growth factor. Cell Proliferation, v. 31, pp. 93–110, 1998.
37. Tyazelova V.G. Dynamics of Haemopoiesis. Moscow: Meditsina, 1988 (Russian).
38. Gozenbuk V.L., Keirim-Markus I.B. Dosimetric Criteria of the Severity of Acute Man Irradiation. Moscow: Energoatomizdat, 1988 (Russian).
39. Sato F., Muramatsu S., Tsuchihashi S., et al. Radiation effects on cell populations in the intestinal epithelium of mice and its theory. Cell and Tissue Kinetics, v. 5, pp. 227–235, 1972.
40. Shiragai A., Sato F., Hiraoka T., et al. Kinetics of cell populations in the intestinal epithelium of mice after partial-body irradiations with X-rays and neutrons. International Journal of Radiation Biology, v. 29, pp. 377–383, 1976.
41. Kaur P., Potten C.S. Cell migration velocities in the crypts of the small intestine after cytotoxic insult are not dependent on mitotic activity. Cell and Tissue Kinetics, v. 19, p. 601, 1986.
42. Strdzidzovsky A.D. Quantitative analysis of the cellular aspects of the intestinal syndrome under ionizing radiation action. Theoretical premises and the models of the radiation damage processes in organism system. Pushchino, pp. 50–57, 1975 (Russian).
43. Romanovsky J.M., Stepanova N.V., Chernavsky D.S. Mathematical Modeling in Biophysics. Introduction to Theoretical Biophysics. Moscow-Izhevsk: Scientific-Publishing Centre "Regular and Chaotic Dynamics," Institute of Computer Science, 2004 (Russian).
44. Romanovsky J.M., Stepanova N.V., Chernavsky D.S. Mathematical Modeling in Biophysics. Moscow: Nauka, 1975 (Russian).
45. Romanovsky J.M., Stepanova N.V., Chernavsky D.S. Kinetische Modelle in der Biophysik. Stuttgart: Gustav Fischer Verlag, 1974.
46. Pontryagin L.S. Ordinary Differential Equations. Moscow: Nauka, 1982 (Russian).
47. Andronov A.A., Vitt A.A., Khikin S.E. Theory of Oscillation. Moscow: Nauka, 1981 (Russian).
48. Andronov A.A., Leontovich E.A., Gordon I.I., Maier A.G. Theory of Bifurcations of Dynamical Systems on Plane. Moscow: Nauka, 1967 (Russian).
49. Hayashi C. Nonlinear Oscillations in Physical Systems. McGraw-Hill Book Company, New York, 1964.
50. Arrowsmith D.K., Place C.M. Ordinary Differential Equations. A Qualitative Approach with Applications. London: Chapman and Hall, 1982.
51. Dulac H. Sur les cycles limités. Bulletin de la Société Mathématique de France, v. 51, pp. 45–188, 1923.
52. Korn G.A., Korn T.M. Mathematical Handbook. McGraw-Hill Book Company, New York, 1968.
53. Lea D.E. Action of Radiation on Living Cells, 2nd ed. Cambridge: Syndics of the Cambridge University Press, 1955.
54. Gruzdev G.P. Problems of Haemopoietic Tissue Damage Under Acute Radiation Pathology. Moscow: Meditsina, 1968 (Russian).
55. Lesher S. Compensatory reactions in intestinal crypt cells after 300 roentgens of Cobalt-60 gamma irradiation. Radiation Research, v. 32(3), pp. 510–519, 1967.
56. Lesher J., Lesher S. Effects of single-dose, whole-body, Cobalt-60 gamma irradiation on number of cells in DNA synthesis and mitosis in the mouse duodenal ephithelium. Radiation Research, v. 43(2), pp. 429–438, 1970.
57. Kononenko A.M. On the influence of cell abnormal growth on crypt cell population kinetics in irradiated intestinal epithelium. Citologiya, v. 10, pp. 1425–1431, 1968 (Russian).
58. Kononenko A.M., Pharaphonov G.V. On changes in the amount of epithelium cells on small intestine fibers of irradiated mice. Radiobiologiya, v. 9, pp. 209–212, 1969 (Russian).
59. Quastder H., Bensted J.P.M., Chir B. Adaptation to continuous irradiation: Observations on the rat intestine. British Journal of Radiology, v. 32(380), pp. 501–512, 1959.
60. Fabrikant J.I. Adaptation of cell renewal systems under continuous irradiation. Health Physics, v. 52(5), pp. 561–570, 1987.

61. Cairnie A.B. Cell proliferation studies in the intestinal epithelium of the rat: Response to continuous irradiation. Radiation Research, v. 32, pp. 240–264, 1967.
62. Matsuzawa T., Wilson R. The intestinal mucosa of germfree mice after whole-body X-irradiation with 3 kiloroentgens. Radiation Research, v. 25(1), pp. 15–24, 1965.

Chapter 4
Radiation and Humoral Immunity

4.1 Introduction

One of the effects of ionizing radiation on mammals is the weakening of the organism's defense against infections. It is exo- and endoinfections that, as a rule, complicate the course of acute radiation sickness and, in some cases, lead to the death of the exposed specimens [1, 2]. These harmful consequences of irradiation are caused by radiation-induced damage to the immune system [3, 4].

Over the past four decades, mathematical modeling has been employed to study a broad spectrum of immunological processes and phenomena. Therefore, one can already speak about a new area of research in immunology: mathematical immunology. The first studies in this area were those of Bell [5–8], the present author and Stepanova [9–13], Jilek et al. [14–17], and Molchanov [18, 19]. All these works were performed at nearly the same time, in the early 1970s. Later, valuable contributions to this subject were made by Marchuk and his co-authors [20–31], as well as by Bell, Bruni, and Mohler and their co-authors [32–44]. Interesting studies were carried out by Vol'kenshtein and his co-workers [45–48], Glushkov et al. [49], and others (see, e.g., [50–73]).

In some of these studies, the phenomenon of immunity was treated either at the level of individual molecules in describing the antigen–antibody reaction, or at the level of individual cells in reproducing the interaction of antigen-presenting cells and lymphocytes. The most interesting models were those in which immunity was studied for the organism as a whole: immunity to infections, immunity to tumors, and immunity in the presence of AIDS. These models were used to check quantitatively the validity of a number of immunological theories, to explain many experimental regularities and clinical observations, and to suggest treatment for some illnesses.

O.A. Smirnova, *Environmental Radiation Effects on Mammals*,
DOI 10.1007/978-3-319-45761-1_4

It is worth noting that the aforementioned models were used to study various aspects of immunity in mammals residing in ecologically favorable conditions.

The primary objectives of our studies [74–80] were to develop and investigate the mathematical models, which describe the dynamics of the system of humoral immunity in mammals unexposed and exposed to acute and chronic irradiation. The models were required to account for the principal regulatory mechanisms of this system and to include explicitly the characteristics of ionizing radiation and the basic immunological and radiobiological parameters of the system under consideration. The results of our investigations of this subject are summarized in this chapter.

4.2 The Essentials of Immunity

Immunity is the system defending mammals and other vertebrates from genetically alien matter (antigens) [3, 4, 81–86]. Antigens may be macromolecules (proteins, carbohydrates, and nucleic acids), bacteria, viruses, cells of foreign organs and tissues, or cells of malignant tumors. When an antigen encounters an organism, it first induces nonspecific reactions. Blood granulocytes and tissue macrophages migrate to its site. These cells are capable of absorbing molecular antigens, viruses, and even entire bacterial cells, and also of splitting them into fragments.

The primary specific immune reaction is humoral immunity. Humoral immunity involves the production of protein molecules (antibodies) by certain cells of the organism. Antibodies can specifically bind to an antigen and hasten its expulsion from the organism.

At present, five basic classes of antibodies (immunoglobulins) are known: *IgG*, *IgM*, *IgA*, *IgD*, and *IgE*. They differ from each other in chemical construction and function. Immunoglobulins of the first two classes play the most important role in the immune reactions developing in an organism with an infectious disease. The *IgG* molecule consists of four chains (two identical heavy ones and two identical light ones) connected to each other by disulfide bonds. Each half of the molecule contains an antigen-binding region (the active center of the antibody). It is formed in a small region of the light and heavy chains and has the form of a shallow "crater" in which a part of the antigen molecule (the antigenic determinant) enters when the antigen–antibody complex is formed. The *IgG* molecules are most effective in neutralizing the toxins produced by sickness-causing organisms. The *IgM* molecule consists of ten light and ten heavy chains. There are ten active centers. However, only five of them can actively combine with an antigen. The *IgM* antibodies play an important role in the early stages of infectious diseases.

The quantity characterizing the ability of an antibody to bind with an antigen is the association constant κ. It is equal to the ratio of the rate constants for the direct and inverse interactions of the antigenic determinant and the active center of the antibody in the formation of the antigen–antibody complex.

The widely accepted theory of antibody production is the clonal selection theory by Burnet [81]. According to this theory, the organism of an adult mammal contains a population of "antigen-sensitive" cells. Only a small fraction of them (10^{-5} of the total) can be stimulated by an antigen. After stimulation, the antigen-sensitive cells (small lymphocytes) are transformed into rapidly dividing blast cells. The division (proliferation) of the latter is accompanied by their development to cells with a more and more complete protein-synthesis apparatus. The final stage of this development is the mature plasma cell, which does not divide. It rapidly produces antibodies, and after a certain time it dies.

Studies have shown that the "antigen-sensitive" cells are the descendants of bone marrow stem cells which follow a route of differentiation to the side of the hematopoietic lymphoid line, and then are "trained" in the bursa of Fabricius in birds or in an analogous organ in mammals. These lymphocytes are called *B*-cells. The *B*-lymphocytes carry receptors on their surface. These receptors are antibody molecules of certain classes or fragments of them. On the average, there are about 10^5 receptors on a *B*-cell. Experimental observations indicate that *B*-lymphocytes are not inert cells regarding the synthesis of immunoglobulins in the absence of an antigen. Immunoglobulins are constantly being produced in *B*-lymphocytes. Some are secreted outside as antibodies, and some become surface receptors, which, in turn, can also be separated from the cell surface. However, the rate of antibody production by *B*-lymphocytes is considerably lower than that by plasma cells. It should be noted that the association constants of the receptors of a *B*-cell and of the antibodies synthesized by it and its descendants are the same.

It is considered a proven fact that the stimulation of a *B*-lymphocyte, which leads to its intense proliferation, is expressed in the binding of some number of receptors on its surface with the corresponding antigen. There is reason to believe that the antigen continues to provide stimulation throughout the entire process of *B*-cell division.

The "delivery" of antigen to immunocompetent *B*-lymphocytes can occur both without and with the participation of other cells—macrophages (*A*-cells) and helper *T*-lymphocytes. Here the antigen is, respectively, named *T*-independent and *T*-dependent. Helper *T*-cells, like *B*-cells, are descendants of bone marrow stem cells, which follow a route of differentiation to the side of the lymphoid line. However, after leaving the bone marrow, these lymphocytes are "trained" in an immune organ—the thymus. In addition to helper *T*-cells, the regulation of the humoral immune response to *T*-dependent antigens involves *T*-lymphocyte-suppressors, which inhibit the stimulation of immunocompetent cells by the antigen. The immune system is also subject to nervous, endocrinal, and mediator effects.

Antibody synthesis occurs in lymphatic organs. These are the spleen, the lymph nodes, Peyer's patches, the lungs, and the appendix. The antibodies are then transferred to the blood. The dynamics of antibody accumulation in the blood has four characteristic phases:

- the latency period, during which antibodies are not seen (the lag-phase);
- the phase of exponentially growing antibody concentration (the log-phase);

- the plateau, a period during which the antibody concentration remains at a high level;
- the phase of falling antibody concentration.

The latency period is due to the time needed for the production and passage to the blood of an antibody concentration that exceeds the sensitivity threshold of the method used to measure it. The other phases result from the superposition of several processes, including cell division, increase in the rate of antibody synthesis by individual cells, stimulation of new cells, natural disintegration of antibody molecules, loss of antibodies to antigen–antibody complexes, and death of mature plasma cells.

The dynamics of the accumulation of antibody-producing cells (APCs) is similar to the antibody dynamics discussed above. The latency period is determined by the time needed to produce a sufficient number of cells intensively synthesizing antibodies. The growth phase is due to cell division, cell influx from other lymphatic organs, and the onset of division of new antigen-sensitive cells, whereas the fall phase is due to the death of APCs.

The basic parameters of the immune response, the maximum concentrations of antibodies and APCs, and the times required to reach these maxima depend on many different factors. However, the antigen is decisive. The response will therefore be more intense as the amount of antigen to be introduced increases (this is true only up to a certain level of initial antigen concentration). The intensity of the immune response is also significantly affected by whether or not the organism has previously come into contact with the antigen. If it has, the maximum antibody concentration is, as a rule, from one to two orders of magnitude higher than the maximum antibody concentration in the primary response to the same quantity of antigen, and the duration of the latency period is smaller. The ability of an organism to give an enhanced and faster response in a repeat encounter with an antigen is referred to as immunological memory. In mammals this memory is preserved for a long time, sometimes the entire lifetime. It is thought that *immunological memory* is due to an increase in the number of cells capable of responding to the stimulus of a given antigen.

Cellular immunity is another type of specific immune reaction. The cellular forms of the immune response are related to the functioning of *T*-lymphocyte-effector cells. These are capable of recognizing an antigen, responding to stimulation by multiplication, and then becoming “killers”—cells that annihilate foreign antigenic substances. Cellular immunity occurs in delayed hypersensitivity, in the rejection of transplants and tumors, in the antiviral immune reaction, and also in autoimmune illnesses. The last type occurs when the natural insensitivity of the organism to its own components is destroyed. The autoimmunity problem will be discussed in detail in the next chapter.

4.3 Dynamical Model of the Humoral Immune Response to a T-Independent Antigen in Nonirradiated Mammals

Let us construct a mathematical model describing the humoral immune response to soluble protein antigens. This is the most thoroughly studied reaction in immunology. In developing this model we limit ourselves to consideration of the primary immune response to a soluble T-independent antigen, when the role of T-lymphocytes, macrophages, and immunological memory cells can be neglected.

The model is based on the clonal selection theory of Burnet [4, 81], according to which the mammalian organism contains only a small number of B-lymphocytes capable of recognizing a certain antigen. It is assumed that these cells transfer into the blood from the bone marrow, and after some time they die. It is also assumed that from the moment they leave the bone marrow, B-lymphocytes can pass through all the developmental stages, including the death of a plasma cell, without antigenic stimulation. In this case this process is not associated with B-cell multiplication [87]. In accordance with experimental data [88, 89], it is assumed that the maturation process of a B-cell is accompanied by an increase in the number of antibody-like receptors on its surface, and that this number then decreases immediately before transformation into a plasma cell. It is also assumed that the binding of cell receptors with antigenic molecules can lead either to cell multiplication or to cell death, depending on the number of bound receptors on the cell.

In the model we deal with B-cells predetermined to produce antibodies of a certain specificity in n different developmental stages [Z_i cells ($i = 1, \ldots, n$)], with their progeny, plasma cells, which are capable of producing antibodies of this specificity (Z_{n+1} cells), as well as with antibody molecules (ABs) and antigen molecules (AGs). We use the concentrations of the aforementioned cells and molecules [z_i ($i = 1, \ldots, n+1$), u, and v, respectively] as variables of the model. With the assumptions mentioned above, the dynamics of these concentrations is described by the following system of nonlinear differential equations:

$$\frac{dz_1}{dt} = a - \sigma z_1 + \varsigma s_1(b_1) z_1, \tag{4.1}$$

$$\frac{dz_i}{dt} = \sigma(z_{i-1} - z_i) + \varsigma s_i(b_i) z_i \qquad (i = 2, \ldots, n), \tag{4.2}$$

$$\frac{dz_{n+1}}{dt} = \sigma z_n - \lambda z_{n+1}, \tag{4.3}$$

$$\frac{du}{dt} = \chi z_{n+1} - \xi u - c\eta u, \tag{4.4}$$

$$\frac{dv}{dt} = -\zeta v - \eta v'. \tag{4.5}$$

In Eq. (4.1) the coefficient a is the rate of influx of predetermined cells from the bone marrow, and σ is the specific rate of transition of a cell from one age

group to another, which is equal to the number of age groups n divided by the B-cell development time. The parameters $s_i(b_i)$ in Eqs. (4.1) and (4.2) describe the outcome of interactions between cell receptors and antigenic molecules. If the number of bound receptors b_i on Z_i cells is smaller than some threshold value $b^{\min}$, then multiplication of Z_i cells is not stimulated, i.e., $s_i(b_i) = 0$. If $b^{\min} \leq b_i \leq b^{\max}$, then the Z_i cells multiply at a constant specific rate ς, i.e., $s_i(b_i) = 1$. If $b_i > b^{\max}$, then all Z_i cells die: $z_i = 0$. In Eq. (4.3) the parameter λ is the specific rate of death of plasma cells Z_{n+1}. In Eq. (4.4) the parameter χ is the rate at which they produce antibody molecules. In Eqs. (4.4) and (4.5), the coefficients ξ and ζ are the specific rates of natural extraction of antibody molecules and antigen, and η is the specific rate of extraction of complexes of them.

In Eq. (4.4) the parameter c is the fraction of antibody molecules for which at least one of the m active centers is bound to an antigen, when the fraction of occupied active centers on the antigen molecule is equal to r:

$$c = \sum_{l=1}^{m} C_m^l \, r^l \, (1-r)^{m-l} \, . \tag{4.6}$$

In Eq. (4.5) v' is the concentration of antigenic determinants bound with active antibody centers. It is given by the following equation:

$$v' = v - f - g \, , \tag{4.7}$$

where f is the concentration of free antigenic determinants and g is the concentration of antigenic determinants bound to cell receptors. The quantity g is equal to the product of the fraction of cell receptors bound with antigenic determinants (r') and the total concentration of receptors q on Z_i cells ($i = 1, \ldots, n$):

$$g = r' q \, , \tag{4.8}$$

where

$$q = \sum_{i=1}^{n} \omega_i \, z_i \, . \tag{4.9}$$

In Eq. (4.9) the parameter ω_i is the number of receptors on the cells of the ith age group (on the Z_i cells). It is defined by the following function:

$$\omega_i = \begin{cases} \omega_1 \exp[\varpi \, (i-1)] & \text{for} \quad i = 1, \ldots, k, \\ \omega_k \exp[\varpi' (k-i)] & \text{for} \quad i = k+1, \ldots, n. \end{cases} \tag{4.10}$$

Here ω_1, ω_k, ϖ, and ϖ' are constant coefficients.

The quantities r, r', and $b_i = \omega_i r'$ are determined by formulas known from immunology [86]:

$$r = \frac{\kappa f}{1 + \kappa f}, \qquad r' = \frac{\kappa' f}{1 + \kappa' f}, \qquad b_i = \omega_i \frac{\kappa' f}{1 + \kappa' f}. \tag{4.11}$$

Here the parameters κ and κ' are the association constants in the interaction of free antibodies and cell receptors with antigenic determinants, whereas f is the concentration of free antigenic determinants. The quantity f is found from the equation of chemical equilibrium among antigenic determinants, active centers of the antibodies, and cell receptors [86]:

$$v = \left(f + \frac{\kappa m u f}{1 + \kappa f} + \frac{\kappa' q f}{1 + \kappa' f} \right). \tag{4.12}$$

For zero antigen concentration ($v = 0$), Eqs. (4.1)–(4.4) represent a model of the dynamics of immunocompetent lymphocytes, plasma cells, and antibodies in the absence of an antigenic stimulus. Equations (4.1)–(4.4) have a single stable stationary solution:

$$\bar{z}_i = a/\sigma \qquad (i = 1, \ldots, n), \tag{4.13}$$

$$\bar{z}_{n+1} = \sigma \bar{z}_n/\lambda = a/\lambda, \tag{4.14}$$

$$\bar{u} = \chi \bar{z}_{n+1}/\xi = \chi a/(\lambda \xi) = \chi \sigma \bar{z}_i/(\xi \lambda). \tag{4.15}$$

The stationary concentrations $\bar{z}_i$ ($i = 1, \ldots, n$), $\bar{z}_{n+1}$, $\bar{u}$ can be identified as the concentrations of immunocompetent lymphocytes of a certain specificity at n different developmental stages and of their plasma cell descendants and also as the concentration of the normal antibodies of the respective specificity in non-immunized mammals. This modeling prediction corresponds to the experimental observations [85, 90, 91], which indicate that the blood of mammals contains normal antibodies, that is, antibodies to antigens the organism has not previously encountered, and the lymphatic organs contain cells capable of producing antibodies without the corresponding antigenic stimulus.

The developed model is studied numerically. Equations (4.1)–(4.5) are solved by the Runge–Kutta method, and Eq. (4.12) by the method of Newton tangents. The model simulates the dynamics of the primary immune response of CBA mice to the abdominal introduction of varying amounts of T-independent antigen, capsular antigen of the plague microbe. The parameter values and the initial conditions are determined from the experimental data [92, 93]. In particular, the number of active centers on the antibody molecule m is taken to be equal to 5, because *IgM* antibodies are produced in the course of the primary immune response of mice to the antigen in question. The number of active antigenic determinants is taken to be 6. The boundary values $b^{\min}$ and $b^{\max}$ of the number of cell receptors occupied by an

antigen-stimulating multiplication are chosen to be 10^3 and 10^5, respectively. These values correspond to the estimates obtained from analysis of experiments in which immunization was performed using very small and very large amounts of capsular antigen of the plague microbe [74, 75]. The association constants in the interaction of free antibodies and cell receptors with antigenic determinants, κ and κ', are taken to be equal to $10^8\,M^{-1}$, where M denotes mole/liter. The number n of different age groups of B-cells is taken to be 44. The studies revealed that the increase in the value of n does not significantly change the model predictions. The values of the remaining model coefficients are the following [74, 75]: $\chi = 9.193 \cdot 10^7\,\mathrm{day}^{-1}$, $\sigma = 4\,\mathrm{day}^{-1}$, $\varsigma = 4 \cdot \ln 2\,\mathrm{day}^{-1}$, $\lambda = 2/3\,\mathrm{day}^{-1}$, $\xi = 2.5 \cdot \ln 2\,\mathrm{day}^{-1}$, $\eta = 2.4\,\mathrm{day}^{-1}$, $\zeta = \ln 7\,\mathrm{day}^{-1}$, $\omega_1 = 100$, $\varpi = 0.1/\log e$, $\varpi' = 1.5/\log e$, $k = 40$.

In turn, the initial conditions for the concentrations of immunocompetent lymphocytes at various developmental stages and for the concentration of plasma cells are calculated in the model proceeding from the concentration of normal antibodies to the plague microbe in mice ($\bar{u}$), which is measured using highly sensitive serological reactions. The initial conditions read

$$\begin{aligned} z_i(0) &= \bar{z}_i = \lambda\,\xi\,\bar{u}/(\sigma\,\chi) \quad (i = 1, \ldots, n)\,, \\ z_{n+1}(0) &= \bar{z}_{n+1} = \xi\,\bar{u}/\chi\,. \end{aligned} \tag{4.16}$$

The quantity $\bar{u}$ is also used to determine the rate of influx of immunocompetent cells from the bone marrow:

$$a = \lambda\,\xi\,\bar{u}/\chi\,. \tag{4.17}$$

As a result, we obtain the following values of the parameter a and of the initial conditions [74, 75]: $a = 16 \cdot 10^{-20}$ M/day, $z_i(0) = (2/3) \cdot 10^{-20}$ $(i = 1, \ldots, n)$, $z_{n+1}(0) = 4 \cdot 10^{-20}$ M, $u(0) = 2.12 \cdot 10^{-12}$ M. Additionally, we use two values for the initial concentration of the antigen: $v(0) = 4 \cdot 10^{-9}$ M and $v(0) = 4 \cdot 10^{-8}$ M. It is worth noting that the initial condition for the concentration of antigenic determinants is calculated taking into account the valence of the antigen molecule (which equals 6) and 80 % loss of the total amount of antigen molecules under their abdominal introduction.

The modeling results corresponding to two aforementioned values of the initial antigen concentration are presented in Figs. 4.1 and 4.2, respectively. These figures show the dynamics of the concentrations of APCs, antibody molecules (ABs), and antigenic molecules (AGs). Here we also present the experimental data on the abdominal immunization of CBA mice by the capsular antigen of the plague microbe [74, 75]. These are the average values and standard deviations of the number of APCs in the spleen and also of antigenic and antibody molecules in the animal blood measured at various times after immunization. It is worthwhile noting that in the experiments, serological reactions were used to determine the number of antibody and antigen molecules in the blood. The serological reactions allow one

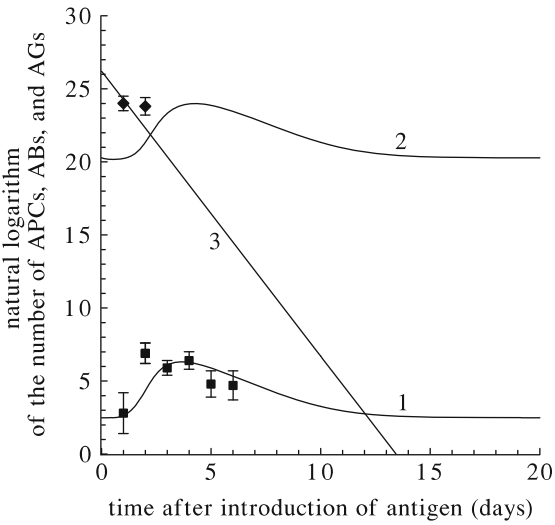

Fig. 4.1 Modeling results (*solid curves*) and experimental data [74, 75] (*symbols*) on the dynamics of the number of antibody-producing cells (APCs) (*curve 1 and box*), antibody molecules (ABs) (*curve 2*), and antigen molecules (AGs) (*curve 3 and diamonds*) during the immune response to 10^{12} molecules of capsular antigen of the plague microbe

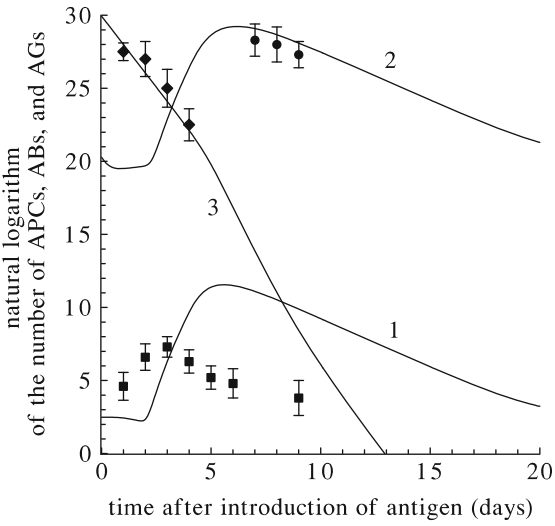

Fig. 4.2 Modeling results (*solid curves*) and experimental data [74, 75] (*symbols*) on the dynamics of the number of antibody-producing cells (APCs) (*curve 1 and box*), antibody molecules (ABs) (*curve 2 and circle*), and antigen molecules (AGs) (*curve 3 and diamonds*) during the immune response to 10^{13} molecules of capsular antigen of the plague microbe

to measure only the excess of antibodies over antigens or the excess of antigens over antibodies. Therefore, experimental data on the antigen dynamics are available for the first few days of the immune response, when the level of antibodies is still low, and data are available on the antibody dynamics for the last days of the immune reaction, when the amount of antigen becomes significantly smaller than the amount of antibody.

In Figs. 4.1 and 4.2 we see that the model qualitatively reproduces all four phases in the dynamics of accumulation of APCs in the spleen and antibodies in the blood of immunized mammals. During first 1–3.5 days after introduction of the antigen, the amounts of APCs and ABs are at very low levels that cannot be reached by

measurements using ordinary methods (the lag-phase). Then these quantities begin to rise exponentially (the log-phase). When high levels are reached, the number of APCs and ABs continues to increase slowly, and then they slowly decrease (the plateau phase). After that a more rapid decrease in these quantities sets in (the fall phase). In Figs. 4.1 and 4.2 we show the initial part of this last phase.

The results shown in these figures imply that the model gives a good reproduction of the experimental data even at the quantitative level. There is good agreement between the model and experimental dynamics of APC accumulation (Fig. 4.1), the dynamics of antigen extraction (Figs. 4.1 and 4.2), and the dynamics of AB accumulation (Fig. 4.2). Even some disagreement between the model and experimental dynamics of the number of APCs in Fig. 4.2 corresponds to the real situation. The point is that for abdominal introduction of large amounts of antigen, up to half of the APCs can be located not in the spleen, but in other lymphatic organs. Therefore, there is a difference between the computed curve describing the dynamics of all the plasma cells producing antibodies of a certain specificity and the experimental data on the dynamics of the number of APCs in the spleen, while there are no discrepancies between the model and experimental results on the dynamics of antibody molecules. The good agreement between the modeling predictions and experimental data testifies to the possibility of using system (4.1)–(4.5) as the basis for modeling the radiation-induced effects on humoral immunity.

4.4 Humoral Immunity in Mammals Exposed to Chronic Irradiation

In modeling studies of the radiation effect on the humoral immunity in mammals, it is possible to limit ourselves to the consideration of the postirradiation damaging and recovering of the bone marrow lymphopoietic system, because the leading role played by the bone marrow in the formation of the *B*-lymphocyte pool is considered as proven [85]. Damage to the functioning of other systems of the organism affecting the immune system indirectly is not taken into account. Proceeding from this, let us describe the radiation effects on the system of bone marrow lymphopoiesis and on the population of immunocompetent cells as its part when constructing the model of the humoral immunity in exposed mammals. For this purpose, we combine the approaches used in developing the model of the dynamics of bone marrow lymphopoiesis in irradiated mammals and the model of the dynamics of the humoral immune response to a *T*-independent antigen in nonirradiated mammals (see Sects. 1.6 and 4.4).

As in Chap. 1, we split all the cells of the lymphopoietic system into the following three compartments according to the degree of maturity and differentiation:

- X, capable of dividing bone marrow lymphocyte precursors (from stem cells in the respective microenvironment to lymphoblasts);
- Y, nondividing maturing bone marrow lymphoid cells;
- Z, mature blood lymphocytes.

We considered the compartment Z to be the collection of the following cells:

- Z_i, B-lymphocytes predetermined to produce antibodies of a certain specificity at the ith developmental stage ($i = 1, \ldots, n$);
- Z_{n+1}, plasma cells (Z_{n+1}) synthesizing antibodies of this specificity;
- Z_{n+2}, B-lymphocytes that are not predetermined to produce antibodies of the specificity in question.

According to experimental data (see, e.g., [94]), the cells of all the aforementioned compartments (with the exception of plasma cells) are radiosensitive. The experimental observations [94] imply that the radiosensitive cells can be split into three groups according to their response to irradiation. The first group includes undamaged cells, the second group includes damaged cells that die within 1–2 days (mitotic death), and the third group includes heavily damaged cells that die within the first 4–7 h following the irradiation (interphase death). Proceeding from this, the model deals with the following groups of cells and molecules:

- X^{ud}, capable of dividing bone marrow lymphocyte precursors undamaged by radiation;
- X^{d}, capable of dividing bone marrow lymphocyte precursors damaged by radiation;
- X^{hd}, capable of dividing bone marrow lymphocyte precursors heavily damaged by radiation;
- Y^{ud}, incapable of dividing bone marrow lymphocyte precursors undamaged by radiation;
- Y^{d}, incapable of dividing bone marrow lymphocyte precursors damaged by radiation;
- Y^{hd}, incapable of dividing bone marrow lymphocyte precursors heavily damaged by radiation;
- Z_i^{ud}, undamaged by radiation B-lymphocytes that are predetermined to produce antibodies of a certain specificity and existing at the ith developmental stage ($i = 1, \ldots, n$);
- Z_i^{d}, damaged by radiation B-lymphocytes that are predetermined to produce antibodies of a certain specificity and existing at the ith developmental stage ($i = 1, \ldots, n$);
- Z_i^{hd}, heavily damaged by radiation B-lymphocytes that are predetermined to produce antibodies of a certain specificity and existing at the ith developmental stage ($i = 1, \ldots, n$);
- Z_{n+1}, the radioresistant plasma cells synthesizing antibodies of this specificity;
- Z_{n+2}^{ud}, undamaged by radiation B-lymphocytes that are not predetermined to produce antibodies of the specificity in question;
- Z_{n+2}^{d}, damaged by radiation B-lymphocytes that are not predetermined to produce antibodies of the specificity in question;
- Z_{n+2}^{hd}, heavily damaged by radiation B-lymphocytes that are not predetermined to produce antibodies of the specificity in question;
- ABs, antibody molecules of the specificity in question;
- AGs, antigen molecules.

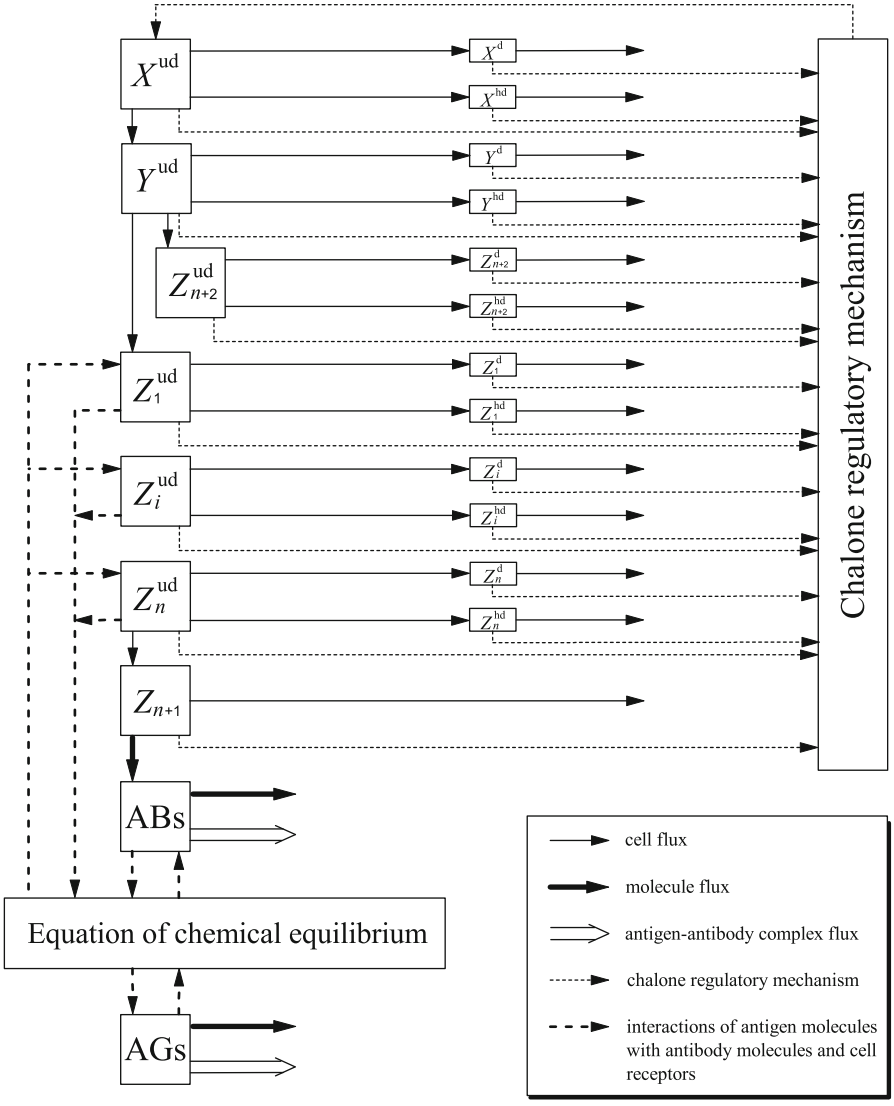

Fig. 4.3 Block diagram of the model (4.18)–(4.31)

The model is also based on the one-target–one-hit theory of cell damage [95]. According to this theory, the specific damage rate is proportional to the radiation dose rate N.

The main ideas and relations forming the basis of the model are displayed in the block diagram presented in Fig. 4.3.

We choose, as the model variables, the concentrations of the aforementioned cells $[x^{ud}, x^d, x^{hd}, y^{ud}, y^d, y^{hd}, z_i^{ud}, z_i^d, z_i^{hd}\ (i = 1, \ldots, n), z_{n+1}, z_{n+2}^{ud}, z_{n+2}^d, z_{n+2}^{hd}]$,

the concentration of the respective antibody molecules (u), and the concentration of antigenic determinants (v). In terms of these variables, the dynamics of the humoral immune response to a T-independent antigen in irradiated mammals is described by the following differential equations:

$$\frac{dx^{\mathrm{ud}}}{dt} = Bx^{\mathrm{ud}} - \gamma x^{\mathrm{ud}} - \frac{N}{D_x^0}x^{\mathrm{ud}}, \tag{4.18}$$

$$\frac{dy^{\mathrm{ud}}}{dt} = \gamma x^{\mathrm{ud}} - \delta y^{\mathrm{ud}} - \frac{N}{D_y^0}y^{\mathrm{ud}}, \tag{4.19}$$

$$\frac{dz_1^{\mathrm{ud}}}{dt} = \varepsilon\delta y^{\mathrm{ud}} - \sigma z_1^{\mathrm{ud}} + \varsigma s_1(b_1)z_1^{\mathrm{ud}} - \frac{N}{D_z^0}z_1^{\mathrm{ud}}, \tag{4.20}$$

$$\frac{dz_i^{\mathrm{ud}}}{dt} = \sigma(z_{i-1}^{\mathrm{ud}} - z_i^{\mathrm{ud}}) + \varsigma s_i(b_i)z_i^{\mathrm{ud}} - \frac{N}{D_z^0}z_i^{\mathrm{ud}} \qquad (i = 2, \ldots, n), \tag{4.21}$$

$$\frac{dz_{n+1}}{dt} = \sigma z_n^{\mathrm{ud}} - \lambda z_{n+1}, \tag{4.22}$$

$$\frac{dz_{n+2}^{\mathrm{ud}}}{dt} = (1-\varepsilon)\delta y^{\mathrm{ud}} - \psi z_{n+2}^{\mathrm{ud}} - \frac{N}{D_z^0}z_{n+2}^{\mathrm{ud}}, \tag{4.23}$$

$$\frac{du}{dt} = \chi z_{n+1} - \xi u - c\eta u, \tag{4.24}$$

$$\frac{dv}{dt} = -\zeta v - \eta v', \tag{4.25}$$

$$\frac{dx^{\mathrm{d}}}{dt} = \frac{N}{D_x^0}\frac{1}{1+\rho_x}x^{\mathrm{ud}} - \mu x^{\mathrm{d}}, \tag{4.26}$$

$$\frac{dy^{\mathrm{d}}}{dt} = \frac{N}{D_y^0}\frac{1}{1+\rho_y}y^{\mathrm{ud}} - \mu y^{\mathrm{d}}, \tag{4.27}$$

$$\frac{dz_i^{\mathrm{d}}}{dt} = \frac{N}{D_z^0}\frac{1}{1+\rho_z}z_i^{\mathrm{ud}} - \mu z_i^{\mathrm{d}} \qquad (i = 1, \ldots, n, n+2), \tag{4.28}$$

$$\frac{dx^{\mathrm{hd}}}{dt} = \frac{N}{D_x^0}\frac{\rho_x}{1+\rho_x}x^{\mathrm{ud}} - \nu x^{\mathrm{hd}}, \tag{4.29}$$

$$\frac{dy^{\mathrm{hd}}}{dt} = \frac{N}{D_y^0}\frac{\rho_y}{1+\rho_y}y^{\mathrm{ud}} - \nu y^{\mathrm{hd}}, \tag{4.30}$$

$$\frac{dz_i^{\mathrm{hd}}}{dt} = \frac{N}{D_z^0}\frac{\rho_z}{1+\rho_z}z_i^{\mathrm{ud}} - \nu z_i^{\mathrm{hd}} \qquad (i = 1, \ldots, n, n+2). \tag{4.31}$$

Here the coefficients σ, ς, λ, ξ, η, ζ, and χ have the same meaning as in Eqs. (4.1)–(4.5), and the variable parameters $s_i(b_i)$, c, and v' are defined by

Eqs. (4.6)–(4.12). In turn, the coefficient γ is the specific rate of transfer of cells from group X^{ud} to group Y^{ud}. The coefficient δ is the specific rate of transfer of cells from group Y^{ud} to groups Z_1^{ud} and Z_{n+2}^{ud}. The coefficient ε is equal to the fraction of cells predetermined to produce antibodies of a certain specificity among all the lymphoid cells leaving the bone marrow. The coefficients μ and ν are the specific decay rates of damaged and heavily damaged cells, respectively. The coefficient ψ is the specific decay rate of lymphocytes, which can be expressed in terms of other model parameters, namely

$$\psi = \frac{1}{n/\sigma + 1/\lambda}. \tag{4.32}$$

To derive the formula determining the reproduction rate of X^{ud} cells, B, it is assumed that a certain tissue-specific substance, chalone, is the material carrier of the feedback in cell division control in lymphopoiesis system, the chalone being the product of vital activity and decay of cells of this hematopoietic lineage [see Eq. (1.12)]. As a result, we have

$$B = \alpha\Bigg[1 + \beta\Big[x^{\mathrm{ud}} + \phi x^{\mathrm{d}} + \varphi x^{\mathrm{hd}} + \theta\big(y^{\mathrm{ud}} + \phi y^{\mathrm{d}} + \varphi y^{\mathrm{hd}}\big) + \vartheta\Big(\sum_{i=1}^{n}\big(z_i^{\mathrm{ud}} + \phi z_i^{\mathrm{d}} + \varphi z_i^{\mathrm{hd}}\big) + z_{n+1} + z_{n+2}^{\mathrm{ud}} + \phi z_{n+2}^{\mathrm{d}} + \varphi z_{n+2}^{\mathrm{hd}}\Big)\Big]\Bigg]^{-1}, \tag{4.33}$$

where α is the maximum specific rate of cell division, and the dimensionless multipliers ϕ and φ represent the dissimilar contributions of damaged and heavily damaged cells to the production of the specific inhibitor of the cell division.

The coefficients ρ_x, ρ_y, and ρ_z in Eqs. (4.26)–(4.31) are expressed through the radiobiological parameters characterizing the radiosensitivity of X, Y, and Z cells (see Sect. 1.4):

$$\rho_x = \frac{1}{D_x^{00}/D_x^0 - 1}, \qquad \rho_y = \frac{1}{D_y^{00}/D_y^0 - 1}, \qquad \rho_z = \frac{1}{D_z^{00}/D_z^0 - 1}. \tag{4.34}$$

The constant parameters D_x^0, D_y^0, and D_z^0 stand for quantities that are traditionally measured in radiobiology and are known as doses D_0. After exposure to these doses, the number of X, Y, and Z_i ($i = 1, \ldots, n, n+2$) cells left undamaged is $e = 2.718\ldots$ times smaller than the initial number of cells of the respective compartment. In turn, the constant parameters D_x^{00}, D_y^{00}, and D_z^{00} are the doses after exposure to which the number of X, Y, and Z_i ($i = 1, \ldots, n, n+2$) cells that have not died in the interphase is $e = 2.718\ldots$ times smaller than the initial number of cells of the respective compartment.

In the absence of an antigenic stimulus [i.e., for $v(0) = 0$], the dynamics of lymphopoietic cells can be described both by the system (4.18)–(4.23), (4.26)–(4.31) with $s_i(b_i)$=0 ($i = 1, \ldots, n$) and by Eqs. (1.7)–(1.11) in Chap. 1, to which

the system (4.18)–(4.23), (4.26)–(4.31) can be reduced. Here the variables of Eqs. (1.7)–(1.11) are expressed in terms of the variables of the system (4.18)–(4.23), (4.26)–(4.31) in the following way:

$$x_1 \equiv x\,, \tag{4.35}$$

$$x_2 \equiv y\,, \tag{4.36}$$

$$x_3 \equiv z_{n+2} + \sum_{i=1}^{n} z_i\,. \tag{4.37}$$

When we simulate the effects of chronic irradiation on the humoral immune response to T-independent antigen in previously unexposed mammals that did not previously come into contact with the respective antigen, then the initial conditions for solving Eqs. (4.18)–(4.31) are defined as follows:

$$\begin{aligned}
&x^{\mathrm{ud}}(0) = \bar{x}, \quad y^{\mathrm{ud}}(0) = \bar{y}, \quad z_i^{\mathrm{ud}}(0) = \bar{z}_i \quad (i = 1, \ldots, n, n+2),\\
&z_{n+1}(0) = \bar{z}_{n+1}, \quad u(0) = \bar{u}, \quad v(0) = 0,\\
&x^{\mathrm{d}}(0) = 0, \quad y^{\mathrm{d}}(0) = 0, \quad z_i^{\mathrm{d}}(0) = 0 \quad (i = 1, \ldots, n, n+2),\\
&x^{\mathrm{hd}}(0) = 0, \quad y^{\mathrm{hd}}(0) = 0, \quad z_i^{\mathrm{hd}}(0) = 0 \quad (i = 1, \ldots, n, n+2).
\end{aligned} \tag{4.38}$$

Here the quantities $\bar{x}$, $\bar{y}$, $\bar{z}_i$ $(i = 1, \ldots, n+2)$, and $\bar{u}$ are the stationary solutions of Eqs. (4.18)–(4.31) with zero values for N and v. The quantities $\bar{x}$, $\bar{y}$, and $\bar{z}_i$ $(i = 1, \ldots, n+2)$ can be identified with the stationary concentrations of X, Y, and Z_i $(i = 1, \ldots, n+2)$ cells in unexposed organism in the absence of antigen. In turn, the quantity $\bar{u}$ can be identified with the concentration of normal antibodies of the specificity in question. The stationary concentrations of X, Y, and Z_i $(i = 1, \ldots, n+2)$ cells are expressed in terms of the stationary concentration of normal antibodies $\bar{u}$ in the following way:

$$\bar{x} = \frac{1}{\varepsilon}\,\frac{\lambda\xi}{\chi\gamma}\,\bar{u}, \tag{4.39}$$

$$\bar{y} = \frac{1}{\varepsilon}\,\frac{\lambda\xi}{\chi\delta}\,\bar{u}, \tag{4.40}$$

$$\bar{z}_i = \frac{\lambda\xi}{\sigma\chi}\,\bar{u} \qquad (i = 1, \ldots, n), \tag{4.41}$$

$$\bar{z}_{n+1} = \frac{\xi}{\chi}\,\bar{u}, \tag{4.42}$$

$$\bar{z}_{n+2} = \frac{1-\varepsilon}{\varepsilon}\,\frac{\lambda\xi}{\chi\psi}\,\bar{u}. \tag{4.43}$$

When solving numerically the system (4.18)–(4.31) with initial conditions (4.38), the variable v is set equal to the initial concentration of antigenic determinants $(v)_0$ at the moment of immunization; the variable parameter N is taken to be equal to the dose rate of the irradiation at the moment of its onset.

The model (4.18)–(4.31) is used to examine the dynamics of the primary humoral immune reaction to the soluble T-independent antigen (the capsular antigen of the plague microbe) in CBA mice exposed to chronic irradiation. Therefore, values of the parameters n, m, $b^{\min}$, $b^{\max}$, κ, κ', ω_1, ϖ, ϖ', σ, ς, λ, ξ, η, ζ, and χ are the same as in the model (4.1)–(4.5) (see Sect. 4.3). The parameter ε is set equal to 10^{-5}, in accordance with the estimates obtained in immunology [81]. The values of some parameters coincide with the values of the corresponding parameters in the lymphopoiesis model (see Table 1.2), namely $\alpha = 2.4\,\text{day}^{-1}$, $\gamma = 1.4\,\text{day}^{-1}$, $\delta = 0.2\,\text{day}^{-1}$, $\mu = 0.5\,\text{day}^{-1}$, $\nu = 6.0\,\text{day}^{-1}$, $D_x^0 = 1.4\,\text{Gy}$, $D_y^0 = 1.4\,\text{Gy}$, $D_z^0 = 1.0\,\text{Gy}$, $D_x^{00} = 13.0\,\text{Gy}$, $D_y^{00} = 13.0\,\text{Gy}$, $D_z^{00} = 6.5\,\text{Gy}$, $\theta = 0.1$, $\vartheta = 0.16$, $\phi = 1$, $\varphi = 12$. The value of parameter ψ was calculated by making use of Eq. (4.32): $\psi = 0.08\,\text{day}^{-1}$. This value is the same as that in the lymphopoiesis model (see Table 1.2).

In the numerical studies of the identified model, the dose rate of chronic irradiation varies over a wide range. Figures 4.4 and 4.5 present the results of

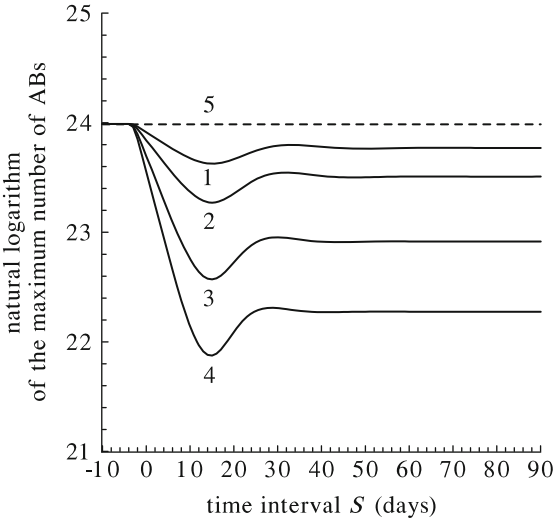

Fig. 4.4 Dependence of the maximum number of antibody molecules ABs on the time interval S between the onset of chronic irradiation at dose rates $N = 0.025, 0.05, 0.1, 0.15$ Gy/day (*curves 1–4*) and introduction of 10^{12} molecules of capsular antigen of the plague microbe. The *dashed line* (5) indicates the respective maximum number of ABs in the unexposed mice ($N = 0$). A zero value of S implies that the introduction of antigen and the onset of chronic irradiation occur simultaneously. Negative values of S correspond to the cases when the introduction of antigen precedes the onset of chronic irradiation. Positive values of S mean that the onset of chronic irradiation precedes the introduction of antigen

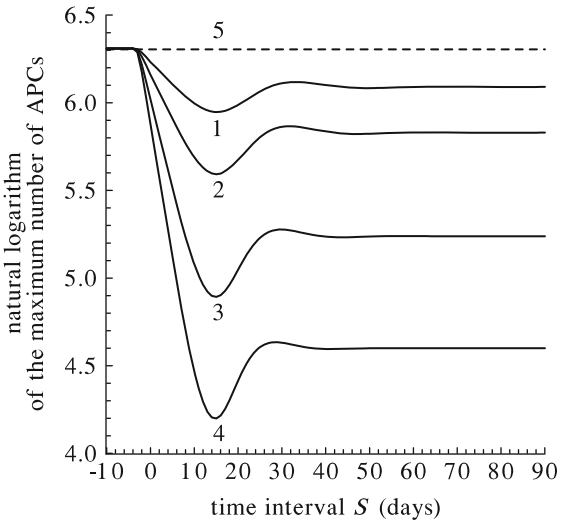

Fig. 4.5 Dependence of the maximum number of antibody-producing cells (APCs) on the time interval S between the onset of chronic irradiation at dose rates $N = 0.025, 0.05, 0.1, 0.15$ Gy/day (*curves 1–4*) and introduction of 10^{12} molecules of capsular antigen of the plague microbe. The *dashed line (5)* indicates the respective maximum number of APCs in the unexposed mice ($N = 0$). A zero value of S implies that the introduction of antigen and the onset of chronic irradiation occur simultaneously. Negative values of S correspond to the cases when the introduction of antigen precedes the onset of chronic irradiation. Positive values of S mean that the onset of chronic irradiation precedes the introduction of antigen

the modeling studies of the dependence of the immune response intensity (i.e., the maximum numbers of ABs and APCs) on the time interval S between the onset of chronic irradiation and the abdominal introduction of 10^{12} molecules of capsular antigen of the plague microbe. The computations are performed for several dose rates N. If the introduction of antigen precedes the onset of exposure by more than 4 days, then the maximum numbers of ABs and APCs coincide for exposed and unexposed animals. In this case, the onset of exposure occurs after the moment when the immune response has reached its maximum level. The decrease in the time interval between the introduction of antigen and the onset of chronic irradiation from 4 days to 0 leads to the decrease in the maximum numbers of ABs and APCs, i.e., to the lowering of the intensity of the immune response. If the onset of exposure precedes the introduction of antigen, the dependence of the maximum numbers of ABs and APCs on S is the following. When S increases from 0 to 15 days, the maximum numbers of ABs and APCs decrease. When S increases from 15 to 28–30 days (depending on N), they grow, being smaller than the respective values for unexposed animals. A further increase in the time interval S between the onset of exposure and the introduction of antigen leads first to lowering of the maximum numbers of ABs and APCs and then to their relaxation to new stationary levels. The latter is lower for higher dose rate N. These modeling results can be interpreted

in the following way. When the duration of radiation exposure that precedes the introduction of antigen increases (i.e., when the accumulated radiation dose grows), the intensity of the humoral immune response in exposed mice first decreases, then increases, being lower than that in unexposed specimens, and then, after a small lowering, relaxes to a new stationary level that is lower than that in unexposed mice. Thus, the model predicts the lowered level of humoral immunity in mammals exposed to low-level chronic irradiation. This prediction qualitatively corresponds to clinical data obtained for some children and juveniles residing in regions with an elevated radiation background [96].

The revealed phenomenon can be considered a result of the process of adaptation of the humoral immune system to low-level long-term irradiation. As revealed by modeling studies, the ability of the humoral immune system to adapt itself to low-level long-term irradiation is due to adaptation processes running in the bone marrow lymphopoietic system under such exposures. In particular, the concentrations of bone marrow lymphocyte precursors that are incapable of dividing and capable of dividing, as well as the mitotic index of the latter, relax to new stationary levels that are higher than those in unexposed specimens. These modeling predictions agree with experimental data for mice [97]. In turn, the concentration of the blood lymphocytes (among them the immunocompetent *B*-lymphocytes) relaxes to a new stationary level that is below the norm. These modeling results qualitatively agree with experimental data for mice [97] and correspond to clinical observations for humans [98].

4.5 Humoral Immunity in Mammals Exposed to Acute Irradiation

In simulating the dynamics of the humoral immune response to a *T*-independent antigen in mammals exposed to acute irradiation, one can employ the model (4.18)–(4.31) with the respective value of the parameter N and with the initial conditions (4.38). One can also use a simplified version of the model. Since the duration of acute irradiation is negligible, the model can be simplified by making use of the approach presented in Sect. 1.4. As a result, the model is reduced to Eqs. (4.18)–(4.31) with a zero value for the parameter N. In the numerical solution of the simplified system (4.18)–(4.31) with initial conditions (4.38), the variable v is set equal to the initial concentration of antigenic determinants $(v)_0$ at the moment of the introduction of the antigen. In turn, at the moment of acute irradiation, the concentrations of undamaged, moderately damaged, and heavily damaged by radiation radiosensitive cells are changed in the following way:

$$x^{\mathrm{ud}}(t_{re}) = \hat{x} \exp\left(-D/D_x^0\right), \tag{4.44}$$

$$y^{\mathrm{ud}}(t_{re}) = \hat{y} \exp\left(-D/D_y^0\right), \tag{4.45}$$

$$z_i^{\mathrm{ud}}(t_{re}) = \widehat{z_i}\exp\left(-D/D_z^0\right) \qquad (i = 1, \ldots, n, n+2), \tag{4.46}$$

$$x^{\mathrm{d}}(t_{re}) = \hat{x}\left[1 - \exp\left(-D/D_x^0\right)\right]\frac{1}{1+\rho_x}, \tag{4.47}$$

$$y^{\mathrm{d}}(t_{re}) = \hat{y}\left[1 - \exp\left(-D/D_y^0\right)\right]\frac{1}{1+\rho_y}, \tag{4.48}$$

$$z_i^{\mathrm{d}}(t_{re}) = \widehat{z_i}\left[1 - \exp\left(-D/D_z^0\right)\right]\frac{1}{1+\rho_z} \quad (i = 1, \ldots, n, n+2), \tag{4.49}$$

$$x^{\mathrm{hd}}(t_{re}) = \hat{x}\left[1 - \exp\left(-D/D_x^0\right)\right]\frac{\rho_x}{1+\rho_x}, \tag{4.50}$$

$$y^{\mathrm{hd}}(t_{re}) = \hat{y}\left[1 - \exp\left(-D/D_y^0\right)\right]\frac{\rho_y}{1+\rho_y}, \tag{4.51}$$

$$z_i^{\mathrm{hd}}(t_{re}) = \widehat{z_i}\left[1 - \exp\left(-D/D_z^0\right)\right]\frac{\rho_z}{1+\rho_z} \quad (i = 1, \ldots, n, n+2), \tag{4.52}$$

where

$$\rho_x = \frac{1 - \exp(-D/D_x^{00})}{\exp(-D/D_x^{00}) - \exp(-D/D_x^0)}, \tag{4.53}$$

$$\rho_y = \frac{1 - \exp(-D/D_y^{00})}{\exp(-D/D_y^{00}) - \exp(-D/D_y^0)}, \tag{4.54}$$

$$\rho_z = \frac{1 - \exp(-D/D_z^{00})}{\exp(-D/D_z^{00}) - \exp(-D/D_z^0)}. \tag{4.55}$$

Here D is the dose of acute irradiation, the quantities $\hat{x}$, $\hat{y}$, and $\hat{z}_i$ are the concentrations of X, Y, and Z_i cells before acute exposure, the parameters D_x^0, D_y^0, D_z^0, D_x^{00}, D_y^{00}, and D_z^{00} are defined above.

The developed model is employed to examine the dynamics of the primary humoral immune reaction to the soluble T-independent antigen (the capsular antigen of the plague microbe) in CBA mice exposed to acute irradiation. The values of all the parameters are the same as before (see Sect. 4.4).

Figures 4.6 and 4.7 show the dynamics of antibody molecules (ABs) and APCs obtained in modeling the immune reaction to the introduction of 10^{12} molecules of capsular antigen of the plague microbe in unexposed mice, in mice exposed to acute irradiation at a dose of 2 Gy 1 and 3 days before immunization, and in mice immunized one and 10 days before acute irradiation at the same dose D. A comparison of the curves shows that exposure both before and after immunization at the chosen time intervals leads to a decrease in the intensity of the immune response. This modeling result agrees qualitatively with the experimental observations [99, 100].

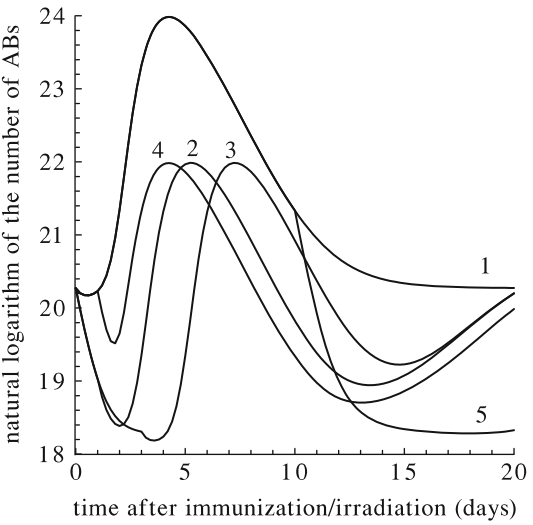

Fig. 4.6 Model dynamics of the number of antibody molecules ABs during the humoral immune response to the abdominal introduction of 10^{12} molecules of capsular antigen of the plague microbe in unexposed mice (*curve 1*) and mice exposed to acute irradiation at a dose of 2 Gy (*curves 2 and 3* are for irradiation 1 and 3 days before immunization, whereas *curves 4 and 5* are for immunization 1 and 10 days before irradiation)

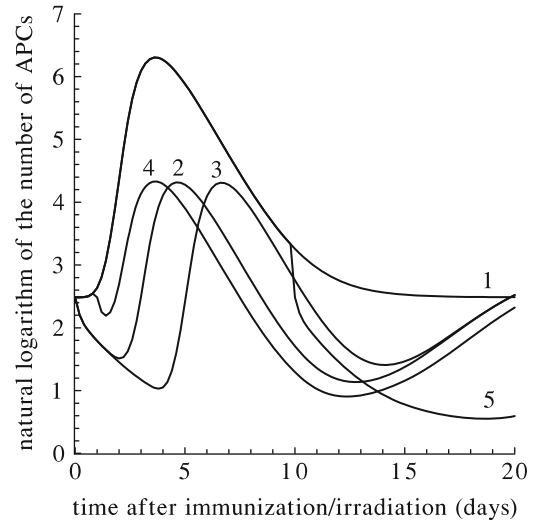

Fig. 4.7 Model dynamics of the number of antibody-producing cells (APCs) during the humoral immune response to the abdominal introduction of 10^{12} molecules of capsular antigen of the plague microbe in unexposed mice (*curve 1*) and mice exposed to acute irradiation at a dose of 2 Gy (*curves 2 and 3* are for irradiation 1 and 3 days before immunization, whereas *curves 4 and 5* are for immunization 1 and 10 days before irradiation)

Each of the five types of the immune response presented in Figs. 4.6 and 4.7 has its own features. As already noted, for unexposed mice in the first 1–1.5 days after immunization, the numbers of APCs and ABs increase very slowly, followed by exponential growth, attainment of the maximum values, and then falloff to the normal level. In the cases when acute irradiation precedes immunization, the initial and final stages of the AB and APC dynamics differ from those studied above. After acute irradiation, the numbers of ABs and APCs decrease as a result of postradiation death of APCs precursors in the blood and bone marrow. After immunization, this falloff continues as long as the rate of replenishing the pool of plasma cells remains smaller than their natural death rate. Then, after certain minimum levels are reached,

the numbers of ABs and APCs begin to increase to the maximum levels, which are lower than in unexposed animals. After that the numbers of ABs and APCs again decrease to levels lower than the norm, and then return to the initial values. This feature of the final stage of the immune response of exposed mammals is due to the superposition of two processes: (1) a decrease in the intensity of AB and APC accumulation as a result of a decrease in the amount of antigen which stimulates the division of immunocompetent *B*-lymphocytes, and (2) an increase in the numbers of ABs and APCs to their normal level in the ongoing process of regeneration of the bone marrow lymphopoietic system. Computations also show that the increase in the time interval between irradiation and immunization leads to shortening and then to complete disappearance of the phase in which the amounts of ABs and APCs decrease right after immunization, and also to a "smoothing" of the final phase of the dynamics of the immune response. However, it should be noted that the values of the radiation dose D and of the time interval between irradiation and immunization have practically no effect on the duration of the time intervals between immunization and the times required to reach the maximum numbers of ABs and APCs. They are the same as in unexposed animals.

In cases when immunization precedes acute irradiation, the nature of the dynamics of the immune reaction depends significantly on the time interval between them. If the time between the introduction of antigen and acute irradiation is small and the immune reaction does not succeed in developing fully by the moment of acute irradiation, the kinetic curves showing the dynamics of APCs and antibodies have a doubly peaked shape. The numbers of APCs and ABs grow slowly during the time between immunization and acute irradiation. After acute irradiation, the numbers of APCs and ABs decrease due to postirradiation death of *B*-lymphocytes predetermined to produce antibodies of a given specificity and their precursors in the bone marrow. Then the antigen-stimulated division of predetermined *B*-lymphocytes undamaged by radiation, together with the increase in the influx of *B*-lymphocytes from the bone marrow, leads to an increase in the numbers of APCs and ABs. They reach maximum values that are lower than in unexposed animals. The final stage of the APC and AB dynamics is the same as that in animals that are first exposed and then immunized. The immune response develops in the same way if the time interval between immunization and irradiation does not exceed 2 days. When the time interval between immunization and irradiation exceeds 2 days, the dynamical curves are different; namely, they have a single peak. This happens because a large number of antibody molecules have been accumulated by the moment of acute irradiation, and these bind to the antigen circulating in the blood and hasten its removal from the organism. Then, after exposure, the numbers of APCs and ABs decrease both as a result of postradiation death of *B*-lymphocytes predetermined to produce antibodies of a given specificity and their precursors in the bone marrow, and as a result of cessation of the division of immunocompetent *B*-lymphocytes in the absence of antigenic stimulation. The final part of the APC and AB dynamics (the rise phase) is due to the regeneration of the bone marrow lymphopoietic system damaged by radiation. The computations revealed that if immunization precedes acute irradiation, the time intervals between

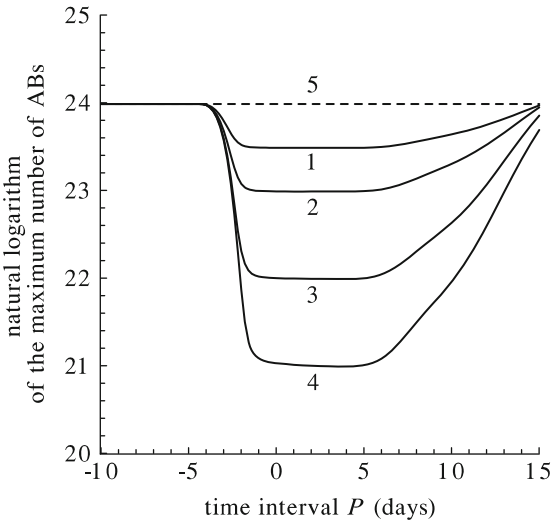

Fig. 4.8 Dependence of the maximum number of antibody molecules ABs on the time interval P between exposure to acute irradiation at doses $D = 0.5, 1, 2, 3$ Gy (*curves 1–4*) and immunization by 10^{12} antigen molecules. The *dashed line (5)* is the level of the maximum number of ABs in unexposed animals. A zero value of P implies that the introduction of antigen and acute irradiation occur simultaneously. Negative values of P correspond to the cases when the introduction of antigen precedes acute irradiation. Positive values of P mean that acute irradiation precedes the introduction of antigen

introduction of the antigen and the times required to reach the maximum numbers of APCs and ABs are nearly independent of the values of the radiation dose and the time interval between immunization and acute irradiation. Moreover, when the value of the time interval between immunization and irradiation exceeds 4 days, the maximum numbers of APCs and ABs in exposed animals are the same as in unexposed ones.

The influence of the value of the time interval P between acute irradiation and immunization on the maximum levels of numbers of APCs and antibodies for a fixed amount of introduced antigen (10^{12} molecules) and for various radiation doses D is also examined. The results are shown in Figs. 4.8 and 4.9.

As one can infer from Figs. 4.8 and 4.9, if the immunization precedes acute irradiation, then the dependence of the maximum numbers of ABs and APCs on the value of P for a fixed radiation dose D is the following. When the introduction of antigen occurs more than 4 days before acute irradiation ($P < -4$ days), the maximum numbers of ABs and APCs are the same as those for unexposed specimens. When the time interval between the introduction of antigen and acute irradiation decreases from 4 to 0 days (i.e., the value of P increases from -4 days to 0), the maximum numbers of ABs and APCs also decrease.

If acute irradiation precedes immunization, then the dependence of the maximum numbers of ABs and APCs on P is quite different (Figs. 4.8 and 4.9). Specifically,

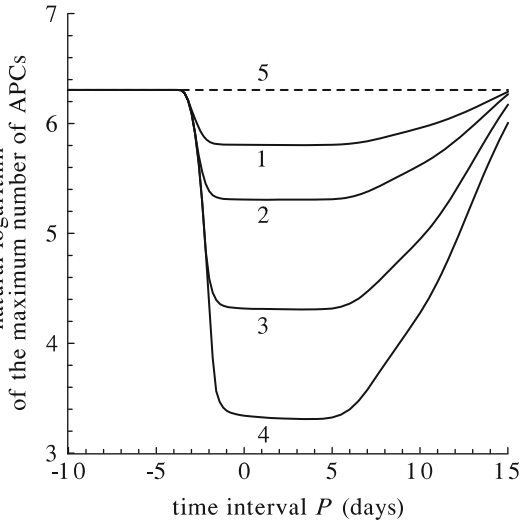

Fig. 4.9 Dependence of the maximum number of antibody-producing cells (APCs) on the time interval P between exposure to acute irradiation at doses $D = 0.5, 1, 2, 3$ Gy (*curves 1–4*) and immunization by 10^{12} antigen molecules. The *dashed line (5)* is the level of the maximum number of APCs in unexposed animals. A zero value of P implies that the introduction of antigen and acute irradiation occur simultaneously. Negative values of P correspond to the cases when the introduction of antigen precedes acute irradiation. Positive values of P mean that acute irradiation precedes the introduction of antigen

when P increases from 0 to 5 days, the dependence of the maximum numbers of ABs and APCs on P is very weak. Namely, within this range of P, the maximum numbers of ABs and APCs assume nearly constant values, the latter being smaller than the respective values for unexposed animals. When P increases from 5 to 15 days, the maximum numbers of ABs and APCs increase and approach values that are close to the respective maximal levels for unexposed animals.

Computations also reveal that a further increase in the time interval P between irradiation and immunization leads first to growth in the maximum numbers of APCs and ABs and then to their lowering. For $P = 30$ days, these quantities return to the levels corresponding to the immune response of unexposed animals and, in practice, do not change with further increases in P. This is caused by the complete restoration of the lymphocyte pool in the blood of exposed animals by the time specified above.

These results agree qualitatively with the experimental data on the dynamics of the humoral immune response in mammals exposed to sublethal doses of radiation at various times before or after immunization [99–104]. In particular, it has been found experimentally that during the period of active biosynthesis of antibodies, exposure to acute irradiation does not lead to a decrease in the maximum levels of antibodies in exposed mammals [102–104]. Meanwhile, during the initial stages of the immune response, the humoral immunity system is sensitive to radiation [104].

The maximum level of antibodies in exposed mammals is significantly lower than the level for unexposed animals. For the same radiation dose and the same amount of introduced antigen, this level decreases as the time interval between immunization and acute irradiation decreases [104].

The modeling results also agree quantitatively with the relevant experimental data. Specifically, CBA mice were exposed to acute irradiation at a dose of 4 Gy [101]. Seven days after the exposure, 50 μg of *T*-independent antigen, *Escherichia coli* lipopolysaccharide, strain 0111:B4, was introduced abdominally. It was found that the maximum amount of APCs in the spleen of the exposed mice was 15 times less than that in unexposed ones. The model reproduces the dynamics of the immune response of mice to the abdominal introduction of 10^{14} molecules of capsular antigen of the plague virus when exposure to acute irradiation at a dose of 4 Gy precedes immunization by 7 days. It was found that the maximum number of APCs in exposed mice is 17.8 times smaller than in unexposed ones. Thus, the model prediction is close to the corresponding experimental data.

In the work [101], CBA mice were exposed to acute irradiation at a dose of 4 Gy. The same antigen, *E. coli* lipopolysaccharide, strain 0111:B4, was introduced abdominally (amount equal to 50 μg) after 30 days. The number of APCs was determined 5 days after immunization. It was found that the numbers of APCs in the spleens of exposed and unexposed mice were practically the same. This implies that 30 days after exposure to acute irradiation at a dose of 4 Gy, the strength of the humoral response to a *T*-independent antigen is fully restored in the animals. These experimental data are consistent with the result obtained in the model: The maximum numbers of APCs in exposed and unexposed mice coincide if the time interval between acute irradiation and immunization exceeds 30 days.

The presented results elucidate the importance of studying the effects of acute irradiation on the dynamics of the humoral immunity system.

4.6 Conclusions

The models of humoral immune response in nonirradiated and irradiated mammals have been developed. The modeling predictions agree with the basic regularities in the dynamics of humoral immunity in nonirradiated and irradiated mammals (mice). These results, obviously, give evidence that the developed model, identified properly, can provide a better understanding of the radiation risks to health from the space radiation environment and enable one to evaluate the need for operational applications of countermeasures for astronauts on long-term space missions such as Lunar colonies and Mars missions.

References

1. Bond V.P., Fliendner T.M., Archambeau J.O. Mammalian Radiation Lethality: A Disturbance in Cellular Kinetics. New York: Academic Press, 1965.
2. Yarmonenko S.P., Vainson A.A. Radiobiology of Humans and Animals. Moscow: Vysshaya shkola, 2004 (Russian).
3. Elgert K.D. Immunology: Understanding the Immune System, 2nd ed. Hoboken, NJ: Wiley-Blackwell, 2009.
4. Coico R., Sunshine G. Immunology: A Short Course, 6th ed. Hoboken, NJ: Wiley-Blackwell, 2009.
5. Bell G.I. Mathematical model of clonal selection and antibody production I. Journal of Theoretical Biology, v. 29, pp. 191–232, 1970.
6. Bell G.I. Mathematical model of clonal selection and antibody production II. Journal of Theoretical Biology, v. 33. pp. 339–378, 1971.
7. Bell G.I. Mathematical model of clonal selection and antibody production III. Journal of Theoretical Biology, v. 33, pp. 379–398, 1971.
8. Bell G.I. Prey-predator equations simulating an immune response. Mathematical Biosciences, v. 16, pp. 291–314, 1973.
9. Smirnova O.A., Stepanova N.V. Mathematical model of oscillations under infection's immunity. In: Proceedings of the Second All-Union Symposium on Oscillatory Processes in Biological and Chemical Systems, Pushchino-na-Oke, 1970. NTsBI AN SSSR, Pushchino-na-Oke, v. 2, pp. 247–251, 1971 (Russian).
10. Smirnova O.A., Stepanova N.V. Computer modeling of immune response dynamics. Vestnik Moskovskogo Universiteta (Fizika, Astronomiya), no. 5, pp. 520–526, 1971 (Russian).
11. Smirnova O.A., Stepanova N.V. Mathematical model of the cooperative interaction in the immune reaction. Zhurnal Mikrobiologii, Epidemiologii i Immunologii, no. 11, pp. 50–53, 1974 (Russian).
12. Smirnova O.A., Stepanova N.V. Mathematical model of infection's immunity. In: Proceedings of the Intercollegiate Meeting on Theoretical and Experimental Biophysics. Kaliningrad: Kaliningrad State University, no. 5, pp. 61–75, 1975 (Russian).
13. Smirnova O.A. Mathematical model of the immune reaction. Vestnik Moskovskogo Universiteta (Fizika, Astronomiya), no. 4, pp. 485–486, 1975 (Russian).
14. Jilek M., Sterzl J. A model of differentiation of immunologically competent cells. In: Developmental Aspects of Antibody Formation and Structure. Prague: Academia; New York: Academic Press, pp. 963–981, 1970.
15. Jilek M., Ursinyova Z. The probability of a contact between immunocompetent cell and antigen. Folia Microbiologica, v. 15, pp. 294–302, 1970.
16. Jilek M., Ursinyova Z. On the distribution of the epoch of the first contact of immunocompetent cell with antigen. Folia Microbiologica, v. 15, pp. 492–499, 1970.
17. Jilek M. On contacts of immunocompetent cell with antigen: Note on a probability model. Folia Microbiologica, v. 16, pp. 83–87, 1971.
18. Molchanov A.V. Multi-barrier immunity. Biofizika, v. 16, pp. 482–487, 1971 (Russian).
19. Molchanov A.M., Nazarenko V.G., Shaturnyi I.G. Analysis of the model of the single-barrier immunity. Biofizika, v. 16, pp. 667–671, 1971 (Russian).
20. Marchuk G.I. The simplest model of viral disease. In: Mathematical Methods in Clinical Practice. Eds. G.I. Marchuk and N.I. Nisevich, Novosibirsk: Nauka, p. 7–19, 1978 (Russian).
21. Marchuk G.I. Mathematical Models in Immunology. Moscow: Nauka, 1980 (Russian).
22. Marchuk G.I. (Ed.). Mathematical Models of Diseases and Methods of Analyzing Medical Information. Novosibirsk: Nauka, 1979 (Russian).
23. Marchuk G.I. (Ed.). Mathematical Modeling in Immunology and Medicine. Novosibirsk: Nauka, 1982 (Russian).
24. Marchuk G.I. Mathematical Modeling in Immunology. Moscow: Nauka, 1991 (Russian).

25. Marchuk G.I. Mathematical Modelling of Immune Response in Infectious Diseases. Dordrecht: Kluwer Academic Publishers, 1997.
26. Belykh L.N. Analysis of Mathematical Models in Immunology. Moscow: Nauka, 1988 (Russian).
27. Zuev S.M. Statistical Estimation of Parameters of Mathematical Models of Diseases. Moscow: Nauka, 1988 (Russian).
28. Romanyukha A.A., Bocharov G.A., Marchuk G.I. Mathematical modelling of infectious diseases. In: Mathematical Aspects of Human Diseases. G. Da Prato (Ed.), Applied Mathematics Monographs, Pisa: Giardini Editori e Stampatori, v. 3, pp. 126–148, 1992.
29. Bocharov G.A., Romanyukha A.A. Mathematical modelling of immune response during acute viral infections. In: Theoretical and Experimental Insights into Immunology. A. Perelson and G. Weisbuch (Eds.), NATO ASI Series H, Heidelberg: Springer-Verlag, v. 66, pp. 309–321, 1992.
30. Marchuk G.I., Romanyukha A.A., Bocharov G.A. Mathematical models of immune response during infectious diseases. In: Mathematics Applied to Biology and Medicine. J. Demongeot and V. Capasso (Eds.), Mathematica Biology Series, Winnipeg, Canada: Wuerz Publishing, pp. 263–273, 1993.
31. Bocharov G.A., Romanyukha A.A. Mathematical model of antiviral immune response. III. Influenza — A virus infection. Journal of Theoretical Biology, v. 167, pp. 323–360, 1994.
32. Bell G., Perelson A., Pimbley G. (Eds.). Theoretical Immunology. New York: Marcel Dekker, 1978.
33. Bell G.I., De Lisi C.P. Antigen binding to receptors on immunocompetent cells. Cellular Immunology, v. 10, pp. 415–431, 1974.
34. De Lisi C.P. A theory of precipitation and agglutination reactions in immunological system. Journal of Theoretical Biology, v. 45, pp. 555–575, 1974.
35. De Lisi C.P. Detection and analysis of recognition and selection in the immune response. Bulletin of Mathematical Biology, v. 39, pp. 705–719, 1977.
36. De Lisi C.P. Some mathematical problems on the initiation and regulation of the immune response. Mathematical Biosciences, v. 21, pp. 251–277, 1974.
37. De Lisi C.P., Perelson A.S. The kinetics of aggregation phenomena. Journal of Theoretical Biology, v. 62, pp. 159–210, 1976.
38. Perelson A.S., Mirmirani M., Oster G.F. Optimal strategies in immunology: I. *B*-cell differentiation and proliferation. Journal of Mathematical Biology, v. 3, pp. 325–365, 1976.
39. Perelson A.S., Mirmirani M., Oster G.F. Optimal strategies in immunology: II. *B*-cell differentiation and proliferation. Journal of Mathematical Biology, v. 5, pp. 213–256, 1976.
40. Pimbley G.H. Periodic solution of predator-prey equations simulating an immune response: I. Mathematical Biosciences, v. 20, pp. 27–51, 1974.
41. Pimbley G.H. Periodic solution of predator-prey equations simulating an immune response: II. Mathematical Biosciences, v. 21, p. 251–277, 1975.
42. Bruni C., Germani A., Koch G., Strom R. Derivation of antibody distribution from experimental binding data. Journal of Theoretical Biology, v. 61, pp. 143–170, 1975.
43. Bruni C., Giovenco M.A., Koch G., Strom R. A dynamical model of humoral immune response. Mathematical Biosciences, v. 27, pp. 191–211, 1975.
44. Mohler R. Bilinear control structures in immunology. In: Modelling and Optimization of Complex System, Proceedings of the IFIP TC, Working Conference, Novosibirsk, USSR, July 1978, G.I. Marchuk (Ed.), Berlin; Heidelberg; New York: Springer-Verlag, pp. 58–68, 1979.
45. Dibrov B.F., Lifshits M.A., Vol'kenshtein M.V. Mathematical model of immune reaction: I. Biofizika, v. 21, pp. 313–317, 1976 (Russian).
46. Dibrov B.F., Lifshits M.A., Vol'kenshtein M.V. Mathematical model of immune reaction: II. Biofizika, v. 22, pp. 905–909, 1977 (Russian).
47. Dibrov B.F., Lifshits M.A., Vol'kenshtein M.V. Mathematical model of immune reaction: III. Biofizika, v. 23, pp. 143–147, 1978 (Russian).

48. Dibrov B.F., Lifshits M.A., Vol'kenshtein M.V. Mathematical model of immune reaction: IV. Biofizika, v. 23, pp. 494–499, 1978 (Russian).
49. Glushkov V.M., Ivanov V.V., Yanenko V.M. Application of one class of models in studies of immune systems. Mathematical Methods in Biology. Kiev: Naukova Dumka, pp. 40–52, 1983 (Russian).
50. Ikegami T. Dynamical behaviors of immune network. Progress of Theoretical Physics, v. 81(2), pp. 309–320, 1989.
51. Stewart J., Varela F.J. Morphogenesis in shape-space. Elementary meta-dynamics in a model of the immune network. Journal of Theoretical Biology, v. 144, pp. 477–498, 1991.
52. De Boer R.J., Kevrekidis I.G., Perelson A.S. Immune network behavior. I. From stationary states to limit cycle oscillations. Bulletin of Mathematical Biology, v. 55, pp. 745–780, 1993.
53. Frost S.D.W., McLean A.R. Germinal centre destruction as a major pathway of HIV pathogenesis. Journal of Acquired Immune Deficiency Syndromes, v. 7(3), pp. 236–244, 1994.
54. Meyer-Hermann M., Deutsch A., Or-Guil M. Recycling probability and dynamical properties of germinal center reactions. Journal of Theoretical Biology, v. 210(3), pp. 265–285, 2001.
55. Frank S.A. Immune response to parasitic attack: Evolution of a pulsed character. Journal of Theoretical Biology, v. 219(3), pp. 281–290, 2002.
56. Kesmir C., De Boer R.J. A spatial model of germinal center reactions: Cellular adhesion based sorting of B cells results in efficient affinity maturation. Journal of Theoretical Biology, v. 222(1), pp. 9–22, 2003.
57. Flores L.E., Aguilar E.J., Barbosa V.C., De Carvalho L.A.V. A graph model for the evolution of specificity in humoral immunity. Journal of Theoretical Biology, v. 229(3), pp. 311–325, 2004.
58. Beauchemin C., Samuel J., Tuszynski J. A simple cellular automaton model for influenza A viral infections. Journal of Theoretical Biology, v. 232(2), pp. 223–234, 2005.
59. Castiglione F., Toschi F., Bernaschi M., Succi S., Benedetti R., Falini B., Liso A. Computational modeling of the immune response to tumor antigens. Journal of Theoretical Biology, v. 237(4), pp. 390–400, 2005.
60. Romanyukha A.A., Rudnev S.G., Sidorov I.A. Energy cost of infection burden: An approach to understanding the dynamics of host-pathogen interactions. Journal of Theoretical Biology, v. 241(1), pp. 1–13, 2006.
61. Na D., Kim D., Lee D. Mathematical modeling of humoral immune response suppression by passively administered antibodies in mice. Journal of Theoretical Biology, v. 241(4), pp. 830–851, 2006.
62. Mallet D.G., De Pillis L.G. A cellular automata model of tumor-immune system interactions. Journal of Theoretical Biology, v. 239(3), pp. 334–350, 2006.
63. Zurakowski R., Teel A.R. A model predictive control based scheduling method for HIV therapy. Journal of Theoretical Biology, v. 238(2), pp. 368–382, 2006.
64. Stilianakis N.I., Schenzle D. On the intra-host dynamics of HIV-1 infections. Mathematical Biosciences, v. 199(1), pp. 1–25, 2006.
65. Meyer-Hermann M.E. Are T cells at the origin of B cell lymphomas? Journal of Theoretical Biology, v. 244(4), pp. 656–669, 2007.
66. Dimitrov D.T., Hallam T.G., Rupprecht C.E., Turmelle A.S., McCracken G.F. Integrative models of bat rabies immunology, epizootiology and disease demography. Journal of Theoretical Biology, v. 245(3), pp. 498–509, 2007.
67. Kim P.S., Lee P.P., Levy D. Modeling regulation mechanisms in the immune system. Journal of Theoretical Biology, v. 246(1), pp. 33–69, 2007.
68. Cappuccio A., Elishmereni M., Agur Z. Optimization of interleukin-21 immunotherapeutic strategies. Journal of Theoretical Biology, v. 248(2), pp. 259–266, 2007.
69. Reluga T.C., Medlock J., Perelson A.S. Backward bifurcations and multiple equilibria in epidemic models with structured immunity. Journal of Theoretical Biology, v. 252(1), pp. 155–165, 2008.

70. Dimitrov D.T., Hallam T.G., Rupprecht C.E., McCracken G.F. Adaptive modeling of viral diseases in bats with a focus on rabies. Journal of Theoretical Biology, v. 255(1), pp. 69–80, 2008.
71. Perelson A.S., Wiegel F.W. Scaling aspects of lymphocyte trafficking. Journal of Theoretical Biology, v. 257(1), pp. 9–16, 2009.
72. Egami C. Bifurcation analysis of the Nowak-Bangham model in CTL dynamics. Mathematical Biosciences, v. 221(1), pp. 33–42, 2009.
73. Golubev A. Exponentially modified Gaussian (EMG) relevance to distributions related to cell proliferation and differentiation. Journal of Theoretical Biology, v. 262(2), pp. 257–266, 2010.
74. Levi M.I., Smirnova O.A. The conveyer hypothesis of the primary immune response to soluble antigen. Zhurnal Obschei Biologii, v. 38, pp. 66–99, 1977 (Russian).
75. Levi M.I., Smirnova O.A. Cyclic kinetics and mathematical expression of the primary immune response to soluble antigen: VII. The conveyer hypothesis and its mathematical expression. Folia Microbiologica, v. 22, pp. 117–127, 1977.
76. Smirnova O.A. Mathematical modeling of radiation effects on immune system. Immunologiya, no. 2, pp. 38–42, 1984 (Russian).
77. Smirnova O.A. Studies of cyclic kinetics of immunity by mathematical modeling methods. Kosmicheskaya Biologiya i Aviakosmicheskaya Meditsina, no. 5, pp. 53–56, 1991 (Russian).
78. Smirnova O.A. Mathematical modeling of the effect of ionizing radiation on the immune system of mammals. Physics of Particles and Nuclei. American Institute of Physics, v. 27(1), pp. 100–120, 1996.
79. Smirnova O.A. Radiation and Organism of Mammals: Modeling approach. Moscow-Izhevsk: Scientific-Publishing Centre "Regular and Chaotic Dynamics," Institute of Computer Science, 2006 (Russian).
80. Smirnova O.A. Mathematical modeling the radiation effects on humoral immunity system. Advances in Space Research, v. 37, pp. 1813–1822, 2006.
81. Burnet F.M. Cellular Immunology. Cambridge: Cambridge University Press, 1970.
82. Nossal G.J.V. Antibodies and Immunity (Russian translation from English original), Moscow: Meditsina, 1973 (Russian).
83. Pol U. (Ed.). Immunology. Moscow: Mir, 3 vol., 1987-1988 (Russian).
84. Petrov R.V. Immunology and Immunogenetics. Moscow: Meditsina, 1976 (Russian).
85. Petrov R.V. Immunology. Moscow: Meditsina, 1987 (Russian).
86. Davis B.D., Dulbecco R., Eisen H.N., et al. (Eds.). Microbiology. New York: Harper and Row, 1968.
87. Osmond D.G., Nossal J.V. Differentiation of lymphocytes in mouse bone marrow: II. Kinetic of maturation and renewal of antibody-binding cells studies by double labeling. Cellular Immunology, v. 13(1), pp. 132–145, 1974.
88. Laefleur L., Underdown B.J., Miller R.G., Phillips R.A. Differentiation of lymphocytes: Characterizing of early precursors of lymphocytes. Series Haematologica, v. 2, pp. 50–63, 1972.
89. Ryser J.E., Vassalli P. Mouse bone marrow lymphocytes and their differentiation. Journal of Immunology, v. 113, pp. 719–729, 1974.
90. Boyden S. Natural antibodies and immune response. Advances in Immunology, v. 5, pp. 1–29, 1966.
91. Fontallin L.N., Pevnitskii L.A. About originating the cells which produce normal antibodies in guinea pigs. Byulleten Eksperimentalnoi Biologii i Meditsini, v. 78(12), pp. 51–54, 1974 (Russian).
92. Levi M.I., Basova N.N. Quantitative relationship between the dose of antigen and duration of its determination in the place of injecting at priming immunization. Zhurnal Mikrobiologii, Epidemiologii i Immunobiologii, no. 2, pp. 42–49, 1972 (Russian).
93. Levi M.I., Saakyan N.N., Livshits M.M. About capability of predicting the level of plasma cell response in mice to soluble antigen. Zhurnal Mikrobiologii, Epidemiologii i Immunobiologii, no. 2, pp. 104–112, 1975 (Russian).

94. Belousova O.I., Gorizontov P.D., Fedorova M.I. Radiation and Haemopoietic System. Moscow: Atomizdat, 1979 (Russian).
95. Lea D.E. Action of Radiation on Living Cells, 2nd ed. Cambridge: The Syndics of the Cambridge University Press, 1955.
96. Kuz'mina E.G., Panteleeva E.S., Neprina G.S., Vatin O.E., Sirotina N.P., Kuzina A.A., Borovikova M.P. Immuno-reactivity of children and juveniles in Ul'yanov district of Kaluga region (data of dynamical study). In: Heritage of the Chernobyl, Proceedings of the Scientific-Practical Conference, MRNC RAMN, Kaluga, pp. 157–164, 1996 (Russian).
97. Muksinova K.N., Mushkacheva G.S. Cellular and molecular bases of haemopoiesis transformation under continuous irradiation. Moscow: Energoatomizdat, 1990 (Russian).
98. Mikhailovskaya E., Chebotarev E. Radiation hormesis as a risk factor. In: Sustainable Development: Environmental Pollution and Ecological Safety, Proceedings of the First Practical Conference, Dnipropetrovsk, Ukraine, December 4-8, 1995, Dnipropetrovsk State University, Dnipropetrovsk, Ukraine, Vol. 1, pp. 173–174, 1995 (Russian).
99. Shuibik V.M. Ionizing Radiation and Immunity. Moscow: Atomizdat, 1977 (Russian).
100. Nezlin R.S. Biochemistry of Antibodies. Moscow: Nauka, 1966 (Russian).
101. Yarilin A.A. Destruction and regeneration of coupled lymphocyte populations after exposure to radiation. Author's Abstract of Dissertation for Doctor of Medical Sciences Degree. Leningrad: IEM, Acad. Med. Sci. USSR, 1981 (Russian).
102. Troitskii V.L., Kaulen D.R., Tumanyan M.A., Fridenshtein A.Y., Chahava O.V. Radiation Immunology. Moscow: Meditsina, 1965 (Russian).
103. Taliaferro W.H., Taliaferro L.G., Jaroslow B.N. Radiation and Immune Mechanisms. New York: Academic Press, 1964.
104. Dixon F.G., Talmage D.W., Maurer P.H. Radiosensitive and radioresistant phases in the antibody response. Journal of Immunology, v. 68(6), pp. 693–700, 1952.

Chapter 5
Modeling of Autoimmune Processes

5.1 Introduction

Radiation exposures can cause the development of autoimmune processes in mammals. In the course of these processes, the organism's own organs and tissues are damaged [1, 2]. Clinical observations show that autoimmunization plays an important role in the pathogenesis of acute radiation sickness arising after acute exposure to sublethal and lethal doses. Autoimmune reactions are one of the possible consequences of chronic exposure to low doses of radiation. Sometimes autoimmune reactions may also develop in unexposed mammals [3–5].

There are a number of works dealing with the modeling of autoimmunity (see, e.g., [6–18]). However, radiation effects on the development of autoimmune processes have not been studied therein.

The primary objectives of our investigations [19–25] were to develop and investigate the mathematical models, which describe the dynamics of autoimmunity in mammals unexposed and exposed to acute and chronic irradiation. The models were required to account for the principal mechanisms of the development of autoimmune processes and to include explicitly the characteristics of ionizing radiation and the basic kinetic and radiobiological parameters of the cell systems under consideration. The results of our studies of this subject are presented in this chapter.

5.2 The Essentials of Autoimmunity

Normally, the immune system of an organism is in a state of tolerance to the components of its own cells and tissues (autoantigens) [4, 5]. The organism of a healthy mammal contains only small concentrations of antibodies against the various antigenic substances of its organs and tissues. It is assumed that the production of

O.A. Smirnova, *Environmental Radiation Effects on Mammals*,
DOI 10.1007/978-3-319-45761-1_5

small quantities of these autoantibodies is a normal process that ensures the transport of macromolecules coming from naturally destroyed cellular and subcellular structures. The loss of tolerance leads to the development of autoimmunity, pathological immune reactions [3–5, 26–28]. Large amounts of autoantibodies and cytotoxic T-lymphocytes appear in the organism and attack the antigens of the organism itself. Autoimmune reactions play the leading pathogenetic role in autoimmune diseases. Examples of such diseases are autoimmune hemolytic anemia, systemic lupus erythematosus, rheumatoid arthritis, dermatomyositis, autoimmune atrophic gastritis, Hashimoto's thyroid disease, and others [4, 5, 29].

At the present time, there is no single viewpoint on how autoimmune diseases develop [30–32]. Some researchers support the hypothesis of Burnet [33], according to which autoimmunity is a pathological process caused by the appearance of a "forbidden" clone of lymphocytes specifically interacting with cells and proteins of the self. Another hypothesis [34] argues that autoimmunity is an ordinary immune reaction against those components of the organism that normally are inaccessible to immunocompetent lymphocytes. "Accessibility" can arise as a result of various types of damage of cells and tissues. The primary injury leads to the appearance of antigen in the blood. This provokes an immune response, which leads to new damage of the tissues, and so on. One more theory of autoimmunity is a development of Burnet's hypothesis [35–38]. According to this theory, the tolerance of an organism to antigens of its own tissues is ensured by an organ of the immune system, the thymus. If its functioning is impaired due to illness (for example, thymomas), the use of cortisone, or exposure to radiation, the result can be the appearance of a forbidden clone of cytotoxic T-lymphocytes.

5.3 Dynamical Model of Autoimmunity in Nonirradiated Mammals

Autoimmune illnesses are extremely diverse. Nevertheless, all of them have a common feature. Namely, all autoimmune illnesses have as their basis a self-sustaining autoimmune reaction directed against some component of the organism, and the course of this reaction is practically independent of the cause of the loss of tolerance to the corresponding antigen. Therefore, we construct, at first, a mathematical model of the final stage of the autoimmune process. Only cellular autoimmunity is considered, because it plays the leading role in long-term autoimmune diseases [35, 36]. The variables of the model are the concentration x of target cells of the organism's own tissue, undamaged and having identical antigen specificity, the concentration y of cytotoxic T-lymphocytes that attack these cells, and the concentration z of tissue-specific antigen produced in the course of the destruction of target cells. The concentrations x, y, and z are expressed in moles per liter of blood.

In constructing the model, we describe the dynamics of the growth of a tissue in the absence of cytotoxic T-lymphocytes by the Ferhulst equation [39–41]:

$$\frac{dx}{dt} = \mu x - \nu x^2, \tag{5.1}$$

where μx is the rate of multiplication of tissue cells and νx^2 is the rate of natural death of these cells, which increases as the tissue grows. The stationary solution of this equation is $\bar{x} = \mu/\nu$. It can be identified with the "normal" concentration of tissue cells.

In constructing the model, we assume the following:

1. the interaction of target-tissue cells with cytotoxic T-lymphocytes leads to their mutual annihilation at rate $\beta\, x\, y$;
2. the rate of production of tissue-specific autoantigen is proportional to the rate of destruction of target-tissue cells by cytotoxic T-lymphocytes ($\sigma\, \beta\, x\, y$);
3. the specific rate of multiplication of cytotoxic T-lymphocytes is proportional to the antigen concentration ($\psi\, z$);
4. cytotoxic T-lymphocytes die at specific rate α;
5. antigen is removed from the organism at specific rate γ.

With these assumptions, the dynamics of concentrations of target-tissue cells x, cytotoxic T-lymphocytes y, and tissue-specific antigen z is described by the following differential equations:

$$\frac{dx}{dt} = \mu\, x - \nu\, x^2 - \beta\, x\, y, \tag{5.2}$$

$$\frac{dz}{dt} = \sigma\, \beta\, x\, y - \gamma\, z, \tag{5.3}$$

$$\frac{dy}{dt} = \psi\, z\, y - \beta\, x\, y - \alpha y. \tag{5.4}$$

Here the coefficients α, β, γ, σ, and ψ are constants.

The model (5.2)–(5.4) can be simplified by taking into account the difference in the time scales of autoimmune processes (months), tissue growth (months), and establishment of equilibrium concentrations of the antigen (days). This makes it possible to consider Eq. (5.3) as "fast" compared to Eqs. (5.2) and (5.4). Then, according to the Tikhonov theorem [39–41], Eq. (5.3) can be replaced by its stationary solution

$$z = \frac{\sigma\, \beta}{\gamma}\, x\, y. \tag{5.5}$$

As a result, Eq. (5.4) takes the form

$$\frac{dy}{dt} = \frac{\psi\, \sigma\, \beta}{\gamma}\, x\, y^2 - \beta\, x\, y - \alpha\, y\,. \tag{5.6}$$

After introducing the dimensionless variables $\xi = (\nu/\mu)\,x$, $\eta = (\beta/\mu)\,y$, $\tau = \mu\,t$ and the dimensionless parameters $a = \psi\,\sigma\,\mu/(\gamma\,\nu)$, $b = \beta\,\gamma/(\psi\,\sigma\,\mu)$, $c = \alpha\,\gamma\,\nu/(\mu^2\,\psi\,\sigma)$, we obtain the following equations:

$$\frac{d\xi}{d\tau} = \xi\,(1 - \xi - \eta), \tag{5.7}$$

$$\frac{d\eta}{d\tau} = a\,\eta\,(\xi\,\eta - b\,\xi - c). \tag{5.8}$$

The system (5.7), (5.8) is investigated by methods of the qualitative theory of differential equations, oscillation theory, and bifurcation theory [42–48]. Figure 5.1 shows the principal isoclines of the system (5.7), (5.8) on the phase plane, i.e., on the plane of states $\{\xi\eta\}$ of the system (5.7), (5.8). The principal isoclines are the isoclines of the horizontal tangents $\eta = 0$, $\eta = b + c/\xi$, and the isoclines of the vertical tangents $\xi = 0$ and $\eta = 1-\xi$. The singular points located at the intersections of the principal isoclines are shown by dots in Fig. 5.1.

It is found that the trivial singular point ($\xi_1 = 0$, $\eta_1 = 0$) is always unstable (a saddle). The singular point 2 with coordinates $\xi_2 = 1$ and $\eta_2 = 0$ is always stable (a node). It corresponds to the state of the healthy organism in which the target tissue has normal size and is not damaged. The singular points 3 and 4 are in the positive quadrant when $b < 1 - 2\sqrt{c}$. The point 3 is always unstable (a saddle), and the point 4 is either a node or focus. When $c < (1/a - b)\,(1 - 1/a)$, the point 4 becomes unstable.

The results of numerical study of the system (5.7), (5.8) confirm the predictions made in the course of its analytical investigations. In Figs. 5.2, 5.3, and 5.4 we give

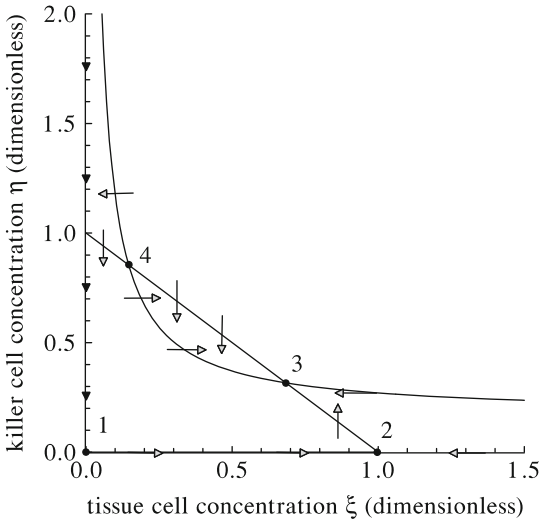

Fig. 5.1 Principal isoclines and singular points of the system (5.7), (5.8) on the phase plane $\{\xi\,\eta\}$. Here ξ is the concentration of target-tissue cells, whereas η denotes the concentration of cytotoxic T-lymphocytes (killer cells). The singular points are labeled by the numbers 1–4

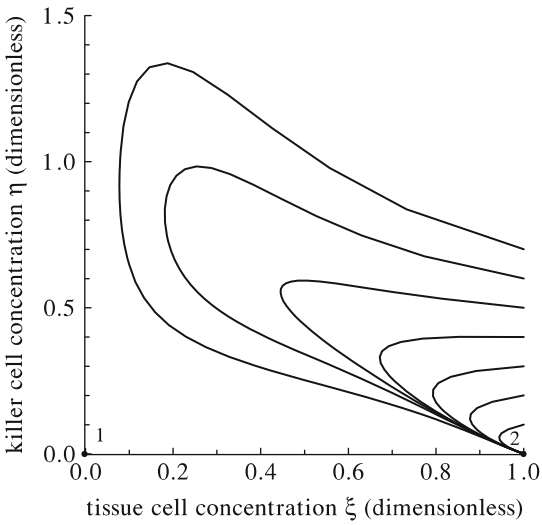

Fig. 5.2 Phase portrait of the system (5.7), (5.8). Results of computation for $a = 1.2$, $b = 0.17$, and $c = 0.21$. The singular points are labeled by the numbers 1 and 2

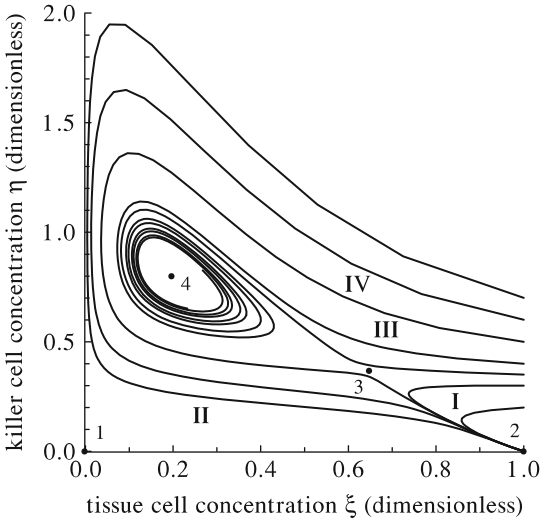

Fig. 5.3 Phase portrait of the system (5.7), (5.8). Results of computation for $a = 1.2$, $b = 0.17$, and $c = 0.125$. The singular points are labeled by the numbers 1–4. The regions of the phase plane with different behavior of integral curves are marked by I–IV

three typical phase portraits of this system. Each of them displays the integral curves of the system (5.7), (5.8) on the phase plane $\{\xi\eta\}$ computed for a certain set of the parameter values.

Figure 5.2 shows a phase portrait of the system when the singular points 3 and 4 do not exist. All the integral curves converge to the singular point 2 (stable node). Such solutions can be identified with the dynamics of autoimmunity in mammals possessing the potential ability to regenerate tissue or organs, no matter what the original damage was. However, in real cases this possibility is often not realized, because death occurs due to weakness of the damaged target tissue or organ.

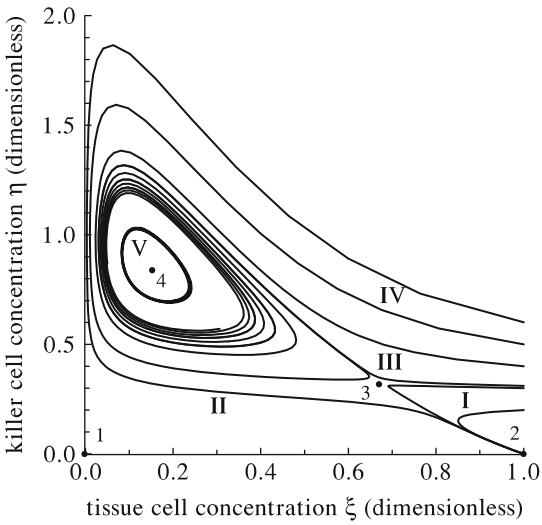

Fig. 5.4 Phase portrait of the system (5.7), (5.8). Results of computation for $a = 1.2$, $b = 0.17$, and $c = 0.1$. The singular points are labeled by the numbers 1–4. The regions of the phase plane with different behavior of integral curves are marked by I–V

In Fig. 5.3 we present a phase portrait of the system when it has all four singular points, the singular point 4 being a stable focus. The phase plane can be divided into regions I–IV according to the behavior of the integral curves. The regions are separated by separatrixes passing through the singular point 3 (a saddle). One of the branches of the emerging separatrix ends at the singular point 2 (a stable node), and the other one has the form of a spiral winding around the singular point 4, converging to the latter. The integral curves in region I converge to the singular point 2. These solutions correspond to the cases of small initial damage of the target tissue and low concentration of cytotoxic T-lymphocytes. Here the organism returns to the normal state.

The solutions of the system in region II can be regarded as the process of regeneration of the target tissue in the presence of cytotoxic T-lymphocytes attacking the cells of this tissue.

Region III lies between the branches of the separatrix going to the third singular point. In this region the integral curves have the form of spirals winding around the fourth singular point. The corresponding dynamical curves are damped oscillations. Such solutions describe the dynamics of progressive autoimmune diseases with periodic aggravation. The solutions in region IV are first characterized by rapid growth in the concentration of cytotoxic T-lymphocytes and decrease in the concentration of undamaged target-tissue cells. Then the integral curves go into region II. Apparently, these solutions are meaningful only in a restricted region of the phase plane, because in living organisms death occurs long before the complete destruction of a vitally important organ or tissue.

Figure 5.4 shows a phase portrait of the system (5.7), (5.8) when it has all four singular points, the singular point 4 being unstable. In this case, the system under consideration has one more particular solution: a stable limit cycle (closed curve on the phase plane $\{\xi\eta\}$). As one can infer from Fig. 5.4, all the integral curves from region III converge to the stable limit cycle. The latter corresponds to the

stable oscillations of the variables ξ and η. Such solutions are the analog of chronic autoimmune diseases.

The study of the system (5.7), (5.8) enables one to explain experiments on artificial autoimmunity induced in laboratory animals by the introduction, together with Freund's adjuvant, of extracts of self tissues or killed microbes (staphylococcus, streptococcus) having the same antigenic specificity as some tissues of the organism. Autoimmune diseases developed in these animals either were cured "spontaneously" or ended in death. In the model, the introduction of these components is equivalent to an abrupt increase in the autoantigen concentration and, eventually, to an increase in the concentration of cytotoxic T-lymphocytes. In turn, this results in the changing of the location of the representative point; namely, it may move either to region I or to region IV of the phase plane (Fig. 5.4). If the representative point appears to be located in region I of the phase plane, then the system will return to the initial state. Such solutions of the system (5.7), (5.8) are equivalent to spontaneous recovery of the tissue. However, if the representative point appears to be located in region IV of the phase plane, then the concentration of undamaged target-tissue cells will decrease so greatly with time that such solutions are equivalent to acute progression of the autoimmune process and death.

The model (5.7), (5.8) is used to simulate the dynamics of the autoimmune process in the case when the disease is cured by means of immunodepressants (cortico-steroidal hormones). An excess of the latter in the blood leads to lymphocyte destruction. Therefore, the introduction of cortico-steroidal hormones into the organism can be simulated in the model by an abrupt decrease in the concentration of cytotoxic T-lymphocytes. This can cause the representative point to move from region III of the phase plane (chronic illness) to region I or II of the phase plane (recovery) (Fig. 5.4). Analysis of the model reveals that the most favorable time for the introduction of medicine is a remission period, when the concentration of cytotoxic T-lymphocytes is minimal.

Thus, the developed model reproduces the main features of the autoimmune process and can be used as a basis for constructing the dynamic model of autoimmunity in mammals exposed to radiation.

5.4 Autoimmune Reactions Induced by Chronic Irradiation

According to the aforementioned theory of autoimmunity, the mechanisms of the development of cellular autoimmune processes in mammals exposed to radiation can be represented in the following way. First, ionizing radiation directly damages a part of the cells of radiation-sensitive tissues, resulting in the release of autoantigens. Second, radiation destroys the proper functioning of the thymus. This may occur as follows. Among the population of medullary cells of the thymus that are resistant to radiation, there are immunocompetent predecessor cells that can recognize certain tissue-specific antigens. These cells can turn into cytotoxic T-lymphocytes, which destroy the cells of the corresponding tissues. Certain lymphocytes of the cortical

layer of the thymus, T-suppressors sensitive to radiation, hinder this transformation. In a healthy organism, T-suppressors completely suppress the production of cytotoxic T-lymphocytes directed against the self tissues. Exposure to radiation leads to a deficit of T-suppressors and damages the immunosuppression function of the thymus. This, in turn, leads to the formation of immunocompetent predecessor cells, relatively insensitive to radiation. After their maturation and release from the thymus, these cells, having been transformed to cytotoxic T-lymphocytes, can interact with target cells of the corresponding tissue and damage them. This damage can be expressed both as a loss of the cell's functions and as death of the cell. The tissue-specific antigen released in the destruction of the cells will stimulate an immune response, which leads to further damage of the self tissue and the development of an autoimmune disease.

Let us proceed to the construction of the model of the cellular autoimmunity developing in mammals exposed to chronic irradiation. In accordance with statements presented above, the variables of the model are the concentration x of target cells of the organism's own tissue (undamaged by irradiation and having identical antigen specificity), the concentration y of cytotoxic T-lymphocytes that attack these cells, the concentration z of tissue-specific antigen produced in the destruction of target-tissue cells, and the concentration S of T-suppressors of the cortical layer of the thymus.

We make the same assumptions as those in the construction of the model (5.2)–(5.4). Additionally, we describe the concentration S of T-suppressors of the cortical layer of the thymus in healthy unexposed mammals by the Ferhulst equation, in which the terms ωS and φS^2 are the rates of multiplication and natural death of T-suppressors. The stationary solution of this equation is $\bar{S} = \omega/\varphi$, representing the concentration of T-suppressors of the cortical layer of the thymus in healthy, unexposed mammals. We also assumed that the destruction of a certain number of T-suppressors of the cortical layer of the thymus leads to loss of tolerance of a proportional number of immunocompetent cell-predecessors from the medullary region. After maturation and release from the thymus, these cells enlarge the pool of cytotoxic T-lymphocytes with the rate ε, which is given by the piecewise-linear function

$$\varepsilon = \begin{cases} 0 & \text{when } S \geq \bar{S}, \\ \chi\,\kappa\,(\bar{S} - S) & \text{when } S < \bar{S}, \end{cases} \tag{5.9}$$

where κ is the coefficient of proportionality and χ is the specific rate at which cytotoxic T-lymphocytes mature in the thymus.

We take into account that tissue cells and T-suppressors of the cortical layer of the thymus are radiosensitive. In describing the radiation effect on the radiosensitive cells, we use the one-target–one-hit theory of cell damage [49], according to which the specific damage rate is proportional to the radiation dose rate N.

Proceeding from everything just stated, we write down the following differential equations that describe the dynamics of autoimmune processes in mammals exposed to chronic irradiation:

$$\frac{dx}{dt} = \mu x - \nu x^2 - \beta x y - \frac{N}{D_k} x, \tag{5.10}$$

$$\frac{dy}{dt} = \psi z y - \beta x y - \alpha y + \varepsilon, \tag{5.11}$$

$$\frac{dz}{dt} = \sigma \beta x y - \gamma z + \frac{\sigma N}{D_k} x, \tag{5.12}$$

$$\frac{dS}{dt} = \omega S - \varphi S^2 - \frac{N}{D_s} S. \tag{5.13}$$

The terms proportional to the dose rate N in (5.10) and (5.13) are specific rates at which radiosensitive tissue cells and T-suppressors are killed by the effects of radiation. The coefficients D_k and D_s characterize the radiosensitivity of the tissue cells and T-suppressors, respectively. In turn, the term $\sigma(N/D_k)x$ in (5.12) is the rate of formation of tissue-specific antigen in the postirradiation destruction of tissue cells.

The system (5.10)–(5.13) can be simplified. The fact that the typical time scale of the development of autoimmune processes (months) significantly differs from that for the establishment of stationary antigen concentrations (days) allows one to consider Eq. (5.12) as "fast" compared to Eqs. (5.10), (5.11), and (5.13). According to the Tikhonov theorem [39–41], the "fast" equation (5.12) can be replaced by its stationary solution $z = (\sigma/\gamma)[\beta x y + (N/D_k) x]$, so that (5.11) takes the form

$$\frac{dy}{dt} = \frac{\psi \sigma \beta}{\gamma} x y^2 - \left(\beta - \frac{\sigma \psi}{\gamma} \frac{N}{D_k}\right) x y - \alpha y + \varepsilon\,. \tag{5.14}$$

After introduction of the dimensionless variables $\xi = \nu x/\mu$, $\eta = \beta y/\mu$, $\zeta = \varphi S/\omega$, $\tau = \mu t$ and the dimensionless parameters $a = \psi \sigma \mu/(\gamma \nu)$, $b = \beta \gamma/(\psi \sigma \mu)$, $q = \omega/\mu$, $c = \alpha \gamma \nu/(\mu^2 \psi \sigma)$, $h = \gamma \nu \beta \kappa \chi \omega/(\psi \sigma \mu^3 \varphi)$, the following system of equations is obtained:

$$\frac{d\xi}{d\tau} = \xi \left[\left(1 - \frac{N}{\mu D_k}\right) - \xi - \eta\right], \tag{5.15}$$

$$\frac{d\eta}{d\tau} = a \left[\xi \eta^2 - \left(b - \frac{N}{\mu D_k}\right) \xi \eta - c \eta + \varepsilon'\right], \tag{5.16}$$

$$\frac{d\zeta}{d\tau} = q \zeta \left[\left(1 - \frac{N}{\omega D_s}\right) - \zeta\right], \tag{5.17}$$

where

$$\varepsilon' = \begin{cases} 0 & \text{for } \zeta \geq 1, \\ h(1-\zeta) & \text{for } \zeta < 1\,. \end{cases} \tag{5.18}$$

The initial conditions for the system (5.15)–(5.17) depend on a type of problem we are going to examine. For example, in the case of irradiation of the healthy organism that has not previously been exposed to radiation, the initial conditions are the following:

$$\xi(0) = 1, \quad \eta(0) = 0, \quad \zeta(0) = 1. \tag{5.19}$$

We study the model of autoimmunity dynamics in chronically irradiated mammals [system (5.15)–(5.17)] by making use of the methods of the qualitative theory of differential equations and oscillation theory. The coordinates of five singular points of the system (5.15)–(5.17) in the space of variables are found and the stability of these singular points is investigated.

We obtained the relations between the dose rate N and other model coefficients that give the conditions for saddle bifurcation and bifurcation of the creation of the stable limit cycle. In addition, we derived the equation that enables one to estimate the critical dose rate of chronic irradiation N_{ca}. The meaning of the latter is the following: Chronic exposure with the dose rate $N \geq N_{\text{ca}}$ leads to irreversible destruction of all tissue cells. It is important to emphasize here that the destruction of tissue cells is due to both direct radiation injury and autoaggression. The derived equation expresses N_{ca} in terms of quantities that characterize the radiosensitivity of tissue cells and T-suppressors in the cortical layer of the thymus, as well as the kinetics of the aforementioned cells, cytotoxic T-lymphocytes, and immunocompetent predecessors in the medullary layer of the thymus:

$$N_{\text{ca}} = \begin{cases} \dfrac{\mu D_k}{1 + h\mu D_k / c\omega D_s} & \text{for} \quad \mu D_k \left(1 - \dfrac{h}{c}\right) < \omega D_s, \\ \mu D_k \left(1 - \dfrac{h}{c}\right) & \text{for} \quad \mu D_k \left(1 - \dfrac{h}{c}\right) \geq \omega D_s. \end{cases} \tag{5.20}$$

It is worthwhile here to note the following. Equation (5.20) accounts for the destruction of tissue cells caused by both direct radiation injury and autoaggression. The latter, in turn, is due to radiation-induced damage of T-suppressors in the cortical layer of the thymus. In accordance with Eq. (5.15), if the autoaggression is neglected, then the critical dose rate of chronic irradiation N_{c} is determined only by the radiosensitivity and proliferative potential of tissue cells:

$$N_{\text{c}} = \mu D_k. \tag{5.21}$$

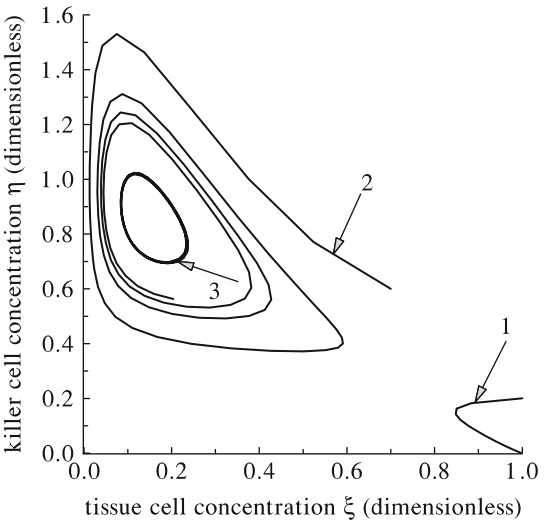

Fig. 5.5 Projections on the plane of states $\{\xi\,\eta\}$ of integral curves of the system (5.15)–(5.17) computed for dose rate of chronic irradiation $N = 0.001$ Gy/day. The presented results correspond to the following values of parameters: $a = 1.2$, $b = 0.17$, $c = 0.1$, $h = 0.1$, $\mu = 0.1\,\text{day}^{-1}$, $\omega = 1\,\text{day}^{-1}$, $D_s = 1$ Gy, and $D_k = 4$ Gy. Three sets of the initial conditions are considered: $\xi(0) = 1.0$, $\eta(0) = 0.2$, $\zeta(0) = 1.0$ (*curve 1*); $\xi(0) = 0.7$, $\eta(0) = 0.6$, $\zeta(0) = 1.0$ (*curve 2*); and $\xi(0) = 0.2$, $\eta(0) = 0.7$, $\zeta(0) = 1.0$ (*curve 3*)

Obviously, the critical dose rate of chronic irradiation N_{ca} is always less than N_{c}. This result testifies to the importance of accounting for damage effects of the autoaggression on the vital body system when estimating the radiation risks.

The dependence of autoimmune processes on the dose rate of chronic irradiation N is studied numerically. The obtained modeling results are presented in Fig. 5.5. For the lowest dose rate considered, as one can see, the system (5.15)–(5.17) has a particular solution: a stable limit cycle, the analog of the chronic autoimmune process. However, computations reveal that this dynamical regime can be reached only if the concentration of cytotoxic T-lymphocytes is sufficiently large and target-tissue cells are damaged before the onset of irradiation. If, before exposure at the low dose rate, the concentration of cytotoxic T-lymphocytes vanishes and the tissue is not damaged, the integral curves converge to a singular point. The latter is nearly indistinguishable from the point ($\xi = 1$, $\eta = 0$, $\zeta = 1$) that characterizes a healthy organism. These results imply that long-term exposure to radiation at low dose rates, which is not dangerous for healthy individuals, can lead to enhancement of autoimmune processes in persons with autoimmune diseases occurring before irradiation.

When the dose rate N of chronic irradiation is increased, autoimmune processes develop even in a healthy organism. As Fig. 5.6 shows, the larger N is, the larger the number of target-tissue cells that will be damaged as a result of autoaggression. When N equals or exceeds the critical dose rate N_{ca}, the concentration of tissue cells

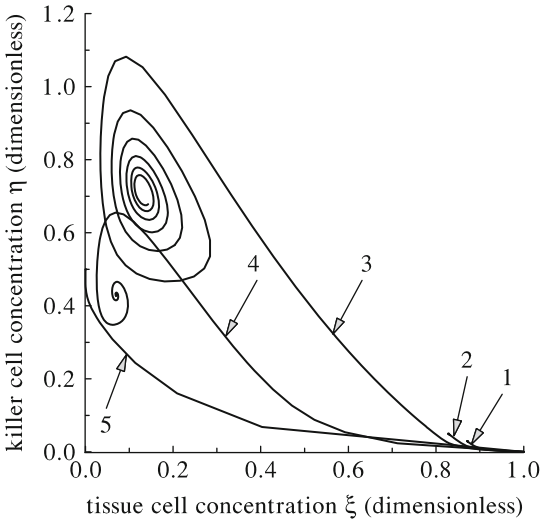

Fig. 5.6 Projection on the plane of states $\{\xi\ \eta\}$ of integral curves of the system (5.15)–(5.17) computed for the initial conditions $\xi(0) = 1$, $\eta(0) = 0$, $\zeta(0) = 1$. Five curves correspond to five values of the dose rates of chronic irradiation: $N = 0.04$ Gy/day (*curve 1*), $N = 0.049$ Gy/day (*curve 2*), $N = 0.063$ Gy/day (*curve 3*), $N = 0.2$ Gy/day (*curve 4*), $N = 0.5$ Gy/day (*curve 5*). The values of the coefficients a, b, c, h, μ, ω, D_s, and D_k are specified in the caption to Fig. 5.5

undamaged by radiation decreases to zero. Such solutions can be viewed as the analog of death of the organism if the tissue in question performs vitally important functions.

The dependence of the autoimmunity dynamics on the radiation sensitivity of tissue cells and T-suppressors of the cortical layer of the thymus is also studied. The parameters D_k and D_s are varied in a wide range. It is found that chronic exposure at the same dose rate N leads to the development of autoimmune processes in which the higher the radiation sensitivity of the cells of this tissue and the T-suppressors, the larger the number of target-tissue cells that are damaged.

The model (5.15)–(5.17) is also used to simulate the effect of shielding of the target tissue and the thymus on autoimmunity dynamics. Here the different degrees of radiation protection are specified by varying the effective dose rate (N_{eff}) acting on the shielded tissue and thymus. In Figs. 5.7, 5.8, 5.9, and 5.10 we show the dynamics of concentrations of target-tissue cells ξ, cytotoxic T-lymphocytes η, and T-suppressors of the cortical layer of the thymus ζ computed at different values of N_{eff} and at fixed values of the parameters a, b, c, h, μ, ω, D_s, D_k, and N. In these figures, we also indicate the stationary levels of concentration of target-tissue cells $\bar{\xi}_R = 1 - N_{\text{eff}}/(\mu D_k)$, to which the value of ξ would be decreased as a result of direct radiation damage of the tissue at the dose rate N_{eff} with neglecting autoaggression.

The dynamics of autoimmune processes presented in Fig. 5.7 corresponds to the case when neither the thymus nor the target tissue is screened (i.e., $N_{\text{eff}} = N$). One can see from this figure that the combined action of radiation and autoaggression leads to damage to a significant number of target-tissue cells, which in some cases can result in death of the mammal. Screening of the target tissue, which decreases the effective dose rate by a factor of 10 (Fig. 5.8), almost completely prevents the development of the autoimmune reaction. The same results are obtained for the simultaneous screening of the tissue and the thymus, decreasing the effective

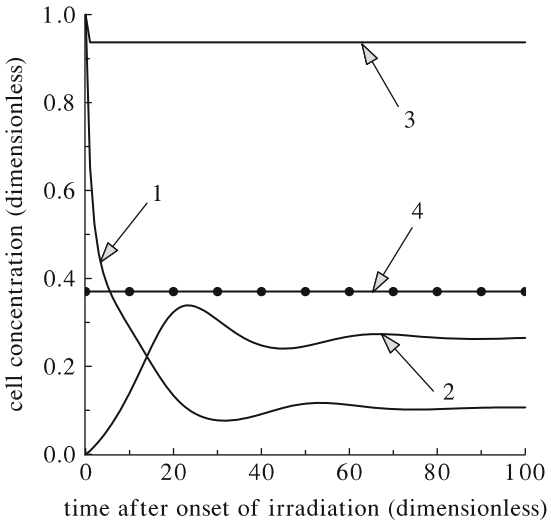

Fig. 5.7 Dynamics of the autoimmune process caused by chronic irradiation with dose rate $N = 0.063$ Gy/day without shielding ($N_{\text{eff}} = N$). The concentrations of target-tissue cells ξ, cytotoxic T-lymphocytes (killer cells) η, and T-suppressors of the cortical layer of the thymus ζ are given by *curves 1–3*, respectively. Line 4 (*with dots*) denotes the stationary level of the concentration of target-tissue cells $\xi_R = 1 - N_{\text{eff}}/(\mu D_k)$, to which the value of ξ would be decreased as a result of direct radiation damage of the tissue at dose rate N_{eff} when neglecting autoaggression. These results correspond to the parameter values $D_s = 1$ Gy and $D_k = 1$ Gy. The values of the coefficients a, b, c, h, μ, and ω are specified in the caption to Fig. 5.5

Fig. 5.8 Effect of radiation screening of the target tissue ($N_{\text{eff}} = 0.1\,N$) on dynamics of the autoimmune process caused by chronic irradiation. The values of the parameters of Eqs. (5.15)–(5.17) and notations are given in the caption to Fig. 5.7

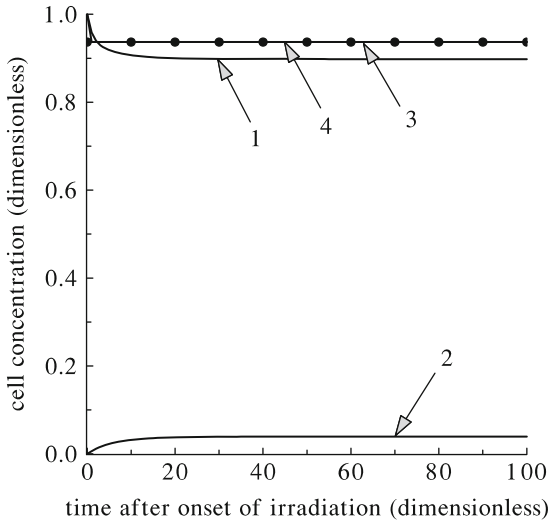

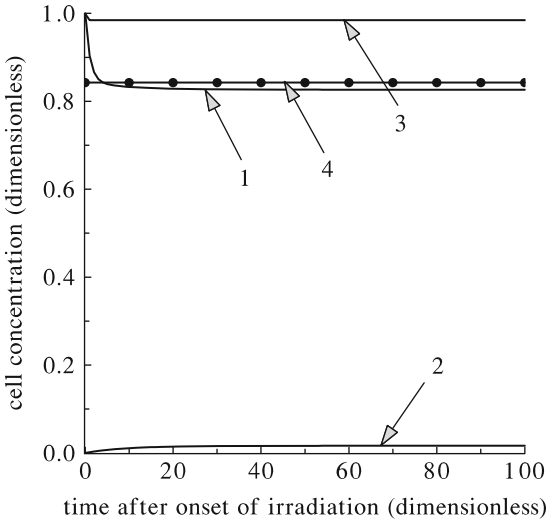

Fig. 5.9 Effect of radiation screening of the target tissue and thymus ($N_{\text{eff}} = 0.25\,N$) on dynamics of the autoimmune process caused by chronic irradiation. The values of the parameters of Eqs. (5.15)–(5.17) and notations are given in the caption to Fig. 5.7

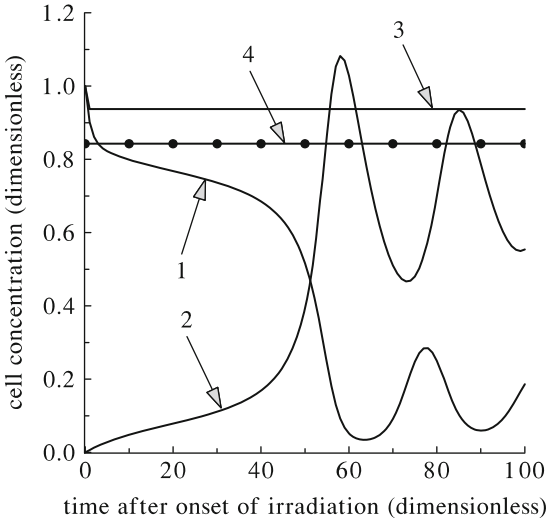

Fig. 5.10 Effect of radiation screening of the target tissue ($N_{\text{eff}} = 0.25\,N$) on dynamics of the autoimmune process caused by chronic irradiation. The values of the parameters of Eqs. (5.15)–(5.17) and notations are given in the caption to Fig. 5.7

dose rate by a factor of 4 altogether (Fig. 5.9). As in Fig. 5.8, the tissue is slightly damaged, mainly by the effect of ionizing radiation. It should be noted that radiation shielding of only the target tissue, which also decreases the effective dose rate by a factor of 4, does not prevent the development of the autoimmune process, although it does lessen the damage of the shielded organ (Fig. 5.10). These results show that screening of the thymus plays an important role in preventing remote consequences of chronic irradiation, namely the development of autoimmune processes that damage radiation-sensitive organs and tissues.

5.5 Autoimmune Reactions Induced by Acute Irradiation

A distinct feature of acute irradiation is its very short duration. This fact should certainly be taken into account in modeling studies of the cellular autoimmunity dynamics in acutely irradiated mammals. In this case, the model (5.15)–(5.17) reduces to Eqs. (5.15) and (5.16) with $N = 0$ and $\varepsilon' = 0$ [i.e., to the system (5.7)–(5.8)] with the following initial conditions:

$$\xi(0) = \exp(-D/D_k), \tag{5.22}$$

$$\eta(0) = l\,[1 - \exp(-D/D_s)]\exp\{m[1 - \exp(-D/D_k)]\}\,. \tag{5.23}$$

Here D is the dose of acute irradiation, and l and m are new dimensionless parameters.

Numerical studies show that the model of autoimmunity dynamics in acutely irradiated mammals reproduces the typical situations observed experimentally. For example, Fig. 5.11 presents the results of simulating autoimmune processes in mammals exposed to various doses of acute irradiation. Three integral curves of the phase portrait correspond to three different doses D. We see from this figure that the small dose [$D \ll \min(D_k, D_s)$] does not induce the development of an autoimmune disease. The concentration of cytotoxic T-lymphocytes vanishes, and the population of cells of the tissue is completely restored. A higher dose [$D < \min(D_k, D_s)$] leads to the establishment in the system of stable oscillations of the concentrations of undamaged target-tissue cells and cytotoxic T-lymphocytes that attack these cells, i.e., to the development of a

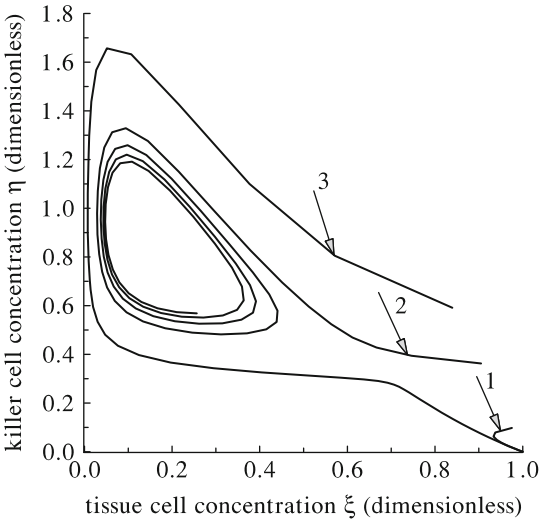

Fig. 5.11 Projection on the plane of states $\{\xi\ \eta\}$ of integral curves of the system (5.7), (5.8) computed with the initial conditions (5.22), (5.23) and with the following values of the parameters: $a = 1.2$, $b = 0.17$, $c = 0.1$, $l = m = 1.0$, $D_s = 1$ Gy, and $D_k = 4$ Gy. *Curves 1, 2, and 3* correspond to $D = 0.1$ Gy, $D = 0.4$ Gy, and $D = 0.7$ Gy, respectively

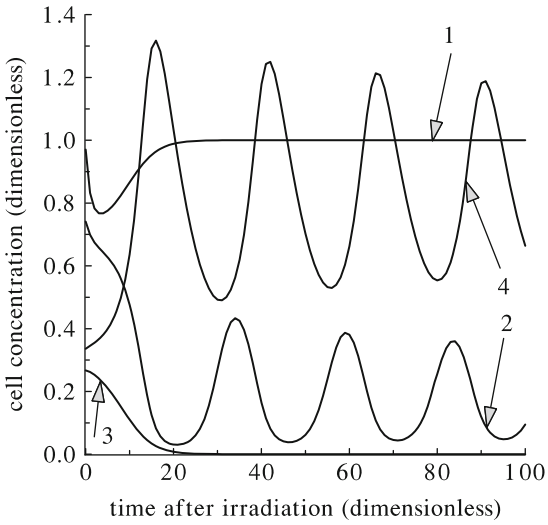

Fig. 5.12 Dynamics of the concentrations of target cells of radioresistant (*curve 1*) and radiosensitive (*curve 2*) tissues (ξ) and of cytotoxic T-lymphocytes (η) attacking target cells of these tissues (*curves 3 and 4*, respectively) after acute irradiation at dose $D = 0.3$ Gy. Results of computation of the system (5.7), (5.8) with the initial conditions (5.22), (5.23) and with two values of the parameter D_k characterizing the radiosensitivity of the tissues in question: $D_k = 10$ Gy and $D_k = 1$ Gy. The values of the coefficients a, b, c, l, m, and D_s are specified in the caption to Fig. 5.11

chronic autoimmune disease. An even higher dose [$D \sim \min(D_k, D_s)$] induces an abrupt increase in the concentration of cytotoxic T-lymphocytes and a decrease in the concentration of undamaged target-tissue cells. Such solutions can be viewed as simulating "acute" autoimmune processes. They can lead either to death of the organism (if the tissue in question performs vitally important functions) or to spontaneous recovery.

The model also reproduces the experimentally observed fact that postirradiation autoimmunity is directed against the tissues most sensitive to radiation. In Fig. 5.12 we show autoimmune processes that are directed against radioresistant and radiosensitive tissues exposed to the same acute dose. We see that the population of cells of the radioresistant tissue is completely restored, and the concentration of the corresponding cytotoxic T-lymphocytes vanishes. The population of cells of the radiosensitive tissue is damaged by a chronic autoimmune disease: The concentration of tissue cells undamaged by cytotoxic T-lymphocytes and the concentration of the corresponding cytotoxic T-lymphocytes oscillate about new stationary values.

Thus, the proposed model reproduces the main features of autoimmune processes developing in mammals after acute irradiation.

5.6 Conclusions

Mathematical models capable of describing autoimmune reactions in nonirradiated mammals and in mammals exposed to acute/chronic radiation are developed. They are based on conventional radiobiological theories and on the current immunological concept concerning the important role of the immunosuppression function of the thymus in the maintenance of autotolerance. The models are implemented as the systems of nonlinear differential equations. The concentrations of target cells of autogenous tissue, of cytotoxic T-lymphocytes, and of T-suppressors are the dynamical variables in these equations, the radiation dose and dose rate being the variable parameters. The models are investigated by making use of the methods of the qualitative theory of differential equations, bifurcation theory, and numerical methods. The models reproduce the well-known fact that radiation-induced autoimmunity is directed against the tissues most sensitive to radiation. Depending on the value of the dose and dose rate, the models describe different dynamical regimes that are observed in experiments: total restoration of target-tissue after low dose acute irradiation, slight damages of target tissue under low dose rate chronic irradiation, cyclic autoimmune processes at moderate doses and dose rates, and irreversible destruction of all target-tissue cells under high-level exposures. The dangerous dose rates of chronic irradiation can be calculated by making use of the derived equation, which involves key immunological and radiobiological parameters. The developed models can be used for elucidation of the origin of radiation-induced autoimmunity, as well as for making practical recommendations. In particular, the effectiveness of the thymus shielding for the prevention of autoimmune diseases is predicted. Finally, the obtained equation for calculation of the dangerous dose rates of chronic irradiation can be applied to estimate the health effects of the space radiation environment on astronauts on long-term space missions such as Lunar colonies and Mars missions.

References

1. Shubik V.M. Immunological Studies in Radiation Hygiene. Moscow: Energoatomizdat, 1987 (Russian).
2. Klemparskaya N.N. Autoantibodies of an Organism Exposed to Radiation. Moscow: Atomizdat, 1972 (Russian).
3. Andras P. (Ed.). Autoimmunity: Methods and Protocols. Totowa, NJ: Humana Press, 2004.
4. Elgert K.D. Immunology: Understanding the Immune System, 2nd ed. Hoboken, NJ: Wiley-Blackwell, 2009.
5. Coico R., Sunshine G. Immunology: A Short Course, 6th ed. Hoboken, NJ: Wiley-Blackwell, 2009.
6. Al'perin L.B., Isavina I.A. Mathematical model of immune response auto-regulation. The Natural Sciences at the Service of Public Health, Novosibirsk: USSR Acad. Med. Sci., Siberian Div., p. 66, 1980 (Russian).

7. Waniewski J., Priklova D. Mathematical modeling of autoimmune decease and its treatment. Abstracts of Reports presented at the International Working Conference on Mathematical Modeling in Immunology and Medicine (Kiev, August-September 1989). Kiev: Glushkov Cybernetics Institute, p. 17, 1989 (Russian).
8. Waniewski J., Priklova D. Autoimmunity and its therapy: Mathematical modelling. Immunology Letters, v. 18, pp. 77–80, 1988.
9. Bar-Or R.L, Segel L.A. On the role of a possible dialogue between cytokine and TCR-presentation mechanisms in the regulation of autoimmune disease. Journal of Theoretical Biology, v. 190(2), pp. 161–178, 1998.
10. Sulzer B., Van Hemmen J.L. Adaptive control: A strategy to treat autoimmunity. Journal of Theoretical Biology, v. 196(1), pp. 73–79, 1999.
11. Uziel A., Schwartz M., Neumann A. Modeling protective autoimmunity following central nervous system (CNS) trauma. Mathematical modeling and computing in biology and medicine. 5th Conference of the European Society of the Mathematical and Theoretical Biology (July 2-6, 2002, Milan, Italy). Book of Abstracts. Milan: Politecnico Di Milano, p. 210, 2002.
12. Nevo U., Golding I., Neumann A.U., Schwartz M., Akselrod S. Autoimmunity as an immune defense against degenerative processes: A primary mathematical model illustrating the bright side of autoimmunity. Journal of Theoretical Biology, v. 227(4), pp. 583–592, 2004.
13. Wang X., He Z., Ghosh S. Investigation of the age-at-onset heterogeneity in type 1 diabetes through mathematical modeling. Mathematical Biosciences, v. 203(1), pp. 79–99, 2006.
14. Kim P.S., Lee P.P., Levy D. Modeling regulation mechanisms in the immune system. Journal of Theoretical Biology, v. 246(1), pp. 33–69, 2007.
15. Iwami S., Takeuchi Y., Miura Y., Sasaki T., Kajiwara T. Dynamical properties of autoimmune disease models: Tolerance, flare-up, dormancy. Journal of Theoretical Biology, v. 246(4), pp. 646–659, 2007.
16. Iwami S., Takeuchi Y., Iwamoto K., Naruo Y., Yasukawa M. A mathematical design of vector vaccine against autoimmune disease. Journal of Theoretical Biology, v. 256(3), pp. 382–392, 2009.
17. Radulescu A. A multi-etiology model of systemic degeneration in schizophrenia. Journal of Theoretical Biology, v. 259(2), pp. 269–279, 2009.
18. Vodovotz Y., Constantine G., Rubin J., Csete M., Voit E.O., An G. Mechanistic simulations of inflammation: Current state and future prospects. Mathematical Biosciences, v. 217(1), pp. 1–10, 2009.
19. Smirnova O.A., Stepanova N.V. Mathematical model of autoimmunity. Biofizika, v. 20, pp. 1095–1998, 1975 (Russian).
20. Smirnova O.A. Mathematical modeling of autoimmunity dynamics under continuous irradiation. In: Modeling of Population Dynamics. Gorky: Gorky University Press, pp. 47–54, 1988 (Russian).
21. Smirnova O.A. Mathematical model for postirradiation autoimmunity. Radiobiologiya, v. 28(3), pp. 331–335, 1988 (Russian).
22. Smirnova O.A. Mathematical modeling of the effect of ionizing radiation on the immune system of mammals. Physics of Particles and Nuclei. American Institute of Physics, v. 27(1), pp. 100–120, 1996.
23. Smirnova O.A. Autoimmunity dynamics in irradiated mammals: Mathematical modeling. BioMedSim'99. 1st Conference on Modelling and Simulation in Biology, Medicine and Biomedical Engineering, Noisy-le-Grand, France, April 20–22, 1999. Proceedings. Paris: Groupe ESIEE, pp. 110–113, 1999.
24. Smirnova O.A. Mathematical modeling of radiation-induced autoimmunity. In: Mathematical Modelling and Computing in Biology and Medicine. 5th ECMTB Conference 2002. V. Capasso (Ed.). Milan: Milan Research Centre for Industrial and Applied Mathematics, pp. 392–402, 2003.
25. Smirnova O.A. Radiation and Organism of Mammals: Modeling Approach. Moscow-Izhevsk: Scientific-Publishing Centre "Regular and Chaotic Dynamics," Institute of Computer Science, 2006 (Russian).

26. Petrov R.V. Immunology. Moscow: Meditsina, 1987 (Russian).
27. Tomer Y., Shoenfeld Y. The significance of natural autoantibodies. Immunological Investigations, v. 17, pp. 389–424, 1988.
28. Pol U. (Ed.). Immunology. Moscow: Mir, 3 vol., 1987-1988 (Russian).
29. Misher P., Forlender K.O. (Eds.). Immunopathology in Clinical Practice and Experiment and the Problem of Autoimmunity (Russian translation from German original). Moscow: Medgiz, 1963.
30. Adams D.D. Three theories which explain the occurrence and inheritance of the autoimmune diseases. Journal of Clinical and Laboratory Immunology, v. 36, pp. 1–14, 1991.
31. Mackay I.R. Autoimmunity: Paradigms of Burnet and complexities of today. Immunology and Cell Biology, v. 70, pp. 159–171, 1992.
32. Silverstein A.M., Rose N.R. On the mystique of the immunological self. Immunological Reviews, v. 159, p. 197–206; discussion pp. 207–218, 1997.
33. Burnet F.M. Cellular Immunology. Cambridge: Cambridge University Press, 1970.
34. Nossal G.J.V. Antibodies and Immunity (Russian translation from English original), Moscow: Meditsina, 1973 (Russian).
35. Lyampert I.M. Autoimmunity. Uspehi Sovremennoi Biologii, v. 75, pp. 183–202, 1973 (Russian).
36. Lyampert I.M. Autoimmunity. Uspehi Sovremennoi Biologii, v. 81, pp. 274–290, 1976 (Russian).
37. Kemileva Z. The Thymus. Moscow: Meditsina, 1984 (Russian).
38. Trufakin V.A. Immuno-morphological aspects of autoimmune processes. Novosibirsk: Nauka, 1983 (Russian).
39. Romanovsky J.M., Stepanova N.V., Chernavsky D.S. Mathematical Modeling in Biophysics. Introduction to Theoretical Biophysics. Moscow-Izhevsk: Scientific-Publishing Centre "Regular and Chaotic Dynamics," Institute of Computer Science, 2004 (Russian).
40. Romanovsky J.M., Stepanova N.V., Chernavsky D.S. Mathematical Biophysics. Moscow: Nauka, 1984 (Russian).
41. Romanovsky J.M., Stepanova N.V., Chernavsky D.S. Kinetische Modelle in der Biophysik. Stuttgart: Gustav Fischer Verlag, 1974.
42. Pontryagin L.S. Ordinary Differential Equations. Moscow: Nauka, 1982 (Russian).
43. Andronov A.A., Vitt A.A., Khikin S.E. Theory of Oscillation. Moscow: Nauka, 1981 (Russian).
44. Andronov A.A., Leontovich E.A., Gordon I.I., Maier A.G. Theory of Bifurcations of Dynamical Systems on Plane. Moscow: Nauka, 1967 (Russian).
45. Hayashi C. Nonlinear Oscillations in Physical Systems. New York: McGraw-Hill Book Company, 1964.
46. Arrowsmith D.K., Place C.M. Ordinary Differential Equations. A Qualitative Approach with Applications. London: Chapman and Hall, 1982.
47. Dulac H. Sur les cycles limités. Bulletin de la Société Mathématique de France, v. 51, pp. 45–188, 1923.
48. Korn G.A., Korn T.M. Mathematical Handbook. New York: McGraw-Hill Book Company, 1968.
49. Lea D.E. Action of Radiation on Living Cells, 2nd ed. Cambridge: The Syndics of the Cambridge University Press, 1955.

Chapter 6
Individual-Based Approach to Radiation Risk Assessment

6.1 Introduction

Ensuring the radiation safety of a population residing in radioactively contaminated areas, persons subjected to occupational exposures, personnel engaged in operations to eliminate nuclear disaster aftereffects, as well as astronauts on long-term space missions is an important and challenging problem [1–10]. Resolving this problem requires, in particular, the invention of new approaches to radiation risk assessment. The present risk-estimation methods [11, 12] are not always applicable in the cases of low-level irradiation due to the nonlinearity of radiobiological effects of such exposures. Therefore, new approaches must not ignore intrinsic properties of irradiated organisms. The implementation of new approaches calls for the development and investigation of mathematical models describing mortality as an ultimate result of radiation-induced damage to the mammalian organism. Our own results obtained in this field [13–27] are summarized in this chapter.

6.2 Model of Radiation-Induced Mortality for a Homogeneous Mammalian Population

Usually, three statistical biometric functions are measured in experiments studying the mortality dynamics of mammals [28–30]. These are the life span probability $v(t)$, the life span probability density $w(t)$, and the mortality rate $\rho(t)$. The last function is also called the mortality intensity or mortality strength [30]. The function $v(t)$ defines the ratio of the number of individuals $\theta(t)$ that have survived to time t (i.e., that reach age t), to the initial number of individuals θ_0: $v(t) = \theta(t)/\theta_0$. In demography $v(t)$ is also called the longevity function. The biometric function $w(t)$ characterizes the rate of decrease in the number of individuals resulting from the deaths at age t normalized to the initial number of individuals: $w(t) = -(d\theta/dt)/\theta_0$.

O.A. Smirnova, *Environmental Radiation Effects on Mammals*,
DOI 10.1007/978-3-319-45761-1_6

The function $\rho(t)$ characterizes the rate of decrease in the number of individuals resulting from the deaths at age t normalized to the number of individuals that reach age t: $\rho(t) = -(d\theta/dt)/\theta(t)$.

It is worthwhile to note here that the average life span A can be expressed in terms of the function $w(t)$, namely [30]:

$$A = \int_0^\infty t\, w(t)\, dt\,. \tag{6.1}$$

To construct a mathematical model simulating the dynamics of population mortality, we use, in the first stage, the approach proposed by Sacher [31, 32]. He modeled a homogeneous population in which every individual was characterized by the same average values of all physiological variables and their fluctuation parameters, and described it by a random variable ξ, which was an index of the physiological state. It was also assumed that the deviation μ of the random variable ξ from its mean value m ($\mu = \xi - m$) obeys the stochastic differential equation

$$\frac{d\mu}{dt} + \omega\,\mu = \eta(t), \tag{6.2}$$

where $\eta(t)$ is a Gaussian random process with a zero mean value and the spectral density $4\Omega = 4S^2\omega$ [ω^{-1} is the mean relaxation time in the system (6.2); S^2 is the variance of the random variable μ].

The distribution function of the variable μ, $P(\mu_0 \,|\, \mu,\, t)$, is a solution to the Fokker–Planck partial differential equation

$$\frac{\partial P}{\partial t} = \omega\,\frac{\partial}{\partial \mu}\,(\mu P) + \Omega\,\frac{\partial^2 P}{\partial \mu^2}\,. \tag{6.3}$$

The quantity $P(\mu_0 \,|\, \mu,\, t)d\mu$ is the probability of observing in the system (6.2) the value of the variable μ between μ and $\mu + d\mu$ at time t if the value μ_0 was observed at $t = 0$. The stationary solution of Eq. (6.3) is given by

$$P(\mu) = \frac{1}{\sqrt{2\pi S^2}}\,\exp(-\mu^2/2S^2). \tag{6.4}$$

Further, it was assumed that when the variable ξ, which characterizes an individual, reaches or exceeds the threshold value L, then the situation could be interpreted as an analog of death. Such individuals then left the population. In accordance with this assumption, the distribution function $P(\mu)$ was modified:

$$P_M(\mu) = \begin{cases} \dfrac{(2\pi S^2)^{-1/2} \exp(-\mu^2/2S^2)}{(2\pi S^2)^{-1/2} \int\limits_{-\infty}^{\lambda} \exp(-\mu^2/2S^2)\, d\mu} & \text{for } \mu < \lambda\,, \\ 0 & \text{for } \mu \geq \lambda\,, \end{cases} \tag{6.5}$$

where

$$\lambda = L - m. \tag{6.6}$$

By virtue of Eq. (6.5), it was found that the rate at which individuals leave the population, i.e., the mortality rate, is described by the formula

$$\rho = \frac{\lambda\omega}{\sqrt{2\pi S^2}} \frac{\exp(-\lambda^2/2S^2)}{\Phi(U)}\,. \tag{6.7}$$

Here $U = \lambda/S$ is a dimensionless constant and $\Phi(U)$ is the standard normal distribution [33] of a standardized random variable $u = \mu/S$:

$$\Phi(U) = \frac{1}{\sqrt{2\pi}} \int\limits_{-\infty}^{U} e^{-u^2/2} du. \tag{6.8}$$

The meaning of the index of the physiological state ξ was not specified by Sacher [31]. He used Eq. (6.7) only to approximate the experimental data.

To specify the meaning of the index of the physiological state ξ, we use as our basis the commonly accepted radiobiological concept of a critical body system [34]. According to this concept, for certain ranges of doses and dose rates of irradiation, one can pick out a specific critical cell system, the radiation damage to which will play a key role in the development of radiation sickness and ultimately in the death of mammals. In turn, the damage to the critical system manifests itself in a reduction in the number of its functional cells below the level needed to sustain vitality. Note that bone marrow hematopoiesis and small intestinal epithelium are considered critical systems at sublethal and lethal radiation doses, respectively [34–36].

Proceeding from the concept of the critical system, we identify ξ with the variable that characterizes the deviation of the physiological state index of a critical cell system from its normal level. We consider the concentration of functional cells $z(t)$ as the index of the physiological state of the critical system. We also assume that when the deviation of the concentration of functional cells from the normal level z_0 in the critical system of an individual exceeds the threshold (life-critical) value L, then the situation can be treated as an analog of death. The reasons for such a deviation in our model are the following:

1. random fluctuation in the concentration of functional cells at time t around the mean value $z(t)$ with the variance S^2;

2. radiation-induced change in the mean value of the concentration of functional cells, which is described by $z_R(t)$ for $t > t_R$, t_R being the time of the onset of irradiation;
3. natural aging process, a result of which is that the mean value $z(t)$ of the concentration of functional cells decreases linearly with time at the low rate κ.

The last assumption is based on the facts known from biology and medicine. According to these facts, the values of many physiological indices decrease insignificantly with age. The following equation for $z(t)$ is obtained as a result:

$$z(t) = \begin{cases} z_0 - \kappa t & \text{for } t < t_R\,, \\ z_R(t) - \kappa t & \text{for } t \geq t_R\,. \end{cases} \tag{6.9}$$

In Eq. (6.9) the parameter κ satisfies the following relation:

$$\kappa\, t \ll z_0 \quad \text{for } t < A_I\,, \tag{6.10}$$

where A_I is an average life span of intact individuals.

Proceeding from the model assumptions and Eq. (6.9), the mean value of the random variable ξ reads

$$m(t) = z_0 - z(t) = \begin{cases} \kappa\, t & \text{for } t < t_R\,, \\ z_0 - z_R(t) + \kappa t & \text{for } t \geq t_R\,. \end{cases} \tag{6.11}$$

Substituting (6.11) into (6.7) and introducing the dimensionless parameters $Q = S/L$ and $q = z_0/L$, the coefficient $k = \kappa/L$ of the dimension of the inverse time, and the dimensionless variable $\tilde{z}_R(t) = z_R(t)/z_0$, we obtain

$$\rho(t) = \rho_1 R \exp\left[\frac{1 - R^2}{2Q^2}\right]\,, \tag{6.12}$$

where

$$\rho_1 = \rho_0 \frac{\Phi(1/Q)}{\Phi(R/Q)}\,, \tag{6.13}$$

$$R = R(t) = \begin{cases} 1 - kt & \text{for } t < t_R\,, \\ 1 - q[1 - \tilde{z}_R(t)] - kt & \text{for } t \geq t_R\,, \end{cases} \tag{6.14}$$

$$\rho_0 = \frac{\omega}{\sqrt{2\pi Q^2}} \frac{\exp[-1/(2Q^2)]}{\Phi(1/Q)}\,. \tag{6.15}$$

The function $R(t)$ [Eq. (6.14)] is proportional to the difference between the threshold (life-critical) deviation in the concentration of functional cells from the

norm and mean value of this deviation at moment t. The assumptions made in the derivation of Eqs. (6.12)–(6.15) imply that the function $R(t)$ is always positive. The function $\tilde{z}_R(t)$ in Eq. (6.14) must be computed within the mathematical model of the respective critical system.

When the mortality dynamics is simulated for nonirradiated mammals, the model (6.12)–(6.15) is reduced to the formula

$$\rho(t) = \rho_0 \frac{\Phi(1/Q)}{\Phi[(1-kt)/Q]} (1-kt) \exp\left[\frac{1-(1-kt)^2}{2Q^2}\right]. \tag{6.16}$$

If t is less than the mean life span A_I [i.e., if the relations (6.10) are satisfied], then we can neglect the following terms in (6.16): the term $-kt/Q$ in the argument of the function Φ; the linear term $-kt$ in the preexponent; and the quadratic term $-k^2t^2/(2Q^2)$ in the exponent. After these simplifications, Eq. (6.16) is reduced to the classical Gompertz equation [29]:

$$\rho(t) = \rho_0 \exp(R_0 t), \tag{6.17}$$

where

$$R_0 = k/Q^2. \tag{6.18}$$

It is important to point out that formula (6.17) is adequate for describing the mortality rate of nonirradiated mammals only about the mean age, but is unable to give the deviation from the exponential dependence in the function $\rho(t)$ at large t.

The function $\rho(t)$ uniquely defines two other biometric functions $w(t)$ and $v(t)$ [30]:

$$w(t) = \rho(t) \exp\left[-\int_0^t \rho(\tau)\, d\tau\right], \tag{6.19}$$

$$v(t) = \exp\left[-\int_0^t \rho(\tau)\, d\tau\right]. \tag{6.20}$$

The function $w(t)$ determines an average life span A [Eq. (6.1)]. In addition, the function $w(t)$ makes it possible to compute a very important characteristic of radiation-induced mortality: the shortening of the mean life span caused by irradiation. It equals the difference between the mean life span of intact (nonirradiated) specimens A_I and the mean life span of irradiated specimens A_R:

$$A_I - A_R = \int_0^\infty t\, w_I(t)\, dt - \int_0^\infty t\, w_R(t)\, dt. \tag{6.21}$$

Here, $w_I(t)$ and $w_R(t)$ are probability densities of the life span for nonirradiated and irradiated specimens and t denotes time. In turn, the function $v(t)$ [Eq. (6.20)] makes it possible to compute the risk function $r(t)$, which represents the probability of dying before age t:

$$r(t) = 1 - v(t). \tag{6.22}$$

Thus, we developed the model describing the mortality dynamics in homogeneous populations of irradiated and nonirradiated mammals. The results of the numerical studies of this model are presented in the next two sections of this chapter.

6.3 Mortality Dynamics in a Homogeneous Population: Gastrointestinal Subsyndrome of Acute Radiation Syndrome

We use the developed model (6.12)–(6.15) to examine the mortality dynamics in a homogeneous population of mice exposed to acute and chronic irradiation within the dose and dose rate ranges for which the small intestinal epithelium is the critical system [36]. The principal reason for animal death in this case is the so-called gastrointestinal subsyndrome of the acute radiation syndrome. The dynamics of the concentration of functional elements of the critical body system, villus enterocytes, is determined within the model presented in Chap. 3. The time interval within which the dynamics of the small intestinal epithelium and mortality are simulated is 12 days. It is a period during which the transitional process under chronic irradiation and the recovery process after acute irradiation are completely finished in the epithelium of the small intestine. Additionally, the duration of real experiments is similar [37].

The following experimental facts are used when estimating the coefficients q and Q. The irradiated mice die if the concentration of functional cells of the small intestinal epithelium (villus enterocytes) drops to 10 % of the normal level (z_0) [36]. Hence, the threshold value L equals $0.9\,z_0$; thus, $q = 1.1$. The mean square deviation from the mean values of the enterocyte concentration in nonirradiated and irradiated mice is about $0.175\,z_0$ [38]. Therefore, we have $Q^2 = 0.038$. The parameters $\rho_0 = \exp(-11.7)\,\text{day}^{-1}$ and $k = 0.0005\,\text{day}^{-1}$ in (6.15) are calculated by the least-squares method from experimental data on the mortality rate of nonirradiated mice of the BCF_1 and LAF_1 strains [28].

First we use the model to examine effects of acute irradiation on mortality dynamics of 100-day-old mice. The obtained results are presented in Figs. 6.1, 6.2, 6.3, and 6.4. They show the biometric functions $\rho(t)$, $w(t)$, $v(t)$, and the risk function $r(t)$ computed for three different doses of acute irradiation.

As one can infer from Fig. 6.1, after irradiation the mortality rate $\rho(t)$ grows to a certain maximal value. This is followed by a decrease in $\rho(t)$ and then by a

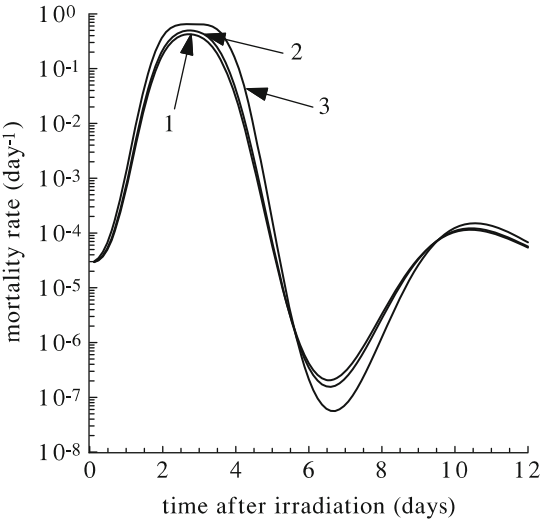

Fig. 6.1 The biometric function $\rho(t)$ (the mortality rate) computed for the homogeneous population of mice exposed to acute irradiation at doses of 8 Gy (*curve 1*), 9 Gy (*curve 2*), and 14 Gy (*curve 3*)

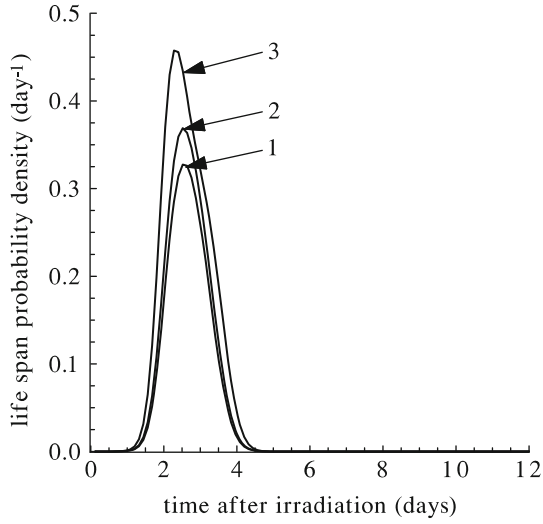

Fig. 6.2 The biometric function $w(t)$ (the life span probability density) computed for the homogeneous population of mice exposed to acute irradiation at doses of 8 Gy (*curve 1*), 9 Gy (*curve 2*), and 14 Gy (*curve 3*)

new ascent. The maximal value of $\rho(t)$ is larger as the dose D increases. These modeling results are qualitatively consistent with experimental data collected and parameterized in [37].

Figure 6.2 shows that the life span probability density $w(t)$ remains at the initial level during the first day after acute irradiation. Then the function $w(t)$ increases to a maximum value; the higher the dose, the greater the maximum level becomes. The time required to reach the maximum level weakly depends on the dose. After reaching its maximum level, the function $w(t)$ decreases. By the end of the fifth day, it returns to the initial value. The subsequent variations of $w(t)$ are insignificant.

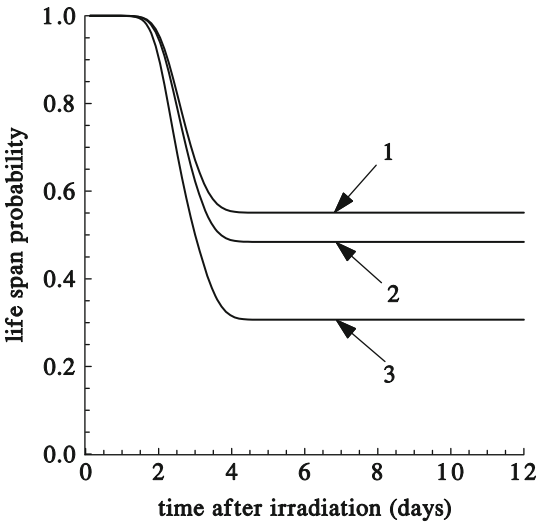

Fig. 6.3 The biometric function $v(t)$ (the life span probability) computed for the homogeneous population of mice exposed to acute irradiation at doses of 8 Gy (*curve 1*), 9 Gy (*curve 2*), and 14 Gy (*Curve 3*)

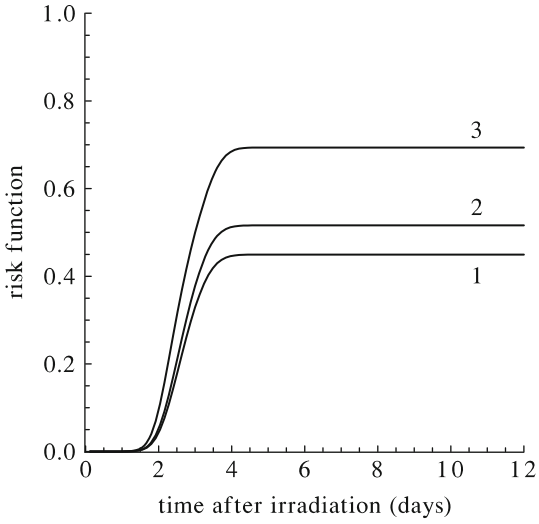

Fig. 6.4 The risk function $r(t)$ (6.22) computed for the homogeneous population of mice exposed to acute irradiation at doses of 8 Gy (*curve 1*), 9 Gy (*curve 2*), and 14 Gy (*curve 3*)

These modeling results qualitatively agree with the diagram of the function $w(t)$ built from experimental observations of mice after an acute exposure to doses of $(10 \div 20)$ Gy [34]. It should be noted that the time parameters obtained in the model are consistently smaller than the corresponding experimental quantities by about 24 h. For example, in the experiments with the dose of 14 Gy, mice started dying at $t_1 = 2$ days, and all mice were dead at $t_2 = 5$ days after irradiation, with the maximum number of deaths at $t_3 = 3.5$ days [34]. The computed values of t_1, t_2, and t_3 are 1.2, 4.5, and 2.5 days, respectively. This discrepancy seems to be due to a delay period between the final stage of sickness (severe impairment of the small

intestinal epithelium) and death. The experiments suggest that this delay is a little less than 24 h [34]. This means that there is quantitative agreement between the modeling results and experimental data.

As one can infer from Fig. 6.3, the life span probability function $v(t)$ does not practically deviate from its initial value within 1.5 days after radiation exposure. For 100-day-old mice, this value is about unity. Then the function $v(t)$ goes down; by the end of the fourth day, it approaches a new stationary level. The higher the radiation dose D is, the lower the stationary level will be. This means that the higher the dose D is, the smaller the fraction of animals alive will be after 4 days of the impact of radiation. For instance, the fraction of surviving animals is about 50 % at $D = 9$ Gy. This modeling prediction agrees with the experimental data [39], which indicate that the dose that induces death of 50 % of 12-week-old mice of the C5761/6 strain within 4 days ($LD_{50/4}$) is 8.8 ± 0.13 Gy. The estimates of mean lethal doses $LD_{50/5}, LD_{50/6}, LD_{50/7}$ by other authors are rather similar: $(8.5 \div 13)$ Gy [40].

It should be noted that the function $v(t)$ remains constant as long as the gastrointestinal subsyndrome is the only cause of death. At given intervals of doses D, this period is restricted to $5 \div 7$ days, according to the experimental data [37].

In turn, Fig. 6.4 shows risk functions $r(t)$ (6.22) calculated proceeding from the functions $v(t)$ given in Fig. 6.3. The function $r(t)$, which represents the probability of dying before age t, does not practically deviate from its initial value within 1.5 days after radiation exposure. For 100-day-old mice, this initial value is about zero. Then the function $r(t)$ increases; by the end of the fourth day, it approaches a new stationary level. The greater the radiation dose D, the higher the stationary level will be.

The model is also used to examine the effects of chronic irradiation on the mortality dynamics of 100-day-old mice. The obtained results are presented in Figs. 6.5, 6.6, 6.7, and 6.8. They show the biometric functions $\rho(t)$, $w(t)$, and $v(t)$ computed for three different dose rates of chronic irradiation.

Figure 6.5 shows that the mortality rate $\rho(t)$ does not practically deviate from its initial value during the first day after the onset of irradiation. Then the function $\rho(t)$ grows, decreases, and increases again, achieving the value that is greater for higher dose rates N.

In turn, the life span probability density $w(t)$ remains at the initial level during the first 2 days after the onset of irradiation (Fig. 6.6). On the third day, $w(t)$ starts to increase and reaches a maximum value; the lower the dose rate, the later the maximum is reached. The maximum value of $w(t)$ is greater when the dose rate N is higher. Then the function $w(t)$ decreases.

As one can infer from Fig. 6.7, the life span probability $v(t)$ does not practically deviate from its initial value for more than 2 days after the onset of chronic irradiation. Then it decreases, and the larger N is, the smaller the level is down to which it drops. These results qualitatively [in the time interval $(0 \div 7)$ days quantitatively] agree with experimental data [37]. Here the experimental data from [37] are presented with a correction to a 1-day delay, discovered in experiments [34], between the final stage of sickness (severe impairment of the small intestinal epithelium) and death. The computed value of the fraction of specimens

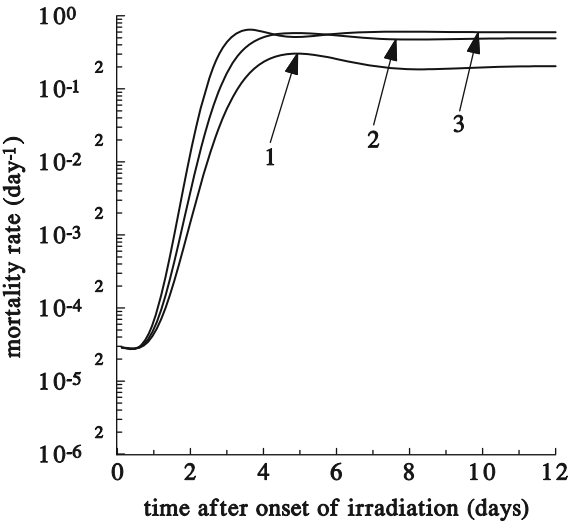

Fig. 6.5 The biometric function $\rho(t)$ (the mortality rate) computed for the homogeneous population of mice exposed to chronic irradiation at dose rates of 2 Gy/day (*curve 1*), 3 Gy/day (*curve 2*), and 5 Gy/day (*curve 3*)

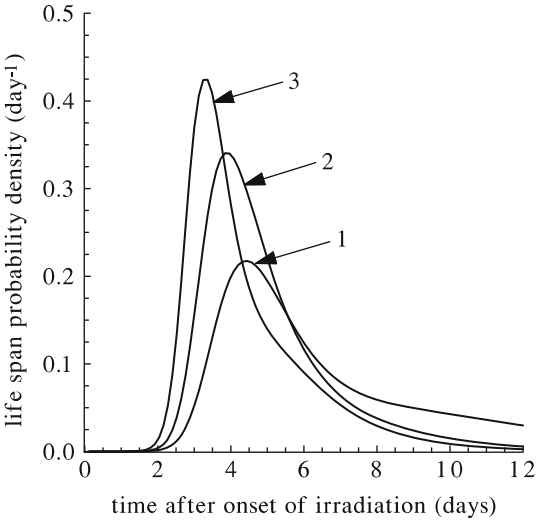

Fig. 6.6 The biometric function $w(t)$ (the life span probability density) computed for the homogeneous population of mice exposed to chronic irradiation at dose rates of 2 Gy/day (*curve 1*), 3 Gy/day (*curve 2*), and 5 Gy/day (*curve 3*)

that survived after 9 days of irradiation at the dose rate $N = 2\,\text{Gy/day}$ slightly exceeds the corresponding experimental values. The discrepancy probably indicates that during this period the damage to the small intestine is already not the sole reason for animal death.

In turn, Fig. 6.8 shows risk functions $r(t)$ (6.22) calculated proceeding from the functions $v(t)$ given in Fig. 6.7. The function $r(t)$ does not deviate in practice from its initial value for more than 2 days after the onset of chronic irradiation.

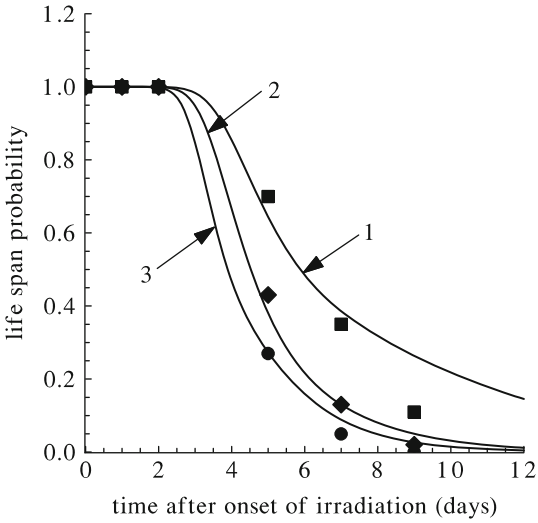

Fig. 6.7 The biometric function $v(t)$ (the life span probability) computed for the homogeneous population of mice exposed to chronic irradiation at dose rates of 2 Gy/day (*curve 1*), 3 Gy/day (*curve 2*), and 5 Gy/day (*curve 3*), and corresponding experimental data [37] (*box, diamond, and circle*, respectively)

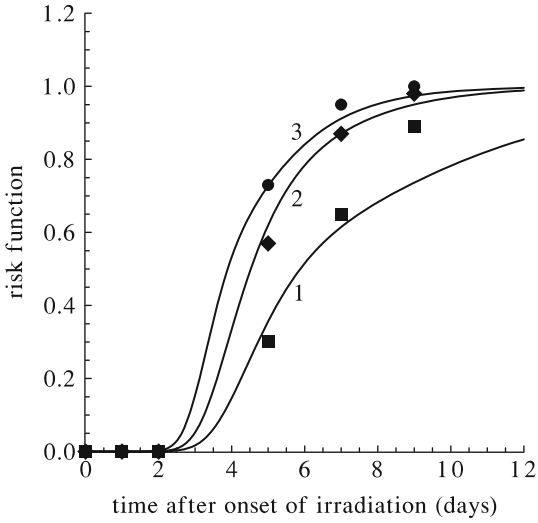

Fig. 6.8 The risk function $r(t)$ (6.22) computed for the homogeneous population of mice exposed to chronic irradiation at doses of 2 Gy/day (*curve 1*), 3 Gy/day (*curve 2*), and 5 Gy/day (*curve 3*), and corresponding values of $r(t)$ (*box, diamond, and circle*, respectively) calculated proceeding from experimental data [37]

For 100-day-old mice, this initial value is about zero. Then $r(t)$ increases, and the greater N is, the higher will be the level it reaches. These results qualitatively [in the time interval $(0 \div 7)$ days quantitatively] agree with the respective values of $r(t)$ calculated proceeding from experimental data [37].

Thus, the modeling results presented above qualitatively, and in most cases quantitatively, agree with the experimental data.

6.4 Mortality Dynamics in a Homogeneous Population: Hematopoietic Subsyndrome of Acute Radiation Syndrome

We apply the model described above to simulate the mortality dynamics of a homogeneous population of mice exposed, from the age t of 100 days, to chronic irradiation at dose rates $0 \leq N \leq 0.088\,\mathrm{Gy/day}$. In this case the hematopoietic system, namely the thrombopoietic system, is the critical one [35]. The main reason for animal death in this case is the so-called hematopoietic subsyndrome of the acute radiation syndrome. The dynamics of the concentration of functional elements of the critical body system system, thrombocytes, is determined within the model developed in Chap. 1. The time interval within which the dynamics of the critical system and mortality are simulated is 1000 days, as in the real experiments [28].

The following experimental facts are used when estimating the coefficients q and Q. The irradiated mice die when the thrombocyte concentration is 10 % of the normal level [35]. Therefore, the threshold value L equals $0.9\,z_0$ and $q = 1.1$. The mean square deviation from the mean thrombocyte concentrations for irradiated and nonirradiated mice is about $0.2\,z_0$ [35]. Hence, we have $Q^2 = 0.05$. The parameters $\rho_0 = \exp(-11.7)\,\mathrm{day}^{-1}$ and $k = 0.0005\,\mathrm{day}^{-1}$, as before, are calculated by the least-squares method from the experimental mortality rates for nonirradiated mice of the $\mathrm{BCF_1}$ and $\mathrm{LAF_1}$ strains [28].

Figures 6.9, 6.10, 6.11, and 6.12 present the functions $\rho(t)$, $w(t)$, $v(t)$, and $r(t)$ computed within the model (6.12)–(6.15). They describe the mortality dynamics of mice unexposed and exposed to chronic irradiation at three dose rates N.

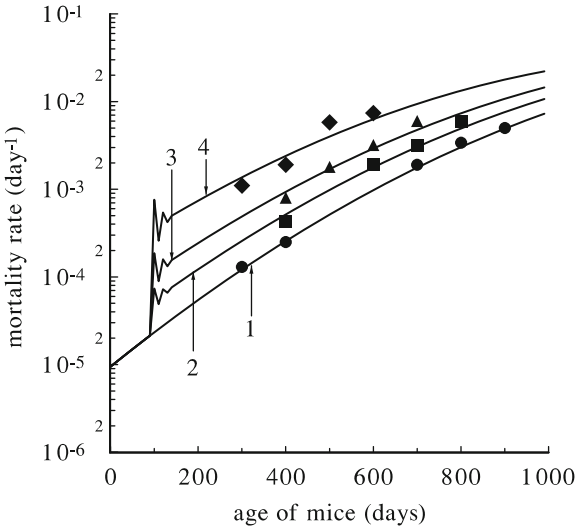

Fig. 6.9 The biometric function $\rho(t)$ (the mortality rate) computed for the homogeneous population of mice unexposed (*curve 1*) and exposed to chronic irradiation at dose rates of 0.022 Gy/day (*curve 2*), 0.044 Gy/day (*curve 3*), and 0.088 Gy/day (*curve 4*), and also corresponding experimental data on the mortality rate for the homogeneous population of $\mathrm{LAF_1}$ mice (*circle, box, triangle, and diamond*) [28]

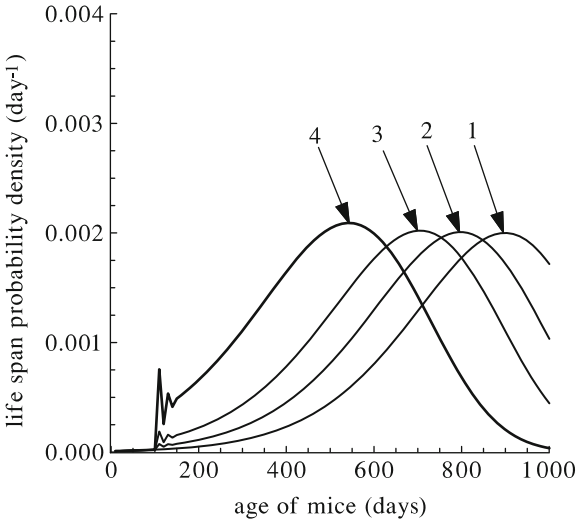

Fig. 6.10 The biometric function $w(t)$ (the life span probability density) computed for the homogeneous population of mice unexposed (*curve 1*) and exposed to chronic irradiation at dose rates of 0.022 Gy/day (*curve 2*), 0.044 Gy/day (*curve 3*), and 0.088 Gy/day (*curve 4*)

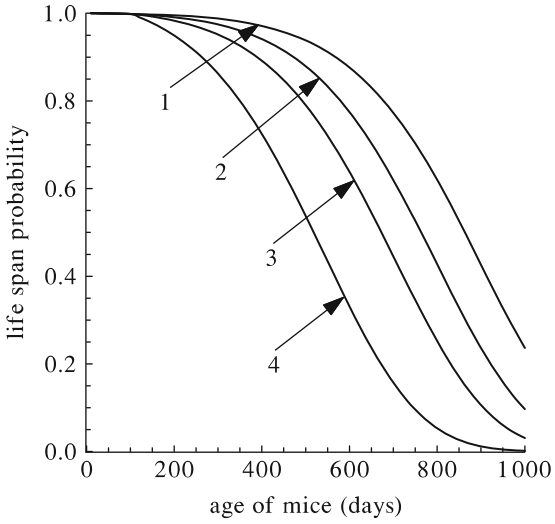

Fig. 6.11 The biometric function $v(t)$ (the life span probability) computed for the homogeneous population of mice unexposed (*curve 1*) and exposed to chronic irradiation at dose rates of 0.022 Gy/day (*curve 2*), 0.044 Gy/day (*curve 3*), and 0.088 Gy/day (*curve 4*)

Figure 6.9 also shows the corresponding experimental data [28] on the mortality rate dynamics of LAF_1 mice nonirradiated and irradiated from the age $t_R = 100$ days at the same dose rates.

As one can infer from Fig. 6.9, the model adequately reproduces the experimental results [28]. Specifically, the mortality rate for nonirradiated mice increases as the age t increases. In contrast to the widely applied Gompertz equation (6.17), the model describes the experimentally observed deviation of the function $\rho(t)$ from the exponential curve in the region of high values of t. Two phases can be distinguished in the dynamics of the mortality rate of irradiated mice. During the first phase, the values of $\rho(t)$ oscillate with damping near a permanently rising level. This phase

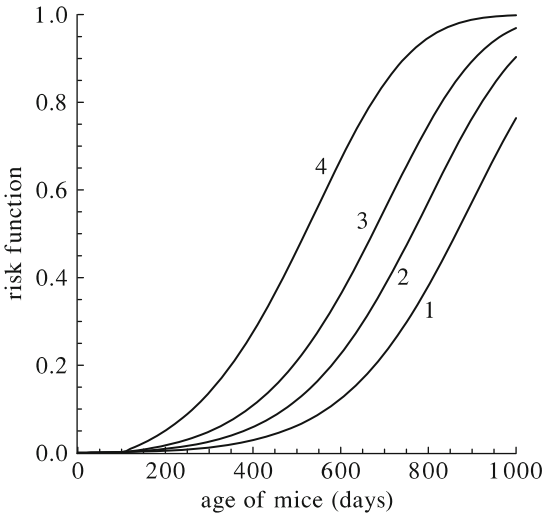

Fig. 6.12 The risk function $r(t)$ (6.22) computed for the homogeneous population of mice unexposed (*curve 1*) and exposed to chronic irradiation at dose rates of 0.022 Gy/day (*curve 2*), 0.044 Gy/day (*curve 3*), and 0.088 Gy/day (*curve 4*)

corresponds to the oscillating transitional process in the dynamics of thrombopoietic system and precedes the establishment of a new homeostasis in the system under consideration (see Chap. 1). During the second phase, the function $\rho(t)$ increases. As in experiments [28], for a fixed age t, the mortality rate for chronically irradiated mice exceeds that for nonirradiated mice by a quantity that increases with increasing dose rate N.

Figure 6.10 shows that the function $w(t)$ describing the life span probability density of nonirradiated mice increases to a maximum and then decreases. In turn, the function $w(t)$ describing the life span probability density of mice exposed to chronic irradiation has, as the function $\rho(t)$, two characteristic regions. From the onset of the irradiation, $w(t)$ reproduces the oscillating transitional process. Further, the function $w(t)$ increases, arrives at the maximum level, and then decreases. At the values N used in computations, the maxima of the function $w(t)$ do not differ from the maximum of the life span probability density of unexposed mice. It is important that increasing of the dose rate entails the shortening of the time required for arriving at the maximum of the function $w(t)$, i.e., the mortality peak occurs earlier.

As one can infer from Fig. 6.11, the function $v(t)$, which describes the life span probability of specimens exposed to chronic irradiation, decreases after the onset of irradiation and takes the smaller value as the dose rate N increases. For a fixed value t, the probability of the life span $v(t)$ computed for irradiated mice is less than that for nonirradiated specimens by a quantity that increases with increasing N. In other words, the probability of surviving to a certain age for irradiated animals is less than that for unexposed specimens. The difference between them increases as the dose rate N increases.

Experimental data are not presented in Figs. 6.10 and 6.11 because in the real experiment [28] simulated here, only the biometric function $\rho(t)$ was measured. Such additional experimental data are not really required because the

function $\rho(t)$ uniquely determines two other biometric functions, $w(t)$ and $v(t)$ (see Eqs. (6.19), (6.20)].

In turn, Fig. 6.12 shows the risk functions $r(t)$ (6.22) computed proceeding from the functions $v(t)$ given in Fig. 6.11. As one can see, the function $r(t)$, which represents the probability of dying before age t, increases after the onset of irradiation and takes the greater value as the dose rate N increases. For a fixed value t, the function $r(t)$ computed for irradiated mice is greater than that for nonirradiated specimens by a quantity that increases with increasing N. In other words, the probability of dying before age t for irradiated mice is greater than that for unexposed specimens. The difference between them increases as the dose rate N increases.

The function $r(t)$ does not practically deviate from its initial value for more than 2 days after the onset of chronic irradiation. For 100-day-old mice, this initial value is about zero. Then $r(t)$ increases, and the greater N is, the higher the level it reaches.

The model is used to evaluate the average shortening of the life span, which is the difference between the values of the average life span computed for nonirradiated and irradiated mammals [Eq. (6.21)]. For N values of 0.013, 0.026, and 0.06 Gy/day, the values of the life span shortening are equal to 30, 64, and 166 days, respectively. As one can see, the average life span decreases with increasing dose rate N. These modeling predictions are fairly close to the experimental estimates of 34, 67, and 146 days [28].

Thus, the developed mathematical model reproduces the dynamics and the integral characteristics of mortality in a homogeneous population of mammals (mice) unexposed and exposed to radiation in broad ranges of doses and dose rates. Therefore, the radiobiological concept of the critical system is confirmed at the quantitative level. According to this concept, the radiosensitivity of the organism as a whole closely correlates with the radiosensitivity of the corresponding critical system and ultimately with the radiosensitivity of its cells. The model can be used for predicting the mortality dynamics in the homogeneous mammalian populations when the main reason of specimen death is either the hematopoietic subsyndrome or the gastrointestinal subsyndrome of the acute radiation syndrome.

6.5 Model of Radiation-Induced Mortality for a Nonhomogeneous (in Radiosensitivity) Mammalian Population

In Sects. 6.2–6.4, the mathematical model of the mammalian mortality dynamics has been presented. Its development involves the simplifying assumption about the homogeneity of the population of the biological objects. This model was found to reproduce fairly well the mortality dynamics in the homogeneous population of mice irradiated in the ranges of acute irradiation doses and chronic irradiation dose rates within which the critical systems are those of thrombopoietic system and

small intestinal epithelium. However, there is significant evidence indicating that there exist human subpopulations hypersensitive to radiation [41–43]. This calls for model investigations of mortality dynamics for a nonhomogeneous population.

In radiobiology it is assumed that the inhomogeneity of a mammalian population with respect to radiation exposure is mainly due to the dissimilarity in the radiosensitivity index of critical system cells among the specimens constituting the population [34]. The index of cell radiosensitivity is the conventional radiobiological dose D_0: After exposure to this dose, the number of cells left undamaged is $e = 2.718\ldots$ times smaller than their initial number [34]. The radiosensitive cells in the two above-considered critical systems, thrombopoietic system and small intestinal epithelium, are capable of dividing precursor cells of thrombocytes in the bone marrow and capable of dividing precursor cells of enterocytes in crypts, respectively. Thus, the parameter D_0 characterizing the radiosensitivity of capable of dividing precursor cells of the relevant critical system can be used in the model as the index of inhomogeneity (in radiosensitivity) of mammalian populations.

Taking all this into account, let us describe the specimen distribution in the radiosensitivity index D_0 in a nonhomogeneous mammalian population by a continuous function $\varphi(D_0)$. Then, for simplification of the problem, let us replace the continuous distribution of the random variable D_0 by a discrete one. To this end we split the range of the continuous random variable D_0 into a finite number of intervals, I. This operation corresponds to the partitioning of the population into I groups of specimens whose critical cell radiosensitivity index D_0 belongs to the respective ith interval (D'_{0i}, D''_{0i}) $(i = 1, \ldots, I)$. The fraction of individuals constituting the ith group is expressed through the probability density function $\varphi(D_0)$ as follows [44]:

$$n_i = \int_{D'_{0i}}^{D''_{0i}} \varphi(D_0)\, dD_0 \,. \tag{6.23}$$

The mean value of D_0 for individuals of the ith group is

$$\bar{D}_{0i} = \frac{1}{n_i} \int_{D'_{0i}}^{D''_{0i}} D_0\, \varphi(D_0)\, dD_0 \,. \tag{6.24}$$

We approximate the original continuous distribution $\varphi(D_0)$ by a discrete distribution in the following way. It is assumed that the random variable D_0 takes the discrete values $\bar{D}_{0i}$ $(i = 1, \ldots, I)$ [Eq. (6.24)] with the probability

$$\mathscr{P}(D_0 = \bar{D}_{0i}) = n_i \quad (i = 1, \ldots, I) \,. \tag{6.25}$$

In this equation, the n_i are determined by Eq. (6.23).

This operation is equivalent to the representation of the original nonhomogeneous population as a set of finite number of homogeneous subpopulations. The number of specimens in the ith homogeneous subpopulation coincides with the number of specimens in the ith group of the original population whose D_0 belongs to the ith interval. The parameter $\bar{D}_{0i}$ that shows the radiosensitivity of the critical system cells for individuals of the ith homogeneous subpopulation is equal to the mean value of D_0 for the individuals of the ith group of the original population. It should be noted that with any method of partitioning the range of continuous random variable D_0 into intervals and irrespective of the number of the latter, the mean values of the radiosensitivity index of the critical system cells for individuals of the original nonhomogeneous population and for individuals of the nonhomogeneous population that is a set of the homogeneous subpopulations [with the parameters n_i and $\bar{D}_{0i}$ $(i = 1, \ldots, I)$] are equal. This follows from the equality of the expected value of the random variable D_0, described by the continuous distribution $\varphi(D_0)$, and of the expected value of the random variable D_0 described by the discrete distribution $\varphi_i(\bar{D}_{0i})$ derived above (6.25).

The dynamics of the radiation-induced mortality of each ith homogeneous subpopulation, whose members have their particular value of the radiosensitivity index $\bar{D}_{0i}$, can be computed by the model described in Sect. 6.2. This will yield a set of values of the biometric functions [the mortality rate $\rho_i(t)$, the probability density $w_i(t)$, and the probability $v_i(t)$ of the life span] that describe the mortality dynamics of the ith subpopulation under a given irradiation regime.

Let us express the biometric functions $\rho_\Sigma(t)$, $w_\Sigma(t)$, and $v_\Sigma(t)$ characterizing the mortality dynamics of the population as a whole through the biometric functions $\rho_i(t)$, $w_i(t)$, and $v_i(t)$ $(i = 1, \ldots, I)$. According to its definition, the biometric function $v_\Sigma(t)$ represents the ratio of individuals that survived to time t, $N_\Sigma(t)$, to their initial number $N_{0\Sigma}$ in the population:

$$v_\Sigma(t) = \frac{N_\Sigma(t)}{N_{0\Sigma}}. \tag{6.26}$$

For each time instant t, we know the values of the functions $v_i(t)$ $(i = 1, \ldots, I)$. They are equal to the ratio of the number of specimens of the ith subpopulation that survived to time t, $N_i(t)$, to their initial number $N_{0i} = N_{0\Sigma} \cdot n_i$:

$$v_i(t) = \frac{N_i(t)}{N_{0i}} = \frac{N_i(t)}{N_{0\Sigma} \cdot n_i}. \tag{6.27}$$

It follows from (6.27) that

$$N_i(t) = N_{0\Sigma} \cdot v_i(t) \cdot n_i. \tag{6.28}$$

Hence, the total number of individuals that survived to time t in the population composed of I homogeneous subpopulations is

$$N_\Sigma(t) = \sum_{i=1}^{I} N_i(t) = N_{0\Sigma} \sum_{i=1}^{I} v_i(t) \cdot n_i \,. \tag{6.29}$$

Substituting (6.29) into (6.26), we obtain

$$v_\Sigma(t) = \sum_{i=1}^{I} v_i(t)\, n_i. \tag{6.30}$$

The biometric function $w_\Sigma(t)$ is equal to the ratio of the decrease rate of the number of individuals in the population as the result of death at time t, dN_Σ/dt, to the initial number of individuals $N_{0\Sigma}$:

$$w_\Sigma(t) = -\frac{dN_\Sigma}{dt} \cdot \frac{1}{N_{0\Sigma}} \,. \tag{6.31}$$

For every instant t, we know the values of the functions $w_i(t)$ $(i = 1, \ldots, I)$. They are equal to the ratio of the decrease rate of the number of individuals in the ith subpopulation as the result of death at time t, dN_i/dt, to the initial number of individuals in this subpopulation $N_{0i} = N_{0\Sigma} \cdot n_i$:

$$w_i(t) = -\frac{dN_i}{dt} \cdot \frac{1}{N_{0i}} = -\frac{dN_i}{dt} \cdot \frac{1}{N_{0\Sigma} \cdot n_i} \,. \tag{6.32}$$

It follows from (6.32) that

$$-\frac{dN_i}{dt} = N_{0\Sigma} \cdot w_i(t) \cdot n_i \,. \tag{6.33}$$

In accordance with (6.33), the decrease rate of the number of individuals in the entire population as the result of death at time t is defined by the expression

$$-\frac{dN_\Sigma}{dt} = -\sum_{i=1}^{I} \frac{dN_i}{dt} = N_{0\Sigma} \sum_{i=1}^{I} w_i(t)\, n_i \,. \tag{6.34}$$

Substituting (6.34) into (6.31), we find that

$$w_\Sigma(t) = \sum_{i=1}^{I} w_i(t)\, n_i \,. \tag{6.35}$$

The biometric function $\rho_\Sigma(t)$ represents the ratio of the decrease rate of the number of individuals in the population as the result of death at time t, dN_Σ/dt, to the number of individuals of the same population that survived to time t, $N_\Sigma(t)$:

$$\rho_\Sigma(t) = -\frac{dN_\Sigma}{dt} \cdot \frac{1}{N_\Sigma(t)}. \tag{6.36}$$

By virtue of relations (6.29), (6.30), (6.34), and (6.35), we obtain

$$\rho_\Sigma(t) = \frac{N_{0\Sigma} \sum_{i=1}^{I} w_i(t)\, n_i}{N_{0\Sigma} \sum_{i=1}^{I} v_i(t)\, n_i} = \frac{w_\Sigma(t)}{v_\Sigma(t)}. \tag{6.37}$$

There is another version of the formula suitable for computation of the function $\rho_\Sigma(t)$. For each time instant t, we know the values of the functions $\rho_i(t)$ ($i = 1, \ldots, I$). They are equal to the ratio of the decrease rate of the number of individuals in the ith subpopulation as the result of death at time t, dN_i/dt, to the number of individuals in the ith subpopulation that survived to time t, $N_i(t)$:

$$\rho_i(t) = -\frac{dN_i}{dt} \cdot \frac{1}{N_i(t)}. \tag{6.38}$$

From (6.38) we have

$$-\frac{dN_i}{dt} = \rho_i(t) \cdot N_i(t). \tag{6.39}$$

According to (6.28) and (6.39), the decrease rate of the number of individuals in the entire population as the result of death at time t is

$$-\frac{dN_\Sigma}{dt} = -\sum_{i=1}^{I} \frac{dN_i}{dt} = \sum_{i=1}^{I} \rho_i(t) \cdot N_i(t) = N_{0\Sigma} \sum_{i=1}^{I} \rho_i(t) \cdot v_i(t) \cdot n_i. \tag{6.40}$$

In turn, N_Σ is defined, according to formulas (6.29) and (6.30), by the expression

$$N_\Sigma(t) = N_{0\Sigma} \sum_{i=1}^{I} v_i(t) \cdot n_i = N_{0\Sigma} \cdot v_\Sigma(t). \tag{6.41}$$

Substituting (6.40) and (6.41) into (6.36), we have

$$\rho_\Sigma(t) = \frac{\sum_{i=1}^{I} \rho_i(t)\, v_i(t)\, n_i}{\sum_{i=1}^{I} v_i(t)\, n_i} = \frac{1}{v_\Sigma(t)} \cdot \sum_{i=1}^{I} \rho_i(t)\, v_i(t)\, n_i. \tag{6.42}$$

Thus, we have constructed, in a general form, a mathematical model that enables one to calculate the statistical biometric functions that describe the mortality dynamics for a nonhomogeneous (in radiosensitivity) population of irradiated mammals.

6.6 Populations with Normal and Log-Normal Distributions of Specimens in Radiosensitivity Index of Critical System Cells

In this section we apply the aforementioned mathematical model for the description of a nonhomogeneous population with two different types of distributions of specimens in the radiosensitivity index D_0 of the critical system cells: normal (Gaussian) and log-normal, most frequently used in biology. First we examine the case when the distribution obeys Gauss's law [44]:

$$\varphi_N(D_0) = \frac{1}{\sigma\sqrt{2\pi}} \exp\left[-\frac{(D_0 - \bar{D}_0)^2}{2\sigma^2}\right]. \tag{6.43}$$

In (6.43) the parameter $\bar{D}_0$ is the expected value of the random variable D_0 [the mean of the density $\varphi_N(D_0)$]. In turn, σ^2 is equal to the variance $V(D_0)$ of the probability density function $\varphi_N(D_0)$ (i.e., σ is the standard deviation of the random variable D_0).

The range of the variable D_0 in (6.43) covers the real numbers from $-\infty$ to $+\infty$. However, since the ratio of the standard deviation to the mean for many biological indices described by the normal distribution does not exceed 0.3 [45], in the model we consider a finite range of the random variable: $\bar{D}_0 - 3\sigma \le D_0 \le \bar{D}_0 + 3\sigma$. It is worth noting that in this range the random variable D_0 is positive, i.e., has a real physical meaning. The probability that a normally distributed random variable goes outside the aforementioned range is negligibly small (namely, it is 0.0027 [33]). Therefore, there is no need to renormalize the probability density function.

To replace the continuous distribution (6.43) by the discrete distribution (6.25), it is convenient to split the aforementioned range of the continuous random variable D_0 into six intervals symmetric with respect to $\bar{D}_0$:

$$\bar{D}_0 - 3\sigma, \quad \bar{D}_0 - 2\sigma, \quad \bar{D}_0 - \sigma, \quad \bar{D}_0, \quad \bar{D}_0 + \sigma, \quad \bar{D}_0 + 2\sigma, \quad \bar{D}_0 + 3\sigma. \tag{6.44}$$

According to Eqs. (6.23), (6.24), and (6.43), the parameters n_i and $\bar{D}_{0i}$ in (6.25) are defined by the formulas

$$n_i = \Phi(U_i'') - \Phi(U_i'), \tag{6.45}$$

$$\bar{D}_{0i} = \bar{D}_0 - \frac{1}{n_i}\frac{\sigma}{\sqrt{2\pi}}\left\{\exp\left[-\frac{(U_i'')^2}{2}\right] - \exp\left[-\frac{(U_i')^2}{2}\right]\right\}. \tag{6.46}$$

In Eqs. (6.45) and (6.46) U_i' and U_i'' are expressed through the boundary values of the intervals D_{0i}' and D_{0i}'':

$$U_i' = \frac{D_{0i}' - \bar{D}_0}{\sigma}, \qquad U_i'' = \frac{D_{0i}'' - \bar{D}_0}{\sigma}. \tag{6.47}$$

In Eq. (6.45) $\Phi(U)$ is the standard normal distribution (6.8).

With the chosen values of D'_{0i} and D''_{0i} (6.44), the parameters n_i and $\bar{D}_{0i}$ ($i = 1, \ldots, 6$) are defined as follows:

$$\begin{aligned} n_1 &= 0.02140, \quad & n_4 &= 0.34134, \\ n_2 &= 0.13591, \quad & n_5 &= 0.13591, \\ n_3 &= 0.34134, \quad & n_6 &= 0.02140, \end{aligned} \tag{6.48}$$

and

$$\begin{aligned} \bar{D}_{01} &= \bar{D}_0 - \sigma \cdot 2.31585, \quad & \bar{D}_{04} &= \bar{D}_0 + \sigma \cdot 0.45986, \\ \bar{D}_{02} &= \bar{D}_0 - \sigma \cdot 1.38312, \quad & \bar{D}_{05} &= \bar{D}_0 + \sigma \cdot 1.38312, \\ \bar{D}_{03} &= \bar{D}_0 - \sigma \cdot 0.45986, \quad & \bar{D}_{06} &= \bar{D}_0 + \sigma \cdot 2.31585\,. \end{aligned} \tag{6.49}$$

Thus, in this approximation, the original nonhomogeneous population with a normal distribution of specimens in the radiosensitivity index of the critical system cells can indeed be represented as a set of the six homogeneous subpopulations. The fraction of specimens in each of the subpopulations is determined by n_i (6.48). The index of individual radiosensitivity of critical system cells in specimens of each of the six subpopulations, $\bar{D}_{0i}$ (6.49), is uniquely expressed by the parameters $\bar{D}_0$ and σ of the normal distribution $\varphi_N(D_0)$ (6.43).

Now let us consider the case of the log-normal distribution of specimens of the population in the radiosensitivity index D_0 of the critical system cells. In what follows we adhere to the standard form of the log-normal distribution [44, 46–48]. Specifically, the log-normal distribution implies that the logarithm of the random variable D_0, $X = \ln D_0$, but not the random variable D_0 itself, is distributed by the normal law. The probability density function $\varphi_{LN}(D_0)$ of the random variable D_0 is expressed in terms of the expected value m and the standard deviation σ of the normal random variable X in the following way [44]:

$$\varphi_{LN}(D_0) = \frac{1}{\sigma\sqrt{2\,\pi}}\,\frac{1}{D_0}\,\exp\left[-\frac{(\ln D_0 - m)^2}{2\,\sigma^2}\right]. \tag{6.50}$$

The parameters m and σ specify the expected value $\bar{D}_0$ of the random variable D_0 and the variance $V(D_0)$ of the probability density function $\varphi_{LN}(D_0)$ [44]:

$$\bar{D}_0 = \exp\left(m + \frac{\sigma^2}{2}\right), \tag{6.51}$$

$$V(D_0) = \exp(2\,m + \sigma^2)\left[\exp(\sigma^2) - 1\right]. \tag{6.52}$$

The range of the normal random variable X covers the real numbers from $-\infty$ to $+\infty$. The corresponding range of the random variable D_0 covers the positive real numbers. Therefore, the random variable D_0 described by the log-normal distribution (6.50) has a real physical meaning within the domain of its definition.

As before, in the model we consider a finite range of the random variable X: $(m - 5\sigma,\ m + 5\sigma)$. The probability that a normally distributed random variable X goes outside the aforementioned range is negligibly small (namely, it is 5.734×10^{-7} [33]). Therefore, there is no need to renormalize the probability density function.

To replace the continuous distribution (6.50) by the discrete distribution (6.25), it is convenient to split the aforementioned range of the continuous random variable X into six intervals symmetric with respect to m:

$$m - 5\,\sigma, \quad m - 2\,\sigma, \quad m - \sigma, \quad m, \quad m + \sigma, \quad m + 2\,\sigma, \quad m + 5\,\sigma\,. \tag{6.53}$$

The corresponding boundaries D'_{0i} and D''_{0i} of the intervals of the range of the random variable D_0 are expressed in terms of the parameters m and σ in the following way:

$$e^{m-5\sigma}, \quad e^{m-2\sigma}, \quad e^{m-\sigma}, \quad e^{m}, \quad e^{m+\sigma}, \quad e^{m+2\sigma}, \quad e^{m+5\sigma}\,. \tag{6.54}$$

According to Eqs. (6.23), (6.24), and (6.50), the parameters n_i and $\bar{D}_{0i}$ in (6.25) are defined by the formulas

$$n_i = \Phi(U'') - \Phi(U'), \tag{6.55}$$

$$\bar{D}_{0i} = \frac{1}{n_i}\,\frac{e^m}{\sqrt{2\,\pi}} \int\limits_{U'_i}^{U''_i} \exp\left(-\frac{u^2}{2} + \sigma\,u\right)\,du. \tag{6.56}$$

In Eqs. (6.55) and (6.56) U'_i and U''_i are expressed by the boundary values of the intervals, D'_{0i} and D''_{0i}:

$$U'_i = \frac{\ln D'_{0i} - m}{\sigma}, \qquad U''_i = \frac{\ln D''_{0i} - m}{\sigma}. \tag{6.57}$$

In Eq. (6.55) $\Phi(U)$ is the standard normal distribution (6.8).

With the above-indicated values of D'_{0i} and D''_{0i} (6.54), the parameters n_i ($i = 1, \ldots, 6$) are as follows:

$$\begin{aligned} n_1 &= 0.02275, \quad & n_4 &= 0.34134, \\ n_2 &= 0.13591, \quad & n_5 &= 0.13591, \\ n_3 &= 0.34134, \quad & n_6 &= 0.02275. \end{aligned} \tag{6.58}$$

In turn, the lower and upper integration limits in formula (6.56) [which defines $\bar{D}_{0i}$ $(i = 1, \ldots, 6)$] are set by the following pairs of numbers:

$$\begin{array}{lll} [-5,\ -2], & [0,\ 1], \\ [-2,\ -1], & [1,\ 2], \\ [-1,\ 0], & [2,\ 5]. \end{array} \tag{6.59}$$

Thus, in the aforementioned approximation, the original nonhomogeneous population with a log-normal distribution of specimens in the radiosensitivity index of critical system cells is replaced by a nonhomogeneous population formed by six homogeneous subpopulations. The fraction of individuals in each subpopulation is determined by n_i (6.58). The index of individual radiosensitivity $\bar{D}_{0i}$ of critical system cells for specimens of these subpopulations [Eq. (6.56)] is uniquely expressed by the parameters m and σ of the log-normal distribution φ_{LN} (6.50).

So, we have proposed two sets of the quantities n_i and formulas for calculating the values $\bar{D}_{0i}$ $(i = 1, \ldots, I)$, which are parameters of the model of radiation-induced mortality in a nonhomogeneous mammalian population. These sets are used when the distribution $\varphi(D_0)$ of specimens of the population in the cell radiosensitivity index D_0 is, respectively, normal or log-normal.

The model is used to study the relationship between the mortality dynamics and the type of probability density function $\varphi(D_0)$. We also examined the correlation between the radiation-induced mortality and the degree of inhomogeneity of the population, that is, the spread of values of the random variable D_0 about a fixed mean $\bar{D}_0$. As a measure of inhomogeneity, we introduce a dimensionless quantity κ, which is equal to the ratio of the square root of the variance, $\sqrt{V(D_0)}$, to the mean $\bar{D}_0$ of the probability density function $\varphi(D_0)$ of the random variable D_0:

$$\kappa = \frac{\sqrt{V(D_0)}}{\bar{D}_0}. \tag{6.60}$$

If the random variable D_0 is described by the normal distribution $\varphi_N(D_0)$ (6.43), then κ is uniquely related to the parameters of this distribution [44]:

$$\sigma = \kappa \bar{D}_0 . \tag{6.61}$$

Therefore, the variation of κ in modeling studies of the effect of population inhomogeneity on the dynamics of its radiation-induced mortality will be manifested in changes, according to (6.61), of the parameter σ in formulas (6.49) for calculation of $\bar{D}_{0i}$.

If the random variable D_0 is described by the log-normal distribution $\varphi_{LN}(D_0)$ (6.50), then in accordance with (6.51) and (6.52), the dimensionless quantity κ is determined by only one parameter, σ, of the log-normal distribution $\varphi_{LN}(D_0)$:

$$\kappa = \frac{\sqrt{V(D_0)}}{\bar{D}_0} = \sqrt{\exp(\sigma^2) - 1}. \tag{6.62}$$

Hence we find

$$\sigma = \sqrt{\ln(\kappa^2 + 1)}. \tag{6.63}$$

According to (6.51), the second parameter, m, of the distribution $\varphi_{LN}(D_0)$ (6.50) can be expressed in terms of σ and a fixed expected value $\bar{D}_0$ of the random variable D_0 as follows:

$$m = \ln \bar{D}_0 - \frac{\sigma^2}{2}. \tag{6.64}$$

Substitution of (6.63) into (6.64) yields

$$m = \ln \bar{D}_0 - \frac{1}{2} \ln(\kappa^2 + 1). \tag{6.65}$$

Therefore, in the case under consideration, when modeling the dependence of the population mortality on the degree of its inhomogeneity, variation of κ leads to changes in both the parameter σ (6.63) and the parameter m (6.65) in the formulas (6.56) for calculation of parameters $\bar{D}_{0i}$.

The model is employed in studies of the mortality dynamics in nonhomogeneous (in radiosensitivity) mammalian populations when the main reason for specimen death is either the hematopoietic subsyndrome or the gastrointestinal subsyndrome of the acute radiation syndrome. The results of these studies are given in subsequent sections of this chapter.

6.7 Mortality Dynamics in a Nonhomogeneous Population: Gastrointestinal Subsyndrome of Acute Radiation Syndrome

We apply the model described in the Sect. 6.6 to examine the impact of extremely high doses and dose rates of acute and chronic irradiation on the mortality dynamics in a nonhomogeneous mammalian population. At these irradiation regimes, the critical system is the small intestinal epithelium. The main reason for specimen death is the gastrointestinal subsyndrome of the acute radiation syndrome. Accordingly, we use the mathematical model describing the dynamics of this critical body system (Sect. 3.3) and the model simulating the mortality dynamics in a homogeneous mammalian population under the gastrointestinal subsyndrome of acute radiation syndrome (Sect. 6.3) as the constituent parts of the mortality model for a nonhomogeneous population. As in Sects. 3.3 and 6.3, mice are considered the object of the modeling. Therefore, all the parameters of the above models are kept unchanged. In turn, the parameter $\bar{D}_0$ of the mortality model for a nonhomogeneous population is taken equal to the parameter D_0 of the model

Table 6.1 Index of individual radiosensitivity $\bar{D}_{0i}$ ($i = 1, \ldots, 6$) of small intestinal epithelium precursor cells for specimens of six subpopulations that constitute the nonhomogeneous population

Parameter	Normal distribution		Log-normal distribution		
κ	0.15	0.3	0.3	1.0	1.5
$\bar{D}_{01}$	7.309	3.419	5.370	1.137	0.500
$\bar{D}_{02}$	8.876	6.553	7.170	2.565	1.441
$\bar{D}_{03}$	10.427	9.655	9.405	5.549	3.948
$\bar{D}_{04}$	11.973	12.745	12.321	11.942	10.731
$\bar{D}_{05}$	13.524	15.847	16.151	25.711	29.161
$\bar{D}_{06}$	15.091	18.981	21.643	59.815	88.725

The normal and log-normal distributions of individuals in the original nonhomogeneous population in the radiosensitivity index D_0 are considered. The distributions have equal means $\bar{D}_0 = 11.2$ Gy and different variances $V(D_0)$. The parameter κ is defined by Eq. (6.60)

of the small intestinal epithelium system, which is the averaged index of the radiosensitivity of small intestinal epithelium precursor cells capable of dividing. It is worthwhile remembering that the parameter $\bar{D}_0$ denotes the expected value of the random variable D_0 (index of radiosensitivity of the above-indicated cells for members of the nonhomogeneous population).

The parameters n_i are determined first, and the parameters $\bar{D}_{0i}$ ($i = 1, \ldots, 6$) are calculated proceeding from the given $\bar{D}_0$ and the chosen value of κ (6.60). Equations (6.48), (6.49), and (6.61) are used for the normal distribution $\varphi_N(D_0)$ (6.43) of the random variable D_0, and Eqs. (6.56), (6.58), (6.63), and (6.65) are used for the log-normal distribution $\varphi_{LN}(D_0)$ (6.50). The obtained values of $\bar{D}_{0i}$ are listed in Table 6.1.

Next, the model presented in Chap. 3 is used to find the dynamics of the small intestinal epithelium for six subpopulations of mice under the chosen irradiation conditions and the corresponding values of $\bar{D}_{0i}$ ($i = 1, \ldots, 6$). Recall that the latter describe the individual radiosensitivity of intestinal epithelium precursor cells in specimens of the ith subpopulation. The obtained values of the functional cell concentration of the critical system on hand are substituted into formula (6.14) of the mortality model for a homogeneous population. In the framework of this model, the biometric functions $\rho_i(t)$, $w_i(t)$, $v_i(t)$ ($i = 1, \ldots, 6$), which describe the mortality of mice in each of the six subpopulations for the chosen irradiation conditions, are computed by Eqs. (6.12)–(6.15), (6.19), and (6.20). Further, these functions are used to calculate the functions $v_\Sigma(t)$, $w_\Sigma(t)$, and $\rho_\Sigma(t)$ by formulas (6.30), (6.35), and (6.42). These functions characterize the mortality dynamics for the nonhomogeneous population as a whole.

The parameter κ, the dose of acute irradiation, and the dose rate of chronic irradiation are varied in the numerical studies of the model. As in Sect. 6.3, the duration of the "model experiment" is 12 days and the age of the animals at the onset of irradiation is taken to be 100 days.

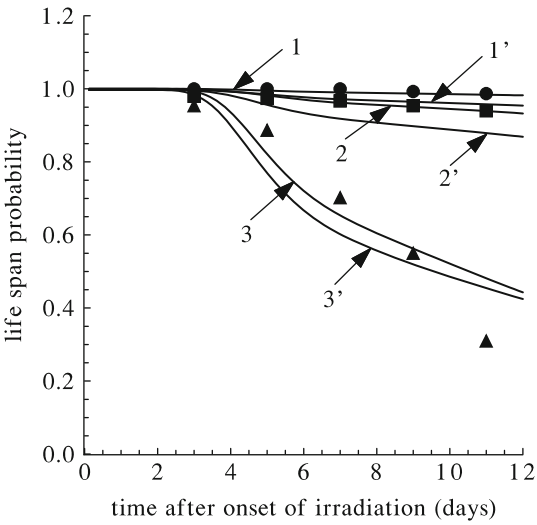

Fig. 6.13 The biometric functions $v(t)$ and $v_\Sigma(t)$ computed for the homogeneous and nonhomogeneous (normal distribution, $\kappa = 0.3$) populations of mice exposed to chronic irradiation at dose rates $N = 0.5$ Gy/day (*curves 1 and* 1′), $N = 0.75$ Gy/day (*curves 2 and* 2′), $N = 1.5$ Gy/day (*curves 3 and* 3′), and also corresponding experimental data for the homogeneous population of mice (*circle, box, and triangle*) [37]

First we examine the mortality dynamics in the nonhomogeneous population of mice exposed to chronic irradiation in the case of the normal specimen distribution in the radiosensitivity index of the intestinal epithelium precursor cells. Figure 6.13 shows the biometric functions $v_\Sigma(t)$. They describe the life span probability for the nonhomogeneous population of mice chronically irradiated with three different dose rates N. The value of the parameter κ [Eq. (6.60)] is close to the maximum possible for this particular distribution type. Figure 6.13 (and other similar ones) also presents the functions $v(t)$. The latter determine the life span probability for the homogenous population of mice under the same irradiation regimes. The radiosensitivity index of the intestinal epithelium precursor cells in the specimens of this population is equal to the expected value $\bar{D}_0$ of the random variable D_0 that describes this radiosensitivity index in animals of the original nonhomogeneous population. Figure 6.13 also shows the corresponding experimental data on the mortality dynamics in a homogeneous population of mice which were collected and parameterized in [37].

As one can infer from Fig. 6.13, the dependence of the life span probability on time t at a constant N and that on N at $t = \text{const}$ for the nonhomogeneous population is similar to those for the homogeneous population. However, some specific features are revealed at the quantitative level. For all three dose rates N used in the computations, the nonhomogeneous population mortality model predicts a lower survival of the animals than the one seen in the data obtained for the homogeneous population of mice [37] and the one predicted by the homogeneous population mortality model: $v_\Sigma(t) < v(t)$.

The modeling studies reveal substantial distinctions in the mortality dynamics of the subpopulations constituting the nonhomogeneous population. Survival at a time t ($0 < t \leq 12$ days) is higher in the subpopulation whose specimens are characterized by lower radiosensitivity of the intestinal epithelium precursor cells, i.e., by larger

values of $\bar{D}_{0i}$. In particular, after 12 days of chronic irradiation at a dose rate of 1.5 Gy/day, the survival in the first and sixth subpopulations, whose members have the most and least radiosensitive intestinal epithelium precursor cells, are 0.41 and 88.12 %, respectively.

Qualitatively similar results are obtained when we examine the mortality of the nonhomogeneous population that is characterized by other values of the parameter κ ($0 < \kappa < 1/3$) and by other (but of the same order of magnitude) values of N. It was found that at the same N, the differences in the predicted mortality for the nonhomogeneous and homogeneous populations, as well as for individual subpopulations, are less pronounced when the parameter κ is smaller, i.e., when the variance $V(D_0)$ of the normal distribution is lower.

Next we examine the mortality dynamics in the nonhomogeneous population of mice exposed to chronic irradiation in the case of the log-normal distribution of population specimens in the radiosensitivity index of the intestinal epithelium precursor cells. Figure 6.14 presents the biometric functions $v_\Sigma(t)$ describing the life span probability for the nonhomogeneous population of mice exposed to chronic irradiation with three different dose rates N. The value of the parameter κ is large enough in this computation. Figure 6.14 also shows the biometric functions $v(t)$ that determine the mortality dynamics of the homogeneous population in the same irradiation conditions. The corresponding experimental data for the homogeneous population of mice [37] are presented in Fig. 6.14, too. One can see that the mortality model with the log-normal distribution of the population specimens, as in the case of the normal distribution, predicts a lower survival of the specimens than the one seen in the experimental data for the homogeneous population of mice [37] and the one predicted by the homogeneous population mortality model: $v_\Sigma(t) < v(t)$.

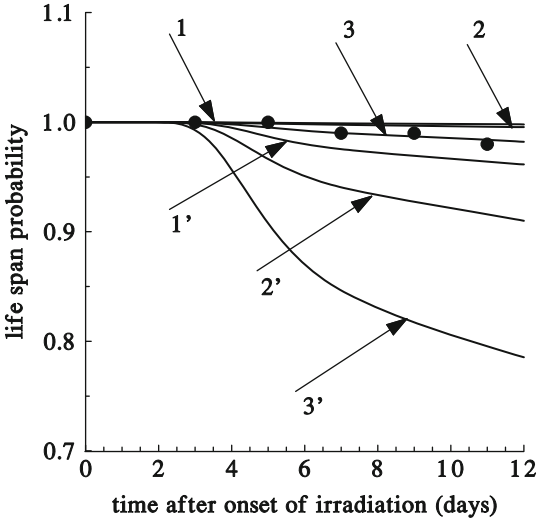

Fig. 6.14 The biometric functions $v(t)$ and $v_\Sigma(t)$ computed for the homogeneous and nonhomogeneous (log-normal distribution, $\kappa = 1.0$) populations of mice exposed to chronic irradiation at dose rates $N = 0.2$ Gy/day (*curves 1 and* 1′), $N = 0.3$ Gy/day (*curves 2 and* 2′), $N = 0.5$ Gy/day (*curves 3 and* 3′), and also experimental data on mortality dynamics for the homogeneous population of mice exposed to chronic irradiation at dose rate $N = 0.5$ Gy/day (*circle*) [37]

In computations within the same model but with other values of κ and other dose rates N (though of the same order of magnitude), we obtain qualitatively similar results. Their quantitative comparison reveals that the nonhomogeneous population mortality model based on the log-normal distribution manifests the same features as does the model with the normal distribution. Specifically, for the same values of the radiation dose rate, the differences in the mortality predictions for the nonhomogeneous and homogeneous populations diminish with decreasing κ, i.e., with decreasing variance $V(D_0)$ of the log-normal distribution. For instance, after 12 days of chronic irradiation at $N = 0.5\,\mathrm{Gy/day}$, the homogeneous population has 98.20 % survival, whereas the nonhomogeneous populations have 96.86 % survival for $\kappa = 0.3$ and 78.53 % survival for $\kappa = 1.0$.

The parameter κ is largely responsible for the extent of differences in mortality dynamics between the individual subpopulations constituting a nonhomogeneous population with the log-normal distribution of specimens. When $\kappa = 1.0$, the amount of the specimens remaining alive after 12 days of chronic irradiation at $N = 0.5\,\mathrm{Gy/day}$ in the first and sixth subpopulations, whose members have the most and least radiosensitive precursor cells, are 0.42 and 99.92 %, respectively. In turn, these quantities computed for the same chronic irradiation dose rate but at a lower parameter $\kappa = 0.3$ are 79.51 and 99.66 %, respectively. Thus, a 3.3-fold increase in the parameter κ brings about a 190-fold increase in the ratio of the survival indices between the specimens with the most radioresistant and the most radiosensitive precursor cells of the critical system under consideration. These results demonstrate that chronic exposure, even to relatively low dose rates, is particularly dangerous for mammals whose precursor cells of the small intestinal epithelium system are hyperradiosensitive.

The performed studies suggest an important conclusion. At the same mean values $\bar{D}_0$ of the individual radiosensitivity index D_0 of the critical system precursor cells in nonhomogeneous populations with both normal and log-normal distributions, the level of hazardous dose rates of chronic irradiation is lower for the population with the wider scatter in the values of D_0 [i.e., with larger variance $V(D_0)$].

Let us now examine the effects of acute irradiation on the mortality dynamics in nonhomogeneous populations. First we consider the case of the normal distribution of specimens in the radiosensitivity index of the intestinal epithelium precursor cells. Figure 6.15 shows the biometric functions $v_\Sigma(t)$ and $v(t)$, which describe the life span probability for the nonhomogeneous and homogeneous populations of mice exposed to three radiation doses D. In this computation the values of the mean $\bar{D}_0$ and the variance $V(D_0)$ are the same as those in Fig. 6.13.

As one can infer from Fig. 6.15, the dependence of the life span probability on time t at a constant D for the nonhomogeneous population is qualitatively similar to those for the homogeneous population. However, some specific features are revealed at the quantitative level. For all three doses D used in the computation, the nonhomogeneous population mortality model predicts a lower survival of specimens than the one predicted by the homogeneous population mortality model: $v_\Sigma(t) < v(t)$.

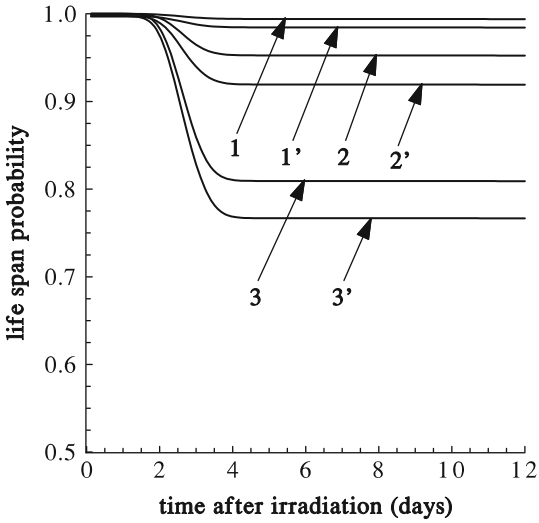

Fig. 6.15 The biometric functions $v(t)$ and $v_\Sigma(t)$ computed for the homogeneous and nonhomogeneous (normal distribution, $\kappa = 0.3$) populations of mice exposed to acute irradiation at doses $D = 1.5$ Gy (*curves 1 and* $1'$), $D = 3$ Gy (*curves 2 and* $2'$), and $D = 5$ Gy (*curves 3 and* $3'$)

The numerical studies of the model reveal that the biometric functions $v_i(t)$ ($i = 1, \ldots, 6$), which describe the mortality dynamics for the six subpopulations constituting the nonhomogeneous population, differ appreciably. The survival is higher in subpopulations whose members possess less radiosensitive intestinal epithelium precursor cells. For example, 12 days after acute irradiation at $D = 5$ Gy, the survival in the first and sixth subpopulations (having the most and least radiosensitive intestinal epithelium precursor cells) are 27.80 and 95.46 %, respectively.

In computations within the same model but with other values of κ and other doses D (but of the same order of magnitude), we obtain qualitatively similar results. Their quantitative comparison reveals the following. Differences in the mortality predictions for the nonhomogeneous and homogeneous populations exposed to acute irradiation diminish with decreasing variance $V(D_0)$ of the normal distribution, i.e., with decreasing κ. In addition, the differences in the mortality dynamics between the different subpopulations in the nonhomogeneous population also decrease with decreasing κ.

Next we consider the case of the log-normal distribution type. Figure 6.16 presents the biometric functions $v_\Sigma(t)$ and $v(t)$, which describe the mortality dynamics for the nonhomogeneous and homogeneous populations of mice exposed to three radiation doses D. The parameter κ in this computation is large enough. As one can see, the effects of the exposures under consideration on the mortality of the homogeneous population are negligible. On the other hand, the effects of the same exposures on the nonhomogeneous population are rather noticeable.

Numerical studies of the model show that the difference in the predicted mortality for the nonhomogeneous and homogeneous populations increases with increasing parameter κ, that is, with increasing variance $V(D_0)$ of the log-normal distribution. For instance, 12 days after acute irradiation at a dose of 1.5 Gy, the survival in the

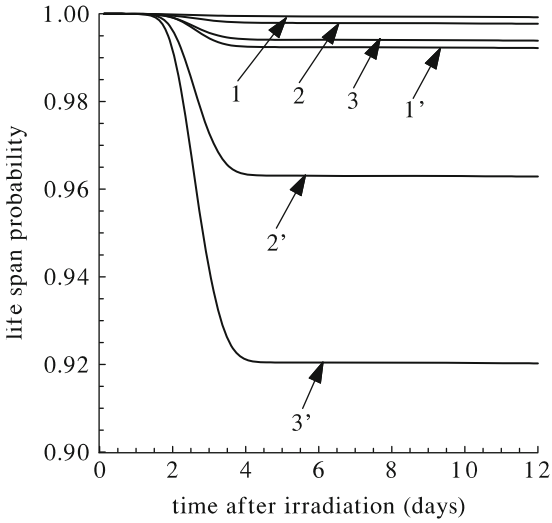

Fig. 6.16 The biometric functions $v(t)$ and $v_\Sigma(t)$ computed for the homogeneous and nonhomogeneous (log-normal distribution, $\kappa = 1.0$) populations of mice exposed to acute irradiation at doses $D = 0.5$ Gy (*curves 1 and* $1'$), $D = 1$ Gy (*curves 2 and* $2'$), and $D = 1.5$ Gy (*curves 3 and* $3'$)

homogeneous population is 99.39 %, while the survival in two nonhomogeneous populations is 99.03 % for $\kappa = 0.3$ and 92.02 % for $\kappa = 1.0$, respectively.

The numerical studies of the model also reveal that for the dose D, the difference in the predicted mortality for individual subpopulations grows with increasing parameter κ, i.e., with increasing variance $V(D_0)$ of the log-normal distribution describing the original nonhomogeneous population. For example, 12 days after acute irradiation at a dose of 1.5 Gy, the survival in the first and sixth subpopulations (having the most and least radiosensitive precursor cells) is 99.55 and 99.86 % ($\kappa = 0.3$) and 29.45 and 99.95 % ($\kappa = 1.0$), respectively.

The mortality dynamics in acutely irradiated nonhomogeneous populations with both the normal and log-normal distribution types shows features similar to those for chronically irradiated nonhomogeneous populations. Specifically, the level of hazardous doses of acute irradiation is lower for populations with wider scatter in the values of individual radiosensitivity index of the small intestinal epithelium precursor cells. For instance, when modeling the mortality dynamics for two nonhomogeneous populations with the log-normal distribution type, we found that 3 % of specimens died in the first population ($\kappa = 1.5$) and 0.08 % of the specimens in the second one ($\kappa = 0.15$) 12 days after the acute irradiation at 0.5 Gy. Accordingly, the mortality in the first and second subpopulations of these populations was 62.12 and 10.05 % ($\kappa = 1.5$) and 0.12 and 0.10 % ($\kappa = 0.15$), respectively. The mortality of the corresponding homogeneous population is 0.08 %. These data demonstrate that acute exposures to relatively low radiation doses are particularly dangerous for specimens whose small intestinal epithelium precursor cells show a hyperradiosensitivity.

It should be noted that the modeling results obtained with both types of D_0 distributions at different values of the variance $V(D_0)$ suggest that there is a direct correlation between the variability in individual radiosensitivity of the small

intestinal epithelium precursor cells and the variability in the overall organism radiosensitivity, which manifests itself in different death probabilities for specimens exposed to extremely high doses and dose rates of acute and chronic irradiation.

6.8 Mortality Dynamics in a Nonhomogeneous Population: Hematopoietic Subsyndrome of Acute Radiation Syndrome

In this section we use our model to examine the mortality dynamics in the nonhomogeneous population of mammals exposed to lifelong low dose rate chronic irradiation. As pointed out above, the critical system under such regimes of radiation impact is hematopoietic system, specifically thrombopoietic system (see Sect. 6.4). The principal reason for specimen death is the hematopoietic subsyndrome of the acute radiation syndrome. Therefore, the constituent parts of the nonhomogeneous population mortality model are the thrombopoiesis model (Sect. 1.5) and the model describing the mortality dynamics in the homogeneous mammalian population under the hematopoietic subsyndrome of the acute radiation syndrome (Sect. 6.2). As before, mice are considered the object of the modeling. The parameter $\bar{D}_0$ of the mortality model for the nonhomogeneous population is taken equal to the parameter D_0 of the thrombopoiesis model, which is the averaged index of the radiosensitivity of bone marrow thrombocyte precursor cells capable of dividing. It is worthwhile remembering that the parameter $\bar{D}_0$ denotes the expected value of the random variable D_0 (index of radiosensitivity of the above-indicated cells for members of the nonhomogeneous population).

For the calculation procedure, the parameters n_i are found first and, proceeding from the given value of $\bar{D}_0$ and the chosen value of κ (6.60), the parameters $\bar{D}_{0i}$ ($i = 1, \ldots, 6$) are calculated. Formulas (6.48), (6.49), and (6.61) for the normal distribution $\varphi_N(D_0)$ (6.43) and formulas (6.56), (6.58), (6.63), and (6.65) for the log-normal distribution $\varphi_{LN}(D_0)$ (6.50) are used. The obtained values of $\bar{D}_{0i}$ are presented in Table 6.2.

The dynamics of thrombopoiesis in six subpopulations of mice characterized by the corresponding values of $\bar{D}_{0i}$ ($i = 1, \ldots, 6$) are computed for the chosen irradiation regimes in the framework of the dynamical model of this system (Sect. 1.3). Using the computed concentrations of the functional elements, thrombocytes, the biometric functions $\rho_i(t)$, $w_i(t)$, $v_i(t)$ ($i = 1, \ldots, 6$) are computed by making use of the model (6.12)–(6.15), (6.19), and (6.20). These functions describe the mortality dynamics for each of the six subpopulations under the chosen irradiation conditions. In turn, the values of these functions and of n_i are used to compute the functions $\rho_\Sigma(t)$, $w_\Sigma(t)$, and $v_\Sigma(t)$ by formulas (6.30), (6.35), and (6.42). These functions reproduce the mortality dynamics for the nonhomogeneous population as a whole. In the course of model studies, the parameter κ and the dose rate N of chronic irradiation are varied. As in Sect. 6.3, the duration of the "model experiment" and the age of the animals at the onset of irradiation are chosen to be 1000 days and 100 days, respectively.

Table 6.2 Index of individual radiosensitivity $\bar{D}_{0i}$ $(i = 1, \ldots, 6)$ of thrombocyte precursor cells for specimens of six subpopulations constituting the nonhomogeneous population

Parameter	Normal distribution		Log-normal distribution		
κ	0.15	0.3	0.3	1.0	1.5
$\bar{D}_{01}$	1.566	0.733	1.151	0.244	0.107
$\bar{D}_{02}$	1.902	1.404	1.536	0.550	0.309
$\bar{D}_{03}$	2.235	2.069	2.015	1.189	0.846
$\bar{D}_{04}$	2.566	2.731	2.640	2.559	2.300
$\bar{D}_{05}$	2.898	3.396	3.461	5.509	6.249
$\bar{D}_{06}$	3.234	4.067	4.638	12.818	19.013

The normal and log-normal distributions of animals of the original nonhomogeneous population in the radiosensitivity index D_0 are considered. These distributions have equal means $\bar{D}_0 = 2.4\,\text{Gy}$ and different variances $V(D_0)$. The parameter κ is defined by Eq. (6.60)

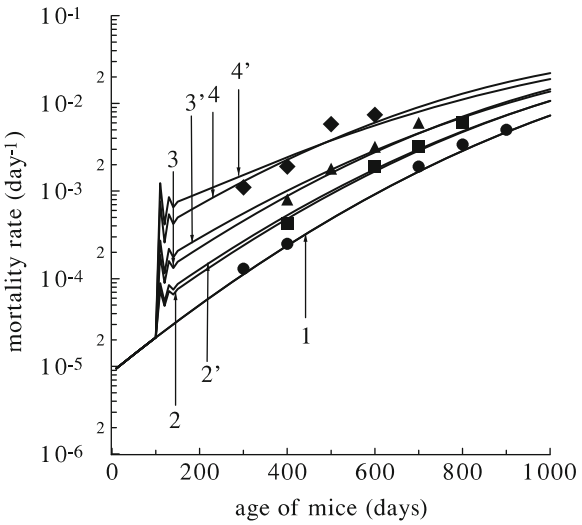

Fig. 6.17 The biometric functions $\rho(t)$ and $\rho_\Sigma(t)$ computed for the homogeneous and nonhomogeneous (normal distribution, $\kappa = 0.3$) populations of mice unexposed (*curve* 1) and exposed to chronic irradiation at dose rates $N = 0.022\,\text{Gy/day}$ (*curves* 2 *and* 2′), $N = 0.044\,\text{Gy/day}$ (*curves* 3 *and* 3′), $N = 0.088\,\text{Gy/day}$ (*curves* 4 *and* 4′), and also corresponding experimental data on the mortality rate for the homogeneous population of LAF_1 mice (*circle, box, triangle, and diamond*) [28]

The results of modeling the mortality dynamics for the nonhomogeneous population of irradiated and nonirradiated mice for the case of the normal distribution of specimens in the radiosensitivity index of bone marrow thrombocyte precursor cells that are capable of dividing are presented in Fig. 6.17. This figure shows the biometric functions $\rho_\Sigma(t)$, which describe the mortality rate for the nonho-

mogeneous population of mice in the absence of irradiation and under chronic irradiation with three different dose rates N. The parameter κ [Eq. (6.60)] in this computation is close to its possible maximum for the distribution type under consideration. Figure 6.17 (as well as the similar figures ahead) shows the functions $\rho(t)$. They describe the mortality rate for the homogeneous population of mice both unexposed and exposed to chronic irradiation at the same dose rates as those for mice of the nonhomogeneous population. The radiosensitivity index of bone marrow thrombocyte precursor cells that are capable of dividing for specimens of the homogeneous population is equal to the expected value $\bar{D}_0$ of the random variable D_0 that describes this index for specimens of the original nonhomogeneous population. Figure 6.17 also shows the experimental data on the mortality rate dynamics for nonirradiated and irradiated LAF_1 mice [28].

As one can infer from Fig. 6.17, the mortality dynamics in the homogeneous and nonhomogeneous populations in the absence of irradiation are the same. This could not be otherwise, because, according to the model construction conditions, any differences between specimens belonging to the homogeneous and nonhomogeneous populations manifest themselves only when irradiation is involved. It is important to note that the mortality dynamics computed for nonirradiated mammals quantitatively agrees with experimental data [28].

The results given in Fig. 6.17 imply that the dependence of the mortality rate on time t at a constant N and on N at $t = \text{const}$ for the nonhomogeneous population is qualitatively similar to those for the homogeneous population. The quantitative comparison of the biometric functions $\rho_\Sigma(t)$ and $\rho(t)$ shows that with the lowest of the dose rates used in the computations, the mortality model for the nonhomogeneous population, over the total time period considered, predicts higher mortality rates than does the mortality model for the homogeneous population: $\rho_\Sigma(t) > \rho(t)$. With the other two dose rates N, the relationship between $\rho_\Sigma(t)$ and $\rho(t)$ is similar to that described above for stage 1, whereas at stage 2 this relationship is reversed: $\rho_\Sigma(t) < \rho(t)$. However, the differences between $\rho_\Sigma(t)$ and $\rho(t)$ are very small, so the change of its sign does not affect the ratio between the average life spans of specimens in the nonhomogeneous and homogeneous populations: The former have a shorter average life span than the latter at each dose rate N used. Hence, the shortening of the average life span for specimens of the nonhomogeneous population is greater than that for animals of the homogenous population. With the dose rates of 0.022 Gy/day, 0.044 Gy/day, and 0.088 Gy/day, values of the average life span shortening are 61, 132, and 266 days for the nonhomogeneous population and 53, 116, and 250 days for the homogeneous one, respectively.

The modeling results demonstrate that there are appreciable differences in the radiation-induced mortality of individual subpopulations constituting the nonhomogeneous population. Comparison of the functions $\rho_i(t)$ $(i = 1, \ldots, 6)$ reveals the following. At any time after the onset of irradiation with the chosen dose rates N, the mortality rate is lower for the subpopulation whose members possess less radiosensitive bone marrow thrombocyte precursor cells capable of dividing. For instance, 900 days after the onset of chronic exposure to a dose rate of $N = 0.022\,\mathrm{Gy/day}$, the first and sixth subpopulations have, respectively, 0.51 and

14.39 % of specimens surviving. Thus, the survival of mice having the least and most radiosensitive bone marrow thrombocyte precursor cells differs by more than a factor of 28 after 900 days. The average life span shortening for the specimens of these two subpopulations under these irradiation conditions is 203 and 30 days, respectively, which gives a quite appreciable difference of 173 days.

Qualitatively similar data are obtained when modeling the nonhomogeneous population mortality at other values of the parameter κ ($0 < \kappa < 1/3$). At the same dose rate N, distinctions in the mortality prediction between the nonhomogeneous and homogeneous populations, as well as between individual subpopulations, are less pronounced with lower κ, i.e., with a lower variance $V(D_0)$.

The modeling results obtained for the case of the log-normal distribution of specimens in the radiosensitivity index of bone marrow thrombocyte precursor cells that are capable of dividing are presented in Fig. 6.18. This figure shows the biometric functions $\rho_\Sigma(t)$ calculated for the same dose rate N of chronic irradiation and the same $\bar{D}_0$ as those in Fig. 6.17. The parameter κ in this computation is large enough. Figure 6.18 also displays the biometric functions $\rho(t)$ defining the mortality dynamics of the corresponding homogeneous population in the absence of irradiation and under chronic irradiation at the same dose rates. Figure 6.18 also shows the experimental data on the mortality of nonirradiated and irradiated LAF_1 mice [28].

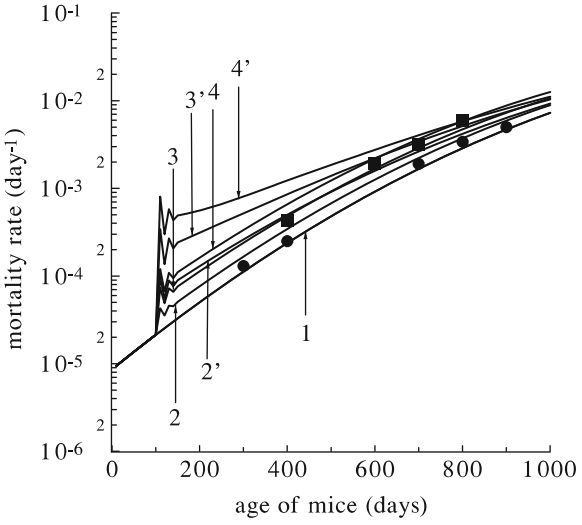

Fig. 6.18 The biometric functions $\rho(t)$ and $\rho_\Sigma(t)$ computed for the homogeneous and nonhomogeneous (log-normal distribution, $\kappa = 1.0$) populations of mice unexposed (*curve* 1) and exposed to chronic irradiation at dose rates $N = 0.011\,\mathrm{Gy/day}$ (*curves* 2 *and* 2′), $N = 0.022\,\mathrm{Gy/day}$ (*curves* 3 *and* 3′), and $N = 0.033\,\mathrm{Gy/day}$ (*curves* 4 *and* 4′), and also corresponding experimental data on the mortality rate for the homogeneous population of LAF_1 mice unexposed (*circle*) and exposed to chronic irradiation at dose rate $N = 0.022\,\mathrm{Gy/day}$ (*box*) [28]

The results presented in Fig. 6.18 imply the following. At the same dose rate N, the differences between the functions $\rho_{\Sigma}(t)$ and $\rho(t)$ are particularly large within the first year after the onset of irradiation, and nearly disappear toward the end of the "model experiment." Respectively, the differences between the function $\rho_{\Sigma}(t)$ and the experimental data on the mortality rate for LAF_1 mice [which practically coincide with the corresponding values of the function $\rho(t)$] also diminish with time.

It should be noted that in this computation the differences in the mortality dynamics between the subpopulations are quite large in the first months of the "model experiment" and diminish toward its concluding stages. At each of the three dose rates, the mortality dynamics of the sixth subpopulation, whose members have the least radiosensitive bone marrow thrombocyte precursor cells capable of dividing, is close to the mortality dynamics of nonirradiated mammals.

Computations performed at other values of the parameter κ and at fixed values of the dose rate N show that the difference between the functions $\rho_{\Sigma}(t)$ and $\rho(t)$ is more pronounced when the parameter κ is larger. Therefore, as κ increases, the difference in the average life span shortening between the homogenous and nonhomogeneous populations also grows. For example, at a dose rate of 0.022 Gy/day, the average life span shortening for mice of a homogeneous population is 53 days and the average life span shortenings for mice of four nonhomogeneous populations are 54 days ($\kappa = 0.15$), 59 days ($\kappa = 0.3$), 113 days ($\kappa = 1.0$), and 160 days ($\kappa = 1.5$), respectively. In turn, as κ increases, the differences in the average life span shortening for different subpopulations also grow. For instance, at $N = 0.022\,\mathrm{Gy/day}$, the values of the average life span shortening for the first and sixth subpopulations, whose specimens have the most and the least radiosensitive bone marrow thrombocyte precursor cells capable of dividing, are 122 and 26 days ($\kappa = 0.3$), 494 and 9 days ($\kappa = 1.0$), and 611 and 6 days ($\kappa = 1.5$), respectively.

It is important to keep in mind that the results of computations performed with both types of D_0 distributions at different values of κ demonstrate a direct relationship between the variability in the individual radiosensitivity of bone marrow thrombocyte precursor cells that are capable of dividing and the variability in the survival of specimens.

The obtained modeling results suggest an important conclusion. The greater the scatter in the values of the individual radiosensitivity index of bone marrow thrombocyte precursor cells in the nonhomogeneous population, the lower the level of the dose rate of chronic irradiation that is harmful for this population.

6.9 Conclusions

This chapter presents the stochastic models of the mortality dynamics for homogeneous and nonhomogeneous populations of mammals exposed to irradiation. In accordance with the radiobiological concept of a critical system, the deviation in the concentration of critical system functional cells from the normal level is chosen as an index of the physiological state and it is assumed that reaching or

exceeding a threshold value by this deviation is an analog of death. The model of radiation-induced mortality for a nonhomogeneous population is also based on the assumption of a non-uniformity of the index of individual radiosensitivity of the critical system cells. Two types of distribution, normal (Gaussian) and log-normal, are employed to describe the distribution of specimens in the population that is nonhomogeneous with respect to the aforementioned index. In the developed models, the statistical biometric functions (mortality rate, life span probability density, and life span probability) are computed proceeding from the dynamics of critical system functional cell concentration and statistical characteristics of this physiological index in the specimens of the respective population.

The models were used to simulate mortality in small laboratory animals (mice) exposed to acute and chronic irradiation at extremely high doses and dose rates, as well as to lifelong chronic irradiation at low dose rates. The critical system is represented by the small intestinal epithelium system (SIES) in the first and second cases, and by the bone marrow thrombopoietic system in the third case. The dynamics of the concentrations of functional elements of these systems, enterocytes and thrombocytes, are computed by the SIES model and by the thrombopoiesis model developed in Chaps. 3 and 1, respectively.

The model of radiation-induced mortality for a homogeneous population reproduces, on qualitative and quantitative levels, the experimental data on mortality dynamics and average life span shortening for the population of LAF_1 mice unexposed and exposed to lifelong low dose rate chronic irradiation. The model also quantitatively describes the mortality dynamics for the population of LAF_1 mice exposed to acute and chronic irradiation at extremely high doses and dose rates.

A major difference and advantage of this model as compared to models of other authors is that the identification of the model's coefficients does not require data on the mortality dynamics of irradiated mammalian populations. Only data on the population's mortality in the absence of radiation are needed, and some limited number of experimental data on the behavior of the respective critical system under acute or chronic irradiation. Therefore, this model, after the proper identification, can be employed to predict the average life span shortening of humans under various radiation conditions.

The model of radiation-induced mortality for a nonhomogeneous population includes, as its constituent parts, the mortality model for the homogeneous population and the mathematical model of the respective critical system. This model structure corresponds to the actual existing levels of manifestation of radiation effects in mammals. The first level is that of a critical system, whose radiation injury is largely determined by the radiosensitivity of the constituent cells. The second is the level of an individual. Here the probable outcome of irradiation mainly depends on the extent of radiation injury of the respective critical system, i.e., on individual cell radiosensitivity of this system. The third level is that of the whole population, which includes individuals with different individual radiosensitivities of the critical system cells. It follows then that the developed model of mortality is

actually a mathematical description of cause–effect relationships setup in the course of radiation injury of mammals.

In the framework of the developed model, the dependence of the radiation-induced mortality in the nonhomogeneous population of mice on the distribution of specimens in the radiosensitivity index of the critical system precursor cells, as well as on the most important distribution parameter, the variance, is studied. Various irradiation conditions are simulated: acute irradiation at extremely high doses, chronic irradiation at extremely high dose rates, as well as lifelong chronic irradiation at low dose rates. The critical system was assumed to be the small intestinal epithelium in the first and second cases and the thrombopoietic system in the third case.

The performed investigations reveal the direct correlation between the variability in specimen mortality in the nonhomogeneous population and the variability in individual radiosensitivity of cells of the respective critical system. It is found that the probability of death from the gastrointestinal subsyndrome resulting from exposures to acute and chronic irradiation at extremely high doses and dose rates increases with increases in the radiosensitivity of the intestinal epithelium precursor cells capable of dividing. In turn, the probability of surviving to a certain age for a specimen exposed to low dose rate chronic irradiation grows as the radiosensitivity of bone marrow thrombocyte precursor cells that are capable of dividing decreases.

It is shown that accounting for the normal and log-normal distributions of specimens of the nonhomogeneous population in the index of radiosensitivity of the critical system precursor cells leads to higher mortality rates and lower survival than could have been predicted proceeding from the averaged radiosensitivity index alone. The differences in predictions increase as the variance in the individual radiosensitivity index for critical system precursor cells in the nonhomogeneous population increases. These differences are particularly pronounced when the log-normal distribution with a large value for the variance is used. This modeling result is of substantial practical significance in view of experimental data [49], which imply that a human population is probably characterized by a log-normal distribution with a fairly large value of the variance. Therefore, the variability in individual radiosensitivity is of crucial importance in the estimation of radiation risk for human populations.

The model studies also suggest practical conclusions. The minimal level of dose rates of chronic exposures that is harmful for nonhomogeneous mammalian populations is lower as the spread of values in the individual radiosensitivity index for the critical system precursor cells in these populations increases, i.e., for greater variance in corresponding distributions. In particular, for specimens having hyperradiosensitive precursor cells, even low-level irradiation can have fatal consequences. These conclusions are especially significant for the development of recommendations for the radiation protection of human populations, since the fraction of hypersensitive individuals is rather high (5–25 %) [41–43].

Thus, the developed models of radiation-induced mortality, after appropriate identification, can be used as a tool for the estimation of the radiation risks for populations residing in areas with elevated radiation background, for persons

exposed to occupational irradiation, for clean-up crew members involved in the elimination of radiation catastrophes, as well as for astronauts on long-term space missions, such as Lunar colonies and Mars missions.

References

1. National Council on Radiation Protection and Measurements. Guidance on Radiation Received in Space Activity (NCRP report no. 98). NCRP, Bethesda, MD, 1989.
2. Schimmerling W., Cucinotta F.A., Wilson J.W. Radiation risk and human space exploration. Advances in Space Research, v. 31(1), pp. 27–34, 2003.
3. Simonsen L.C., Wilson J.W., Kim, M.H., Cucinotta F.A. Radiation exposure for human Mars exploration. Health Physics, v. 79(5), pp. 515–525, 2000.
4. Blakely E.A. Biological effects of cosmic radiation: Deterministic and stochastic. Health Physics, v. 79(5), pp. 495–506, 2000.
5. Hagen U., Harder D., Jung H., Streffer C. (Eds.). Radiation research 1895–1995. Congress Proceedings. Volume 2: Congress Lectures. Wurzburg: Universitatsdruckerei H. Sturtz AG, pp. 1–1210, 1995.
6. Gottlober P., Steinert M., Weiss M., Bebeshko V., Belyi D., Nadejina N., Stefani F.H., Wagemaker G., Fliedner T.M., Peter R.U. The outcome of local radiation injuries: 14 years of follow-up after the Chernobyl accident. Radiation Research, v. 155(3), pp. 409–416, 2001.
7. Ivanov V.K., Tzyb A.F. Medical radiobiological effects of the Chernobyl catastrophe on the population of Russia: Estimation of radiation risks. Moscow: Meditsina, 2002 (Russian).
8. Akleev A.V., Kisselyov M.F. (Eds.). Medical–biological and ecological impacts of radioactive contamination of the Techa river. Moscow: "Medbioextrem," 2001 (Russian).
9. Barsukov O.A., Barsukov K.A. Radiation Ecology. Moscow: Scientific Word, 2003.
10. Canu I.G., Ellis E.D., Tirmarche M. Cancer risk in nuclear workers occupationally exposed to uranium — Emphasis on internal exposure. Health Physics, v. 94(1), pp. 1–17, 2008.
11. ICRP. Radiation protection: Recommendations of the International Commission on Radiological Protection, ICRP Publication 60, Oxford: Pergamon Press, 1991.
12. ICRP. The 2007 Recommendations of the International Commission on Radiological Protection, ICRP Publication 103, Elsevier, 2008.
13. Smirnova O.A. The mathematical model of mortality dynamics for irradiated mammals which is based on the model of hematopoiesis. Radiobiologiya, v. 27, p. 713. Dep. in VINITI N 2443–1387, 06.07.87, 1987 (Russian).
14. Smirnova O.A. Mathematical modelling of the death rate dynamics in mammals with intestinal form of radiation sickness. Radiobiologiya, v. 30, pp. 814–820, 1990 (Russian).
15. Kovalev E.E., Smirnova O.A. Life-span of irradiated mammals. Mathematical modelling. Acta Astronautica, v. 32, pp. 649–652, 1994.
16. Kovalev E.E., Smirnova O.A. Radiation risk assessment based on the concept of individual variability of radiosensitivity. Radiation research 1895–1995. Congress Proceedings. Vol. 1. U. Hagen, H. Jung, C. Streffer (Eds.). Tenth International Congress of Radiation Research, Wurzburg, Germany, August 27 – September 1, 1995. Wurzburg: Universitatsdruckerei H. Strtz AG, p. 335, 1995.
17. Kovalev E.E., Smirnova O.A. Estimation of radiation risk based on the concept of individual variability of radiosensitivity. AFRRI Contract Report 96-1. Bethesda, MD: Armed Forces Radiobiology Research Institute, 1996.
18. Kovalev E.E., Smirnova O.A. New approach to radiation risk assessment. 12th Man in Space Symposium: The Future of Humans in Space, Washington, DC, June 8–13, 1997. Abstract Volume. Houston, TX: USRA, p. 324, 1997.

19. Smirnova O.A. Mathematical modeling of the mortality dynamics of mammals exposed to acute and chronic irradiation. Mathematics, Computers, Education. Moscow: Progress-Tradiciya, v. 5, pp. 299–303, 1998 (Russian).
20. Smirnova O.A. Mathematical modeling of mortality dynamics of mammalian population exposed to radiation. Mathematical Biosciences, v. 167, pp. 19–30, 2000.
21. Smirnova O.A. Simulation of mortality dynamics for mammalian populations exposed to radiation. The 4th International EUROSIM Congress "Shaping Future with Simulation," Delft, the Netherlands, June 26–29, 2001. Abstracts, Delft: TUDelft, pp. 109–110, 2001.
22. Smirnova O.A. Comparative risk assessment for homogeneous and nonhomogeneous mammalian populations exposed to low level radiation. NATO Advanced Research Workshop "Comparative Risk Assessment and Environmental Decision Making," Rome, Anzio, Italy, October 13–16, 2002. Book of Abstracts, p. 35, 2002.
23. Smirnova O.A. Mathematical model for assessment of radiation risk on long space mission. Advances in Space Research, v. 30(4), pp. 1005–1010, 2002.
24. Sakovich V.A., Smirnova O.A. Modeling radiation effects on life span of mammals. Physics Particles and Nuclei, v. 34(6), pp. 743–766, 2003.
25. Smirnova O.A. Comparative risk assessment for homogeneous and nonhomogeneous mammalian populations exposed to low level radiation. In: I. Linkov and A.B. Ramadan (Eds.), Comparative Risk Assessment and Environmental Decision Making. NATO Science Series. IV. Earth and Environmental Sciences, Vol. 38. Dordrecht, the Netherlands: Kluwer Academic Publishers, pp. 385–392, 2004.
26. Smirnova O.A. Simulation of mortality dynamics for populations of mammals (mice) exposed to radiation. In: Simulation Modelling Practice and Theory: Advances in Modelling and Simulation in Biology and Medicine. Y. Hamam and F. Rocaries (Eds.). v. 12(2), pp. 171–182, 2004.
27. Smirnova O.A. Radiation and Organism of Mammals: Modeling Approach. Moscow-Izhevsk: Scientific-Publishing Centre "Regular and Chaotic Dynamics," Institute of Computer Science, 2006 (Russian).
28. United Nations Scientific Committee on the Effects of Atomic Radiation. Ionizing radiation: Sources and biological effects. Report to the General Assembly, 1982. New York: United Nations Organization, Volume II, 1982.
29. Cox D.R., Oakes D. Analysis of Survival Data. London: Chapman and Hall, 1984.
30. Boleslawski L. Cohort Tables of Life Span. Moscow: Statistika, pp. 12–38, 1977 (Russian).
31. Sacher G.A. On the statistical nature of mortality with a special reference to chronic radiation mortality. Radiology, v. 67(2), pp. 250–258, 1955.
32. Sacher G.A., Trucco E. The stochastic theory of mortality. Annals of the New York Academy of Sciences, v. 96, pp. 985–1007, 1962.
33. Korn G.A., Korn T.M. Mathematical Handbook. London: McGraw-Hill Book Company, 1968.
34. Bond V.P., Fliendner T.M., Archambeau J.O. Mammalian Radiation Lethality: A Disturbance in Cellular Kinetics. New York: Academic Press, 1965.
35. Kalina I., Praslichka M. Changes in haemopoiesis and survival of continuously irradiated mice. Radiobiologiya, v. 17, pp. 849–853, 1977 (Russian).
36. Matsuzawa T., Wilson R. The intestinal mucosa of germfree mice after whole-body *X*-irradiation with 3 kiloroentgens. Radiation Research, v. 25(1), pp. 15–24, 1965.
37. Iberall A.S. Quantitative modeling of the physiological factors in radiation lethality. Annals of the New York Academy of Sciences, v. 147, Art. I, pp. 1–81, 1967.
38. Lesher S. Compensatory reaction in intestinal crypt cells after 300 roentgens of Cobalt-60 gamma irradiation. Radiation Research, v. 32(3), pp. 510–519, 1967.
39. Konoplyannikova O.A., Konoplyannikov A.G. Age-related changes in radiosensitivity of animals and critical cell systems: Survival of stem cells of small intestine epithelium, and 4-5-day death of mice of different age after irradiation. Radiobiologiya, v. 24, pp. 249–252, 1984 (Russian).

40. Potten C.S. Radiosensitivity and kinetics of target cells in relation to tissue responses as exemplified by the epidermis and the intestine. Radiation Research. Proceedings of the 8th International Congress of Radiation Research. Edinburgh, July 1987. London: Taylor Francis, v. 2, pp. 782–788, 1987.
41. Ivanov I.V. Initial reactivity of organism and radiation effects: Medical-prophylactic aspects of the problem. In: Scientific-Practical Manual. N.G. Darenskaya (Ed.). Moscow: RMAPO, 2005.
42. Arlett C.F., Cole J., Green M.H.L. Radiosensitive individuals in the population. In: Low Dose Radiation: Biological Bases of Risk Assessment. K.F. Baverstock and J.W. Stather (Eds.). London: Taylor and Francis, pp. 240–252, 1989.
43. Gentner N.E., Morrison D.P. Determination of the proportion of persons in the population-at-large who exhibit abnormal sensitivity to ionizing radiation. In: Low Dose Radiation: Biological Bases of Risk Assessment. K.F. Baverstock and J.W. Stather (Eds.). London: Taylor and Francis, pp. 259–268, 1989.
44. Eadie W.T., Drijard D., James F.E., Roos M., Sadoulet B. Statistical Methods in Experimental Physics. Amsterdam: North-Holland Publishing Company, 1971.
45. Report of the Task Group on Reference Man. ICRP Publication 23. Oxford: Pergamon Press, 1975.
46. Balakrishnan N., Chen W.W.S. Handbook of Tables for Order Statistics from Lognormal Distributions with Applications. Amsterdam: Kluwer, 1999.
47. Crow E.L., Shimizu K. (Eds.). Lognormal Distributions: Theory and Applications. New York: Marcel Dekker, 1988.
48. Kenney J.F., Keeping E.S. Mathematics of Statistics, Pt. 2, 2nd ed. Princeton, NJ: Van Nostrand, p. 123, 1951.
49. Cox R., Haskingand G.P., Wilson J. Ataxia telangiectasia. Evaluation of radiosensitivity in cultured skin fibroblasts as a diagnostic test. Archives of Disease in Childhood, v. 53, pp. 386–390, 1978.

Chapter 7
Effects of Acute and Chronic Irradiation on Human Hematopoiesis

7.1 Introduction

The hematopoietic system is known as one of the most radiosensitive vital body systems in humans, as well as in the other mammalian species. In particular, the major hematopoietic lineages (thrombopoietic, granulopoietic, lymphopoietic, and erythropoietic systems) demonstrate characteristic patterns of dose-dependent radiation responses [1–6].

Modeling studies of radiation effects on the human hematopoiesis remains a subject of increased interest over past decades, for recent works see, e.g., [7–15]. This is basically caused by a vital necessity to predict, on quantitative level, the effects of various regimes of irradiation on this vital body system and estimate on this basis the health hazards of radiation exposures to large groups of people, as well as to individuals. In particular, it concerns the problem of the assessment of health hazards of radiation exposures to people residing in contaminated areas after accidents and to clean-up crew members taking part in the elimination of consequences of such accidents (especially, in view of the recent Fukushima disaster), to astronauts engaging in long-term space missions (such as voyages to Mars or the manning of Lunar colonies), and to patients treated with radiotherapy.

The primary objectives of our studies [16–23] were to develop and thoroughly investigate mathematical models, which describe the dynamics of the thrombopoietic, granulopoietic, lymphopoietic, and erythropoietic systems in chronically and acutely irradiated humans. The models were required to account for the principal regulatory mechanisms of the human hematopoietic system and to include explicitly the characteristics of ionizing radiation and the basic kinetic and radiobiological parameters of the human major hematopoietic lineages. The results of our studies on this subject are presented in this chapter.

O.A. Smirnova, *Environmental Radiation Effects on Mammals*,
DOI 10.1007/978-3-319-45761-1_7

7.2 Mathematical Models

7.2.1 Models of the Dynamics of the Major Hematopoietic Lineages Under Chronic Irradiation

The thrombopoietic, granulopoietic, lymphopoietic, and erythropoietic systems, as it has been noted above, are the major hematopoietic lineages in mammals including humans. Mature cells of these systems circulate in the peripheral blood, whereas their precursor cells are located in the bone marrow. The principal stages of the development of cells, as well as the regulatory mechanism of cell renewing, are, in general, quite similar for the major hematopoietic lineages in humans, as well as in other mammalian species (see Chap. 1 and the references therein for the details, as well as, e.g., [24–28]).

The mathematical models of the dynamics of the thrombopoietic, granulopoietic, lymphopoietic, and erythropoietic systems in irradiated humans are developed in the framework of the biologically motivated dynamic approach to the modeling of responses of self-renewing cell systems in mammalian organism to irradiation. This approach was elaborated by the author and successfully used in the modeling studies of the effects of chronic and acute irradiation on the dynamics of the major hematopoietic lineages and the small intestinal epithelium system in other mammalian species (rats, mice) (see Chaps. 1 and 3, as well as [16, 29–50]).

Specifically, basing on the theories and experimental facts concerning the structure and function of the human hematopoietic system in the norm and under radiation exposures [1–6, 24–28], the models of the human major hematopoietic lineages take into account the principal stages of the development of hematopoietic cells and consider the basic cell compartments depending on to the degree of maturity and differentiation of cells in the respective hematopoietic lineage:

- X_1, the capable of dividing precursor cells (from stem cells in the microenvironment, which predetermine their differentiation toward the respective hematopoietic lineage, to morphologically identifiable dividing maturing bone marrow cells in this hematopoietic lineage, namely to megakaryocytoblasts in the thrombopoietic system, to myelocytes in the granulopoietic system, to polychromatophilic erythroblasts in the erythropoietic system, and to lymphoblasts in the lymphopoietic system);
- X_2, the incapable of dividing precursor cells (nondividing maturing bone marrow cells in the hematopoietic lineage on hand, namely from promegakaryocytes to mature megakaryocytes in the thrombopoietic system, from metamyelocytes to granulocytes in the granulopoietic system, and from orthochromatic erythroblasts to reticulocytes in the erythropoietic system, and bone marrow lymphoid cells in the lymphopoietic system);
- X_3, the mature cells (blood cells in the hematopoietic lineage on hand, namely thrombocytes (blood platelets) in the thrombopoietic system, blood granulocytes in the granulopoietic system, blood erythrocytes in the erythropoietic system, and blood lymphocytes in the lymphopoietic system);
- X_4, the tissue granulocytes (appears only in the granulopoiesis model).

The cells of a radiosensitive compartment X_i ($i = 1, \ldots, n$) are split into several groups, with regard for their response to irradiation [1, 51]:

- X_i^{ud}, undamaged cells;
- X_i^{d}, damaged cells that die within several days following irradiation;
- X_i^{hd}, heavily damaged cells that die within several hours following irradiation (interphase death).

In addition to undamaged, damaged, and heavily damaged cells of the radiosensitive compartments [X_i^{ud}, X_i^{d}, and X_i^{hd} ($i = 1, \ldots, n$)], the models consider the cells of the radioresistant compartments, which are denoted as X_i^{ud} ($i = n + 1, \ldots, m$). Here m is the total number of cell compartments considered in the model of the respective hematopoietic lineage and n is the number of radiosensitive cell compartments among them. Specifically, only X_1 cells are radiosensitive in the thrombopoietic system (i.e., $n = 1$, $m = 3$). In the granulopoietic system, X_1, X_2, X_3, and X_4 cells are radiosensitive, though in a rather different degree (i.e., $n = m = 4$). In the lymphopoietic system, X_1, X_2, and X_3 cells are radiosensitive (i.e., $n = m = 3$). In the erythropoietic system, only X_1 and X_2 cells are radiosensitive (i.e., $n = 2$, $m = 3$).

The models of the human major hematopoietic lineages take into account the feedback loop regulatory mechanisms of the reproduction rate of the bone marrow precursor cells, which is implemented by the tissue-specific inhibitor of cell division, chalones [52–55]. Chalones, which belong to the cytokine family, are the product of the growth and decay of cells of some self-renewing systems in the mammalian organism, including the major hematopoietic lineages.

The models of the human major hematopoietic lineages employ the one-target–one-hit theory of cell damage [56], which assumes the damage rate of radiosensitive cells to be proportional to the dose rate N.

Additionally, the models of the human thrombopoietic and granulopoietic systems consider peculiarities of the regulation of these major hematopoietic lineages. Namely, the model of the thrombopoietic system takes into account the regulatory mechanism of megacaryocyte ploidy [57, 58]. In turn, the model of granulopoietic system accounts for the regulatory mechanism of the specific rate of the granulocyte supply from the bone marrow to the blood flow [26, 57]. Modeling implementations of these regulatory mechanisms are presented below.

The models of the major hematopoietic lineages in chronically irradiated humans also originate in the following:

1. the dynamics of X_1^{ud} cells is determined by the rate of their reproduction and by the rate of their transition to cell group X_2^{ud}, as well as by the rates of their transition to the cell groups X_1^{d} and X_1^{hd} (in the thrombopoiesis, granulopoiesis, lymphopoiesis, and erythropoiesis models);
2. the dynamics of X_2^{ud} cells is determined by the rate of arrival of cells from group X_1^{ud} and by the rate of their transition to the cell group X_3^{ud}, as well as by the rates of their transition to the cell groups X_2^{d} and X_2^{hd} (in the granulopoiesis, lymphopoiesis, and erythropoiesis models);

3. the dynamics of X_3^{ud} cells is determined by the rate of arrival of cells from group X_2^{ud} and by the rate of their natural death (in the thrombopoiesis, lymphopoiesis, and erythropoiesis models) or by the rate of their transition to the cell group X_4^{ud} (in the granulopoiesis model), as well as by the rates of their transition to the cell groups X_3^{d} and X_3^{hd} (in the granulopoiesis and lymphopoiesis models);
4. the dynamics of X_4^{ud} cells is determined by the rate of arrival of cells from group X_3^{ud}, by the rate of their natural death, and by the rates of their transition to cell groups X_4^{d} and X_4^{hd} (in the granulopoiesis model only);
5. the dynamics of X_i^{d} $(i = 1, \ldots, n)$ cells is determined by the rate of arrival of cells from group X_i^{ud} $(i = 1, \ldots, n)$ and by the rate of their death;
6. the dynamics of X_i^{hd} $(i = 1, \ldots, n)$ cells is determined by the rate of arrival of cells from group X_i^{ud} $(i = 1, \ldots, n)$ and by the rate of their death.

Schematic diagrams of the models of the major hematopoietic lineages in chronically irradiated humans are presented in Figs. 7.1, 7.2, 7.3, and 7.4.

The variables of the models are the concentrations of radiosensitive cells X_i^{ud}, X_i^{d}, X_i^{hd} $(i = 1, \ldots, n)$ and radioresistant cells X_i^{ud} $(i = n + 1, \ldots, m)$: x_i^{ud}, x_i^{d}, x_i^{hd} $(i = 1, \ldots, n)$ and x_i^{ud} $(i = n + 1, \ldots, m)$, respectively. By cell concentration, we mean the ratio of the total number of cells of a certain group to the total blood volume.

Proceeding from the foregoing statements, the models of the dynamics of the major hematopoietic lineages in chronically irradiated humans can be written in the following general form (see Chap. 1 and the references therein for the details):

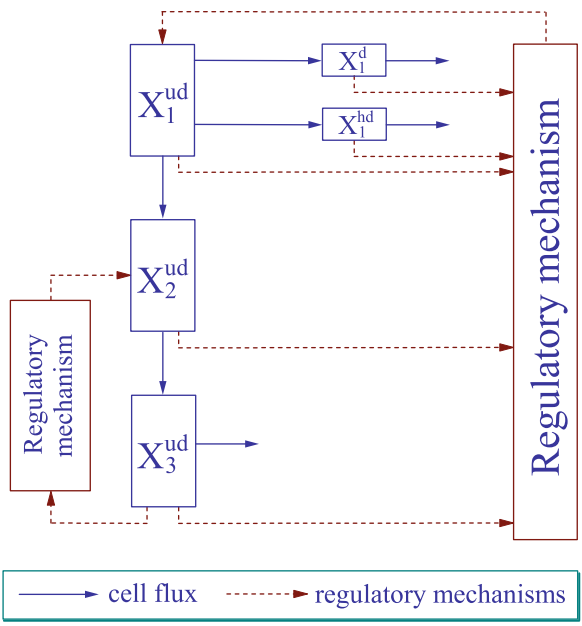

Fig. 7.1 Schematic diagram of the thrombopoiesis model

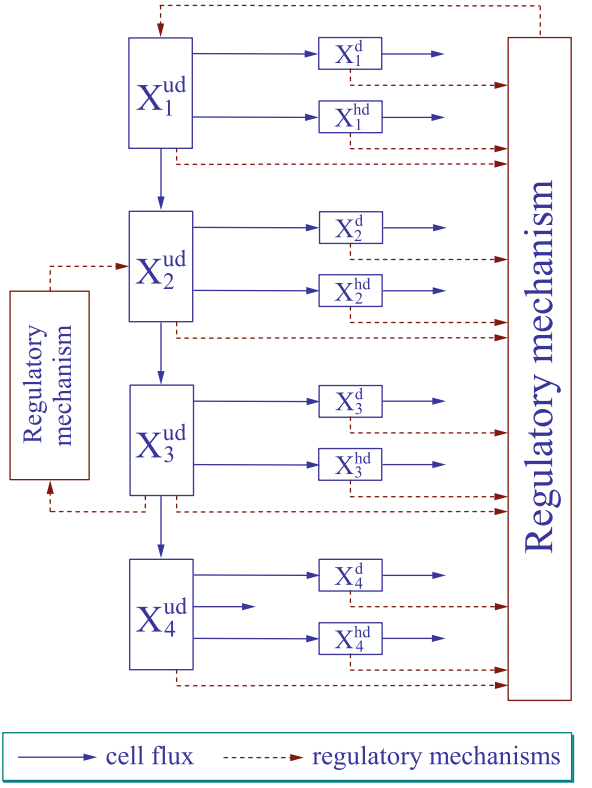

Fig. 7.2 Schematic diagram of the granulopoiesis model

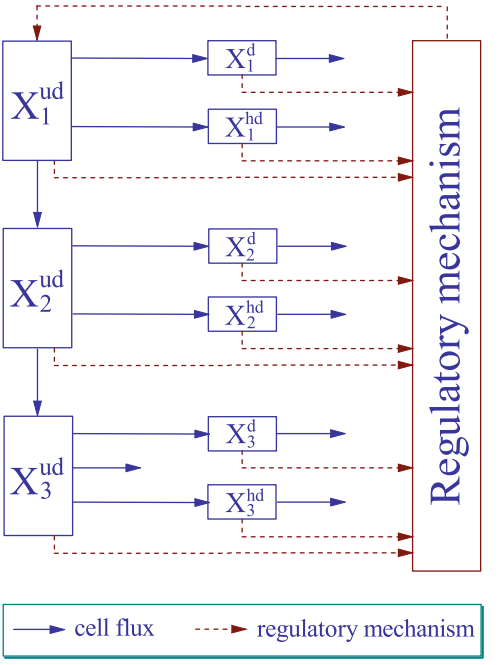

Fig. 7.3 Schematic diagram of the lymphopoiesis model

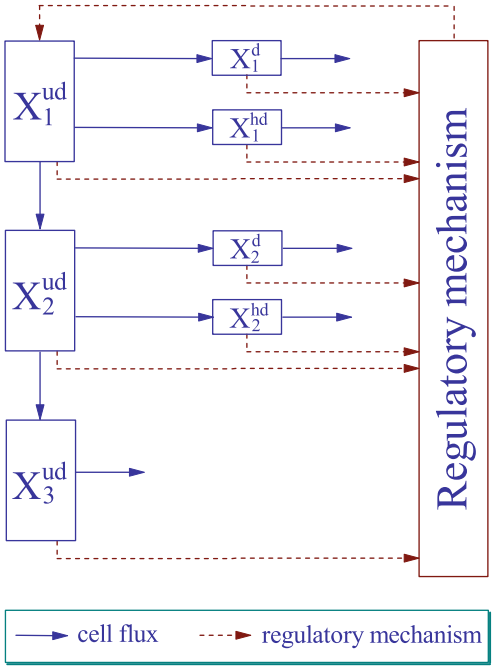

Fig. 7.4 Schematic diagram of the erythropoiesis model

$$\frac{dx_1^{ud}}{dt} = Bx_1^{ud} - \gamma x_1^{ud} - \frac{N}{D_1^0} x_1^{ud}, \tag{7.1}$$

$$\frac{dx_2^{ud}}{dt} = \gamma x_1^{ud} - Fx_2^{ud} - \frac{N}{D_2^0} x_2^{ud}, \tag{7.2}$$

$$\frac{dx_3^{ud}}{dt} = Fx_2^{ud} - \psi x_3^{ud} - \frac{N}{D_3^0} x_3^{ud}, \tag{7.3}$$

$$\frac{dx_4^{ud}}{dt} = \psi x_3^{ud} - \xi x_4^{ud} - \frac{N}{D_4^0} x_4^{ud}, \tag{7.4}$$

$$\frac{dx_i^{d}}{dt} = \frac{N}{D_i^0} \frac{1}{1+\rho_i} x_i^{ud} - \mu x_i^{d} \quad (i = 1, \ldots, n), \tag{7.5}$$

$$\frac{dx_i^{hd}}{dt} = \frac{N}{D_i^0} \frac{\rho_i}{1+\rho_i} x_i^{ud} - \nu x_i^{hd} \quad (i = 1, \ldots, n). \tag{7.6}$$

The coefficients γ and F in Eqs. (7.1)–(7.3) are the specific rates of transfer of cells from group X_1^{ud} to group X_2^{ud} and from group X_2^{ud} to group X_3^{ud}, respectively. In the thrombopoiesis, lymphopoiesis, and erythropoiesis models, the coefficient ψ in Eq. (7.3) denotes the specific rate of the natural death of X_3^{ud} cells. In the granulopoiesis model, the coefficient ψ in Eqs. (7.3) and (7.4) stands for the specific rate of transfer of cells from group X_3^{ud} to group X_4^{ud} (from blood to tissues) and the coefficient ξ in Eq. (7.4) denotes the specific rate of the natural death of X_4^{ud} cells.

The term $[(N/D_i^0)x_i]$ on the right-hand side of an equation describing the dynamics of concentration of radiosensitive cells X_i^{ud} is the rate of decrease of the concentration of these cells due to their radiation-induced damage. One part of them transfers into the group of damaged cells X_i^{d} [Eq. (7.5)] and the other part passes to the group of heavily damaged cells X_i^{hd} [Eq. (7.6)]. The ratio of these parts is denoted by ρ_i. The parameters ρ_i $(i = 1, \ldots, n)$ are determined below (see Sect. 7.2.2). The coefficients μ and ν in Eqs. (7.5) and (7.6) stand for the specific death rates of damaged and heavily damaged cells, respectively.

In Eqs. (7.1)–(7.6), the parameter D_i^0 is equivalent to the conventional radiobiological dose D_0. Namely, after exposure to such dose, the number of X_i^{ud} cells left undamaged is $e = 2.718\ldots$ times smaller than their initial number [1]. In the equations, which describe the dynamics of concentrations of radioresistant cells X_i^{ud} $(i = n+1, \ldots, m)$, the parameters D_i^0 $(i = n+1, \ldots, m)$ tend to infinity, that results in the absence of the term expressing the radiation effect on these cells.

The formula describing the specific reproduction rate B of X_1^{ud} cells takes into account the contributions of the radiosensitive cells X_i^{ud}, X_i^{d}, X_i^{hd} $(i = 1, \ldots, n)$ and the radioresistant cells X_i^{ud} $(i = n+1, \ldots, m)$ to the feedback loop regulatory mechanism of the reproduction rate of the aforementioned cells. In its final form, this formula reads (see Chap. 1 and the references therein for the details):

$$B = \frac{\alpha}{1 + \beta\left[\sum_{i=1}^{n} \theta_i \left(x_i^{\mathrm{ud}} + \phi x_i^{\mathrm{d}} + \varphi x_i^{\mathrm{hd}}\right) + \sum_{i=n+1}^{m} \theta_i x_i^{\mathrm{ud}}\right]}, \tag{7.7}$$

where α is the maximum specific rate of reproduction of X_1^{ud} cells, the coefficient θ_1 is equal to unity by definition, the parameters θ_i $(i = 2, \ldots, m)$, ϕ, φ, and β are constants.

As noted above, the models of the human thrombopoietic and granulopoietic systems consider the specific regulatory mechanisms in these hematopoietic lineages. In particular, the specific feature of the thrombopoietic system is the variation of an average ploidy of bone marrow precursor cells incapable of dividing (megakaryocytes) caused by the variation of the concentration of their progeny (blood thrombocytes). The model of the human thrombopoietic system takes into account the regulatory mechanism of megakaryocyte ploidy by the introduction of the ploidy coefficient f, similar to the model of this system in some other mammalian species (rats, mice) (see Chap. 1). The coefficient f is the ratio of the average ploidy of megakaryocytes, which corresponds to the current thrombocyte concentration, to the average ploidy of megakaryocytes, which corresponds to the normal thrombocyte concentration. The coefficient f is described by the decreasing function of the concentration of blood thrombocytes (X_3 cells) (see Chap. 1 and the references therein for the details):

$$f = \frac{1}{\lambda + (1-\lambda)(x_3^{\mathrm{ud}}/\bar{x}_3)}. \tag{7.8}$$

Here λ is a dimensionless constant and $\bar{x}_3$ is the normal concentration of blood thrombocytes. In the thrombopoiesis model, the additional factor f [Eq. (7.8)] appears in front of the first term on the right-hand side of Eq. (7.2). In turn, the additional factor σ, which denotes the average number of thrombocytes produced by one megakaryocyte in the norm, appears in front of the first term on the right-hand side of Eq. (7.3).

In turn, the specific feature of the granulopoietic system is the variation of the specific rate F of granulocyte supply from the bone marrow to the blood flow caused by the variation of the blood granulocyte concentration. The model of the human granulopoietic system considers the regulatory mechanism of the specific rate of the granulocyte supply from the bone marrow to the blood flow by the introduction of the variable parameter F, likewise the model of this system in some other mammalian species (rats, mice) (see Chap. 1). The parameter F accounts for the contributions of the undamaged, damaged, and heavily damaged blood granulocytes (X_3^{ud}, X_3^{d}, and X_3^{hd} cells) to this regulatory mechanism:

$$F = \delta \frac{1 + M\left(x_3^{\mathrm{ud}} + x_3^{\mathrm{d}} + x_3^{\mathrm{hd}}\right)^2}{1 + L\left(x_3^{\mathrm{ud}} + x_3^{\mathrm{d}} + x_3^{\mathrm{hd}}\right)^2}. \tag{7.9}$$

Here constants δ and $\delta M/L$ are, respectively, the maximal and minimal values of the specific rate of granulocyte supply from the bone marrow to the blood flow.

It is worthwhile to note that the parameter F in the models of the thrombopoietic, lymphopoietic, and erythropoietic systems is a constant $F \equiv \delta$. In turn, the parameters γ, ψ, and ξ are also constants in the models on hand.

Initial conditions for Eqs. (7.1)–(7.6) are determined by the concentrations of X_i^{ud}, X_i^{d}, X_i^{hd} $(i = 1, \ldots, n)$ and X_i^{ud} $(i = n+1, \ldots, m)$ cells before the onset of irradiation. In particular, in the case of irradiation of a healthy individual that has not previously been exposed to radiation, the initial concentrations of X_i^{ud} $(i = 1, \ldots, m)$ cells are equal to their normal values $\bar{x}_i$, whereas the initial concentrations of X_i^{d} $(i = 1, \ldots, n)$ cells and X_i^{hd} $(i = 1, \ldots, n)$ cells are equal to zero:

$$(x_i^{\mathrm{ud}})_0 = \bar{x}_i, \quad (x_i^{\mathrm{d}})_0 = 0, \quad (x_i^{\mathrm{hd}})_0 = 0 \quad (i = 1, \ldots, n),$$

$$(x_i^{\mathrm{ud}})_0 = \bar{x}_i \quad (i = n+1, \ldots, m). \tag{7.10}$$

It is important to emphasize that the developed models explicitly embody the main characteristics of irradiation, namely the dose rate N of chronic irradiation, as well as the radiobiological parameters D_i^0 $(i = 1, \ldots, n)$, which specify the radiosensitivity of the hematopoietic cells in the respective major hematopoietic lineages in humans.

7.2.2 *Models of the Dynamics of the Major Hematopoietic Lineages After Acute Irradiation*

A distinctive feature of the postirradiation dynamics of the major hematopoietic lineages in humans, as well as in some other mammalian species (e.g., monkeys, dogs), is the so-called abortive rise, the latter being the short-term elevation of concentrations of functional blood cells and their bone marrow precursors soon after acute irradiation. At present, there is no single point of view on the nature of the abortive rise. A hypothesis proposed by Bond et al. in [1] assumes the existence of weakly damaged cells in the respective hematopoietic lineages after acute irradiation. It is also suggested that these weakly damaged cells divide and differentiate as ordinary intact cells within the first few days. After that they die together with their progeny.

This hypothesis is implemented in the models of the postirradiation dynamics of the major hematopoietic lineages [16–20] in the following way. According to this hypothesis, the models consider the subgroup of weakly damaged cells X_i^{wd} and the subgroup of moderately damaged cells X_i^{md} instead of the entire group of damaged cells X_i^{d}. The moderately damaged cells die within 1–2 days following irradiation (mitotic death). Their concentrations, x_i^{md}, are described by Eq. (7.5) with $N = 0$. In turn, the concentrations of the weakly damaged cells, x_i^{wd}, are described by equations identical to those for the concentrations of the undamaged cells X_i^{ud} in the time interval between the onset of irradiation and the moment of maximum abortive rise T_{ar} ($0 \le t \le T_{ar}$). After the moment of maximum abortive rise ($t > T_{ar}$), the concentrations x_i^{wd} are described by equations, which consider only the death of weakly damaged cells at a specific rate η. The concentrations of undamaged cells X_i^{ud} and heavily damaged cells X_i^{hd} are described by Eqs. (7.1)–(7.4) and (7.6) with $N = 0$. Eventually, the models of the postirradiation dynamics of the human major hematopoietic lineages acquire the following form:

$$\frac{dx_1^{\mathrm{ud}}}{dt} = Bx_1^{\mathrm{ud}} - \gamma x_1^{\mathrm{ud}}, \tag{7.11}$$

$$\frac{dx_2^{\mathrm{ud}}}{dt} = \gamma x_1^{\mathrm{ud}} - Fx_2^{\mathrm{ud}}, \tag{7.12}$$

$$\frac{dx_3^{\mathrm{ud}}}{dt} = Fx_2^{\mathrm{ud}} - \psi x_3^{\mathrm{ud}}, \tag{7.13}$$

$$\frac{dx_4^{\mathrm{ud}}}{dt} = \psi x_3^{\mathrm{ud}} - \xi x_4^{\mathrm{ud}}, \tag{7.14}$$

$$\frac{dx_1^{\mathrm{wd}}}{dt} = \Theta(T_{ar} - t)[Bx_1^{\mathrm{wd}} - \gamma x_1^{\mathrm{wd}}] - \Theta(t - T_{ar})\eta x_1^{\mathrm{wd}}, \tag{7.15}$$

$$\frac{dx_2^{\mathrm{wd}}}{dt} = \Theta(T_{ar} - t)[\gamma x_1^{\mathrm{wd}} - Fx_2^{\mathrm{wd}}] - \Theta(t - T_{ar})\eta x_2^{\mathrm{wd}}, \tag{7.16}$$

$$\frac{dx_3^{\mathrm{wd}}}{dt} = \Theta(T_{ar} - t)[Fx_2^{\mathrm{wd}} - \psi x_3^{\mathrm{wd}}] - \Theta(t - T_{ar})\eta x_3^{\mathrm{wd}}, \tag{7.17}$$

$$\frac{dx_4^{\mathrm{wd}}}{dt} = \Theta(T_{ar} - t)[\psi x_3^{\mathrm{wd}} - \xi x_4^{\mathrm{wd}}] - \Theta(t - T_{ar})\eta x_4^{\mathrm{wd}}, \tag{7.18}$$

$$\frac{dx_i^{\mathrm{md}}}{dt} = -\mu x_i^{\mathrm{md}} \quad (i = 1, \ldots, n), \tag{7.19}$$

$$\frac{dx_i^{\mathrm{hd}}}{dt} = -\nu x_i^{\mathrm{hd}} \quad (i = 1, \ldots, n). \tag{7.20}$$

Here $\Theta(t)$ is the unit step-function [59]:

$$\Theta(t) = \begin{cases} 1, & t \geq 0, \\ 0, & t < 0. \end{cases} \tag{7.21}$$

In the models of the postirradiation dynamics of the human major hematopoietic lineages [Eqs. (7.11)–(7.20)], the contributions of X_i^{wd} and X_i^{md} cells to the feedback loop regulatory mechanism of the reproduction rate of X_1^{ud} cells are taken into account by the appropriate modification of Eq. (7.7):

$$B = \frac{\alpha}{1 + \beta\left[\sum_{i=1}^{n} \theta_i \left(x_i^{\mathrm{ud}} + \Phi x_i^{\mathrm{wd}} + \phi x_i^{\mathrm{md}} + \varphi x_i^{\mathrm{hd}}\right) + \sum_{i=n+1}^{m} \theta_i \left(x_i^{\mathrm{ud}} + \Phi x_i^{\mathrm{wd}}\right)\right]}, \tag{7.22}$$

where

$$\Phi = \Theta(T_{ar} - t) + \varsigma\Theta(t - T_{ar}). \tag{7.23}$$

In Eq. (7.22), the parameters α, θ_i $(i = 1, \ldots, m)$, ϕ, φ, and β are the same as those in Eq. (7.7). In Eq. (7.23), $\Theta(t)$ is the unit step-function [Eq. (7.21)] and ς is a constant.

In accordance with the clinical data [60, 61], the variable parameter T_{ar} in Eqs. (7.15)–(7.18) and (7.23) is taken as the linear function of the dose D of acute irradiation in the considered dose range:

$$T_{ar} = \tau - \upsilon D. \tag{7.24}$$

Here the constant parameters τ and υ have the dimensions of day and day Gy^{-1}, respectively.

In the model of the postirradiation dynamics of the human thrombopoietic system, the contribution of X_3^{wd} cells to the regulatory mechanism of the megakaryocyte ploidy is taken into account by the appropriate modification of Eq. (7.8):

$$f = \frac{1}{\lambda + (1 - \lambda)[(x_3^{\mathrm{ud}} + x_3^{\mathrm{wd}})/\bar{x}_3]}. \tag{7.25}$$

In Eq. (7.25), the constant parameter λ is the same as that in Eq. (7.8); the parameter $\bar{x}_3$ denotes the normal concentration of thrombocytes as in Eq. (7.8). In the model of the postirradiation dynamics of the human thrombopoietic system, the additional factor f [Eq. (7.25)] appears in front of the first terms on the right-hand sides of Eqs. (7.12) and (7.16). In turn, the additional factor σ appears in front of the first terms on the right-hand sides of Eqs. (7.13) and (7.17). Remind that the constant parameter σ denotes the average number of thrombocytes produced by one megakaryocyte in the norm.

In the model of the postirradiation dynamics of the human granulopoietic system, the contributions of X_3^{wd} and X_3^{md} cells to the regulatory mechanism of the specific rate of the granulocyte supply from the bone marrow to the blood flow are taken into account by the appropriate modification of Eq. (7.9):

$$F = \delta \frac{1 + M\left(x_3^{\mathrm{ud}} + x_3^{\mathrm{wd}} + x_3^{\mathrm{md}} + x_3^{\mathrm{hd}}\right)^2}{1 + L\left(x_3^{\mathrm{ud}} + x_3^{\mathrm{wd}} + x_3^{\mathrm{md}} + x_3^{\mathrm{hd}}\right)^2}. \tag{7.26}$$

In Eq. (7.26), the constant parameters δ, M, and L are the same as those in Eq. (7.9). Remind that δ and $\delta(M/L)$ are the maximal and minimal values of the specific rate of granulocyte supply from the bone marrow to the blood flow.

As noted above, the parameter F is a constant ($F \equiv \delta$) in the models of the postirradiation dynamics of the human thrombopoietic, lymphopoietic, and erythropoietic systems. In turn, the parameters γ, ψ, and ξ are also constants in the models on hand.

The initial conditions for Eqs. (7.11)–(7.20), which describe the postirradiation dynamics of the human major hematopoietic lineages, read

$$x_i^{\mathrm{ud}}(0) = \bar{x}_i \exp(-D/D_i^0) \quad (i = 1, \ldots, n), \tag{7.27}$$

$$x_1^{\mathrm{wd}}(0) = \bar{x}_1 \frac{1}{1+\rho_1} \frac{\kappa}{1+\kappa} [1 - \exp(-D/D_1^0)], \tag{7.28}$$

$$x_1^{\mathrm{md}}(0) = \bar{x}_1 \frac{1}{1+\rho_1} \frac{1}{1+\kappa} [1 - \exp(-D/D_1^0)], \tag{7.29}$$

$$x_i^{\mathrm{wd}}(0) = 0 \quad (i = 2, \ldots, m), \tag{7.30}$$

$$x_i^{\mathrm{md}}(0) = \bar{x}_i \frac{1}{1+\rho_i} [1 - \exp(-D/D_i^0)] \quad (i = 2, \ldots, n), \tag{7.31}$$

$$x_i^{\mathrm{hd}}(0) = \bar{x}_i \frac{\rho_i}{1+\rho_i} [1 - \exp(-D/D_i^0)] \quad (i = 1, \ldots, n), \tag{7.32}$$

$$x_i^{\mathrm{ud}}(0) = \bar{x}_i \quad (i = n+1, \ldots, m). \tag{7.33}$$

Here D is the dose of acute irradiation. Remind that the parameter D_i^0 is equivalent to the conventional radiobiological dose D_0. Namely, after exposure to such dose, the number of X_i cells left undamaged is $e = 2.718\ldots$ times smaller than their

initial number [1]. In turn, the parameter ρ_i $(i = 1, \ldots, n)$ is the ratio of the parts of X_i^{ud} cells that transfer to the groups of weakly and moderately damaged cells (X_i^{wd} and X_i^{md} cells) and to the group of heavily damaged cells (X_i^{hd} cells) after acute irradiation. The parameter κ is the ratio of the parts of X_1^{ud} cells that transfer to weakly damaged cells X_1^{wd} and moderately damaged cells X_1^{md} after acute irradiation. Note that Eqs. (7.27)–(7.33) were derived in the similar way as Eqs. (1.17)–(1.19) in Chap. 1.

In the models [Eqs. (7.11)–(7.20)], which describe the postirradiation dynamics of the human thrombopoietic, granulopoietic, lymphopoietic, and erythropoietic systems, the parameters ρ_i $(i = 1, \ldots, n)$ and κ are given by the following formulae:

$$\rho_i = \frac{1 - \exp(-D/D_i^{00})}{\exp(-D/D_i^{00}) - \exp(-D/D_i^{0})} \quad (i = 1, \ldots, n), \tag{7.34}$$

$$\kappa = \frac{\exp(-D/D_1^{000}) - \exp(-D/D_1^{0})}{\exp(-D/D_1^{00}) - \exp(-D/D_1^{000})}. \tag{7.35}$$

The parameters D and D_i^0 appearing in Eqs. (7.34) and (7.35) are defined above. The parameter D_i^{00} is the dose, after exposure to which the number of X_i cells, which did not undergo the interphase death, is $e = 2.718\ldots$ times smaller than their initial number. In turn, the coefficient D_1^{000} is the dose, after exposure to which the number of X_1 cells, which did not undergo either the interphase death or the mitotic death, is $e = 2.718\ldots$ times smaller than their initial number. Note that Eq. (7.34) is derived in Chap. 1. In turn, Eq. (7.35) is derived in a similar way.

As it follows from Eqs. (7.34) and (7.35), the parameters ρ_i $(i = 1, \ldots, n)$ and κ are physically meaningful, if the inequalities $D_1^0 < D_1^{000} < D_1^{00}$ and $D_i^0 < D_i^{00}$ $(i = 2, \ldots, n)$ are fulfilled.

For $D \ll \min(D_i^0)$, the coefficients ρ_i $(i = 1, \ldots, n)$ and κ, at a first approximation, are

$$\rho_i = \frac{1}{(D_i^{00}/D_i^0 - 1)} \quad (i = 1, \ldots, n), \tag{7.36}$$

$$\kappa = \frac{(D_1^{000}/D_1^0 - 1)}{(1 - D_1^{000}/D_1^{00})}. \tag{7.37}$$

In this case, they depend only on the parameters, which determine the radiosensitivity of X_i $(i = 1, \ldots, n)$ cells.

From physical considerations it is obvious that the simplified versions of the expressions for the coefficients ρ_i $(i = 1, \ldots, n)$ and κ [Eqs. (7.36) and (7.37)] can be used in the model describing the hematopoiesis dynamics under chronic irradiation. The reason is that for any small interval of time dt, the condition of the applicability of formulae (7.36) and (7.37), namely $D = N \cdot dt \ll \min(D_i^0)$ will certainly be satisfied in the studied range of N.

To reproduce in details the dynamics of the erythropoiesis dynamics in acutely irradiated humans, Eqs. (7.11)–(7.20) are used instead of Eqs. (7.11)–(7.13), (7.15)–(7.17), (7.19), (7.20). In this case Eq. (7.13) describes the dynamics of the concentration of undamaged blood reticulocytes (X_3^{ud} cells), whereas Eq. (7.14) describes the dynamics of the concentration of undamaged mature blood erythrocytes (X_4^{ud} cells). In turn, Eq. (7.17) describes the dynamics of the concentration of weakly damaged blood reticulocytes (X_3^{wd} cells), whereas Eq. (7.18) describes the dynamics of the concentration of weakly damaged mature blood erythrocytes (X_4^{wd} cells). The parameter ψ entering Eqs. (7.13), (7.14), (7.17), and (7.18) denotes the specific rate of transfer of cells from the subgroup of X_3^{ud} cells and X_3^{wd} cells to the subgroup of X_4^{ud} cells and X_4^{wd} cells, respectively. This parameter is renamed by ψ'. The coefficient ξ in Eqs. (7.14) and (7.18) denotes the specific rate of the cell leaving the subgroup of X_4^{ud} cells and X_4^{wd} cells. The parameter θ_4 in Eq. (7.22) is taken to equal to θ_3. Such a modification of the erythropoiesis model allows one to compare the modeling results with relevant clinical data in more profound way.

It is important to emphasize that the developed models of the postirradiation dynamics of the human major hematopoietic lineages in acutely irradiated humans explicitly embody the main characteristics of irradiation, namely the dose D of acute exposure, as well as the radiobiological parameters D_i^0, D_i^{00} ($i = 1, \ldots, n$), and D_1^{000}, which characterize the radiosensitivity of the hematopoietic cells.

7.2.3 Parameter Estimation

The independent parameters of the models of the human thrombopoietic, granulopoietic, lymphopoietic, and erythropoietic systems were specified in [16–18, 20, 23] (see Tables 7.1, 7.2, 7.3, and 7.4).

Table 7.1 presents the values of independent parameters of the model of the human thrombopoietic system. The values of the parameters α, γ, δ, ψ, σ, μ, ν, τ, υ are determined on the basis of empirical data [26, 51, 57, 60–62]. The parameters λ, η, ϕ, φ, ς, θ_2, $\theta_3' = \sigma\,\theta_3$, D_1^0, D_1^{00}, D_1^{000} are evaluated in the course of numerical studies of the model and consequent juxtaposition of the modeling results with empirical data on the dynamics of the thrombopoiesis in humans after acute irradiation [62, 63].

Table 7.2 shows the values of independent parameters of the model of the human granulopoietic system. The values of the parameters α, γ, δ, ψ, ξ, μ, ν, τ, υ D_2^0, D_2^{00}, D_3^0, D_3^{00}, D_4^0, D_4^{00} are determined on the basis of empirical data [26, 51, 57, 60–62, 64, 65] The parameters $m = M\bar{x}_3^2$, $l = L\bar{x}_3^2$, η, ϕ, φ, ς, θ_2, θ_3, θ_4, D_1^0, D_1^{00}, D_1^{000} are evaluated in the course of numerical studies of the model and consequent juxtaposition of the modeling results with empirical data on the dynamics of the granulopoietic system in humans after acute irradiation [62, 63].

Table 7.3 contains the values of independent parameters of the model of the human lymphopoietic system. The values of the parameters γ, ψ, μ, ν, τ, υ, D_2^0, D_2^{00}, D_3^0, and D_3^{00} are determined on the basis of empirical data [26, 51, 60, 61, 66–

Table 7.1 Parameters of the thrombopoiesis model for humans

Parameter	Value	Dimension
α	2.4	day^{-1}
γ	1.4	day^{-1}
δ	0.2	day^{-1}
ψ	0.2	day^{-1}
μ	0.5	day^{-1}
ν	6.0	day^{-1}
η	0.2	day^{-1}
τ	14.0	day
υ	2.0	day Gy^{-1}
D_1^0	0.2	Gy
D_1^{00}	2.0	Gy
D_1^{000}	1.95	Gy
ϕ	1.0	1
φ	12.0	1
ς	12.0	1
θ_1	1.0	1
θ_2	0.1	1
$\theta_3' = \sigma\,\theta_3$	0.3	1
λ	0.25	1
σ	3000	1

70]. The values of the parameters η, ϕ, φ, and ς are taken to be equal to those in the thrombopoiesis and granulopoiesis models. The values of the parameters α, δ, θ_2, θ_3 are taken to be equal to those in [23]. The parameters D_1^0, D_1^{00}, and D_1^{000} are evaluated in the course of numerical studies of the model and subsequent juxtaposition of the modeling results with empirical data on the dynamics of the lymphopoietic system in acutely irradiated humans [60, 61, 69, 70].

Table 7.4 gives the values of independent parameters of the model of the human erythropoietic system. The values of the parameters α, γ, δ, ψ, ψ', ξ, μ, ν, τ, and υ are determined on the basis of empirical data [26, 51, 57, 60–62]. The values of the parameters η, ϕ, φ, and ς are taken to be the same as those in the thrombopoiesis, granulopoiesis, and lymphopoiesis models. The parameters θ_2, θ_3, D_1^0, D_1^{00}, D_1^{000}, D_2^0, and D_2^{00} are evaluated in the course of numerical studies of the model and subsequent juxtaposition of the modeling results with empirical data on the erythropoiesis dynamics in acutely irradiated humans [61]. The parameter θ_4 is taken to be equal to θ_3.

The developed and identified models of the thrombopoietic, granulopoietic, lymphopoietic, and erythropoietic systems are used to study the dynamics of these major hematopoietic lineages in humans under normal conditions and under acute and chronic irradiation. The obtained modeling results are presented in the next sections.

Table 7.2 Parameters of the granulopoiesis model for humans

Parameter	Value	Dimension
α	2.4	day^{-1}
γ	0.4	day^{-1}
δ	0.2	day^{-1}
ψ	2.2	day^{-1}
ξ	0.2	day^{-1}
μ	0.5	day^{-1}
ν	6	day^{-1}
η	0.2	day^{-1}
τ	19.0	day
υ	2.0	day Gy^{-1}
D_1^0	0.5	Gy
D_1^{00}	2.0	Gy
D_1^{000}	1.5	Gy
D_2^0	5	Gy
D_2^{00}	50	Gy
D_3^0	5	Gy
D_3^{00}	50	Gy
D_4^0	5	Gy
D_4^{00}	50	Gy
m	0.5	1
l	1.0	1
θ_1	1.0	1
θ_2	0.1	1
θ_3	0.05	1
θ_4	0.25	1
ϕ	1	1
φ	12	1
ς	12	1

7.3 Dynamics of the Human Major Hematopoietic Lineages Under Normal Conditions

7.3.1 Thrombopoietic System

To describe the dynamics of the thrombopoietic system under normal conditions, Eqs. (7.1)–7.3), (7.5), (7.6) can be reduced to Eqs. (7.1)–(7.3) with $N = 0$ and $x_i^{\text{ud}} \equiv x_i$ $(i = 1, 2, 3)$ in them. In turn, Eqs. (7.11)–(7.13), (7.15)–(7.17), (7.19), (7.20) can be reduced to Eqs. (7.11)–(7.13) with $x_i^{\text{ud}} \equiv x_i$ $(i = 1, \ldots, 3)$ in them. Remind that the first terms on the right-hand sides of Eqs. (7.2) and (7.12) are multiplied by the ploidy coefficient f. The latter is determined by Eq. (7.8) with $x_3^{\text{ud}} \equiv x_3$ and by Eq. (7.25) with $x_3^{\text{ud}} \equiv x_3$ and $x_3^{\text{wd}} = 0$, respectively. In turn, the first terms on the right-hand sides of Eqs. (7.3) and (7.13) are multiplied by factor σ, which

Table 7.3 Parameters of the lymphopoiesis model for humans

Parameter	Value	Dimension
α	0.8	day^{-1}
γ	0.2	day^{-1}
δ	0.6	day^{-1}
ψ	0.02	day^{-1}
μ	0.5	day^{-1}
ν	6.0	day^{-1}
η	0.2	day^{-1}
τ	16.0	day
υ	2.0	day Gy^{-1}
D_1^0	1.0	Gy
D_1^{00}	1.45	Gy
D_1^{000}	1.4	Gy
D_2^0	1.4	Gy
D_2^{00}	13.0	Gy
D_3^0	1.6	Gy
D_3^{00}	6.5	Gy
θ_1	1.0	1
θ_2	0.06	1
θ_3	0.01	1
ϕ	1.0	1
φ	12.0	1
ς	12.0	1

denotes the average number of thrombocytes produced by one megakaryocyte in the norm. Obviously, the systems of differential equations obtained in this way are identical to each other and to Eqs. (1.28)–(1.30), which describe the dynamics of the thrombopoietic system in mammals under normal conditions (see Chap. 1).

The system of Eqs. (1.28)–(1.30) was investigated by methods of the qualitative theory of differential equations, oscillation theory, and bifurcation theory [71–76] (see Chap. 1). As it was found, the system of Eqs. (1.28)–(1.30) has two singular points in the space of variables. The first of them is trivial. If $\alpha < \gamma$, then the second singular point has negative coordinates in the space of variables, i.e., it has no physical sense. If $\alpha = \gamma$, then the second singular point coincides with the first one. In both these cases, the trivial singular point is stable and can be identified with the state of the extinction of the thrombopoietic system. This range of parameters ($\alpha \leq \gamma$) of the thrombopoiesis model is not considered in what follows.

If $\alpha > \gamma$, then the first (trivial) singular point is unstable, whereas the second singular point with positive coordinates $\bar{x}_i$ can be stable or unstable depending on the values of model parameters. When the second singular point is stable, it can be identified with the state of the stable dynamic equilibrium (the homeostasis state) of the thrombopoietic system and the values of its coordinates $\bar{x}_i$ [Eqs. (1.33)–(1.35)] can be considered the normal concentrations of blood thrombocytes and

Table 7.4 Parameters of the erythropoiesis model for humans

Parameter	Value	Dimension
α	2.4	day^{-1}
γ	0.15	day^{-1}
δ	0.5	day^{-1}
ψ	0.015	day^{-1}
ψ'	4.0	day^{-1}
ξ	0.015	day^{-1}
μ	0.5	day^{-1}
ν	6	day^{-1}
η	0.2	day^{-1}
τ	20.0	day
υ	2.0	day Gy^{-1}
D_1^0	0.8	Gy
D_1^{00}	1.5	Gy
D_1^{000}	1.45	Gy
D_2^0	5	Gy
D_2^{00}	50	Gy
θ_1	1.0	1
θ_2	0.1	1
θ_3	0.05	1
θ_4	0.05	1
ϕ	1	1
φ	12	1
ς	12	1

their bone marrow precursor cells. When the second singular point is unstable, one more particular solution appears: a stable limit cycle. This particular solution can be identified with stable oscillations of the concentrations of blood thrombocytes and their bone marrow precursor cells. Conditions of appearance of the cyclic thrombopoiesis are given by inequalities (1.36)–(1.38) (see Chap. 1).

The developed model [Eqs. (1.28)–(1.30)] is used to study numerically the dynamics of the thrombopoietic system in humans under normal conditions. For the convenience, Eqs. (1.28)–(1.30) are rewritten in terms of the new dimensionless variables, the latter being the ratios of the dimension concentrations of X_i ($i = 1, 2, 3$) cells, x_i ($i = 1, 2, 3$), to their stationary values $\bar{x}_i$ ($i = 1, 2, 3$).

Specifically, the model (1.28)–(1.30) is employed to simulate the homeostasis state of the thrombopoietic system in healthy humans under normal conditions. This state is characterized by the normal concentrations of blood thrombocytes and their bone marrow precursors cells. After deviation from the homeostasis state, the system returns to it. Such a behavior of the thrombopoietic system in healthy humans is reproduced by the model (1.28)–(1.30) with the normal values of its independent parameters α, γ, δ, ψ, σ, λ, θ_1, θ_2, and $\theta_3' = \sigma\,\theta_3$ (Table 7.1). Results

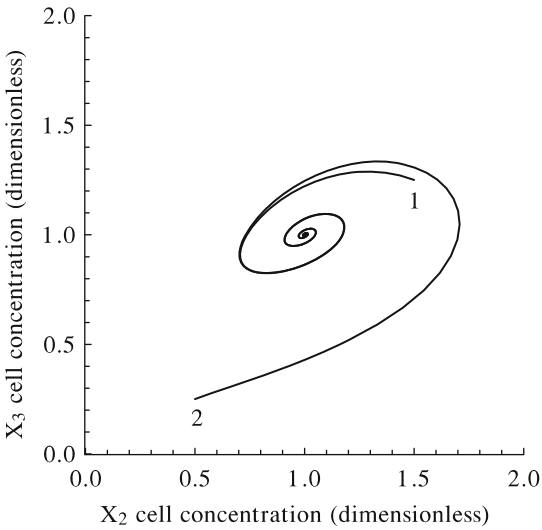

Fig. 7.5 Results of numerical studies of the human thrombopoiesis model. Projections of two integral curves of the system of Eqs. (1.28)–(1.30) onto the plane of states $\{x_2\, x_3\}$. *Curves 1 and 2* converge to the stable second singular point [Eqs. (1.33)–(1.35)]

of the numerical study of the thrombopoiesis model with these normal values of the independent parameters are presented in Fig. 7.5.

Figure 7.5 shows projections of two integral curves of the system of Eqs. (1.28)–(1.30) onto the plane of states $\{x_2\, x_3\}$. The concentrations of X_i $(i = 1, 2, 3)$ cells are computed in the dimensionless units as the ratios of the dimension concentrations of these cells, x_i $(i = 1, 2, 3)$, to their normal values, i.e., to the respective coordinates of the stable second singular point $\bar{x}_i$ $(i = 1, 2, 3)$. The values of coordinates of the stable second singular point in these dimensionless units is $(1, 1, 1)$ by definition. As one can see from Fig. 7.5, the integral curves converge to this point. In other words, the concentrations of X_i $(i = 1, 2, 3)$ cells return to their normal values $\bar{x}_i$ $(i = 1, 2, 3)$ after deviations from them. The obtained results demonstrate that the model (1.28)–(1.30) with the normal values of its independent parameters is capable of reproducing the homeostasis state of the thrombopoietic system under normal conditions.

The model (1.28)–(1.30) is also applied to simulate the cyclic dynamics of the thrombopoietic system in humans under normal conditions. To reproduce such a behavior of this hematopoietic lineage by the model (1.28)–(1.30), it turns out to be sufficient to increase the parameters α, λ, and θ_3'. Values of the rest of the independent parameters are taken to be equal to their normal values (Table 7.1). A set of these "oscillatory" values of the independent parameters of the thrombopoiesis model $(\tilde{\alpha}, \tilde{\gamma}, \tilde{\delta}, \tilde{\psi}, \tilde{\sigma}, \tilde{\lambda}, \tilde{\theta}_1, \tilde{\theta}_2, \tilde{\theta}_3' = \tilde{\sigma}\, \tilde{\theta}_3)$ is given in Table 7.5. Results of the numerical studies of the thrombopoiesis model with these "oscillatory" values of the independent parameters are presented in Figs. 7.6, 7.7, 7.8, and 7.9.

Figure 7.6 shows projections of three integral curves of the system of Eqs. (1.28)–(1.30) onto the plane of states $\{x_2\, x_3\}$. The concentrations of X_i $(i = 1, 2, 3)$ cells are

Table 7.5 "Oscillatory" values of parameters of the thrombopoiesis model for humans

Parameter	Value	Dimension
$\alpha \equiv \tilde{\alpha}$	4.0	day^{-1}
$\gamma \equiv \tilde{\gamma}$	1.4	day^{-1}
$\delta \equiv \tilde{\delta}$	0.2	day^{-1}
$\psi \equiv \tilde{\psi}$	0.2	day^{-1}
$\theta_1 \equiv \tilde{\theta}_1$	1.0	1
$\theta_2 \equiv \tilde{\theta}_2$	0.1	1
$\theta_3' \equiv \tilde{\theta}_3'$	4.5	1
$\lambda \equiv \tilde{\lambda}$	0.9	1
$\sigma \equiv \tilde{\sigma}$	3000	1

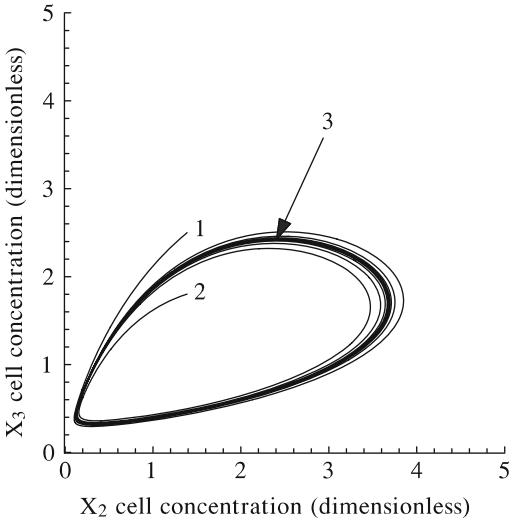

Fig. 7.6 Results of numerical studies of the human thrombopoiesis model. Projections of three integral curves of the system of Eqs. (1.28)–(1.30) onto the plane of states $\{x_2\, x_3\}$. *Curves 1 and 2* converge to the limit cycle (*closed curve* labeled by 3)

computed in the dimensionless units as the ratios of the dimension concentrations of these cells, x_i $(i = 1, 2, 3)$, to their stationary values, i.e., to the values of the respective coordinates of the unstable second singular point $\widetilde{\widetilde{x}}_i$ $(i = 1, 2, 3)$. The coordinates of the unstable second singular point in the dimensionless units are $(1, 1, 1)$ by definition. In Fig. 7.6, the closed curve is the limit cycle and two other curves converge to it from the outside and inside. These modeling results demonstrate the existence of the stable limit cycle in the system (1.28)–(1.30), which corresponds to the stable oscillations of the concentrations of the cells in the thrombopoietic system.

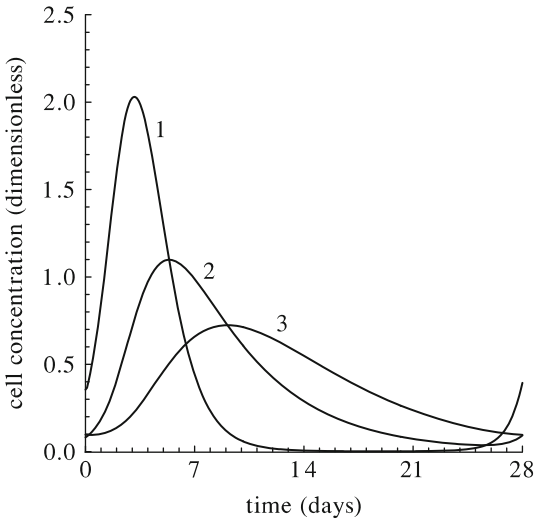

Fig. 7.7 Results of numerical studies of the human thrombopoiesis model [Eqs. (1.28)–(1.30)]. The cyclic dynamics of dimensionless concentrations of X_1, X_2, and X_3 cells (*curves 1–3*)

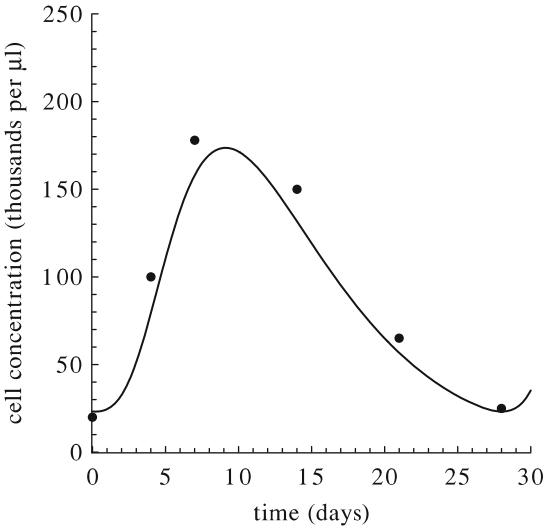

Fig. 7.8 The cyclic dynamics of the thrombocyte concentration in a human with cyclic thrombocytopenia. The results of the numerical studies of the human thrombopoiesis model [Eqs. (1.28)–(1.30)] (*curve*) and the clinical data [80] (*circle*)

Next, the concentrations of X_i $(i = 1, 2, 3)$ cells are expressed in the dimensionless units as the ratios of the dimension concentrations of these cells, x_i $(i = 1, 2, 3)$, to their normal values, i.e., to the respective coordinates of the stable second singular point $\bar{x}_i$ $(i = 1, 2, 3)$. For this purpose, the computed values of the dimensionless concentrations of X_i $(i = 1, 2, 3)$ cells, $x_i/\widetilde{\bar{x}}_i$ $(i = 1, 2, 3)$, are multiplied by factors R_i $(i = 1, 2, 3)$. The latter are equal to ratios of coordinates of the unstable singular point $\widetilde{\bar{x}}_i$ $(i = 1, 2, 3)$ to the respective coordinates of the stable singular point $\bar{x}_i$ $(i = 1, 2, 3)$:

$$R_i = \frac{\widetilde{\bar{x}}_i}{\bar{x}_i} \quad (i = 1, 2, 3). \tag{7.38}$$

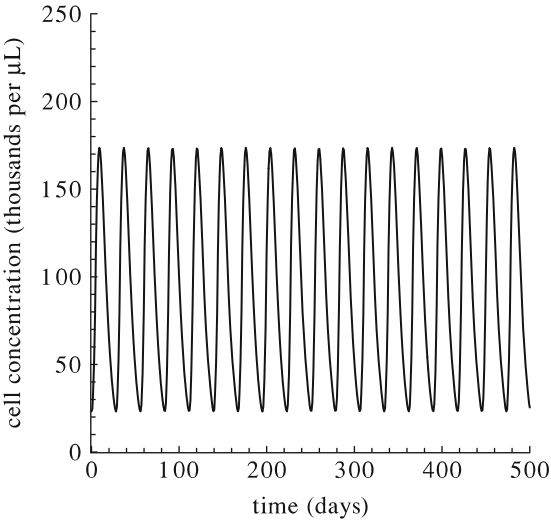

Fig. 7.9 Results of numerical studies of the human thrombopoiesis model [Eqs. (1.28)–(1.30)]. The cyclic dynamics of the blood thrombocyte concentration given in the standard units

As it follows from Eqs. (1.28)–(1.30), the quantity R_3 is equal to a positive root of the quadratic equation [77]:

$$R_3 = \frac{-a_1 + \sqrt{a_1^2 - 4a_0a_2}}{2a_0}, \tag{7.39}$$

where

$$a_0 = 1 - \tilde{\lambda}, \tag{7.40}$$

$$a_1 = \tilde{\lambda} + \widetilde{\theta}_2 \frac{\tilde{\gamma}}{\tilde{\delta}} + \widetilde{\theta}_3' \frac{\tilde{\gamma}}{\tilde{\psi}}, \tag{7.41}$$

$$a_2 = -\frac{\tilde{\alpha} - \tilde{\gamma}}{\alpha - \gamma} \frac{\tilde{\sigma}}{\sigma} \frac{\psi}{\tilde{\psi}} \left(1 + \theta_2 \frac{\gamma}{\delta} + \theta_3' \frac{\gamma}{\psi}\right). \tag{7.42}$$

In turns, the quantities R_1 and R_2 are expressed in terms of R_3 in the following way:

$$R_2 = R_3 \frac{\tilde{\psi}}{\psi} \frac{\sigma\delta}{\tilde{\sigma}\,\tilde{\delta}}, \tag{7.43}$$

$$R_1 = R_3 \left[\tilde{\lambda} + (1 - \tilde{\lambda})\, R_3\right] \frac{\tilde{\psi}}{\psi} \frac{\sigma\gamma}{\tilde{\sigma}\,\tilde{\gamma}}. \tag{7.44}$$

Remind that the normal and "oscillatory" values of the independent parameters of the thrombopoiesis model (α, γ, δ, ψ, θ_1, θ_2, θ_3', λ, σ and $\tilde{\alpha}$, $\tilde{\gamma}$, $\tilde{\delta}$, $\tilde{\psi}$, $\tilde{\theta}_1$, $\tilde{\theta}_2$, $\tilde{\theta}_3'$, $\tilde{\lambda}$, $\tilde{\sigma}$, respectively) are given in Tables 7.1 and 7.5.

Figure 7.7 shows one period of oscillations of concentrations of blood thrombocytes (X_3 cells) and their bone marrow precursor cells capable and incapable of dividing (X_1 cells and X_2 cells, respectively). The cell concentrations are presented here in the dimensionless units as the ratios of the dimension cell concentrations, x_i $(i = 1, 2, 3)$, to their normal values $\bar{x}_i$ $(i = 1, 2, 3)$. As one can infer from Fig. 7.7, the concentration of X_3 cells oscillates around the level, which is lower than its normal one. These modeling results can be identified with the dynamics of the thrombopoiesis in patients with cyclic thrombocytopenia [78]. This rare hematological disorder is characterized by stable oscillations of the concentration of blood thrombocytes around the level decreased in comparison with the normal one [25, 78–80]. As one can also see from Fig. 7.7, the concentration of X_1 cells oscillates in parallel with the concentration of X_2 cells with the phase advance of about 2 days. In turn, the concentration of X_2 cells oscillates in parallel with the concentration of X_3 cells with the phase advance of about 4 days that coincides with the respective clinical data [78].

To compare the modeling dynamics of blood thrombocytes (X_3 cells) with the kinetics of these cells in patients with cyclic thrombocytopenia in more profound way, the concentration of X_3 cells is expressed in the standard units. For this purpose, the computed values of the dimensionless concentration of X_3 cells, $x_3/\bar{x}_3$, are multiplied by the factor R_3 [Eq. (7.39)] and by the normal thrombocyte concentration in humans, which is given in the standard units. This concentration is equal to 240 thousands per μl [26]. The obtained modeling results are displayed in Figs. 7.8 and 7.9.

Figure 7.8 shows one period of oscillations of the thrombocyte concentration given in the standard units. As one can see, these modeling results are in a good agreement with the data on the kinetics of the thrombocyte concentration in a patient with cyclic thrombocytopenia [80]. It is important to emphasize that the developed model is capable of reproducing even the typical shape of the kinetic curves describing the thrombocyte concentration in patients with cyclic thrombocytopenia [78, 80].

Figure 7.9 presents the cyclic dynamics of the blood thrombocyte concentration, which is given in the standard units. As one can see from this figure, the concentration of the blood thrombocytes oscillates between 23 thousands per μl and 174 thousands per μl around the level of 98.5 thousands per μl. These modeling results lie within the range of clinical observations [78–80]. The period of these oscillations is about 28 days, which also agrees with clinical data (21–39 days) [78–80]. All this demonstrates that the developed model is capable of reproducing the dynamics of the thrombopoietic system in patients with cyclic thrombocytopenia.

Proceeding from the results of analytical and numerical studies of the thrombopoiesis model, the following biological interpretation of the causes of cyclic thrombocytopenia in humans can be proposed. This hematological disorder is due to failures in some regulatory mechanisms in the thrombopoietic system. They are manifested in (1) the weakening of the regulatory mechanism of the megakaryocyte ploidy, (2) the enhancing of the influence of the contribution of X_3 cells to the regulatory mechanism of the reproduction rate of X_1 cells, and (3)

the increasing of the maximal specific rate α of the reproduction of X_1 cells. The first two of them lead to the decrease of timely production of thrombocytes (X_3 cells). The third one is not able to compensate completely the decrease in the thrombocyte production. The modeling predictions concerning the nature of the cyclic thrombocytopenia are consistent with the assumptions made on the basis of the clinical studies. According to the latter, the cyclic thrombocytopenia is the consequence of the decrease of thrombocyte production rather than their increased destruction [78].

All this implies that the model takes into account the key regulatory mechanisms in thrombopoietic system in humans under normal conditions. The qualitative and quantitative agreement of the modeling predictions with relevant clinical observations testifies to the successful identification and verification of this model. Thus, the latter can be used as a basis in modeling studies of radiation effects on thrombopoiesis in humans.

7.3.2 Granulopoietic System

To describe the dynamics of the granulopoietic system in humans under normal conditions, Eqs. (7.1)–(7.6) can be reduced to Eqs. (7.1)–(7.4) with $N = 0$ and $x_i^{\mathrm{ud}} \equiv x_i$ ($i = 1, \ldots, 4$) in them. In turn, Eqs. (7.11)–(7.20) can be reduced to Eqs. (7.11)–(7.14) with $x_i^{\mathrm{ud}} \equiv x_i$ ($i = 1, \ldots, 4$) in them. The parameter F in Eqs. (7.2) and (7.3) is determined by Eq. (7.9) with $x_3^{\mathrm{ud}} \equiv x_3$, $x_3^{\mathrm{d}} = 0$, and $x_3^{\mathrm{hd}} = 0$. The parameter F in Eqs. (7.12) and (7.13) is determined by Eq. (7.26) with $x_3^{\mathrm{ud}} \equiv x_3$, $x_3^{\mathrm{wd}} = 0$, $x_3^{\mathrm{md}} = 0$, and $x_3^{\mathrm{hd}} = 0$. Obviously, the systems of the differential equations obtained in this way are identical to each other and to Eqs. (1.60)–(1.63), which describe the dynamics of the granulopoietic system in mammals under normal conditions (see Chap. 1).

To study analytically the dynamics of the granulopoietic system in humans under normal conditions, the simplified version of the model [Eqs. (1.60)–(1.63)] was used (see Chap. 1). This version of the model considers the dynamics of the concentration of granulocytes outside the bone marrow instead of the dynamics of the concentration of blood granulocytes and the concentration of tissue granulocytes. As a result, Eqs. (1.60)–(1.63) are reduced to Eqs. (1.49)–(1.51).

The system of Eqs. (1.49)–(1.51) was investigated by methods of the qualitative theory of differential equations, oscillation theory, and bifurcation theory [71–76] (see Chap. 1). It was found that the system of Eqs. (1.49)–(1.51) has two singular points in the space of variables. The first of them is trivial. If $\alpha < \gamma$, then the second singular point has negative coordinates in the space of variables, i.e., it has no physical sense. If $\alpha = \gamma$, then the second singular point coincides with the first one. In both these cases, the trivial singular point is stable and can be identified with the state of the extinction of the granulopoietic system. This range of parameters of the granulopoiesis model ($\alpha \leq \gamma$) is not considered in what follows. If $\alpha > \gamma$, the first (trivial) singular point is unstable, whereas the second singular point with

positive coordinates $\bar{x}_i$ [Eqs. (1.53)–(1.55)] can be stable or unstable depending on the model parameter values. When the second singular point is stable, it can be identified with the state of the stable dynamic equilibrium (the homeostasis state) of the granulopoietic system and the values $\bar{x}_i$ ($i = 1, 2, 3$) are considered the normal concentrations of mature granulocytes and their bone marrow precursor cells. When the second singular point is unstable, one more particular solution appears. It is a stable limit cycle. This particular solution can be identified with stable oscillations of concentrations of mature granulocytes and their bone marrow precursor cells. Conditions of appearance of the cyclic granulopoiesis are given by inequalities (1.56)–(1.58) (see Chap. 1).

To study numerically the dynamics of the granulopoietic system in humans under normal conditions, the basic version of the model of this major hematopoietic lineage [Eqs. (1.60)–(1.63)] is used. For the convenience, Eqs. (1.60)–(1.63) are rewritten in terms of the new dimensionless variables, the latter being the ratios of the dimension concentrations of X_i ($i = 1, \ldots, 4$) cells, x_i ($i = 1, \ldots, 4$), to their stationary values $\bar{x}_i$ ($i = 1, \ldots, 4$) [Eqs. (1.64)–(1.67)].

The model of the granulopoietic system [Eqs.(1.60)–(1.63)] is employed to simulate the homeostasis state of this major hematopoietic lineage in healthy humans under normal conditions. This state is characterized by the normal concentrations of blood and tissue granulocytes and their bone marrow precursor cells. After deviation from this state, the granulopoietic system returns to it. It is found that such a dynamics of this major hematopoietic lineage is reproduced by the model [Eqs. (1.60)–(1.63)] with the normal values of its independent parameters α, γ, δ, ξ, ψ, m, l, θ_2, θ_3, and θ_4 (Table 7.2). The obtained modeling results are presented in Fig. 7.10.

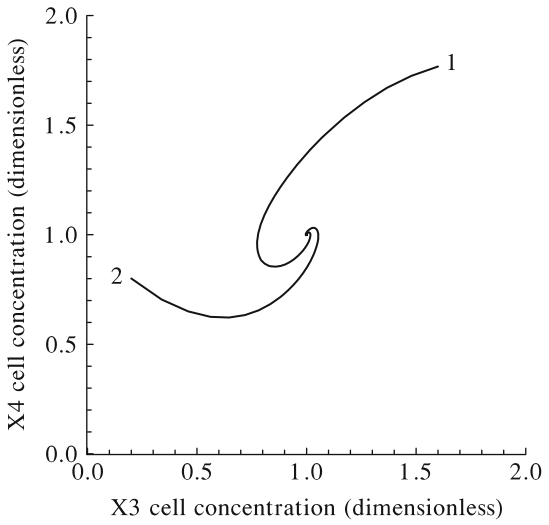

Fig. 7.10 Results of numerical studies of the human granulopoiesis model. Projections of two integral curves of the system of Eqs. (1.60)–(1.63) onto the plane of states $\{x_3\, x_4\}$. *Curves 1 and 2* converge to the stable second singular point [Eqs. (1.64)–(1.67)]

Figure 7.10 shows projections of two integral curves of the system of Eqs. (1.60)–(1.63) onto the plane of states $\{x_3\, x_4\}$. The concentrations of X_i $(i = 1, \ldots, 4)$ cells are computed in the dimensionless units as the ratios of the dimension concentrations of these cells, x_i $(i = 1, \ldots, 4)$, to their normal values, i.e., to the respective coordinates of the stable second singular point $\bar{x}_i$ $(i = 1, \ldots, 4)$. The values of coordinates of the stable second singular point in the dimensionless units are $(1, 1, 1, 1)$ by definition. As one can infer from Fig. 7.10, the integral curves converge to this point. In other words, the concentrations of X_i $(i = 1, \ldots, 4)$ cells return to their normal values $\bar{x}_i$ $(i = 1, \ldots, 4)$ after deviations from them. The obtained results imply that the model (1.60)–(1.63) with the normal values of its independent parameters is capable of reproducing the homeostasis state of the granulopoietic system under normal conditions.

The model of the granulopoietic system [Eqs. (1.60)–(1.63)] is also applied to simulate the cyclic dynamics of this system in humans under normal conditions. To reproduce such a behavior of this hematopoietic lineage by the model [Eqs. (1.60)–(1.63)], it turns out to be sufficient to increase the parameters γ and θ_4. The values of the rest of the parameters are taken to be equal to their normal values (Table 7.2). A set of these "oscillatory" values of the independent parameters of the granulopoiesis model ($\tilde{\alpha}$, $\tilde{\gamma}$, $\tilde{\delta}$, $\tilde{\psi}$, $\tilde{\xi}$, $\tilde{\theta}_1$, $\tilde{\theta}_2$, $\tilde{\theta}_3$, $\tilde{\theta}_4$, $\tilde{l}$, $\tilde{m}$) is given in Table 7.6. Results of the numerical studies of the granulopoiesis model with these "oscillatory" values of the independent parameters are presented in Figs. 7.11 and 7.12.

Figure 7.11 shows projections of three integral curves of the system of Eqs. (1.60)–(1.63) onto the plane of states $\{x_3\, x_4\}$. The concentrations of X_i $(i = 1, \ldots, 4)$ cells are computed in the dimensionless units as the ratios of the dimension cell concentrations x_i $(i = 1, \ldots, 4)$ to their stationary values, i.e., to values of the respective coordinates of the unstable second singular point $\widetilde{\bar{x}}_i$ $(i = 1, \ldots, 4)$. The values of coordinates of the unstable second singular point in the dimensionless units are $(1, 1, 1, 1)$ by definition. In Fig. 7.11, the closed curve is a limit cycle and two other curves converge to it from the outside and inside. These modeling results prove the existence of the stable limit cycle in the system of

Table 7.6 "Oscillatory" values of parameters of the granulopoiesis model for humans

Parameter	Value	Dimension
$\alpha \equiv \tilde{\alpha}$	2.4	day^{-1}
$\gamma \equiv \tilde{\gamma}$	1.4	day^{-1}
$\delta \equiv \tilde{\delta}$	0.2	day^{-1}
$\psi \equiv \tilde{\psi}$	2.2	day^{-1}
$\xi \equiv \tilde{\xi}$	0.2	day^{-1}
$m \equiv \tilde{m}$	0.5	1
$l \equiv \tilde{l}$	1.0	1
$\theta_1 \equiv \tilde{\theta}_1$	1.0	1
$\theta_2 \equiv \tilde{\theta}_2$	0.1	1
$\theta_3 \equiv \tilde{\theta}_3$	0.05	1
$\theta_4 \equiv \tilde{\theta}_4$	2.5	1

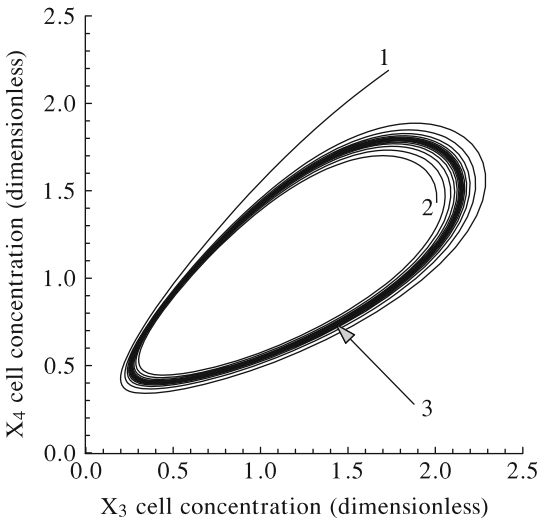

Fig. 7.11 Results of numerical studies of the human granulopoiesis model. Projections of three integral curves of the system of Eqs. (1.60)–(1.63) onto the plane of states $\{x_3\, x_4\}$. *Curves 1 and 2* converge to the limit cycle (*closed curve* labeled by 3)

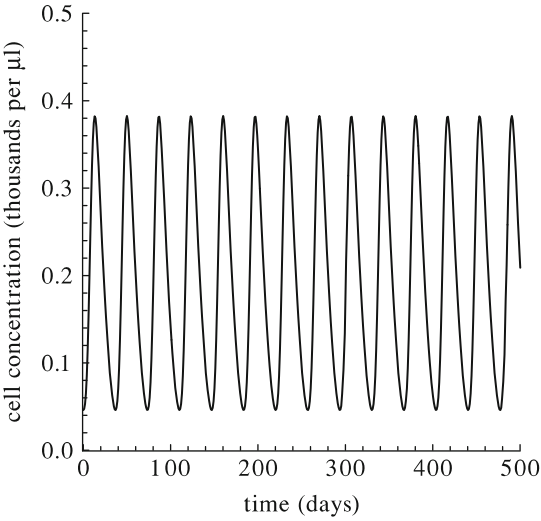

Fig. 7.12 Results of numerical studies of the human granulopoiesis model [Eqs. (1.60)–(1.63)]. The cyclic dynamics of the blood granulocyte concentration given in the standard units

Eqs. (1.60)–(1.63). This behavior of system of Eqs. (1.60)–(1.63) can be identified with the stable oscillations of the cell concentrations in the granulopoietic system.

Next, the concentrations of X_i $(i = 1, \ldots, 4)$ cells are expressed in the dimensionless units as the ratios of the dimension cell concentrations x_i $(i = 1, \ldots, 4)$ to their normal values, i.e., to the respective coordinates of the stable second singular point $\bar{x}_i$ $(i = 1, \ldots, 4)$. For this purpose, computed values of the dimensionless concentrations of X_i $(i = 1, \ldots, 4)$ cells, $x_i/\widetilde{\bar{x}}_i$ $(i = 1, \ldots, 4)$, are multiplied by factors R_i $(i = 1, \ldots, 4)$. The latter are equal to the ratios of the coordinates of the unstable singular point $\widetilde{\bar{x}}_i$ $(i = 1, \ldots, 4)$ to the respective coordinates of the stable singular point $\bar{x}_i$ $(i = 1, \ldots, 4)$.

As it follows from Eqs. (1.60)–(1.63), the ratio of the coordinate $\widetilde{\bar{x}_3}$ of the unstable second singular point to the coordinate $\bar{x}_3$ of the stable second singular point, if the dimensionless quantities $m = M\bar{x}_3^2$ and $l = L\bar{x}_3^2$ are invariants, is determined by the following formula:

$$R_3 = \frac{\psi}{\tilde{\psi}} \frac{(\tilde{\alpha} - \tilde{\gamma})}{(\alpha - \gamma)} \frac{[1 + \theta_2(\gamma/\delta)(1 + l)/(1 + m) + \theta_3(\gamma/\psi) + \theta_4(\gamma/\xi)]}{[1 + \widetilde{\theta_2}(\tilde{\gamma}/\tilde{\delta})(1 + \tilde{l})/(1 + \tilde{m}) + \widetilde{\theta_3}(\tilde{\gamma}/\tilde{\psi}) + \widetilde{\theta_4}(\tilde{\gamma}/\tilde{\xi})]}. \tag{7.45}$$

In turn, the quantities R_1, R_2, and R_4 are expressed in terms of R_3 in the following way:

$$R_1 = R_3 \frac{\tilde{\psi}}{\psi} \frac{\gamma}{\tilde{\gamma}}, \tag{7.46}$$

$$R_2 = R_3 \frac{\tilde{\psi}}{\psi} \frac{\delta}{\tilde{\delta}}, \tag{7.47}$$

$$R_4 = R_3 \frac{\tilde{\psi}}{\psi} \frac{\xi}{\tilde{\xi}}. \tag{7.48}$$

Remind that the normal and "oscillatory" values of the independent parameters of the granulopoiesis model (α, γ, δ, ψ, ξ, θ_1, θ_2, θ_3, θ_4, m, l and $\tilde{\alpha}$, $\tilde{\gamma}$, $\tilde{\delta}$, $\tilde{\psi}$, $\tilde{\xi}$, $\tilde{\theta}_1$, $\tilde{\theta}_2$, $\tilde{\theta}_3$, $\tilde{\theta}_4$, $\tilde{l}$, $\tilde{m}$, respectively) are given in Tables 7.2 and 7.6.

Further on, the concentration of X_3 cells is expressed in the standard units. For this purpose, the computed values of the dimensionless concentration of X_3 cells, $x_3/\widetilde{\bar{x}_3}$, is multiplied by R_3 [Eq. (7.45)] and by the normal value of the concentration of blood neutrophils prevailing in the pool of blood granulocytes. This normal value given in the standard units is 3.9 thousands per μl [26].

Figure 7.12 shows the modeling dynamics of the blood neutrophil concentration. As one can see, the blood neutrophil concentration fluctuates around the level of 0.214 thousands per μl, which is less than its normal level (3.9 thousands per μl). These modeling results can be identified with the dynamics of the concentration of blood neutrophils in patients with cyclic neutropenia [81–84]. This rare hematological disorder is characterized by stable oscillations of the concentration of blood neutrophils around the levels decreased in comparison with the normal one [25, 81–84]. As one can infer from Fig. 7.12, the period of oscillations of the blood neutrophil concentration predicted by the model is about 37 days. This result lies within the range of the clinical observations (15–50 days) [79, 81–84]. In turn, the concentration of the blood neutrophil oscillates between 0.046 thousands per μl and 0.382 thousands per μl. This modeling result also lies within the range of the clinical observations [79, 81–84]. Moreover, the modeling results are in a good agreement with the clinical data [83], according to which the concentration of the blood neutrophil oscillates between 0.05 thousands per μl and 0.5 thousands per μl in a patient.

Proceeding from the results of analytical and numerical investigations of the granulopoiesis model, the following biological interpretation of the causes of cyclic neutropenia in humans can be proposed. This hematological disorder is due to failures of some regulatory mechanisms in the granulopoietic system. They are manifested in (1) the decrease of the time the cells spend passing through X_1 compartment, i.e., the decrease of the period, during which bone marrow precursor cells are capable of dividing, and (2) the enhancing of the influence of the contribution of X_3 cells to the regulatory mechanism of the reproduction rate of X_1 cells. These failures lead to the decrease of timely production of granulocytes.

All this shows that the model takes into account the key regulatory mechanisms in the granulopoietic system in humans under normal conditions. The qualitative and quantitative agreement of the modeling predictions with relevant clinical observations testifies to the successful identification and verification of this model. Thus, it can be used as a basis in modeling studies of radiation effects on the granulopoietic system in humans.

7.3.3 Lymphopoietic System

To describe the dynamics of the lymphopoietic system in humans under normal conditions, Eqs. (7.1)–(7.3), (7.5), (7.6) can be reduced to Eqs. (7.1)–(7.3) with $N = 0$ and $x_i^{\mathrm{ud}} \equiv x_i$ $(i = 1, \ldots, 3)$ in them. In turn, Eqs. (7.11)–(7.13), (7.15)–(7.17), (7.19), (7.20) can be reduced to Eqs. (7.11)–(7.13) with $x_i^{\mathrm{ud}} \equiv x_i$ $(i = 1, \ldots, 3)$ in them. Remind that the parameter F in Eqs. (7.2) and (7.3), as well as in Eqs. (7.12) and (7.13), is a constant ($F \equiv \delta$) in the lymphopoiesis model. Obviously, the systems of the differential equations obtained in this way are identical to each other and to Eqs. (1.40)–(1.42), which describe the dynamics of the lymphopoietic system in mammals under normal conditions (see Chap. 1).

The system of Eqs. (1.40)–(1.42) was investigated by methods of the qualitative theory of differential equations, oscillation theory, and bifurcation theory [71–76] (see Chap. 1). It was found that the system of Eqs. (1.40)–(1.42) has two singular points in the space of variables. The first of them is trivial. If $\alpha < \gamma$, then the second singular point has negative coordinates in the space of variables, i.e., it has no physical sense. If $\alpha = \gamma$, then the second singular point coincides with the first one. In both these cases, the trivial singular point is stable and can be identified with the state of the extinction of the lymphopoietic system. This range of parameters of the lymphopoiesis model ($\alpha \leq \gamma$) is not considered in what follows. If $\alpha > \gamma$, then the first (trivial) singular point is unstable, whereas the second singular point with positive coordinates $\bar{x}_i$ [Eqs. (1.43)–(1.45)] can be stable or unstable depending on the values of model parameters. When the second singular point is stable, it can be identified with the state of the stable dynamic equilibrium (the homeostasis state) of the lymphopoietic system under normal conditions and the values $\bar{x}_i$ can be

considered the normal concentrations of blood lymphocytes and their bone marrow precursor cells. When the second singular point is unstable, one more particular solution appears: a stable limit cycle. This particular solution can be identified with stable oscillations of the concentrations of blood lymphocytes and their bone marrow precursor cells. Conditions of appearance of the cyclic lymphopoiesis are given by inequalities (1.46)–(1.48) (see Chap. 1).

The model [Eqs. (1.40)–(1.42)] is used to study numerically the dynamics of the lymphopoietic system in humans under normal conditions. For the convenience, Eqs. (1.40)–(1.42) are rewritten in terms of the new dimensionless variables, the latter being the ratios of the dimension concentrations of X_i ($i = 1, 2, 3$) cells, x_i ($i = 1, 2, 3$), to their stationary values $\bar{x}_i$ ($i = 1, 2, 3$) [Eqs. (1.43)–(1.45].

Specifically, the model of the lymphopoietic system [Eqs. (1.40)–(1.42)] is applied to simulate the state of the stable dynamic equilibrium (the homeostasis state) of this system in healthy humans under normal conditions. The homeostasis state is characterized by the normal concentrations of blood lymphocytes and their bone marrow precursors cells. After deviation from this state, the lymphopoietic system returns to it. Such a behavior of the lymphopoietic system in healthy humans is reproduced by the lymphopoiesis model [Eqs. (1.40)–(1.42)] with the normal values of the independent parameters α, γ, δ, ψ, θ_1, θ_2, and θ_3 (Table 7.3). The respective modeling results are presented in Fig. 7.13.

Figure 7.13 shows projections of two integral curves of the system of Eqs. (1.40)–(1.42) onto the plane of states $\{x_2\, x_3\}$. The concentrations of X_i ($i = 1, 2, 3$) cells are computed in dimensionless units as the ratios of the dimension concentrations of these cells, x_i ($i = 1, 2, 3$), to their normal values, i.e., to the respective coordinates of the stable second singular point $\bar{x}_i$ ($i = 1, 2, 3$). The values of coordinates of the

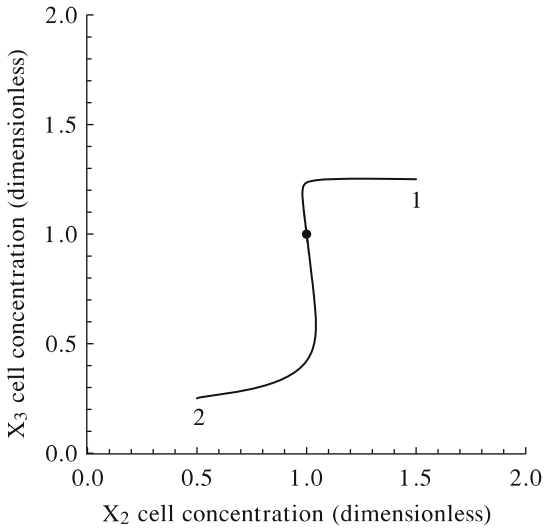

Fig. 7.13 Results of numerical studies of the human lymphopoiesis model. Projections of two integral curves of the system of Eqs. (1.40)–(1.42) onto the plane of states $\{x_2\, x_3\}$. *Curves 1 and 2* converge to the stable second singular point [Eqs. (1.43)–(1.45)]

stable second singular point in these dimensionless units is $(1, 1, 1)$ by definition. As one can see, the integral curves converge to this point. The obtained results argue that the model [Eqs. (1.40)–(1.42)] with the normal values of the parameters is capable of reproducing the homeostasis state of the lymphopoietic system under normal conditions. In other words, this model is capable of reproducing the returning of concentrations of X_1, X_2, and X_3 cells to their normal values $\bar{x}_i$ $(i = 1, 2, 3)$ [Eqs. (1.43)–(1.45)] after deviations from them.

It is worthwhile to note that the similar behavior of the lymphopoietic system was observed in patients received allogeneic stem cell transplantation [85]. The model of the lymphopoietic system [Eqs. (1.40)–(1.42)] is employed to simulate the dynamics of this major hematopoietic lineage in such patients. Initial concentrations of X_1, X_2, and X_3 cells in the modeling simulation are chosen in such a way as to reproduce the real dynamics of the blood lymphocyte concentration in those patients. The obtained modeling results and the respective clinical data [85] are presented in Fig. 7.14. As one can infer from this figure, they agree with each other. The obtained agreement of the modeling results and the clinical data [85] demonstrates the potential application of the developed model as a tool in the theoretical studies of recovering processes in the human lymphopoietic system after allogenic stem cell transplantation.

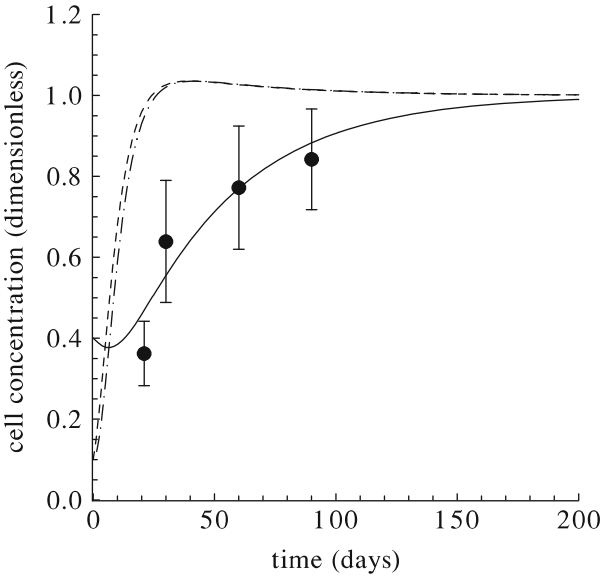

Fig. 7.14 The dynamics of dimensionless concentrations of X_1 cells (*dashed curve*), X_2 cells (*dot-dashed curve*), and X_3 cells (*solid curve*) obtained in the framework of the human lymphopoiesis model [Eqs. (1.40)–(1.42)], where the initial concentrations of the aforementioned cells are below norm. The clinical data [85] on the dynamics of the dimensionless concentration of blood lymphocytes (X_3 cells) in patients, who had received allogeneic stem cell transplantation, are presented by mean values of the dimensionless concentration of blood lymphocytes (*circle*) and mean square deviations from these mean values

The model [Eqs. (1.40)–(1.42)] is also used to simulate the cyclic lymphopoiesis in humans under normal conditions. To reproduce such a behavior of the lymphopoietic system by the developed model, it turns out to be sufficient to increase the values of parameters α, γ, ψ, and θ_3 and to decrease the value of parameter δ. The parameter θ_2 is taken to be equal to its normal value (Table 7.3). The set of these "oscillatory" values of the independent parameters of the lymphopoiesis model is given in Table 7.7. Results of the numerical studies of the lymphopoiesis model with these "oscillatory" values of the independent parameters ($\tilde{\alpha}$, $\tilde{\gamma}$, $\tilde{\delta}$, $\tilde{\psi}$, $\tilde{\theta}_1$, $\tilde{\theta}_2$, and $\tilde{\theta}_3$) are presented in Figs. 7.15 and 7.16.

Figure 7.15 shows projections of three integral curves of the system of Eqs. (1.40)–(1.42) onto the plane of states $\{x_2\, x_3\}$. The concentrations of X_i ($i = 1, 2, 3$) cells are computed in the dimensionless units as the ratios of the dimension cell concentrations x_i ($i = 1, 2, 3$) to their stationary values, i.e., to the respective coordinates of the unstable singular point $\widetilde{\widetilde{x}_i}$ ($i = 1, 2, 3$). The values of coordinates of the unstable second singular point in these dimensionless units is $(1, 1, 1)$ by definition. In Fig. 7.15, the closed curve is the limit cycle. Two other curves converge to the limit cycle from the outside and inside. These results

Table 7.7 "Oscillatory" values of parameters of the lymphopoiesis model for humans

Parameter	Value	Dimension
$\alpha \equiv \tilde{\alpha}$	10.0	day^{-1}
$\gamma \equiv \tilde{\gamma}$	1.0	day^{-1}
$\delta \equiv \tilde{\delta}$	0.2	day^{-1}
$\psi \equiv \tilde{\psi}$	0.1	day^{-1}
$\theta_1 \equiv \tilde{\theta}_1$	1.0	1
$\theta_2 \equiv \tilde{\theta}_2$	0.06	1
$\theta_3 \equiv \tilde{\theta}_3$	1.5	1

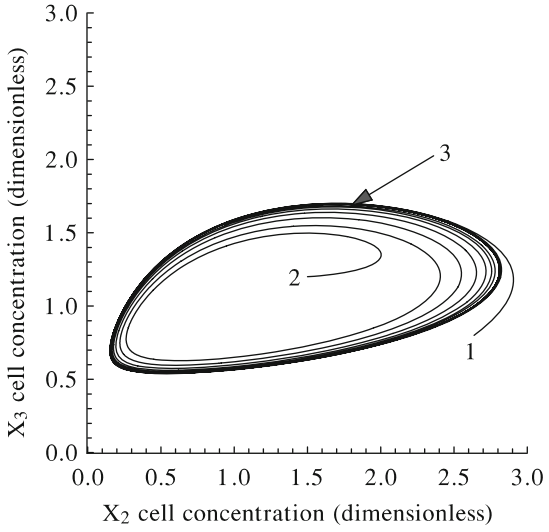

Fig. 7.15 Results of numerical studies of the human lymphopoiesis model. Projections of three integral curves of the system of Eqs. (1.40)–(1.42) onto the plane of states $\{x_2\, x_3\}$. *Curves 1 and 2* converge to the limit cycle (*closed curve* labeled by 3)

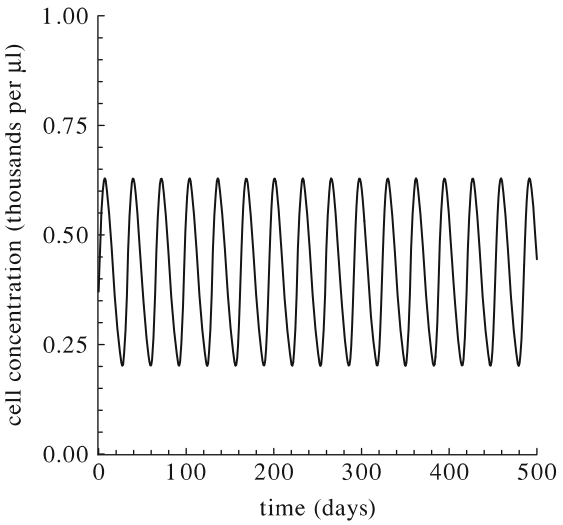

Fig. 7.16 Results of numerical studies of the human lymphopoiesis model [Eqs. (1.40)–(1.42)]. The cyclic dynamics of the blood lymphocyte concentration given in the standard units

attest to the stability of the limit cycle, i.e., they argue that the developed model is capable of reproducing the stable oscillations of cell concentrations in the human lymphopoietic system.

Next, the concentrations of the aforementioned cells are expressed in the dimensionless units as the ratios of the dimension concentrations of X_i $(i = 1, 2, 3)$ cells, x_i $(i = 1, 2, 3)$, to their normal values, i.e., to the respective coordinates of the stable second singular point $\bar{x}_i$ $(i = 1, 2, 3)$ [Eqs. (1.33)–(1.35)]. For this purpose, computed values of the dimensionless concentrations of X_i $(i = 1, 2, 3)$ cells, $x_i/\widetilde{\bar{x}}_i$ $(i = 1, 2, 3)$, are multiplied by factors R_i $(i = 1, 2, 3)$. The latter are equal to the ratios of the coordinates of the unstable singular point $\widetilde{\bar{x}}_i$ $(i = 1, 2, 3)$ to the respective coordinates of the stable singular point $\bar{x}_i$ $(i = 1, 2, 3)$ [Eq. (7.38)].

As it follows from Eqs. (1.43)–(1.45), the ratio of the coordinate $\widetilde{\bar{x}}_3$ of the unstable second singular point to the coordinate $\bar{x}_3$ of the stable second singular point is determined by the following formula:

$$R_3 = \frac{\psi}{\tilde{\psi}} \frac{(\tilde{\alpha} - \tilde{\gamma})}{(\alpha - \gamma)} \frac{[1 + \theta_2(\gamma/\delta) + \theta_3(\gamma/\psi)]}{[1 + \widetilde{\theta}_2(\tilde{\gamma}/\tilde{\delta}) + \widetilde{\theta}_3(\tilde{\gamma}/\tilde{\psi})]}. \tag{7.49}$$

In turns, the quantities R_1 and R_2 are expressed in terms of R_3 in the following way:

$$R_1 = R_3 \frac{\tilde{\psi}}{\psi} \frac{\gamma}{\tilde{\gamma}}, \tag{7.50}$$

$$R_2 = R_3 \frac{\tilde{\psi}}{\psi} \frac{\delta}{\tilde{\delta}}. \tag{7.51}$$

Remind that the normal and "oscillatory" values of the independent parameters of the lymphopoiesis model (α, γ, δ, ψ, θ_1, θ_2, θ_3 and $\tilde{\alpha}$, $\tilde{\gamma}$, $\tilde{\delta}$, $\tilde{\psi}$, $\tilde{\theta}_1$, $\tilde{\theta}_2$, $\tilde{\theta}_3$, respectively) are given in Tables 7.3 and 7.7.

To compare the modeling dynamics of blood lymphocytes (X_3 cells) with the kinetics of these cells in patients with cyclic lymphocytopenia in more profound way, the modeling results on the concentration of blood lymphocytes (X_3 cells) are presented in the standard units. For this purpose, the computed values of the dimensionless concentration of X_3 cells, $x_3/\widetilde{x}_3$, are multiplied by the factor R_3 [Eq. (7.49)] and by the normal concentration of blood lymphocytes, $\bar{x}_3$, which is given in the standard units. This normal value is 1.8 thousands per μl [26].

Figure 7.16 shows the modeling results on the dynamics of the blood lymphocyte concentration given in standard units. As one can infer from this figure, the concentration of the blood lymphocytes oscillates between 0.20 thousands per μl and 0.63 thousands per μl around the level of 0.515 thousands per μl, which is lower than its normal level (1.8 thousands per μl). These modeling results can be identified with the dynamics of the concentration of blood lymphocytes in patients with the cyclic lymphocytopenia [79]. This rare hematological disorder is characterized by stable oscillations of the concentration of blood lymphocytes around a level lowered in comparison with the norm [79]. As one can see from Fig. 7.16, the period of these oscillations predicted by the lymphopoiesis model is about 32 days that conforms with clinical observations (15–35 day) [79].

Proceeding from the results of analytical and numerical investigations of the lymphopoiesis model, the following biological interpretation of the causes of cyclic lymphocytopenia in humans can be proposed. This hematological disorder is due to failures in some regulatory mechanisms in the lymphopoietic system. They are manifested in (1) the decrease of the time the cells spend passing through X_1 compartment, i.e., the decrease of the period, during which bone marrow precursor cells are capable of dividing, (2) the increase of the time the cells spend passing through X_2 compartment, i.e., the increase of the period of maturation of bone marrow precursor cells incapable of dividing, (3) the enhancing of the influence of the contribution of X_3 cells to the regulatory mechanism of the reproduction rate of X_1 cells, (4) the increase of the maximal specific rate α of the reproduction of X_1 cells, and (5) the decrease of the time the cells spend passing through X_3 compartment. The first three of them lead to the decrease of timely production of lymphocytes (X_3 cells). The fourth one is not able to compensate completely the decrease in the lymphocyte production. The fifth one leads to shortening of the mature lymphocyte life span and, as a consequence, to additional decrease of the blood erythrocyte concentration.

All this demonstrates that the model takes into account the key regulatory mechanisms in lymphopoietic system in humans under normal conditions. The qualitative and quantitative agreement of the modeling predictions with relevant clinical observations testifies to the successful identification and verification of this model. Thus, the latter can be used as a basis in modeling studies of radiation effects on the lymphopoietic system in humans.

7.3.4 *Erythropoietic System*

The dynamics of the erythropoietic system in human under normal conditions, as it was shown in Chap. 1, is described by same system of Eqs. (1.40)–(1.42), as the lymphopoietic system. Therefore, all the results of the analytic investigation of the lymphopoiesis model are valid for the erythropoiesis model.

The model of the erythropoietic system [Eqs. (1.40)–(1.42)] is used to study numerically the dynamics of this major hematopoietic lineage in humans under normal conditions. For the convenience, Eqs. (1.40)–(1.42) are rewritten in terms of the new dimensionless variables, the latter being the ratios of the dimension concentrations of X_i $(i = 1, 2, 3)$ cells, x_i $(i = 1, 2, 3)$, to their stationary values $\bar{x}_i$ $(i = 1, 2, 3)$ [Eqs. (1.43)–(1.45)].

The model [Eqs. (1.40)–(1.42)] is employed to simulate the state of the stable dynamic equilibrium (the homeostasis state) of the erythropoietic system in healthy humans under normal conditions. The homeostasis state is characterized by the normal concentrations of blood erythrocytes and their bone marrow precursors cells. After deviation from this state, the erythropoietic system returns to it. Such a behavior of the erythropoietic system in healthy humans is reproduced by the model [Eqs. (1.40)–(1.42)] with the normal values of the independent parameters α, γ, δ, ψ, θ_1, θ_2, and θ_3. The latter are given in Table 7.4. Results of the numerical study of the erythropoiesis model with these normal values of its parameters are presented in Fig. 7.17.

Figure 7.17 shows projections of two integral curves of the system of Eqs. (1.40)–(1.42) onto the plane of states $\{x_2\, x_3\}$. The concentrations of X_i $(i = 1, 2, 3)$ cells are computed in the dimensionless units as the ratios of the dimension concentrations of these cells, x_i $(i = 1, 2, 3)$, to their normal values, i.e., to the respective coordinates

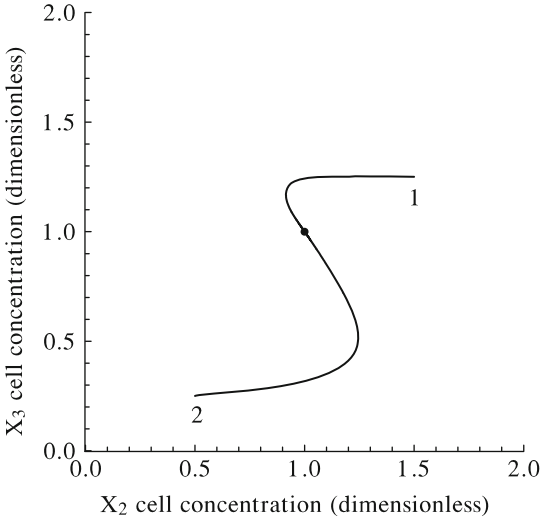

Fig. 7.17 Results of numerical studies of the human erythropoiesis model. Projections of two integral curves of the system of Eqs. (1.40)–(1.42) onto the plane of states $\{x_2\, x_3\}$. *Curves 1 and 2* converge to the stable second singular point [Eqs. (1.43)–(1.45)]

of the stable second singular point $\bar{x}_i$ $(i = 1, 2, 3)$. The values of coordinates of the stable second singular point in these dimensionless units are $(1, 1, 1)$ by definition. As one can see, the integral curves converge to this point. In other words, the concentrations of X_i $(i = 1, 2, 3)$ cells return to their normal values $\bar{x}_i$ $(i = 1, 2, 3)$ after deviations from them. The obtained results imply that the model (1.40)–(1.42) with the normal values of the parameters is capable of reproducing the homeostasis state of the erythropoietic system under normal conditions.

The model [Eqs. (1.40)–(1.42)] is also applied to simulate the cyclic erythropoiesis in humans under normal conditions. To reproduce such a behavior of the erythropoietic system by the developed model, it turns out to be sufficient to increase the parameters α, γ, and θ_3 and to decrease the parameter δ. The rest of the model parameters (namely, ψ, θ_1, and θ_2) are taken to be equal to their normal values (Table 7.4). A set of these "oscillatory" values of the independent parameters of the erythropoiesis model (namely, $\tilde{\alpha}$, $\tilde{\gamma}$, $\tilde{\delta}$, $\tilde{\psi}$, $\tilde{\theta}_1$, $\tilde{\theta}_2$, $\tilde{\theta}_3$) is given in Table 7.8. Results of the numerical studies of the erythropoiesis model with these "oscillatory" values of the independent parameters are presented in Figs. 7.18 and 7.19.

Table 7.8 "Oscillatory" values of parameters of the erythropoiesis model for humans

Parameter	Value	Dimension
$\alpha \equiv \tilde{\alpha}$	10.0	day^{-1}
$\gamma \equiv \tilde{\gamma}$	0.4	day^{-1}
$\delta \equiv \tilde{\delta}$	0.1	day^{-1}
$\psi \equiv \tilde{\psi}$	0.015	day^{-1}
$\theta_1 \equiv \tilde{\theta}_1$	1.0	1
$\theta_2 \equiv \tilde{\theta}_2$	0.1	1
$\theta_3 \equiv \tilde{\theta}_3$	1.0	1

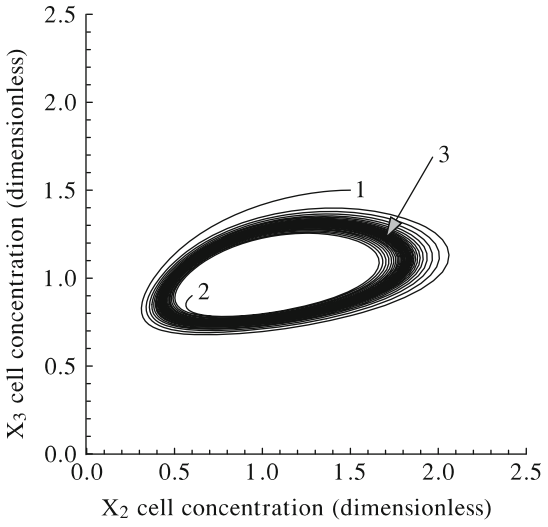

Fig. 7.18 Results of numerical studies of the human erythropoiesis model. Projections of three integral curves of the system of Eqs. (1.40)–(1.42) onto the plane of states $\{x_2\, x_3\}$. *Curves 1 and 2* converge to the limit cycle (*closed curve* labeled by 3)

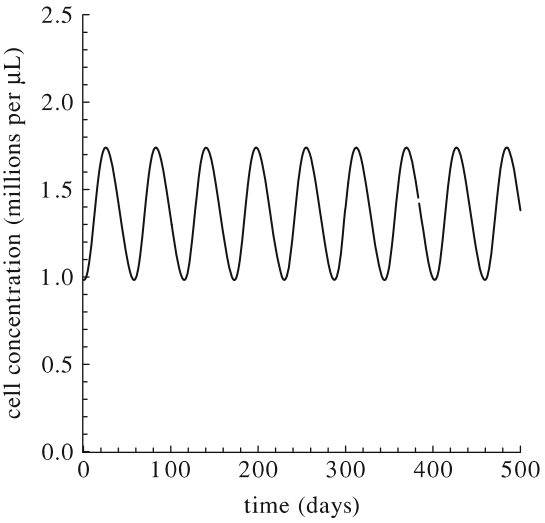

Fig. 7.19 Results of numerical studies of the human erythropoiesis model [Eqs. (1.40)–(1.42)]. The cyclic dynamics of the blood erythrocyte concentration given in the standard units

Figure 7.18 shows projections of three integral curves of the system of Eqs. (1.40)–(1.42) onto the plane of states $\{x_2, x_3\}$. The concentrations of X_i ($i = 1, 2, 3$) cells are computed in the dimensionless units as the ratios of the dimension concentrations of these cells, x_i ($i = 1, 2, 3$), to their stationary values, i.e., to the respective coordinates of the unstable singular point $\widetilde{\bar{x}}_i$ ($i = 1, 2, 3$). The values of coordinates of the unstable second singular point in these dimensionless units are $(1, 1, 1)$ by definition. In Fig. 7.18, the closed curve is the limit cycle. Two other curves converge to the limit cycle from the outside and inside. These results testify to the stability of the limit cycle, i.e., they prove that the developed model is capable of reproducing the stable oscillations of cell concentrations in the erythropoietic system in humans under normal conditions.

Next, the concentration of blood erythrocytes (X_3 cells) are expressed in the standard units. For this purpose, the computed values of the dimensionless concentration of X_3 cells, $x_3/\widetilde{\bar{x}}_3$, are multiplied by the factor R_3, which is the ratio of the coordinate $\widetilde{\bar{x}}_3$ of the unstable second singular point to the coordinate $\bar{x}_3$ of the stable second singular point, as well as by the normal value of the blood erythrocyte concentration given in the standard units. This normal value is 4.5 millions per μl [26]. In turn, the factor R_3 is determined by Eq. (7.49). The normal and "oscillatory" values of the independent parameters of the erythropoiesis model (α, γ, δ, ψ, θ_1, θ_2, θ_3 and $\tilde{\alpha}$, $\tilde{\gamma}$, $\tilde{\delta}$, $\tilde{\psi}$, $\tilde{\theta}_1$, $\tilde{\theta}_2$, $\tilde{\theta}_3$, respectively) entering Eq. (7.49) are given in Tables 7.4 and 7.8.

Figure 7.19 presents the modeling results on the cyclic dynamics of the blood erythrocyte concentration given in the standard units. As one can see, the concentration of the blood erythrocytes oscillates between 0.98 millions per μl and 1.74 millions per μl around the level of 1.36 millions per μl, which is lower than its normal level (4.5 millions per μl). These modeling results can be identified with the cyclic dynamics of the concentration of blood erythrocytes in patients with cyclic erythrocytopenia [25, 81–84]. This rare hematological disorder is characterized by

stable oscillations of the concentration of blood erythrocytes around a level lowered in comparison with the norm. As one can see from Fig. 7.19, the period of these oscillations predicted by the model is about 53 days that conforms with clinical observations (14–90 day) [79].

Proceeding from the results of analytical and numerical investigations of the erythropoiesis model, the following biological interpretation of the causes of cyclic erythrocytopenia in humans can be proposed. This hematological disorder is due to failures in some regulatory mechanisms in the erythropoietic system. They are manifested in (1) the decrease of the time the cells spend passing through X_1 compartment, i.e., the decrease of the period, during which bone marrow precursor cells are capable of dividing, (2) the increase of the time the cells spend passing through X_2 compartment, i.e., the increase of the period of maturation of bone marrow precursor cells incapable of dividing, (3) the enhancing of the influence of the contribution of X_3 cells to the regulatory mechanism of the reproduction rate of X_1 cells, and (4) the increase of the maximal specific rate α of the reproduction of X_1 cells. The first three of them lead to the decrease of timely production of erythrocytes (X_3 cells). The fourth one is not able to compensate completely the decrease in the erythrocyte production. Put together, these modeling findings indicate that the causes of the cyclic erythrocytopenia can be failure of timely production of erythrocytes.

All this attests that the model takes into account the key regulatory mechanisms in erythropoietic system in humans under normal conditions. The qualitative and quantitative agreement of the modeling predictions with relevant clinical observations testifies to the successful identification and verification of this model. Thus, the latter can be used as a basis in modeling studies of radiation effects on erythropoiesis in humans.

7.4 Effects of Acute Irradiation on the Human Major Hematopoietic Lineages

The developed models of the thrombopoietic, granulopoietic, lymphopoietic, and erythropoietic systems, which are presented in Sect. 7.2.2, are employed to investigate numerically the dynamics of these systems in humans exposed to acute irradiation. For the convenience, these models are rewritten in terms of the new dimensionless variables. The latter are the ratios of the dimension cell concentrations to their normal values.

In the modeling studies of effects of acute irradiation on the thrombopoietic, granulopoietic, lymphopoietic, and erythropoietic systems in humans, the radiation dose is varied in a wide range. The obtained results are presented in Figs. 7.20, 7.21, 7.22, 7.23, 7.24, 7.25, 7.26, 7.27, 7.28, 7.29, 7.30, 7.31, 7.32, 7.33, 7.34, 7.35, 7.36, 7.37, 7.38, and 7.39. Specifically, the dynamics of the concentrations of blood cells (X_3 cells) and their bone marrow precursor cells (X_1 and X_2 cells) in the

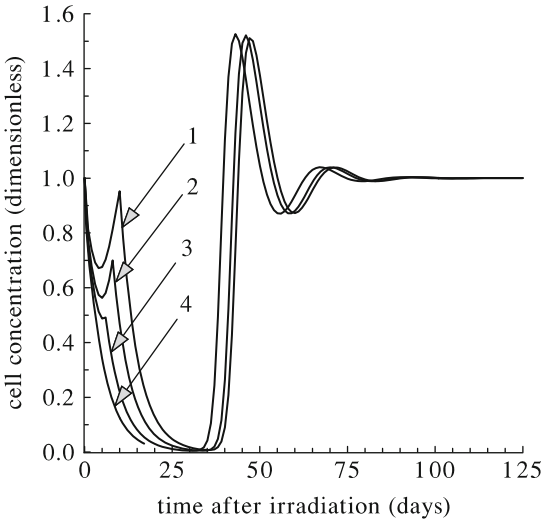

Fig. 7.20 The modeling dynamics of the dimensionless concentration of bone marrow precursor cells (X_1 and X_2 cells) in the thrombopoietic system of humans exposed to acute radiation with doses of 2.0, 3.0, 3.9, and 6.0 Gy (*curves 1–4*, respectively)

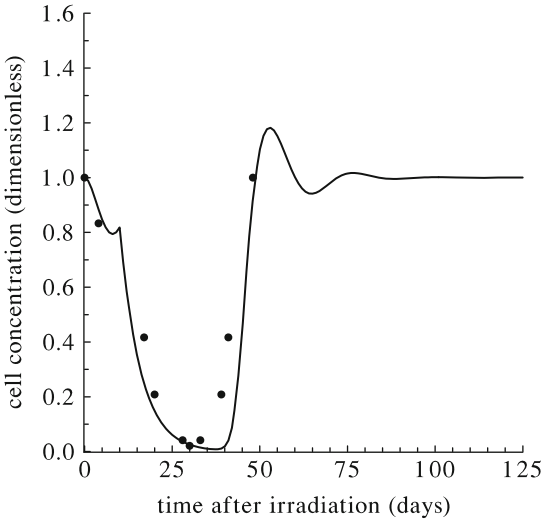

Fig. 7.21 The modeling dynamics of the dimensionless concentration of blood thrombocytes (X_3 cells) in the thrombopoietic system of humans exposed to acute irradiation with a dose of 2.0 Gy (*curve*) and the corresponding clinical data [69] (*circles*)

aforementioned major hematopoietic lineages in acutely irradiated humans are given in Figs. 7.21, 7.22, 7.23, 7.24, Figs. 7.26, 7.27, 7.28, 7.29, Figs. 7.31, 7.32, 7.33, 7.34, Figs. 7.36, 7.37, 7.38, 7.39 and in Figs. 7.20, 7.25, 7.30, 7.35, respectively.

For the beginning, let us consider the modeling dynamics of the thrombopoietic, granulopoietic, lymphopoietic, and erythropoietic systems in humans exposed to acute irradiation with not high doses. As one can infer from Figs. 7.20, 7.25, 7.30, and 7.35, the concentrations of bone marrow precursor cells in the systems on hand start to decrease after such exposures and soon achieve the first minimum values. Then the concentrations increase in the course of the abortive rise and reach the respective maximum abortive rise values. After that the concentrations

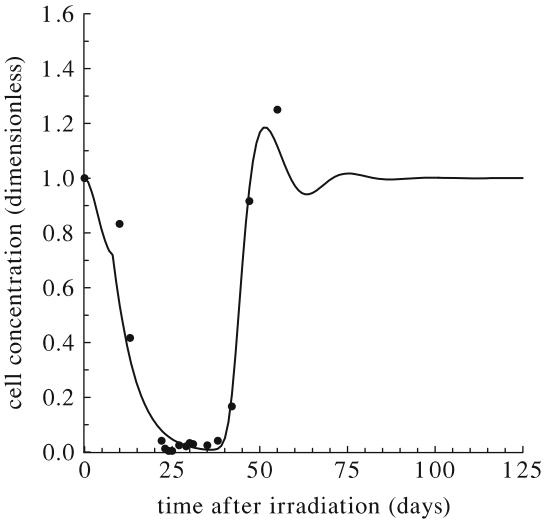

Fig. 7.22 The modeling dynamics of the dimensionless concentration of blood thrombocytes (X_3 cells) in the thrombopoietic system of humans exposed to acute irradiation with a dose of 3.0 Gy (*curve*) and the corresponding clinical data [60] (*circles*)

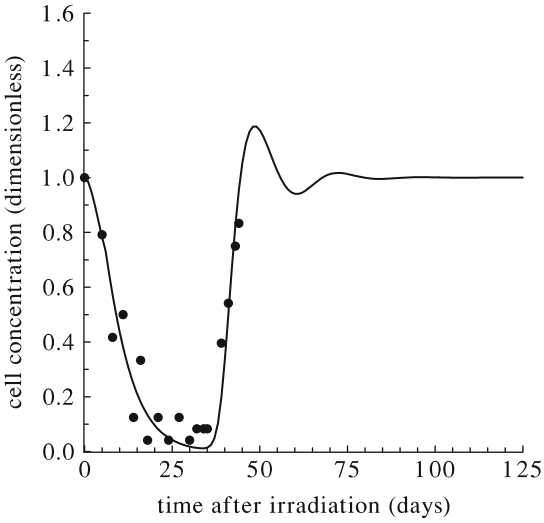

Fig. 7.23 The modeling dynamics of the dimensionless concentration of blood thrombocytes (X_3 cells) in the thrombopoietic system of humans exposed to acute irradiation with a dose of 3.9 Gy (*curve*) and the corresponding clinical data [70] (*circles*)

of bone marrow precursor cells decrease to the second minimal values. Then these concentrations increase again and, after damped oscillations in the thrombopoietic and granulopoietic systems and overdamped oscillations in the lymphopoietic and erythropoietic systems, return to their normal levels.

As it follows from Figs. 7.21, 7.22, 7.23, 7.24, 7.26, 7.27, 7.28, 7.29, 7.31, 7.32, 7.33, 7.34, and 7.36, 7.37, 7.38, 7.39, the dynamics of the concentrations of blood cells in the thrombopoietic, granulopoietic, lymphopoietic, and erythropoietic systems is similar to that of the concentrations of their bone marrow precursor cells. Though, the abortive rises of the concentrations of thrombocytes, granulocytes, and lymphocytes are much less pronounced in comparison with abortive rises

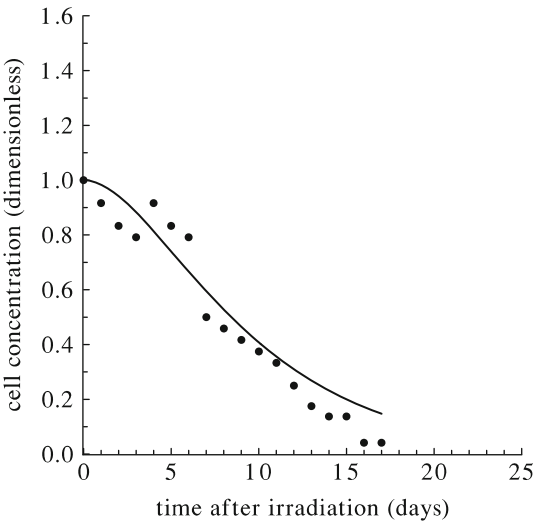

Fig. 7.24 The modeling dynamics of the dimensionless concentration of blood thrombocytes (X_3 cells) in the thrombopoietic system of humans exposed to acute irradiation with a dose of 6.0 Gy (*curve*) and the corresponding clinical data [60] (*circles*)

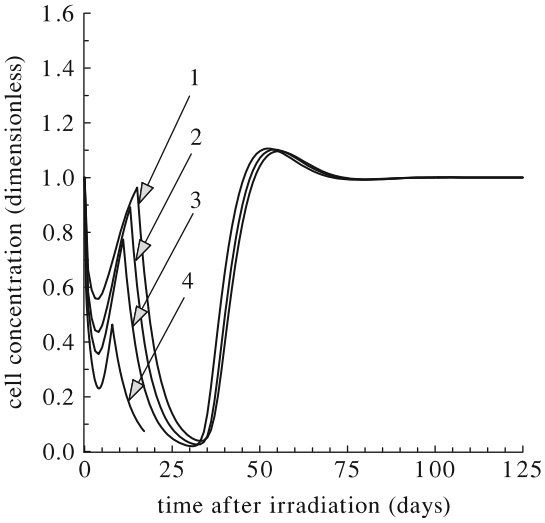

Fig. 7.25 The modeling dynamics of the dimensionless concentration of bone marrow precursor cells (X_1 and X_2 cells) in the granulopoietic system of humans exposed to acute radiation with doses of 2.0, 3.0, 3.9, and 6.0 Gy (*curves 1–4*, respectively)

of concentrations of their bone marrow precursor cells. The abortive rise of the concentration of mature blood erythrocytes is also much less pronounced in comparison with that of the concentrations of their bone marrow precursor cells and blood reticulocytes.

The juxtaposition of the obtained modeling predictions with real clinical data [60, 61, 69, 70, 86], which are also presented in Figs. 7.21, 7.22, 7.23, 7.24, 7.26, 7.27, 7.28, 7.29, 7.31, 7.32, 7.33, 7.34, and 7.36, 7.37, 7.38, 7.39, demonstrates that the models provide a qualitative and quantitative description of the postirradiation injury and recovery of the thrombopoietic, granulopoietic, lymphopoietic, and

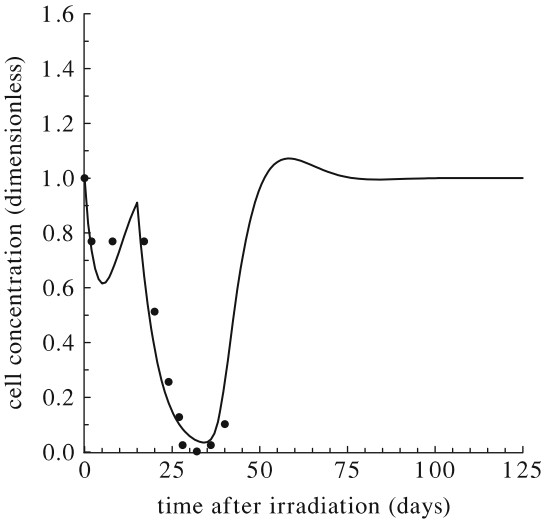

Fig. 7.26 The modeling dynamics of the dimensionless concentration of blood granulocytes (X_3 cells) in the granulopoietic system of a human exposed to acute irradiation with a dose of 2.0 Gy (*curve*) and the corresponding clinical data [69] (*circles*)

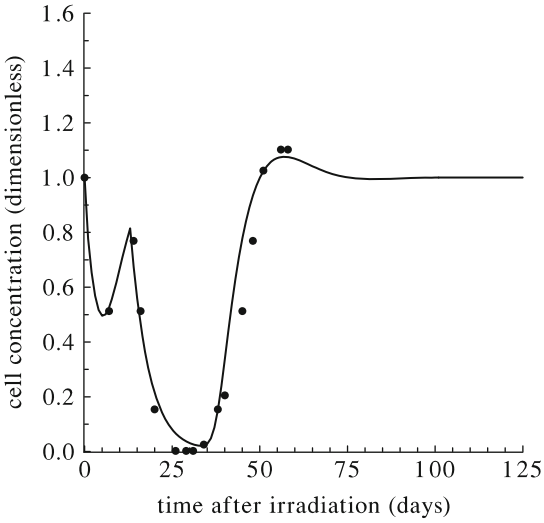

Fig. 7.27 The modeling dynamics of the dimensionless concentration of blood granulocytes (X_3 cells) in the granulopoietic system of a human exposed to acute irradiation with a dose of 3.0 Gy (*curve*) and the corresponding clinical data [60] (*circles*)

erythropoietic systems in humans exposed to acute irradiation in the considered range of doses.

It is worthwhile to note the following modeling findings. As one can infer from Figs. 7.20, 7.21, 7.22, 7.23, 7.24, 7.25, 7.26, 7.27, 7.28, 7.29, 7.30, 7.31, 7.32, 7.33, 7.34, 7.35, 7.36, 7.37, 7.38, and 7.39, the first and the second minimal values of concentrations of blood cells and their bone marrow precursor cells in the systems on hand, as well as their maximum abortive rise values, are smaller at larger doses of acute irradiation in the dose range under consideration. It is important to emphasize that these modeling predictions agree with clinical observations [60, 63].

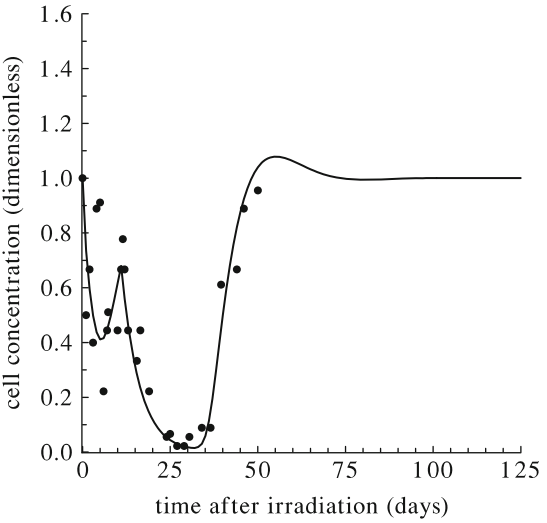

Fig. 7.28 The modeling dynamics of the dimensionless concentration of blood granulocytes (X_3 cells) in the granulopoietic system of a human exposed to acute irradiation with a dose of 3.9 Gy (*curve*) and the corresponding clinical data [70] (*circles*)

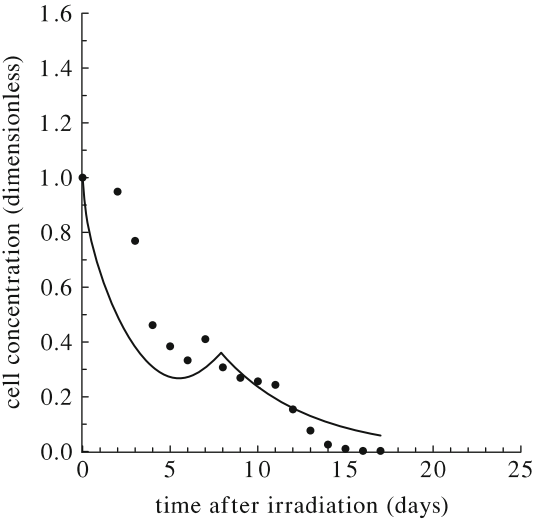

Fig. 7.29 The modeling dynamics of the dimensionless concentration of blood granulocytes (X_3 cells) in the granulopoietic system of a human exposed to acute irradiation with a dose of 6.0 Gy (*curve*) and the corresponding clinical data [60] (*circles*)

Modeling studies reveal the following reason-consequence relations, which cause these features of the dynamics of the thrombopoietic, granulopoietic, lymphopoietic, and erythropoietic systems in humans exposed to acute radiation in the considered range of doses. Specifically, the first minimal values of the concentrations of blood cells and their bone marrow precursor cells in these systems are smaller at smaller total amounts of the respective capable of dividing bone marrow precursor cells, which did not obtain any damages or obtained weak damages in the result of acute irradiation. The second minimal values of the concentrations of blood cells and their bone marrow precursor cells in the systems on hand are smaller at smaller amounts of the respective capable of dividing bone marrow precursor cells, which

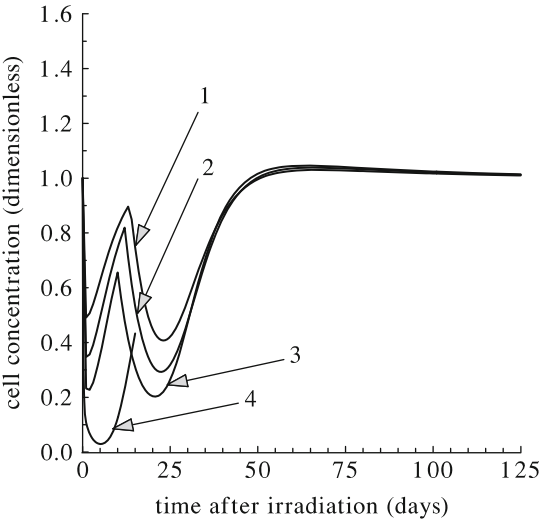

Fig. 7.30 The modeling dynamics of the dimensionless concentration of bone marrow precursor cells (X_1 and X_2 cells) in the lymphopoietic system of humans exposed to acute radiation with doses of 1.1, 2.0, 3.0, and 6.0 Gy (*curves 1–4*, respectively)

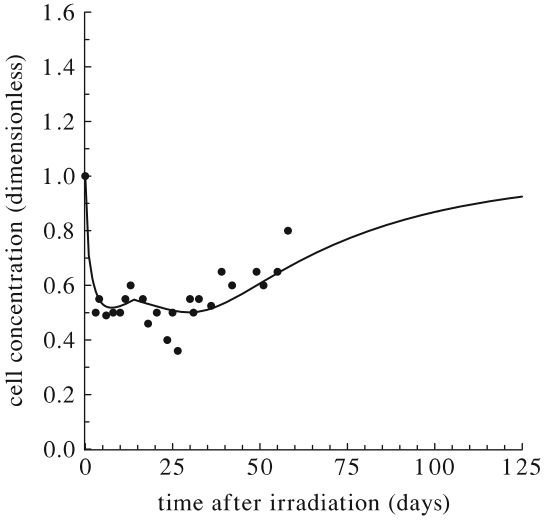

Fig. 7.31 The modeling dynamics of the dimensionless concentration of blood lymphocytes (X_3 cells) in the lymphopoietic system of humans exposed to acute irradiation with a dose of 1.1 Gy (*curve*) and the corresponding clinical data [86] (*circles*)

did not obtain any damages in the result of acute exposure. The maximum abortive rise values of the concentrations of blood cells and their bone marrow precursor cells in the systems under consideration are smaller at smaller total amounts of the respective capable of dividing bone marrow precursor cells, which did not obtain any damages or obtained weak damages in the result of acute irradiation. In turn, as it is found, the aforementioned quantities (namely, the total amounts of the respective capable of dividing bone marrow precursor cells without any damages and with weak damages and the amounts of the respective capable of dividing bone marrow precursor cells without any damages in the systems on hand after acute

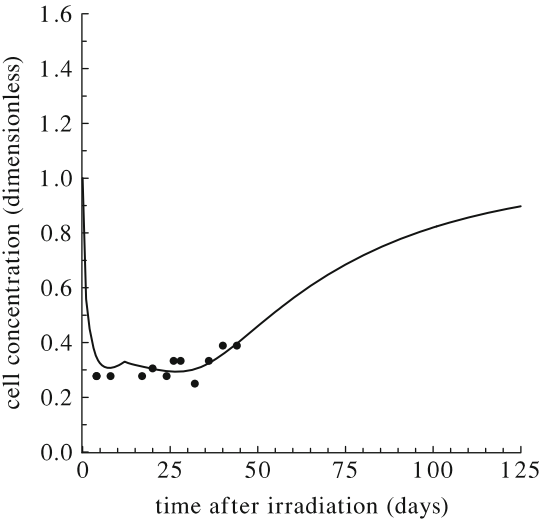

Fig. 7.32 The dynamics of the dimensionless concentration of blood lymphocytes (X_3 cells) in the lymphopoietic system of humans exposed to acute irradiation with a dose of 2.0 Gy (*curve*) and the corresponding clinical data [69] (*circles*)

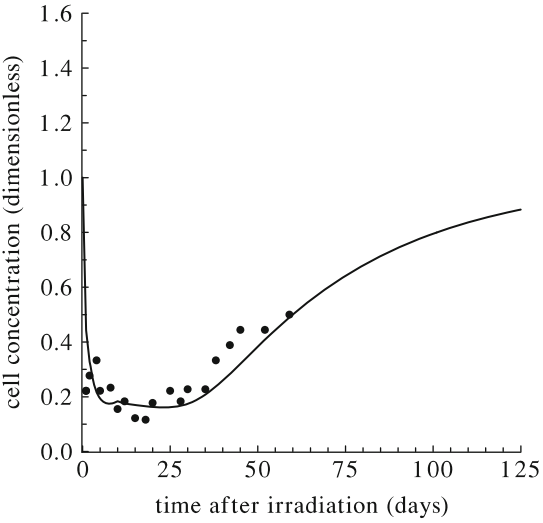

Fig. 7.33 The modeling dynamics of the concentration of blood lymphocytes (X_3 cells) in the lymphopoietic system of humans exposed to acute irradiation at the dose of 3.0 Gy (*curve*) and the corresponding clinical data [61] (*circles*)

irradiation), which are determined by Eqs. (7.27), (7.28), (7.34), and (7.35), really decrease with the increase of the dose of acute irradiation in the dose range under consideration.

Let us proceed now to the modeling dynamics of the thrombopoietic, granulopoietic, lymphopoietic, and erythropoietic systems in humans exposed to acute irradiation with high doses. Figures 7.20, 7.24, 7.25, 7.29, 7.30, 7.34, 7.35, and 7.39 show that the concentrations of the blood cells (X_3 cells) and their bone marrow precursor cells (X_1 and X_2 cells) in these systems abruptly decrease to very low levels after such exposures. The juxtaposition of the obtained modeling results with the relevant clinical data [60, 61] presented in Figs. 7.24, 7.29, 7.34, and 7.39

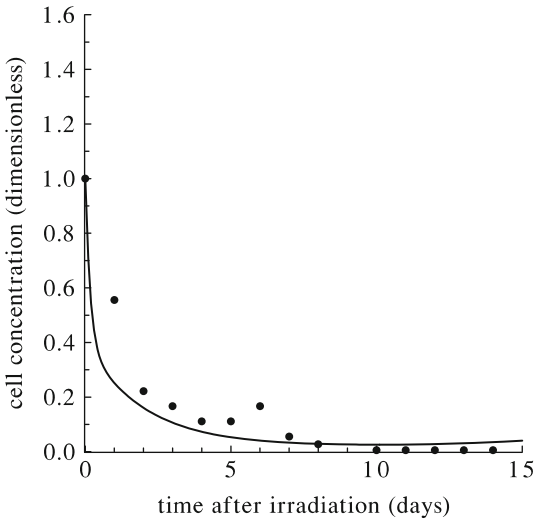

Fig. 7.34 The modeling dynamics of the dimensionless concentration of blood lymphocytes (X_3 cells) in the lymphopoietic system of humans exposed to acute irradiation with a dose of 6.0 Gy (*curve*) and the corresponding clinical data [60] (*circles*)

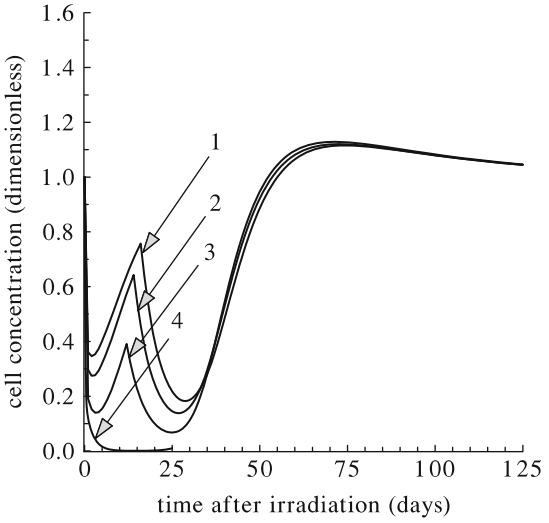

Fig. 7.35 The modeling dynamics of the dimensionless concentration of bone marrow precursor cells (X_1 and X_2 cells) in the erythropoietic system of humans exposed to acute irradiation with doses of 2.0, 3.0, 4.0, and 9.8 Gy (*curves 1–4*, respectively)

shows that the models reproduce, on qualitative and quantitative levels, the deep depletion of the aforementioned hematopoietic lineages in individuals exposed to high doses of acute irradiation. As a result, these individuals die, as it follows from the respective clinical data [60, 61].

Thus, the developed models of the human thrombopoietic, granulopoietic, lymphopoietic, and erythropoietic systems are capable of predicting both the postirradiation damage and recovery of these systems after not high doses of acute irradiation and their deep depletion after high doses of acute irradiation.

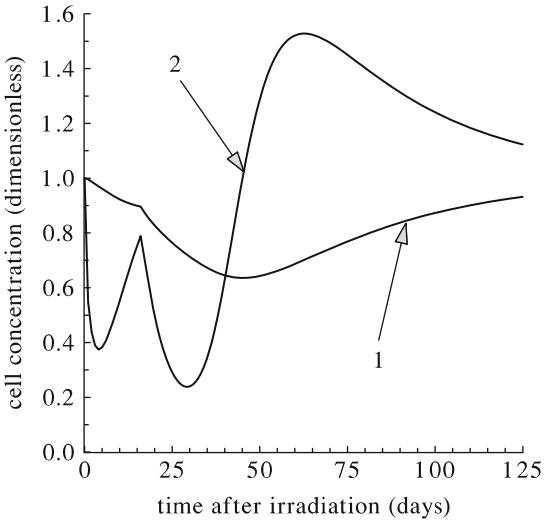

Fig. 7.36 The modeling dynamics of dimensionless concentrations of blood erythrocytes and reticulocytes in humans exposed to acute irradiation with a dose of 2.0 Gy (*curves 1 and 2*, respectively)

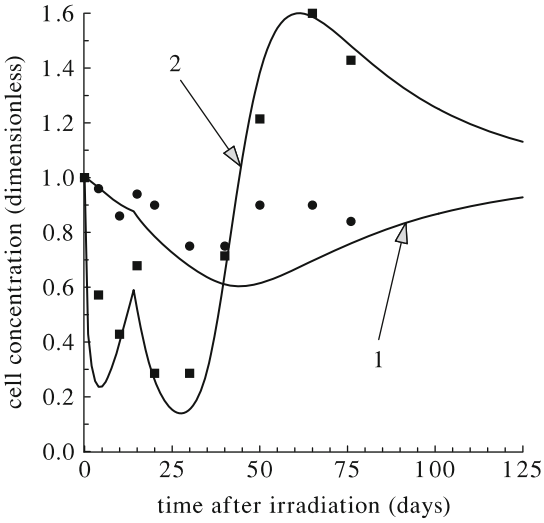

Fig. 7.37 The modeling dynamics of dimensionless concentrations of blood erythrocytes and reticulocytes in humans exposed to acute irradiation with a dose of 3.0 Gy (*curves 1 and 2*, respectively) and the corresponding clinical data [61] (*circles and boxes*, respectively)

7.5 Effects of Chronic Irradiation on the Human Major Hematopoietic Lineages

The developed models of the thrombopoietic, granulopoietic, lymphopoietic, and erythropoietic systems [Eqs.(7.1)–(7.6)], which are presented in Sect. 7.2.1, are employed to investigate numerically the dynamics of these systems in humans exposed to chronic irradiation. Remind that these models of the major hematopoietic lineages consider the entire group of damaged cells instead of the subgroups of weakly and moderately damaged cells. This is due to the following reasons. The

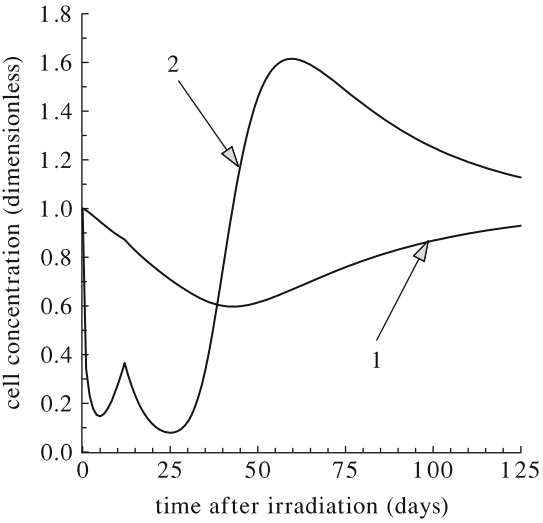

Fig. 7.38 The modeling dynamics of dimensionless concentrations of blood erythrocytes and reticulocytes in humans exposed to acute irradiation with a dose of 4.0 Gy (*curves 1 and 2*, respectively)

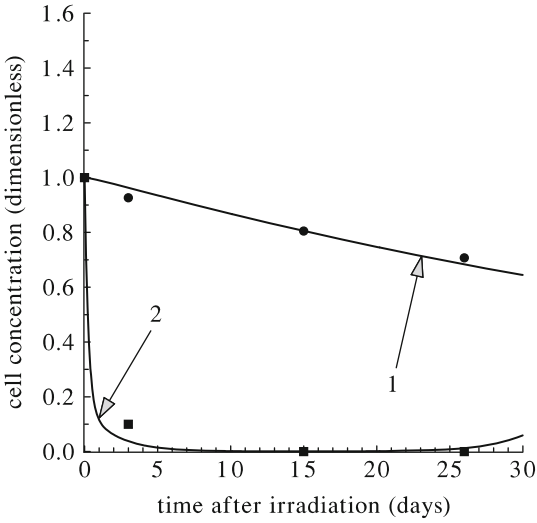

Fig. 7.39 The modeling dynamics of dimensionless concentrations of blood erythrocytes and reticulocytes in humans exposed to acute irradiation with a dose of 9.8 Gy (*curves 1 and 2*, respectively) and the corresponding clinical data [61] (*circles and boxes*, respectively)

values of the parameter κ in the thrombopoiesis, granulopoiesis, lymphopoiesis, and erythropoiesis models, which are calculated by Eq. (7.35), are about 350, 8, 12, and 24, respectively. This implies that the parts of undamaged capable of dividing precursor cells X_1^{ud}, which transfer to the subgroup of weakly damaged cells X_1^{wd} in the thrombopoietic, granulopoietic, and erythropoietic systems in chronically irradiated humans, are in 350, 8, 12, and 24 times greater than the parts of undamaged precursor cells X_1^{ud}, which transfer to the subgroup of moderately damaged cells X_1^{md} in the respective systems. Additionally, the specific death rate of the weakly damaged cells is smaller than that of the moderately damaged cells. Therefore, the weakly damaged cells dominate in the groups of the damaged cells

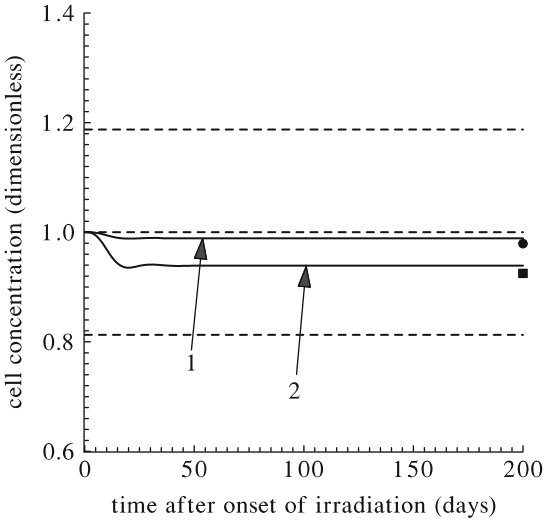

Fig. 7.40 The modeling dynamics of the dimensionless concentration of blood thrombocytes in humans exposed to chronic irradiation with dose rates of 0.17 mGy day^{-1} (*curve 1*) and 1.00 mGy day^{-1} (*curve 2*) and the corresponding clinical data [61] obtained for particle accelerator facility employees exposed to chronic irradiation with dose rate of 0.17 mGy day^{-1} (*circle*) and for nuclear power plant employees exposed to chronic irradiation in the interval of dose rates (0.2–1.0) mGy day^{-1} (*box*). The normal level of the dimensionless concentration of blood thrombocytes and the mean square deviations from this level given in the dimensionless units are shown by *dashed lines* [26]

in all the hematopoietic lineages on hand. Hence, the contributions of moderately damaged cells to the dynamics of the concentrations of the damaged cells can be neglected. Therefore the values of the parameter μ in Eq. (7.5) and the parameter ϕ in Eq. (7.7) are taken to be equal to the values of the parameters η and ς, respectively.

For the numerical studies, the developed models of the dynamics of the major hematopoietic lineages in chronically irradiated humans are rewritten in terms of the new dimensionless variables. The latter are the ratios of the dimension cell concentrations to their normal values.

In the modeling studies of the effects of chronic radiation on the major hematopoietic lineages in humans, the dose rate is varied in a wide range. The obtained modeling results are presented in Figs. 7.40, 7.41, 7.42, 7.43, 7.44, 7.45, 7.46, and 7.47. Specifically, Figs. 7.40, 7.42, 7.44, and 7.46 show the modeling dynamics of concentrations of blood cells (X_3 cells) in the thrombopoietic, granulopoietic, lymphopoietic, and erythropoietic systems in humans exposed to chronic irradiation with low and moderate dose rates. In turn, Figs. 7.41, 7.43, 7.45, and 7.47 display the modeling dynamics of concentrations of bone marrow precursor cells (X_1 and X_2 cells) and the modeling dynamics of the specific reproduction rate B of X_1 cells in the aforementioned systems in humans exposed to chronic irradiation with the same dose rates.

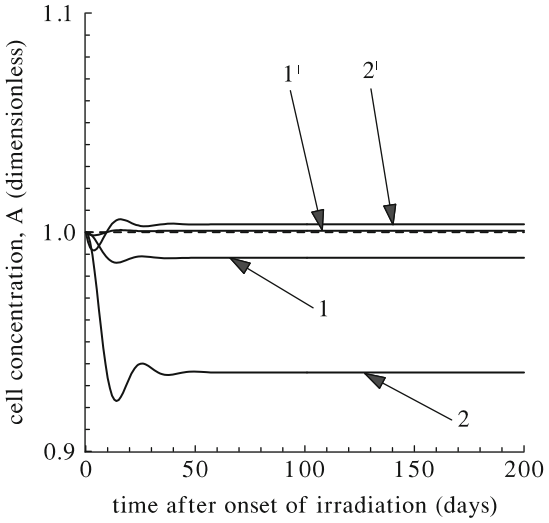

Fig. 7.41 The modeling dynamics of the dimensionless concentrations of the bone marrow precursor cells (X_1 and X_2 cells) and the dimensionless reproduction rate B of undamaged X_1 cells in the thrombopoietic system of humans exposed to chronic irradiation with dose rates of 0.17 mGy day^{-1} (*curves 1 and 2*, respectively) and with the dose rate of 1.00 mGy day^{-1} (*curves 1′ and 2′*, respectively). The normal level for the dimensionless concentration of the aforementioned cells and for the dimensionless reproduction rate B is given by *dashed line*

As one can infer from Figs. 7.40, 7.41, 7.42, 7.43, 7.44, 7.45, 7.46, and 7.47, the models reproduce the transition processes, which start after the onset of such exposures. In the thrombopoietic and granulopoietic systems, these processes are characterized by damped oscillations of the concentrations of blood cells (X_3 cells) and their bone marrow precursor cells (X_1 and X_2 cells), as well as by damped oscillations of the concentrations of the specific reproduction rates B of X_1 cells. The transition processes in the lymphopoietic and erythropoietic systems are characterized by overdamped oscillations of the concentration of bone marrow precursor cells (X_1 and X_2 cells) and by overdamped oscillations of the reproduction rate B of X_1 cells. In turn, the dynamics of the concentration of blood cells (X_3 cells) in these two systems has an aperiodic character. When the transition processes are over, the concentrations of blood cells (X_3 cells) and their bone marrow precursor cells (X_1 and X_2 cells), as well as the values of the reproduction rates B of X_1 cells in the systems on hand acquire new stationary values. In other words, the new stable dynamic equilibrium states (i.e., the new homeostasis states) are established in the thrombopoietic, granulopoietic, lymphopoietic, and erythropoietic systems of humans exposed to chronic irradiation with low and moderate dose rates N. The establishment of these states can be regarded as an adaptation of these systems to chronic irradiation. Note that such adaptation of cellular self-renewing systems in mammals to chronic radiation was observed in [87–89].

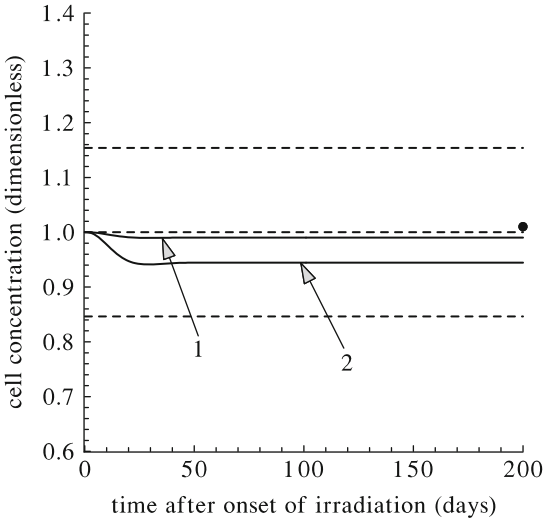

Fig. 7.42 The modeling dynamics of the dimensionless concentration of blood granulocytes in humans exposed to chronic irradiation with dose rates of 0.17 mGy day^{-1} (*curve 1*) and 1.00 mGy day^{-1} (*curve 2*) and the corresponding clinical data [61] obtained for particle accelerator facility employees exposed to chronic irradiation with dose rate of 0.17 mGy day^{-1} (*circle*). The normal level of the dimensionless concentration of blood granulocytes and the mean square deviations from this level given in the dimensionless units are shown by *dashed lines* [26]

It is worthwhile to emphasize the following. The new homeostasis states of the thrombopoietic, granulopoietic, lymphopoietic, and erythropoietic systems in humans exposed to low and moderate dose rates of chronic irradiation are characterized by reduced, in comparison with the norm, stationary concentrations of blood cells (X_3 cells) and their bone marrow precursor cells (X_1 and X_2 cells) (Figs. 7.40, 7.41, 7.42, 7.43, 7.44, 7.45, 7.46, and 7.47). These new homeostasis states of the major hematopoietic lineages are also characterized by elevated, in comparison with the norm, reproduction rates B of X_1 cells, i.e., by enhanced mitotic activity of these cells (Figs. 7.41, 7.43, 7.45, and 7.47). Hence, the models are capable of predicting the "overstrain" in functioning of these systems, which is required to maintain the new stable dynamic equilibrium states in them under chronic irradiation with low and moderate dose rates N. These predictions of the models are also supported by experimental and clinical data [88–90].

Note that the first dose rate of 0.17 mGy day^{-1}, which is used in the modeling studies of the effects of chronic irradiation on the major hematopoietic lineages in humans, coincides with the dose rate of long-term chronic irradiation of employees of the particle accelerator facilities [61]. The second dose rate of 1.0 mGy day^{-1}, which is used in the modeling studies, is taken to be equal to the upper boundary of the interval of dose rates, (0.2–1.0) mGy day^{-1}, which employees of the nuclear power plants were exposed to [61]. The averaged concentrations of thrombocytes, granulocytes, lymphocytes, and erythrocytes for the first group of employees and

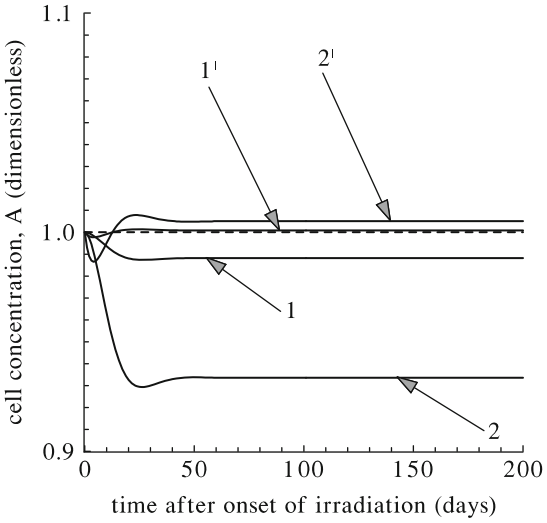

Fig. 7.43 The modeling dynamics of the dimensionless concentrations of the bone marrow precursor cells (X_1 and X_2 cells) and the dimensionless reproduction rate B of undamaged X_1 cells in the granulopoietic system of humans exposed to chronic irradiation with dose rates of 0.17 mGy day^{-1} (*curves 1 and 2*, respectively) and with the dose rate of 1.00 mGy day^{-1} (*curves 1′ and 2′*, respectively). The normal level for the dimensionless concentration of the aforementioned cells and for the dimensionless reproduction rate B is given by *dashed line*

the averaged concentration of thrombocytes for the most irradiated individuals from the second group of employees are given in Figs. 7.40, 7.42, 7.44, and 7.46. As one can infer from these figures, the modeling predictions of the stationary concentrations of blood cells (X_3 cells) in the major hematopoietic lineages of chronically irradiated humans agree with the respective clinical data. Note that the stationary concentrations of blood thrombocytes, granulocytes, lymphocytes and erythrocytes, which are established in the corresponding systems under such exposures, are greater than the respective lower boundaries of physiological norm for these cells in humans [26]. The obtained results testify to a high recovery capability of the major hematopoietic lineages in humans exposed to chronic irradiation in the considered range of dose rates.

The modeling studies of the dynamics of the thrombopoietic, granulopoietic, lymphopoietic, and erythropoietic systems in humans exposed to chronic irradiation with high dose rates reveal both resemblances and distinctions in the responses of these systems on such exposures. Specifically, the concentrations of blood cells in these systems decrease after the onset of such exposures. Note that the concentrations of blood lymphocytes, granulocytes, and thrombocytes decrease considerably faster than the concentration of blood erythrocytes does. As a result, in the same time interval, the lymphocyte, granulocyte, and thrombocyte concentrations reach considerably lower levels in comparison with that of the erythrocyte concentration does.

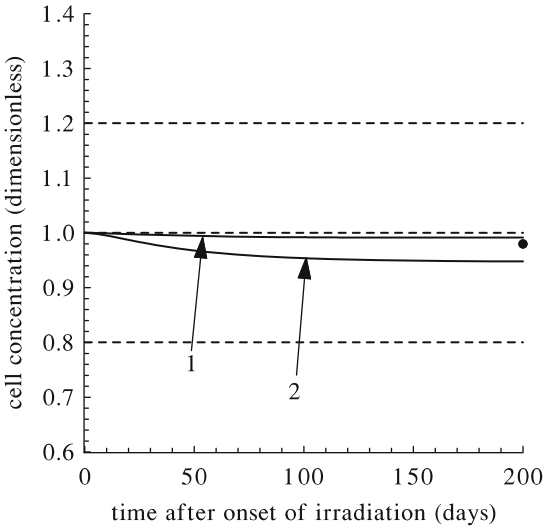

Fig. 7.44 The modeling dynamics of the dimensionless concentration of blood lymphocytes in humans exposed to chronic irradiation with dose rates of 0.17 mGy day^{-1} (*curve 1*) and 1.00 mGy day^{-1} (*curve 2*) and the corresponding clinical data [61] obtained for particle accelerator facility employees exposed to chronic irradiation with dose rate of 0.17 mGy day^{-1} (*circle*). The normal level of the dimensionless concentration of blood lymphocytes and the mean square deviations from this level given in the dimensionless units are shown by *dashed lines* [26]

Figures 7.48 and 7.49 show the modeling results on the dose dependence of stationary concentrations of blood cells and their bone marrow precursor cells, which are established in the thrombopoietic, granulopoietic, lymphopoietic, and erythropoietic system in chronically irradiated humans, on the dose rate N of chronic irradiation exposures. As one can see, these stationary concentrations decrease with growing of N and vanish when N becomes equal to or exceeds the respective critical dose rates N_c. The values of the critical dose rates N_c for the thrombopoietic, granulopoietic, lymphopoietic, and erythropoietic systems are determined, in terms of the model parameters, by a simple formula (see Chap. 1 and the references therein for the details):

$$N_c = D_1^0(\alpha - \gamma). \tag{7.52}$$

This equation implies that the critical dose rate N_c depends on both the radiosensitivity of the bone marrow precursor cells capable of dividing (X_1 cells) and the proliferation potential of these cells. The values of the critical dose rate N_c for the thrombopoietic, granulopoietic, lymphopoietic, and erythropoietic systems in humans are equal to 0.2 Gy day^{-1}, 1.0 Gy day^{-1}, 0.6 Gy day^{-1}, and 1.8 Gy day^{-1}, respectively.

It is worthwhile to note that the irradiated mammals die, if the concentration of functional cells in the respective critical body system reaches 10 % of its normal

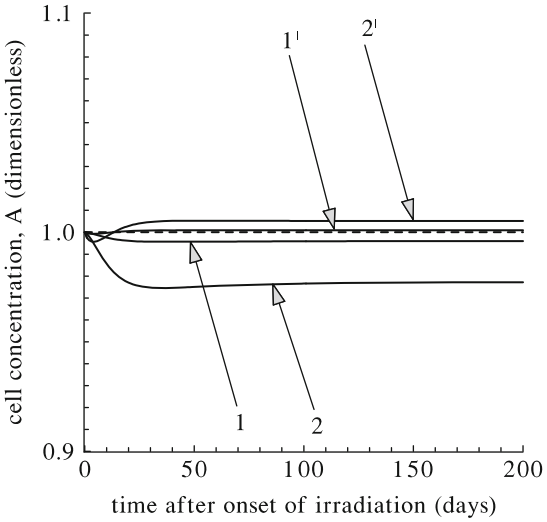

Fig. 7.45 The modeling dynamics of the dimensionless concentrations of the bone marrow precursor cells (X_1 and X_2 cells) and the dimensionless reproduction rate B of undamaged X_1 cells in the lymphopoietic system of humans exposed to chronic irradiation with dose rates of 0.17 mGy day^{-1} (*curves 1 and 2*, respectively) and with the dose rate of 1.00 mGy day^{-1} (*curves 1′ and 2′*, respectively). The normal level for the dimensionless concentration of the aforementioned cells and for the dimensionless reproduction rate B is given by *dashed line*

level [91, 92]. This "lethal" level of 0.1, which is incompatible with a life, is shown by dashed line in Fig. 7.48. Remind that this figure presents the dependence of the new dimensionless stationary concentrations of blood cells, which are established in the thrombopoietic, granulopoietic, lymphopoietic, and erythropoietic systems in chronically irradiated humans, on the dose rate N of chronic irradiation (solid curves). The dose rates corresponding to the points of intersection of these curves with the "lethal" level are the minimal dose rates of chronic irradiation, which lead to the death of exposed individuals. These "lethal" dose rates of chronic irradiation obtained in the framework of the thrombopoiesis, granulopoiesis, lymphopoiesis, and erythropoiesis models are 0.11 Gy day^{-1}, 0.10 Gy day^{-1}, 0.06 Gy day^{-1}, and 0.13 Gy day^{-1}, respectively. The averaged value of the "lethal" dose rates of chronic irradiation, which are obtained for the major hematopoietic lineages, is equal to 0.10 Gy day^{-1}. It is worthwhile to emphasize that this "lethal" dose rate, which is predicted by the developed models, coincides with the real minimal dose rate of lethal chronic irradiation found on the basis of analysis of numerous clinical data for chronically irradiated individuals in [93]. These modeling findings are also supported by clinical observations, according to which the main manifestations of the hematopoietic subsyndrome of the acute radiation syndrome resulted in a death of individuals are endo- and exoinfections, hemorrhage, and anemia caused by the deep depletion of the lymphopoietic, granulopoietic, thrombopoietic, and erythropoietic systems, respectively [1, 5, 6]. Thus, the developed models are

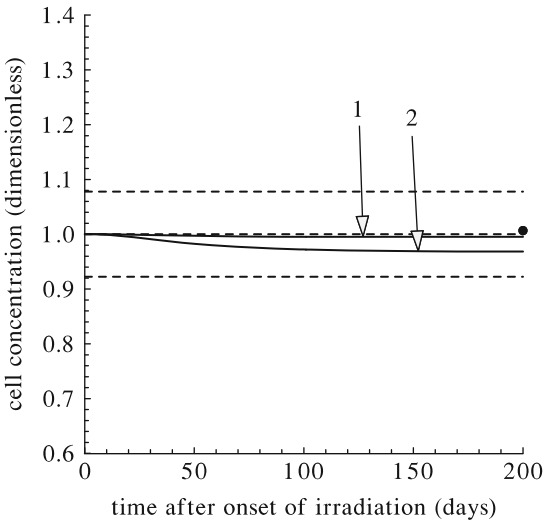

Fig. 7.46 The modeling dynamics of the dimensionless concentration of blood erythrocytes in humans exposed to chronic irradiation with dose rates of 0.17 mGy day^{-1} (*curve 1*) and 1.00 mGy day^{-1} (*curve 2*) and the corresponding clinical data [61] obtained for particle accelerator facility employees exposed to chronic irradiation with dose rate of 0.17 mGy day^{-1} (*circle*). The normal level of the dimensionless concentration of blood erythrocytes and the mean square deviations from this level given in the dimensionless units are shown by *dashed lines* [26]

capable of predicting the effects of chronic irradiation in the wide range of dose rates on the human thrombopoietic, granulopoietic, lymphopoietic, and erythropoietic systems.

7.6 Space Radiation and Human Hematopoiesis

The developed models of the thrombopoietic, granulopoietic, erythropoietic, and lymphopoietic systems [Eqs. (7.1)–(7.6)] are applied to simulate the dynamics of these major hematopoietic lineages in astronauts in a typical spacecraft traveling in interplanetary space. In the simulations, the variable parameter N in Eqs. (7.1)–(7.6) is given in terms of the dose rate equivalent (Sv day^{-1}). In this way, one properly takes into account the various biological effectiveness of the components of the space radiation environment [94].

The following hypothetic scenario of irradiation during the 3-year-long mission is adopted. It is assumed that five 1-day-long solar particle events (SPEs) happen. The dose rate equivalent for the chronic exposure to galactic cosmic rays (GCR) is taken to be equal to 1.5 mSv day^{-1}. This value corresponds to the dose rate equivalent for the chronic exposure to the GCR near solar minimum [8, 95]. The dose rate equivalent for the exposure within an SPE is taken to be equal to

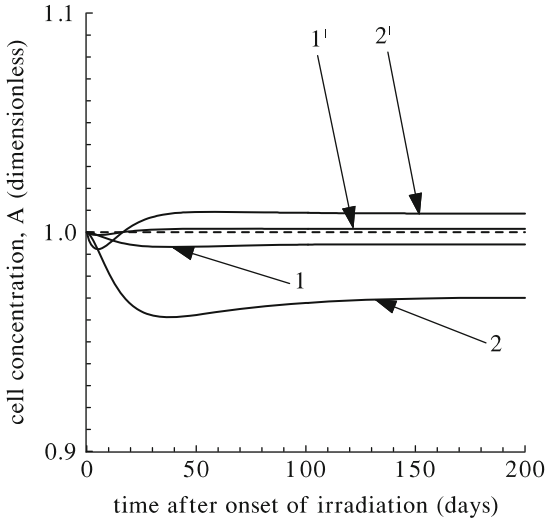

Fig. 7.47 The modeling dynamics of the dimensionless concentrations of the bone marrow precursor cells (X_1 and X_2 cells) and the dimensionless reproduction rate B of undamaged X_1 cells in the erythropoietic system in humans exposed to chronic irradiation with dose rates of 0.17 mGy day^{-1} (*curves 1 and 2*, respectively) and with the dose rate of 1.00 mGy day^{-1} (*curves 1′ and 2′*, respectively). The normal level for the dimensionless concentration of the aforementioned cells and for the dimensionless reproduction rate B is given by *dashed line*

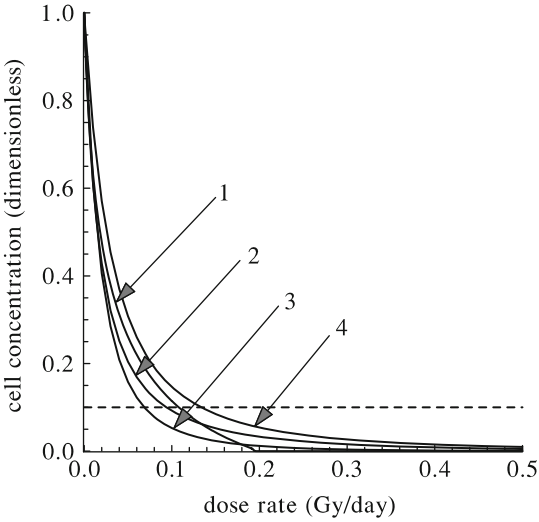

Fig. 7.48 Dimensionless values of new stationary concentrations of blood thrombocytes, granulocytes, lymphocytes, and erythrocytes (X_3 cells) (*curves 1–4*) in the thrombopoietic, granulopoietic, lymphopoietic, and erythropoietic systems of humans versus the dose rate N of chronic irradiation. Critical level of the dimensionless concentrations of these cells (0.1) is given by *dashed line*

0.4 Sv day^{-1}. This quantity corresponds to the dose equivalent for the exposure at the historical worst SPE (August 2, 1972) [8, 96]. It is assumed that five 1-day-long SPEs happen 250, 500, 507, 750, and 780 days after the mission's onset in simulating the dynamics of the thrombopoietic system; 250, 500, 507, 750, and

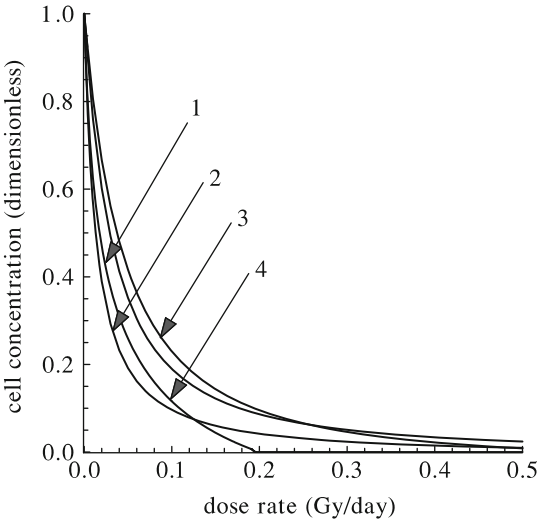

Fig. 7.49 Dimensionless values of new stationary concentrations of bone marrow precursor cells (X_1 and X_2 cells) in the thrombopoietic, granulopoietic, lymphopoietic, and erythropoietic systems of humans versus the dose rate N of chronic irradiation

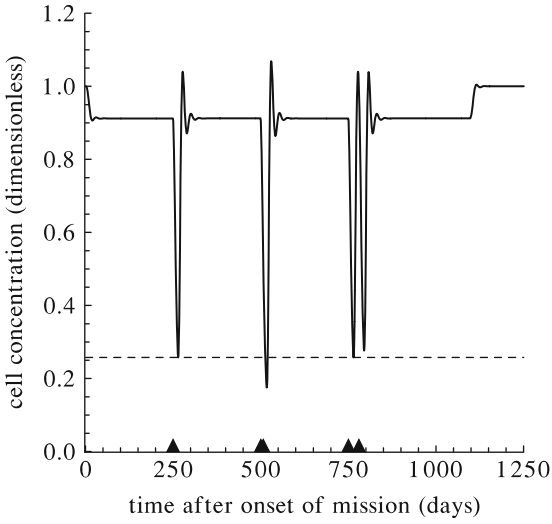

Fig. 7.50 Modeling results on the dynamics of the dimensionless concentration of blood thrombocytes in humans during the 3-year-long mission to Mars. The dose rate equivalent of exposure to the galactic cosmic rays (GCR) is $N_{GCR} = 1.5\,\text{mSv day}^{-1}$. The dose rate equivalent of exposure to 1-day-long solar particle event (SPE) is $N_{SPE} = 0.4\,\text{Sv day}^{-1}$. *Triangles* indicate the onsets of SPEs

790 days after the mission's onset in simulating the dynamics of the granulopoietic system; 250, 500, 507, 750, and 800 days after the mission's onset in simulating the dynamics of the lymphopoietic system; 250, 500, 507, 750, and 810 days after the mission's onset in simulating the dynamics of the erythropoietic system. The intervals between the moments of the beginning of the fourth and fifth SPEs are different in these four scenarios of irradiation. This is due to the necessity to elucidate the effects of the fourth and fifth SPEs on these hematopoietic lineages more evident way. The results of the respective modeling simulations are presented in Figs. 7.50, 7.51, 7.52, and 7.53.

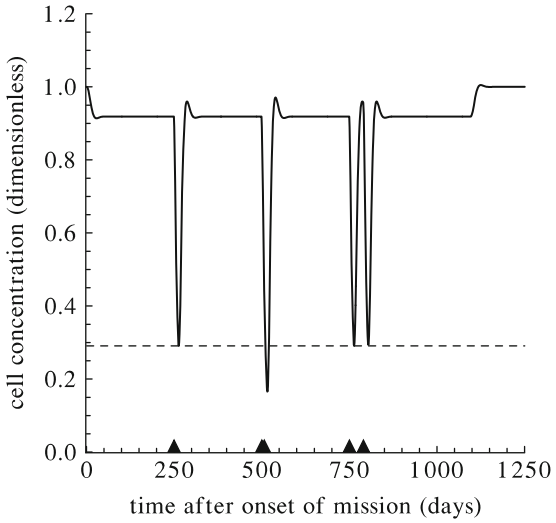

Fig. 7.51 Modeling results on the dynamics of blood granulocytes in humans during the 3-year-long mission to Mars. The dose rate equivalent of exposure to the galactic cosmic rays (GCR) is $N_{GCR} = 1.5\,\mathrm{mSv\,day^{-1}}$. The dose rate equivalent of exposure to the 1-day-long solar particle event (SPE) is $N_{SPE} = 0.4\,\mathrm{Sv\,day^{-1}}$. The *dashed line* denotes the minimum of the granulocyte concentration after the first SPE. *Triangles* indicate the onsets of SPEs

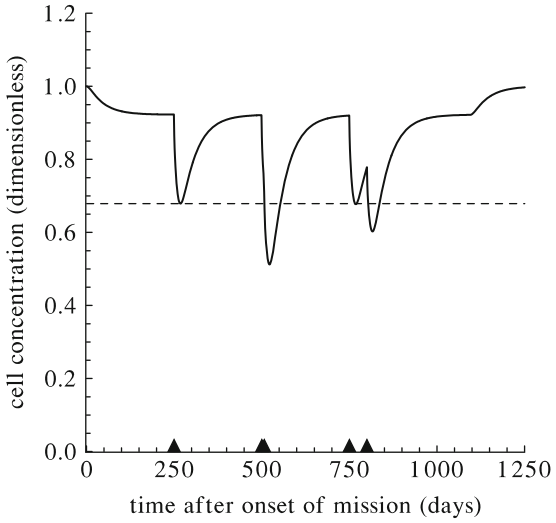

Fig. 7.52 Modeling results on the dynamics of blood lymphocytes in humans during the 3-year-long mission to Mars. The dose rate equivalent of exposure to the galactic cosmic rays (GCR) is $N_{GCR} = 1.5\,\mathrm{mSv\,day^{-1}}$. The dose rate equivalent of exposure to the 1-day-long solar particle event (SPE) is $N_{SPE} = 0.4\,\mathrm{Sv\,day^{-1}}$. The *dashed line* denotes the minimum of the lymphocyte concentration after the first SPE. *Triangle arrows* indicate the onsets of SPEs

First of all, let us consider the dynamics of concentration of blood thrombocytes, granulocytes, lymphocytes, and erythrocytes in time intervals between the onset of space mission and the onset of the first SPE and between the end of the space mission and the end of the observation. As one can see from Figs. 7.50 and 7.51, the dynamics of concentrations of blood thrombocytes and granulocytes are quite similar to each other in the aforementioned time intervals. Specifically, after the onset of space mission, the concentrations of these cells decrease and reach their local minima. After that they slightly increase and, after damped and overdamped oscillations, reach their new stationary levels. The latter are slightly lowered in comparison with their normal levels. These modeling results imply that the human

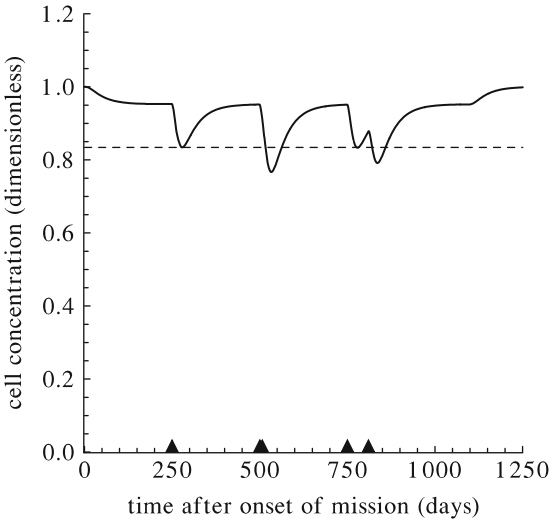

Fig. 7.53 Modeling results on the dynamics of blood erythrocytes in humans during the 3-year-long mission to Mars. The dose rate equivalent of exposure to the galactic cosmic rays (GCR) is $N_{GCR} = 1.5\,\mathrm{mSv\,day^{-1}}$. The dose rate equivalent of exposure to 1-day-long solar particle event (SPE) is $N_{SPE} = 0.4\,\mathrm{Sv\,day^{-1}}$. The *dashed line* denotes the minimum of the erythrocyte concentration after the first SPE. *Triangles arrows* indicate the onsets of SPEs

thrombopoietic and granulopoietic systems are capable of adapting themselves to exposure to the GCR. After the end of the space mission, concentrations of blood thrombocytes and granulocytes increase and, after damped and overdamped oscillations, return to their normal levels. As one can infer from Figs. 7.52 and 7.53, the dynamics of concentrations of blood lymphocytes and erythrocytes are also similar to each other in the aforementioned time intervals. Specifically, after the onset of the space mission, the concentrations of these cells decrease and, without any oscillations, reach their new stationary levels. The latter are also slightly lowered in comparison with their normal levels. These modeling results imply that the human lymphopoietic and erythropoietic systems are capable of adapting themselves to exposure to the GCR. After the end of the space mission, concentrations of blood lymphocytes and erythrocytes increase and return aperiodically to their normal levels.

Let us consider now the dynamics of the concentrations of blood thrombocytes, granulocytes, lymphocytes, and erythrocytes before, during, and after the first SPE (Figs. 7.50, 7.51, 7.52, and 7.53). Before the first SPE, the concentrations of these cells are maintained on the stationary levels, which are lowered in comparison with their normal ones. After the first SPE, the concentrations of blood thrombocytes and granulocytes decrease to local minima. Then the concentrations of these cells increase and reach local maxima. The latter are above their normal levels. Further on, the concentrations of blood thrombocytes and granulocytes decrease again and, after damped and overdamped oscillations, return to the stationary levels (Figs. 7.50 and 7.51). In turn, the concentrations of blood lymphocytes and erythrocytes decrease to local minima. Then they increase and return aperiodically to the stationary levels (Figs. 7.52 and 7.53).

Let us consider the dynamics of the concentrations of blood thrombocytes, granulocytes, lymphocytes, and erythrocytes before, during, and after the second

and third SPEs. The latter follows shortly after the second SPE (7 days). As one can see from Figs. 7.50, 7.51, 7.52, and 7.53, the concentrations of these cells are maintained on the same stationary levels before the second SPE, as well as those before the first SPE. This modeling findings imply that the time interval between the first and second SPEs (250 days) exceeds the time needed to restore the stable dynamic equilibrium states in the considered systems after the first SPE.

Figures 7.50 and 7.51 show that the concentrations of blood thrombocytes and granulocytes decrease after the second SPE. They continue to decrease after the next (third) SPE and eventually reach local minima. After that, the concentrations of blood thrombocytes and granulocytes increase and approach local maxima. The latter are above their normal levels. Further on, the concentrations of blood thrombocytes and granulocytes decrease again and, after damped and overdamped oscillations, return to the stationary levels. In turn, Figs. 7.52 and 7.53 exhibit that the concentrations of blood lymphocytes and erythrocytes decrease after the second SPE. They continue to decrease after the next (third) SPE and eventually reach local minima. Further on, the concentrations of blood lymphocytes and erythrocytes increase and return aperiodically to the stationary levels.

As one can infer from Figs. 7.50, 7.51, 7.52, and 7.53, the concentrations of blood thrombocytes, granulocytes, lymphocytes, and erythrocytes approach smaller minimal values after the third SPE than those after the first SPE. This modeling findings imply that the damage effect of exposure to the third SPE, which follows in the short-term interval after the previous (second) SPE, is superimposed on the damage effect of exposure to the second SPE.

Let us consider the dynamics of concentrations of blood thrombocyte, granulocyte, lymphocyte, and erythrocyte before, during, and after the fourth and fifth SPEs (Figs. 7.50, 7.51, 7.52, and 7.53). As one can see from Figs. 7.50, 7.51, 7.52, and 7.53, the concentrations of these cells are maintained on the same stationary levels before the fourth SPE, as well as those before the first and second SPEs. This modeling findings imply that the time interval between the third and fourth SPEs (243 days) exceeds the time needed to restore the new stable dynamic equilibrium states in the considered systems after the third SPE.

Figures 7.50 and 7.51 show that the concentrations of blood thrombocytes and granulocytes decrease to local minima after the fourth SPE. Then, these concentrations increase and reach local maxima at the onset of the fifth SPE. Note that these local maxima of the concentrations of blood thrombocytes and granulocytes are above their normal levels. After that, the concentrations of these cells decrease and reach next local minima. Then, they increase and reach local maxima. Further on, the concentrations of blood thrombocytes and granulocytes decrease again and, after damped and overdamped oscillations, return to the stationary levels. In turn, Figs. 7.52 and 7.53 exhibit that the concentrations of blood lymphocytes and erythrocytes also decrease to local minima after the fourth SPE. Then these concentrations increase and reach local maxima at the onset of the fifth SPE. Note that these local maxima of the concentrations of blood lymphocytes and erythrocytes are below their normal levels. After that, the concentrations of these cells decrease again and reach next local minima. Further on, the concentrations of blood lymphocytes and erythrocytes return aperiodically to the stationary levels.

As one can infer from Figs. 7.50, 7.51, 7.52, and 7.53, the minimal values of the concentrations of blood thrombocyte, granulocyte, lymphocyte, and erythrocyte after the fourth SPE coincide with those after the first SPE. In turn, after the fifth SPE, which follows, respectively, 30 and 40 days after the onset of the fourth SPE, the concentrations of thrombocytes and granulocytes decrease to minimal values, which are higher than the minimal values of the concentrations of these cells after the first SPE (Figs. 7.50 and 7.51). After the fifth SPE, which follows, respectively, 50 and 60 days after the onset of the fourth SPE, the concentrations of blood lymphocytes and erythrocytes decrease to minimal values, which are lower than those after the first SPE, but higher than those after the third SPE (Figs. 7.52 and 7.53).

The modeling results presented above argue that exposure to SPE may induce changes in the radiosensitivity of the thrombopoietic, granulopoietic, lymphopoietic, and erythropoietic systems to the forthcoming SPE. This interpretation of the modeling predictions is based on the conventional radiobiological concept [1]. According to this concept, the radiosensitivity of an organism's cell system can be characterized by a severity of postirradiation injury of this system, namely by a depth of postirradiation depletion of its functional cell pool. Manifestations of elevated and lowered radiosensitivity of the system are, respectively, more severe and less severe depletion of its functional cell pool. Therefore, one can take, as the indexes of radiosensitivity of the thrombopoietic, granulopoietic, lymphopoietic, and erythropoietic systems, the minimal levels up to which the concentrations of functional cells in these systems (blood thrombocytes, granulocytes, lymphocytes, and erythrocytes) are reduced after radiation exposure.

Proceeding from this, the following interpretations of the obtained modeling results can be proposed. The exposure to the previous SPE can induce the radioprotection or radiosensitization effects on the thrombopoietic and granulopoietic systems depending on the time interval between the previous and forthcoming SPEs. In the first case, these systems manifest the acquired radioresistance at the moment the forthcoming SPE, whereas in the second case they demonstrate the acquired radiosensitivity. In turn, the exposure to the previous SPE can induce the radiosensitization effect on the lymphopoietic and erythropoietic systems, if the interval between the previous and forthcoming SPEs does not exceed the time needed for each of these systems to restore the stable dynamic equilibrium state after the previous SPE. In other words, these systems demonstrate the acquired radiosensitivity in the aforementioned period.

Note that these modeling results agree with the results obtained in the modeling and experimental studies of acquired radioresistance and radiosensitivity in the respective major hematopoietic lineages in rodents, which are induced by previous continuous irradiation (Chap. 1).

7.7 Conclusions

The mathematical models of the dynamics of the major hematopoietic lineages (the thrombopoietic, granulopoietic, lymphopoietic, and erythropoietic systems) in both nonirradiated and acutely/chronically irradiated humans are developed and thoroughly investigated [16–23]. These models consider the principal stages of development of hematopoietic cells and take into account the general and specific regulatory mechanisms of the major hematopoietic lineages. The models also embody the mechanism of forming the abortive rise, which is a characteristic feature of responses of the human major hematopoietic lineages to acute irradiation. The mathematical implementations of the models of the human major hematopoietic lineages are the systems of nonlinear ordinary differential equations, whose variables and parameters have clear biological meaning. The dose rate of chronic irradiation and the dose of acute exposure are variable parameters of the models.

The developed models are used to study the dynamics of the major hematopoietic lineages (the thrombopoietic, granulopoietic, lymphopoietic, and erythropoietic systems) in humans under normal conditions. It is shown that the developed models are capable of describing the homeostasis states of these systems in healthy humans. It is found that the model of the human lymphopoietic system is capable of simulating the dynamics of the blood lymphocytes in patients received allogenic stem cell transplantation. It is also demonstrate that the developed models are capable of reproducing the dynamical regimes, which are typical for patients with cyclic hematological disorders (cyclic thrombocytopenia, cyclic neutropenia, cyclic lymphocytopenia, and cyclic erythrocytopenia). Proceeding from the results of analytical and numerical investigations of these models, the biological interpretation of the causes of these disorders are proposed. It will be interesting to conduct further investigations to verify these modeling predictions, which may provide hints of cure for these rare hematological disorders.

The developed models of major hematopoietic lineages are employed to study the dynamics of these systems in humans exposed to acute radiation in a wide range of doses. It is found that the models reproduce, on qualitative and quantitative levels, the deep depletion of these systems in humans exposed to high doses of acute irradiation. It is also revealed that the models provide a qualitative and quantitative description of the postirradiation injury and recovery of the aforementioned hematopoietic lineages in humans exposed to lower doses of acute irradiation. The dose dependence of the main characteristics of the abortive rise is reproduced. The interpretation of the obtained results is proposed.

The developed models are applied to investigate the dynamics of the thrombopoietic, granulopoietic, lymphopoietic, and erythropoietic systems in humans exposed to chronic radiation in a wide range of dose rates. The obtained results demonstrate that the models are capable of reproducing the observed ability of these systems in humans to adapt themselves to chronic irradiation with low and moderate dose rates. Specifically, the models reproduce the ability of these systems to establish the new stable dynamic equilibrium states under such exposures.

These states are characterized by new, lower than normal, stationary values of the concentrations of blood cells, and their bone marrow precursor cells in the aforementioned hematopoietic lineages. These stationary values are smaller at higher dose rates of chronic irradiation. The new stable dynamic equilibrium states are also characterized by new, higher than normal, stationary values of the specific reproduction rate of the bone marrow precursor cells in the systems on hand. Thus, the models simulate the observed "overstrain" in the functioning of the human major hematopoietic lineages under chronic irradiation. It is also found that the developed models are capable of reproducing the complete irreversible depletion of the thrombopoietic, granulopoietic, lymphopoietic, and erythropoietic systems in humans, if the dose rate of chronic irradiation is equal to or exceeds the respective critical values N_c. The latter are found in the framework of the models. Additionally, the "lethal" dose rates of chronic irradiation for the aforementioned hematopoietic lineages in humans are evaluated in the framework of the models. These "lethal" dose rates for the thrombopoiesis, granulopoiesis, lymphopoiesis, and erythropoiesis models are $0.11\,\mathrm{Gy\,day^{-1}}$, $0.10\,\mathrm{Gy\,day^{-1}}$, $0.06\,\mathrm{Gy\,day^{-1}}$, and $0.13\,\mathrm{Gy\,day^{-1}}$, respectively. The averaged value of the "lethal" dose rates of chronic irradiation evaluated in the models of these major hematopoietic lineages is equal to $0.10\,\mathrm{Gy\,day^{-1}}$. It is crucial to stress that this averaged "lethal" dose rate, which is predicted by the developed models, coincides with the real minimal dose rate of lethal chronic irradiation obtained on the basis of analysis of numerous clinical data for chronically irradiated individuals in [93].

The obtained modeling findings clearly demonstrate that the developed models are capable of predicting, on the quantitative level, the dynamics of the major hematopoietic lineages in humans exposed to various irradiation conditions. Therefore they can be applied in the studies of a variety vital aspects of radiation research.

In particular, the developed models of human thrombopoietic, granulopoietic, lymphopoietic, and erythropoietic systems are used to simulate the dynamics of these major hematopoietic lineages in astronauts in a typical spacecraft traveling in interplanetary space. The dose rate equivalent for space radiation [galactic cosmic rays (GCR) and solar particles events (SPE)] is taken as a variable parameter of the models. It is found that the aforementioned major hematopoietic lineages can adapt themselves to GCR exposure. This manifests in the establishment of new stable dynamic equilibrium states in these systems. These states are characterized by the new stationary concentrations of the functional blood cells, which are slightly below their normal levels. It is revealed that the concentrations of the functional blood cells in the thrombopoietic, granulopoietic, lymphopoietic, and erythropoietic systems decrease after an SPE and then return to the same new stationary levels. It is also elucidated that, in the case of two and more SPEs during the space mission, a previous SPE can influent on the response of the aforementioned major hematopoietic lineages to a forthcoming SPE, if the interval between the previous and forthcoming SPEs does not exceed the time needed for each of these systems to restore the new stable dynamic equilibrium state after the previous SPE. In particular, the exposure to a previous SPE can induce the radioprotection or radiosensitization effects on the thrombopoietic and granulopoietic systems

depending on the time interval between the previous and forthcoming SPEs. These effects of a previous SPE manifest, respectively, in the acquired radioresistance or acquired radiosensitivity of these two systems at the moment the forthcoming SPE and, respectively, in their weaker or heavier injury, respectively. In turn, the exposure to the previous SPE can induce only radiosensitization effect on the lymphopoietic and erythropoietic systems that manifests in acquired radiosensitivity of these two systems at the moment the forthcoming SPE and, respectively, in their heavier injury. The obtained results convincingly demonstrate the importance of the study of radiation effects on the human major hematopoietic lineages in the dynamic way. These results also testify to the efficiency of employment of the developed models in the investigation and prediction of the effects of space radiation on the human major hematopoietic lineages. Thus, the developed models of the human major hematopoietic lineages could be employed in the investigation and prediction of effects of space radiation on these systems in astronauts on long-term space missions, such as voyages to Mars or Lunar colonies. The obtained modeling predictions would provide a better understanding of the risks to health from the space radiation environment and enable one to evaluate the need for operational applications of countermeasures for astronauts.

The developed models of the human major hematopoietic lineages could also be applied to predict the radiation injury of these systems in individuals exposed to radiation in the result of an incident. Obtained results would help to select an appropriate treatment.

Additionally, the developed models of the human major hematopoietic lineages could be used for predicting the radiation injury of these systems for people residing in contaminated areas after nuclear power plant accidents. Obtained results would help the decision makers to evaluate the hazard for the health of such people and to take justified decisions for operational applications of all necessary countermeasures including their settling out, as well as for their subsequent resettling. These models could also be applied to assessment of the health hazard for clean-up crew members taking part in the elimination of consequences of such accidents.

References

1. Bond V.P., Fliendner T.M., Archambeau J.O. Mammalian Radiation Lethality: A Disturbance in Cellular Kinetics. New York: Academic Press, 1965.
2. Fliedner T.M. The role of blood stem cells in hematopoietic cell renewal. Stem Cells (Dayton, Ohio), v. 16(6), pp. 361–374, 1998.
3. Fliedner T.M., Graessle D., Paulsen C., Reimers K. Structure and function of bone marrow hemopoiesis: Mechanisms of response to ionizing radiation exposure. Cancer Biotherapy and Radiopharmaceuticals, v. 17(4), pp. 405–426, 2002.
4. Fliedner T.M., Graessle D., Meineke V., Dorr H. Pathophysiological principles underlying the blood cell concentration responses used to assess the severity of effect after accidental whole-body radiation exposure: An essential basis for an evidence-based clinical triage. Experimental Hematology, v. 35(4), pp. 8–16, 2007.
5. Nias A.H.W. An Introduction to Radiobiology, 2nd ed. Chichester, UK: Wiley, 1998.

6. Yarmonenko S.P., Vainson A.A. Radiobiology of Humans and Animals. Moscow: Vysshaya shkola, 2004 (Russian).
7. Graessle D.H., Fliedner T.M. Computer-assisted severity of effect assessment of hematopoietic cell renewal after radiation exposure based on mathematical models. Health Physics, v. 98, pp. 282–289, 2010.
8. Hu S., Cucinotta F.A. A cell kinetic model of granulopoiesis under radiation exposure: extension from rodents to canines and humans. Radiation Protection Dosimetry, v. 143, pp. 207–213, 2011.
9. Hu S, Cucinotta FA. Characterization of the radiation-damaged precursor cells in bone marrow based on modeling of the peripheral blood granulocytes response. Health Physics, v. 101(1), pp. 67–78, 2011.
10. Hu S., Cucinotta F.A. Modeling the depressed hematopoietic cells for immune system under chronic radiation. In: Computational Intelligence Methods for Bioinformatics and Biostatistics. Berlin, Heidelberg: Springer, pp. 26–36, 2013.
11. Hu S., Cucinotta F.A. Radiation dose assessment by using lymphocyte counts. Nuclear Terrorism and National Preparedness, NATO Science for Peace and Security Series B: Physics and Biophysics, S. Apikyan, D. Diamond (eds.). Netherlands: Springer, pp. 253–263, 2015.
12. Hu S., Blakely W.F., Cucinotta F.A. HEMODOSE: A Biodosimetry Tool Based on Multi-type Blood Cell Counts. Health Physics, v. 109(1), pp. 54–68, 2015.
13. Wentz J., Oldson D., Stricklin D. Modeling the Thrombopoietic Effects of Burn. Letters in Biomathematics, v. 1(1), pp. 111–126, 2014.
14. Wentz J.M., Vainstein V., Oldson D., Gluzman-Poltorak Z., Basile L.A., Stricklin D. Mathematical model of radiation effects on thrombopoiesis in rhesus macaques and humans. Journal of Theoretical Biology, V. 383, pp. 44–60, 2015.
15. Carnell L., Blattnig S., Hu S., Huff J.L., Kim M.H., Norman R., Patel Z., Simonsen L., Wu H., Casey R., Cucinotta F.A. Risk of Acute Radiation Syndromes Due to Solar Particle Events. NASA Technical Report JSC-CN-35747, 2016.
16. Smirnova O.A. Blood and small intestine kinetics under radiation exposure: Mathematical modeling. Advances in Space Research, v. 44, pp. 1457–1469, 2009.
17. Smirnova O.A. Modeling study of radiation effects on thrombocytopoietic and granulopoietic systems in humans. Advances in Space Research, v. 48, pp. 184–198, 2011.
18. Smirnova O.A. Comparative analysis of the dynamics of thrombocytopoietic, granulopoietic, and erythropoietic systems in irradiated humans: A modeling approach. Health Physics, v. 103(6), pp. 787–801, 2012.
19. Smirnova O.A. Modeling Analysis of the Dynamics of Thrombocytopoietic, Granulopoietic, and Erythropoietic Systems in Irradiated Humans. Journal of Radiation Research, v. 55, pp. i36, 2014.
20. Smirnova O.A., Hu S., and Cucinotta F.A. Analysis of the Lymphocytopoiesis Dynamics in Nonirradiated and Irradiated Humans: A Modeling Approach. Radiation Research, v. 181, pp. 240–250, 2014.
21. Smirnova O.A., Akleyev A.V., Dimov G.P. Analysis of hematopoiesis dynamics in residents of Techa riverside villages chronically exposed to nonuniform radiation: modeling approach. Health Physics, v. 106(4), pp. 445–458, 2014.
22. Smirnova O.A., Akleyev A.V., Dimov G.P. Modeling analysis of the lymphocytopoiesis dynamics in chronically irradiated residents of Techa riverside villages. Radiation and Environmental Biophysics, v. 53(3), pp. 515–523, 2014.
23. Hu S., Smirnova O.A., Cucinotta F.A. A biomathematical model of lymphopoiesis following severe radiation accidents–potential use for dose assessment. Health physics, v. 102(4), pp. 425–436, 2012.
24. Munker R., Hiller E., Glass J., Paquette R. (Eds.). Modern Hematology, 2nd ed. Totowa, NJ: Humana Press, 2007.
25. Young N.S., Gerson S.L., High K.A. (Eds.). Clinical Hematology. Philadelphia: Mosby/Elsevier, 2005.

26. Fedorov N.A.(Ed.). Normal haemopoiesis and its regulation. Moscow: Meditsina, 1976 (Russian).
27. Loeffler M., Potten C.S. Stem cells and cellular pedigrees — A conceptual introduction. In: Potten C.S. (Ed.) Stem Cells. Cambridge: Academic Press, pp. 1–27, 1997.
28. Loeffler M., Roeder I. Tissue stem cells: Definition, plasticity, heterogeneity, self-organization and models — A conceptual approach. Cells Tissues Organs, v. 171, pp. 8–26, 2002.
29. Smirnova O.A. Mathematical modeling of thrombocytopoiesis dynamics in mammals exposed to radiation, Radiobiologiya, v. 25, p. 571. Dep. in VINITI N 2552-85, 16.04.85, 1985 (Russian).
30. Smirnova O.A. Mathematical model of cyclic kinetics of granulocytopoiesis. Kosmicheskaya Biologiya i Aviakosmicheskay Meditsina, no. 1, pp. 77–80, 1985 (Russian).
31. Zukhbaya T.N., Smirnova O.A. Experimental and theoretical investigation of the dynamics of lymphopoiesis upon prolonged exposure to ionizing radiation. Radiobiologiya, v. 28, pp. 626–631, 1988 (Russian).
32. Smirnova O.A. The model of homeostasis of hematopoiesis system under chronic irradiation. In: Modeling of Population Dynamics. Gorky: Gorky University Press, pp. 39–45, 1989 (Russian).
33. Smirnova O.A. Mathematical modeling of cyclic kinetics of hematopoiesis. Kosmicheskaya Biologiya i Aviakosmicheskaya Meditsina, no. 1, pp. 41–45, 1989 (Russian).
34. Smirnova O.A. Mathematical modeling of dynamics of erythropoiesis and granulocytopoiesis under acute irradiation. Radiobiologiya, v. 30, pp. 627–633, 1990 (Russian).
35. Smirnova O.A. Mathematical modeling of bone-marrow erythropoiesis dynamics in nonirradiated and irradiated mammals. In: Dynamics of Biological Populations. Gorky: Gorky University Press, pp. 51–58, 1990 (Russian).
36. Zukhbaya T.M., Smirnova O.A. An experimental and mathematical analysis of lymphopoiesis dynamics under continuous irradiation. Health Physics, v. 61, pp. 87–95, 1991.
37. Smirnova O.A. Effect of chronic irradiation at high dose rate on the hematopoietic system: Mathematical simulation. Radiobiologiya, v. 32, pp. 757–763, 1992 (Russian).
38. Smirnova O.A. Hematopoiesis dynamics in mammals under combined exposures to radiation: Mathematical modeling. Aviakosmicheskaya i Ekologicheskaya Meditsina, no. 3, pp. 45–49, 1995 (Russian).
39. Kovalev E.E., Smirnova O.A. Estimation of radiation risk based on the concept of individual variability of radiosensitivity. AFRRI Contract Report 96-1. Bethesda, MD: Armed Forces Radiobiology Research Institute, 1996.
40. Smirnova O.A. Mathematical models of hematopoiesis dynamics in nonirradiated and irradiated mammals. BioMedSim'99. 1st Conference on Modeling and Simulation in Biology, Medicine and Biomedical Engineering, Noisy-le-Grand, France, April 20–22, 1999. Proceedings. Paris: Groupe ESIEE, pp. 105–109, 1999.
41. Smirnova O.A. Paradoxical effects of low level irradiation on radiosensitivity of mammals: Modeling investigation. In: "Problems of Biochemistry, Radiation, and Space Biology," II International Symposium under the auspices of UNESCO dedicated to the memory of Academician N. Sissakian and II Sissakian Readings, Moscow, Dubna, Russia, 2001: Proceedings. ISBN 5-85165-697-2. Dubna: JINR, v. I, pp. 177–182, 2002 (Russian).
42. Smirnova O.A., Yonezawa M. Radioprotection effect of low level preirradiation on mammals: modeling and experimental investigations. Health Physics, v. 85, pp. 150–158, 2003.
43. Smirnova O.A., Yonezawa M. Radioresistance in mammals induced by low-level chronic irradiation: modeling and experimental investigations. Health Physics, v. 87, pp. 366–374, 2004.
44. Smirnova O., Yonezawa M. Effects of chronic low-level irradiation on radiosensitivity of mammals: Modeling and experimental studies. In: Radiation Risk Estimates in Normal and Emergency Situations. Proceedings of the NATO Advanced Research Workshop on Impact of Radiation Risk Estimates in Normal and Emergency Situations, Yerevan, Armenia, September 8–11, 2005. A.A. Cigna and M. Durante (Eds.), Springer, XX, pp. 291–301, 2006.

45. Smirnova O.A. Radiation and organism of mammals: Modeling approach. Moscow-Izhevsk: Scientific-Publishing Centre "Regular and Chaotic Dynamics," Institute of Computer Science, 2006 (Russian).
46. Smirnova O.A. Effects of low-level chronic irradiation on the radiosensitivity of mammals: Modeling studies. Advances in Space Research, v. 40, pp. 1408–1413, 2007.
47. Smirnova O.A. Mathematical simulation of the dynamics of postirradiation damage and recovery of intestinal epithelium. Radiobiologiya, v. 28, pp. 817–821, 1988 (Russian).
48. Smirnova O.A. Mathematical simulation of the intestinal epithelium dynamics in nonirradiated and irradiated mammals. Radiobiologiya, v. 32, pp. 751–756, 1992 (Russian).
49. Smirnova O.A. Mathematical models of dynamics of small intestine epithelium system in nonirradiated and irradiated mammals. Abstracts of the 24th Meeting of the European Study Group for Cell Proliferation (ESGCP), Leipzig, Germany, June 12–17, 2001. Cell Proliferation, v. 34(3), pp. 193–194, 2001.
50. Smirnova O.A. Radiation effects on small intestine epithelium system: Mathematical modeling. Proceedings of III International Symposium "Problems of Biochemistry, Radiation and Space Biology" dedicated to the centenary of Academician N.M. Sissakian's birth, Dubna: JINR, pp. 250–256, 2007.
51. Belousova O.I., Gorizontov P.D., Fedorova M.I., Radiation and Haemopoietic System. Moscow: Atomizdat, 1979 (Russian).
52. Bullough W.S. The chalones. Science, v. 5, pp. 71–76, 1969.
53. Romanov J.A., Ketlinsky S.A., Antokhin A.I., Okulov V.B. Chalones and Regulation of Cell Division. Moscow: Meditsina, 1984 (Russian).
54. Ketlinsky S.A., Simbircev A.S., Vorob'ev A.A. Endogenous Immunomodulators. Sankt-Peterburg: Hippokrat, 1992 (Russian).
55. Blanpain C., Fuchs E. Epidermal homeostasis: a balancing act of stem cells in the skin. Nature Reviews Molecular Cell Biology, v. 10, pp. 207–217, 2009.
56. Lea D.E. Action of Radiation on Living Cells, 2nd ed. Cambridge: The Syndics of the Cambridge University Press, 1955.
57. Mosyagina E.N., Vladimirskaya E.B., Torubarova N.A., Mizina N.V. Kinetics of the Blood Constituents of the Blood. Moscow: Meditsina, 1976 (Russian).
58. Harker L.A. Platelet production. New England Journal of Medicine, v. 282(9), pp. 492–494, 1970.
59. OldhamH K.B., Myland J.C., Spanier J. An atlas of functions. New York, USA: Springer, pp. 405–415, 2009.
60. Pyatkin E.K., Baranov A.E. Byological indication of a dose on the basis of the analysis of chromosome aberrations and quantity of cells in peripheral blood. In: Results of sciences and technics. Radiation biology, v. 3, pp. 103–179, 1980 (Russian).
61. Guskova A.K., Baysogolov G.D. Radiation sickness of human. Moscow: Meditsina, 1971 (Russian).
62. Gruzdev G.P. Acute Radiation Bone-Marrow Syndrome. Moscow: Meditsina, 1988 (Russian).
63. Yarmonenko S.P. Radiobiology of Humans and Animals. Moscow: Vysshaya shkola, 1988 (Russian).
64. Hulse E.V. The depletion of the myelopoietic cells of the irradiated rat. British Journal of Haematology, v. 5, pp. 369–378, 1959.
65. Darenskaya N.G., Ushakov I.B., Ivanov I.V., Nasonova T.A., Esaulenko I.E., Popov V.I. Extrapolation of the experimental data on man: principles, approaches, substantiation of methods and their use in physiology and radiobiology (Manual). Moscow-Voronezh: Istoki, 2004 (Russian).
66. Hofer E.P., Briicher S., Mehr K., Tibken B. An Approach to a biomathematical model of lymphocytopoiesis. Stem Cells, v. 13, pp. 290–300, 1995.
67. Hulse E.V. Lymphocyte depletion of the blood and bone marrow of the irradiated rat: a quantitative study. British Journal of Haematology, v. 5, pp. 278–283, 1959.

68. Hirama T., Tanosaki S., Kandatsu S., Kuroiwa N., Kamada T., Tsuji H., Yamada S., Katoh H., Yamamoto N., Tsujii H., Suzuki G., Akashi M. Initial medical management of patients severely irradiated in the Tokai-mura criticality accident. The British Journal of Radiology, v. 76, pp. 246–253, 2003.
69. Baranov A.E. Assessment of doses and prediction of the dynamics of neutrophil number in blood by making use of hematological data for gamma-irradiation of humans. Meditsinskaya radiologiya, v. 26, pp. 11–16, 1981 (Russian).
70. Guskova A.K., Baranov A.E., Barabanova A.V., Gruzdev G.P., Pyatkin E.K., Nadezhina N.M., Metlyaeva N.A., Selidovkin G.D., Gusev I.A., Moiseev A.A., Dorofeeva E.M., Zykova I.E., Konchalovsky M.V. Acute radiation effects in exposed persons at the Chernobyl atomic power station accident. Meditsinskaya radiologiya, v. 32, pp. 3–18, 1987 (Russian).
71. Pontryagin L.S. Ordinary Differential Equations. Moscow: Nauka, 1982 (Russian).
72. Andronov A.A., Vitt A.A., Khikin S.E. Theory of Oscillations. Moscow: Nauka, 1981 (Russian).
73. Andronov A.A., Leontovich E.A., Gordon I.I., Maier A.G. Theory of Bifurcations of Dynamical Systems on Plane. Moscow: Nauka, 1967 (Russian).
74. Hayashi C. Nonlinear Oscillations in Physical Systems. New York: McGraw-Hill Book Company, 1964.
75. Arrowsmith D.K., Place C.M. Ordinary Differential Equations. A Qualitative Approach with Applications. London: Chapman and Hall, 1982.
76. Dulac H. Sur les cycles limités. Bulletin de la Société Mathématique de France, v. 51, pp. 45–188, 1923.
77. Korn G.A., Korn T.M. Mathematical Handbook. New York: McGraw-Hill Book Company, 1968.
78. Dan K., Inokuchi K., An E., Nomura T. Cell-mediated cyclic thrombocytopenia treated with azathioprine. British Journal of Haematology, v. 77, pp. 365–370, 1991.
79. Reimann H.A. Haemocytic periodicity and periodic disorders: Periodic neutropenia, thrombocytopenia, lymphocytosis and anaemia. Postgraduate Medical Journal, v. 47, pp. 504–510, 1971.
80. Lewis M.L. Cyclic thrombocytopenia: A thrombopoietin deficiency? Journal of Clinical Pathology, v. 27, pp. 242–246, 1974.
81. Morley A., Haurie C., Mackey M.C., Daled D.C., Periodic hematological disorders. Blood, v. 93, pp. 4023–4024, 1999.
82. Hauriea, C., Daled, D.C., Mackey, M.C., Cyclic neutropenia and other periodic hematological disorders: A review of mechanisms and mathematical models. Blood, v. 92(8), pp. 2629–2640, 1998.
83. Hauriea C., Daled D.C., Mackey M.C. Occurrence of periodic oscillations in the differential blood counts of congenital, idiopathic, and cyclical neutropenic patients before and during treatment with G-CSF. Experimental Hematology, v. 27(3), pp. 401–409, 1999.
84. Hansen N.E., Andersen V., Kable H. Plasma lysozyme in drug-induced and spontaneous cyclic neutropenia. British Journal of Hematology, v. 25, pp. 485–495, 1973.
85. Kim D.H., Kim J.G., Sohn S.K., Sung W.J., Suh J.S., Lee K.S., Lee K.B. Clinical impact of early absolute lymphocyte count after allogeneic stem cell transplantation. British Journal of Haematology, v. 125(2), pp. 217–224, 2004.
86. Guskova A.K., Baranov A.E., Gusev I.A. Acute radiation sickness: underlying principles and assessment. In: Gusev I.A., Guskova A.K., Mettler F.A. Jr., (Eds). Medical management of radiation accidents. Boca Raton, Fl: CRC Press, pp. 33–51, 2001.
87. Quastler H., Bensted J.P.M., Chir B. Adaptation to continuous irradiation: observations on the rat intestine. British Journal of Radiology, v. 32, pp. 501–512, 1959.
88. Fabrikant J.I. Adaptation of cell renewal systems under continuous irradiation. Health Physics, v. 52, pp. 561–570, 1987.
89. Muksinova K.N., Mushkacheva G.S. Cellular and molecular bases of haemopoiesis transformation under continuous irradiation. Moscow: Energoatomizdat, 1990 (Russian).

90. Akleyev A.V., Kisselyov M.F. (Eds.). Medical-biological and ecological impacts of radioactive contamination of the Techa river. Moscow: Medbioextrem, 2001 (Russian).
91. Matsuzawa T., Wilson R. The intestinal mucosa of germfree mice after whole-body *X*-irradiation with 3 kiloroentgens. Radiation Research, v. 25(1), pp. 15–24, 1965.
92. Kalina I., Praslichka M. Changes in haemopoiesis and survival of continuously irradiated mice. Radiobiologiya, v. 17, pp. 849–853, 1977 (Russian).
93. Fliedner T.M., Graessle D.H. Hematopoietic cell renewal systems: mechanisms of coping and failing after chronic exposure to ionizing radiation. Radiation and environmental biophysics, v. 47(1), pp. 63–69, 2008.
94. National Council on Radiation Protection and Measurements. Guidance on Radiation Received in Space Activity (NCRP report no. 98). Bethesda, MD: NCRP, 1989.
95. Cucinotta F.A., Kim M.Y., Ren L. Evaluating shielding effectiveness for reducing space radiation cancer risks. Radiation Measurements, v. 41, pp. 1173–1185, (2006).
96. Hu S., Kim M.Y., McClellan G.E., Cucinotta F.A. Modeling the acute health effects of astronauts from exposure to large solar particle events. Health Physics, v. 96, pp. 465–476, 2009.

Chapter 8
Radiogenic Leukemia Risk Assessment

8.1 Introduction

Ionizing radiation is a human leukemogen [1, 2]. In particular, statistically significant increases of the leukemia risk were observed among atomic bomb survivors, uranium miners, radium dial workers, radiologists, patients undergoing repeated fluoroscopic or radiographic diagnostic examinations, and patients treated with radiotherapy [3–8]. Radiogenic leukemia has the shortest minimal latency period among all cancers (about 2 years) [8].

A leukemogenic effect of a radiation exposure is characterized by the relative risk (*RR*) for leukemia. The value of *RR* is determined as the ratio of odds for leukemia among exposed individuals (P_R) to odds for leukemia among unexposed individuals (P_G) [8]:

$$RR = \frac{P_R}{P_G}. \tag{8.1}$$

The other characteristic of a leukemogenic effect of a radiation exposure is the excess relative risk (*ERR*) for leukemia. The value of *ERR* is equal to *RR* minus unity [8]:

$$ERR = RR - 1 = \frac{P_R - P_G}{P_G}. \tag{8.2}$$

The risk of radiation-induced leukemia depends on an exposure dose, as well as on an exposure dose rate [1]. In particular, the excess relative risk for leukemia among atomic bomb survivors, who received an instantaneous whole-body exposure, increases with the growth of an exposure dose, reaches a peak at an exposure dose of 3–4 Gy, and decreases with its further growth [1].

O.A. Smirnova, *Environmental Radiation Effects on Mammals*,
DOI 10.1007/978-3-319-45761-1_8

To fit the dependence of the excess relative risk for leukemia on the dose D of acute irradiation, the linear–quadratic–exponential equation can be used (see, e.g., [1, 9]). In particular, it is this equation that was successfully employed for fitting the data on the dose dependence of the excess relative risk for leukemia among atomic bomb survivors, which were exposed to acute irradiation in a wide range of doses [10]. In turn, to fit the dose dependence of the excess relative risk for leukemia among atomic bomb survivors, which were exposed to acute irradiation with comparatively low doses, the linear equation, the linear–quadratic equation, the pure-quadratic equation, and some other ones can also be used [1, 3].

The primary objectives of our studies [11] were the development of a dynamical modeling approach to the estimation of the excess relative risk for myeloid and lymphocytic leukemia among humans exposed to acute and continuous irradiation.

8.2 Foundations of the Dynamical Modeling Approach to Radiogenic Leukemia Risk Assessment

The dynamical modeling approach to the estimation of the excess relative risk for myeloid and lymphocytic leukemia among humans exposed to acute and continuous irradiation is based on the conventional radiobiological concepts:

1. Radiation-induced damage of cells can initiate the production of changes that make a cell premalignant, such as chromosomal aberrations (stage of initiation) [1, 2].
2. Cells with the aforementioned cytogenetic abnormalities may become (under certain factors) malignant cells that, in turn, may lead (under certain factors) to the development of cancer (stages of promotion and progression) [1, 2, 12, 13].
3. Target cells, radiation-induced damages of which may, eventually, lead to the development of myeloid leukemia, are bone marrow granulopoietic cells capable of dividing in the granulopoietic system [2, 14].
4. Target cells, radiation-induced damages of which may, eventually, lead to the development of lymphocytic leukemia, are bone marrow lymphopoietic cells capable of dividing in the lymphopoietic system [2, 14].

Proceeding from these concepts, it is reasonable to suppose that certain characteristics of the dynamics of the above-indicated granulopoietic cells in the granulopoietic system of irradiated individuals can correlate with the odds for the appearance of myeloid leukemia among those individuals, whereas certain characteristics of the dynamics of the above-indicated lymphopoietic cells in the lymphopoietic system of irradiated individuals can correlate with the odds for the appearance of lymphocytic leukemia among those individuals.[1]

[1]Note that examples of correlations between certain characteristics of deterministic effects of ionizing radiation and its stochastic effects were revealed in, e.g., [15–17].

To discover such correlations, mathematical models of the dynamics of the granulopoietic and lymphopoietic systems in acutely and chronically irradiated humans, which were developed by the author (see Chap. 7, as well as [18–24]), are employed. Specifically, the mathematical models of the granulopoietic and lymphopoietic systems are implied to simulate the dynamics of these major hematopoietic lineages in humans under the radiation exposures, which correspond to those reported for historical data on the excess relative risk for myeloid and lymphocytic leukemia among atomic bomb survivors exposed to acute irradiation and among patients exposed to continuous irradiation in a course of brachytherapy. In turn, the obtained modeling results are used to reveal correlations between key characteristics of the dynamics of above-indicated granulopoietic and lymphopoietic cells in the granulopoietic and lymphopoietic systems in acutely or continuously irradiated individuals and the data on the excess relative risk for myeloid and lymphocytic leukemia among the relevant groups of exposed individuals. The results of such studies are presented in this chapter.

8.3 Risks for Acute and Chronic Myeloid Leukemia Among Acutely Irradiated Humans

The model of the granulopoietic system [Eqs. (7.11)–(7.20) with the initial conditions (7.27)–(7.32) and the parameters given in Table 7.2] (see Chap. 7) is applied to examine the response of this system to acute irradiation. A particular attention is paid to the modeling study of the dynamics of the dimensionless concentration of weakly damaged bone marrow granulopoietic cells capable of dividing (X_1^{wd} cells). It is these cells that can be considered as the cells having radiation-induced cytogenetic abnormalities that make a cell premalignant (see Sect. 8.1).

Figures 8.1, 8.2, 8.3, and 8.4 present the modeling results on the dynamics of the dimensionless concentration of blood granulocytes (X_3 cells) in the granulopoietic system of humans exposed to acute irradiation with doses D reported in [25–27] and the respective empirical data [25–27]. As one can see from these figures the modeling results and empirical data are in a good agreement with each other.

Figures 8.1, 8.2, 8.3, and 8.4 also display the modeling results on the dynamics of the dimensionless concentration of weakly damaged bone marrow precursor cells capable of dividing (X_1^{wd} cells) in the granulopoietic system of humans exposed to acute irradiation with the same doses D. As one can infer from Figs. 8.1, 8.2, 8.3, and 8.4, the dimensionless concentration of X_1^{wd} cells increases after acute irradiation and reaches its maximum. Then the dimensionless concentration of X_1^{wd} cells decreases, practically, to zero over considered period of time.

The juxtaposition of the modeling results given in Figs. 8.1, 8.2, 8.3, and 8.4 with each other elucidates that the dose dependence of the maximum of the dimensionless concentration of X_1^{wd} cells resembles to the dose dependencies of the excess relative risk for acute and chronic myeloid leukemia among atomic bomb survivors of all age groups together [10].

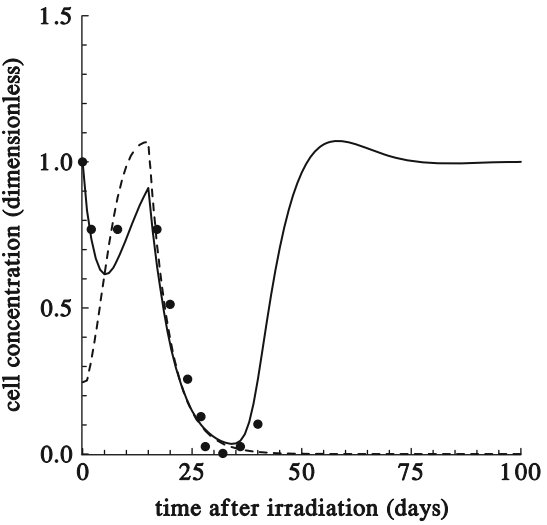

Fig. 8.1 Modeling results on the dynamics of dimensionless concentrations of the blood granulocytes (X_3 cells) (*solid curve*) and their weakly damaged bone marrow precursor cells capable of dividing (X_1^{wd} cells) (*dashed curve*) in the granulopoietic system of a human exposed to acute irradiation at the dose D of 2.0 Gy. Relevant empirical data on the blood granulocyte concentration [25] are shown by *circles*

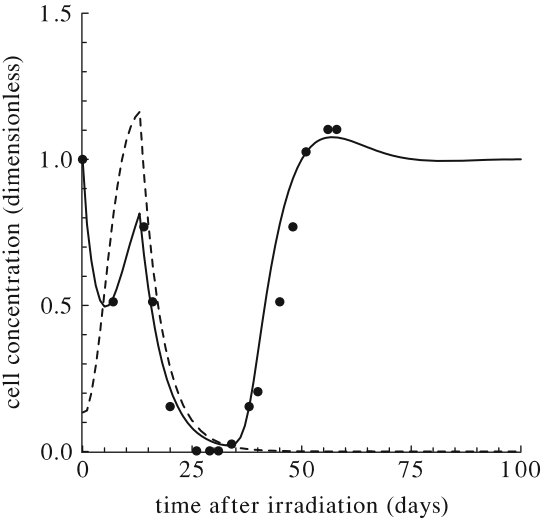

Fig. 8.2 Modeling results on the dynamics of dimensionless concentrations of the blood granulocytes (X_3 cells) (*solid curve*) and their weakly damaged bone marrow precursor cells capable of dividing (X_1^{wd} cells) (*dashed curve*) in the granulopoietic system of a human exposed to acute irradiation at the dose D of 3.0 Gy. Pertinent empirical data on the blood granulocyte concentration [26] are shown by *circles*

Accounting for these modeling findings and basing on the conventional radiobiological concepts of the leukemogenic effect of ionizing radiation (see Sect. 8.1), it is reasonable to assume that the odds for acute myeloid leukemia and the odds for chronic myeloid leukemia among acutely exposed individuals are greater when the levels of X_1^{wd} cells in the granulopoietic system in those individuals are higher. To verify this assumption on the quantitative level, values of the maximum of the dimensionless concentration of X_1^{wd} cells over the period of the response of the granulopoietic system to acute irradiation in the wide range of doses D ($0 \leq D \leq 8$ Gy) are computed in the framework of the model of this system. Then the obtained

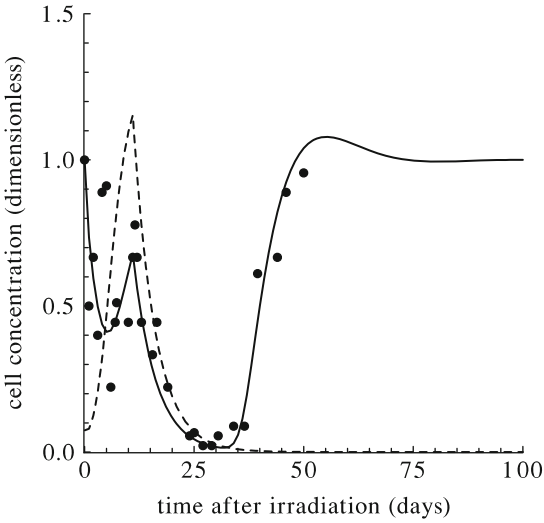

Fig. 8.3 Modeling results on the dynamics of dimensionless concentrations of the blood granulocytes (X_3 cells) (*solid curve*) and their weakly damaged bone marrow precursor cells capable of dividing (X_1^{wd} cells) (*dashed curve*) in the granulopoietic system of a human exposed to acute irradiation at the dose D of 3.9 Gy. Respective empirical data on the blood granulocyte concentration [27] are shown by *circles*

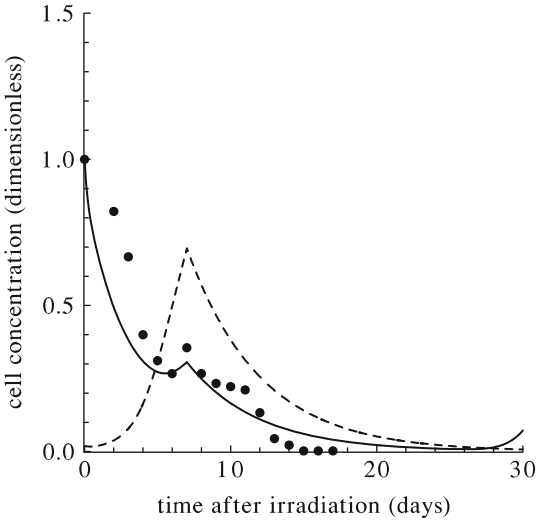

Fig. 8.4 Modeling results on the dynamics of dimensionless concentrations of the blood granulocytes (X_3 cells) (*solid curve*) and their weakly damaged bone marrow precursor cells capable of dividing (X_1^{wd} cells) (*dashed curve*) in the granulopoietic system of a human exposed to acute irradiation at the dose D of 6.0 Gy. Corresponding empirical data on the blood granulocyte concentration [26] are shown by *circles*

dose dependence of the maximum of the dimensionless concentration of X_1^{wd} cells is juxtaposed with the dose dependence of the excess relative risk for the acute myeloid leukemia and with the dose dependence of the excess relative risk for the chronic myeloid leukemia among atomic bomb survivors of all age groups together, which were fitted by the following linear–quadratic–exponential equations [10]:

$$ERR_F^{AML} = (a_1 D + a_2 D^2) \exp(-a_3 D - a_4 D^2), \tag{8.3}$$

$$ERR_F^{CML} = (b_1 D + b_2 D^2) \exp(-b_3 D - b_4 D^2), \tag{8.4}$$

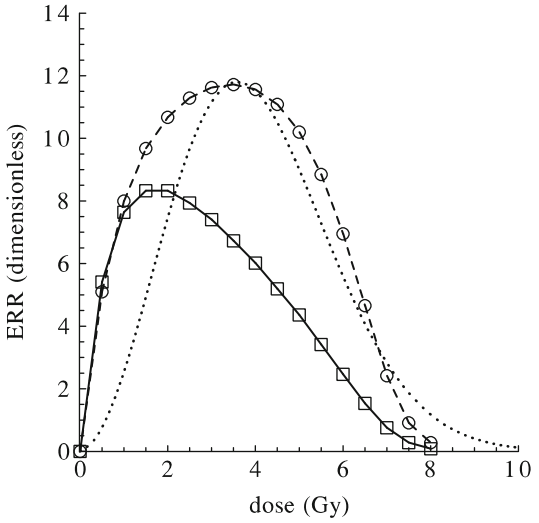

Fig. 8.5 The dose dependence of the properly scaled maximum concentration of X_1^{wd} cells (*dashed curve* marked by *empty circle*) and the dose dependence of the properly scaled integral of the dimensionless concentration of X_1^{wd} cells (*solid curve* marked by *empty box*) over the period of the response of the granulopoietic system to acute irradiation, which are computed in the framework of the model of this major hematopoietic lineage. The *dotted curve* displays the function ERR_F^{AML} [Eq. (8.3)], which fits the dose dependence of the excess relative risk for acute myeloid leukemia among atomic bomb survivors of all age group together [10]

where $a_1 = 0.423\,\mathrm{Gy}^{-1}$, $a_2 = 2.32\,\mathrm{Gy}^{-2}$, $a_3 = 0$, $a_4 = 0.076\,\mathrm{Gy}^{-2}$, $b_1 = 5.05\,\mathrm{Gy}^{-1}$, $b_2 = 0$, $b_3 = 0.345\,\mathrm{Gy}^{-1}$, and $b_4 = 0$.

It is found that the dose dependence of the maximum of the dimensionless concentration of X_1^{wd} cells, which is multiplied by the scale factor $S_M^{AML} = 10$, corresponds to the function ERR_F^{AML} [Eq. (8.3)] in the considered range of doses D ($0 \le D \le 8\,\mathrm{Gy}$) (Fig. 8.5). Specifically, as one can infer from this figure, both the properly scaled maximum of the dimensionless concentration of X_1^{wd} cells and the function ERR_F^{AML} increase with the growth of an exposure dose D, reach their peaks at the exposure dose D of 3.5 Gy and 3.6 Gy, respectively, and decrease with its further growth. It is important that the doses, at which the properly scaled maximum of the dimensionless concentration of X_1^{wd} cells and the function ERR_F^{AML} approach their peaks, are very close to each other. The peak values, practically, coincide.

These results attest that the computed values of the properly scaled maximum of the dimensionless concentration of X_1^{wd} cells over the period of the response of the granulopoietic system to acute irradiation in the considered range of doses D ($0 \le D \le 8\,\mathrm{Gy}$) can be used to predict the excess relative risk ERR_M^{AML} for acute myeloid leukemia among humans exposed to the acute radiation in the above-indicated range of doses D ($0 \le D \le 8\,\mathrm{Gy}$).

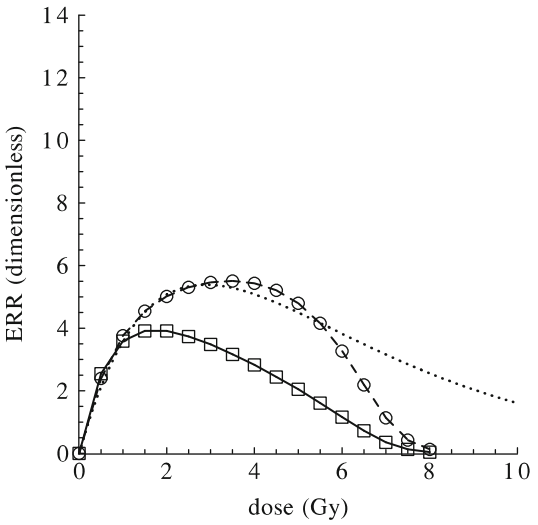

Fig. 8.6 The dose dependence of the properly scaled maximum of the dimensionless concentration of X_1^{wd} cells (*dashed curve* marked by *empty circle*) and the dose dependence of the properly scaled integral of the dimensionless concentration of X_1^{wd} cells (*solid curve* marked by *empty box*) over the period of the response of the granulopoietic system to acute irradiation, which are computed in the framework of the model of this major hematopoietic lineage. The *dotted line* displays the function ERR_F^{CML} [Eq. (8.4)], which fits the dose dependence of the excess relative risk for chronic myeloid leukemia among atomic bomb survivors of all age group together [10]

In turn, it is revealed that the dose dependence of the maximum of the dimensionless concentration of X_1^{wd} cells, which is multiplied by the scale factor $S_M^{CML} = 4.7$, conforms to the function ERR_F^{CML} [Eq. (8.4)] in the considered range of doses D ($0 \leq D \leq 8$ Gy) (Fig. 8.6). Specifically, as one can see from this figure, both the properly scaled maximum of the dimensionless concentration of X_1^{wd} cells and the function ERR_F^{CML} increase with the growth of an exposure dose D, reach their peaks at the exposure dose D of 3.5 Gy and 3.0 Gy, respectively, and decrease with its further growth. It is worth noting that the doses, at which the properly scaled maximum of the dimensionless concentration of X_1^{wd} cells and the function ERR_F^{CML} approach their peaks, are close to each other. In turn, the peak values, practically, coincide.

These results testify that the computed values of the properly scaled maximum of the dimensionless concentration of X_1^{wd} cells over the period of the response of the granulopoietic system to acute irradiation in the considered range of doses D ($0 \leq D \leq 8$ Gy) can be used to predict the excess relative risk ERR_M^{CML} for chronic myeloid leukemia among humans exposed to the acute irradiation in the above-indicated range of doses D ($0 \leq D \leq 8$ Gy).

Basing on the conventional radiobiological concepts of the leukemogenic effect of ionizing radiation (see Sect. 8.1), it is also reasonable to assume that the odds for acute myeloid leukemia, as well as the odds for chronic myeloid leukemia, among

acutely exposed individuals are greater when the total amount of premalignant granulopoietic cells in the granulopoietic system in those individuals over the period of the response of this system to acute irradiation are higher. To verify this assumption on the quantitative level, values of the integral of the dimensionless concentration of X_1^{wd} cells over the period of the response of the granulopoietic system to acute irradiation in the considered range of doses D ($0 \leq D \leq 8$ Gy) are computed in the framework of the model of this major hematopoietic lineage. Then the obtained dose dependence of the integral of the dimensionless concentration of X_1^{wd} cells is juxtaposed with the dose dependence of the excess relative risk for the acute myeloid leukemia ERR_F^{AML} [Eq. (8.3)] and the dose dependence of the excess relative risk for the chronic myeloid leukemia ERR_F^{cML} [Eq. (8.4)] among atomic bomb survivors of all age groups together.

It is discovered that the dose dependence of the integral of the dimensionless concentration of X_1^{wd} cells, which is multiplied by the scale factor $S_I^{AML} = 0.5$, and the function ERR_F^{AML} [Eq. (8.3)], which fits the dose dependence of the excess relative risk for acute myeloid leukemia among atomic bomb survivors of all age groups together, agree with each other in the range of comparatively low doses D ($0 \leq D \leq 1$ Gy) (Fig. 8.5). Note that the scale factor S_I^{AML} is equal to the product of the above-indicated scale factor S_M^{AML} and a new scale factor $Q = 0.05$ (i.e., $S_I^{AML} = S_M^{AML} \times Q$).

These findings attest that the computed values of the properly scaled integral of the dimensionless concentration of X_1^{wd} cells over the period of the response of the granulopoietic system to acute irradiation in the range of comparatively low doses D ($0 \leq D \leq 1$ Gy) can be used to predict the excess relative risk for acute myeloid leukemia ERR_I^{AML} among humans exposed to acute irradiation in the above-indicated range of doses D ($0 \leq D \leq 1$ Gy).

It is determined that the dose dependence of the integral of the dimensionless concentration of X_1^{wd} cells, which is multiplied by the scale factor $S_I^{CML} = 0.235$, and the function ERR_F^{CML} [Eq. (8.4)], which fits the dose dependence of the excess relative risk for chronic myeloid leukemia among atomic bomb survivors of all age groups together, are in a good agreement with each other in the range of comparatively low doses D ($0 \leq D \leq 1$ Gy) (Fig. 8.6). Note that the scale factor S_I^{CML} is equal to the product of the above-indicated scale factor S_M^{CML} and the same scale factor $Q = 0.05$ (i.e., $S_I^{CML} = S_M^{CML} \times Q$).

These results testify that the computed values of the properly scaled integral of the dimensionless concentration of X_1^{wd} cells over the period of the response of the granulopoietic system to acute irradiation in the range of comparatively low doses D ($0 \leq D \leq 1$ Gy) can be used to predict the excess relative risk for chronic myeloid leukemia ERR_I^{CML} among humans exposed to acute irradiation in the above-indicated range of doses D ($0 \leq D \leq 1$ Gy).

8.4 Risks for Acute Lymphocytic Leukemia Among Acutely Irradiated Humans

The model of the lymphopoietic system [Eqs. (7.11)–(7.13), (7.15)–(7.17), (7.19), and (7.20) with the initial conditions (7.27)–(7.32) and the parameters given in Table 7.3] (see Chap. 7) is applied to examine the response of this system to acute irradiation in a wide range of doses. A particular attention is paid to the modeling study of the dynamics of the concentration of weakly damaged bone marrow lymphopoietic cells capable of dividing (X_1^{wd} cells). It is these cells that can be considered as the cells having radiation-induced cytogenetic abnormalities that make a cell premalignant (see Sect. 8.1).

Figures 8.7, 8.8, 8.9, and 8.10 present the modeling results on the dynamics of the dimensionless concentration of blood lymphocytes (X_3 cells) in the lymphopoietic system in humans exposed to acute irradiation with doses D reported in [25, 26, 28, 29] and the respective empirical data [25, 26, 28, 29]. As one can infer from these figures, the modeling results are in a good agreement with these empirical data [25, 26, 28, 29].

Figures 8.7, 8.8, 8.9, and 8.10 also display the modeling results on the dynamics of the dimensionless concentration of weakly damaged bone marrow precursor cells capable of dividing (X_1^{wd} cells) in the lymphopoietic system of humans exposed to acute irradiation with the same doses D. As one can see from these figures, the dimensionless concentration of X_1^{wd} cells increases after acute irradiation and reaches its maximum. Then the dimensionless concentration of X_1^{wd} cells decreases, practically, to zero over considered period of time.

The juxtaposition of the modeling results given in Figs. 8.7, 8.8, 8.9, and 8.10 with each other elucidates that the dose dependence of the maximum of the

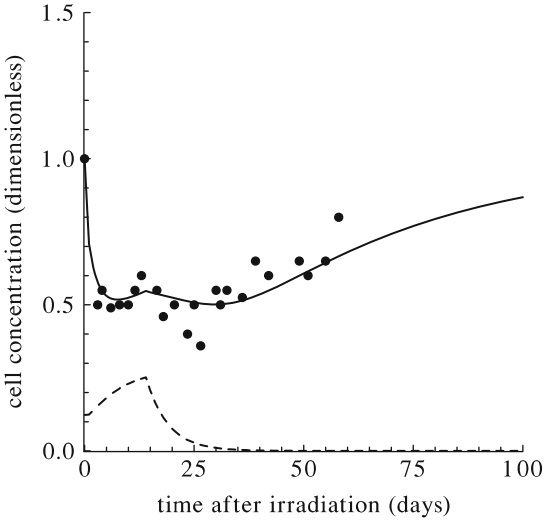

Fig. 8.7 Modeling results on the dynamics of dimensionless concentrations of the blood lymphocytes (X_3 cells) (*solid curve*) and their weakly damaged bone marrow precursor cells capable of dividing (X_1^{wd} cells) (*dashed curve*) in the lymphopoietic system of a human exposed to acute irradiation at the dose D of 1.1 Gy. Relevant empirical data on the blood granulocyte concentration [28] are shown by *circles*

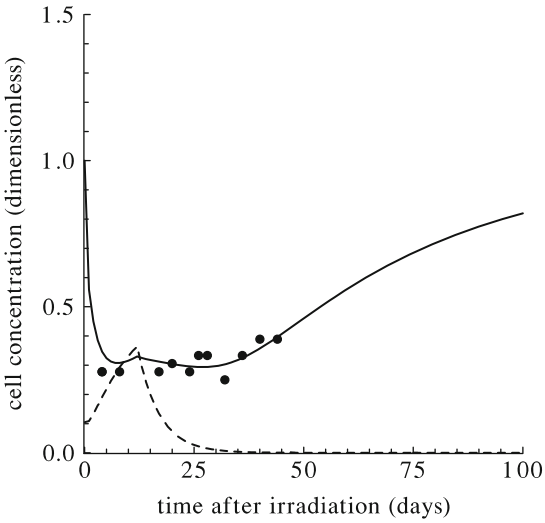

Fig. 8.8 Modeling results on the dynamics of dimensionless concentrations of the blood lymphocytes (X_3 cells) (*solid curve*) and their weakly damaged bone marrow precursor cells capable of dividing (X_1^{wd} cells) (*dashed curve*) in the lymphopoietic system of a human exposed to acute irradiation at the dose D of 2.0 Gy. Pertinent empirical data on the blood lymphocyte concentration [25] are shown by *circles*

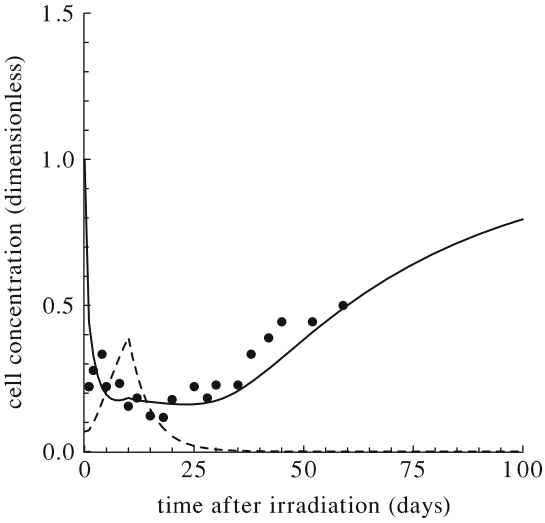

Fig. 8.9 Modeling results on the dynamics of dimensionless concentrations of the blood lymphocytes (X_3 cells) (*solid curve*) and their weakly damaged bone marrow precursor cells capable of dividing (X_1^{wd} cells) (*dashed curve*) in the lymphopoietic system of a human exposed to acute irradiation at the dose D of 3.0 Gy. Respective empirical data on the blood lymphocyte concentration [29] are shown by *circles*

dimensionless concentration of X_1^{wd} cells resembles to the dose dependence of the excess relative risk for acute lymphocytic leukemia among atomic bomb survivors of all age groups together [10].[2]

Accounting for these modeling findings and basing on the conventional radiobiological concepts of the leukemogenic effect of ionizing radiation (see Sect. 8.1), it is reasonable to assume that the odds for acute lymphocytic leukemia among acutely exposed individuals are greater when the levels of X_1^{wd} cells in the lymphopoietic

[2]Note that the chronic lymphocytic leukemia (*CLL*) is very seldom in Japan [3].

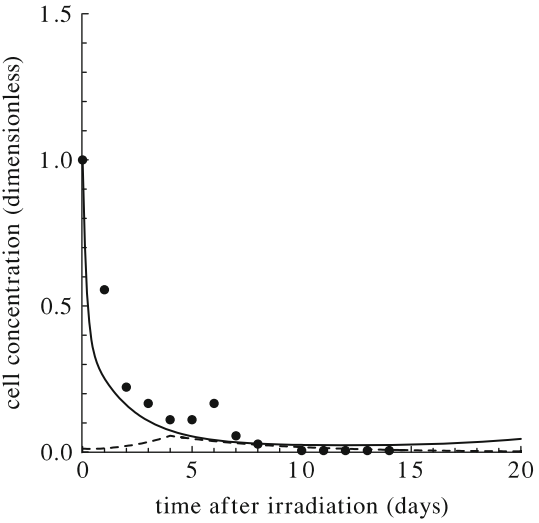

Fig. 8.10 Modeling prediction of the dynamics of dimensionless concentrations of the blood lymphocytes (X_3 cells) (*solid curve*) and their weakly damaged bone marrow precursor cells capable of dividing (X_1^{wd} cells) (*dashed curve*) in the lymphopoietic system of a human exposed to acute irradiation at the dose D of 6.0 Gy. Corresponding empirical data on the blood lymphocyte concentration [26] are shown by *circles*

system in those individuals are higher. To verify this assumption on the quantitative level, values of the maximum of the dimensionless concentration of X_1^{wd} cells in the period of the response of the lymphopoietic system to acute irradiation in the wide range of doses D ($0 \le D \le 8$ Gy) are computed in the framework of the model of this major hematopoietic lineage. Then the dose dependence of the maximum of the dimensionless concentration of X_1^{wd} cells is juxtaposed with the dose dependence of the excess relative risk for the acute lymphocytic leukemia among atomic bomb survivors of all age groups together, which was fitted by the following linear–quadratic–exponential equation [10]:

$$ERR_F^{ALL} = (c_1 D + c_2 D^2) \exp(-c_3 D - c_4 D^2), \tag{8.5}$$

where $c_1 = 2.23\,\text{Gy}^{-1}$, $c_2 = 4.15\,\text{Gy}^{-2}$, $c_3 = 0$, and $c_4 = 0.0344\,\text{Gy}^{-2}$.

It is found that the dose dependence of the maximum of the dimensionless concentration of X_1^{wd} cells, which is multiplied by the scale factor $S_M^{ALL} = 25$, agrees with the function ERR_F^{ALL} in the considered range of doses D ($0 \le D \le 8$ Gy) (Fig. 8.11). Specifically, as one can infer from this figure, both the properly scaled maximum of the dimensionless concentration of X_1^{wd} cells and the function ERR_F^{ALL} increase with the growth of an exposure dose D, reach their peaks at the exposure dose D of 3.0 Gy and 2.5 Gy, respectively, and decrease with its further growth. It is worth noting that the doses, at which the properly scaled maximum of the dimensionless concentration of X_1^{wd} cells and the function ERR_F^{ALL} approach their peaks, are close to each other. In turn, the peak values are also close to each other.

These results attest that the computed values of the properly scaled maximum of the dimensionless concentration of X_1^{wd} cells over the period of the response of the lymphopoietic system to acute irradiation in the considered range of doses D ($0 \le D \le 8$ Gy) can be used to predict the excess relative risk for acute lymphocytic leukemia ERR_M^{ALL} among humans exposed to the acute radiation in the above-indicated range of doses D ($0 \le D \le 8$ Gy).

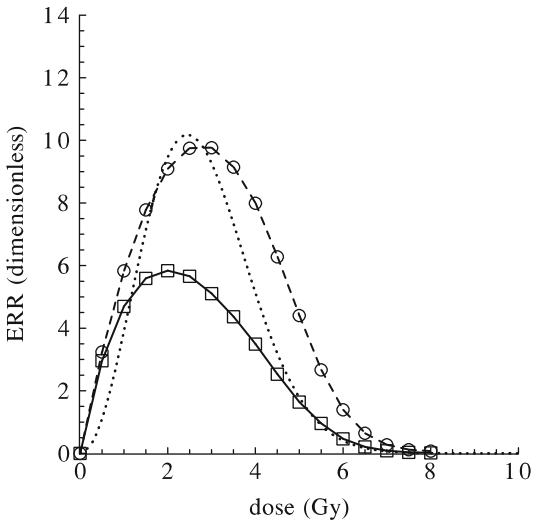

Fig. 8.11 The dose dependence of the properly scaled maximum concentration of X_1^{wd} cells (*dashed curve* marked by *empty circle*) and the dose dependence of the properly scaled integral of the dimensionless concentration of X_1^{wd} cells (*solid curve* marked by empty box) over the period of the response of the lymphopoietic system to acute irradiation, which are computed in the framework of the model of this major hematopoietic lineage. The *dotted curve* shows the function ERR_F^{ALL} [Eq. (8.5)], which fits the dose dependence of the excess relative risk for acute lymphocytic leukemia among atomic bomb survivors of all age group together [10]

Basing on the conventional radiobiological concepts of the leukemogenic effect of ionizing radiation (see Sect. 8.1), it is also reasonable to assume that the odds for acute lymphocytic leukemia among acutely exposed individuals are greater when the total amounts of premalignant lymphopoietic cells in the lymphopoietic system in those individuals over the period of the response of this system to acute irradiation are higher. To verify this assumption on the quantitative level, values of the integral of the dimensionless concentration of X_1^{wd} cells over the period of the response of the lymphopoietic system to acute irradiation in the considered range of doses D ($0 \leq D \leq 8$ Gy) are computed in the framework of the model of this major hematopoietic lineage.

It is revealed that the dose dependence of the integral of the dimensionless concentration of X_1^{wd} cells, which is multiplied by the scale factor $S_I^{ALL} = 1.25$, and the function ERR_F^{ALL} [Eq. (8.5)], which fits the dose dependence of the excess relative risk for acute lymphocytic leukemia among atomic bomb survivors of all age groups together, agree with each other in the range of comparatively low doses D ($0 \leq D \leq 1$ Gy) (Fig. 8.11). It is important to note that the scale factor S_I^{ALL} is equal to the product of the above-indicated scale factor S_M^{ALL} and the scale factor $Q = 0.05$ (i.e., $S_I^{ALL} = S_M^{ALL} \times Q$).

These results testify that the computed values of the properly scaled integral of the dimensionless concentration of X_1^{wd} cells over the period of the response of the lymphopoietic system to acute irradiation in the range of comparatively low doses D ($0 \leq D \leq 1$ Gy) can be used to predict the excess relative risk for the acute lymphocytic leukemia ERR_I^{ALL} among humans exposed to acute irradiation in the above-indicated range of doses D ($0 \leq D \leq 1$ Gy).

8.5 Risks for Myeloid Leukemia Among Acutely Irradiated Humans

The values of the excess relative risks for acute myeloid leukemia and for chronic myeloid leukemia among humans exposed to acute irradiation with various doses D, which are obtained in the framework of the developed modeling approach (see Sect. 8.3), are used to determine the dose dependence of the excess relative risk for both acute and chronic myeloid leukemia, i.e., for myeloid leukemia among acutely irradiated humans. Specifically, the following modeling results are used for this aim:

- two sets of the values of the excess relative risk for acute myeloid leukemia, ERR_M^{AML} and ERR_I^{AML}, which were obtained in the frameworks of the granulopoiesis model proceeding from the values of the properly scaled maximum of the dimensionless concentration of X_1^{wd} cells and the properly scaled integral of the dimensionless concentration of X_1^{wd} cells over the period of the response of the granulopoietic system to acute irradiation in the considered ranges of doses D;
- two sets of the values of the excess relative risk for chronic myeloid leukemia, ERR_M^{CML} and ERR_I^{CML}, which were obtained in the frameworks of the granulopoiesis model proceeding from the values of the properly scaled maximum of the dimensionless concentration of X_1^{wd} cells and the properly scaled integral of the dimensionless concentration of X_1^{wd} cells over the period of the response of the granulopoietic system to acute irradiation in the considered ranges of doses D.

Taking into account of the definition of the relative risk for leukemia (RR) [Eq. (8.1)] and the definition of the excess relative risk for leukemia (ERR) [Eq. (8.2)], the dose dependence of the excess relative risk for myeloid leukemia among acutely irradiated humans ERR_M^{ML} can be expressed in terms of ERR_M^{AML} and ERR_M^{CML} in the following way:

$$ERR_M^{ML} = \frac{(ERR_M^{AML} + 1)P_G^{AML} + (ERR_M^{CML} + 1)P_G^{CML}}{P_G^{AML} + P_G^{CML}} - 1. \tag{8.6}$$

Here the parameters P_G^{AML} and P_G^{CML} are the background levels of odds for acute myeloid leukemia and for chronic myeloid leukemia, respectively. Their values are equal to $P_G^{AML} = 0.295$ and $P_G^{CML} = 0.095$ [10].

In turn, the function ERR_F^{ML}, which describes the dose dependence of the excess relative risk for myeloid leukemia among atomic bomb survivors of all age groups together, can be expressed in terms of the functions ERR_F^{AML} [Eq. (8.3)] and ERR_F^{CML} [Eq. (8.4)] by the formula analogous to Eq. (8.6):

$$ERR_F^{\mathrm{ML}} = \frac{(ERR_F^{\mathrm{AML}} + 1)P_G^{\mathrm{AML}} + (ERR_F^{\mathrm{CML}} + 1)P_G^{\mathrm{CML}}}{P_G^{\mathrm{AML}} + P_G^{\mathrm{CML}}} - 1, \tag{8.7}$$

where the parameters P_G^{AML} and P_G^{CML} are specified above.

Figure 8.12 shows the dose dependence of the excess relative risk for myeloid leukemia among acutely irradiated humans ERR_M^{ML} [Eq. (8.6)], which is predicted in the framework of the developed modeling approach, and the function ERR_F^{ML} [Eq. (8.7)], which describes the dose dependence of the excess relative risk for myeloid leukemia among atomic bomb survivors of all age groups together. As one can infer from this figure, they are in a good agreement with each other in the considered range of doses D ($0 \leq D \leq 8$ Gy). Specifically, both the functions ERR_M^{ML} and ERR_F^{ML} increase with the growth of an exposure dose D, reach their peaks at the exposure doses D of 3.5 Gy and 3.6 Gy, respectively, and decrease with its further growth. It is worth noting that the doses, at which the functions ERR_M^{ML} and ERR_F^{ML} approach their peaks, are very close to each other. In turn, the peak values, practically, coincide.

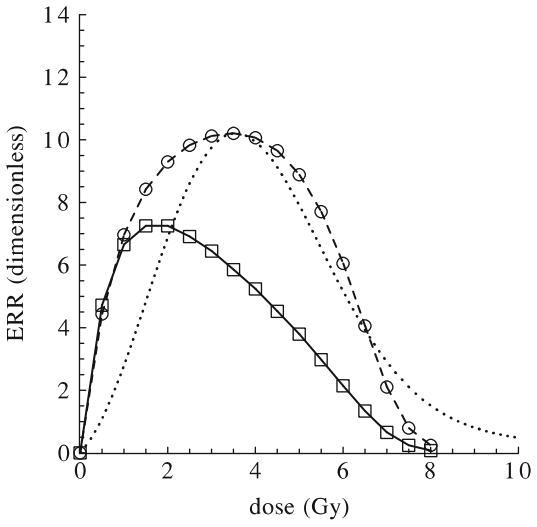

Fig. 8.12 The modeling prediction of the dose dependence of the excess relative risk ERR_M^{ML} [Eq. (8.6)] for myeloid leukemia among acutely irradiated humans (*dashed curve* marked by *empty circle*) and the dose dependence of the excess relative risk ERR_I^{ML} [Eq. (8.8)] for myeloid leukemia among acutely irradiated humans (*solid curve* marked by *empty box*). The *dotted curve* displays the function ERR_F^{ML} [Eq. (8.7)], which describes the dose dependence of the excess relative risk for myeloid leukemia among atomic bomb survivors of all age groups together [10]

These findings prove that the values of the excess relative risk for the acute myeloid leukemia ERR_M^{AML} and the excess relative risk for chronic myeloid leukemia ERR_M^{CML}, which are obtained proceeding from the computed values of the properly scaled maximum of the dimensionless concentration of X_1^{wd} cells over the period of the response of the granulopoietic system to acute irradiation in the considered range of doses D ($0 \leq D \leq 8$ Gy), can be used to predict the excess relative risk for myeloid leukemia ERR_M^{ML} among humans exposed to acute irradiation in the above-indicated range of doses D ($0 \leq D \leq 8$ Gy).

The values of the excess relative risk for acute myeloid leukemia ERR_I^{AML} and the excess relative risk for chronic myeloid leukemia ERR_I^{CML}, which are obtained proceeding from the computed values of the properly scaled integral of the dimensionless concentration of X_1^{wd} cells over the period of the response of the granulopoietic system to acute irradiation in the range of comparatively low doses D ($0 \leq D \leq 1$ Gy), are used to determine the respective values of the excess relative risk for both acute and chronic myeloid leukemia, i.e., the excess relative risk for myeloid leukemia ERR_I^{ML} among acutely irradiated humans. For this aim, the equation analogous to Eq. (8.6) is applied:

$$ERR_I^{ML} = \frac{(ERR_I^{\mathrm{AML}} + 1)P_G^{\mathrm{AML}} + (ERR_I^{\mathrm{CML}} + 1)P_G^{\mathrm{CML}}}{P_G^{\mathrm{AML}} + P_G^{\mathrm{CML}}} - 1, \tag{8.8}$$

where the parameters P_G^{AML} and P_G^{CML} are specified above.

Figure 8.12 presents the dose dependence of the excess relative risk for myeloid leukemia among acutely irradiated humans ERR_I^{ML} [Eq. (8.8)], which is predicted in the framework of the developed modeling approach. As one can infer from this figure, the function ERR_I^{ML} and the function ERR_F^{ML} [Eq. (8.7)], which describes the dose dependence of the excess relative risk for myeloid leukemia among atomic bomb survivors of all age groups together, agree with each other in the range of comparatively low doses D ($0 \leq D \leq 1$ Gy).

These findings argue that the values of the excess relative risk for the acute myeloid leukemia ERR_I^{AML} and for chronic myeloid leukemia ERR_I^{CML}, which are obtained proceeding from the computed values of the properly scaled integral of the dimensionless concentration of X_1^{wd} cells over the period of the response of the granulopoietic system to acute irradiation in the range of comparatively low doses D ($0 \leq D \leq 1$ Gy), can be used to predict the excess relative risk for myeloid leukemia ERR_I^{ML} among humans exposed to acute irradiation in the above-indicated range of doses D ($0 \leq D \leq 1$ Gy).

8.6 Risks for Leukemia Among Acutely Irradiated Humans

The modeling values of the excess relative risks for acute myeloid leukemia, chronic myeloid leukemia, and acute lymphocytic leukemia among humans exposed to acute irradiation with various doses D (see Sects. 8.3 and 8.4) are used to determine

the dose dependence of the excess relative risk for leukemia except for chronic lymphocytic leukemia (non-CLL) among acutely irradiated humans. Specifically, the following modeling results are used for this aim:

- two sets of the values of the excess relative risk for acute myeloid leukemia, ERR_M^{AML} and ERR_I^{AML}, which were obtained in the frameworks of the granulopoiesis model proceeding from the values of the properly scaled maximum of the dimensionless concentration of X_1^{wd} cells and the properly scaled integral of the dimensionless concentration of X_1^{wd} cells over the period of the response of the granulopoietic system to acute irradiation in the considered ranges of doses D;
- two sets of the values of the excess relative risk for chronic myeloid leukemia, ERR_M^{CML} and ERR_I^{CML}, which were obtained in the frameworks of the granulopoiesis model proceeding from the values of the properly scaled maximum of the dimensionless concentration of X_1^{wd} cells and the properly scaled integral of the dimensionless concentration of X_1^{wd} cells over the period of the response of the granulopoietic system to acute irradiation in the considered ranges of doses D;
- two sets of the values of the excess relative risk for acute lymphocytic leukemia, ERR_M^{ALL} and ERR_I^{ALL}, which were obtained in the frameworks of the lymphopoiesis model proceeding from the values of the properly scaled maximum of the dimensionless concentration of X_1^{wd} cells and the properly scaled integral of the dimensionless concentration of X_1^{wd} cells over the period of the response of the lymphopoietic system to acute irradiation in the considered ranges of doses D;

Taking into account of the definition of the relative risk for leukemia (RR) [Eq. (8.1)] and the definition of the excess relative risk for leukemia (ERR) [Eq. (8.2)], the dose dependence of the excess relative risk for non-CLL leukemia ERR_M^{L} among acutely irradiated humans is expressed in terms of ERR_M^{AML}, ERR_M^{CML}, and ERR_M^{ALL} in the following way:

$$ERR_M^{\mathrm{L}} = \frac{(ERR_M^{\mathrm{AML}} + 1)P_G^{\mathrm{AML}} + (ERR_M^{\mathrm{CML}} + 1)P_G^{\mathrm{CML}} + (ERR_M^{\mathrm{ALL}} + 1)P_G^{\mathrm{ALL}}}{P_G^{\mathrm{AML}} + P_G^{\mathrm{CML}} + P_G^{\mathrm{ALL}}} - 1. \tag{8.9}$$

Here the parameters P_G^{AML} and P_G^{CML} are specified above. The parameter P_G^{ALL} is the background levels of odds for acute lymphocytic leukemia. Its value is equal to $P_G^{\mathrm{ALL}} = 0.0687$ [10].

In turn, the dose dependence of the excess relative risk for non-CLL leukemia among acutely irradiated humans ERR_I^{L} is expressed in terms of ERR_I^{AML}, ERR_I^{CML}, and ERR_I^{ALL} by the formula analogous to Eq. (8.9):

$$ERR_I^{\mathrm{L}} = \frac{(ERR_I^{\mathrm{AML}} + 1)P_G^{\mathrm{AML}} + (ERR_I^{\mathrm{CML}} + 1)P_G^{\mathrm{CML}} + (ERR_I^{\mathrm{ALL}} + 1)P_G^{\mathrm{ALL}}}{P_G^{\mathrm{AML}} + P_G^{\mathrm{CML}} + P_G^{\mathrm{ALL}}} - 1, \tag{8.10}$$

where the parameters P_G^{AML}, P_G^{CML}, and P_G^{ALL} are specified above.

The obtained functions ERR_M^{L} [Eq. (8.9)] and ERR_I^{L} [Eq. (8.10)] are compared with the function ERR_F^{L}, which describes the dose dependence of the excess relative risk for non-CLL leukemia among atomic bomb survivors of all age groups together. The function ERR_F^{L} is expressed in terms of the functions ERR_F^{AML} [Eq. (8.3)], ERR_F^{CML} [Eq. (8.4)], and ERR_F^{ALL} [Eq. (8.5)] by the formula analogous to Eqs. (8.9) and (8.10):

$$ERR_F^{\mathrm{L}} = \frac{(ERR_F^{\mathrm{AML}} + 1)P_G^{\mathrm{AML}} + (ERR_F^{\mathrm{CML}} + 1)P_G^{\mathrm{CML}} + (ERR_F^{\mathrm{ALL}} + 1)P_G^{\mathrm{ALL}}}{P_G^{\mathrm{AML}} + P_G^{\mathrm{CML}} + P_G^{\mathrm{ALL}}} - 1, \tag{8.11}$$

where the parameters P_G^{AML}, P_G^{CML}, and P_G^{ALL} are specified above.

The functions ERR_M^{L} [Eq. (8.9)] and ERR_I^{L} [Eq. (8.10)] are also juxtaposed with the dose dependence of the excess relative risk for non-CLL leukemia among atomic bomb survivors exposed to comparatively low doses (the ages at the exposure exceed 20 years), which was fitted in [1] by the linear–quadratic–exponential equation:

$$ERR_H^{\mathrm{L}} = (h_1 D + h_2 D^2)\exp(-h_3 D - h_4 D^2), \tag{8.12}$$

where $h_1 = 0.243\,\mathrm{Gy}^{-1}$, $h_2 = 0.271\,\mathrm{Gy}^{-2}$, $h_3 = 2.367$, and $h_4 = 0$.

Figure 8.13 presents the functions ERR_M^{L} [Eq. (8.9)], ERR_I^{L} [Eq. (8.10)], ERR_F^{L} [Eq. (8.11)], and ERR_H^{L} [Eq. (8.12)]. As one can see from this figure, the dose dependence of the excess relative risk for non-CLL leukemia among acutely irradiated humans ERR_M^{L} [Eq. (8.9)], which is obtained in the framework of the developed modeling approach, and the function ERR_F^{L} [Eq. (8.11)], which describes the dose dependence of the excess relative risk for non-CLL leukemia among atomic bomb survivors of all age groups together, agree with each other in the wide range of doses D ($0 \le D \le 8\,\mathrm{Gy}$). Specifically, both the function ERR_M^{L} and the function ERR_F^{L} increase with the growth of an exposure dose D, reach their peaks at the exposure dose D of 3.0 Gy and 3.3 Gy, respectively, and decrease with its further growth. It is important to emphasize that the peak value of the excess relative risk for non-CLL leukemia ERR_M^{L}, which is predicted in the framework of the modeling approach, is quite close to the peak value of the function ERR_F^{L}, which describes the excess relative risk for non-CLL leukemia among atomic bomb survivors of all age groups together. It is also important to note that the modeling prediction of the dose D, at which the excess relative risk for non-CLL leukemia ERR_M^{L} reaches its peak, is quite close to the dose D, at which the function ERR_F^{L} approaches its peak. Additionally, the modeling value of dose D, at which the excess relative risk for non-CLL leukemia ERR_M^{L} reaches its peak, lies within the range of the dose values of 3–4 Gy, at which the excess relative risk for non-CLL leukemia among atomic bomb survivors reaches its peak [1].

These findings prove that the values of the excess relative risk for the acute myeloid leukemia ERR_M^{AML}, chronic myeloid leukemia ERR_M^{CML}, and acute lymphocytic leukemia ERR_M^{ALL}, which are obtained in the framework of the models of the granulopoietic and lymphopoietic systems proceeding from the values of the properly scaled maximum of the dimensionless concentrations of X_1^{wd} cells over the periods of the responses of these systems to acute irradiation in the wide range of

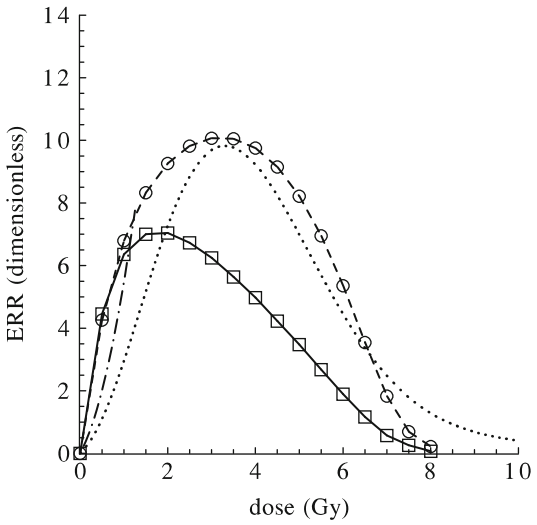

Fig. 8.13 The modeling prediction of the dose dependence of the excess relative risk ERR_M^{L} [Eq. (8.9)] (*dashed curve* marked by *empty circle*) and the dose dependence of the excess relative risk ERR_I^{L} [Eq. (8.10)] (*solid curve* marked by *empty box*) for non-CLL leukemia among acutely irradiated humans. The *dotted curve* displays the function ERR_F^{L} [Eq. (8.11)], which describes the dose dependence of the excess relative risk for non-CLL leukemia among atomic bomb survivors of all age groups together [10]. The *point-dashed curve* shows the function ERR_H^{L} [Eq. (8.12)], which fits the dose dependence of the excess relative risk for non-CLL leukemia among atomic bomb survivors exposed to comparatively low doses (the ages at the exposure did not exceed 20 years) [1]

doses D ($0 \leq D \leq 8$ Gy), can be used to predict the excess relative risk for non-CLL leukemia among humans exposed to acute irradiation in the above-indicated range of doses ($0 \leq D \leq 8$ Gy).

As one can also infer from Fig. 8.13, the dose dependence of the excess relative risk for non-CLL leukemia among acutely irradiated humans ERR_I^{L} [Eq. (8.10)], which is predicted in the framework of the developed modeling approach, and the function ERR_F^{L} [Eq. (8.11)], which describes the dose dependence of the excess relative risk for non-CLL leukemia among atomic bomb survivors of all age groups together, agree with each other in the range of comparatively low doses D ($0 \leq D \leq 1$ Gy). It is important to note that the function ERR_I^{L} also agrees with the function ERR_H^{L}, which fits the dose dependence of the excess relative risk for non-CLL leukemia among atomic bomb survivors exposed to comparatively low doses (the ages at the exposure exceed 20 years) [1].

These findings argue that the values of the excess relative risk for the acute myeloid leukemia ERR_I^{AML}, chronic myeloid leukemia ERR_I^{CML}, and acute lymphocytic leukemia ERR_I^{ALL}, which are obtained in the framework of the models of the granulopoietic and lymphopoietic systems proceeding from the values of the properly scaled integral of the dimensionless concentrations of X_1^{wd} cells over

the periods of the responses of these systems to acute irradiation in the range of comparatively low doses D ($0 \leq D \leq 1$ Gy), can be used to predict the excess relative risk for non-CLL leukemia among humans exposed to acute irradiation in the above-indicated range of doses ($0 \leq D \leq 1$ Gy).

8.7 Risks of Leukemia Among Continuously Irradiated Humans

The model of the human granulopoietic system [Eqs. (7.1)–(7.6) with the initial conditions (7.10) and the parameters given in Table 7.2] (see Chap. 7) and the model of the human lymphopoietic system [Eqs. (7.1)–(7.3), (7.5), (7.6) with the initial conditions (7.10) and the parameters given in Table 7.3] (see Chap. 7) are applied to examine the responses of these major hematopoietic lineages to continuous irradiation. In these modeling studies, the conditions of continuous exposures of patients with uterine corpus cancer, which were treated with brachytherapy [8], are simulated. As in the case of the investigation of the responses of the human granulopoietic and lymphopoietic systems to acute irradiation (see Sects. 8.3 and 8.4), a particular attention is paid to the study of the dynamics of the dimensionless concentration of weakly damaged bone marrow granulopoietic cells capable of dividing and the dynamics of the dimensionless concentration of weakly damaged bone marrow lymphopoietic cells capable of dividing under such exposures.

Figure 8.14 shows the modeling results on the dynamics of the dimensionless concentrations of blood granulocytes (X_3 cells) and weakly damaged bone marrow granulopoietic cells capable of dividing (X_1^{wd} cells) in humans exposed to continuous

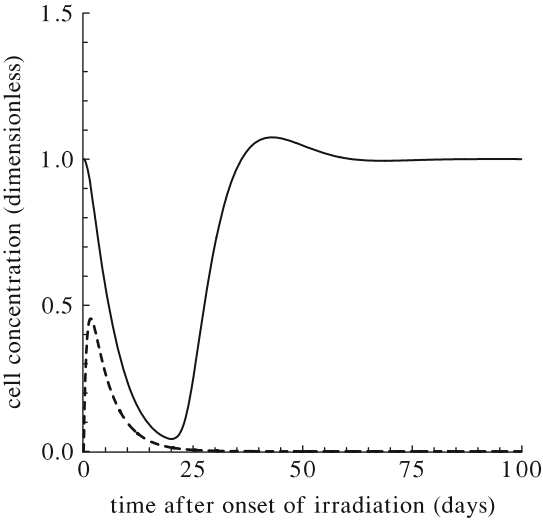

Fig. 8.14 Modeling results on the dynamics of dimensionless concentrations of the blood granulocytes (X_3 cells) (*solid curve*) and the weakly damaged bone marrow granulopoietic cells capable of dividing (X_1^{wd} cells) (*dashed curve*) in the granulopoietic system of humans exposed to continuous irradiation with the dose rate N of 0.576 Gy day^{-1}, with the duration of 4 day, and with the total exposure dose of 2.304 Gy

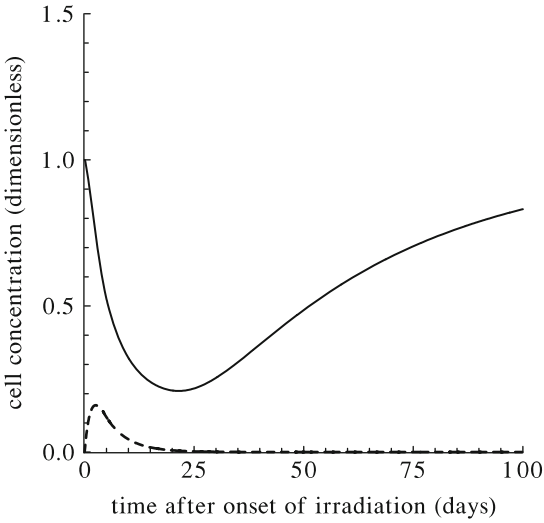

Fig. 8.15 Modeling results on the dynamics of dimensionless concentrations of the blood lymphocytes (X_3 cells) (*solid curve*) and the weakly damaged bone marrow lymphoid cells capable of dividing (X_1^{wd} cells) (*dashed curve*) in the lymphopoietic system of humans exposed to continuous irradiation with the dose rate N of 0.576 Gy day^{-1}, with the duration of 4 day, and with the total exposure dose of 2.304 Gy

irradiation with the dose rate N, which is equal to the dose rate of continuous irradiation of patients with uterine corpus cancer [8], and with the duration T, which does not exceed the largest duration of the exposure of those patients [8]. As one can infer from Fig. 8.14, the concentration of blood granulocytes (X_3 cells) decreases up to a minimum and then, after overdamped oscillations, returns to its normal level. In turn, the dimensionless concentration of X_1^{wd} cells increases to a maximum and then decreases, practically, to zero over considered period of time.

Figure 8.15 shows the modeling results on the dynamics of the dimensionless concentrations of blood lymphocytes (X_3 cells) and weakly damaged bone marrow lymphopoietic cells capable of dividing (X_1^{wd} cells) in humans exposed to continuous irradiation with the dose rate N, which is equal to the dose rate of continuous irradiation of patients with uterine corpus cancer [8], and with the duration T, which does not exceed the largest duration of the exposure of those patients [8]. As one can infer from Fig. 8.15, the concentration of blood lymphocytes (X_3 cells) decreases up to a minimum and after that goes back to its normal level. In turn, the concentration of X_1^{wd} cells increases to a maximum and then decreases, practically, to zero over considered period of time.

In the framework of the model of the human granulopoietic system, the values of the maximum of the dimensionless concentration of X_1^{wd} cells and the integral of the dimensionless concentration of X_1^{wd} cells over the period of the response of this major hematopoietic lineages to continuous irradiation with various duration T and with the dose rate N reported in [8] are computed.

In turn, in the framework of the model of the human lymphopoietic system, the values of the maximum of the dimensionless concentration of X_1^{wd} cells and the integral of the dimensionless concentration of X_1^{wd} cells over the period of the response of this major hematopoietic lineage to continuous irradiation with various duration T and with the dose rate N reported in [8] are computed.

The modeling values of the maximum of the dimensionless concentration of X_1^{wd} cells and the integral of the dimensionless concentration of X_1^{wd} cells over the period of the response of the granulopoietic system to continuous irradiation with various duration T and with the dose rate N, which is equal to the dose rate of continuous irradiation of patients with uterine corpus cancer [8], are used to predict the values of the excess relative risk, ERR_M^{AML} and ERR_I^{AML}, for acute myeloid leukemia among such patients. For this aim, the modeling values of the maximum of the dimensionless concentration of X_1^{wd} cells and the integral of the dimensionless concentration of X_1^{wd} cells are multiplied by the scale factors $S_M^{\mathrm{AML}} = 10.0$ and $S_I^{\mathrm{AML}} = 0.5$, respectively. The latter are the same as those, which are used in the case of the prediction of the excess relative risk for acute myeloid leukemia among humans exposed to acute irradiation (see Sect. 8.3).

The modeling values of the maximum of the dimensionless concentration of X_1^{wd} cells and the integral of the dimensionless concentration of X_1^{wd} cells over the period of the response of the granulopoietic system to the continuous irradiation with various duration T and with the dose rate N, which is equal to the dose rate of continuous irradiation of patients with uterine corpus cancer [8], are also used to predict the values of the excess relative risk, ERR_M^{CML} and ERR_I^{CML}, for chronic myeloid leukemia among such patients. For this aim, the modeling values of the maximum of the dimensionless concentration of X_1^{wd} cells and the integral of the dimensionless concentration of X_1^{wd} cells are multiplied by the scale factors $S_M^{\mathrm{CML}} = 4.7$ and $S_I^{\mathrm{CML}} = 0.235$, respectively. These factors are the same as those, which are used in the case of the prediction of the excess relative risk for chronic myeloid leukemia among humans exposed to acute irradiation (see Sect. 8.3).

The modeling values of the maximum of the dimensionless concentration of X_1^{wd} cells and the integral of the dimensionless concentration of X_1^{wd} cells over the period of the response of the lymphopoietic system to continuous irradiation with various duration T and with the dose rate N, which is equal to the dose rate of continuous irradiation of patients with uterine corpus cancer [8], are used to predict the values of the excess relative risk, ERR_M^{ALL} and ERR_I^{ALL}, for acute lymphocytic leukemia among such patients. For this aim, the modeling values of the maximum of the dimensionless concentration of X_1^{wd} cells and the integral of the dimensionless concentration of X_1^{wd} cells are multiplied by the scale factors $S_M^{\mathrm{ALL}} = 25.0$ and $S_I^{\mathrm{ALL}} = 1.25$, respectively. The latter are the same as those, which are used in the case of the prediction of the excess relative risk for acute lymphocytic leukemia among humans exposed to acute irradiation (see Sect. 8.4).

In turn, the values of ERR_M^{AML}, ERR_M^{CML}, and ERR_M^{ALL}, as well as the values of ERR_I^{AML}, ERR_I^{CML}, and ERR_I^{ALL}, which are predicted in the framework of the developed modeling approach, are used to determine the respective values of the excess relative risk for non-CLL leukemia, ERR_M^{L} and ERR_I^{L}, among humans exposed to continuous irradiation with various duration T and with the dose rate N, which is equal to the dose rate of continuous irradiation of patients with uterine corpus cancer [8].[3] For this aim, Eqs. (8.9) and (8.10) are applied (see Sect. 8.5).

[3]Note that the chronic lymphocytic leukemia (*CLL*) is not observed among those patients [8].

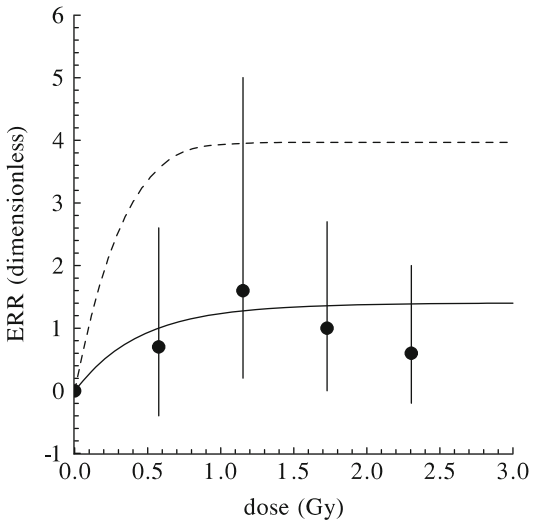

Fig. 8.16 The modeling prediction of the dose dependence of the excess relative risk ERR_M^{L} [Eq. (8.9)] (*dashed curve*) and the dose dependence of the excess relative risk ERR_I^{L} [Eq. (8.10)] (*solid curve*) for non-CLL leukemia among humans exposed to continuous irradiation with various duration T and with the dose rate N of 0.576 Gy day^{-1}, which is equal to the dose rate of continuous irradiation of patients with uterine corpus cancer [8]. The *circles* display the relevant empirical data on the dose dependence of the excess relative risk for non-CLL leukemia among those patients [8]

The values of ERR_M^{L} [Eq. (8.9)] and ERR_I^{L} [Eq. (8.10)], which are obtained at various duration T of continuous irradiation and at the dose rate N reported in [8] (i.e., at various total doses D of the considered exposures), are presented in Fig. 8.16. This figure also shows the respective empirical data on the dose dependence of the excess relative risk for non-CLL leukemia among patients with uterine corpus cancer, which were earlier treated with brachytherapy [8]. As one can infer from this figure, the dose dependence of the excess relative risk for non-CLL leukemia ERR_I^{L} among humans exposed to continuous irradiation with various duration T and with the dose rate N reported in [8], which is determined proceeding from the values of functions ERR_I^{AML}, ERR_I^{CML}, and ERR_I^{ALL}, conforms to the empirical data on the dose dependence of the excess relative risk for non-CLL leukemia among the respective groups of patients with uterine corpus cancer, which were earlier treated with brachytherapy [8]. In turn, the dose dependence of the values of ERR_M^{L}, which is determined proceeding from the values of functions ERR_M^{AML}, ERR_M^{CML}, and ERR_M^{ALL}, exceeds the respective empirical data [8].

These findings testify that the values of the excess relative risk for the acute myeloid leukemia ERR_I^{AML}, for chronic myeloid leukemia ERR_I^{CML}, and for acute lymphocytic leukemia ERR_I^{ALL}, which are obtained in the framework of the developed modeling approach proceeding from the values of the properly scaled integral of the dimensionless concentrations of X_1^{wd} cells over the periods of the responses

of the granulopoietic and lymphopoietic systems to continuous irradiation, can be used to predict the excess relative risk for non-CLL leukemia among continuously irradiated individuals.

8.8 Conclusions

A biologically motivated dynamical modeling approach to the assessment of the excess relative risks for myeloid and lymphocytic leukemia among acutely and continuously irradiated humans is developed. The basic tools of this approach are the mathematical models of the granulopoietic and lymphopoietic systems, which are capable of predicting the dynamics of functional blood cells and their bone marrow precursor cells in these major hematopoietic lineages in humans exposed to acute and chronic irradiation in wide ranges of doses and dose rates. These models are employed for simulating the dynamics of the granulopoietic and lymphopoietic systems in acutely and continuously irradiated humans. A particular attention is paid to the modeling studies of the dynamics of the concentration of weakly damaged bone marrow granulopoietic and lymphopoietic cells capable of dividing in these systems under such exposures. It is these cells that can be considered as premalignant cells.

It is revealed that the modeling values of the properly scaled maximum of the dimensionless concentrations of weakly damaged bone marrow granulopoietic cells capable of dividing over the period of the response of the granulopoietic system to acute irradiation can be used to predict the excess relative risk for acute myeloid leukemia and the excess relative risk for chronic myeloid leukemia among humans exposed to acute irradiation in the wide range of doses D ($0 \leq D \leq 8\,\mathrm{Gy}$). The respective two scale factors were evaluated from the comparison of the dose dependence of the scaled maximum of the dimensionless concentrations of weakly damaged bone marrow granulopoietic cells capable of dividing over the period of the response of the granulopoietic system to acute irradiation with the dose dependence of the excess relative risk for acute myeloid leukemia and the dose dependence of the excess relative risk for chronic myeloid leukemia among the atomic bomb survivors of all age groups together, which were fitted by the linear–quadratic–exponential equations [10]. It is also found that the modeling values of the properly scaled maximum of the dimensionless concentrations of weakly damaged bone marrow lymphopoietic cells capable of dividing over the period of the response of the lymphopoietic systems to acute irradiation can be used to predict the excess relative risk for acute lymphocytic leukemia among humans exposed to acute irradiation in the same range of doses D ($0 \leq D \leq 8\,\mathrm{Gy}$). The respective scale factor was evaluated from the comparison of the dose dependence of the scaled maximum of the dimensionless concentrations of weakly damaged bone marrow lymphopoietic cells capable of dividing over the period of the response of the lymphopoietic system to acute irradiation, with the dose dependence of the excess relative risk for acute lymphocytic leukemia among atomic bomb survivors of all age groups together, which was fitted by the linear–quadratic–exponential equation [10].

It is discovered that the modeling values of the properly scaled integral of the dimensionless concentration of weakly damaged bone marrow granulopoietic cells capable of dividing over the period of the response of the granulopoietic system to acute irradiation can be used to predict the excess relative risk for acute myeloid leukemia and the excess relative risk for chronic myeloid leukemia among humans exposed to acute irradiation in the range of comparatively low doses D ($0 \leq D \leq 1\,\mathrm{Gy}$). The respective two scale factors were evaluated from the comparison of the dose dependence of the scaled integral of the dimensionless concentration of weakly damaged bone marrow granulopoietic cells capable of dividing over the period of the response of the granulopoietic system to acute irradiation with the dose dependence of the excess relative risk for acute myeloid leukemia and the dose dependence of the excess relative risk for chronic myeloid leukemia among atomic bomb survivors of all age groups together, which were fitted by the linear–quadratic–exponential equations [10]. It is also shown that the modeling values of the properly scaled integral of the dimensionless concentration of weakly damaged bone marrow lymphopoietic cells capable of dividing over the period of the response of the lymphopoietic system to acute irradiation can be used to predict the excess relative risk for acute lymphocytic leukemia among humans exposed to acute irradiation in the range of comparatively low doses D ($0 \leq D \leq 1\,\mathrm{Gy}$). The respective scale factor was evaluated from the comparison of the dose dependence of the scaled integral of the dimensionless concentration of weakly damaged bone marrow lymphopoietic cells capable of dividing over the period of the response of the lymphopoietic system to acute irradiation with the dose dependence of the excess relative risk for acute lymphocytic leukemia among the atomic bomb survivors of all age groups together, which was fitted by the linear–quadratic–exponential equation [10]. It is worth noting that the found values of these scale factors are equal to the above-mentioned scale factors, multiplied by one and the same additional scale factor.

It is argued that the values of the excess relative risk for acute myeloid leukemia and the excess relative risk for chronic myeloid leukemia, which are determined in the framework of the model of the granulopoietic system proceeding from values of the properly scaled maximum of the dimensionless concentration of weakly damaged bone marrow granulopoietic cells capable of dividing over the period of the response of this major hematopoietic lineage to acute irradiation, can be used to predict the excess relative risk for myeloid leukemia among humans exposed to acute irradiation in the wide range of doses D ($0 \leq D \leq 8\,\mathrm{Gy}$). Specifically, the dose dependence of the excess relative risk for myeloid leukemia among human exposed to acute irradiation, which is predicted in the framework of the developed modeling approach, and the function, which describes the dose dependence of the excess relative risk for myeloid leukemia among atomic bomb survivors of all age groups together [10], are in a good agreement with each other in the wide range of doses D ($0 \leq D \leq 8\,\mathrm{Gy}$). It is important that the modeling prediction of the dose D of 3.5 Gy, at which the excess relative risk for myeloid leukemia reaches its peak, is very close to the dose D of 3.6 Gy, at which the function describing the dose dependence of the excess relative risk for myeloid leukemia among atomic bomb survivors of all age groups together approaches its peak [10]. In turn, the peak values, practically, coincide.

It is demonstrated that the values of the excess relative risk for acute myeloid leukemia and the excess relative risk for chronic myeloid leukemia, which are determined proceeding from values of the properly scaled integral of the dimensionless concentration of weakly damaged bone marrow granulopoietic cells capable of dividing over the period of the response of the granulopoietic system to acute irradiation, can be used to predict the excess relative risk for myeloid leukemia among humans exposed to acute irradiation in the range of comparatively low doses D ($0 \leq D \leq 1$ Gy). Specifically, the dose dependence of the excess relative risk for myeloid leukemia among human exposed to acute irradiation, which is predicted in the framework of the developed modeling approach, and the function, which describes the dose dependence of the excess relative risk for myeloid leukemia among atomic bomb survivors of all age groups together [10], are in a good agreement with each other in the above-indicated range of doses D ($0 \leq D \leq 1$ Gy).

It is proved that the values of the excess relative risk for acute myeloid leukemia, the excess relative risk for chronic myeloid leukemia, and the excess relative risk for acute lymphocytic leukemia, which are determined proceeding from values of the properly scaled maximum of the dimensionless concentrations of weakly damaged bone marrow granulopoietic and lymphopoietic cells capable of dividing over the periods of the responses of the granulopoietic and lymphopoietic systems to acute irradiation, can be used to predict the excess relative risk for leukemia except for chronic lymphocytic leukemia (non-CLL) among humans exposed to acute irradiation in the wide range of doses D ($0 \leq D \leq 8$ Gy). Specifically, the dose dependence of the excess relative risk for non-CLL leukemia among human exposed to acute irradiation, which is obtained in the framework of the developed modeling approach, and the function, which describes the dose dependence of the excess relative risk for non-CLL leukemia among the atomic bomb survivors of all age groups together [10], are in a good agreement with each other in the wide range of doses D ($0 \leq D \leq 8$ Gy). It is important that the modeling prediction of the dose D of 3 Gy, at which the excess relative risk for non-CLL leukemia reaches its peak, is close to the dose D of 3.3 Gy, at which the function describing the dose dependence of the excess relative risk for non-CLL leukemia among atomic bomb survivors of all age groups together approaches its peak [10]. The peak values are also close.

It is demonstrated that the values of the excess relative risk for acute myeloid leukemia, the excess relative risk for chronic myeloid leukemia, and the excess relative risk for acute lymphocytic leukemia, which are determined proceeding from the modeling values of the properly scaled integral of the dimensionless concentrations of weakly damaged bone marrow granulopoietic and lymphopoietic cells capable of dividing over the periods of the responses of the granulopoietic and lymphopoietic systems to acute irradiation, can be used to predict the excess relative risk for non-CLL leukemia among humans exposed to acute irradiation in the range of comparatively low doses D ($0 \leq D \leq 1$ Gy). Specifically, the dose dependence of the excess relative risk for non-CLL leukemia among human exposed to acute irradiation, which is predicted in the framework of the developed modeling approach, is in a good agreement with the function, which describes the

dose dependence of the excess relative risk for non-CLL leukemia among the atomic bomb survivors of all age groups together [10], as well as with the function, which fits the dose dependence of the excess relative risk for non-CLL leukemia among atomic bomb survivors exposed to comparatively low doses (the ages at the exposure exceed 20 years) [1].

It is argued that the values of the excess relative risks for acute myeloid leukemia, chronic myeloid leukemia, and acute lymphocytic leukemia, which are determined proceeding from modeling values of the properly scaled integral of the dimensionless concentrations of weakly damaged bone marrow granulopoietic and lymphopoietic cells capable of dividing over the periods of the responses of the granulopoietic and lymphopoietic systems to continuous irradiation, can be used to predict the excess relative risk for non-CLL leukemia among humans underwent to such exposures. Specifically, the modeling prediction of the dose dependence of the excess relative risk for non-CLL leukemia among patients exposed to continuous irradiation in the course of brachytherapy [8] conforms to the relevant empirical data on the dose dependence of the excess relative risk for non-CLL leukemia among the respective groups of patients [8]. It is important to emphasize that the scale factors used in the case of the estimation of the excess relative risks for acute myeloid leukemia, chronic myeloid leukemia, and lymphocytic leukemia among continuously irradiated humans are equal to the respective scale factors used in the case of the estimation of the excess relative risks for acute myeloid leukemia, chronic myeloid leukemia, and lymphocytic leukemia among acutely irradiated humans.

Thus, the developed dynamical modeling approach to leukemia risk assessment enables one to relate (by making use of only four scale factors) the excess relative risks for acute myeloid leukemia, chronic myeloid leukemia, myeloid leukemia, acute lymphocytic leukemia, and non-CLL leukemia among acutely and continuously irradiated humans with two key characteristics of the dynamics of the lymphopoietic and granulopoietic systems under such radiation exposures. They are the maximum and/or the integral of the dimensionless concentration of the weakly damaged bone marrow granulopoietic and/or lymphopoietic cells capable of dividing over the periods of the responses of the granulopoietic and/or lymphopoietic systems to the respective radiation exposures. In turn, these quantities (for various radiation regimes) are evaluated in the framework of the granulopoiesis and lymphopoiesis models. All this demonstrates the potential to use the developed dynamical modeling approach for estimating the leukemia risk among humans exposed to various radiation regimes. Obviously, it is especially important in assessing the risk of radiogenic leukemia among people residing in contaminated areas after nuclear power plant accidents, among astronauts in long-term space missions, as well as among patients treated with radiotherapy.

References

1. Committee on the Biological Effects of Ionizing Radiations, National Research Council: Health Effects of Exposure to Low Levels of Ionizing Radiation (BEIR V). Washington, DC: Natl Acad Press, 1990.
2. Committee to Assess Health Risks from Exposure to Low Levels of Ionizing Radiation, National Research Council: Health risks from exposure to low levels of ionizing radiation (BEIR VII—Phase 2). Washington, DC: Natl Acad Press, 2006.
3. Hsu W.L., Preston D.L., Soda M., Sugiyama H., Funamoto S., Kodama K., Kimura A., Kamada N., Dohy H., Tomonaga M., Iwanaga M., Miyazaki Y., Cullings H.M., Suyama A., Ozasa K., Shore R.E., Mabuchi K. The incidence of leukemia, lymphoma, and multiple myeloma among atomic bomb survivors: 1950–2001. Radiation Research, v. 179, pp. 361–382, 2013.
4. Preston D.L., Kusumi S., Tomonaga M., Izumi S., Ron E., Kuramoto A., Kamada N., Dohy H., Matsui T., Nonaka H., Thompson D.E., Soda M., Mabuchi K. Cancer incidence in atomic bomb survivors. Part III: leukemia, lymphoma, and multiple myeloma, 1950–1987. Radiation Research, v. 137, pp. 568–597, 1994.
5. Shimizu Y., Kato H., Schull W.J. Studies of the mortality of A-bomb survivors. 9. Mortality, 1950–1985: Part 2. Cancer mortality based on the recently revised doses (DS86). Radiation Research, v. 121, pp. 120–141, 1990.
6. Linet M.S., Slovis T.L., Miller D.L., Kleinerman R., Lee C., Rajaraman P., Gonzalez A.B. Cancer risks associated with external radiation from diagnostic imaging procedures. CA: A Cancer Journal for Clinicians, v. 62, pp. 75–100, 2012.
7. Wang J.X., Inskip P.D., Boice J.D. Jr., Li B.X., Zhang J.Y., Fraumeni J.F. Jr. Cancer incidence among medical diagnostic X-ray workers in China, 1950 to 1985. International Journal of Cancer, v. 45, pp. 889–895, 1990
8. Curtis R.E., Boice J.D., Jr., Stovall M., Bernstein L., Holowaty E., Karjalainen S., Langmark F., Nasca P.C., Schwartz A.G., Schymura M.J., Storm H.H., Toogood P., Weyer P., Moloney W.C. Relationship of leukemia risk to radiation dose following cancer of the uterine corpus. Journal of the National Cancer Institute, v. 86, pp. 1315–1324, 1994.
9. Bennett J., Little M.P., Richardson S. Flexible dose-response models for Japanese atomic bomb survivor data: Bayesian estimation and prediction of cancer risk. Radiation and Environmental Biophysics, v. 43, pp. 233–245, 2004.
10. Kuni H. Dose-Response Relationship of Low and High LET Radiation. In: Radiation Exposures by Nuclear Facilities, Evidence of the Impact on Health. Proceedings International Workshop, University of Portsmouth, GB, 1996. I. Schmitz-Feuerhake and M. Schmidt (Eds.). Berlin: Strahlentelex Inh. Thomas Dersee, pp.20–34, 1998.
11. Smirnova O.A. Myeloid leukemia risk assessment and dynamics of the granulocytopoietic system in acutely and continuously irradiated humans: modeling approach Health Physics, v. 108(5), pp. 492–502, 2015.
12. Whang-Peng J., Young R.C., Lee E.C., Longo D.L., Schechter G.P., DeVita V.T. Jr. Cytogenetic studies in patients with secondary leukemia/ dysmyelopoietic syndrome after different treatment modalities. Blood, v. 71, pp. 403–414, 1988.
13. Christiansen D.H., Andersen M.K., Desta F., Pedersen-Bjergaard J. Mutations of genes in the receptor tyrosine kinase (RTK)/RAS-BRAF signal transduction pathway in therapy-related myelodysplasia and acute myeloid leukemia. Leukemia, v. 19, pp. 2232–2240, 2005.
14. Akleyev A.V. Chronic Radiation Syndrome. Heidelberg: Springer, 2014.
15. Seed T.M. Hematopoietic tissue repair under chronic low daily dose irradiation. Advances in Space Research, v. 18, pp. 65–70, 1996.
16. Seed T.M., Fritz T.E., Tolle D.V., Jackson W.E. Hematopoietic responses under protracted exposures to low daily dose gamma irradiation. Advances in Space Research, v. 30, pp. 945–955, 2002.

17. Veremeyeva G., Akushevich I., Pochukhailova T., Blinova E., Varfolomeyeva T., Ploshchanskaya O., Khudyakova O., Vozilova A., Kozionova O., Akleyev A. Long-term cellular effects in humans chronically exposed to ionizing radiation. Health Physics, v. 99, pp. 337–346, 2010.
18. Smirnova O.A. Blood and small intestine cell kinetics under radiation exposures: Mathematical modeling. Advances in Space Research, v. 44, pp. 1457–1469, 2009.
19. Smirnova O.A. Modeling study of radiation effects on thrombocytopoietic and granulocytopoietic systems in humans. Advances in Space Research, v. 48, pp. 184–198, 2011.
20. Smirnova O.A. Comparative analysis of the dynamics of thrombocytopoietic, granulocytopoietic, and erythropoietic systems in irradiated humans: a modeling approach. Health Physics, v. 103(6), pp. 787–801, 2012.
21. Smirnova O.A. Modeling Analysis of the dynamics of thrombocytopoietic, granulocytopoietic, and erythropoietic systems in irradiated humans. Journal of Radiation Research, v. 55, p. i36, 2014.
22. Smirnova O.A., Hu S., Cucinotta F.A. Analysis of the lymphocytopoiesis dynamics in nonirradiated and irradiated humans: a modeling approach. Radiation Research, v. 181, pp. 240–250, 2014.
23. Smirnova O.A., Akleyev A.V., Dimov G.P. Analysis of hematopoiesis dynamics in residents of Techa riverside villages chronically exposed to nonuniform radiation: modeling approach. Health Physics, v. 106, pp. 445–458, 2014.
24. Smirnova O.A., Akleyev A.V., Dimov G.P. Modeling analysis of the lymphocytopoiesis dynamics in chronically irradiated residents of Techa riverside villages. Radiation and Environmental Biophysics, v. 53, pp. 515–523, 2014.
25. Baranov A.E. Dosage assessment and prognosis of peripheral neutrophil count dynamics based on the hematological indices of human gamma irradiation. Medical Radiology and Radiation Safety, v. 26(8), pp. 11–16, 1981 (Russian).
26. Pyatkin E.K., Baranov A.E. Biological indication of a dose on the basis of the analysis of chromosome aberrations and quantity of cells in peripheral blood. In: Results of sciences and technics. Radiatsionnaya Biologiya, v. 3, pp. 103–179, 1980 (Russian).
27. Guskova A.K., Baranov A.E., Barabanova A.V., Gruzdev G.P., Pyatkin E.K., Nadezhina N.M., et al. Acute radiation effects in exposed persons at the Chernobyl atomic power station accident. Medical Radiology and Radiation Safety, v. 32, pp. 3–18, 1987 (Russian).
28. Guskova A.K., Baranov A.E., Gusev I.A. Acute radiation sickness: underlying principles and assessment. In: Medical management of radiation accidents. I.A. Gusev, A.K. Guskova, and F.A.J. Mettler (Eds.). Boca Raton, Fl: CRC Press, pp. 33–51, 2001.
29. Guskova A.K., Baysogolov G.D. Radiation sickness of human. Moscow: Meditsina, 1971 (Russian).

Chapter 9
Radiation and Skin

9.1 Introduction

The skin is one of the vital body systems [1–3]. It forms a protective barrier at outer surface of an organism. The skin is related to the radiosensitive systems in mammals [4–10]. Its radiation-induced damage can lead to erythema, pigmentation, dry and moist desquamation in early phase (<4 weeks), and atrophy and fibrosis (or necrosis) in later phase (>6 weeks) [5, 7, 8, 11, 12]. They are the main manifestations of the cutaneous subsyndrome of the acute radiation syndrome. The ED_{10} (a dose in which 10 % of a population receives the effect) has been estimated to be 4 Gy for erythema and 14 Gy for the more serious moist desquamation [13, 14].

The problem of the estimation of the risks of the development of the pathophysiological reactions in skin in accident victims, in astronauts on long-term space missions (e.g., voyages to Mars or Lunar colonies), and in patients treated with the radiotherapy is vital and actual one [15]. Its solution requires, in particular, the development of reliable tools that enable one to predict the dynamics of radiation-induced processes in the skin, which may lead to the malfunction of the latter and various manifested illnesses. One of such tools is the biologically motivated mathematical models, which are capable of simulating, in dynamical way, the responses of this radiosensitive vital body system to various radiation exposures.

The primary objectives of our studies [16, 17] were to develop and investigate the mathematical model of skin, which is capable of predicting the dynamics of this system under the normal conditions and under single and fractionated irradiation. The model was required to account for the principal regulatory mechanisms of this vital body system and its basic kinetic and radiobiological parameters, as well as to include explicitly the characteristics of ionizing radiation. The results of our investigations of this subject are summarized in this chapter.

O.A. Smirnova, *Environmental Radiation Effects on Mammals*,
DOI 10.1007/978-3-319-45761-1_9

9.2 The Essentials of Skin

The skin plays an important part in maintaining the vitality of mammals [1–3]. Specifically, it forms a protective barrier at outer surface of an organism. The skin consists of the epidermal epithelium (epidermis) and the underlying dermis. The dermal–epidermal junction serves as a partial barrier against exchange of molecules and cells.

The dermis consists of two layers: the superficial papillary dermis and the reticular dermis. The dermis is composed largely of collagen fibers, as well as of elastin fibers. The cellular constituents of the dermis are fibroblasts, mast cells, and histiocytes (monocytes/macrophages). The dermis has a very rich blood supply, which is provided by the cutaneous arteries and the segmental arteries (perforating vessels). In particular, the papillary dermis is highly vascularized (about 70 capillary loops/mm^2, that is one order of magnitude greater than in the reticular dermis). Though, vessels do not pass through the dermal–epidermal junction.

In turn, the skin epidermal epithelium consists of keratinocytes (95 % of the total amount of cells), as well as of Langerhans' cells, which have immunological functions, Merkel cells, and melanocytes. The keratinocytes move from the attachment to the epidermal basement membrane toward the skin surface forming basal, spinous, granular, and corneal layers. Progenitors of keratinocytes are stem cells. The latter are located in small clusters in the basal interfollicular epidermis and in the bulge region of follicles. Stem cells have an unlimited capacity for self-renewing, as well as the ability to generate daughter cells. The daughter cells, which are destined to undergo terminal differentiation, can first divide a number of times. The stem cells and their dividing maturing daughter cells constitute the basal layer. In turn, their nondividing maturing progenies, spinous cells and granular cells, constitute, respectively, the spinous layer and the granular layer. These keratinocytes are also known as prickle cells. The keratinocytes of the corneal layer are flattened anucleate cells (corneal cells or squame). These cells, which form approximately 25 % of total thickness of the epidermis [7], protect the underlying viable cell layers. Corneal cells are continually shed from the skin surface. In the norm, the rate of production of cells in the basal layer corresponds to the rate of their loss from the corneal layer providing the normal skin thickness.

9.3 Mathematical Model

9.3.1 Dynamical Model of the Skin Epidermis Under Normal Conditions

A basic model of the dynamics of skin epidermal epithelium under normal conditions is developed proceeding from the contemporary concepts of the structure and functioning of this system [1–3]. The object of the modeling is the population of

epidermal keratinocytes. In the model, the keratinocytes are split into three groups according to the degree of their maturity and differentiation:

- X, the dividing maturing cells of the basal layer (from stem cells to mature basal cells);
- Y, the maturing cells of the joint spinous/granular layer (from spinous cells to granular cells, i.e., prickle cells);
- Z, the cells of the corneal layer (corneal cells or squame).

It is assumed that

1. the dynamics of X cells is determined by the rates of their reproduction and transition to the group of Y cells;
2. the dynamics of Y cells is determined by the rate of arrival of cells from the group of X cells and by the rate of their transition to the group of Z cells;
3. the dynamics of Z cells is determined by the rate of arrival of cells from the group of Y cells and by the rate of leaving the group of Z cells.

The model accounts for the negative-feedback control of the specific reproduction rate of X cells, which is implemented by the tissue-specific inhibitor of cell division, the epidermal chalone [1, 18–21]. The chalones, which belong to cytokines, are the product of the vital activity and decay of capable of dividing cells and their progeny [21].

The concentrations of X, Y, and Z cells (x, y, and z, respectively) and the concentration of the epidermal chalone (I) are used as variables of the model. By cell concentration, we mean the ratio of the total number of cells of a certain group to the normal epidermal epithelium volume. By the epidermal chalone concentration, we mean the ratio of its total amount to the normal epidermal epithelium volume. Proceeding from the aforementioned statements, the dynamics of the skin epidermal epithelium is described by the system of ordinary differential equations, which resembles those, which describe the dynamics of the major hematopoietic lineages and the small intestinal epithelium under normal conditions (see Chaps. 1 and 4, as well as [22–24]):

$$\frac{dx}{dt} = B\,x - C\,x, \tag{9.1}$$

$$\frac{dy}{dt} = C\,x - F\,y, \tag{9.2}$$

$$\frac{dz}{dt} = F\,y - E\,z, \tag{9.3}$$

$$\frac{dI}{dt} = G\,(x + \vartheta_y y + \vartheta_z z) - HI. \tag{9.4}$$

In Eqs. (9.1)–(9.3), the coefficients B, C, F, and E are the specific rates of X cell reproduction, cell transition from the group of X cells to the group of Y cells, cell transition from the group of Y cells to the group of Z cells, and cell leaving the

group of Z cells, respectively. In Eq. (9.4), the factors G, $G\vartheta_y$, and $G\vartheta_z$ are the specific rates of chalone production by X, Y, and Z cells during their vital activity and decay, whereas H is the rate of natural decay of the chalone.

Accounting for the negative-feedback control of the specific reproduction rate of X cells, which is implemented by the inhibitor of cell division, the epidermal chalone, the specific rate B of reproduction of X cells is given by the Ierusalimskii equation [25–27]:

$$B = \frac{\alpha}{1 + I/K}, \tag{9.5}$$

where I is the concentration of the epidermal chalone, the coefficient α is a maximum specific rate of cell division, and the coefficient K is an inhibitor constant.

In view of the fact that the chalones keep their activity for a few hours [21], whereas the skin epidermal cells live, differentiate, and maturate over several days [3], Eq. (9.4) can be considered as "fast" compared to Eqs. (9.1)–(9.3). Therefore, according to the Tikhonov theorem [25–27], Eq. (9.4) can be replaced by its stationary solution $I = (G/H)\,(x + \vartheta_y y + \vartheta_z z)$, by virtue of which Eq. (9.5) acquires the form

$$B = \frac{\alpha}{1 + \beta(x + \vartheta_y y + \vartheta_z z)}, \qquad \beta = \frac{G}{HK}. \tag{9.6}$$

Note that Eq. (9.6) can be used for the computation of the mitotic index M of X cells. The latter is related to the specific reproduction rate B by the following formula [28]:

$$M = B \cdot T_m \cdot 100\,\%. \tag{9.7}$$

In Eq. (9.7), the parameter T_m is the true time of mitosis.

Accounting for the data presented in [7], the specific rate C of cell transition from group X to group Y (i.e., the specific rate of cell displacement from the basal layer to the joint spinous/granular layer) is assumed to be a constant: $C = \gamma$.

Proceeding from the data presented in [29], it is assumed that the specific rate F of cell transition from group Y to group Z (i.e., the specific rate of cell displacement from the joint spinous/granular layer to corneal layer) and the specific rate E of cell leaving the group of Z cells (i.e., the specific rate of cell shed from the skin surface) depend on the mitotic activity of X cells, i.e., on the specific rate B of reproduction of X cells. The exact form of the dependence of F and E on B in the skin epidermal epithelium system has not been determined experimentally yet. As a first approximation, we assume them to be linear in B, as those in the model of the small intestinal epithelium system (see Chap. 3 and the references therein):

$$F = \delta(1 + \sigma B), \tag{9.8}$$

$$E = \psi(1 + \lambda B). \tag{9.9}$$

Here δ, ψ, σ, and λ are constants.

Thus, the developed model, which describes the dynamics of the skin epidermal epithelium system under normal conditions, includes three nonlinear ordinary differential equations (9.1)–(9.3).

9.3.2 *Dynamical Model of the Skin Epidermis Under Acute Irradiation*

The basic model of the dynamics of the skin epidermal epithelium under normal conditions [Eqs. (9.1)–(9.3)] is extended to describe the dynamics of this vital body system under acute irradiation. The extended model is developed in the framework of the dynamic approach to the modeling of the response of renewing cell systems to irradiation. The approach was elaborated and successfully applied earlier to the modeling of such vital body systems, as the hematopoietic system and the small intestinal epithelium system (see Chaps. 1, 7, and 3, as well as [22–24, 30–32]).

Specifically, the effects of acute irradiation on the skin epidermis are accounted for in the model of this vital body system on the basis of the conventional radiobiological concepts and experimental facts:

1. The experimental findings [4–10], according to which the basal cells (X cells) are radiosensitive, whereas their progenies, prickle cells (Y cells) and corneal cells (Z cells), are radioresistant ones.
2. The one-target–one-hit theory of cell damage [33], according to which the damage rate of radiosensitive cells is assumed to be proportional to the dose rate N.
3. The experimental findings and the concept proposed by V.P. Bond, T.M. Fliedner, J.O. Archambeau in [34], which concern the types of reaction of radiosensitive cells in renewing systems to radiation impact. According to them, the radiosensitive cells may stay undamaged ones, or become heavily damaged, moderately damaged, or weakly damaged ones. Heavily damaged cells die within several hours following irradiation (interphase death). Moderately damaged cells can divide few (at least, one) times and die within 1–2 days following irradiation (mitotic death). The weakly damaged cells are able to proliferate and differentiate as undamaged ones over a certain period ($0 < t < T_{ar}$), forming the pools of weakly damaged progenies. After the time moment T_{ar}, which is known as the time of maximum abortive rise, all weakly damaged cells and their progenies die within several days.

Proceeding from these concepts and facts, the radiosensitive basal cells (X cells) are split into four groups:

- X^{ud}, undamaged cells;
- X^{hd}, heavily damaged cells that die within several hours following irradiation (interphase death);

- X^{md}, moderately damaged cells that die within several days following irradiation (mitotic death);
- X^{wd}, weakly damaged cells, which are capable of dividing and maturing and then transfer to the group of Y^{wd} cells, if the time passed after irradiation does not exceed the time interval T_{ar}, and which only die within several days, if the time passed after irradiation equals or exceeds the time interval T_{ar}.

The prickle cells (Y cells) are split into two groups:

- Y^{ud}, progenies of undamaged basal cells (X^{ud} cells);
- Y^{wd}, progenies of weakly damaged basal cells (X^{wd} cells), which are capable of maturing and then transfer to the group of Z^{wd} cells, if the time passed after irradiation does not exceed the time interval T_{ar}, and which only die within several days, if the time passed after irradiation equals or exceeds the time interval T_{ar}.

The corneal cells (Z cells) are also split into two groups:

- Z^{ud}, progenies of Y^{ud} cells;
- Z^{wd}, progenies of Y^{wd} cells, which are functioning as undamaged Z^{ud} cells, if the time passed after irradiation does not exceed the time interval T_{ar}, and which leave the group of Z^{wd} cells within several days, if the time passed after irradiation equals or exceeds the time interval T_{ar}.

The concentrations of the foregoing cells (x^{ud}, y^{ud}, z^{ud}, x^{wd}, y^{wd}, z^{wd}, x^{md}, and x^{hd}, respectively) are taken as the variables of the model.

It is assumed that the dynamics of undamaged X^{ud}, Y^{ud}, and Z^{ud} cells after acute irradiation is determined by Eqs. (9.1)–(9.3). The dynamics of weakly damaged X^{wd}, Y^{wd}, and Z^{wd} cells is determined in the same way as that of X^{ud}, Y^{ud}, and Z^{ud} cells until a time moment T_{ar}. After the time moment T_{ar}, the dynamics of X^{wd} and Y^{wd} cells is determined only by the death rate, whereas the dynamics of Z^{wd} cells is determined by the rate of leaving the group of Z^{wd} cells. In turn, the dynamics of moderately damaged X^{md} cells and the dynamics of heavily damaged X^{hd} cells are determined only by death rates of these cells.

Originating in the aforementioned statements, the model of acutely irradiated skin epidermal epithelium is implemented as the system of the differential equations, which resemble those of the models of the major hematopoietic lineages in acutely irradiated humans (see Chap. 7):

$$\frac{dx^{ud}}{dt} = B\,x^{ud} - \gamma\,x^{ud}, \tag{9.10}$$

$$\frac{dy^{ud}}{dt} = \gamma\,x^{ud} - F\,y^{ud}, \tag{9.11}$$

$$\frac{dz^{ud}}{dt} = F\,y^{ud} - E\,z^{ud}, \tag{9.12}$$

$$\frac{dx^{\mathrm{wd}}}{dt} = \Theta(T_{ar} - t)[Bx^{\mathrm{wd}} - \gamma x^{\mathrm{wd}}] - \Theta(t - T_{ar})\eta x^{\mathrm{wd}}, \tag{9.13}$$

$$\frac{dy^{\mathrm{wd}}}{dt} = \Theta(T_{ar} - t)[\gamma x^{\mathrm{wd}} - Fy^{\mathrm{wd}}] - \Theta(t - T_{ar})\eta y^{\mathrm{wd}}, \tag{9.14}$$

$$\frac{dz^{\mathrm{wd}}}{dt} = \Theta(T_{ar} - t)[Fy^{\mathrm{wd}} - Ez^{\mathrm{wd}}] - \Theta(t - T_{ar})Ez^{\mathrm{wd}}, \tag{9.15}$$

$$\frac{dx^{\mathrm{md}}}{dt} = -\mu x^{\mathrm{md}}, \tag{9.16}$$

$$\frac{dx^{\mathrm{hd}}}{dt} = -\nu x^{\mathrm{hd}}. \tag{9.17}$$

Here the parameters B, γ, F, and E are, respectively, the specific rate of reproduction of X^{ud} cells and of X^{wd} cells (at $t < T_{ar}$), cell transition from the group of X^{ud} cells to the group of Y^{ud} cells and from the group of X^{wd} cells to the group of Y^{wd} cells (at $t < T_{ar}$), cell transition from the group of Y^{ud} cells to the group of Z^{ud} cells and from the group of Y^{wd} cells to the group of Z^{wd} cells (at $t < T_{ar}$), and cell leaving the groups of Z^{ud} and Z^{wd} cells. Coefficients μ and ν are the specific death rates of X^{md} and X^{hd} cells, whereas η is the specific death rates of X^{wd} and Y^{wd} cells (at $t > T_{ar}$). The coefficients γ, μ, ν, and η are constants. In turn, $\Theta(t)$ denotes the unit step-function:

$$\Theta(t) = \begin{cases} 1, & t \geq 0, \\ 0, & t < 0. \end{cases} \tag{9.18}$$

To describe the specific reproduction rate B of the basal cells (X cells) in acutely irradiated skin epidermal epithelium, it is necessary to account for the negative-feedback control mechanism of cell division specified above, as well as an additional regulation mechanism. To specify the latter, it is taken into account the following conventional concepts and experimental facts. Namely, the response of the skin epidermis to acute irradiation with a not high dose includes degenerative and regenerative phases, which correspond to the processes of damage and recover running in this vital body system after such exposure. In turn, the response of the skin epidermis to acute irradiation with a high dose includes an additional (postregenerative) phase, which follows after degenerative and regenerative ones. The postregenerative phase in the response of skin epidermal epithelium system to high dose acute irradiation is characterized by the second descend of the concentrations of the epidermal cells [35–37]. This phenomenon is explained in the framework of the concept proposed by Archambeau et al. [37]. According to this concept, the second descend of the concentrations of the epidermal cells is a consequence of the radiation-induced damage of the dermal microvasculature, which provides the nutrient flow. The delay (of about 1 month) in the manifestation of the influence of damaged dermal microvasculature on the processes running in

the epidermal epithelium is due to the great sustainability of this system. Namely, as little as about 10 % of the vessels in the papillary dermis disposed beneath the epidermal epithelium is enough to provide the nutrient flow, which is sufficient for the normal functioning of the epidermal cells [6].

Proceeding from all this, it is natural to assume that the damaged dermal microvasculature affects the reproduction rate of the basal cells (X cells) in the aforementioned period after acute irradiation. In the model, this influence can be taken into account in the following way:

$$B = B_0\, V. \tag{9.19}$$

Here B_0 is the function, which describes the negative-feedback control of the specific reproduction rate of X cells, which is implemented by the epidermal chalone, whereas V is a weight function, which describes the influence of damaged dermal microvasculature on the reproduction rate of X cells.

The expression for the function B_0 is derived taking into account of the contributions of undamaged cells and weakly, moderately, and heavily damaged cells into the negative-feedback control mechanism. As it is found, the function B_0 in the model of the dynamics of acutely irradiated skin epidermal epithelium is described by the formula, which resembles the formula for the function B in the models of the dynamics of the major hematopoietic lineages in acutely irradiated humans (see Chap. 7):

$$B_0 = \frac{\alpha}{1 + \beta\left[\left(x^{\mathrm{ud}} + \Phi_x + \phi x^{\mathrm{md}} + \varphi x^{\mathrm{hd}}\right) + \vartheta_y\left(y^{\mathrm{ud}} + \Phi_y\right) + \vartheta_z\left(z^{\mathrm{ud}} + \Phi_z\right)\right]}, \tag{9.20}$$

where

$$\Phi_x = [\Theta(T_{ar} - t) + \varsigma\Theta(t - T_{ar})]x^{\mathrm{wd}}, \tag{9.21}$$

$$\Phi_y = [\Theta(T_{ar} - t) + \varsigma\Theta(t - T_{ar})]y^{\mathrm{wd}}, \tag{9.22}$$

$$\Phi_z = [\Theta(T_{ar} - t) + \varsigma\Theta(t - T_{ar})]z^{\mathrm{wd}}. \tag{9.23}$$

Here $\Theta(t)$ is the unit step-function [Eq. (9.18)]. Parameters α, β, ϑ_y, ϑ_z, ϕ, φ, and ς are constants. Proceeding from the analysis of experimental data [35], the variable parameter T_{ar} in Eqs. (9.21)–(9.23), as well as in Eqs. (9.13)–(9.15), is described by the linear function of the dose of acute irradiation D:

$$T_{ar} = \tau_{ar} - \upsilon\, D. \tag{9.24}$$

Here the constant parameters τ_{ar} and υ have the dimensions of day and day Gy^{-1}, respectively. Note that Eq. (9.24) coincides with Eq. (7.24), which describes the parameter T_{ar} in the models of the dynamics of the major hematopoietic lineages in acutely irradiated humans.

To shape the function V, we take into account the following experimental facts [35–37]. The influence of the damaged dermal microvasculature on the processes running in the epidermal epithelium is not observed in the first period after high dose acute irradiation (at $t \leq T_{ed}$) and it is observed in the subsequent period (at $t > T_{ed}$). Proceeding from this, the function V is defined as follows:

$$V = P + \Theta(T_{ed} - t)(1 - P). \tag{9.25}$$

Here $\Theta(T_{ed} - t)$ denotes the unit step-function [Eq. (9.18)]. As a result, $V = 1$ if $t \leq T_{ed}$, and $V = P$ if $t > T_{ed}$. The functions T_{ed} and P are specified below.

The function P in Eq. (9.25) can be determined proceeding from the experimental data [35–37] on the dose dependence of the magnitude of the second descent of the concentration of basal cells. Specifically, the second descent is not observed if the radiation dose D does not exceed a certain critical level D_c (i.e., if $D \leq D_c$). In turn, the second descent strongly depends on the radiation dose D if the radiation dose D exceeds this critical level D_c (i.e., if $D > D_c$). Namely, it becomes much more pronounced at a higher dose D. Therefore, it is natural to assume that the effect of the damaged dermal microvasculature on the reproduction rate B of X cells depends on the radiation dose D in the respective way. In the reported dose range, the effect is negligible ($P \to 1$) if $D \leq D_c$, whereas the effect strongly increases (the function P strongly decreases) with growing the radiation dose D if $D > D_c$. Proceeding from this, the function P in our model is described by making use of the so-called complementary error function (see, e.g., [38]):

$$P = \frac{1}{2}\,\mathrm{erfc}\left(\frac{D - D_w}{D_v}\right). \tag{9.26}$$

Here D is the dose of acute irradiation, D_w and D_v are constants with the dimension of Gy, and

$$\mathrm{erfc}(U) = \frac{2}{\sqrt{\pi}} \int_U^\infty e^{-\xi^2} d\xi. \tag{9.27}$$

The function T_{ed} in Eq. (9.25) can be specified proceeding from the following experimental findings. In the reported dose range, the moment of beginning of the second descent of concentration of basal cells (X cells) slightly depends on the radiation dose D [35–37]. Namely, the second descend begins earlier if the dose D is higher [35–37]. Therefore, it is natural to assume that the moment T_{ed} of the beginning of influence of damaged dermal microvasculature on the processes running in the epidermis depends on the radiation dose D in the respective way: the function T_{ed} slightly decreases with the growing of the dose D. In the dose range under consideration, this dependence is taken as the linear function of the dose D:

$$T_{ed} = \tau_{ed} - \zeta\, D. \tag{9.28}$$

Here the constant parameters τ_{ed} and ζ have the dimensions of day and day Gy^{-1}, respectively.

The model takes also into account the influence of damaged dermal microvasculature on the dynamics of prickle cells and corneal cells. On the basis of the analysis of the experimental data [35, 36], it is assumed that the damaged dermis induces the increase of the specific rate F of transition of prickle cells (Y cells) to the group of corneal cells (Z cells) and the increase of the specific rate E of leaving the group of Z cells in the respective period after acute irradiation ($t \geq T_{ed}$). Accordingly, it is supposed that, starting from the moment $t = T_{ed}$, the specific rates F and E gain an additional contribution ε:

$$F = \delta(1 + \sigma B) + \varepsilon\Theta(t - T_{ed}), \tag{9.29}$$

$$E = \psi(1 + \lambda B) + \varepsilon\Theta(t - T_{ed}). \tag{9.30}$$

Here δ, ψ, σ, and λ are constant parameters, the parameter T_{ed} is determined by Eq. (9.28), and $\Theta(t - T_{ed})$ is the unit step-function [Eq. (9.18)].

Analysis of experimental data [35, 36] shows that the parameter ε in Eqs. (9.29) and (9.30) depends on the radiation dose D. Namely, in the reported dose range, it grows with the growing of the dose D. In our model, this dependence is taken to be the linear function of D:

$$\varepsilon = \omega + \varpi D, \tag{9.31}$$

with the constant parameters ω and ϖ being of the dimensions of day^{-1} and day^{-1} Gy^{-1}, respectively.

The corresponding initial conditions for Eqs. (9.10)–(9.17) are derived proceeding from the fact that the duration of acute irradiation is extremely short. Therefore the characteristic time scales of Eqs. (9.10)–(9.17) considerably exceed the duration of acute irradiation. Therefore, during acute irradiation, the concentrations of radioresistant cells can be considered as constant ones, whereas the concentrations of undamaged, weakly damaged, moderately damaged, and heavily damaged radiosensitive cells, according to the one-target–one-hit theory of cell damage [33], can be described by the system of "fast" equations:

$$\frac{dx^{\mathrm{ud}}}{dt} = -\frac{N}{D_x^0} x^{\mathrm{ud}}, \tag{9.32}$$

$$\frac{dy^{\mathrm{ud}}}{dt} = 0, \tag{9.33}$$

$$\frac{dz^{\mathrm{ud}}}{dt} = 0, \tag{9.34}$$

$$\frac{dx^{\mathrm{wd}}}{dt} = \frac{1}{1 + \rho} \frac{\kappa}{1 + \kappa} \frac{N}{D_x^0} x^{\mathrm{ud}}, \tag{9.35}$$

$$\frac{dy^{\mathrm{wd}}}{dt} = 0, \tag{9.36}$$

$$\frac{dz^{\mathrm{wd}}}{dt} = 0, \tag{9.37}$$

$$\frac{dx^{\mathrm{md}}}{dt} = \frac{1}{1+\rho}\,\frac{1}{1+\kappa}\,\frac{N}{D_x^0}\,x^{\mathrm{ud}}, \tag{9.38}$$

$$\frac{dx^{\mathrm{hd}}}{dt} = \frac{\rho}{1+\rho}\,\frac{N}{D_x^0}\,x^{\mathrm{ud}}. \tag{9.39}$$

The term on the right-hand side of Eq. (9.32) describes the rate of decrease of the concentration of X^{ud} cells, which is proportional to the radiation dose N. One part of these cells transfers to the group of heavily damaged X^{hd} cells, whereas the other part of these cells transfers to the groups of weakly damaged X^{wd} cells and moderately damaged X^{md} cells. The ratio of these parts is denoted by ρ. In turn, the ratio of the part of X^{ud} cells, which transfers to the group of weakly damaged X^{wd} cells, to the part of X^{ud} cells, which transfers to the groups of moderately damaged X^{md} cells, is denoted by κ.

The initial conditions for Eqs. (9.32)–(9.39) are the initial concentrations of X^{ud}, Y^{ud}, Z^{ud}, X^{wd}, Y^{wd}, Z^{wd}, X^{md}, and X^{hd} cells before the onset of irradiation. In particular, in the case of irradiation of a healthy individual, which has not previously been exposed to radiation, the initial concentrations of radiosensitive X^{ud} cells and radioresistant Y^{ud} and Z^{ud} cells are equal to their normal values ($\bar{x}$, $\bar{y}$, and $\bar{z}$, respectively), whereas the concentrations of X^{wd}, Y^{wd}, Z^{wd}, X^{md}, and X^{hd} cells are equal to zero. For the case of the constant dose rate N, Eqs. (9.32)–(9.39) with the aforementioned initial conditions can be integrated explicitly. The obtained expressions for the concentrations of X^{ud}, Y^{ud}, Z^{ud}, X^{wd}, Y^{wd}, Z^{wd}, X^{md}, and X^{hd} can be used as the initial conditions for Eqs. (9.10)–(9.17):

$$x^{\mathrm{ud}}(0) = \bar{x}\,\exp(-D/D_x^0), \tag{9.40}$$

$$y^{\mathrm{ud}}(0) = \bar{y}, \tag{9.41}$$

$$z^{\mathrm{ud}}(0) = \bar{z}, \tag{9.42}$$

$$x^{\mathrm{wd}}(0) = \bar{x}\,\frac{1}{1+\rho}\,\frac{\kappa}{1+\kappa}\,[1-\exp(-D/D_x^0)], \tag{9.43}$$

$$y^{\mathrm{wd}}(0) = 0, \tag{9.44}$$

$$z^{\mathrm{wd}}(0) = 0. \tag{9.45}$$

$$x^{\mathrm{md}}(0) = \bar{x}\,\frac{1}{1+\rho}\,\frac{1}{1+\kappa}\,[1-\exp(-D/D_x^0)], \tag{9.46}$$

$$x^{\mathrm{hd}}(0) = \bar{x}\,\frac{\rho}{1+\rho}[1-\exp(-D/D_x^0)], \tag{9.47}$$

where

$$\rho = \frac{1 - \exp(-D/D_x^{00})}{\exp(-D/D_x^{00}) - \exp(-D/D_x^{0})}, \tag{9.48}$$

$$\kappa = \frac{\exp(-D/D_x^{000}) - \exp(-D/D_x^{0})}{\exp(-D/D_x^{00}) - \exp(-D/D_x^{000})}. \tag{9.49}$$

The quantities $\bar{x}$, $\bar{y}$, and $\bar{z}$ in Eqs. (9.40)–(9.43), (9.46), and (9.47), the parameter ρ in Eqs. (9.43), (9.46), (9.47), and the parameter κ in Eqs. (9.43) and (9.46) are defined above. The variable parameters D in Eqs. (9.40), (9.43), and (9.46)–(9.49) is a dose of acute irradiation. The coefficient D_x^0 in Eqs. (9.32), (9.35), (9.38), (9.39), (9.40), (9.43), (9.46)–(9.49) is equivalent to the conventional radiobiological dose D_0. After exposure to such dose, the number of X cells left undamaged is $e = 2.718\ldots$ times smaller than their initial number [34]. The coefficient D_x^{00} in Eqs. (9.48) and (9.49) is the dose, after exposure to which the number of X cells that did not undergo the interphase death is $e = 2.718\ldots$ times smaller than their initial number. In turn, the coefficient D_x^{000} in (9.49) is the dose, after exposure to which the number of X cells that did not undergo either the interphase death or the mitotic death is $e = 2.718\ldots$ times smaller than their initial number.

Thus, the developed model of the dynamics of acutely irradiated skin epidermis, in its final form, is implemented by Eqs.(9.10)–(9.17) with the initial conditions (9.40)–(9.47).

9.3.3 Dynamical Model of the Skin Epidermis Under Fractionated Irradiation

The model, which describes the dynamics of skin epidermis under single acute irradiation [Eqs. (9.10)–(9.17)], is extended to reproduce the effects of n-fractionated irradiation on this vital body system. It is taken into account that n-fractionated irradiation can be considered as a composition of n single acute exposures with doses D_i ($i = 1, \ldots, n$) and with time intervals between the exposures τ_i ($i = 1, \ldots, n-1$).

First of all, let us address the response of the skin epidermis to the first exposure. In the system on hand, before this exposure ($t = 0$), there are undamaged X^{ud}, Y^{ud}, and Z^{ud} cells, which concentrations are equal to their normal values ($\bar{x}$, $\bar{y}$, $\bar{z}$). In the result of the first exposure, a part of undamaged X^{ud} cells remains undamaged ones (X^{ud} cells), whereas the rest of the cells transfer to the groups of heavily damaged cells (X^{hd} cells), moderately damaged cells (X^{md} cells), and weakly damaged cells (X_1^{wd} cells). In turn, progenies of X_1^{wd} cells form the groups of Y_1^{wd} and Z_1^{wd} cells. Behavior of X_1^{wd}, Y_1^{wd}, and Z_1^{wd} cells is the same as that for X^{ud}, Y^{ud}, and Z^{ud} cells until time moment T_{ar}, after which the dynamics of X_1^{wd} and Y_1^{wd} cells is determined only by their death rate and the dynamics of Z_1^{wd} cells is determined by the rate of

leaving the group of Z_1^{wd} cells. Thus, the first exposure leads to the forming of five new groups of cells with the different degree of their radiation-induced damage.

Then, let us address the response of the skin epidermis to the second exposure. In the system on hand, before this exposure ($t = \tau_1$), there are undamaged X^{ud}, Y^{ud}, and Z^{ud} cells, moderately damaged X^{md} cells, and heavily damaged X^{hd} cells, as well as weakly damaged X_1^{wd}, Y_1^{wd}, and Z_1^{wd} cells. In the result of the second radiation exposure, a part of undamaged X^{ud} cells remains undamaged ones (X^{ud} cells), whereas the rest of the cells transfer to groups of heavily damaged cells (X^{hd} cells), moderately damaged cells (X^{md} cells), and weakly damaged cells (X_2^{wd} cells). In turn, progenies of weakly damaged X_2^{wd} cells forms the groups of weakly damaged Y_2^{wd} and Z_2^{wd} cells. The behavior of X_2^{wd}, Y_2^{wd}, and Z_2^{wd} cells is the same as the behavior of undamaged X^{ud}, Y^{ud}, and Z^{ud} cells until time moment $t = T_{ar} + \tau_1$, after which the dynamics of X_2^{wd} and Y_2^{wd} cells is determined only by their death rate, whereas the dynamics of Z_2^{wd} cells is determined by the rate of leaving the group of Z_2^{wd} cells. As for the weakly damaged X_1^{wd} cells, one part of these cells is not damaged in the result of the second exposure and remains weakly damaged ones, whereas the other part of these cells is damaged by radiation in the different extent and, as it is supposed, transfer to groups of heavily damaged cells (X^{hd} cells) and moderately damaged cells (X^{md} cells). Thus, the second exposure leads to the forming of three new groups of cells.

Finally, let us address the response of the skin epidermis to the i-th exposure. In the system on hand, before this exposure ($t = \tau_1 + \ldots + \tau_{i-1}$), there are undamaged X^{ud}, Y^{ud}, and Z^{ud} cells, moderately damaged X^{md} cells, heavily damaged X^{hd} cells, as well as $[3(i-1)]$ groups of weakly damaged cells, namely X_1^{wd}, Y_1^{wd}, Z_1^{wd}, X_2^{wd}, Y_2^{wd}, Z_2^{wd}, …, X_{i-1}^{wd}, Y_{i-1}^{wd}, and Z_{i-1}^{wd} cells. In the results of the i-th exposure, a part of undamaged X^{ud} cells remains undamaged ones (X^{ud} cells), whereas the rest of the cells transfer to groups of heavily damaged cells (X^{hd} cells), moderately damaged cells (X^{md} cells), and weakly damaged cells (X_i^{wd} cells). In turn, progenies of X_i^{wd} cells form the groups of weakly damaged Y_i^{wd} cells and weakly damaged Z_i^{wd} cells. The behavior of X_i^{wd}, Y_i^{wd}, and Z_i^{wd} cells is the same as the behavior of undamaged X^{ud}, Y^{ud}, and Z^{ud} cells until the time moment ($t = T_{ar} + \tau_1 + \tau_2 + \ldots + \tau_{i-1}$), after which the dynamics of X_i^{wd} and Y_i^{wd} cells is determined only by their death rate, whereas the dynamics of Z_i^{wd} cells is determined by the rate of leaving the group of Z_i^{wd} cells. As for $(i-1)$ groups of the weakly damaged cells (X_1^{wd}, …, X_{i-1}^{wd} cells), a part of the cells in each such group is not damaged in the result of the i-th exposure and remains weakly damaged ones, whereas the other part of these cells is damaged and transfers to groups of heavily damaged cells (X^{hd} cells) and moderately damaged cells (X^{md} cells). Thus, the i-th exposure leads to the forming of three new groups of cells. For the total number n of the exposures, the number of the groups of the skin epidermal cells under consideration is equal to $3 + 2 + 3n = 5 + 3n$. Hence, the extended model, which describes the response of the skin epidermal epithelium to n-fractionated irradiation, considers $5 + 3n$ aforementioned groups of the skin epidermal cells, namely:

- X^{ud}, undamaged basal cells;
- Y^{ud}, prickle cells, which are progenies of X^{ud} cells;

- Z^{ud}, corneal cells, which are progenies of Y^{ud} cells;
- X^{hd}, heavily damaged basal cells that die within several hours (interphase death);
- X^{md}, moderately damaged basal cells that die within several days (mitotic death);
- X_i^{wd}, weakly damaged basal cells, which appear in the result of the i-th ($i = 1, \ldots, n$) exposure; these cells are capable of dividing and maturing and then transfer to the group of Y_i^{wd} cells, if the time passed after the i-th exposure does not exceed the time interval T_{ar}, and they only die within several days, if the time passed after the i-th exposure equals or exceeds the time interval T_{ar};
- Y_i^{wd}, prickle cells that are progenies of weakly damaged basal cells (X_i^{wd} cells); these cells are capable of functioning as Y^{ud} cells, if the time passed after the i-th exposure ($i = 1, \ldots, n$) does not exceed the time interval T_{ar}, and they only die within several days, if the time passed after the i-th exposure equals or exceeds the time interval T_{ar};
- Z_i^{wd}, corneal cells that are progenies of Y_i^{wd} cells; these cells are capable of functioning as Z^{ud} cells, if the time passed after the i-th exposure ($i = 1, \ldots, n$) does not exceed the time interval T_{ar}, and they leave the group of Z_i^{wd} cells within several days, if the time passed after the i-th exposure equals or exceeds the time interval T_{ar}.

The concentrations of the foregoing cells, namely x^{ud}, y^{ud}, z^{ud}, x^{hd}, x^{md}, x_i^{wd}, y_i^{wd}, and z_i^{wd} ($i = 1, \ldots, n$), are the model variables.

Proceeding from the aforementioned assumptions, the version of the model, which describes the dynamics of the skin epidermis after n-fractionated irradiation with exposure doses D_i ($i = 1, \ldots, n$) and time intervals τ_i ($i = 1, \ldots, n-1$) between the exposures, takes the following form:

$$\frac{dx^{\mathrm{ud}}}{dt} = B\,x^{\mathrm{ud}} - \gamma\,x^{\mathrm{ud}}, \tag{9.50}$$

$$\frac{dy^{\mathrm{ud}}}{dt} = \gamma\,x^{\mathrm{ud}} - F\,y^{\mathrm{ud}}, \tag{9.51}$$

$$\frac{dz^{\mathrm{ud}}}{dt} = F\,y^{\mathrm{ud}} - E\,z^{\mathrm{ud}}, \tag{9.52}$$

$$\begin{aligned}\frac{dx_i^{\mathrm{wd}}}{dt} &= \Theta\left(T_{ar} - t + \sum_{j=1}^{i-1}\tau_j\right)[Bx_i^{\mathrm{wd}} - \gamma x_i^{\mathrm{wd}}] \\ &\quad -\Theta(t - T_{ar} - \sum_{j=1}^{i-1}\tau_j)\eta x_i^{\mathrm{wd}} \qquad (i = 1, \ldots, n),\end{aligned} \tag{9.53}$$

$$\begin{aligned}\frac{dy_i^{\mathrm{wd}}}{dt} &= \Theta(T_{ar} - t + \sum_{j=1}^{i-1}\tau_j)[\gamma x_i^{\mathrm{wd}} - Fy_i^{\mathrm{wd}}] \\ &\quad -\Theta(t - T_{ar} - \sum_{j=1}^{i-1}\tau_j)\eta y_i^{\mathrm{wd}} \qquad (i = 1, \ldots, n),\end{aligned} \tag{9.54}$$

$$\frac{dz_i^{\mathrm{wd}}}{dt} = \Theta(T_{ar} - t + \sum_{j=1}^{i-1}\tau_j)[Fy_i^{\mathrm{wd}} - Ez_i^{\mathrm{wd}}]$$

$$-\Theta(t - T_{ar} - \sum_{j=1}^{i-1}\tau_j)Ez_i^{\mathrm{wd}} \qquad (i = 1, \ldots, n), \tag{9.55}$$

$$\frac{dx^{\mathrm{md}}}{dt} = -\mu x^{\mathrm{md}}, \tag{9.56}$$

$$\frac{dx^{\mathrm{hd}}}{dt} = -\nu x^{\mathrm{hd}}, \tag{9.57}$$

where $\Theta(t)$ is the unit step-function [Eq. (9.18)].

In the case of n-fractionated irradiation, the specific reproduction rate B of X cells, which enters Eqs. (9.50) and (9.53), is determined by Eq. (9.19), as that in the case of acute irradiation. The formula, which describes the parameter B_0 entering Eq. (9.19), is derived taking account of the contributions of all considered cells into the negative-feedback control mechanism. As a result, it takes the following form:

$$B_0 = \frac{\alpha}{1 + \beta\left[\left(x^{\mathrm{ud}} + \Phi_x^{'} + \phi x^{\mathrm{md}} + \varphi x^{\mathrm{hd}}\right) + \vartheta_y\left(y^{\mathrm{ud}} + \Phi_y^{'}\right) + \vartheta_z\left(z^{\mathrm{ud}} + \Phi_z^{'}\right)\right]}, \tag{9.58}$$

where

$$\Phi_x^{'} = \sum_{i=1}^{n} x_i^{\mathrm{wd}}\left[\Theta(T_{ar} - t + \sum_{j=1}^{i-1}\tau_j) + \varsigma\Theta(t - T_{ar} - \sum_{j=1}^{i-1}\tau_j)\right], \tag{9.59}$$

$$\Phi_y^{'} = \sum_{i=1}^{n} y_i^{\mathrm{wd}}\left[\Theta(T_{ar} - t + \sum_{j=1}^{i-1}\tau_j) + \varsigma\Theta(t - T_{ar} - \sum_{j=1}^{i-1}\tau_j)\right], \tag{9.60}$$

$$\Phi_z^{'} = \sum_{i=1}^{n} z_i^{\mathrm{wd}}\left[\Theta(T_{ar} - t + \sum_{j=1}^{i-1}\tau_j) + \varsigma\Theta(t - T_{ar} - \sum_{j=1}^{i-1}\tau_j)\right]. \tag{9.61}$$

In turn, the function V entering Eq. (9.19) is determined, as in the case of acute irradiation, by Eqs. (9.25)–(9.28), in which the parameter D is taken to be equal to the total dose of n-fractionated irradiation: $D = \sum_{i=1}^{n} D_i$.

In the case of n-fractionated irradiation, the functions F and E entering Eqs. (9.51), (9.52, (9.54), and (9.55) are described, as in the case of acute irradiation, by Eqs. (9.29)–(9.31) with the parameter D taken to be equal to the total dose of n-fractionated irradiation: $D = \sum_{i=1}^{n} D_i$.

It is obvious that the concentrations of X^{ud}, Y^{ud}, Z^{ud}, X^{hd}, X^{md}, X_1^{wd}, Y_1^{wd}, and Z_1^{wd} cells just after the first exposure of n-fractionated irradiation are determined by the

same Eqs. (9.40)–(9.47), as the concentrations of the respective cells just after acute irradiation. In turn, the concentrations of the rest of the cells under consideration are equal to zero. Therefore the initial conditions for Eqs. (9.50)–(9.57) take the following form:

$$x^{\mathrm{ud}}(0) = \bar{x}\,\exp(-D_1/D_x^0), \tag{9.62}$$

$$y^{\mathrm{ud}}(0) = \bar{y}, \tag{9.63}$$

$$z^{\mathrm{ud}}(0) = \bar{z}, \tag{9.64}$$

$$x^{\mathrm{hd}}(0) = \bar{x}\,\frac{\rho_1}{1+\rho_1}[1-\exp(-D_1/D_x^0)], \tag{9.65}$$

$$x^{\mathrm{md}}(0) = \bar{x}\,\frac{1}{1+\rho_1}\,\frac{1}{1+\kappa_1}\,[1-\exp(-D_1/D_x^0)], \tag{9.66}$$

$$x_1^{\mathrm{wd}}(0) = \bar{x}\,\frac{1}{1+\rho_1}\,\frac{\kappa_1}{1+\kappa_1}\,[1-\exp(-D_1/D_x^0)], \tag{9.67}$$

$$y_1^{\mathrm{wd}}(0) = 0, \tag{9.68}$$

$$z_1^{\mathrm{wd}}(0) = 0, \tag{9.69}$$

$$x_i^{\mathrm{wd}}(0) = 0 \qquad (i = 2,\ldots,n), \tag{9.70}$$

$$y_i^{\mathrm{wd}}(0) = 0 \qquad (i = 2,\ldots,n), \tag{9.71}$$

$$z_i^{\mathrm{wd}}(0) = 0 \qquad (i = 2,\ldots,n). \tag{9.72}$$

Here $\bar{x}$, $\bar{y}$, and $\bar{z}$ are the normal concentrations of X, Y, and Z cells.

The concentrations of the considered cells just after the i-th ($i = 2,\ldots,n$) exposure ($t = T_i = \sum_{j=1}^{i-1}\tau_j$) of n-fractionated irradiation take the following values:

$$x^{\mathrm{ud}}(T_i) = \tilde{x}_i^{\mathrm{ud}}\,\exp\left(-\frac{D_i}{D_x^0}\right) \qquad (i = 2,\ldots,n), \tag{9.73}$$

$$y^{\mathrm{ud}}(T_i) = \tilde{y}_i^{\mathrm{ud}} \qquad (i = 2,\ldots,n), \tag{9.74}$$

$$z^{\mathrm{ud}}(T_i) = \tilde{z}_i^{\mathrm{ud}} \qquad (i = 2,\ldots,n), \tag{9.75}$$

$$x^{\mathrm{hd}}(T_i) = \tilde{x}_i^{\mathrm{hd}} + \tilde{x}_i^{\mathrm{ud}}\,\frac{\rho_i}{1+\rho_i}\left[1-\exp\left(-\frac{D_i}{D_x^0}\right)\right] + \sum_{j=1}^{i-1}\tilde{x}_{ij}^{\mathrm{wd}}\,\frac{\xi_i}{1+\xi_i}\left[1-\exp\left(-\frac{D_i}{D_{xwd}^0}\right)\right] \qquad (i = 2,\ldots,n), \tag{9.76}$$

$$x^{\mathrm{md}}(T_i) = \tilde{x}_i^{\mathrm{md}} + \tilde{x}_i^{\mathrm{ud}}\,\frac{1}{1+\rho_i}\,\frac{1}{1+\kappa_i}\,[1-\exp(-\frac{D_i}{D_x^0})] + \sum_{j=1}^{i-1}\tilde{x}_{ij}^{\mathrm{wd}}\,\frac{1}{1+\xi_i}\,[1-\exp(-\frac{D_i}{D_{xwd}^0})] \qquad (i = 2,\ldots,n), \tag{9.77}$$

$$x_i^{\mathrm{wd}}(T_i) = \tilde{x}_i^{\mathrm{ud}} \frac{1}{1+\rho_i} \frac{\kappa_i}{1+\kappa_i} [1 - \exp(-\frac{D_i}{D_x^0})] \qquad (i = 2, \ldots, n), \tag{9.78}$$

$$y_i^{\mathrm{wd}}(T_i) = 0 \qquad (i = 2, \ldots, n), \tag{9.79}$$

$$z_i^{\mathrm{wd}}(T_i) = 0 \qquad (i = 2, \ldots, n), \tag{9.80}$$

$$x_j^{\mathrm{wd}}(T_i) = \tilde{x}_{ij}^{\mathrm{wd}} \exp(-\frac{D_i}{D_{xwd}^0}) \qquad (j = 1, \ldots, i-1; i = 2, \ldots, n), \tag{9.81}$$

$$y_j^{\mathrm{wd}}(T_i) = \tilde{y}_{ij}^{\mathrm{wd}} \qquad (j = 1, \ldots, i-1; i = 2, \ldots, n), \tag{9.82}$$

$$z_j^{\mathrm{wd}}(T_i) = \tilde{z}_{ij}^{\mathrm{wd}} \qquad (j = 1, \ldots, i-1; i = 2, \ldots, n), \tag{9.83}$$

where $\tilde{x}_i^{\mathrm{ud}}$, $\tilde{y}_i^{\mathrm{ud}}$, $\tilde{z}_i^{\mathrm{ud}}$, $\tilde{x}_i^{\mathrm{hd}}$, $\tilde{x}_i^{\mathrm{md}}$ $(i = 2, \ldots, n)$ and $\tilde{x}_{ij}^{\mathrm{wd}}$, $\tilde{y}_{ij}^{\mathrm{wd}}$, $\tilde{z}_{ij}^{\mathrm{wd}}$ $(j = 1, \ldots, i-1; i = 2, \ldots, n)$ are concentrations of X^{ud}, Y^{ud}, Z^{ud}, X^{hd}, X^{md} and X_j^{wd}, Y_j^{wd}, Z_j^{wd} $(j = 1, \ldots, i-1; i = 2, \ldots, n)$ cells just before the time moment of i-th exposure T_i $(i = 2, \ldots, n)$.

The parameter ρ_i $(i = 1, \ldots, n)$ in Eqs. (9.65)–(9.67) and Eqs. (9.76)–(9.78) is the ratio of the fractions of undamaged X^{ud} cells, which transfer to heavily damaged X^{hd} cells and to moderately damaged X^{md} and weakly damaged X_i^{wd} $(i = 1, \ldots, n)$ cells, respectively, after i-th exposure with the dose D_i $(i = 1, \ldots, n)$:

$$\rho_i = \frac{1 - \exp(-D_i/D_x^{00})}{\exp(-D_i/D_x^{00}) - \exp(-D_i/D_x^0)} \qquad (i = 1, \ldots, n). \tag{9.84}$$

The parameter κ_i $(i = 1, \ldots, n)$ entering Eqs. (9.66) and (9.67), as well as in Eqs. (9.77) and (9.78), is the ratio of the fractions of X^{ud} cells, which transfer to weakly damaged X_i^{wd} $(i = 1, \ldots, n)$ cells and to moderately damaged X^{md} cells, respectively, after i-th exposure with the dose D_i $(i = 1, \ldots, n)$:

$$\kappa_i = \frac{\exp(-D_i/D_x^{000}) - \exp(-D_i/D_x^0)}{\exp(-D_i/D_x^{00}) - \exp(-D_i/D_x^{000})} \qquad (i = 1, \ldots, n). \tag{9.85}$$

The parameter ξ_i $(i = 2, \ldots, n)$ appearing in Eqs. (9.76) and (9.77) is the ratio of the fractions of weakly damaged X_j^{wd} $(j = 1, \ldots, i-1; i = 2, \ldots, n)$ cells, which transfer to heavily damaged X^{hd} cells and to moderately damaged X^{md} cells, respectively, after i-th exposure with the dose D_i $(i = 2, \ldots, n)$:

$$\xi_i = \frac{1 - \exp(-D_i/D_{xwd}^{00})}{\exp(-D_i/D_{xwd}^{00}) - \exp(-D_i/D_{xwd}^0)} \qquad (i = 2, \ldots, n). \tag{9.86}$$

The parameters D_x^0, D_x^{00}, and D_x^{000} characterizing the radiosensitivity of undamaged X^{ud} cells were specified above (Sect. 9.3.2). Remind that the parameter D_x^0 is equivalent to the conventional radiobiological dose D_0. After exposure to such dose, the number of X^{ud} cells left undamaged is $e = 2.718\ldots$ times smaller than

their initial number [34]. The parameter D_x^{00} is the dose, after exposure to which the number of X^{ud} cells that did not undergo the interphase death is $e = 2.718\ldots$ times smaller than their initial number. The parameter D_x^{000} is the dose, after exposure to which the number of X^{ud} cells that did not undergo either the interphase death or the mitotic death is $e = 2.718\ldots$ times smaller than their initial number. In turn, the parameters D_{xwd}^{0} and D_{xwd}^{00} characterize the radiosensitivity of weakly damaged X^{wd} cells. Specifically, the coefficient D_{xwd}^{0} is the dose, after exposure to which the number of weakly damaged X_j^{wd} $(j = 1,\ldots,i-1; i = 2,\ldots,n)$ cells left weakly damaged ones is $e = 2.718\ldots$ times smaller than their initial number. The coefficient D_{xwd}^{00} is the dose, after exposure to which the number of X_j^{wd} $(j = 1,\ldots,i-1; i = 2,\ldots,n)$ cells that did not undergo the interphase death is $e = 2.718\ldots$ times smaller than their initial number.

It is worthwhile to note that Eqs. (9.50)–(9.57), which describe the dynamics of the skin epidermis under n-fractionated irradiation, are reduced to Eqs. (9.10)–(9.17), which describe the dynamics of this vital body system under acute irradiation, if the parameter n in them is taken to be equal to unity and the parameter D_1 is considered as the dose of acute irradiation D. In turn, Eqs. (9.10)–(9.17), which describe the dynamics of the skin epidermis under acute irradiation, are reduced to Eqs. (9.1)–(9.3), which describe the dynamics of this system under normal conditions, if the parameter D in them is taken to be equal to zero. Thus, the developed model of skin epidermis can be used to study the dynamics of this vital body system under normal conditions and under single and fractionated irradiation.

9.3.4 Parameter Estimation

The developed model is applied to the studies of the dynamics of the epidermal epithelium in young swine skin under normal conditions and under single and fractionated irradiation. It is worthwhile to note that young swine is regarded as the best animal model for the studies of the radiation effects on the human skin. The point is that the swine skin bears many characteristics similar to human skin [7]. Specifically, the dimensions of epidermis and dermis are approximately the same in the young swine and adult human [39]; the swine skin and human skin have the similar histological appearance [40, 41]; the structural organization of the epidermis in the young swine, at the microscopic level, is similar to that in adult human [42]. In addition, the population kinetics, the density of the basal cells, and cell-cycle parameters in swine epidermis are comparable to those in human epidermis [6, 7]. The similarities between these two species provide the impetus to special attention to swine skin in radiobiological studies [35–37, 43–51].

The values of the independent parameters in the developed model are given in Table 9.1. The values of parameters γ, δ, and ψ are estimated proceeding from experimental data, which characterize the swine skin epidermal epithelium in the norm [35, 41]. The values of parameters α, σ, and λ are taken to be the same as

Table 9.1 Parameters of the model of the skin epidermis in swine

Parameter	Value	Dimension
α	5.6	day^{-1}
γ	0.3	day^{-1}
δ	0.06	day^{-1}
ψ	0.141	day^{-1}
μ	0.5	day^{-1}
ν	6	day^{-1}
η	0.1	day^{-1}
ω	0.016	day^{-1}
σ	1.25	day
λ	1.25	day
τ_{ar}	10	day
τ_{ed}	40.67	day
T_m	0.0333	day
D_x^0	2.55	Gy
D_x^{00}	1000	Gy
D_x^{000}	25	Gy
D_{xwd}^0	4	Gy
D_{xwd}^{00}	1000	Gy
D_w	21	Gy
D_v	6.7	Gy
υ	0.001	dayGy^{-1}
ζ	0.333	dayGy^{-1}
ϖ	0.002	$\text{day}^{-1}\text{Gy}^{-1}$
ϑ_y	0.25	1
ϑ_z	0.001	1
ϕ	1	1
φ	3	1
ς	1	1

those in the model of the small intestinal epithelium system (see Chap. 3 and the references therein). The values of the parameters μ and ν are taken from [52]. The value of the parameter D_x^0 is taken from [36]. The value of the parameter T_m is taken from [7]. The other parameters are evaluated by matching the modeling results with appropriate sets of experimental data [35, 36, 41].

The results of investigations of the developed model, which describes the dynamics of the epidermal epithelium in swine skin under normal conditions and under single and fractionated irradiation, are presented in the next sections.

9.4 Basic Dynamic Regimes of the Swine Skin Epidermis Under Normal Conditions

The model (9.1)–(9.3) is investigated by methods of the qualitative theory of differential equations and oscillation theory [53–57]. It is found that this system has two singular points in the space of variables (x, y, z). The first singular point is trivial (variables x, y, and z vanish). The coordinates of the second singular point in the space of variables are the following:

$$\bar{x} = \frac{(\alpha/\gamma) - 1}{\beta \left\{1 + \vartheta_y \gamma/[\delta(1 + \sigma\gamma)] + \vartheta_z \gamma/[\psi(1 + \lambda\gamma)]\right\}}, \tag{9.87}$$

$$\bar{y} = \bar{x}\,\frac{\gamma}{\delta(1 + \sigma\gamma)}, \tag{9.88}$$

$$\bar{z} = \bar{x}\,\frac{\gamma}{\psi(1 + \lambda\gamma)}. \tag{9.89}$$

When $\alpha < \gamma$, the first (trivial) singular point is stable and the second singular point has no physical sense because its coordinates are negative ($\bar{x} < 0$, $\bar{y} < 0$, $\bar{z} < 0$). If $\alpha = \gamma$, the second singular point coincides with the first one. In both the cases the stable trivial singular point can be identified with the state of the extinction of the skin epidermal epithelium system. This range of parameters is not considered in what follows.

When $\alpha > \gamma$, the first (trivial) singular point is unstable. The coordinates of the second singular point are positive. The second singular point can be either stable or unstable, depending on the values of the model parameters. If the second singular point with positive coordinates $\bar{x}$, $\bar{y}$, and $\bar{z}$ [Eqs. (9.87)–(9.89)] is stable, then it can be identified with the state of the stable dynamical equilibrium (the homeostasis state) in the skin epidermal epithelium system. In turn, the values $\bar{x}$, $\bar{y}$, and $\bar{z}$ can be considered as the normal concentrations of basal cells (X cells), prickle cells (Y cells), and corneal cells (Z cells), respectively. When the second singular point with positive coordinates $\bar{x}$, $\bar{y}$, and $\bar{z}$ [Eqs. (9.87)–(9.89)] is unstable, there is one more particular solution: stable oscillations of the variables x, y, and z (a stable limit cycle). This particular solution can be identified with the stable oscillations of concentrations of X, Y, and Z cells.

Equations (9.1)–(9.3) are investigated numerically. It is found that the second singular point with positive coordinates $\bar{x}$, $\bar{y}$, and $\bar{z}$ [Eqs. (9.87)–(9.89)] is stable at the normal values of the model parameters given in Table 9.1.

The results of the numerical studies of the model of the swine skin epidermis [Eqs. (9.1)–(9.3)] with the normal values of its parameters are presented in Fig. 9.1. This figure shows projections of two integral curves of Eqs. (9.1)–(9.3) onto the plane of states $\{yz\}$. The concentrations of X, Y, and Z cells are computed in the dimensionless units as the ratios of the dimension cell concentrations x, y, and z, and to their normal values $\bar{x}$, $\bar{y}$, and $\bar{z}$. The latter are determined by Eqs. (9.87)–(9.89) with the normal values of the model parameters. Obviously, the values of the

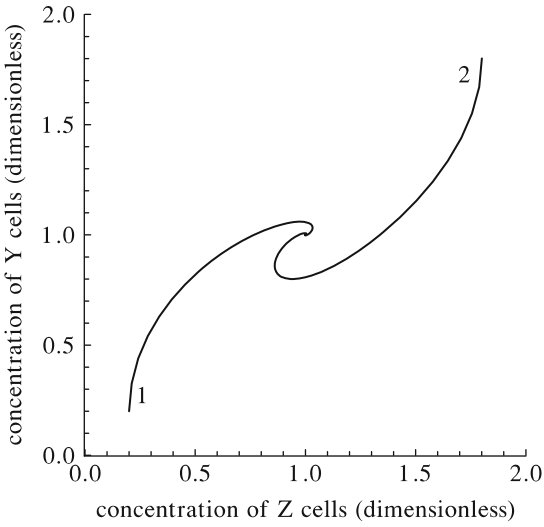

Fig. 9.1 Projections of two integral curves of the system (9.1)–(9.3) onto the plane of states $\{yz\}$. *Curves 1 and 2* converge to the stable second singular point (1, 1, 1). Results of computations of Eqs. (9.1)–(9.3) with the normal values of their parameters and with two sets of the initial values of the dimensionless concentrations of X, Y, and Z cells: 1.8, 0.2, and 0.2 (*curve 1*) and 0.2, 1.8, and 1.8 (*curve 2*), respectively

coordinates of the second singular point in these dimensionless units are (1, 1, 1) by definition. As one can infer from Fig. 9.1, the integral curves converge to this point. In other words, the concentrations of X, Y, and Z, cells return to their normal values $\bar{x}$, $\bar{y}$, and $\bar{z}$ after deviations from them. The obtained modeling results demonstrate that the developed model [Eqs. (9.1)–(9.3)] with the normal values of its parameters (Table 9.1) is capable of reproducing the homeostasis state in the swine skin epidermis under normal conditions.

It is also found that the second singular point with positive coordinates $\bar{x}$, $\bar{y}$, and $\bar{z}$ [Eqs. (9.87)–(9.89)] is unstable at $\vartheta_z = 17$ and $\alpha = 30$ day^{-1} and at the values of parameters γ, δ, ψ, σ, and λ, which coincide with their normal values (Table 9.1). The results of the numerical studies of the model of the swine skin epidermis [Eqs. (9.1)–(9.3)] with the set of "oscillatory" values of its parameters are presented in Figs. 9.2, 9.3, and 9.4.

Figure 9.2 displays projections of three integral curves of Eqs. (9.1)–(9.3) onto the plane of states $\{yz\}$. The concentrations of X, Y, and Z cells are computed in the dimensionless units as the ratios of the dimension cell concentrations x, y, and z to the values $\bar{x}$, $\bar{y}$, and $\bar{z}$. The latter are determined by Eqs. (9.87)–(9.89) with the "oscillatory" values of the model parameters specified above. Obviously, the values of the coordinates of the unstable second singular point [Eqs. (9.87)–(9.89)] in these dimensionless units are (1, 1, 1) by definition. In Fig. 9.2, the closed curve is the limit cycle, which corresponds to oscillations of cell concentrations. Two other curves converge to the limit cycle from the outside and inside. These modeling results testify to the stability of the limit cycle, i.e., they prove that the developed model is capable of reproducing the stable oscillations of cell concentrations in the swine skin epidermis under normal conditions.

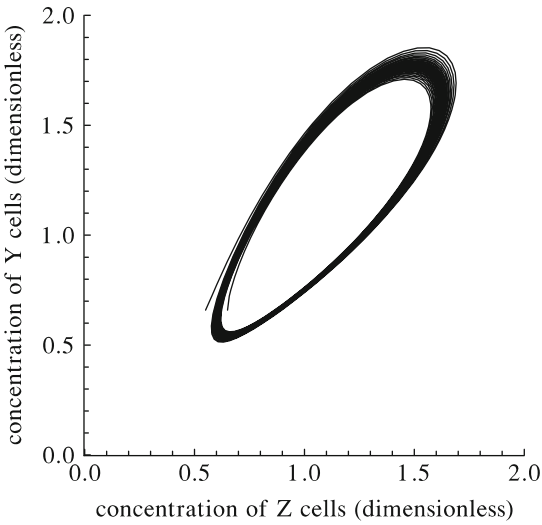

Fig. 9.2 Projections of three integral curves of the system (9.1)–(9.3) onto the plane of states $\{yz\}$. Two curves converge to the limit cycle (*closed curve*). Results of computations of Eqs. (9.1)–(9.3) with the "oscillatory" values of their parameters

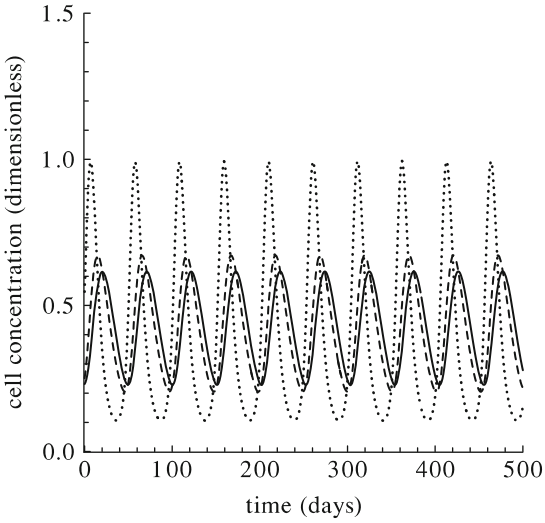

Fig. 9.3 The cyclic dynamics of the dimensionless concentration of X cells (*dotted curve*), Y cells (*dashed curve*), and Z cells (*solid curve*). Results of computations of Eqs. (9.1)–(9.3) with the "oscillatory" values of their parameters

Figure 9.3 shows the dynamics of the concentrations of basal cells (X cells), prickle cells (Y cells), and corneal cells (Z cells). These concentrations are given in the dimensionless units as the ratios of the dimension cell concentrations of X, Y, and Z cells (x, y, and z) to their normal values $\bar{x}$, $\bar{y}$, and $\bar{z}$. The latter are determined by Eqs. (9.87)–(9.89) with the normal values of the model parameters (Table 9.1). As numerical studies show, the values of the coordinates of the unstable second singular point [Eqs. (9.87)–(9.89)] in these dimensionless units are smaller than unity. As one can infer from Fig. 9.3, the dimensionless concentrations of basal, prickle, and corneal cells (X, Y, and Z cells) oscillate around the levels, which are below their normal levels (unity). Note that the concentration of Y cells oscillates in parallel

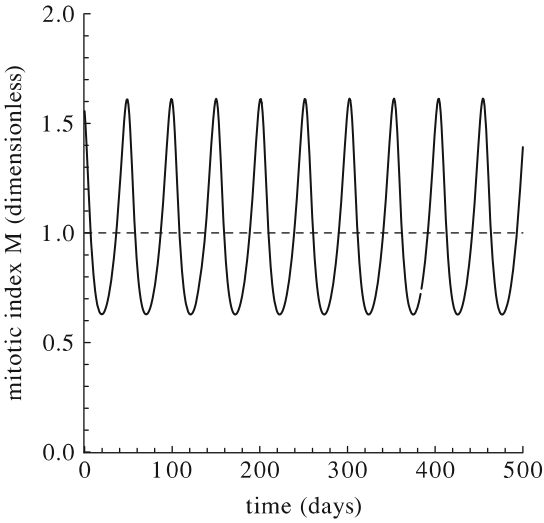

Fig. 9.4 The cyclic dynamics of the mitotic index M of X cells (*solid curve*) and its normal level (*dashed line*). Results of computations of Eqs. (9.1)–(9.3) and (9.7)

with the concentration of Z cells with the phase advance of 5 days. In turn, the concentration of X cells oscillates in parallel with the concentration of Y cells with the phase advance of 8 days. The amplitude of oscillations of the concentration of Y cells is less than that of X cells. The amplitude of oscillations of the concentration of Z cells is less than that of Y cells. The period of the oscillations of the epidermal cell concentrations is 51 days. The results presented in Fig. 9.3 demonstrate that the developed model is capable of reproducing the stable oscillations of dimensionless concentrations of basal, prickle, and corneal cells (X, Y, and Z cells) around the levels, which are below their normal ones.

Figure 9.4 presents the dynamics of the mitotic index M of basal cells (X cells), which is computed in the framework of the model (9.1)–(9.3) by making use of Eq. (9.7). The mitotic index M is given here in the dimensionless units as the ratio of its dimension value to the normal one. As one can infer from this figure, the mitotic index M of X cells oscillates around the level, which exceeds the normal one. The period of these oscillations (51 days) coincides with the period of oscillation of the epidermal cell concentrations. It is interesting to note that M oscillates in parallel with the concentration of X cells with the phase delay of 41 days. The results shown in Fig. 9.4 demonstrate that the developed model is capable of reproducing the stable oscillations of the mitotic index of the basal cells around the level, which is above its normal one.

The developed model [Eqs. (9.1)–(9.3)] with the "oscillatory" values of the parameters specified above is employed to predict the dynamics of the moist desquamation in swine skin. For this purpose, Eq. (9.90) is used. This equation is derived below (Sect. 9.6). The obtained modeling results are given in Fig. 9.5. This figure shows the dynamics of the fraction of area of the skin without moist desquamation $W(t)$. As one can infer from Fig. 9.5, the function $W(t)$ has the periodic character. After the period of the skin healing, which is characterized by

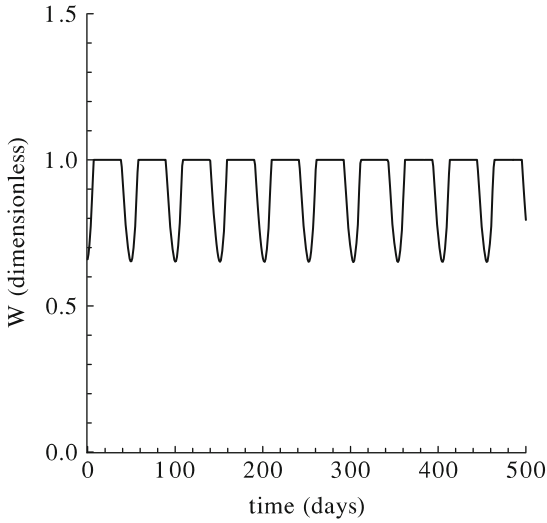

Fig. 9.5 The dynamics of the fraction of area of irradiated skin without moist desquamation $W(t)$ (*solid curve*). Results of computations of Eqs. (9.1)–(9.3) and (9.90)

the absence of the moist desquamation [$W(t) = 1$], the period of the exacerbations of the disease follows. The latter is characterized by the decrease and following increase of the fraction of area of the skin without moist desquamation $W(t)$. The moments of the minimum levels of $W(t)$ (i.e., the maximal exacerbations of the disease) coincide with the moments of the minimum of the concentration of Z cells. Obviously, the time interval between such moments is equal to the period of the oscillations of the epidermal cell concentrations (51 days).

Proceeding from the obtained modeling results, the following biological interpretation of causes of the cyclic dynamics of the skin epidermis can be proposed. Namely, such dynamical regime can arise (1) if the influence of the tissue-specific inhibitor of cell division produced by Z cells on the specific reproduction rate B of X cells is intensified in comparison with the norm and (2) if the maximal specific reproduction rate α of X cells increases in comparison with the norm.

It is important to note that the modeling results presented in Figs. 9.3, 9.4, and 9.5 resemble the dynamics of the skin epidermis in the cases of skin diseases, which are characterized by the periodicity of exacerbations, as well as increased mitotic activity of keratinocytes.

Thus, the developed model reproduces the basic dynamic regimes of the skin epidermal epithelium system under the normal conditions.

9.5 Effects of Acute Irradiation on the Swine Skin Epidermis

The developed model [Eqs. (9.10)–(9.17)] is used to study numerically the effects of acute irradiation on the swine skin epidermis. For the convenience, Eqs. (9.10)–(9.17) are rewritten in terms of the new dimensionless variables. The latter are

the ratios of the dimension concentrations of the epidermal cells to their normal values. In the course of the numerical studies of the model, the dynamics of the dimensionless concentrations of the epidermal cells and the dynamics of the mitotic index of basal cells are computed. For the verification of the modeling results, experimental data [35] are employed. These data represent a particular interest. Specifically, as it was shown in [35], the experiment was conducted in such way, that the reepithelialization of irradiated field of skin is due to the proliferation of survival cells within this field, the ingrowth from the nonirradiated edge being negligible. Obviously, this feature implies that these experimental data can be directly compared with the predictions of the developed model, which neglects the cell ingrowth from the nonirradiated edge as a contributing factor of recovering the epidermal epithelium within the irradiated field of skin.

The obtained modeling results and the respective experimental data [35] are given in Figs. 9.6, 9.7, 9.8, 9.9, 9.10, 9.11, 9.12, 9.13, 9.14, 9.15, 9.16, and 9.17. Specifically, Figs. 9.6, 9.10, and 9.14 display the modeling results on the dynamics of the dimensionless concentration of the basal cells (X cells), the dimensionless concentration of the prickle cells (Y cells), and the dimensionless concentration of the corneal cells (Z cells), which are computed at three doses of acute irradiation D reported in [35]. The experimental data [35] are presented here by mean values of the dimensionless cell density of all basal cells and mean square deviations

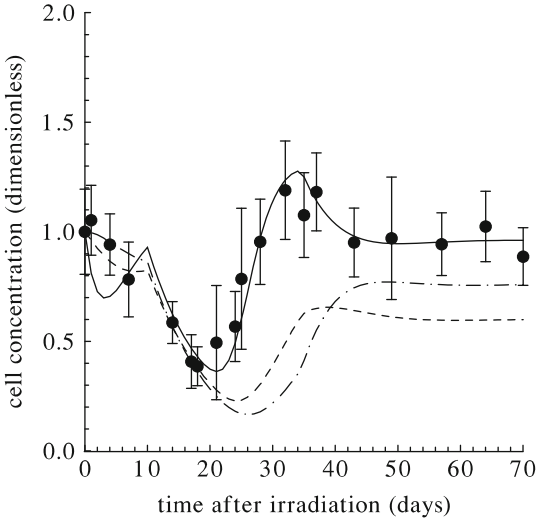

Fig. 9.6 The response of the swine skin to acute irradiation with the dose of $D = 16.49$ Gy: the modeling dynamics of the dimensionless total concentration of undamaged, weakly damaged, moderately damaged, and heavily damaged basal cells (*solid curve*), the dimensionless total concentration of undamaged and weakly damaged prickle cells (*dashed curve*), and the dimensionless total concentration of undamaged and weakly damaged corneal cells (*dot-dashed curve*), as well as the respective experimental data [35], which are given by mean values of the dimensionless total concentrations of basal cells (*circles*) and mean square deviations from these mean values

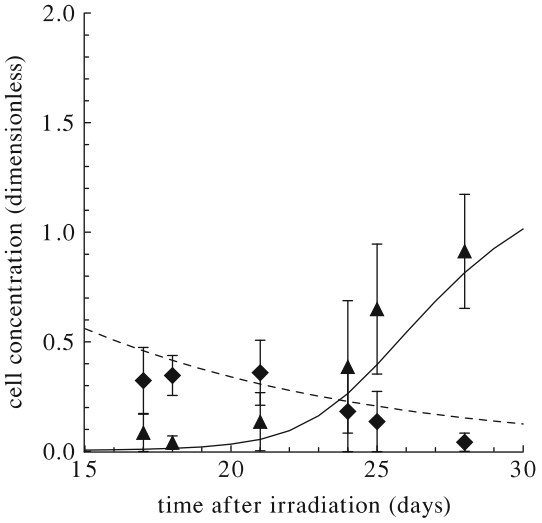

Fig. 9.7 The response of the swine skin to acute irradiation with the dose of $D = 16.49\,\text{Gy}$: the modeling dynamics of the dimensionless concentration of undamaged basal cells (*solid curve*) and the dimensionless total concentration of weakly damaged, moderately damaged, and heavily damaged basal cells (*dashed curve*), as well as the respective experimental data [35], which are given by mean values of the dimensionless concentrations of the aforementioned cells (*triangles and diamonds*, respectively) and mean square deviations from these mean values

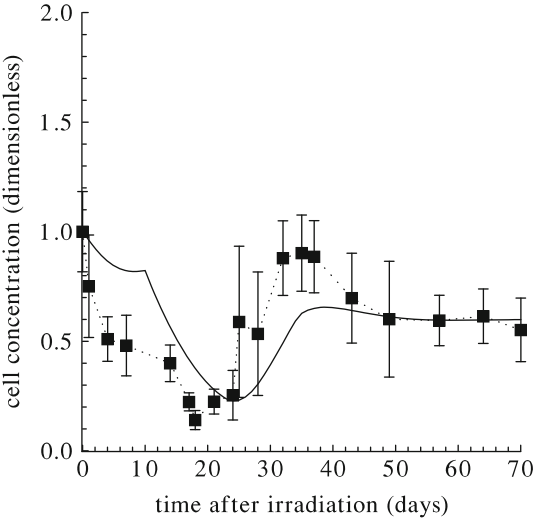

Fig. 9.8 The response of the swine skin to acute irradiation with the dose of $D = 16.49\,\text{Gy}$: the modeling dynamics of the dimensionless total concentration of undamaged and weakly damaged prickle cells (*solid curve*), as well as the respective experimental data [35], which are given by mean values of the dimensionless total concentration of the aforementioned cells (*boxes and dotted curve*) and mean square deviations from these mean values

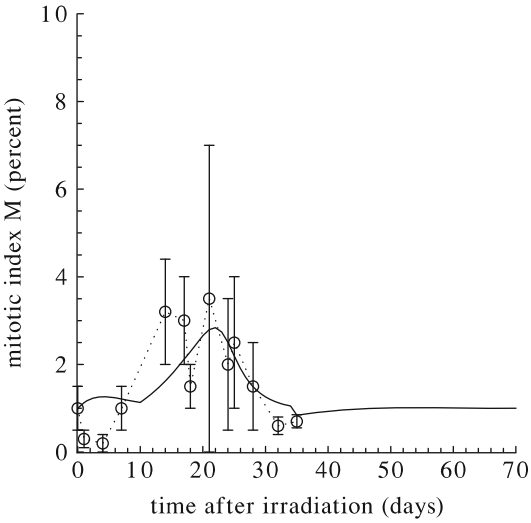

Fig. 9.9 The response of the swine skin to acute irradiation with the dose of $D = 16.49\,\text{Gy}$: the modeling dynamics of the mitotic index of the basal cells (*solid curve*), as well as the respective experimental data [35], which are given by mean values of the mitotic index of the aforementioned cells (*empty circles and dotted curve*) and mean square deviations from these mean values

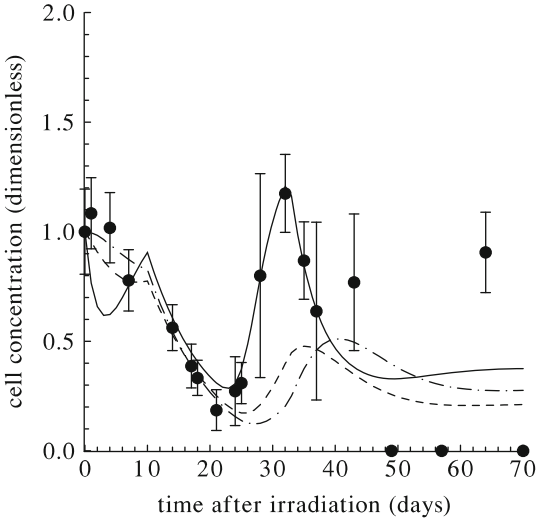

Fig. 9.10 The response of the swine skin to acute irradiation with the dose of $D = 22.31\,\text{Gy}$: the modeling dynamics of the dimensionless total concentration of undamaged, weakly damaged, moderately damaged, and heavily damaged basal cells (*solid curve*), the dimensionless total concentration of undamaged and weakly damaged prickle cells (*dashed curve*), and the dimensionless total concentration of undamaged and weakly damaged corneal cells (*dot-dashed curve*), as well as the respective experimental data [35], which are given by mean values of the dimensionless total concentrations of basal cells (*circles*) and mean square deviations from these mean values

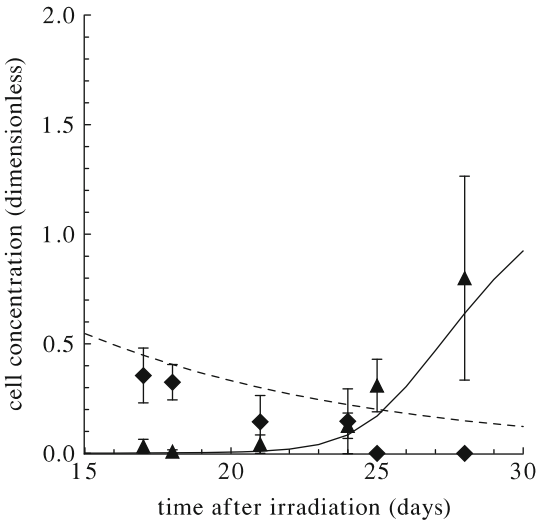

Fig. 9.11 The response of the swine skin to acute irradiation with the dose of $D = 22.31$ Gy: the modeling dynamics of the dimensionless concentration of undamaged basal cells (*solid curve*) and the dimensionless total concentration of weakly damaged, moderately damaged, and heavily damaged basal cells (*dashed curve*), as well as the respective experimental data [35], which are given by mean values of the dimensionless concentrations of the aforementioned cells (*triangles and diamonds*, respectively) and mean square deviations from these mean values

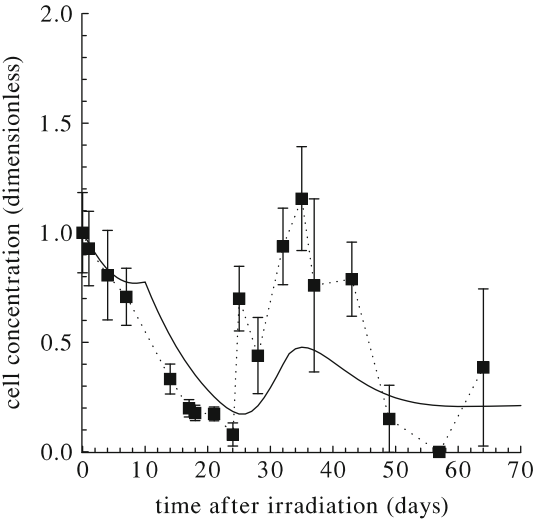

Fig. 9.12 The response of the swine skin to acute irradiation with the dose of $D = 22.31$ Gy: the modeling dynamics of the dimensionless total concentration of undamaged and weakly damaged prickle cells (*solid curve*), as well as the respective experimental data [35], which are given by mean values of the dimensionless total concentration of the aforementioned cells (*boxes and dotted curve*) and mean square deviations from these mean values

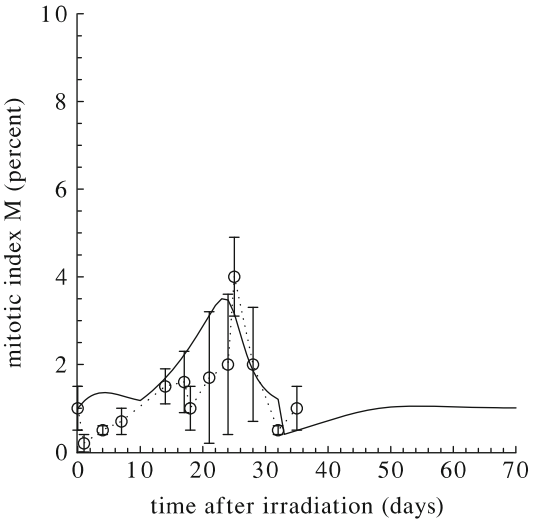

Fig. 9.13 The response of the swine skin to acute irradiation with the dose of $D = 22.31$ Gy: the modeling dynamics of the mitotic index of the basal cells (*solid curve*), as well as the respective experimental data [35], which are given by mean values of the mitotic index of the aforementioned cells (*empty circles and dotted curve*) and mean square deviations from these mean values

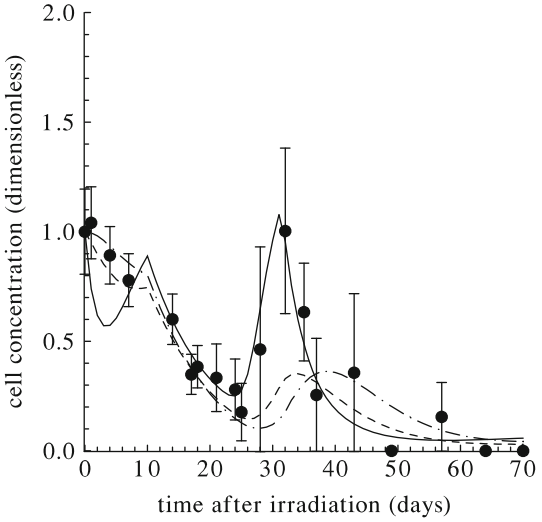

Fig. 9.14 The response of the swine skin to acute irradiation with the dose of $D = 26.19$ Gy: the modeling dynamics of the dimensionless total concentration of undamaged, weakly damaged, moderately damaged, and heavily damaged basal cells (*solid curve*), the dimensionless total concentration of undamaged and weakly damaged prickle cells (*dashed curve*), and the dimensionless total concentration of undamaged and weakly damaged corneal cells (*dot-dashed curve*), as well as the respective experimental data [35], which are given by mean values of the dimensionless total concentrations of basal cells (*circles*) and mean square deviations from these mean values

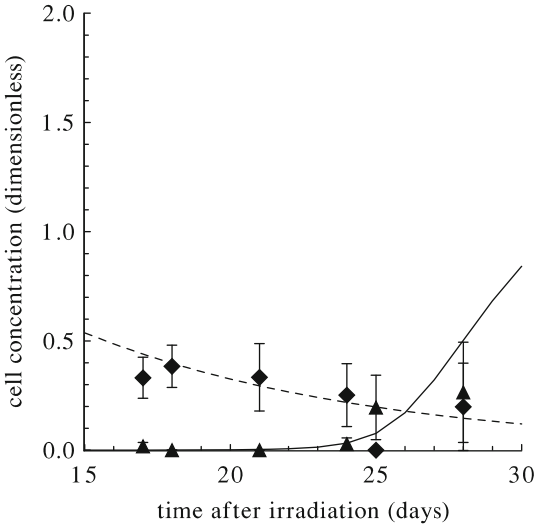

Fig. 9.15 The response of the swine skin to acute irradiation with the dose of $D = 26.19\,\text{Gy}$: the modeling dynamics of the dimensionless concentration of undamaged basal cells (*solid curve*) and the dimensionless total concentration of weakly damaged, moderately damaged, and heavily damaged basal cells (*dashed curve*), as well as the respective experimental data [35], which are given by mean values of the dimensionless concentrations of the aforementioned cells (*triangles and diamonds*, respectively) and mean square deviations from these mean values

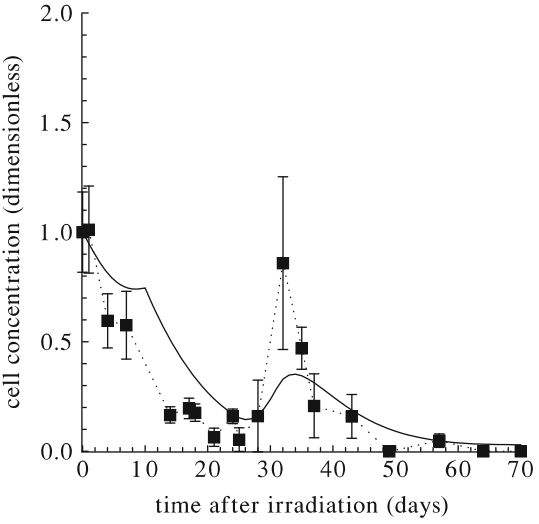

Fig. 9.16 The response of the swine skin to acute irradiation with the dose of $D = 26.19\,\text{Gy}$: the modeling dynamics of the dimensionless total concentration of undamaged and weakly damaged prickle cells (*solid curve*), as well as the respective experimental data [35], which are given by mean values of the dimensionless total concentration of the aforementioned cells (*boxes and dotted curve*) and mean square deviations from these mean values

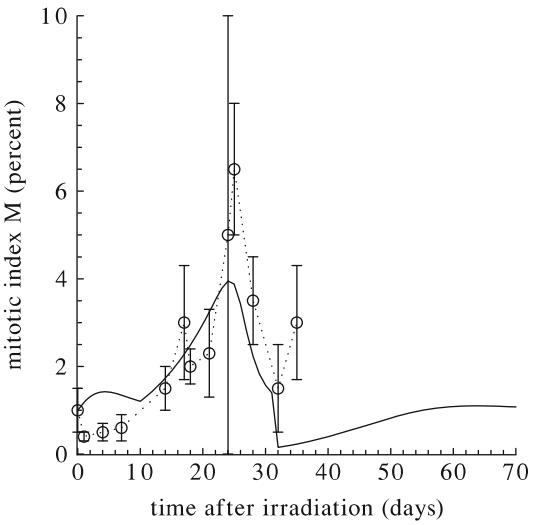

Fig. 9.17 The response of the swine skin to acute irradiation with the dose of $D = 26.19\,\text{Gy}$: the modeling dynamics of the mitotic index of the basal cells (*solid curve*), as well as the respective experimental data [35], which are given by mean values of the mitotic index of the aforementioned cells (*empty circles and dotted curve*) and mean square deviations from these mean values

from these mean values. As one can infer from these figures, the dynamics of dimensionless concentrations of the basal cells (X cells) and the dynamics of dimensionless concentrations of the prickle cells (Y cells) after acute irradiation with three considered doses D have a similar character. The dimensionless concentrations of the aforementioned cells decrease after irradiation and approach their first local minima, the latter being smaller at a higher dose D of acute irradiation. Then, the dimensionless concentrations of X cells and Y cells increase and approach their first local maxima, the latter being higher at a smaller dose D. This increase of the cell concentrations, which is known as the abortive rise, is more pronounced in the dynamics of the dimensionless concentration of the basal cells (X cells) than that in the dynamics of the dimensionless concentration of the prickle cells (Y cells). After the abortive rise, the dimensionless concentrations of X cells and Y cells decrease again and reach their second local minima, the latter being lower at a higher dose D of acute irradiation. After that, the dimensionless concentrations of X cells and Y cells increase again and approach their second local maxima, the latter being higher at a smaller dose D of acute irradiation. Then the dimensionless concentrations of X cells and Y cells decrease again and, at the end of the considered period, reach the values, which are smaller at a higher dose D. Note that these values are below their normal levels in the considered range of doses D of acute irradiation. The obtained modeling results show that the dimensionless concentration of X cells changes, practically, in parallel with the dimensionless concentration of Y cells with the phase advance of several days in the considered period of time.

In turn, the dimensionless concentration of the corneal cells (Z cells) decreases after acute irradiation and reaches its minimum, the latter being smaller at a higher dose D. Then, this concentration increases and approaches its maximum, the latter being higher at a smaller dose D. After that, the dimensionless concentration of corneal cells (Z cells) decreases again and, at the end of the considered period,

reaches the value, which is smaller at a higher dose D of acute irradiation. Note that this value is below their normal level in the considered range of doses D of acute irradiation.

The juxtaposition of the modeling results on the dynamics of the dimensionless concentration of the basal cells (X cells) at the doses D reported in [35] with the respective experimental data [35] reveals their good agreement (Figs. 9.6, 9.10, and 9.14). In particular, the developed model reproduces the degenerative, regenerative, and postregenerative phases of the response of the swine skin epidermal epithelium to acute irradiation in the considered range of doses D. It is important to emphasize that the duration of these phases predicted by the model, practically, coincide with the experimentally observed ones [35]. Moreover, the values of the dimensionless concentration of the basal cells (X cells) computed at three doses D reported in [35] are close to the respective experimental data [35] (Figs. 9.6, 9.10, and 9.14).

In the framework of the model, as well as in the experiments [35], the dynamics of the basal cells is investigated in details. Specifically, Figs. 9.7, 9.11, and 9.15 show the modeling results on the dynamics of the dimensionless concentration of undamaged basal cells and the dimensionless total concentration of all damaged basal cells (i.e., weakly damaged, moderately damaged, and heavily damaged basal cells), which are computed at three considered doses D of acute irradiation. The respective experimental data [35] are given here by mean values of the dimensionless cell density of the aforementioned cells and mean square deviations from these mean values. The juxtaposition of the modeling results and these experimental data reveals their good agreement. Within the considered period (15–30 days), the dimensionless concentration of undamaged basal cells increases from a small value up to a certain value, the latter being greater at a lower radiation dose D. In turn, the dimensionless total concentration of weakly damaged, moderately damaged, and heavily damaged basal cells (i.e., all damaged basal cells) decreases within the period under consideration. It is important to emphasize that the values of the dimensionless concentration of undamaged basal cells and the dimensionless total concentration of all damaged basal cells, which are computed at three doses D reported in [35], are close to the respective experimental data [35] (Figs. 9.7, 9.11, and 9.15).

Figures 9.8, 9.12, and 9.16 present the modeling results on the dynamics of the dimensionless concentration of the prickle cells (Y cells), which are computed at three considered doses D of acute irradiation. The respective experimental data [35] are given here by mean values of the dimensionless cell density of the aforementioned cells and mean square deviations from these mean values. As one can infer from these figures, the modeling results conform to the experimental data [35] in the period under consideration.

Figures 9.9, 9.13, and 9.17 display the dynamics of the mitotic index M of the basal cells (X cells) computed in the framework of model at three considered doses D of acute irradiation, as well as the respective experimental data [35], which are given by mean values of the mitotic index of the basal cells and mean square deviations from these mean values. The modeling results show that the mitotic

index M weakly increases after irradiation and soon achieves a local maximum, the latter being a bit greater at a higher dose D. After that, the mitotic index M weakly decreases and soon reaches a local minimum, the latter being a bit smaller at a lower dose D. Then the mitotic index M starts growing again and attains next local maximum, the latter being greater at a higher dose D. After that, the mitotic index decreases again and reaches the next local minimum, the latter being smaller at a higher dose D. Then the mitotic index M increases again and approaches a level, which is higher at a higher dose D. As one can see, these modeling results correspond, in a general way, with the respective experimental data [35].

The obtained agreement between the modeling results and the respective experimental data testify to the validity of employment of the developed model in the study and prediction of the dynamics of concentrations of the basal, prickle, and corneal cells, as well as of the mitotic activity of basal cells in the swine skin epidermis under acute irradiation.

9.6 Epidermal Cell Kinetics and Moist Reaction in Swine Skin After Acute Irradiation

To interpret the obtained modeling results and to compare them with one of the pathophysiological reactions of the skin on acute irradiation, namely with the moist reaction or moist desquamation, it is necessary to take into account the concept, according to which the moist reaction in irradiated skin is a consequence of the loss of a sufficient amount of cells in the epidermal epithelium to permit a leakage of serum [7, 35, 43]. Proceeding from this concept, the experimental data [35, 43] on the dynamics of the moist desquamation in acutely irradiated swine skin are juxtaposed with the respective modeling results on the dynamics of the dimensionless concentrations of epidermal cells (X, Y, and Z cells). It is found that the correlation between the experimental data [35, 43] on the dynamics of the moist desquamation in acutely irradiated swine skin and the respective modeling results on the dynamics of the dimensionless concentration of the corneal cells (Z cells) is most pronounced.

Figures 9.18, 9.19, 9.20, and 9.21 show the modeling dynamics of the dimensionless concentration of Z cells computed at four doses D reported in [35, 43] and the respective experimental data [35, 43] on the dynamics of the fraction of area of irradiated skin without moist desquamation $W(t)$. As one can infer from Figs. 9.18, 9.19, 9.20, and 9.21, the moist desquamation is not observed (i.e., $W(t) = 1$), if the dimensionless concentration of corneal cells (Z cells) is above a certain threshold level ($THL = 0.35$). In turn, the moist desquamation is observed (i.e., $W(t) < 1$), if the dimensionless concentration of the aforementioned cells is below this threshold level. As one can also see from Figs. 9.18, 9.19, 9.20, and 9.21, the fraction of area of irradiated skin without moist desquamation, $W(t)$, decreases with decreasing the dimensionless concentration of corneal cells and increases with

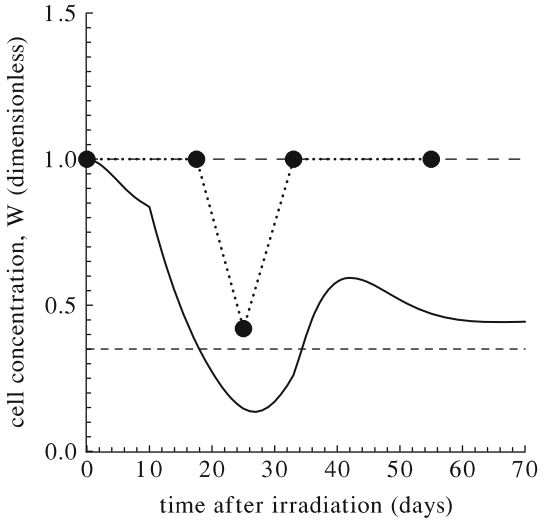

Fig. 9.18 The response of the swine skin to acute irradiation with the dose of $D = 20.37$ Gy: the modeling dynamics of the dimensionless concentration of corneal cells (Z cells) (*solid curve*) and the respective experimental values of the fraction of area of irradiated skin without moist desquamation $W(t)$ [43] (*circles and dotted curve*). The normal level of $W(t)$ and the normal level of the dimensionless concentration of Z cells are shown by *medium-dashed line*; the threshold level of the dimensionless concentration of Z cells is shown by *short-dashed line*

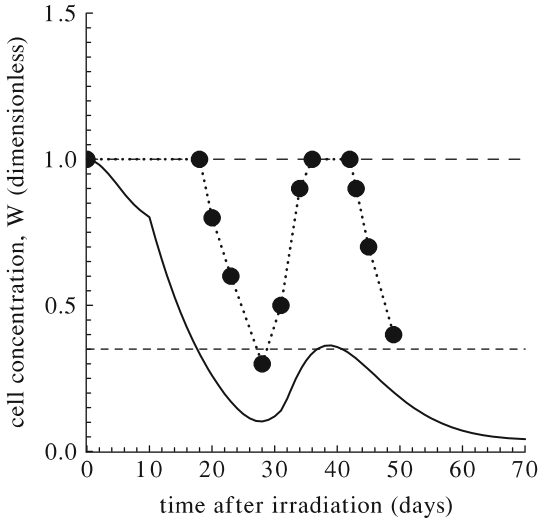

Fig. 9.19 The response of the swine skin to acute irradiation with the dose of $D = 26.19$ Gy: the modeling dynamics of the dimensionless concentration of corneal cells (Z cells) (*solid curve*) and the respective experimental values of the fraction of area of irradiated skin without moist desquamation $W(t)$ [35] (*circles and dotted curve*). The normal level of $W(t)$ and the normal level of the dimensionless concentration of Z cells are shown by *medium-dashed line*; the threshold level of the dimensionless concentration of Z cells is shown by *short-dashed line*

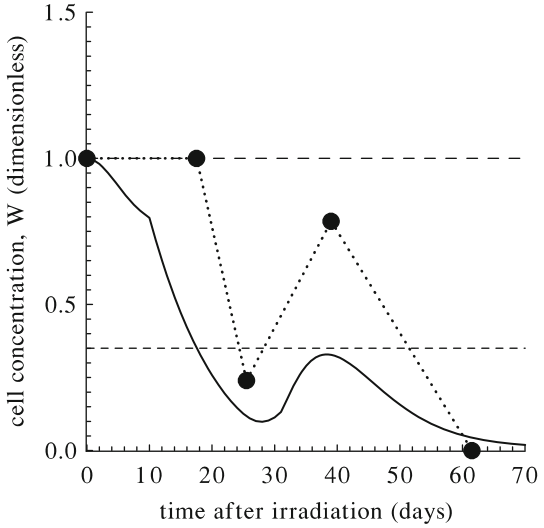

Fig. 9.20 The response of the swine skin to acute irradiation with the dose of $D = 27.16$ Gy: the modeling dynamics of the dimensionless concentration of corneal cells (Z cells) (*solid curve*) and the respective experimental values of the fraction of area of irradiated skin without moist desquamation $W(t)$ [43] (*circles and dotted curve*). The normal level of $W(t)$ and the normal level of the dimensionless concentration of Z cells are shown by *medium-dashed line*; the threshold level of the dimensionless concentration of Z cells is shown by *short-dashed line*

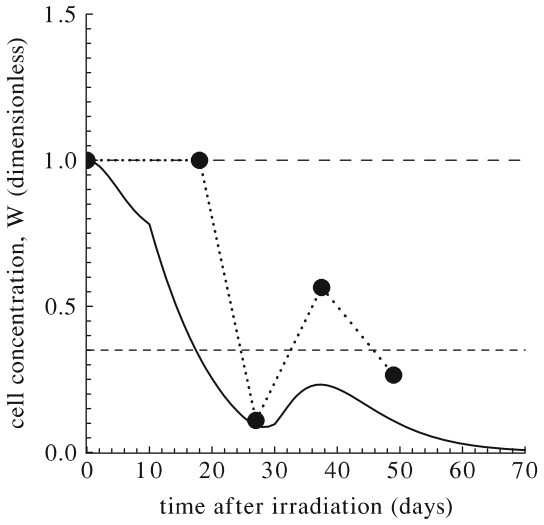

Fig. 9.21 The response of the swine skin to acute irradiation with doses of $D = 30.07$ Gy: the modeling dynamics of the dimensionless concentration of corneal cells (Z cells) (*solid curve*) and the respective experimental values of the fraction of area of irradiated skin without moist desquamation $W(t)$ [43] (*circles and dotted curve*). The normal level of $W(t)$ and the normal level of the dimensionless concentration of Z cells are shown by *medium-dashed line*; the threshold level of the dimensionless concentration of Z cells is shown by *short-dashed line*

growing this concentration, if the latter does not exceed the threshold level. It is important to emphasize that the time of appearance of the moist desquamation and its healing, practically, coincides with the moments, when the dimensionless concentration of corneal cells (Z cells) approaches the threshold level (Figs. 9.18, 9.19, 9.20, and 9.21. In turn, the time of the local minimum of the fraction of area of irradiated skin without moist desquamation $W(t)$ (i.e., the time of the minimum of the noninvolvement of irradiated skin into the moist desquamation) is close to the time of the local minimum of the dimensionless concentration of Z cells in the considered range of doses D.

For effective juxtapositions of the modeling results on the dynamics of the dimensionless concentration of corneal cells (Z cells) computed at the doses D of acute irradiation reported in [35, 43] with the respective experimental values of the fraction of the area of irradiated skin without moist desquamation ($W(t)$) [35, 43], the values of $W(t)$ are multiplied by the scale factor THL. It is obvious that the scaled value of $W(t)$, i.e., $THL \times W(t)$, is equal to THL (i.e., 0.35) in the case of the absence of moist desquamation, whereas it becomes smaller than THL in the case of the appearance of moist desquamation. This is illustrated by the results given in Figs. 9.22, 9.23, 9.24, and 9.25.

Figures 9.22, 9.23, 9.24, and 9.25 show the modeling dynamics of the dimensionless concentration of the corneal cells (Z cells) computed at the doses D reported in [35, 43] and the respective scaled experimental values of $W(t)$, i.e., $THL \times W(t)$

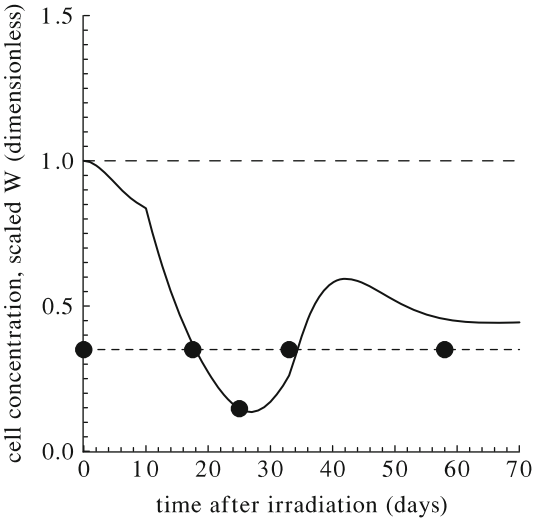

Fig. 9.22 The response of the swine skin to acute irradiation with the dose of $D = 20.37$ Gy: the modeling dynamics of the dimensionless concentration of corneal cells (Z cells) (*solid curve*) and the respective scaled experimental values of the fraction of area of irradiated skin without moist desquamation $W(t)$ [43] (*circles*). *Medium-dashed line* is the normal level of the dimensionless concentration of Z cells; *short-dashed line* is the threshold level of the dimensionless concentration of Z cells

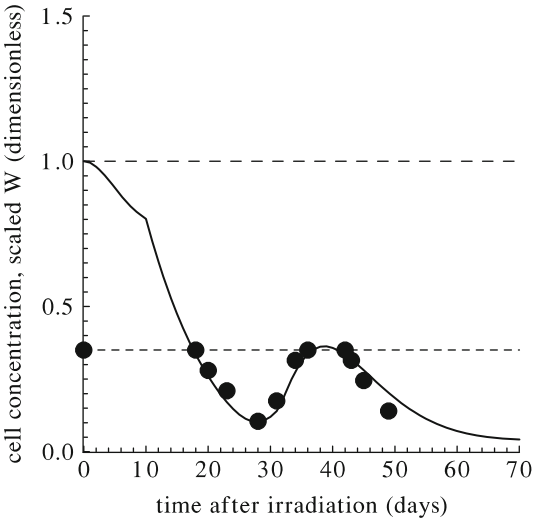

Fig. 9.23 The response of the swine skin to acute irradiation with the dose of $D = 26.19$ Gy: the modeling dynamics of the dimensionless concentration of corneal cells (Z cells) (*solid curve*) and the respective scaled experimental values of the fraction of area of irradiated skin without moist desquamation $W(t)$ [35] (*circles*). *Medium-dashed line* is the normal level of the dimensionless concentration of Z cells; *short-dashed line* is the threshold level of the dimensionless concentration of Z cells

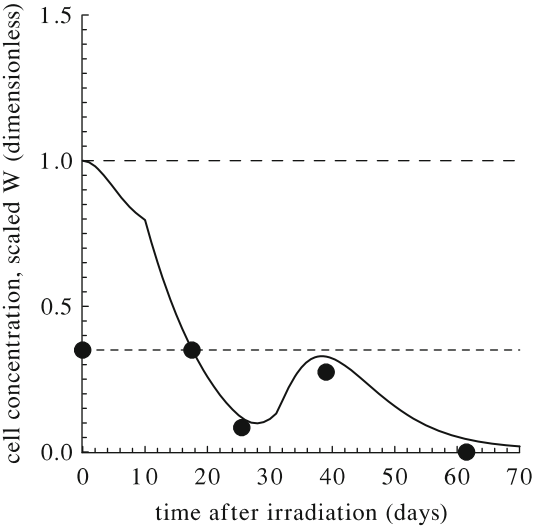

Fig. 9.24 The response of the swine skin to acute irradiation with the dose of $D = 27.16$ Gy: the modeling dynamics of the dimensionless concentration of corneal cells (Z cells) (*solid curve*) and the respective scaled experimental values of the fraction of area of irradiated skin without moist desquamation $W(t)$ [43] (*circles*). *Medium-dashed line* is the normal level of the dimensionless concentration of Z cells; *short-dashed line* is the threshold level of the dimensionless concentration of Z cells

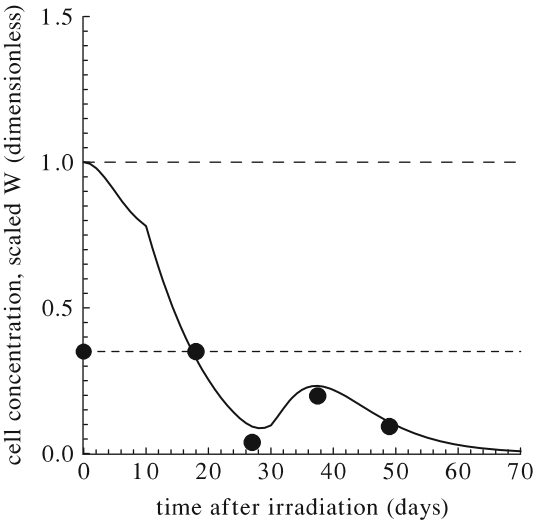

Fig. 9.25 The response of the swine skin to acute irradiation with the dose of $D = 30.07$ Gy: the modeling dynamics of the dimensionless concentration of corneal cells (Z cells) (*solid curve*) and the respective scaled experimental values of the fraction of area of irradiated skin without moist desquamation $W(t)$ [43] (*circles*). *Medium-dashed line* is the normal level of the dimensionless concentration of Z cells; *short-dashed line* is the threshold level of the dimensionless concentration of Z cells

[35, 43]. As one can see, they are in a good agreement. Specifically, the scaled experimental values of the fraction of the area of irradiated swine skin without moist desquamation obtained at several time moments after acute irradiation with the considered doses D [35, 43] almost coincide with the respective modeling results on the dynamics of the dimensionless concentration of the corneal cells (Z cells).

The revealed good agreement of the modeling results on the dynamics of the dimensionless concentration of Z cells with the respective scaled experimental values of the fraction of the area of irradiated skin without moist desquamation $[THL \times W(t)]$ implies that the developed model can be used to predict the dynamics of the moist desquamation in swine skin exposed to acute irradiation in the considered dose range. As it is evident from the results presented above, the fraction of area of irradiated skin without moist desquamation, $W(t)$, can be defined as the dimensionless concentration of Z cells multiplied by the inverse value of THL:

$$W(t) = [z(t)/\bar{z}] \times (1/THL). \tag{9.90}$$

Here $z(t)$ is the concentration of Z cells, $\bar{z}$ is the normal value of the concentration of Z cells, and THL is the threshold level specified above.

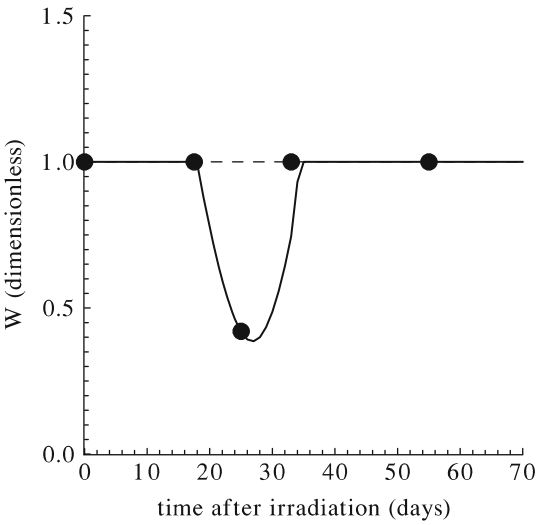

Fig. 9.26 The response of the swine skin to acute irradiation with the dose of $D = 20.37$ Gy: the modeling dynamics of the fraction of area of irradiated skin without moist desquamation $W(t)$ [Eq. (9.90)] (*solid curve*) and the respective experimental values of the fraction of area of irradiated skin without moist desquamation $W(t)$ [43] (*circles*). *Medium-dashed line* is the normal level of $W(t)$

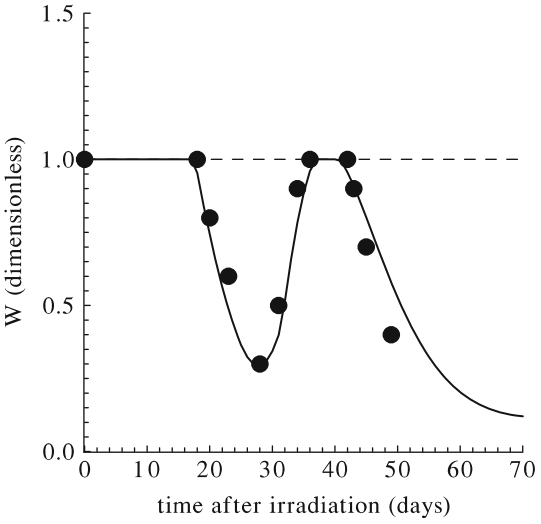

Fig. 9.27 The response of the swine skin to acute irradiation with the dose of $D = 26.19$ Gy: the modeling dynamics of the fraction of area of irradiated skin without moist desquamation $W(t)$ [Eq. (9.90)] (*solid curve*) and the respective experimental values of the fraction of area of irradiated skin without moist desquamation $W(t)$ [35] (*circles*). *Medium-dashed line* is the normal level of $W(t)$

Figures 9.26, 9.27, 9.28, and 9.29 show the modeling dynamics of the fraction of the area of swine skin without moist desquamation $W(t)$ [Eq. 9.90] computed at the doses D reported in [35, 43]. These figures also display the respective experimental values of the fraction of the area of irradiated skin without moist desquamation $W(t)$ [35, 43].

As one can infer from Figs. 9.26 and 9.27, the function $W(t)$ computed at two lesser doses D (from four doses under consideration) stays at its normal level (unity) within a certain period. Then the function $W(t)$ decreases and reaches its local minimum, the latter being lower at a higher dose D. After that, the function $W(t)$ increases and approaches the normal level (unity). In the case of the first dose D,

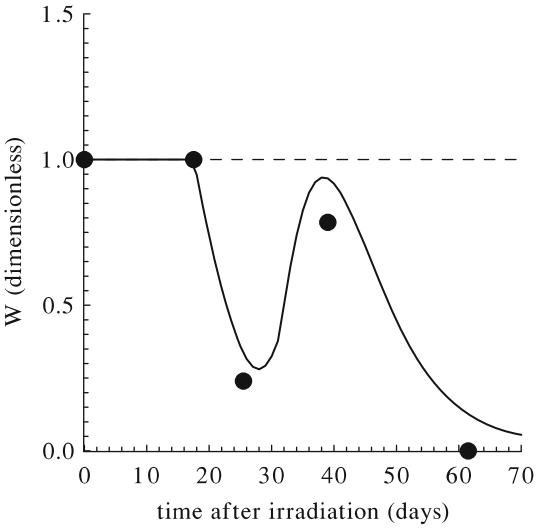

Fig. 9.28 The response of the swine skin to acute irradiation with the dose of $D = 27.16$ Gy: the modeling dynamics of the fraction of area of irradiated skin without moist desquamation $W(t)$ [Eq. (9.90)] (*solid curve*) and the respective experimental values of the fraction of area of irradiated skin without moist desquamation $W(t)$ [43] (*circles*). *Medium-dashed line* is the normal level of $W(t)$

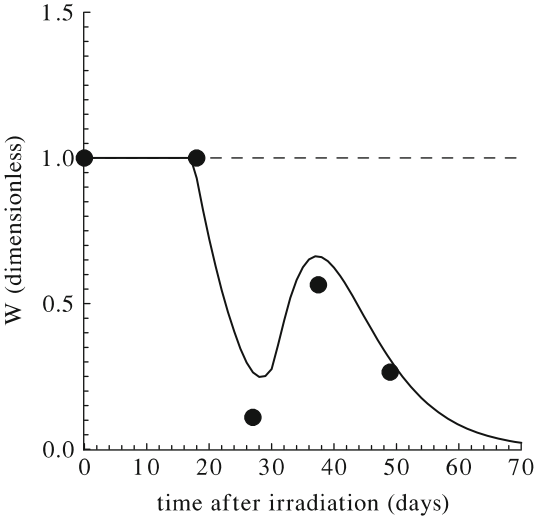

Fig. 9.29 The response of the swine skin to acute irradiation with the dose of $D = 30.07$ Gy: the modeling dynamics of the fraction of area of irradiated skin without moist desquamation $W(t)$ [Eq. (9.90)] (*solid curve*) and the respective experimental values of the fraction of area of irradiated skin without moist desquamation $W(t)$ [43] (*circles*). *Medium-dashed line* is the normal level of $W(t)$

which is a bit lower than the second one, the function $W(t)$ stays at its normal level up to the end of the period under consideration (Figs. 9.26). In the case of the second dose D, the function $W(t)$ stays at the normal level within a certain period, after which the function $W(t)$ decreases again (Figs. 9.27).

As one can infer from Figs. 9.28 and 9.29, the function $W(t)$ computed at two higher doses D (from four doses under consideration) stays at its normal level (unity) within a certain period. Then the function $W(t)$ decreases and reaches its local minimum, the latter being lower at a higher dose D. After that, the function $W(t)$ increases and approaches its maximum, which, contrary to the cases of two lower doses D, is below its normal level. After the reaching of the maximum, which is lower at a higher dose D, the function $W(t)$ decreases again.

All these modeling findings correspond with the respective experimentally observed peculiarities of the dynamics of the fraction of the area of swine skin without moist desquamation $W(t)$ under acute irradiation [35, 43]. Moreover, the values of $W(t)$, which are predicted by the model, almost coincide with the respective experimental values of the fraction of the area of irradiated skin without moist desquamation $W(t)$ within 10 weeks after acute irradiation in the considered range of doses (20.37–30.07 Gy).

The obtained agreement between the modeling findings and the respective experimental observations testify to the validity of employment of the developed model in the prediction of the dynamics of the moist desquamation in the swine skin exposed to acute irradiation in the wide range of doses D.

9.7 Epidermal Cell Kinetics and Moist Reaction in Swine Skin Under Fractionated Irradiation

The developed model of the swine skin epidermis [Eqs. (9.50)–(9.57)] is applied to study the effects of n-fractionated irradiation on this vital body system. For the convenience, Eqs. (9.50)–(9.57) are rewritten in terms of the new dimensionless variables, the latter being the ratios of the dimension concentrations of the epidermal cells to their normal values.

In the modeling studies, four scenarios of two-fractionated irradiation reported in [58] and two scenarios of five-fractionated irradiation reported in [58] are considered. The obtained results are given in Figs. 9.30, 9.31, 9.32, 9.33, 9.34, 9.35, 9.36, 9.37, 9.38, 9.39, 9.40, and 9.41.

Specifically, Figs. 9.30, 9.31, 9.32, 9.33, and 9.34 show the modeling dynamics of the dimensionless concentration of the corneal cells (Z cells) computed at the above-mentioned six scenarios of fractionated irradiation and the respective scaled experimental values [58] of the fraction of the area of swine skin epidermis without moist desquamation [$THL \times W(t)$]. Each of these figures also shows the modeling dynamics of the dimensionless concentration of corneal cells (Z cells) computed at such a dose of single acute irradiation, under which the local minimum of the dimensionless concentration of corneal cells coincides with that under the respective fractionated irradiation.

The juxtaposition of the modeling results on the dynamics of the dimensionless concentration of the corneal cells (Z cells), which are obtained at the aforementioned six scenarios of fractionated irradiation, with the respective scaled experimental values [$THL \times W(t)$] [58] elucidates their agreement (Figs. 9.30, 9.31, 9.32, 9.33, and 9.34). In particular, the moist desquamation is not observed [i.e., $THL \times W(t) = 0.35$], if the dimensionless concentration of the corneal cells (Z cells) is equal or above the threshold level ($THL = 0.35$). In turn, moist desquamation is observed [i.e., $THL \times W(t) < 0.35$], if the dimensionless concentration of the aforementioned cells is below the threshold level ($THL = 0.35$). It is important to emphasize

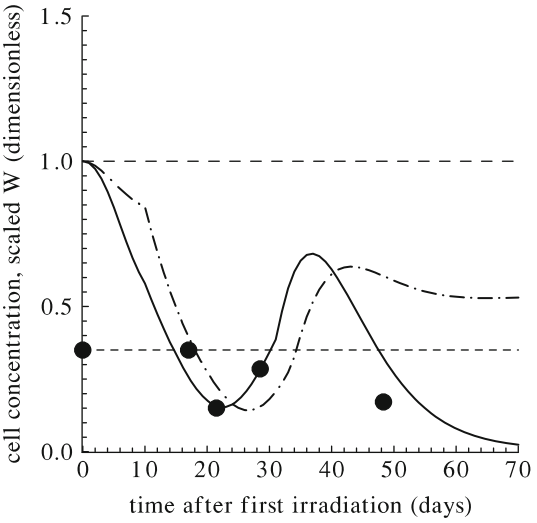

Fig. 9.30 The response of the swine skin to two-fractionated irradiation with the exposure doses of $D_1 = D_2 = 13.58$ Gy and with the time interval between the exposures of $\tau_1 = 0.25$ day: scaled experimental values of the fraction of area of swine skin without moist desquamation $W(t)$ [58] (*circles*) and the modeling dynamics of the dimensionless concentration of the corneal cells (Z cells) (*solid curve*). The response of the swine skin to single acute irradiation with the dose of $D = 19.4$ Gy: the modeling dynamics of the dimensionless concentration of Z cells (*dot-dashed curve*). *Medium-dashed line* is the normal level of the dimensionless concentration of Z cells; *short-dashed line* is the threshold level of the dimensionless concentration of Z cells

that the time moments of appearance of moist desquamation and its healing are close to the moments, when the dimensionless concentration of corneal cells approaches the threshold level. In turn, the time moment of the local minimum of the noninvolvement of irradiated skin into moist desquamation is close to the time moment, when the dimensionless concentration of corneal cells reaches its local minimum. Additionally, the results presented in Figs. 9.30, 9.31, 9.32, 9.33, and 9.34 demonstrate that the scaled experimental value of the fraction of the area of irradiated skin without moist desquamation [$THL \times W(t)$] decreases as the dimensionless concentration of the corneal cells (Z cells) decreases, and it increases with increasing the dimensionless concentration of Z cells up to the threshold level. It is important to emphasize that the scaled experimental values of the fraction of the area of irradiated skin without moist desquamation [$THL \times W(t)$], which are obtained at several time moments after the onset of fractionated irradiation reported in [58], are close to the respective values of the dimensionless concentration of Z cells computed in the framework of the developed model.

The obtained agreement between the scaled experimental values of the fraction of the area of swine skin epidermis without moist desquamation [$THL \times W(t)$] obtained at various regimes of fractionated irradiation in [58] and the respective modeling results on the dynamics of the dimensionless concentration of Z cells computed

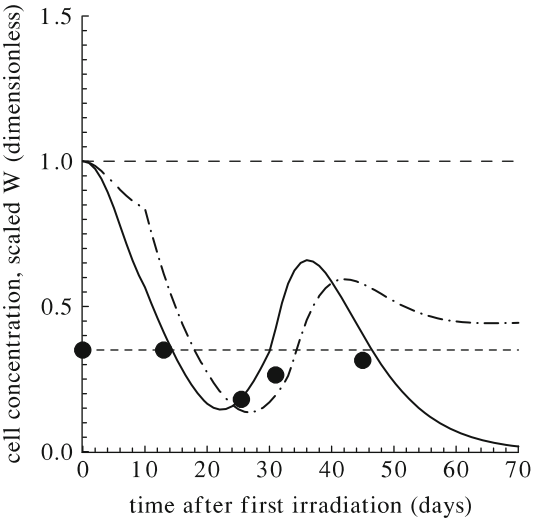

Fig. 9.31 The response of the swine skin to two-fractionated irradiation with the exposure doses of $D_1 = D_2 = 14.55$ Gy and with the time interval between the exposures of $\tau_1 = 0.25$ day: scaled experimental values of the fraction of area of swine skin without moist desquamation $W(t)$ [58] (*circles*) and the modeling dynamics of the dimensionless concentration of the corneal cells (Z cells) (*solid curve*). The response of the swine skin to single acute irradiation with the dose of $D = 20.37$ Gy: the modeling dynamics of the dimensionless concentration of Z cells (*dot-dashed curve*). *Medium-dashed line* is the normal level of the dimensionless concentration of Z cells; *short-dashed line* is the threshold level of the dimensionless concentration of Z cells

at the same radiation regimes (Figs. 9.30, 9.31, 9.32, 9.33, and 9.34 implies that Eq. (9.90) can also be used to predict the dynamics of moist desquamation under fractionated irradiation.

The comparison of the modeling results on the dynamics of the dimensionless concentration of corneal cells (Z cells) under six scenarios of fractionated irradiation with the modeling results on the dynamics of the dimensionless concentration of Z cells under six corresponding regimes of single acute irradiation allows one to reveal peculiarities of the effect of n-fractionated irradiation on swine skin (Figs. 9.30, 9.31, 9.32, 9.33, 9.34, and 9.35). Specifically, as one can infer from Fig. 9.30, the local minimum of the dimensionless concentration of the corneal cells after two-fractionated irradiation with the doses of $D_1 = D_2 = 13.58$ Gy and with the time interval between the first and second exposures τ_1 of 0.25 day is the same as that after single acute irradiation with the dose D of 19.4 Gy. This implies that the ratio of the total dose of two-fractionated irradiation ($D_{tot} = 27.16$ Gy) to the dose of single acute irradiation ($D = 19.4$ Gy), which lead to the same local minimum of the dimensionless concentration of the corneal cells and, hence, to the same local minimum of the fraction of the area of irradiated skin without moist desquamation, is equal to 1.4. In turn, as one can see from Fig. 9.31, the local minimum of the dimensionless concentration of the corneal cells after two-fractionated irradiation

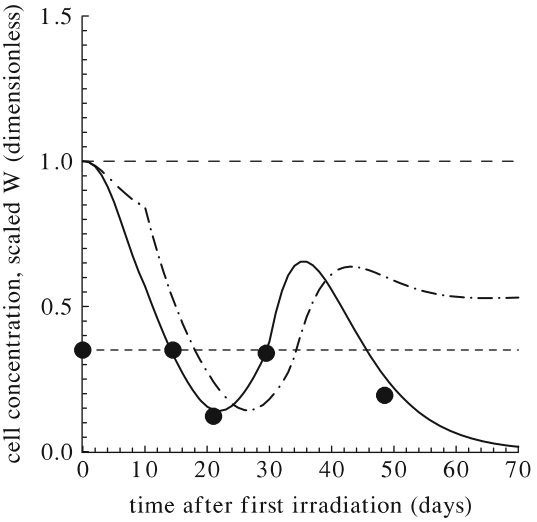

Fig. 9.32 The response of the swine skin to two-fractionated irradiation with the exposure doses of $D_1 = D_2 = 15.52$ Gy and with the time interval between the exposures of $\tau_1 = 1.0$ day: scaled experimental values of the fraction of area of swine skin without moist desquamation $W(t)$ [58] (*circles*) and the modeling dynamics of the dimensionless concentration of the corneal cells (Z cells) (*solid curve*). The response of the swine skin to single acute irradiation with the dose of $D = 19.4$ Gy: the modeling dynamics of the dimensionless concentration of Z cells (*dot-dashed curve*). *Medium-dashed line* is the normal level of the dimensionless concentration of Z cells; *short-dashed line* is the threshold level of the dimensionless concentration of Z cells

with the higher doses of $D_1 = D_2 = 14.55$ Gy and with the same time interval between the first and second exposures τ_1 of 0.25 day is the same as that after single acute irradiation with the dose D of 20.37 Gy. This implies that the ratio of the total dose of two-fractionated irradiation ($D_{tot} = 29.1$ Gy) to the dose of single acute irradiation ($D = 20.37$ Gy), which lead to the same local minimum of the dimensionless concentration of the corneal cells and, hence, to the same local minimum of the fraction of the area of irradiated skin without moist desquamation, is equal to 1.43.

Figure 9.32 demonstrates that the local minimum of the dimensionless concentration of the corneal cells after two-fractionated irradiation with the doses of $D_1 = D_2 = 15.52$ Gy and with the time interval between the first and second exposures τ_1 of 1.0 day is the same as that after single acute irradiation with the dose D of 19.4 Gy. This implies that the ratio of the total dose of two-fractionated irradiation ($D_{tot} = 31.04$ Gy) to the dose of single acute irradiation ($D = 19.4$ Gy), which lead to the same local minimum of the dimensionless concentration of the corneal cells and, hence, to the same local minimum of the fraction of the area of irradiated skin without moist desquamation, is equal to 1.6. In turn, as one can see from Fig. 9.33, the local minimum of the dimensionless concentration of the corneal cells after two-fractionated irradiation with the higher doses of $D_1 = D_2 = 16.49$ Gy and with

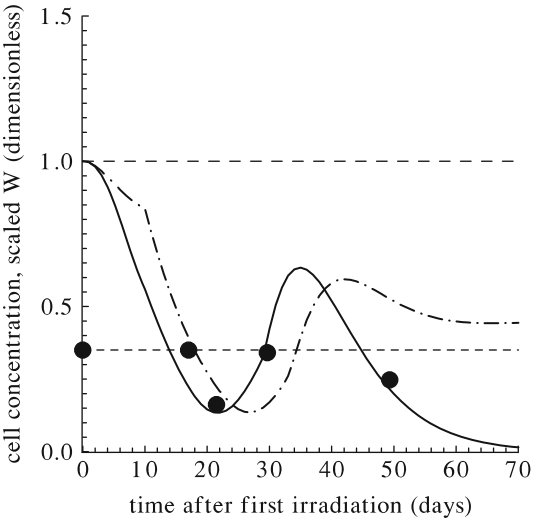

Fig. 9.33 The response of the swine skin to two-fractionated irradiation with the exposure doses of $D_1 = D_2 = 16.49$ Gy and with the time interval between the exposures of $\tau_1 = 1.0$ day: scaled experimental values of the fraction of area of swine skin without moist desquamation $W(t)$ [58] (*circles*) and the modeling dynamics of the dimensionless concentration of the corneal cells (Z cells) (*solid curve*). The response of the swine skin to single acute irradiation with the dose of $D = 20.37$ Gy: the modeling dynamics of the dimensionless concentration of Z cells (*dot-dashed curve*). *Medium-dashed line* is the normal level of the dimensionless concentration of Z cells; *short-dashed line* is the threshold level of the dimensionless concentration of Z cells

the same time interval between the first and second exposures τ_1 of 1.0 day is the same as that after single acute irradiation with the dose D of 20.37 Gy. This implies that the ratio of the total dose of two-fractionated irradiation ($D_{tot} = 32.98$ Gy) to the dose of single acute irradiation ($D = 20.37$ Gy), which lead to the same local minimum of the dimensionless concentration of the corneal cells and, hence, to the same local minimum of the fraction of the area of irradiated skin without moist desquamation, is equal to 1.62.

Figure 9.34 shows that the local minimum of the dimensionless concentration of the corneal cells after five-fractionated irradiation with the doses of $D_1 = D_2 = D_3 = D_4 = D_5 = 6.79$ Gy and with the time intervals between the exposures of $\tau_1 = \tau_2 = \tau_3 = \tau_4 = 1.0$ day is the same as that after single acute irradiation with the dose D of 19.4 Gy. This implies that the ratio of the total dose of five-fractionated irradiation ($D_{tot} = 33.95$ Gy) to the dose of single acute irradiation ($D = 19.4$ Gy), which lead to the same local minimum of the dimensionless concentration of the corneal cells and, hence, to the same minimal level of the fraction of the area of irradiated skin without moist desquamation, is equal to 1.75. It is important to stress that this modeling prediction completely coincides with the experimental estimation of this value (1.75) obtained at the same radiation conditions in [59]. In turn, as one can infer from Fig. 9.35, the local minimum of the dimensionless

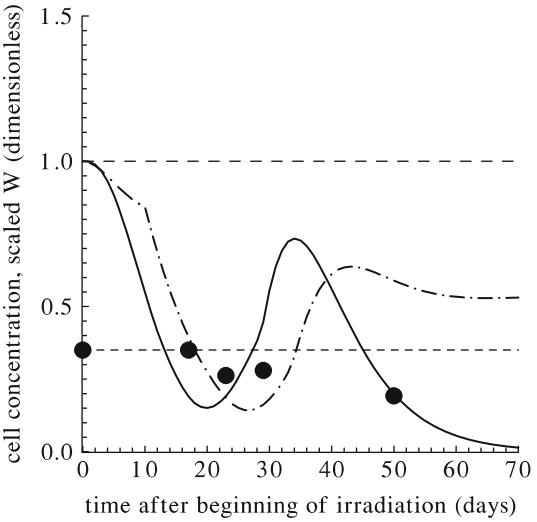

Fig. 9.34 The response of the swine skin to five-fractionated irradiation with the exposure doses of $D_1 = D_2 = D_3 = D_4 = D_5 = 6.79$ Gy and with the time interval between the exposures of $\tau_1 = \tau_2 = \tau_3 = \tau_4 = 1.0$ day: scaled experimental values of the fraction of area of swine skin without moist desquamation $W(t)$ [58] (*circles*) and the modeling dynamics of the dimensionless concentration of the corneal cells (Z cells) (*solid curve*). The response of the swine skin to single acute irradiation with the dose of $D = 19.4$ Gy: the modeling dynamics of the dimensionless concentration of Z cells (*dot-dashed curve*). *Medium-dashed line* is the normal level of the dimensionless concentration of Z cells; *short-dashed line* is the threshold level of the dimensionless concentration of Z cells

concentration of the corneal cells after five-fractionated irradiation with the higher doses of $D_1 = D_2 = D_3 = D_4 = D_5 = 8.73$ Gy and with the same time intervals between the exposures of $\tau_1 = \tau_2 = \tau_3 = \tau_4 = 1.0$ day is the same as that after single acute irradiation with the dose D of 22.31 Gy. This implies that the ratio of the total dose of five-fractionated irradiation ($D_{tot} = 43.65$ Gy) to the dose of single acute irradiation ($D = 22.31$ Gy), which lead to the same local minimum of the dimensionless concentration of the corneal cells and, hence, to the same local minimum of the fraction of the area of irradiated skin without moist desquamation, is equal to 1.96. It is worthwhile to note that this quantity, practically, coincides with the experimental estimation of this value (2.0) obtained at the same radiation regimes in [59].

These modeling findings can be interpreted in the following way. First, the employment of n-fractionated irradiation allows one to use a higher total dose of such irradiation in comparison with the respective dose of single acute irradiation to provide the same minimal level of the noninvolvement of irradiated skin into the moist desquamation. Second, the increase of the time interval between the exposures allows one to use a higher total dose of fractionated irradiation in comparison with the respective dose of single acute irradiation to provide the same minimal level

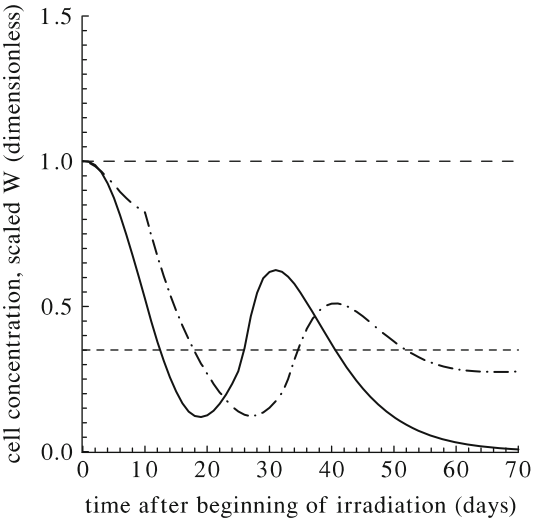

Fig. 9.35 The response of the swine skin to five-fractionated irradiation with the exposure doses of $D_1 = D_2 = D_3 = D_4 = D_5 = 8.73$ Gy and with the time interval between the exposures of $\tau_1 = \tau_2 = \tau_3 = \tau_4 = 1.0$ day: the modeling dynamics of the dimensionless concentration of the corneal cells (Z cells) (*solid curve*). The response of the swine skin to single acute irradiation with the dose of $D = 22.31$ Gy: the modeling dynamics of the dimensionless concentration of Z cells (*dot-dashed curve*). *Medium-dashed line* is the normal level of the dimensionless concentration of Z cells; *short-dashed line* is the threshold level of the dimensionless concentration of Z cells

of the noninvolvement of irradiated skin into the moist desquamation. Third, the increase of the number of fractions n allows one to use a higher total dose of n-fractionated irradiation in comparison with the dose of single acute exposure to provide the same minimal level of the noninvolvement of irradiated skin into the moist desquamation. All these modeling predictions correspond to experimental observations [58].

Figures 9.36, 9.37, 9.38, 9.39, 9.40, and 9.41 present the function $W(t)$ [Eq. 9.90], which is computed in the framework of the developed model [Eqs. (9.50)–(9.57)] at the aforementioned six scenarios of fractionated irradiation reported in [58, 59]. Figures 9.36, 9.37, 9.38, 9.39, and 9.40 also show the respective experimental values of the fraction of the area of irradiated skin without moist desquamation [58]. As one can infer from these figures, the function $W(t)$ obtained at the considered six scenarios of fractionated irradiation stays at its normal level (unity) within a certain period. Then the function $W(t)$ decreases and reaches its local minimum. After that, the function $W(t)$ increases and approaches the normal level (unity). The function $W(t)$ stays at its normal level within a certain period, after which it decreases again. All these modeling findings correspond qualitatively to the experimental observation [58, 59]. Moreover, the values of $W(t)$, which are computed by the developed model at the scenarios of fractionated irradiation reported in [58],

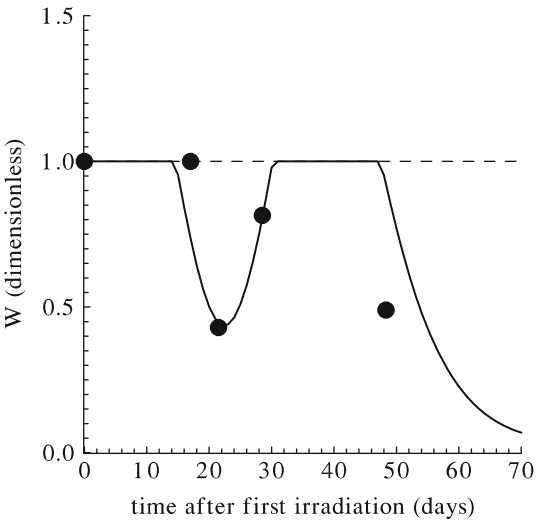

Fig. 9.36 The response of the swine skin to two-fractionated irradiation with the exposure doses of $D_1 = D_2 = 13.58$ Gy and with the time interval between the exposures of $\tau_1 = 0.25$ day: the modeling dynamics of the fraction of area of irradiated skin without moist desquamation $W(t)$ [Eq. (9.90)] (*solid curve*) and the respective experimental values of the fraction of area of irradiated skin without moist desquamation $W(t)$ [58] (*circles*). *Medium-dashed line* is the normal level of $W(t)$

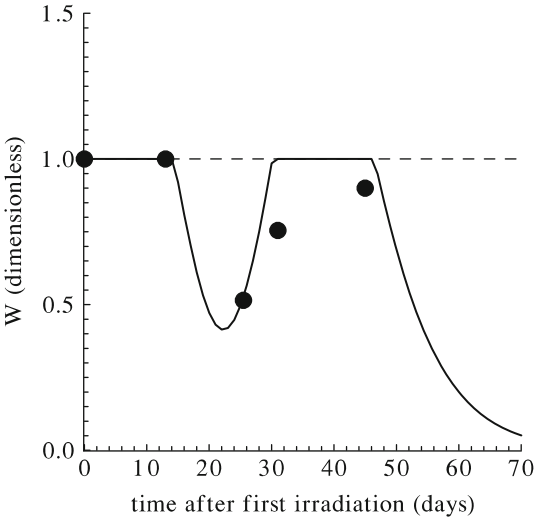

Fig. 9.37 The response of the swine skin to two-fractionated irradiation with the exposure doses of $D_1 = D_2 = 14.55$ Gy and with the time interval between the exposures of $\tau_1 = 0.25$ day: the modeling dynamics of the fraction of area of irradiated skin without moist desquamation $W(t)$ [Eq. (9.90)] (*solid curve*) and the respective experimental values of the fraction of area of irradiated skin without moist desquamation $W(t)$ [58] (*circles*). *Medium-dashed line* is the normal level of $W(t)$

practically, coincide with the respective experimental values of the fraction of the area of irradiated skin without moist desquamation obtained at the same scenarios of fractionated irradiation [58].

All this testifies to the validity of employment of the developed model in the prediction of the dynamics of the moist desquamation in swine skin exposed to n-fractionated irradiation in the wide dose range. The developed model of the skin epidermis can also be useful in the elaboration of optimal regimes of fractionated irradiation to minimize such negative physiological reaction of skin as the moist desquamation.

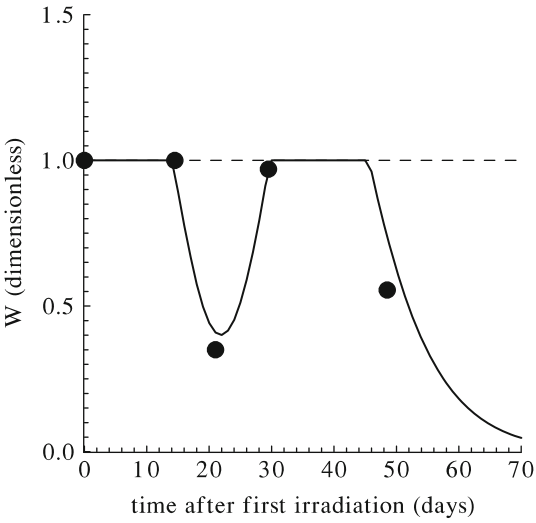

Fig. 9.38 The response of the swine skin to two-fractionated irradiation with the exposure doses of $D_1 = D_2 = 15.52$ Gy and with the time interval between the exposures of $\tau_1 = 1.0$ day: the modeling dynamics of the fraction of area of irradiated skin without moist desquamation $W(t)$ [Eq. (9.90)] (*solid curve*) and the respective experimental values of the fraction of area of irradiated skin without moist desquamation $W(t)$ [58] (*circles*). *Medium-dashed line* is the normal level of $W(t)$

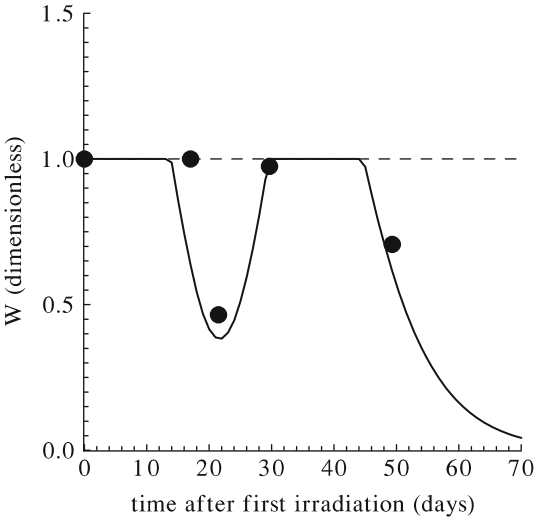

Fig. 9.39 The response of the swine skin to two-fractionated irradiation with the exposure doses of $D_1 = D_2 = 16.49$ Gy and with the time interval between the exposures of $\tau_1 = 1.0$ day: the modeling dynamics of the fraction of area of irradiated skin without moist desquamation $W(t)$ [Eq. (9.90)] (*solid curve*) and the respective experimental values of the fraction of area of irradiated skin without moist desquamation $W(t)$ [58] (*circles*). *Medium-dashed line* is the normal level of $W(t)$

9.8 Conclusion

The biologically motivated mathematical model, which describes the dynamics of the skin epidermal epithelium under the normal conditions and under single and fractionated irradiation, is developed and thoroughly investigated. The model accounts for the principal stages of development of keratinocytes prevailing in this system, as well as peculiarities of its functioning. The identification and verification of the model are performed by making use of experimental data on the dynamics of this vital body system in young swine, which is regarded as the best animal model for the studies of the radiation effects on the human skin.

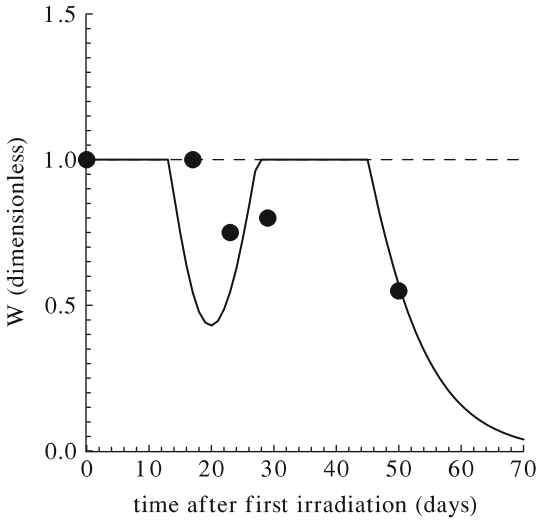

Fig. 9.40 The response of the swine skin to five-fractionated irradiation with the exposure doses of $D_1 = D_2 = D_3 = D_4 = D_5 = 6.79$ Gy and with the time interval between the exposures of $\tau_1 = \tau_2 = \tau_3 = \tau_4 = 1.0$ day: the modeling dynamics of the fraction of area of irradiated skin without moist desquamation $W(t)$ [Eq. (9.90)] (*solid curve*) and the respective experimental values of the fraction of area of irradiated skin without moist desquamation $W(t)$ [58] (*circles*). *Medium-dashed line* is the normal level of $W(t)$

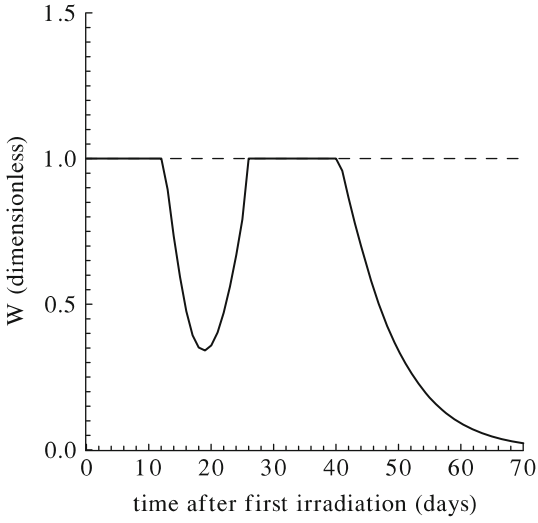

Fig. 9.41 The response of the swine skin to five-fractionated irradiation with the exposure doses of $D_1 = D_2 = D_3 = D_4 = D_5 = 8.73$ Gy and with the time interval between the exposures of $\tau_1 = \tau_2 = \tau_3 = \tau_4 = 1.0$ day: the modeling dynamics of the fraction of area of irradiated skin without moist desquamation $W(t)$ [Eq. (9.90)] (*solid curve*). *Medium-dashed line* is the normal level of $W(t)$

It is shown that the developed model is capable of reproducing the stable dynamical equilibrium state (the homeostasis state) in the system in question under the normal conditions. The model is also capable of reproducing the stable oscillations of concentrations of keratinocytes (basal, prickle, and corneal cells) around the

level decreased in comparison with the norm, as well as the stable oscillations of the mitotic index of basal cells around the level increased in comparison with the norm. Additionally, the model is capable of reproducing the periodic character of the dynamics of the moist desquamation of the skin. Such dynamical regime can be interpreted as a skin disease characterized by periodic exacerbations. The reasons of the appearance of such abnormal dynamical regime in the skin epidermal epithelium are elucidated. The obtained results attest that the developed model of the skin epidermal epithelium accounts for the principal regulatory mechanisms governing the functioning of the skin epidermal epithelium under the normal conditions. The obtained results also testify that the developed model can be used in studies of cyclic skin diseases.

It is demonstrated that the developed model is capable of reproducing the dynamics of concentrations of keratinocytes (basal, prickle, and corneal cells) and the dynamics of mitotic index of basal cells in the swine skin epidermis within 10 weeks after acute irradiation with doses of $16 \div 26$ Gy. The obtained agreement of the modeling results with relevant experimental data attests that the developed model of the skin epidermal epithelium accounts for the principal regulatory mechanisms governing the functioning of this system during the aforementioned period after acute irradiation. The obtained agreement also testifies that the developed model can be used in studies and prediction of the response of the swine skin epidermal epithelium to acute irradiation in the wide range of doses (16–26 Gy).

It is revealed that the dynamics of the dimensionless concentration of corneal cells in acutely irradiated swine skin, which is predicted by the developed model, correlates with the corresponding experimental data on the dynamics of the fraction of the area of the swine skin without moist desquamation. Basing on these modeling findings, the formula, which allows one to predict the dynamics of the moist desquamation in acutely irradiated skin proceeding from the respective dynamics of the aforementioned skin epidermal cells, is proposed. It is demonstrated that the modeling predictions of the dynamics of the moist desquamation in swine skin under acute irradiation in the wide range of doses are in a good agreement with the respective experimental data.

It is also found that the dynamics of the dimensionless concentration of corneal cells in swine skin under fractionated irradiation, which is predicted by the developed model, correlates with the corresponding experimental data on the dynamics of the fraction of the area of the swine skin without moist desquamation. It is demonstrated that the aforementioned formula allows one to predict the dynamics of the moist desquamation in skin epidermis under fractionated irradiation proceeding from the respective dynamics of the skin epidermal cells computed in the framework of the developed model. Specifically, the modeling predictions of the dynamics of the moist desquamation in swine skin under fractionated irradiation in the wide range of total doses ($27 \div 44$ Gy) are in a good agreement with the respective experimental data.

All these modeling results testify to the validity of employment of the developed model in the prediction of the dynamics of the swine skin epidermal epithelium and the dynamics of the moist desquamation in swine skin under the normal conditions and under single and fractionated irradiation.

The developed model of the skin epidermal epithelium constitutes an universal tool of the investigation and prediction of the dynamics of this vital body system under normal conditions and under single and fractionated irradiation in wide ranges of doses and total doses. All the modeling finding implies that this model, after appropriate identification, can be used in the investigation and prediction of radiation effects on the skin epidermal epithelium in humans. In particular, the properly identified model could be applied to predict the radiation injury of the skin epidermis for accidents victims. The modeling results would help to elaborate an appropriate tactics of their treatment. Such model could also be used for predicting the radiation injury of the skin epidermis in patients exposed to fractionated irradiation in courses of cancer therapy. One more area of the application of such model is the investigation and prediction of effects of space radiation on the skin epidermis of astronauts in long-term space missions, such as voyages to Mars or Lunar colonies. The obtained modeling predictions would provide a better understanding of the risks to health from the solar particles events and enable one to evaluate the need for operational applications of countermeasures for astronauts.

References

1. Blanpain C., Fuchs E. Epidermal homeostasis: a balancing act of stem cells in the skin. Nature Reviews. Molecular Cell Biology, v. 10, pp. 207–217, 2009.
2. Kumar V., Abbas A.K., Fausto N., Aster J. (Eds.). Pathologic Basis of Disease, 8th edition. Philadelphia, PA, USA: Saunders Elsevier, pp. 79–110, 2010.
3. McGrath J.A., Uitto J. Anatomy and organization of human skin. In: Burns T., Breathnach S., Cox N., Griffiths C. (Eds.). Rook's textbook of dermatology, 8th edition. Oxford, UK: Wiley-Blackwell, 3-1–3-15, 2010.
4. Langham W.H. (Ed.). Radiobiological factors in manned space flight. Publication 1487. Washington, DC: National Academy of Sciences, 1967.
5. Malkinson F.D., Keane J.T. Radiobiology of the skin: Review of some effects on epidermis and hair. The Journal of Investigative Dermatology, v. 77, pp. 133–138, 1981.
6. Hopewell JW. Mechanisms of the action of radiation on skin and underlying tissues. In: Radiation Damage to Skin. British Journal of Radiology, Suppl. 19. London: British Institute of Radiology, pp. 39–47, 1986.
7. Hopewell J.W. The skin: its structure and response to ionizing radiation. International Journal of Radiation Biology, v. 57(4), pp. 751–773, 1990.
8. NCRP Report No. 106. Limit for exposure to "hot particles" on the skin. Bethesda, MD: NCRPM, 1989.
9. ICRP Publication No 85. Radiopathology of skin and eye and radiation risk. Annals of the ICRP, v. 30, pp. 25–31, 2000.
10. Ryan J.L. Ionizing Radiation: the good, the bad, and the ugly. Journal of Investigative Dermatology, v. 132, pp. 985–993, 2012.
11. Hegazy M.A.H., Fowler J.F. Cell population kinetics and desquamation skin reactions in plucked and unplucked mouse skin. Cell and Tissue Kinetics, v. 6, pp. 587–602, 1973.
12. Davalia H.L., Mansfield L. Radiotherapy and wound healing. International Wound Journal, v. 5, pp. 40–44, 2008.
13. Strom D.J. Health impacts from acute radiation exposure. Report PNNL-14424. Richland, Washington: Pacific Northwest National Laboratory, 2003.

14. Haskin F.E., Harper F.T., Gooseens L.H., Kraan B.C.P., Grupa J.B., Randall J. Probabilistic accident consequence uncertainty analysis: early health effects uncertainty assessment. Main Report. NUREG/CR-6545, EUR 15855 Vol. 1. Washington, D.C.: US Nuclear Regulatory Commission, 1997.
15. Carnell L., Blattnig S., Hu S., Huff J.L., Kim M.H., Norman R., Patel Z., Simonsen L., Wu H., Casey R., Cucinotta F.A. Risk of Acute Radiation Syndromes Due to Solar Particle Events. NASA Technical Report JSC-CN-35747, 2016.
16. Smirnova O.A., Hu S., Cucinotta F.A. Dynamics of acutely irradiated skin epidermal epithelium in swine: modeling studies. Health Physics, v. 107, pp. 47–59, 2014.
17. Smirnova O.A., Cucinotta F.A. Skin response to single and fractionated irradiation: dynamical modeling approach. Health Physics (in press).
18. Bullough W.S. The chalones. Science, v. 5, pp. 71–76, 1969.
19. Bullough W.S. Chalone control mechanism. Life Sciences, v. 16(3), pp. 323–330, 1975.
20. Elgjo K., Devik F. Growth regulation in *X*-irradiated mouth skin. The possible role of chalones. International Journal of Radiation Biology, v. 34(2), pp. 119–127, 1978.
21. Romanov J.A., Ketlinsky S.A., Antokhin A.I., Okulov V.B. Chalones and regulation of cell division. Moscow: Meditsina, 1984 (Russian).
22. Smirnova O.A. Blood and small intestine cell kinetics under radiation exposures: Mathematical modeling. Advances in Space Research, v. 44, pp. 1457–1469, 2009.
23. Smirnova O.A. Modeling study of radiation effects on thrombocytopoietic and granulocytopoietic systems in humans. Advances in Space Research, v. 48, pp. 184–198, 2011.
24. Smirnova O.A., Hu S., Cucinotta F.A. Analysis of the lymphocytopoiesis dynamics in nonirradiated and irradiated humans: a modeling approach. Radiation Research, v. 181, pp. 240–250, 2014.
25. Romanovsky J.M., Stepanova N.V., Chernavsky D.S. Kinetische Modelle in der Biophysik. Stuttgart: Gustav Fischer Verlag, 1974.
26. Romanovsky J.M., Stepanova N.V., Chernavsky D.S. Mathematical modeling in biophysics. Moscow: Nauka, 1975 (Russian).
27. Romanovsky J.M., Stepanova N.V., Chernavsky D.S. Mathematical modeling in biophysics. Introduction to theoretical biophysics. Moscow-Izhevsk: Scientific-Publishing Centre Regular and Chaotic Dynamics, 2004 (In Russian).
28. Gruzdev G.P. Problems of Haemopoietic Tissue Damage Under Acute Radiation Pathology. Moscow: Meditsina, 1968 (In Russian).
29. Loeffler M., Potten C.S., Wichmann H.E. Epidermal cell proliferation. Virchows Archiv B v. 53, pp. 286–300, 1987.
30. Smirnova OA. Comparative analysis of the dynamics of thrombocytopoietic, granulocytopoietic, and erythropoietic systems in irradiated humans: a modeling approach. Health Physics, v. 103(6), pp. 787–801, 2012.
31. Smirnova O.A. Modeling Analysis of the dynamics of thrombocytopoietic, granulocytopoietic, and erythropoietic systems in irradiated humans. Journal of Radiation Research, v. 55, p. i36, 2014.
32. Smirnova O.A. Myeloid leukemia risk assessment and dynamics of the granulocytopoietic system in acutely and continuously irradiated humans: modeling approach. Health Physics, v. 108(5), pp. 492–502, 2015.
33. Lea D.E. Action of radiation on living cells, 2nd edition. Cambridge: The Syndics of the Cambridge University Press, 1955.
34. Bond V.P., Fliendner T.M., Archambeau J.O. Mammalian radiation lethality: a disturbance in cellular kinetics. New York: Academic Press, 1965.
35. Archambeau J.O., Bennet G.W., Abata J.J., Brenneis H.J. Response of swine skin to acute exposure to *X* rays: quantification of the epidermal cell changes. Radiation Research, v. 79, pp. 298–337, 1979.

36. Archambeau J.O., Ines A., Fajardo L.F. Response of swine skin microvasculature to acute single exposures of *X* rays: quantification of endothelial changes. Radiation Research, v. 98, pp. 37–51, 1984.
37. Archambeau J.O., Ines A., Fajardo L.F. Correlation of the dermal microvasculature morphology with the epidermal and the endothelial population changes produced by single *X* ray fractions of 1649, 2231 and 2619 rad in swine. International Journal of Radiation Oncology, Biology, Physics, v. 11, pp. 1639–1646, 1985.
38. Oldham K.B., Myland J.C., Spanier J. An atlas of functions. New York, USA: Springer, pp. 405–415, 2009.
39. Morris G.M., Hopewell J.W. Pig epidermis: a cell kinetic study. Cell and Tissue Kinetics, v. 18, pp. 407–415, 1985.
40. Montagna W., Yun J.S. The skin of the domestic pig. Journal of Investigative Dermatology, v. 42, pp. 11–21, 1964.
41. Archambeau J.O., Bennett G.W. Quantification of morphologic, cytologic, and kinetic parameters of unirradiated swine skin: a histologic model. Radiation Research, v. 98, pp. 254–273, 1984.
42. Morris G.M., Hopewell J.W. Changes in the cell kinetics of pig epidermis after repeated daily doses of X-rays. In: Radiation damage to skin. British Journal of Radiology, Suppl. 19. London: British Institute of Radiology, pp. 34–38, 1986.
43. Archambeau J.O., Mathieu G.R., Brenneis H.J., Tompson K.H., and Fairchild R.G. Response of skin of swine to increasing single exposures of 250-KVp *X*-rays. Radiation Research, v. 36, pp. 299–326, 1968.
44. Hopewell J.W., Young C.M. Changes in the microcirculation of normal tissues after irradiation. International Journal of Radiation Oncology, Biology, Physics, v. 4(1-2), pp. 53–58, 1978.
45. Hopewell J.W., Young C.M. The effect of field size on the reaction of pig skin to single doses of X rays. The British Journal of Radiology, v. 55(653), pp. 356–361, 1982.
46. Redpath J.L., Peel D.M., Dodd P., Simmonds R.H., Hopewell J.W. Repopulation in irradiated pig skin: late versus early effects. Radiotherapy and Oncology, v. 3(2), pp. 173–176, 1985.
47. Morris G.M., Hopewell J.W. Changes in the cell kinetics of pig epidermis after single doses of *X* rays. The British Journal of Radiology, v. 61, pp. 205–211, 1988.
48. Mahl J.A., Vogel B.E., Court M., Kolopp M., Roman D., Nogues V. The minipig in dermatotoxicology: methods and challenges. Experimental and Toxicologic Pathology, v. 57, pp. 341–345, 2006.
49. Agay D., Scherthan H., Forcheron F., Grenier N., Herodin F., Meineke V., Drouet M. Multipotent mesenchymal stem cell grafting to treat cutaneous radiation syndrome: development of a new minipig model. Experimental Hematology, v. 38, pp. 945–956, 2010.
50. Ahmed E.A., Agay D., Schrock G., Drouet M., Meineke V., Scherthan H. Persistent DNA damage after high dose in vivo gamma exposure of minipig skin, PLoS One, v. 7(6), pp. e39521, 2012.
51. Forcheron F., Agay D., Scherthan H., Riccobono D., Herodin F., Meineke V., Drouet M. Autologous adipocyte derived stem cells favour healing in a minipig model of cutaneous radiation syndrome. PLoS One, V. 7, pp. e31694, 2012.
52. Belousova O.I., Gorizontov P.D., Fedotova M.I. Radiation and blood forming system. Moscow: Atomizdat, pp. 6–23, 1979.
53. Pontryagin L.S. Ordinary Differential Equations. Moscow: Nauka, 1982 (Russian).
54. Arrowsmith D.K., Place C.M. Ordinary Differential Equations. A Qualitative Approach with Applications. London: Chapman and Hall, 1982.
55. Andronov A.A., Vitt A.A., Khikin S.E. Theory of Oscillations. Moscow: Nauka, 1981 (Russian).
56. Hayashi C. Nonlinear Oscillations in Physical Systems. McGraw-Hill Book Company, New York, 1964.

57. Dulac H. Sur les cycles limités. Bulletin de la Société Mathématique de France, v. 51, pp. 45–188, 1923.
58. Archambeau J.O., Mathieu G.R., Brenneis H.J., Tompson K.H. The response of skin of swine to increasing multiple exposures of *X*-rays (250-kVp). Radiation Research, v. 37, pp. 141–160, 1969.
59. Fowler J.F., Morgan R.L., Silvester J.A., Bewley D.K., Turner B.A. Experiments with fractionated X-ray treatment of the skin of pigs. The British Journal of Radiology, v. 36, pp. 188–196, 1963.

Conclusions

The monograph presents the biologically motivated dynamic modeling approach to the study and prediction of radiation effects on mammals. This approach embodies the author's mathematical models, which are capable of predicting the dynamics of vital body systems in mammals (namely, the hematopoietic system in rodents and humans, the immune system in rodents, the small intestine in rodents, and the skin in young swine) under normal conditions and under various irradiation regimes (acute/chronic/fractionated/non-uniform irradiation). The developed approach also includes the author's mathematical models, which are capable of prognosticating the mortality dynamics and the average life span shortening for homogeneous and nonhomogeneous (in radiosensitivity) mammalian populations exposed to acute and chronic irradiation in wide ranges of doses and dose rates on the basis of the statistical characteristics and the modeling dynamics of the respective critical body system (the hematopoietic system or the small intestine) in exposed specimens composing the population. The developed approach demonstrates its efficiency in the assessment of the excess relative risks for leukemia among acutely and continuously irradiated humans (the atomic bomb survivors and patients treated with brachytherapy) proceeding from two key characteristics of the respective modeling dynamics of human major hematopoietic lineages (the granulopoietic and lymphopoietic systems). The developed approach also proves its reliability in the prediction of the dynamics of the pathophysiological reaction (moist desquamation) in skin exposed to single and fractionated irradiation in wide ranges of doses and total doses on the basis of the respective modeling dynamics of epidermal cells of the upper skin layer.

A principal advantage of the developed approach consists in the fact that the elaborated mathematical models enable one to reveal and describe the main reason–consequence relationships between the formation of radiobiological effects at various levels of organization of biological objects: from isolated cells and vital body systems to entire organism and whole population, which includes specimens with various radiosensitivity.

O.A. Smirnova, *Environmental Radiation Effects on Mammals*,
DOI 10.1007/978-3-319-45761-1

The monograph summarizes the formulation and construction of the aforementioned mathematical models, their analytical and numerical analysis, and the obtained results. The performed theoretical investigations make a valuable contribution to radiation biology and ecology. In particular, these studies elucidate the major regulatory mechanisms of the damage and recovery processes running in the vital body systems of exposed mammals. The proposed explanations of a number of nonlinear effects of the low-level acute/chronic irradiation on the vital body systems, on the organism as a whole, and on entire nonhomogeneous mammalian population are of a particular theoretical significance, since these effects still have no unambiguous interpretation. The proposed explanation of experimentally observed distinctive features of effects of non-uniform and uniform acute irradiation on the major hematopoietic lineages in rodents is of a definite theoretical significance, too. Furthermore, the models of the radiation-induced mortality lay down the theoretical foundations for a new individual-based approach to radiation risk assessment. The most appealing feature of these mortality models consists in the fact that they account for the intrinsic properties of the exposed organism and the individual variability of radiosensitivity. These models enable one to predict the mortality dynamics and the average life span shortening for homogeneous and nonhomogeneous, in radiosensitivity, populations exposed to both acute and, most importantly, low-level chronic irradiation.

The materials presented in the monograph can be applied to a broad range of practical tasks related to environmental radiation safety. In particular, performed studies of the dynamical models of the major hematopoietic lineages (the thrombopoietic, erythropoietic, granulopoietic, and lymphopoietic systems) in humans testify to the efficiency of employment of these models in the investigation and prediction of effects of space radiation on these major hematopoietic lineages. These models of the human hematopoietic system, as well as the models of other vital body systems (after appropriate identification), could provide a better understanding of the risks to health from the space radiation environment and enable one to evaluate the need for operational applications of countermeasures for astronauts on long-term space missions. The developed models of the human hematopoietic system, as well as the properly identified models of other vital body systems, could also be used for predicting the radiation injury of these systems for people residing in contaminated areas after nuclear power plant accidents. Obtained results would help the decision makers to evaluate the hazard for the health of such people and to take proper decisions for operational applications of all necessary countermeasures including their settling out, as well as for their subsequent resettling. These models could also be applied to assessment of the health hazard for clean-up crew members taking part in the elimination of consequences of such accidents.

The demonstrated efficiency of the employment of the biologically motivated dynamic modeling approach in estimating the excess relative risks for leukemia among acutely and continuously irradiated humans attests to its applicability to the assessment of the radiogenic leukemia risk among people residing in contaminated areas after nuclear power plant accidents, among clean-up crew members taking part in the elimination of consequences of such accidents, among astronauts on

long-term space missions, among person subjected to occupational irradiation (uranium miners, radiologists, and others), as well as among patients treated with radiotherapy.

The properly identified mortality models could be employed as a tool for estimating the risks for populations residing in contaminated areas. These models could also be applied to estimate the risk of long-term irradiation in manned space missions, such as voyages to Mars and Lunar colonies.

Index

O.A. Smirnova, *Environmental Radiation Effects on Mammals*,
DOI 10.1007/978-3-319-45761-1